

©2012

David A. Harrison

ALL RIGHTS RESERVED

IDENTIFICATION AND CHARACTERIZATION OF CRITICAL LAMININ-111
SEQUENCES REQUIRED FOR POLYMERIZATION AND CELL SURFACE
ANCHORAGE AND THE REQUIREMENT OF BOTH ACTIVITIES FOR PROPER
BASEMENT MEMBRANE FORMATION AND OTHER EVENTS

by

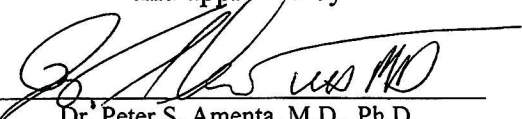
DAVID A. HARRISON

A Dissertation submitted to the Graduate School-New Brunswick; Rutgers, The State
University of New Jersey and The Graduate School of Biomedical Sciences; University
of Medicine and Dentistry of New Jersey

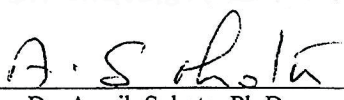
In partial fulfillment of the requirements for the degree of
Doctor of Philosophy

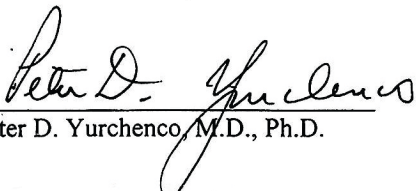
Joint Graduate Program in Biochemistry and Molecular Biology
Rutgers University & The University of Medicine and Dentistry of New Jersey
written under the direction of Dr. Peter D. Yurchenco

and approved by


Dr. Peter S. Amenta, M.D., Ph.D.


Dr. Chavela M. Carr, Ph.D.


Dr. Amrik Sahota, Ph.D.


Dr. Peter D. Yurchenco, M.D., Ph.D.

New Brunswick, New Jersey

May 2012

ABSTRACT OF THE DISSERTATION

Identification and Characterization of Critical Laminin-111 Sequences Required for Polymerization and Cell Surface Anchorage and the Requirement of Both Activities for Proper Basement Membrane Formation and Other Events

by David A. Harrison

Dissertation Advisor:

Peter D. Yurchenco, M.D., Ph.D.

A system was developed for expression and purification of various recombinant $\alpha 1$ LG4-5 and heterotrimeric laminin-111 proteins. A number of combinations involving different promoters, 5'UTRs, signal sequences, epitope tags, selectable antibiotics, and purification schemes were tested in order to optimize the system. A homology model of laminin $\alpha 1$ LG4-5 was generated and utilized to identify candidates for mutation and expression as recombinant $\alpha 1$ LG4-5 proteins. The crystal structure of $\alpha 1$ LG4-5 was also determined. Heparin, α -dystroglycan (α DG), and sulfatide binding of the generated mutants demonstrated wide differences and dependence upon contributions from basic residues on the surface of LG4, including: RKR₂₇₂₁ and KRK₂₇₉₃ for heparin; RAR₂₈₃₃, KDR₂₈₆₀, the Asn₂₈₁₁ glycation moiety, and the LG4 Ca²⁺ ion for α DG; the LG4 Ca²⁺, Arg₂₈₃₃ of RAR₂₈₃₃, and Lys₂₇₆₆ residue of RKGRTK₂₇₇₀ for one sulfatide binding site, and the Arg₂₈₃₁ of RAR₂₈₃₃ for a second sulfatide site.

The produced recombinant heterotrimeric laminin-111s demonstrated a requirement for the N-terminal LN domains of laminin-111's constituent $\alpha 1$, $\beta 1$, and $\gamma 1$ chains in self-polymerization. The inability of embryoid bodies, derived from laminin $\gamma 1$ null embryonic stem cells, to express Lm-111 and develop past formation of an outer endodermal layer of cells without laminin, was utilized via the addition of exogeneous recombinant laminin-

111s, to test the various functions of the recombinant laminins and their ability to form a basement membrane and induce both differentiation of an epiblast layer and formation of a central cavity. Laminins' containing defective polymerization or $\alpha 1$ LG4 anchorage failed to form a BM or undergo any further development after endodermal differentiation.

Experiments with Schwann cells, C2C12 myotubes, and mouse embryonic fibroblasts demonstrated the requirement for both polymerization and $\alpha 1$ LG4 mediated anchorage in laminin-111 for proper BM formation, cytoskeletal attachment, and laminin induced cell signaling via Src. The results also suggest a role for laminin-111 polymerization and anchorage in providing a means for aggregation and accumulation of low affinity interactions in a complex, thereby attaining very high net affinities for binding interactions and attaining otherwise unattainable thresholds necessary for these interactions to exert their effects through manipulation of the cytoskeleton, as well as, laminin induced differentiation and cell signaling.

Acknowledgements

I would like to thank my advisor Peter Yurchenco for his support and encouragement, especially his willingness to let me explore new ideas, make mistakes, and develop as a scientist. I am also thankful for members of the Yurchenco lab, past and present, and the many people in the department who have been great colleagues. Of these colleagues I want to particularly thank Raj Patel, Holly Colognato, Todd Mathus, Yi-Shan Cheng, Shaohua Li, Tricia Liquari, Nancy Martin, John Togneri, David Foran, Don Winkelman, Cathy Hanus, Gautam Kao, Karen McKee, Stephanie Capizzi, Sergei Smirnov, and Ann Latrielle. I am tremendously grateful for Peter Amenta's support and that of my other committee members who were always very helpful and understanding: Barbara Brodsky, Amrik Sahota, and Bob Trelstad. I would also like to acknowledge that actual mice and rabbits were harmed in the making of this work and that their sacrifices were greatly appreciated, for without them, much of this work could not have been accomplished. I would also like to thank my family for their support, and especially my daughter Samantha, without whose smile and infectious laughter life would be less bright. Thank you all for letting me play for so long.

TABLE OF CONTENTS

Abstract	p. iii
Acknowledgements	p. v
Chapter 1. Introduction & Background	p. 1
I. Laminin	p. 5
A. The laminin family	p. 5
B. Individual laminin chains	p. 7
C. Laminin-111	p. 10
II. Laminin activities and basement membrane formation	p. 11
A. Laminin polymerization	p. 11
B. Laminin binding interactions	p. 11
1. Laminin binding to other ECM and BM components	p. 13
a. Type IV collagen	p. 13
b. Nidogen	p. 14
c. Perlecan	p. 14
d. Agrin	p. 16
2. Laminin binding to cellular receptors and anchors	p. 17
a. Integrins	p. 17
b. Dystroglycan	p. 18
c. Heparin, heparan sulfate, and other sulfated glycans	p. 20
1.) HNK-1	p. 20
2.) Syndecans	p. 21
3.) Glypicans	p. 22
d. Sulfatide and other sulfated glycolipids	p. 23

C. Extracellular matrix genes and their related diseases	p. 23
D. The resulting phenotype observed from targeted deletion of ECM and BM proteins, as well as their receptors	p. 24
E. Laminins and early embryonic development	p. 25
1. The role of laminin-111 in dystroglycan null ES cell differentiation, BM formation, and EB formation	p. 27
2. The role of laminin-111 in β 1 integrin null ES cell differentiation, BM formation, and EB formation	p. 27
3. The role of laminin-111 in γ 1 laminin null ES cell differentiation, BM formation, and EB formation	p. 29
F. The role of laminin in the peripheral and central nervous systems	p. 30
1. Src activation and downstream cell signaling events induced in Schwann cells by the addition of exogenous Lm-111	p. 33
2. FAK activation induced in Schwann cells by the addition of exogenous Lm-111	p. 34
G. Laminin binding to mouse embryonic fibroblasts and their response	p. 35
1. Lm-111 induced cell signalling in MEFs	p. 35
Chapter 2. Materials and Methods	p. 38
Selection of the promoter for α 1LG4-5 and other recombinant laminin expression constructs	p.38
Selection of 5'UTR for recombinant α 1LG4-5 constructs	p. 39
Selection of signal sequence for recombinant α 1LG4-5 constructs	p. 40
Selection of epitope tags for recombinant α 1LG4-5 constructs	p. 40
Designed proteolytic cleavage of epitope tags from recombinant proteins	p. 41

Selectable markers and antibiotics	p. 41
Expression vectors	p. 42
Secondary structure prediction, homolgy modeling, refinement of the generated predicted three dimensional structure, and selection of amino acid residues to analyze in α 1LG4-5	p.43
Recombinant α 1LG4-5 protein production and purification	p. 44
Proteoyltic cleavage with EK and TEV	p. 45
Rotary shadow electron microscoy of recombinant α 1LG4-5 proteins	p. 46
Heparin binding of laminin α 1LG4-5 (EHS E3 fragment) and recombinant α 1LG4-5 proteins	p. 47
Analysis of recombinant α 1LG4-5 proteins binding to α DG	p. 47
Analysis of recombinant α 1LG4-5 binding to galactosyl sulfatide and other lipids as well as lipids utilized in other experiments	p. 48
Antibiotics utilized and kill curves generated	p. 51
Antibodies	p. 52
Antibodies and immunofluorescence microscopy	p. 53
Immunoprecipitation (IP) and immunoblotting (IB)	p. 55
Protein visulatizations and quantifications	p. 56
Polymerization assays with laminin, collagen, and nidogen	p. 56
Sulfatide (and other lipids) loading of cells	p. 56
Flourescence microscopy of Schwann and fibroblast cells	p. 57
Electron microscopy	p. 57
Schwann cell culturing	p. 58
Mouse embryonic lung fibroblasts	p. 59
Lipid raft visualization in MEFs	p. 59

Culturing of embryonic stem cells and embryoid bodies	p. 60
Other proteins utilized in this study	p. 61
Expression constructs	p. 64
Construction of recombinant α 1LG4-5 constructs	p. 64
Construction of mouse α 1 based expression constructs other than α 1LG4-5	p. 69
Construction of β 1 laminin based expression constructs	p. 84
Construction of γ 1 laminin based expression constructs	p. 87
Transfection and Establishment of Heterotrimeric Recombinant Lm-111s	p. 89
 Chapter 3. Production and Characterization of α1LG4-5s	 p. 91
I. Recombinant mouse α 1LG4-5s	p. 93
A. Promoter selection	p. 94
B. 5' UTR sequence selection	p. 94
C. Signal sequence selection	p. 95
D. Epitope tag selection	p. 96
E. Engineered proteolytic cleavage sequence	p. 97
F. Selection of selectable markers, antibiotics, and expression vectors	p. 99
G. Creation of a three dimensional model for α 1 LG4-5 and selection of amino acid residues to examine	p. 100
H. Generation and expression of recombinant mouse α 1LG4-5s	p. 103
II. Characterization of recombinant mouse α 1LG4-5s	p. 106
A. Heparin binding affinity of recombinant α 1LG4-5s	p. 107
B. α -Dystroglycan binding affinity of recombinant α 1LG4-5s	p. 107
C. Sulfatide binding affinity of recombinant α 1LG4-5s	p. 109
D. Ability of recombinant α 1LG4-5s to inhibit binding of Lm-111 to sulfatide	p. 111

E. Crystalization and structure determination of mouse laminin $\alpha 1$ LG4-5	p. 111
F. Structural comparison of $\alpha 1$ LG4-5 and $\alpha 2$ LG4-5, as well as, identification of the similarities and differences between the two proteins in the spatial location of key amino acid residues	p. 114
III. Summary	p. 119
A. Expression of recombinant $\alpha 1$ LG4-5 proteins	p. 119
B. Generation of a homology model for $\alpha 1$ LG4-5 and selection of amino acid residues to mutate	p. 131
C. Characterization of recombinant $\alpha 1$ LG4-5s	p. 132
1. Heparin affinity	p. 132
2. α DG affinity	p. 133
3. Sulfatide affinity	p. 136
D. The three dimensional structure of mouse $\alpha 1$ LG4-5 and its implications for amino acid residues identified to interact with heparin, sulfatide, and α -dystroglycan.	p. 140

Chapter 4. Production, Characterization, and Biological Activity of

Heterotrimeric Recombinant Laminin-111s.	p. 144
I. Establishment of a mixed species strategy for reliable production of recombinant heterotrimeric laminin-111s	p. 145
A. Establishment of an all mouse recombinant heterotrimeric laminin-111	p. 145
B. Establishment of an all human recombinant heterotrimeric laminin-111	p. 147
C. Adoption of a recombinant mouse $\alpha 1$ / human $\beta 1$ / human $\gamma 1$ containing laminin-111 strategy	p. 149
II. Characterization of recombinant laminin-111s	p. 153

A. Polymerization of recombinant laminin-111s	p. 154
B. Heparin affinity of recombinant laminin-111s and laminin-211s	p. 156
C. Sulfatide affinity of recombinant laminin-111s and laminin-211s	p. 157
III. The role of laminin-111 and its receptors in Schwann cells	p. 159
A. Individual domain and amino acid residue requirements of Lm-111 for BM formation on the surface of cultured Schwann cells	p. 159
B. Ultrastructure of Schwann cell surfaces with and without the addition of exogenous Lm-111s	p. 164
C. Comparison of laminin-111 and laminin-211 binding and BM formation on Schwann cell surfaces	p. 166
IV. The role of laminin-111 in embryonic stem cell differentiation, basement membrane formation, and embryoid body formation	p. 167
A. The role of laminin-111 in γ 1 laminin null ES/EB BM formation and differentiation.	p. 169
V. The role of laminin-111 and its receptors in C2C12 myotubes	p. 172
VI. The role of laminin-111 and its receptors in embryonic fibroblasts	p. 173
A. The accumulation and condensation of exogeneous Lm-111 on the cell surfaces of MEFs without the aid of sulfatide loading	p. 173
B. Inhibition of exogenous Lm-111 accumulation on MEF cell surfaces by the simultaneous addition of recombinant α 1LG4-5 proteins	p. 176
C. Accumulation of various exogenous recombinant heterotrimeric Lm-111s on the cell surfaces of MEFs	p. 176
VII. Summary	p. 178
A. Expression and characterization of recombinant heterotrimeric laminin-111s.	p. 180

B. The role of laminin, its domains, individual amino acid residues, binding activities, and anchors/receptors in binding, accumulation and basement membrane formation on Schwann cell surfaces	p. 183
C. Interactions of recombinant laminins with type IV collagen and nidogen.	p. 189
D. The effect of AEBSF treatment upon laminin-111 activities and ability to form a BM	p. 190
E. Implications of potential $\beta 1$ integrin inhibition by the C-terminal FLAG epitope tag on the $\gamma 1$ chain of recombinant heterotrimeric laminins	p. 190
F. The role of Lm-111 in ES cell differentiation, BM formation, and embryoid body formation	p. 191
G. The role of laminin-111 and its receptors in C2C12 myotubes	p. 194
H. Insights derived from the role of laminin-111 and its receptors in MEFs	p. 195
 Chapter 5. Summary and Conclusions	 p. 203
 Figure Legends	 p. 213
 Figures	 p. 251
 Tables	 p. 325
 Appendix	 p. 350
 Appendix Figure Legends	 p. 359

Appendix Figures	p. 366
Appendix Tables	p. 385
References	p. 386
Abbreviations	p. 429
Acknowledgements	p. 432

Note: 1) The new domain nomenclature described by Aumailley et al. (2005) is used throughout this thesis.

LIST OF ILLUSTRATIONS

p. 252	Figure 1.	Potential laminin interactions.
p. 253	Figure 2.	The laminin family.
p. 254	Figure 3.	The proteolytic fragments of laminin-111.
p. 255	Figure 4.	The summation of EST expression results for laminin α chains in NCBI's GEO repository.
p. 256	Figure 5.	The summation of EST expression results for laminin β chains in NCBI's GEO repository.
p. 257	Figure 6.	The summation of EST expression results for laminin γ chains in NCBI's GEO repository.
p. 258	Figure 7.	The number of amino acid residues composing laminin-111, its constituent $\alpha 1$, $\beta 1$, and $\gamma 1$ chains, and other proteins it interacts with, as well as the location in Lm-111 of these binding interactions.
p. 259	Figure 8.	Extracellular matrix genes and related diseases.
p. 260	Figure 9.	Mouse knockout results of ECM proteins, their receptors, and related BM components.
p. 261	Figure 10.	Embryoid body development.
p. 262	Figure 11.	Amino acid sequence of mouse laminin $\alpha 1$ LG1-5.
p. 263	Figure 12.	The amino acid sequence of the elastase proteolytic fragment E3 derived from mouse Lm-111.
p. 264	Figure 13.	Optimization of recombination protein production – selection of promoter, signal sequence, and 5'UTR for expression constructs.
p. 265	Figure 14.	Determination of signal sequence cleavage sites.

p. 266	Figure 15.	Epitope tagging of recombinant mouse $\alpha 1$ LG4-5 laminins.
p. 267	Figure 16.	Puromycin based expression construct DHpuro and the mouse $\alpha 1$ laminin construct, $\alpha 1_{Nf}$, derived from DHpuro.
p. 268	Figure 17.	Conservation of the primary sequence between the LG4-5 of mouse $\alpha 1$ and $\alpha 2$ laminin.
p. 269	Figure 18.	Conservation of both primary sequence and predicted potential secondary structure between mouse $\alpha 1$ and $\alpha 2$ LG4-5 of laminin.
p. 270	Figure 19.	Homology model of mouse $\alpha 1$ LG4-5 (recombinant E3 analog).
p. 271	Figure 20.	Comparison of both the spatial and primary location of Arg, Lys, His, and Cys residues in mouse laminin $\alpha 1$ and $\alpha 2$ LG4-5.
p. 272	Figure 21.	Mutational combinations of Arg and Lys residues in initial recombinant $\alpha 1$ LG4-5 screen.
p. 273	Figure 22.	Generation, production, and purification of recombinant mouse $\alpha 1$ LG4-5 laminins.
p. 274	Figure 23.	Heparin affinity of recombinant mouse $\alpha 1$ LG4-5 laminins.
p. 275	Figure 24.	α DG affinity of recombinant mouse $\alpha 1$ LG4-5 laminins.
p. 276	Figure 25.	Sulfatide specificity and affinity of recombinant mouse $\alpha 1$ LG4-5 laminins.
p. 277	Figure 26.	Sulfatide affinity of mutant recombinant mouse $\alpha 1$ LG4-5 laminins.
p. 278	Figure 27.	Comparing the three dimensional crystal structure, Cys residues, and disulfide linkages of $\alpha 1$ and $\alpha 2$ LG4-5.
p. 279	Figure 28.	Crystal structure of mouse laminin $\alpha 1$ LG4-5.

p. 280	Figure 29.	Comparing the crystal structure of the individual LG4 and LG5 domains of mouse $\alpha 1$ and $\alpha 2$ laminin.
p. 281	Figure 30.	Comparing the three dimensional crystal structure, domain separation, and domain interface interactions of $\alpha 1$ and $\alpha 2$ LG4-5.
p. 282	Figure 31.	Secondary structure, charge distribution, and spatial location of mutated amino acid residues on the surface of the crystal derived three dimensional structure of $\alpha 1$ LG4-5.
p. 283	Figure 32.	Characterization of endogeneous and transfected laminin mRNA expression in HEK 293 cells.
p. 284	Figure 33.	Recombinant heterotrimeric laminin-111 and laminin-211 composed entirely of all mouse derived α , β , and γ chains.
p. 285	Figure 34.	Recombinant heterotrimeric laminin-111 composed entirely of all human derived α , β , and γ chains.
p. 286	Figure 35.	Recombinant full length $\alpha 1$ laminin chains constructed and utilized to make rLm-111s.
p. 287	Figure 36.	Recombinant $\alpha 1$ laminin N-terminal deletions constructed and utilized to make rLm-111s.
p. 288	Figure 37.	Recombinant $\alpha 1$ laminin G domain manipulated constructs utilized to make rLm-111s.
p. 289	Figure 38.	Recombinant $\beta 1$ laminins constructed and utilized to make rLm-111s.
p. 290	Figure 39.	Recombinant $\gamma 1$ laminin chains constructed and utilized to make rLm-111s .

p. 291	Figure 40.	Coomassie blue stained SDS-PAGE gels of various recombinant heterotrimeric Lm-111s.
p. 292	Figure 41.	Examination of different N-terminal epitope tags on the N-terminus of full length mouse α 1 laminin chains in recombinant heterotrimeric laminin-111s.
p. 293	Figure 42.	Accumulation of recombinant LN-LEb constructs in a solid phase association assay.
p. 294	Figure 43.	Heparin binding affinities of recombinant Lm-111s and Lm-211s.
p. 295	Figure 44.	Sulfatide binding affinities of recombinant Lm-111s and Lm-211s.
p. 296	Figure 45.	Laminin-111 binding to sulfatide albumin complexes.
p. 297	Figure 46.	Inhibition of Lm-111 binding to Schwann cell surfaces.
p. 298	Figure 47.	Inhibition of Lm-111 binding to the cell surface of Schwann cells via contemporary addition of recombinant α 1LG4-5 proteins.
p. 299	Figure 48.	Assembly of heterotrimeric recombinant Lm-111s on the surface of Schwann cells.
p. 300	Figure 49.	The binding of recombinant heterotrimeric laminins to the cell surface of Schwann cells.
p. 301	Figure 50.	The binding of heterotrimeric α 1LG4 point mutations Lm-111s, as well as, the effect of concurrent addition of exogenous Nd-1 and Coll IV, to the cell surface of Schwann cells.

p. 302	Figure 51.	Electron microscopy images depicting the accumulation of recombinant heterotrimeric Lm-111s and BM formation on the cell surface of Schwann cells (1 of 2).
p. 303	Figure 52.	Electron microscopy images depicting the accumulation of recombinant heterotrimeric Lm-111s and BM formation on the cell surface of Schwann cells (2 of 2).
p. 304	Figure 53.	Comparison of recombinant Lm-111 and Lm-211 BM formation on Schwann cell surfaces.
p. 305	Figure 54.	Basement membrane formation and epiblast differentiation in wild-type, $\beta 1$ integrin null and $\gamma 1$ laminin null embroid bodies.
p. 306	Figure 55.	Exogenous Lm-111 induced BM formation and epiblast differentiation in $\gamma 1$ laminin null EBs.
p. 307	Figure 56.	Binding of various recombinant heterotrimeric Lm-111s on the surface of C2C12 myotubes.
p. 308	Figure 57.	Inhibition of Lm-111 binding to C2C12 myotube surfaces via laminin receptor blocking antibodies and recombinant $\alpha 1$ LG4-5.
p. 309	Figure 58.	Inhibition of EHS Lm-111 binding to C2C12 myotubes by various recombinant $\alpha 1$ LG4-5s.
p. 310	Figure 59.	Accumulation of exogenous Lm-111 on cell surfaces of MEFs without sulfatide loading.
p. 311	Figure 60.	Accumulation of exogenous Lm-111 and other macromolecules on the surface of MEFs in the absence of sulfatide (1 of 2).

p. 312	Figure 61.	Accumulation of exogeneous Lm-111 and other macromolecules on the surface of MEFs in the absence of sulfatide (2 of 2).
p. 313	Figure 62.	Accumulation and condensation of exogeneous Lm-111 on MEF cell surfaces over time, in the absence of sulfatide.
p. 314	Figure 63.	Inability to form higher order aggregates and a BM on the surface of MEFs without the presence of sulfatide.
p. 315	Figure 64.	Time course of multiple loadings of Alexa 488 labeled Lm-111 onto the surface of MEFs in the absence of sulfatide.
p. 316	Figure 65.	Sulfated glycolipid specificity of Lm-111 binding to the surface of MEFs.
p. 317	Figure 66.	Inhibition of exogeneous Lm-111 accumulation on MEF cell surfaces (in the absence of sulfatide) by contemporaneous addition of recombinant α 1LG4-5 proteins.
p. 318	Figure 67.	Accumulation of various exogeneous recombinant heterotrimeric laminins on the cell surface of MEFs in the absence of sulfatide.
p. 319	Figure 68.	Differences in accumulation patterns on MEF cell surfaces (sulfatide not present) between recombinant heterotrimeric laminins, as a consequence of their polymerization capability.
p. 320	Figure 69.	Recombinant α 1G4-5 inhibition of Lm-111 binding.
p. 321	Figure 70.	Embryoid body summary.
p. 322	Figure 71.	Basement membrane formation and epiblast differentiation in γ 1 laminin null embryoid bodies treated with Lm-111, modified Lm-111, Lm-111 fragments, and recombinant Lm-111s.

p. 323	Figure 72.	Lm-111 binding, accumulation, condensation, formation of higher order complexes, BM formation, and cell signaling.
p. 324	Figure 73.	Spatial location of binding activities in mouse $\alpha 1$ LG4.

LIST OF TABLES

p. 326	Table 1.	Temporal and spatial expressin patterns of individual laminin chains.
p. 327	Table 2.	Primer table and diagram for construction of recombinant α 1LG4-5/WT.
p. 328	Table 3.	Oligonucleotide primer table and diagram for construction of mutant recombinant α 1LG4-5s.
p. 329	Table 4.	Individual recombinant laminin constructs - mouse α 1 LG4-5s.
p. 331	Table 5.	Individual recombinant laminin chain constructs - α 1 based constructs.
p. 332	Table 6.	Construction of mouse laminin α chain expression constructs and other assorted information.
p. 341	Table 7.	Individual recombinant laminin chain constructs - β 1 based constructs.
p. 342	Table 8.	Construction of laminin β chain expression constructs and other assorted information.
p. 345	Table 9.	Individual recombinant laminin chain constructs - γ 1 based constructs.
p. 346	Table 10.	Construction of laminin γ chain expression constructs and other assorted information.
p. 347	Table 11.	Recombinant heterotrimeric laminin - construct composition.
p. 349	Table 12.	Summary of recombinant mouse α 1 LG4-5 binding data.

APPENDIX – LIST OF TABLES & LIST OF ILLUSTRATIONS

p. 366	Figure 1.	Laminin chain expression profiles suggested by analysis of EST counts.
p. 367	Figure 2.	Rotary shadow EM of heterotrimeric Lm-111s.
p. 368	Figure 3.	Higher magnification rotary shadow EM of heterotrimeric Lm-111s.
p. 369	Figure 4.	Polymerization ability of recombinant heterotrimeric Lm-111s – SDS-PAGE results.
p. 370	Figure 5.	Polymerization ability of recombinant heterotrimeric Lm-111s – plotted results.
p. 371	Figure 6.	Accumulation, aggregation, and condensation of exogeneous Lm-111 on cell surfaces of sparsely plated Schwann cell cultures.
p. 372	Figure 7.	Accumulation, aggregation, and condensation of exogeneous Lm-111 on cell surfaces of near confluent Schwann cell cultures.
p. 373	Figure 8.	Accumulation, aggregation, and condensation of exogeneous Alexa-488 labeled Lm-111 on Schwann cell surfaces.
p. 374	Figure 9.	Accumulation, aggregation, and condensation of exogeneous Alexa-488 labeled Lm-111 on Schwann cell surfaces – single cell.
p. 375	Figure 10.	α Dystroglycan, nidogen-1, and type IV collagen expression in cultured Schwann cells.
p. 376	Figure 11.	Perlecan, syndecan-1, and syndecan-3 expression in cultured Schwann cells.

p. 377	Figure 12.	β 1 integrin, sulfatide, and agrin expression in cultured Schwann cells.
p. 378	Figure 13.	Contributions of type IV collagen and nidogen to ECM assembly.
p. 379	Figure 14.	Electron microscopy images depicting the accumulation of recombinant heterotrimeric Lm-111s and BM formation on the cell surface of Schwann cells in the presence or absence of type IV collagen and nidogen-1.
p. 380	Figure 15.	The different stages of differentiation and development WT ES cells undergo during embryoid body development.
p. 381	Figure 16.	Immunofluorescence and electron microscopy of exogenous Laminin-111 induction of BM formation, epiblast differentiation, and cavitation in γ 1 laminin null EBs: aggregation and condensation.
p. 382	Figure 17.	Immunofluorescence and electron microscopy of exogenous Laminin-111 induction of BM formation, epiblast differentiation, and cavitation in γ 1 laminin null EBs: BM formation, formation and elongation of epiblast layer.
p. 383	Figure 18.	Immunofluorescence and electron microscopy of exogenous Laminin-111 induction of BM formation, epiblast differentiation, and cavitation in γ 1 laminin null EBs: cavitation.
p. 384	Figure 19.	Basement membrane formation and epiblast differentiation in γ 1 laminin null embryoid bodies treated with Lm-111, modified Lm-111, Lm-111 fragments, and recombinant Lm-111s.
p. 385	Table 1.	Crystallographic statistics for recombinant mouse α 1 LG4-5.

Chapter 1. Introduction & Background

Laminins represent a major glycoprotein family of the cell surface extracellular matrices (ECMs) known as basement membranes (BMs). BMs are cell surface-associated extracellular matrices usually found either as sheets separating cell layers or as enveloping cell coats and are the first extracellular matrices to appear during embryogenesis [1, 2]. They first appear prior to the onset of gastrulation, as the embryo develops two cell layers and can be found associated with several different cell types in many different tissues. These BMs contain networks of laminin (Lm) and type IV collagen that become enmeshed and form a scaffolding that other extracellular matrix proteins, such as nidogens, agrin, perlecan, biglycan, type XVIII collagen, fibronectin, and growth factors can bind to (figure 1). Furthermore, BMs are anchored to various cell surfaces through receptors such as integrins, dystroglycan, syndecans, glypicans, and sulfated glycolipids such as sulfatide. BMs contribute to the permeability-selectivity between tissue compartments, serve as substrates for cell adhesion and migration, and regulate cell behavior and differentiation. Members of the laminin family are thought to be essential for the assembly and proper functioning of BMs during and after embryonic development. Mutations of different laminin chain have been found to cause debilitating and even life-threatening diseases of peripheral nerve, skeletal muscle, brain, skin, and kidney. Each laminin molecule consists of three different subunits, each substantial in size and composed of a linear array of domains, and joined together through a long heterotrimeric coiled-coil arrangement. One of the longstanding goals in the ECM field has been to understand the molecular basis of laminin interactions with itself, with other BM components, and with cell surface binding molecules and receptors. This knowledge is important if one is to gain mechanistic insights into the complex functions of BMs during development and in the pathogenesis of different diseases.

Early work suggested (1) that laminins attach to cell surfaces through their C-terminal α subunit LG domains; binding to sulfatides, heparan sulfates, and the receptor alpha dystroglycan (α DG), and (2) that laminins polymerize through their N-terminal LN domains, creating initial extracellular scaffoldings for attachment of other ECM components. However, advancement of these analyses to formulate a detailed molecular model with predictive value has been hampered by the existence of only a relatively small repertoire of protein fragments that are quite large and that contain several to very many domains each with multiple binding interactions. This problem, recognized by various laboratories, was approached by combining the tools of molecular genetics with those of protein biochemistry and cell biology. Success was variable (e.g. proteins expressed in prokaryotic cells usually lacked proper folding and function) and often slow, particularly in the case of laminins with their large size, complex carbohydrate modifications, and heterotrimeric complexity. The need to generate recombinant fragments and whole laminins became further apparent when it was realized that the different activities of laminin acted cooperatively on cells.

In order to overcome the technical difficulties and begin to learn about laminin adhesive and self-assembly functions at a domain and sequence level, I embarked on a project to develop a library of recombinant laminin fragments and laminin-111 heterotrimers that contained various deletion and point mutations. Many conditions of construct design, epitope tag usage, antibiotic selection, mammalian cell transfection strategies, and recombinant protein purification needed to be first worked out before it was even possible to examine function. In time, a library of secreted and glycosylated recombinant α 1 LG4-5 domains and recombinant heterotrimeric laminins was developed that could then be analyzed for binding properties and cellular interactions. The project was of such magnitude that there were collaborations developed with different

laboratory members from within and outside our own laboratory. I have attempted to credit individuals where appropriate.

The first major project was to generate an all mouse heterotrimeric laminin-111, however, there were issues with the γ 1 chain being secreted by itself, chain imbalance, degradation, and failure to establish a permanent line with sustained expression of the heterotrimeric Lm-111s and Lm-211s. Effort was then put into developing an all human heterotrimeric Lm-111, however, despite trying several construct variations, the vast majority of the produced heterotrimeric Lm-111 contained an α 1 chain which was proteolytically cleaved in the coiled-coil region and also had some minor proteolytic degradation associated with it.

In the meanwhile another major project was initiated: generation of recombinant laminin α 1 fragments containing the LG4 domain previously implicated in cell adhesion. The crystal coordinates of laminin α 1's homolog, α 2 LG4-5, were utilized with the aid of several homology modeling and energy minimization computer programs to generate a three dimensional model of α 1 LG4-5. Based on this generated model and previous binding study data, a series of point mutations altering the lysine and arginine residues thought to be involved in heparin, sulfatide, and dystroglycan binding were introduced into the protein sequence and tested. The proteins were purified by virtue of an N-terminal FLAG epitope tag and analyzed for intactness and correct size. Wild type recombinant protein bound to all three ligands examined: heparin, sulfatide, and α DG (purified recombinant protein was supplied to Dr. James Ervasti who performed the α DG binding analysis). The different mutant α 1 LG4-5 recombinant proteins exhibited reduced ligand binding to various extents. The recombinant protein and expression constructs were then utilized by another collaborator, Erhard Hohenester, to crystallize and determine the structure of mouse α 1 LG4-5. The α DG, sulfatide, and heparin

binding sites were mapped to the generated structure and appear to be partially overlapping patches on the surface of the LG4 domain. This project also provided a system for more easily examining and perfecting the components and procedures necessary for establishing an efficient heterotrimeric recombinant system. Combinations of different promoters, signal sequences, 5'UTRs, epitope tags, and antibiotic selectable markers, were utilized in a multitude of expression constructs and both the quality and quantity of expressed recombinant proteins examined and compared in order to determine which elements worked best in combination with each other.

It was found that the mouse $\alpha 1$ chain could be expressed along with the human $\beta 1$ and $\gamma 1$ chains to make a stable non-proteolytically processed heterotrimeric laminin-111. This project became the focus of several people in the lab over the years. The system was utilized to analyze the role of the individual chain N-terminal LN domains in laminin polymerization, as well as, the role of laminin polymerization in laminin's ability to form a basement membrane and induce differentiation and cell signaling events. C-terminal $\alpha 1$ LG domain deletions and point mutations were also generated in order to test their role in these same processes.

Section I. Laminin.

Not only is laminin (Lm) the most abundant glycoprotein in BMs [1], but also, the first detectable matrix protein to be expressed during embryogenesis. The protein products of both the $\beta 1$ and $\gamma 1$ chains of Lm are detectable at the 2-4 cell stage of mouse embryogenesis [1, 2], however, the $\alpha 1$ chain product is not detectable until the 16-cell stage. The first BMs appear around embryonic day (E) 3.5-4.

Section IA. The laminin family.

Laminin was first identified in a mouse teratocarcinoma, the EHS-tumor (Englebreth-Holm-Swarm, named after its discoverers). All Lms are heterotrimeric; consisting of an α chain and two shorter chains, the β and γ chains (figure 2A). Presently, there have been 5 α , 3 β , and 3 γ chains identified (figure 2B). The combination of the various chains determine the respective Lm type: laminin-111 (is composed of an $\alpha 1$, $\beta 1$, and $\gamma 1$ chain), laminin-211 (consists of an $\alpha 2$, $\beta 1$, and $\gamma 1$ chain), etc. [3]. It is believed that the molecules are not expressed in every possible $\alpha/\beta/\gamma$ combination, however, at least 15 of the potential 54 Lm isoforms have been positively identified so far. The molecular weights of the individual laminin chains range from 140-400 kDa and the heterotrimeric Lms range in size from 400-900 kDa.

Heterotrimeric laminins are cross or T shaped with two or three short arms and one long arm ending in a cluster of five globular domains. The short arms are composed of the N-terminal parts of each of the three chains and consist of globular domains separated by varying numbers of laminin epidermal growth factor-like domains (LE). The beginning N-terminal globular domain of each chain is called an LN domain and the LE domains vary in number, size, and may contain 6, 8, or 10 cysteines. The long arm

is a triple α -helical coiled-coil formed by all three chains. Heterotrimer formation is due to the hydrophobic and polar interactions of the heptad repeats which compose this coiled-coil region [4]. Disulfide linkages of the three chains occur at the beginning of the coiled-coil domain and at the end of the coiled-coil between the β 1 and γ 1 chain. The β and γ chains' C-termini are found at the end of the coiled-coil, while the α chain extends further to form five C-terminal globular domains termed LG1-5 (see figure 2 for a more detailed description of domain nomenclature).

While all Lm chains are characterized by a homologous domain structure, the α 3 and α 4 chains differ from the α 1 and α 2 chains in that the chain is shorter in the former, with the absence of the globular LN and L4 domains as well as the majority of the LE repeats from the N-terminus. Despite all Lm chains sharing a relatively high degree of homology (figure 2C), only 1 of each chain from each subfamily (α , β , and γ) is represented in the heterotrimeric Lm. The α 5 chain, resembles the α 1 and α 2 chains in structure; however, it shows more sequence similarity to the α 3 and α 4 chains. Furthermore, it demonstrates its greatest homology, not to the mammalian α 1- α 4, but to the only known *Drosophila* α chain.

At least four of the laminin chains (α 2, α 3, α 4, and γ 3) possess alternative splice variants [5-7], however, there is no evidence this occurs with any of the chains which compose Lm-111 (α 1, β 1, or γ 1). Furthermore, all of the alpha chains, with the exception of α 1, have demonstrated proteolytic processing variations within the LG1-5 domains due to posttranslational, and possibly post-secretion, modifications [8-11]. In many cases the cleaved fragment remains bound to the remainder of the G domain. Some laminins, such as Lm-332 are highly proteolytically processed [12, 13] and others such as those containing α 2 [7] and α 4 [14] show minor processing of their C-terminal G domain, however, neither α 1 nor Lm-111 show any evidence of proteolytic processing.

Furthermore, to date, all Lms have been shown to exhibit distinct temporal and spatial expression patterns.

Enzymatic digestion of laminin-111 purified from EHS tumor with cathepsin-G, elastase, pepsin, or trypsin yields proteolytic fragments often used for inhibition and binding studies. Of particular relevance for this study are the cathepsin-G C1-4 fragment (figure 3A) and elastase digestion fragments: E1', E4, E8, and E3 (figure 3B).

Section IB. Individual laminin chains.

The temporal and spatial expression pattern of the 11 individual laminin chains is very diverse. There has only been a few attempts at any sort of comprehensive analysis of laminin chain distribution. Table 1 provides a generalized summary based upon *in situ* hybridizations, Northern, Western, and immunohistochemical staining results. As a general rule: the $\beta 1$ and $\gamma 1$ chains are widely expressed and it is the α chain expression which provides specificity to the individual heterotrimeric laminins; which is understandable since the α chain also provides most of the Lm binding activities observed so far.

The laminin $\alpha 1$ chain is mainly expressed by developing epithelial cells during organogenesis in developing embryos and is the major α chain in early embryogenesis. It is not present (or its expression is at extremely low levels) in embryonic and adult muscle, heart, endothelium, fat, and nerves. In adults the highest levels of $\alpha 1$ are present in placenta, kidney, testis, eye, and liver and exceed that of the other α chains in some parts of these tissues. The liver sinusoids do contain $\alpha 1$ laminin and may be the one exception to the epithelial specific expression and distribution of $\alpha 1$ [15].

The laminin $\alpha 1$ chain is often replaced by $\alpha 2$ and $\alpha 5$ during development and organogenesis [15]. There is more $\alpha 1$ than $\alpha 2$ or $\alpha 5$ in adult kidney, otherwise $\alpha 2$ is in higher concentration than $\alpha 1$ in most other adult tissues [16]. Laminin $\alpha 1$ knock-out mice die around embryonic day E6.5 due to the lack of Reichert's membrane and defective epiblast polarization [17]. Recently, mutant mice that express a truncated laminin-111 molecule that is specifically missing the LG4-5 portion of the laminin $\alpha 1$ chain were generated [18]. The mutant mice die from defective Reichert's membrane, just like the laminin $\alpha 1$ knock-out mice [19]. The $\alpha 2$ chain is most prominent in muscle and peripheral nerve, $\alpha 3$ in stratified epithelia such as skin, $\alpha 4$ in mesenchyme or mesenchyme derived cells such as fat cells, bone marrow, and blood vessels, and $\alpha 5$ is the most ubiquitously expressed α chain. Many cells types produce several laminin isoforms or are exposed to them due to production by adjacent cells [20, 21]. Furthermore, the heterotrimeric nature of laminin makes analysis of its distribution difficult since any given subunit chain may belong to a number of different laminin types, however, the distribution of several heterotrimeric laminins has been discerned.

Due to the growing popularity of high-throughput gene expression methodologies in the last 10 years and the ability of microarray hybridization and serial analysis of gene expression (SAGE) to simultaneously quantify tens of thousands of gene transcripts, NCBI created the Gene Expression Omnibus (GEO) to act as a public repository and user interface to store, organize, analyze, and view all the collected data [22]. GEO is linked to UniGene [23] a system for automatically partitioning GenBank sequences, including ESTs, into a non-redundant set of gene-oriented clusters. UniGene clusters ESTs and links related information, such as: the tissue types in which the gene is expressed, model organism protein similarities, the LocusLink report for the gene, source, and other information. In the human UniGene database there are over 3.6

million human ESTs represented and over 1 billion mouse EST results. These programs and their databases were utilized to create a summary of the number of EST hits for each laminin chain found per tissue/cell line and assay. The results were examined and the theoretical number of ESTs identified per screen equilibrated in order to generate an *in silico* derived representation of the expression profile for each laminin chain. The results were grouped by tissue and are presented by chain subtype: figure 4 - α chains, figure 5 - β chains, and figure 6 - γ chains of laminin (the actual numbers are listed in [appendix figure 1](#)). The results not only allow for quick identification of tissue distribution and theoretical expression level comparisons of individual chains but direct comparison of levels between chains across all tissues examined. This is possible because of the nature of the data obtained. Rather than measuring mRNA or protein levels with probes which will vary from chain to chain, the actual number of transcripts obtained is recorded and is representative of the number of transcripts per tissue for each given chain being expressed in the tissue examined and as such is directly comparable to the data generated from any other chain or tissue examined. For example, figure 4 shows that the $\alpha 1$ chain is the most highly expressed transcript in fetal stages of development, followed by $\alpha 5$, and has the highest level of mRNA expression in the adult kidney of all the laminin α chains. Of course, a limitation of this data is that the number of mRNA transcripts will not necessarily reflect expressed protein levels. However, the results from this analysis compliments those obtained by others via *in situ* hybridization, Northern, Western, immunoprecipitation, and immunohistochemical means.

Section IC. Laminin-111.

Laminin-111 is composed of the $\alpha 1$, $\beta 1$, and $\gamma 1$ chains and was the first laminin identified, sequenced, and studied [25-29]. Laminin-111 appears to be the major laminin expressed during early embryogenesis [30-33]. As a matter of fact, embryogenesis will not proceed without this laminin; a situation we capitalized upon when studying embryoid bodies derived from embryonic stem cells. Expressed in the blastocyst, it appears early during epithelial morphogenesis in most tissues of the embryo [15, 19, 34-36], however, it is mostly absent from adult tissues and remains present as a major epithelial laminin in just a few adult tissues [11, 37-43]. Lm-111 has many binding ligands, including: integrins ($\alpha 1\beta 1$, $\alpha 2\beta 1$, $\alpha 6\beta 1$, $\alpha 6\beta 4$, $\alpha 7\beta 1$, and $\alpha 3\beta 1$), nidogen, agrin, α DG, sulfatide, HNK-1, syndecan-1, perlecan, and fibulin-1.

Section II. Laminin activities and basement membrane formation.

Laminin has been shown to enhance cellular attachment, spreading, growth, and differentiation [45-49]. It performs these functions via specific domains (figures 1 and 7B) of the molecule and its interaction with both other extracellular matrix molecules and via direct connection to the cell surface.

Section IIA. Laminin polymerization.

The N-terminal LN domains from all three laminin chains ($\alpha 1$, $\beta 1$, and $\gamma 1$) which compose Lm-111, participate in the formation of a calcium dependent reversible non-covalent polymerization reaction [50-55]. The critical concentration for polymerization in solution is 70-140 nM, however, the apparent critical concentration can be significantly reduced by interactions on artificially created lipid bilayers layers and on cell surfaces, via laminin's binding and accumulation on these surfaces [56].

Section IIB. Laminin binding interactions.

Both type IV collagen and laminin-111 can self-polymerize to form meshes [51, 54, 57-59]. Electron micrographs of freeze-etched samples reveal a laminin polymer composed of interconnecting struts and vertices separate from the type IV collagen network [54]. Perlecan can bind the NC1 domain of type IV collagen, sulfatide, dystroglycan [60], $\alpha 2\beta 1$ integrin, and the G2 domain of nidogen, while its N-terminal heparan sulfate chains can bind the C-terminal LG4-5 domain of Lm-111 (figure 1). Agrin can bind dystroglycan [61], syndecans, $\alpha V\beta 3$ integrin, and $\alpha 7\beta 1$ integrin. Furthermore, the NtA (~~N~~-terminal

agrin) domain of agrin can bind the coiled-coil domain region of Lm-111. Type IV collagen can bind to both $\alpha 2\beta 1$ and $\alpha 1\beta 1$ integrins, as well as, the G2 and G3 domains of nidogen. The N-terminal domains of nidogen can bind to type IV collagen, fibulin, and perlecan [62-65], while the C-terminal, G3 domain of nidogen, can bind to the NIDPNAV₈₀₄ sequence [66] of the fourth EGF-repeat in domain III of the $\gamma 1$ chain of laminin [21], thus providing a bridge among these components of the BM [43, 53, 55, 63, 65, 67-70]. However, knockout evidence reveals that neither nidogen nor its binding to laminin are essential for basement membrane formation [21, 71, 72]. As stated earlier, the HS chains of perlecan can bind LG4 of laminin. The binding epitope for the HNK-1 carbohydrate motif present on several proteins and lipids has also been mapped to LG2 of the $\alpha 1$ chain [73]. The sulfated glycolipid, sulfatide, has been shown to bind both the N-terminal LN domain and C-terminal LG4 domain of laminin-111 [74, 75]. Both $\alpha 1\beta 1$ and $\alpha 2\beta 1$ integrin can bind the N-terminal LN domain of the $\alpha 1$ chain of Lm while $\alpha 6\beta 1$, $\alpha 6\beta 4$, and $\alpha 7\beta 1$ integrins can bind the LG1-3 domains of the $\alpha 1$ chain [36, 76-79]. Fibulin-1 also binds LG4-5 of the $\alpha 1$ chain. Furthermore, α -dystroglycan, a surface protein that is part of the dystrophin-receptor complex in muscle [80, 81] and syndecans, have been shown to bind LG4 of the $\alpha 1$ chain. These transmembrane receptors link laminin to the cellular cytoskeleton and via these associations, it is thought that laminin mediates some of its effects on cell behavior [82-86]. Figure 7 depicts, not only, the amino acid residue size of Lm-111, its component chains, and $\alpha 1$ LG4-5, but also, the size of Lm-111, other ECM proteins, and several cellular receptors.

Section IIB1. Laminin binding to other extracellular matrix and basement membrane components.

Type IV collagen

The collagen family is ubiquitously expressed and contains at least 28 types. The typical interstitial collagen or “collagen molecule” is a rod about 300nm long and 1.5nm in diameter and consists of three polypeptide strands, each of which is present as a left-handed helix. The three strands are twisted together into a right-handed coiled coil, a triple helix, whose quaternary structure is stabilized by numerous hydrogen bonds. Collagen subunits will self-assemble in regular staggered formations into even larger covalently crosslinked, both within the individual triple helices and between neighboring tropocollagen helices, collagen fibrils. These collagen fibrils can also further associate into organized overlapping bundles termed collagen fibers. A distinctive feature of collagens is their repeating pattern of Gly-X-Pro or Gly-X-Hyp), where X may be any of a number of various amino acid residues. This regular repetition and high Gly content is necessary for proper packing and triple helical formation. The structure of the triple helix necessitates glycine at every third position because there is no room in the interior of the triple helix for any side group other than glycine’s single hydrogen atom. Conversely, the rings of Pro and Hyp must point outward from the triple helix. The high Pro and Hyp (Hydroxyproline) content enables the spontaneous formation and stabilization of left-handed helices without intrachain hydrogen bond formation.

Type IV collagen is found primarily in the basal lamina and like the other collagen family members is composed of a triple helix, however, the long collagenous domain of the individual chains, composed of approximately 1,400 amino acid residues, containing Gly-Xaa-Yaa repeats are not well conserved and are interrupted at several sites by short noncollagenous sequences. There is also a 15 amino acid N-terminal noncollagenous 7S domain, and a 230 residue C-terminal non-collagenous globular NC1 domain which

is not removed during post-translational processing [87-89]. Furthermore, the triple helical monomers associate via their carboxyl termini (NC1 to NC1) to form dimers [90] and via their amino termini (7S-7S-7S-7S) to form tetramers [91], as well as laterally [58, 59, 91, 92] rather than in parallel and form a mesh rather than fibrils. Type IV collagen also lacks the regular repeating Gly at every third position that is required for a tight collagen triple helix. The individual collagen chains are encoded by six genes: COL4A1, COL4A2, COL4A3, COL4A4, COL4A5, and COL4A6. Mutations in these genes lead to Alport syndrome [93-95] and the generation of autoantibodies which lead to Goodpasture syndrome [96-101].

Nidogen

Nidogen has been thought to serve as bridge between laminin and type IV collagen [21, 71, 62, 65, 66, 102, 103]. In 2003, Takagi et al. [104] determined the crystal structure of the nidogen-1 G3-III complex with laminin at a resolution of 2.3 angstroms. The structure of the interacting domains revealed a 6-bladed Tyr-Trp-Thr-Asp (YWTD) beta-propeller domain in nidogen bound to laminin epidermal growth factor-like (LE) modules III3-5 (LE3-5) in laminin. Laminin LE module 4 (LE4) binds to an amphitheater-shaped surface on the pseudo-6-fold axis of the beta-propeller, and laminin LE3 binds over its rim. A Phe residue that shutters the water-filled central aperture of the beta-propeller, the rigidity of the amphitheater, and high shape complementarity enabled the construction of an evolutionarily conserved binding surface for LE4 of unprecedentedly high affinity for its small size.

Perlecan

Perlecan is a major HSPG molecule of the basement membrane. The core protein of perlecan is a 467 KDa HSPG (human) composed of 4,370 amino acids and five

domains. The N-terminal domain I is a unique sulfate-binding region containing three HS chains, domain II has four class A low-density lipoprotein (LDL) receptor like repeats, domain III contains three laminin domain IV (L4) like modules and eight laminin epidermal growth factor (EGF)-like repeats (LE), domain IV contains Ig-like repeats similar to those found in NCAM (domain IV), and the C-terminal domain V possess three C-terminal LG domains of α 1 laminin and four EGF-like repeats (C-terminal domain V), respectively [105, 106].

Mammalian perlecan in the BM is substituted with HS, but may also include chondroitin sulfate (CS), dermatan sulfate (DS), hybrid mixtures, and may even be secreted GAG free [107-113]. The HS chains are heterogeneous in size, however, each HS chain averaged 380 KDa in molecular mass and 87 nm in length when examine by electron microscopy. In addition to HS chains, perlecan bears a further 20 KDa of N- and O-linked oligosaccharide chains, which are suggested to function in the secretion of perlecan. The N-terminal HS chains of perlecan can bind laminin, type IV collagen, and fibronectin [63, 114]. Domain IV can bind to the G2 and G3 domains of nidogen-1 [103], nidogen-2 [78], fibulin-2, and fibronectin [115]. Domain V can bind laminin, nidogen, and fibulin-2 [60].

Perlecan is ubiquitously expressed, found in most BMs and a few connective tissues which do not contain a classic BM, such as cartilage (CS-modified), spleen, lymph nodes, and the sinusoids of the liver [116, 117]. Many different cell types can synthesize perlecan, including: fibroblasts [118], epithelial [119], epidermal [120], endothelial [121], chondrocytes [122], and smooth muscle cells [123]. Because many early embryonic BMs can be formed without perlecan participation, targeted deletion of perlecan does not lead to lethality until approximately E10.

Perlecan and other HSPGs act as low affinity receptors, potentiating the binding of the growth factors such as FGF-2 [121, 124-129] and VEGF [130-133] to their

receptors. Perlecan has also been shown to interact with other growth factors and HSPGs [121, 134-136].

Agrin

Agrin is a heparan sulfate proteoglycan with multiple splice variations, is widely expressed, and induces the aggregation of acetylcholine receptors [137] and other postsynaptic proteins on muscle fibers and is crucial for the formation of the neuromuscular junction (NMJ) [138-143]. It is a 200 kDa HSPG consisting of 1,940 amino acid residues, including 141 Cys residues [144]. The morphological appearance of agrin is an elongated structure (approximately 95 nm long), with an N-terminal globular domain on one end and three globular domains, homologous to the laminin LG domains on the other end [139]. Alternative splicing generates multiple agrin variants which differ in their ability to bind heparin and α DG, as well as, AChR clustering efficiency. The 4 residue (Lys-Ser-Arg-Lys), Y splice site variant in rat agrin (A site in chick agrin) is required for agrin binding to heparin. The neuronal-specific isoforms of agrin contain 8, 11, or 19 amino acids at a splice site referred to as the Z site in rat agrin and the B site in chick agrin [145, 146]. Inclusion of the 8 amino acids at the Z splice site result in an agrin that, not only, binds α DG less tightly by affecting the Ca^{2+} binding dependency, but also, demonstrate a 1,000 fold increase in AcChR clustering activity [141, 147].

Agrin induces the clustering of acetylcholine receptors through the skeletal muscle tyrosine kinase receptor MuSK [148] to activate signaling cascades responsible for multiple aspects of synapse formation, including: organization of the postsynaptic membrane, synapse-specific transcription, and presynaptic differentiation. The tyrosine kinases Ab11 and Ab12 are concentrated at the postsynaptic neuromuscular junction

and mediate postsynaptic AChR clustering downstream of agrin and MuSK signaling [149] via interaction with cytoskeletal regulatory molecules important for synapse assembly and remodeling. Interaction between the AChR beta subunit and APC may also link AChRs to the cytoskeleton and help localize the AChR to the neuromuscular junction [150]. Agrin has also been implicated in inducing the aggregation of signaling proteins in both T-cells and nervous tissue via kinase rich lipid raft microdomains [151]. Neuromuscular differentiation is defective in the agrin knockout mice [152, 153], however, some postsynaptic differentiation does occur.

Section IIB2. Laminin binding to cellular receptors and anchors.

There are several known cellular receptors for laminin, including: integrins, dystroglycan, syndecans, glypicans, and sulfated glycolipids. Several other membrane associated, laminin binding proteins, including: the α -amyloid precursor protein [154, 155], galactosidases [156], a galactosyltransferase [157], and the Lutheran glycoprotein erythrocyte receptors (α 5 laminin specific) [158], have been found, however, with the exception of the Lutheran antigen, the significance of these interactions is largely unknown and, therefore, will not be discussed.

Integrins

Although both α 1 β 1 and α 2 β 1 integrin binding sites are located in the N-terminus of the α 1 chain [159-162] their contribution to cell adhesion may be minor. Of greater impact is the α 6 β 1, α 6 β 4, and α 7 β 1 integrin binding sites found in the C-terminal LG1-3 of the α 1 chain [12, 163-168]. This binding probably also requires the C-terminal portion of the coiled-coil as represented by the elastase proteolytic fragment E8 [169]. As it is, *in vivo*,

the $\alpha 7\beta 1$ integrin and Lm-111 have very different temporal and spatial expression and distribution patterns, therefore, they are seldom present in the same tissue, thereby having very few chances of interacting. One exception, however, is in developing muscle [166, 170, 171]. The $\alpha 6$ integrin subunit has a much broader expression distribution and appears to be specific for members of the laminin family, with the exception perhaps of fertilin, a member of the ADAM family [172-174]. The $\alpha 6$ integrin subunit is detected in many cell type throughout development as different splice variants associated with either the $\beta 1$ or $\beta 4$ integrin subunit. The $\alpha 6\beta 1$ integrins are often associated with focal adhesion complexes, while $\alpha 6\beta 4$ integrins are found in hemidesmosomes [175]. Integrin $\alpha 6$ knockouts were perinatal lethal due to defects in epithelial formation, loss of dermal-epidermal adhesion, and subsequent skin blistering [176], as well as central nervous system defects [177]. However, the expected defects in many tissues, such as the kidney and lung, never manifested [176, 178-180].

Dystroglycan

The dystroglycan (DG) gene encodes for both alpha-dystroglycan (α DG) and beta-dystroglycan (β DG), which are derived by posttranslational cleavage of a precursor polypeptide. The 43 kDa (241 amino acid) β DG is an integral membrane protein, whereas, the 156 kDa (623 amino acid) α DG is membrane-associated through its noncovalent interaction with the extracellular domain of β DG [181, 182]. Dystroglycan provides a linkage between components of basement membranes and cytoplasmic proteins that bind to the actin cytoskeleton [94] and initiate cytoskeletal rearrangements, as well as, cell signaling complexes. α DG binds both agrin and perlecan [142, 183, 184]. It has also been shown that α DG present in Schwann cells can bind both agrin and Lm-211 [185], as well as Lm-111. Utrophin colocalizes with agrin induced AcChR

clusters through binding to β DG [186]. Furthermore, the structural integrity of the sarcolemma, in both skeletal and cardiac muscle, depends not only upon binding of the cytoplasmic protein dystrophin to both actin and the cytoplasmic tail of β DG, but also, binding of α DG to laminin-211 in the basal lamina.

Carbohydrates contained within the "neck" region of the α DG subunit are required [165, 187, 188] for binding to specific basic residues within the LG4 domain of the α 1 laminin chain [165, 189, 190]. DAG mutations are a source of several autosomal recessive muscular dystrophies [191, 192]. Furthermore, defective glycosylation of DG is also the cause of several muscular dystrophies, including: Fukuyama congenital muscular dystrophy (FCMD), due to a deficiency of fukutin (FKTN) [193] or fukutin-related protein (FKRP) [194], and both muscle-eye-brain disease and FCMD caused by defective LARGE, a putative glycosyl transferase [195, 196].

Homozygous deletion of the gene encoding dystroglycan is peri-implantation lethal at around day 6.5 of gestation due to disruption of the extra-embryonic Reichert membrane [197]. Williamson et al., [197] also demonstrated the co-localization of laminin and type IV collagen was disrupted in the homozygous nulls. In chimeric mice devoid of DG [198], the BM and laminin deposition in muscles appears unaffected, leading to the conclusion that DG is required for myofiber survival and synapse differentiation and stability, but not BM formation on muscle cells. Henry and Campbell [199], on the other hand, incorrectly concluded that the DG missing in DAG-1 null embryonic stem cells was required for basement membrane formation in embryoid bodies. Furthermore, DG is widely expressed in early development of many tissues where it may play several diverse roles [200], however, they will not be discussed.

Heparin, heparan sulfate, and other sulfated glycans

Heparin and heparan sulfates (HS) are present in cell membranes and on several cell surface proteoglycans. They can bind both the N-terminal LN domain and C-terminal G domain of the $\alpha 1$ laminin chain [69, 160, 201-205]. Furthermore, heparin binding sites are often found in the same general vicinity as the integrin binding sites on laminin. There are several heparin sulfate proteoglycan (HSPG) molecules present in basement membranes as either extracellular matrix components or cellular receptors, including: agrin, perlecan, syndecan and glypican. In addition there is also bamacan, a chondroitin sulfate proteoglycan, known to be another anionic component of the basement membrane.

HNK-1

The HNK-1 carbohydrate epitope (CD57), $\text{HSO}_3\text{-3GlcA}\beta 1\text{-3Gal}\beta 1\text{-4GlcNAc}$ [179, 180], is a sulfated glucuronic acid present on the non-reducing terminus of several glycans present on several molecules, including: glycolipids, such as SGGL-1 and SGGL-2 [179, 181], and glycoproteins, such as the cell adhesion molecules (CAMs) NCAM (neural cell adhesion molecule), telencephalin, tenascin-R, L1, MAG (myelin-associated glycoprotein), TAG-1, P0, and others [182-187]. The HNK-1 epitope has been shown to be involved in the functioning of these molecules in cell adhesion, migration, and neurite outgrowth [188-190].

The HNK-1 epitope is spatially and temporally regulated in the developing nervous system [191, 192], where it is specifically associated with migrating neural crest cells [193], neuron-glial cell adhesion [194], astrocyte migration and outgrowth of processes [189], and neurite outgrowth from motor neurons [195]. Several HNK-1 carbohydrate binding proteins have been identified, including: laminin, L- and P-selectins, SBP-1, and

brevican [196, 197]. The HNK-1 epitope has been shown to bind the laminin α 1 LG2 domain, furthermore, the binding is completely eliminated by desulfation of the HNK-1 epitope [64].

Syndecans

The syndecans are a transmembrane heparan sulfate/chondroitin sulfate proteoglycan family that contains four members: the 33 KDa syndecan-1 (syndecan-1), the 23 KDa syndecan-2 (fibroglycan), the 43 KDa syndecan-3 (N-syndecan), and the 22 KDa syndecan-4 (ryudocan, amphyglycan) [198, 199]. Each syndecan is composed of a short cytoplasmic domain, a single span transmembrane domain, and an extracellular domain with attachment sites for three to five heparan sulfate (HS) and chondroitin sulfate (CS) chains. Syndecans differentially possess both HS and CS glycosaminoglycan (GAG) chains based upon their temporal and spatial expression due to specific post translational modifications. The HS chains interact with a large number of proteins, including: FGFs, VEGFs, and transforming growth factor-B (TGF-B) leading to cell signaling activation events [199]. The CS chains may cooperate with the HS chains in binding the HS binding growth factors, pleiotrophin and midkine [200, 201], as well as laminin [202-204].

Syndecan-1 interacts with the LG4 domain of α 1 laminin and the LG4-5 domain of α 3 laminin [202, 204], as well as intracellular microfilaments through its cytoplasmic tail, whereas, syndecan-4's cytoplasmic tail binds several focal adhesion molecules and is required for activation of several kinases, including focal adhesion kinase (FAK) [205-207]. Both syndecan-1 [208] and syndecan-2 may be involved in ephrin signaling. Ephrin-Eph signaling induces clustering of syndecan-2 and recruitment of several cytoplasmic molecules, which then leads via the Arp2/3 complex, Rho family GTPases,

and N-Wiscott-Aldrich syndrome protein, to localized polymerization of intracellular actin [209]. Ezrin provides a link between syndecan-2, via its cytoplasmic tail, and the actin cytoskeleton [210-212]. Syndecan-3 is involved in the development and differentiation of skeletal muscle, as well as regeneration [213-216]. In Schwann cells, syndecan-3 binds the N-terminal domain of Type V collagen ($\alpha 4$ chain), leading to actin assembly and activation of the Erk1/Erk2 protein kinases [217]. Syndecan-4 has been the most studied syndecan due to its interactions with FGF2 and $\beta 1$ integrin. Syndecan-4 also binds fibronectin and together they create a complex with integrin and initiate cell signaling events to induce cytoskeletal rearrangements [218, 219].

Furthermore, syndecan-1, -2, and -4 appear to affect, not only, other molecules', but also, each others' recruitment into raft structures [220-222]. For example, during cell migration, syndecan-1, syndecan-4, and caveolin-1 condense to the same region of the moving cell [223-225] but do not co-localize [220]. Furthermore, internalization of caveolae requires Src and PKC α activation [226], both of which can be activated by interaction with syndecan-4 [211, 227, 228].

Glypicans

The glypican family is composed of six cell surface HSPG members: the 64 KDa glypican-1 (glypican), the 57 KDa glypican-2 (cerebroglycan), the 69 KDa glypican-3 (OCI-5), the 57KDa glypican-4 (K-glypican), and the 84 KDa glypican-5 (GCP5) [229-231]. Glypicans are composed of an extracellular region which contains varied GAG attachment sites and 14 conserved Cys residues which stabilize a highly compact tertiary structure connected to a C-terminal glycosylphosphatidylinositol (GPI) anchor. Glypican family members are differentially expressed on different cell types and are normally targeted to apical surfaces.

Sulfatide and other sulfated glycolipids

Sulfatides, such as galactosyl-3'-sulfate ceramide, are acidic glycosphingolipids containing sulfate esters on their oligosaccharide chains. In mammals, sulfatides are ubiquitously expressed at low levels, but are present in high levels primarily in nervous tissue, kidney, testis, erythrocytes, platelets, and granulocytes. Sulfatide is found in the outer layer of the lipid bilayer in the cell membrane of Schwann cells and is found *in vivo* adjacent to BMs in peripheral nerve where it may provide anchorage for Lm-111 and Lm-211 through binding to the C-terminal LG4-5 domains of the $\alpha 1$ and $\alpha 2$ chains. Furthermore, sulfatides interact with a variety of cell adhesion molecules involved in hemostasis, such as von Willebrand factor, thrombospondin, and selectins, as well as laminin. In addition, it has been shown that sulfatides are one of the major lipids in serum and activate plasma coagulation factor XII. Sulfatide is also bound by several other proteins besides the $\alpha 1$ and $\alpha 2$ laminin chains; including midkine and perlecan.

Section IIC. Extracellular matrix genes and their related diseases.

Defects of laminins and other genes which encode molecules which comprise extracellular matrices and basement membranes are associated with several diseases (figure 8). For instance, several laminin chains have been shown to play a role in the pathogenesis of severe blistering diseases such as Herlitz junctional epidermolysis bullosa (JEB; Lm-332: $\alpha 3$, $\beta 3$, and $\gamma 2$) and muscular dystrophies ($\alpha 2$). JEB is characterized by the detachment of the squamous epithelium from the dermis. Also, certain forms of muscular dystrophy are due to mutations of the $\alpha 2$ laminin chain. Figure 1 diagrams the complex of the dystrophin associated glycoproteins and their linkages to the cytoskeleton and the extracellular matrix. In skeletal muscle, dystrophin, a

subplasma membrane protein, interacts with actin at its N-terminus and with dystroglycan at its cysteine rich domain near the C-terminus. Dystroglycan forms an integral component with the sarcolemmal complex of adhalin and other dystrophin associated glycoproteins (DAGs). The alpha subunit of dystroglycan, α DG, is also a laminin-receptor which binds to several sites in the G-domain (LG1-5) of the α 2 chain of Lm-211, as well as the LG4 domain of the α 1 chain of Lm-111. This complex of proteins is thought to stabilize the muscle cell membrane during contraction and abnormalities in this linkage complex are thought to predispose muscle cells to necrosis. Furthermore, the well known animal model of muscular dystrophy, the dystrophic mouse (the dy mouse), develops a severe muscular dystrophy in which the BM of both skeletal and cardiac muscle and peripheral nerve cells lack α 2 laminin. It appears that mutations in this Lm chain are responsible for the muscle abnormalities present in these mice.

Section IID. The resulting phenotype observed from targeted deletion of ECM and BM proteins, as well as their receptors.

Targeted deletion (knockouts) of basement membrane components and their receptors in mice, often mimic the disease states observed due to mutation of the targeted gene (figure 9). Deletion of laminin α 1, laminin γ 1, integrin β 1, dystroglycan, and EXT-1 all lead to early embryonic lethality due to basement membrane formation and differentiation failures, whereas, mutation of laminin α 5, nidogen-1+2, deletion of the nidogen binding site, III4, in γ 1 laminin, type IV collagen (α 1, α 2), and perlecan are lethal due to failures of organogenesis. Furthermore, mutation of laminin α 2, laminin α 3, laminin α 4, type IV collagen α 3, and carbohydrate linkages of dystroglycan which interfere with its binding to laminin, perlecan, and agrin result in phenotypes which

mimic disease states and allow for survival past birth. An examination of the phenotypes of the null states that were early embryonic lethal and whose gene product was normally present in BMs, suggest a critical role or requirement of laminin-111, integrin $\beta 1$, and dystroglycan in early embryogenesis and basement membrane formation.

Section IIE. Laminins and early embryonic development.

During embryogenesis, basement membranes first appear shortly before implantation (figure 10A). After implantation the inner cell mass (ICM) of the blastocyst gives rise to two endodermal cell layers: the visceral and parietal endoderm. BM accumulates underneath the two endodermal layers; between both the visceral endoderm and ICM and the parietal endoderm and the trophoctoderm. The ICM then undergoes apoptosis, clearing a cavity which will eventually develop into the pro-amniotic cavity. Concurrently, a layer of surviving cells from the ICM which are adjacent to the BM zone will differentiate forming a layer of elongated epithelium. This layer of epiblasts will eventually give rise to all three primitive germ cell lines from which all cells present in the adult mammalian organism are derived [232-235].

The development of the epithelial layer during embryogenesis requires formation of a BM [70, 236, 237]. Of the multitude of extracellular matrix components only seven have been shown to be present during early embryogenesis: laminin-111, laminin-511, nidogen-1, nidogen-2, collagen IV ($\alpha 1, \alpha 2$), perlecan, and agrin. These matrix proteins appear prior to implantation or shortly after formation of the first embryonic epithelial layers [238]. Early embryogenesis requires laminin-111 as demonstrated by the knockouts of each of the laminin chains which comprised laminin-111: $\alpha 1$ [17, 239, 240], $\beta 1$ [241], and $\gamma 1$ [242], all of which demonstrated day E5.5 lethality.

This *in vivo* phenomenon can be modeled with embryonic stem cells cultured to form embryoid bodies, which recapitulate/mimic many of the processes of embryogenesis just discussed. Dispersed stem cells can be cultured to aggregate and condense; forming an ICM (figure 10B). The ICM will then differentiate to form an outer endodermal cell layer, under which a BM will form. The ICM will undergo apoptosis, cavitation (eventually leading to the formation of a large central cavity), and further differentiation to form a polarized epiblast layer between the ICM and the BM on the basal side of the outer endodermal cell layer. Embryoid bodies derived from null embryonic stem cell lines which fail to produce laminin-111 also fail to produce a BM, differentiate to form an epiblast layer, or cavitate [31, 70, 240-242]. The targeted gene deletion of other BM components do not affect early embryogenesis and lead to death only at midgestation stages or have no effect upon embryogenesis at all (figure 9).

Embryonic development requires basement membrane formation which requires laminin. The early stages of development can be modeled through the use of embryonic stem cells to form embryoid bodies. Just as *in vivo*, basement membrane formation is an integral part of this process and requires laminin. As work done in our laboratory and others has shown, neither $\beta 1$ integrin nor DG are directly required for basement membrane formation, however, laminin-111 is and requires both its polymerization activity, through the N-terminal LN domains of its constituent chains, and its anchorage activity, through $\alpha 1$ LG4.

Section IIE1. The role of Lm-111 in dystroglycan null ES cell differentiation, BM formation, and EB formation.

Contrary to previous published work [170, 172], DG null ES cell lines in our laboratory spontaneously, i.e. without addition of exogenous Lm-111, formed EBs, developed an outer endodermal layer, formed a BM underneath this outer endodermal layer, underwent further differentiation and developed a polarized and elongated epiblast layer underneath the newly formed BM layer, and the inner cell mass underwent apoptosis, developing a large central cavity (most of this work was performed by Dr. Shaohua Li) [70]. By day 5 of culturing, most DG null EBs possessed a BM containing Lm-111, type IV collagen, nidogen, and perlecan. By day 7, many EBs possessed an unusually thick BM and completely lost their epiblast layer via apoptotic degradation by day 9. Both light microscopy of methylene blue stained sections and electron microscopy of developing DG null embryoid bodies revealed the development of an unusually thick BM between the endodermal and epiblast layer. IP/Westerns of DG null EBs demonstrated an overexpression of Lm-111, nidogen, and type IV collagen by day 7 when compared to media and lysates of WT EBs, however, $\beta 1$ integrin expression was not increased.

Section IIE2. The role of Lm-111 in $\beta 1$ integrin null ES cell differentiation, BM formation, and EB formation.

With the addition of exogenous Lm-111, both $\beta 1$ integrin and $\gamma 1$ laminin null EBs were able to overcome their differentiation blockage, form a BM layer on the basal side of a well defined and differentiated outer endodermal layer, further differentiate to form a distinctive second cell layer consisting of a polarized pseudo-stratified columnar epiblast layer interior to this BM, and cavitate to form a sharply demarcated central cavity. Phase

contrast and methylene blue stained light microscopy of $\beta 1$ integrin null EBs clearly showed that EBs “rescued” with the addition of exogenous Lm-111 develop an outer endodermal layer of cells, a BM on the basal side of the endodermal layer, an elongated epithelial layer, and a central cavity, whereas, without the addition of exogenous Lm-111, the $\beta 1$ integrin null ES cells failed to reach these stages of development. A BM was clearly observable in the EM photographs of WT and $\beta 1$ null rescued EBs, and absent in non-rescued EBs. Immuno-flourescent microscopy of $\beta 1$ integrin null EBs revealed the co-localization, accumulation, and deposition of the ECM proteins: Lm-111, type IV collagen, nidogen, and perlecan; in a clear BM pattern between the outer endodermal and inner epiblast layer of “rescued” $\beta 1$ integrin null EBs and not in EBs in which exogenous Lm-111 was not added.

WT and $\beta 1$ integrin null EBs were examined for expression and accumulation of BM components. Conditioned media and cell lysates from EBs were evaluated directly in Westerns or first immunoprecipitated (IP) then analyzed via Westerns. An antibody specific to LG4-5 of $\alpha 1$ laminin (rG50) detected no $\alpha 1$ laminin secreted by the $\beta 1^{-/-}$ EBs, however, antibodies to Lm-111, the LN of $\beta 1$ laminin (anti-E4), and the $\gamma 1$ laminin chain did detect both $\beta 1$ and $\gamma 1$ laminin chains within the EBs but no expressed $\alpha 1$ chain. No laminin $\alpha 1$ expression was detectable in either the conditioned medium or EB cell lysates of the $\beta 1$ -integrin null line. Both nidogen and type IV collagen were expressed and secreted into the medium of the $\beta 1$ -integrin null line, however, they did not accumulate on or in the EBs. Furthermore, despite the presence of $\beta 1$ and $\alpha 6$ integrin in the BM zone of differentiated WT EBs, $\alpha 6$ integrin was not expressed and remained absent from the BM even during rescue of the $\beta 1$ integrin null EBs via addition of exogenous Lm-111 and subsequent differentiation and BM formation [70].

Section IIE3. The role of Lm-111 in γ 1 laminin null ES cell differentiation, BM formation, and EB formation.

Without the addition of exogenous Lm-111, γ 1 laminin null EBs are unable to form a BM layer, epiblast layer, or cavitate. These developmental stages can be reached by γ 1 laminin null EBs if exogenous Lm-111 is supplied. The production and accumulation of BM components of γ 1 laminin null EBs was investigated by Dr. Shaohua Li [70] and compared to WT, β 1 integrin, and DG null EBs. The γ 1 null EB and β 1 integrin null EBs did not produce Lm-111. Eventhough both did produce the β 1 and γ 1 laminin chains of Lm-111, neither expressed the α 1 chain, whereas, WT and DG null EBs both produced and accumulated Lm-111. DG null EBs also overexpressed and accumulated more Lm-111 than WT EBs. Similarly, both γ 1 laminin null and β 1 integrin null EBs produced and secreted nidogen, however, they did not retain appreciable levels within the EBs. WT and DG null EBs both produced and retained nidogen. Again, DG null EBs overexpressed and retained nidogen and despite not retaining the nidogen to appreciable levels, γ 1 laminin null EBs also overexpressed nidogen. EBs derived from all four ES cell lines expressed type IV collagen, with the γ 1 laminin null and β 1 integrin null EBs unable to retain much of it and the DG null line overexpressing it.

No β 1 integrin, as expected, was detectable in the β 1 integrin null EBs and was present in WT, γ 1 laminin null, and DG null EBs. However, there was a noticeable decrease of β 1 integrin expression in the γ 1 laminin null EBs. Both β 1 integrin and γ 1 laminin null EBs overexpressed DG. The expression of DG in β 1 integrin null EBs was much higher than in γ 1 null EBs, however, upon addition of exogenous Lm-111 the expression of DG increased in β 1 null EBs and decreased in γ 1 laminin null EBs. Furthermore, neither null EB line demonstrated altered DG expression when exposed to exogeneous AEBSF treated, polymerization incompetent, Lm-111 [70].

Without the addition of specific exogenous laminins, $\gamma 1$ laminin null EBs will not differentiate, form a BM, undergo epiblast differentiation, or cavitate. The exogenous addition of either Lm-211 ($\alpha 2\beta 1\gamma 1$) or a Lm-211($\alpha 2\beta 1\gamma 1$)/Lm-221($\alpha 2\beta 2\gamma 1$) mixture were able to rescue some of the $\gamma 1$ laminin null EBs, however, at only about half the BM formation efficiency of Lm-111 ($\alpha 1\beta 1\gamma 1$); 37% and 40% versus 74% respectively. Furthermore, the percentage of EBs with epiblast differentiation dropped from 45% for Lm-111 to 9% for Lm-211/Lm-221 and 20% for Lm-221. The addition of either Lm-332 ($\alpha 3\beta 3\gamma 2$) or Lm-411 ($\alpha 4\beta 1\gamma 1$) resulted in neither BM formation nor epiblast differentiation. Furthermore, both immunohistochemical and electron microscopy of $\gamma 1$ laminin null EBs rescued with the addition of various exogenous recombinant heterotrimeric laminins, revealed BM formation and epiblast differentiation in only those EBs grown in the presence of recombinant laminins with both intact polymerization and LG4-5 anchorage activities.

Section IIF. The role of laminin in the peripheral and central nervous systems.

Several laminin receptors exist in the developing peripheral nervous system (PNS), where laminins have been shown to be required for attachment, migration, differentiation, and cell survival [243]. Laminin deficient Schwann cells exhibit defects in cell survival, proliferation, and myelination [244-248]. The laminin receptor $\beta 1$ integrin is required for normal radial sorting of axons and Schwann cells. Another, laminin receptor, αDG is necessary for proper myelination in the PNS. DG null mice [249] possess Schwann cells in which the majority are capable of radial sorting of axons and myelination; however, they demonstrate abnormalities in myelin ensheathment and organization of the nodes of Ranvier that cause myelin instability and a resulting

neuropathy. The laminin $\alpha 2$ deficient PNS phenotype mirrors the loss of both integrin and dystroglycan signaling, whereby each receptor plays a distinct role in the different stages of myelination.

There are at least eight murine Src family nonreceptor tyrosine kinases (SFKs) known: Src, Yes, and Fyn are expressed ubiquitously; Hck, Fgr, Blk, and Lck are restricted to hematopoietic cell lineages; and Lyn is expressed in hematopoietic and neuronal tissues. Targeted gene deletion of Src, Fyn, and Yes, either individually or in combinations, lead to perinatal death or postnatal defects in specific cell types. The frequency of lethality and severity of defects is increased in mice harboring compound mutations, suggesting redundancy of biological functions of the SFKs during development. It is well known, that Src, Yes, and Fyn promote normal development, proliferation, and gene expression, as well as extracellular matrix promoted adhesion, spreading, migration, and protection from apoptosis; executing various cell signaling cascades initiated by activation of cell surface receptors. For instance, adherence of cells to extracellular matrix proteins, results in the tyrosine phosphorylation of several focal adhesion proteins, including: FAK (focal adhesion kinase: FAK- pTyr₁₂₅). Potential SFK members responsible for phosphorylation of FAK include Fyn and Src. Furthermore, FAK-integrin associations driven by extracellular matrix protein interaction with integrin have been demonstrated to interact with Src and Fyn. Upon phosphorylation FAK functions to direct phosphorylation of other cellular substrates by recruitment of Src kinases.

The question arises, not just whether or not the myelinating glia of the central nervous system (CNS), oligodendrocytes, use the same receptors, but also, if Lm-211 plays the same role and through the same mechanisms as in the Schwann cells of the PNS. In the CNS, myelination of axons occurs after oligodendrocyte progenitors undergo terminal differentiation and initiate process formation and axonal ensheathment.

Oligodendrocyte-neuron contact initiates this process and the appearance of several tyrosine phosphorylated proteins which are only found in the differentiated cells. The required increased tyrosine kinase activity is due to Fyn, as the other SFK family members are not active in oligodendrocytes. Early in oligodendrocyte differentiation SFK Lyn drives $\alpha V\beta 3$ integrin dependent progenitor proliferation through PDGF α R. Fyn is maintained in an inactive state by Csk phosphorylation of Fyn's inhibitory C-terminal Tyr₅₃₁. However, at later stages in differentiation, after axonal contact and ligation of the $\alpha 6\beta 1$ integrin by the laminin $\alpha 2$ chain expressed in myelinating axon tracts, Lyn dissociates from the integrin growth factor complex, resulting in Csk downregulation, and reduced Fyn phosphorylation at Tyr₅₃₁, thereby promoting Fyn activity. The active Fyn- $\alpha 6\beta 1$ integrin complex can then trigger PI3K signaling through the PDGF α R receptor promoting cell survival and trigger MAPK signaling through the ErbB2/4 receptor enhancing survival and promoting differentiation and myelination. Hence the change in extracellular matrix proteins and the integrins they engage, can affect a response change in oligodendrocytes from proliferation to differentiation and myelin formation.

With the aid of some of our reagents, Colognato et. al, [243] were able to demonstrate that similar to Schwann cells in the PNS, oligodendrocytes of the CNS express both $\alpha 6\beta 1$ integrin and DG, DG appears to mediate interactions between laminin and oligodendrocytes, and DG plays a role in laminin regulated oligodendrocyte survival and differentiation. Just as in the PNS, different laminin receptors are required at different developmental stages and laminin-integrin interactions amplify the survival effects of soluble growth factors, whereas, laminin-DG interactions contribute to differentiation and myelin membrane formation [243].

Section IIF1. Src activation and downstream cell signaling events induced in Schwann cells by the addition of exogenous Lm-111.

Dr. Shaohua Li [71] performed a series of experiments examining the induction of phosphorylation and activation of Src and FAK in Schwann cells due to the addition of exogenous Lm-111. Phosphorylation of Tyr₄₁₆ of Src was detected within 15 minutes of the addition of exogenous Lm-111 to cultured SCs. The activation of Src peaked by 30 to 60 minutes. Furthermore, the disperse intracellular Src was observed to condense with the condensing Lm-111 and pSrc (Src-pY₄₁₆) accumulated in the nucleus. Another Src family member, Fyn, which the Src activation antibody also recognizes, was also activated by Lm-111 treatment.

Cultured Schwann cells treated with arylsulfatase, failed to accumulate exogenous Lm-111 and did not induce Src activation. Therefore, sulfatide must be required for Src activation and/or at least for its ability to anchor Lm-111 to the cell surface. Furthermore, Schwann cell detergent lysates immunoprecipitated with β DG antibody, followed by immunoblotting with cSrc antibody, revealed that Src was associated with the DG complex irregardless of whether or not Lm-111 was added to the Schwann cells nor did the level of cSrc associated with β DG change in the prescence or absence of exogenous Lm-111. Concurrent addition of α DG antibody IIH6, which blocks α DG's ability to bind to Lm-111, severely reduced the Src phosphorylation otherwise observed upon addition of exogeneous Lm-111. Conversely, treatment of SCs with β 1 integrin antibody, Ha2/5, that blocks β 1 integrin's ability to bind Lm-111 treatment, did not block exogeneous Lm-111 induced Src phosphorylation.

Schwann cells were incubated with Lm-111 in the prescence of excess Lm-111 elastase digest fragments and recombinant α 1LG4-5s. Lm-111 polymerization inhibiting fragment E1' blocked Src activation as did recombinant α 1LG4-5/WT_{Nf} but not a mutant

recombinant $\alpha 1$ LG4-5, $\alpha 1$ LG4-5/KRK₂₇₉₃, which demonstrated reduced sulfatide and α DG binding affinity, nor fragment E8, site of Lm-111's $\alpha 6$ integrin binding activity. Src activation in Schwann cells in response to the addition of exogenous laminin-111 was inhibited by inhibitors of either laminin polymerization or laminin $\alpha 1$ LG4 dependent anchorage.

A similar study was performed on Schwann cells grown in suspension cultures in order to further examine the potential roles of $\beta 1$ integrin and FAK activation, as well as Src signalling. Schwann cells grown in suspension formed spherical cell aggregates. When the suspended Schwann cell clusters were treated with Lm-111, Src phosphorylation was observed even in the presence of concurrent treatment with $\beta 1$ integrin blocking antibody, however, laminin- α DG blocking antibody, IIH6, effectively blocked Src phosphorylation.

Section IIF2. FAK activation induced in Schwann cells by the addition of exogenous Lm-111.

The analysis of adherent Schwann cells revealed that there was no colocalization of Lm-111 with $\beta 1$ integrin and that Lm-111 anchorage and resulting BM formation could occur in the absence of $\beta 1$ integrin [71]. In developing peripheral nerves, $\beta 1$ integrin and Lm-111 do colocalize [250, 251], however, analysis of Schwann cells adherent to solid phase substrates (tissue culture plastic and treated glass) may have resulted in most of the $\beta 1$ integrin being recruited to the basal side of the cells, leaving little if any to interact on the exposed apical cell surface. Therefore, Schwann cells were grown in suspension culture where they formed spherical cell aggregates [71]. When exogenous Lm-111 was added to the medium, it was observed to accumulate between the cells of the

cluster and colocalized with $\beta 1$ integrin. Furthermore, incubation overnight with exogenous Lm-111 also induced FAK phosphorylation, whereas, adherent confluent monolayers of cultured Schwann cells demonstrated a constitutively high basal level of FAK phosphorylation, obscuring any potential Lm-111 induction.

Section IIG. Laminin binding to mouse embryonic fibroblasts and their response.

Despite being “factories” for the production of many extracellular matrix components *in vivo*, the same ECM components rarely accumulate on the surface of the fibroblasts producing them nor do basement membranes form on the cell surfaces of these cells. Therefore, these cells must by necessity be devoid of some of the receptors and anchors which these components would normally bind to. It was the absence of certain of these receptors/anchors which our laboratory hoped to take advantage of.

Section IIG1. Lm-111 induced cell signalling in MEFs.

Sulfatide loaded MEFs were examined by Dr. Shaohua Li [71] for Src tyrosine phosphorylation activation in response to the addition of exogenous Lm-111. Phosphorylation of amino acid residue Tyr₄₁₆ on Src was observed 15 minutes after addition of exogenous Lm-111 and peaked at 1 hour only if the MEFs were first loaded with sulfatide. No phosphorylation event was observed if the MEFs were not loaded with sulfatide prior to the addition of exogenous Lm-111. Sulfatide loaded MEF Src activation in response to Laminin-111 was also inhibited by inhibitors of either laminin polymerization, fragment E1', or laminin anchorage through LG4, either through use of recombinant $\alpha 1\text{LG4-5/WT}_{\text{NF}}$ or antibody I1H6 which blocks laminin-111 binding to αDG .

Inhibition of laminin-111 binding to $\beta 1$ integrins, through fragment E8 or laminin-111- $\beta 1$ integrin blocking antibody Ha2/5, had no effect upon Src phosphorylation.

In order to further evaluate the role of DG and $\beta 1$ integrin mediated activation of Src by exogenous Lm-111, differentiated fibroblasts were isolated and cultured from embryonic stem cell lines null for either DG or $\beta 1$ integrin and compared to fibroblasts derived from WT ES cells or ones which had been transfected with a construct to enable constitutive expression of $\beta 1$ integrin ($\beta 1$ AGD25 cells). All cells were loaded with sulfatide and incubated with Lm-111. A dramatic increase in phosphorylation of Src-Tyr₄₁₆ was observed in WT ES, $\beta 1$ integrin null, and $\beta 1$ integrin expressing ES derived fibroblasts but not DG null derived fibroblasts. Therefore, it is likely that the Src activation by laminin-111 is primarily through DG and not dependent upon $\beta 1$ integrin, since: exogenous Lm-111 induced Src activation in the $\beta 1$ integrin null fibroblasts, the $\beta 1$ integrin blocking antibody was unable to inhibit Lm-111 induced Src activation, and $\beta 1$ integrin did not colocalize with Lm-111 staining nor affect its ability to activate Src when absent. Whereas, DG null fibroblasts did bind Lm-111 once loaded with sulfatide but failed to activate Src and the DG-laminin blocking antibody IIH6 did inhibit Src phosphorylation [71].

Caveolin-1 was also phosphorylated in much the same sulfatide/laminin-111/time dependant manner as Src. In MEFs first loaded with sulfatide and then incubated with Lm-111, phosphorylation of Tyr₁₄ of caveolin-1 was observed starting at 15 minutes and peaking at 60 minutes post addition of laminin-111. This phosphorylation was not observed without sulfatide loading and was inhibited when the MEFs were concurrently treated with either of two structurally different Src kinase inhibitors, PP2 or SU6656. This data suggested that caveolin-1 is a potential downstream target in the laminin-111 induced Src signaling cascade.

My analysis of adherent MEFs revealed that there was no colocalization of Lm-111 with $\beta 1$ integrin and that Lm-111 anchorage and resulting BM formation could occur in the absence of $\beta 1$ integrin as long as the cells were first loaded with sulfatide. In developing peripheral nerves $\beta 1$ integrin and Lm-111 do colocalize [250, 251], however, analysis of MEFs adherent to solid phase substrates (tissue culture plastic and treated glass) may have resulted in most of the integrin being recruited to the basal side of the cells, leaving little if any to interact with exogenous laminin on the exposed apical cell surface. Furthermore, adherent MEF cultures expressed constitutively high basal levels of phosphorylated FAK. Therefore, both MEFs null for $\beta 1$ integrin (DG25) and transfected with a construct that expressed $\beta 1$ integrin ($\beta 1_A$ GD25) were first treated with sulfatide and then grown in suspension culture where they formed spherical cell aggregates [71]. When exogenous Lm-111 was added to the medium, it was observed to accumulate mostly on the surface of the outer layer of cells belonging to the cluster. There was no observable difference in phosphorylated FAK levels of $\beta 1$ integrin null (GD25) cells, whether or not Lm-111 was added, however, there was a threefold increase in phosphorylation of FAK in $\beta 1$ integrin expressing ($\beta 1_A$ GD25) fibroblast cell clusters if exogenous Lm-111 was supplied.

Chapter 2. Materials and Methods

Selection of the promoter for α 1LG4-5 and other recombinant laminin expression constructs.

Three different expression constructs were made by first cloning mouse α 1 LG4-5 into the expression construct pRCX3 (supplied by Billy Hudson at Vanderbilt University) to generate m α 1LG4-5/WT-pRCX3_{Nf}, then replacing the CMV (cytomegalovirus) promoter of m α 1LG4-5/WT-pRCX3 with either the RSV (rous sarcoma virus) promoter to generate m α 1LG4-5/WT-RSV_{Nf} or the mouse β 1 Lm promoter to generate m α 1LG4-5/WT-m β 1_{Nf} (see “constructs” section of “Materials and Methods” for details on the construction of the constructs) (figure 13A and B). The “_{Nf}” on the end of the construct designation signifies that the expressed recombinant protein contains an N-terminal (“_N”) FLAG (“_f”) epitope tag. The plasmids were linearized with Sca I (NEB), transfected into the HEK 293 cell line with Lipofectamine 2000 (Invitrogen), and 12 stable clones from each construct isolated. The cells were grown in media containing: 1X DMEM (Invitrogen) + 10% Fetal Bovine Serum (FBS; Atlanta Biologicals) + 1X P/S (1,000 u/ml Penicillin and 1,000ug/ml Streptomycin; Invitrogen) + 500 ug/ml G418 (Sigma-Aldrich). Media from cells were harvested, the cells from the dish isolated, and a portion of the media from each clone, normalized based upon cell number, solubilized in Laemmli sample buffer (LSB) and reduced with β -mercaptoethanol and boiling, then loaded and run on a 6-12% gradient SDS-PAGE gels. Proteins were either stained with Coomassie Brilliant Blue R-250 for direct visualization or blotted onto PVDF membranes (BioRad) using a BioRad electroblotter for Western detection. Bound protein was detected with either rabbit anti-mouse α 1LG4-5 polyclonal antibody rG50 and a secondary HRP-linked goat anti-rabbit IgG or with the monoclonal HRP linked FLAG M2 antibody from Sigma-Aldrich, specific for the FLAG epitope present on each of the expressed α 1LG4-5s. Autoradiographs

were scanned and band intensity correlating to expression level of recombinant α 1LG4-5s determined by imaging with a BioRad Gel Doc 2000, analyzed, and quantitated with Quantity One software (BioRad).

Selection of 5'UTR for recombinant α 1LG4-5 constructs.

A total of nine different expression constructs were created, each, containing the mouse laminin α 1 LG4-5 WT coding sequence, with an N-terminal FLAG tag, and a BM40 signal sequence. The constructs are: α 1LG4-5/WT_{Nf}, α 1LG4-5/WT-pRCX3_{Nf}, α 1LG4-5/WTcon2_{Nf}, α 1LG4-5/WTh2b_{Nf}, α 1LG4-5/WTtomm7_{Nf}, α 1LG4-5/WTiars_{Nf}, α 1LG4-5/WTfdft1_{Nf}, α 1LG4-5/WTube2s_{Nf}, and α 1LG4-5/WTeif4a1_{Nf}. The construct designation format is as follows: “ α 1LG4-5/WT” describes an expression construct that will produce a mouse α 1 laminin LG4-5 recombinant protein; “con2” “h2b”, “tomm7”, “iars”, “fdft1”, “ube2s, and “eif4a1” represent the 5' untranslated region (UTR) sequence utilized in the expression construct for the expressed recombinant protein (figure 13A, D, and E); and the “_{Nf}” on the end of the construct designation signifies that the expressed recombinant protein contains an N-terminal (“_N”) FLAG (“_f”) epitope tag. The nine constructs were transfected into 293 cells, stable clones isolated, media harvested, and recombinant α 1LG4-5 expression levels compared via FLAG detection of straight media loads compensated for by determining the cell number at time of media collection. Quantitation and comparison was same as previously stated. Clones transfected with the construct utilizing the “consensus-1” 5' UTR (construct α 1LG4-5/WT) had a 3-4 fold higher expression of the recombinant α 1LG4-5 than any other construct.

Selection of signal sequence for recombinant α 1LG4-5 constructs.

Three signal sequences were examined for secretion of recombinant α 1LG4-5. The BM40 signal sequence of α 1LG4-5/WT was replaced with either the IG κ signal sequence or the endogenous mouse α 1 laminin signal sequence (figure 13A and C). The three constructs α 1LG4-5/WT_{Nf}, α 1LG4-5/WT-IG κ _{Nf}, and α 1LG4-5/WT-m α 1_{Nf}, were utilized to generate stably transfected cell lines (see “constructs” section of “Materials and Methods” for details on the construction of the constructs). Relative recombinant protein expression was determined as described earlier utilizing the N-terminal FLAG epitope tag common to all the expressed recombinant α 1LG4-5 proteins. Neural network software programs ACN, SignalP, Signal-NN, and SignalP-HMM were used to predict signal cleavage points in the recombinant proteins expressed.

Selection of epitope tags for recombinant α 1LG4-5 constructs.

Seven epitope tags were tested on the N-terminus of recombinant α 1LG4-5: FLAG (constructs: α 1LG4-5/WT_{Nf} and m α 1LG4-5/WT-pRCX3_{Nf}), c-myc (construct: α 1LG4-5/WT_{Nm}), c-myc X3 (construct: α 1LG4-5/WT_{Nm3}), HA (construct: α 1LG4-5/WT_{Nh}), VSV-G (construct: α 1LG4-5/WT_{Nv}), V5 (construct: α 1LG4-5/WT_{Nv5}), and protein-C (construct: α 1LG4-5/WT_{Np}) (see “constructs” section of “Materials and Methods” for details on the construction of the constructs). The construct designation format is as follows: “ α 1LG4-5/WT” describes an expression construct that will produce a mouse α 1 laminin LG4-5 recombinant protein; a terminal “_{Nf}” signifies an N-terminal (“_N”) FLAG (“_f”) epitope tag, a “_{Nm}” signifies an N-terminal (“_N”) myc (“_m”) epitope tag, a “_{Nm3}” signifies an N-terminal (“_N”) triple myc (“_{m3}”) epitope tag, a “_{Nh}” signifies a N-terminal (“_N”) HA (“_h”) epitope tag, a “_{Nv}” a N-terminal (“_N”) VSV-G (“_v”) epitope tag, a “_{Nv5}” signifies a N-terminal (“_N”) V5 (“_{v5}”) epitope tag, and a “_{Np}” signifies a N-terminal (“_N”) protein-C (“_p”) epitope tag on the

expressed recombinant protein (figure 15). Media from stably transfected cell lines were tested and the results analyzed as previously discussed. The epitope specific antibodies employed are listed in the “antibody” sub-section of this “Materials and Methods” section.

Designed proteolytic cleavage of epitope tags from recombinant proteins.

Purified recombinant laminin proteins, E3, and EHS Lm-111 were digested with either enterokinase (EK; Invitrogen) or tobacco etch virus protease (TEV; Invitrogen). Furthermore, purified recombinant α 1LG4-5 proteins with various N-terminal epitope tags separated from the α 1LG4-5 sequence by an engineered EK cleavage sequence were incubated with EK. Incubations were performed utilizing 1unit of EK (EKMax; Invitrogen) per 10ug of α 1LG4-5 in 50mM Tris-HCl, pH 7.4, 90mM NaCl, 1mM CaCl_2 for 1 hr. at RT or 4 hrs. at 4⁰C. EK was left in the reaction or removed via either it's inability to bind heparin or the use of EK-Away resin (Invitrogen) to precipitate it out. TEV incubations were performed in 50mM Tris-HCl, pH8.0, 90mM NaCl, 1 mM EDTA for 1 hr. at RT or 4 hrs. at 4⁰C. Samples were run on SDS-PAGE and analyzed as previously described.

Selectable markers and antibiotics.

“Kill” curves, for determining the optimal antibiotic concentrations for growing transfected cell lines in, were generated for five antibiotics in the fibroblast HEK 293 cell line by growing the cells in 8 different concentrations of each antibiotic over a period of 3 weeks. The optimal concentration at which to use each was determined and then tested on a transfected 293 cell line expressing the appropriate selectable marker. The final determination of appropriate antibiotic was: 500ug/ml G418 for neomycin (Sigma-Aldrich), 80-100 ug/ml for zeocin (Invitrogen), 5 ug/ml for hygromycin (Sigma-Aldrich), 1

ug/ml for puromycin (Sigma-Aldrich), and 5ug/ml for blasticidin (Invitrogen). A similar process was then performed to generate kill curves for eleven unique combinations each consisting of three out of the five antibiotics examined. The triple antibiotic mixtures were tested at 100% and 80% of their determined optimal killing concentration.

Expression vectors.

The recombinant mouse α 1LG4-5s were cloned into the neomycin resistance expression vector pRCX3 [252] and zeocin resistance expression vector pcDNA3.1/zeo(+) (Invitrogen). Laminin α 1 chains were cloned into the hygromycin resistance expression vector pcDNA3.1/hygro(+) (Invitrogen), pRCX3, and puromycin expression vector DHPuro. There were no acceptable commercially available puromycin based expression vectors, therefore, a unique puromycin based expression vector, DHPuro, was constructed (figure 16). The construct provides for the CMV promoter driven expression of recombinant genes placed in a unique MCS which is followed by the bovine growth hormone polyadenylation sequence (BGH pA) for high efficiency expression and polyadenylation of recombinant mRNA. The construct also contains the *Streptomyces alboniger* puromycin-N-acetyl-transferase (pac, puromycin, PuroR) gene under the control of the SV40 early promoter and followed by the SV40 polyadenylation sequence, allowing for simultaneous puromycin resistance selection. There is also a pBR322 origin of replication and ampicillin resistance gene for propagation and selection in *E. coli*. Human β 1 Lm chains were cloned into both pCEP4 and pcDNA3.1/zeo(+), while human γ 1 Lm chains were cloned into neomycin expression vector pRc/CMV2 (Invitrogen) and pcDNA3.1/neo(+) (Invitrogen).

Secondary structure prediction, homology modeling, refinement of the generated predicted three dimensional structure, and selection of amino acid residues to analyze in $\alpha 1$ LG4-5.

The amino acid sequences for the laminin chains were assembled in the OMIGA software suite of programs, then aligned using either ClustalW [253, 254] hosted by the European Bioinformatics Institute (EMBL-EBI) in Cambridge UK, which is part of the European Molecular Biology Laboratory (EMBL), or MUSCLE (Multiple Sequence Comparison by Log-Expectation) [255, 256] hosted on a server, kindly provided by Kimmen Sjolander's group at UC Berkeley, USA. The preliminary alignment was then outputted in FASTA format [257, 258], imported back into OMIGA for fine tuning of each alignment by hand, and then the PHYLIP (PHYLogeny Inference Package) package of programs [259, 260] was utilized to generate a phylogenetic tree.

Twelve secondary structure programs were used to analyze laminin $\alpha 1$ and $\alpha 2$ via the NPS@ (Network Protein Sequence @nalysis) analysis suite (<http://npsa-pbil.ibcp.fr/>) [261]. The NPS@ server was utilized to perform the following secondary structure prediction programs: DPM (Double Prediction Method) [262], DSC (Discrimination of protein Secondary structure Class) [263], GOR IV (Garnier Osguthorpe and Robson 4th version) [264], HNN (Hierarchical Neural Network) [265], PHD [266, 267], PREDATOR [268], SIMPA96 [269, 270], SOPM (Self-Optimized Prediction Method) [271], SOPMA (Self-Optimized Prediction Method with Alignment) [272], MLRC (Multivariate Linear Regression Combination) [273], GOR I (Garnier Osguthorpe and Robson 1st version) [274], and GOR III (Garnier Osguthorpe and Robson 3rd version) [275].

A homology model of mouse $\alpha 1$ LG4-5 was constructed utilizing Swiss-Model, Swiss-Pdb Viewer/DeepView (<http://www.expasy.org/spdbv/>) [276-279] and MODELLER [280]. The generated structure and earlier generated table of sequence

secondary characteristics were used along with the aid of CHARMM (Chemistry at HARvard Molecular Mechanics; <http://www.charmm.org/html>) [281, 282], AMBER [283-287], GROMOS96 [288], ENCAD [289], MEAD (Macroscopic Electrostatics with Atomic Detail [290], WHAT IF [291], and WHAT_CHECK [292] to further improve the theoretical structure and identify likely amino acid residue candidates for mutational analysis.

Recombinant α 1LG4-5 protein production and purification.

Constructs were linearized with Bgl II and transfected into the human kidney fibroblast cell line HEK 293 (ATCC) using Lipofectamine 2000 (Invitrogen). Stable clones were selected for secretion of recombinant α 1LG4-5 by growth in DMEM media containing either 80-100ug/ml zeocin or 500 ug/ml G418, depending upon the construct utilized. Cells were grown in DMEM (Invitrogen) supplemented with 10% FBS (Atlanta Biological), 1,000 u/ml penicillin (Invitrogen), 1,000 ug/ml streptomycin (Invitrogen) and the appropriate selection antibiotic. Once cells were 80% confluent the media was replaced with fresh media minus antibiotic and then both the cells and media collected 72 hours later. The genomic DNA was isolated (GenElute Mammalian Genomic DNA Miniprep kit; SIGMA) and sequenced from the cells after media harvesting to verify identity of the various recombinant α 1LG4-5s. Collected media was purified at 4°C through a gravity column (Econo-Pac Chromatography Columns; Bio-Rad Laboratories) packed with FLAG M2 agarose (SIGMA) and eluted with FLAG peptide (SIGMA) in 90mM NaCl, 1mM CaCl₂, 50mM Tris-HCl; pH7.4 at room temperature (TBS50/Ca). The eluted material was then run through a TosoHass heparin 5PW column on a Pharmacia AKTA FPLC, where the FLAG peptide was recovered for re-use and the recombinant α 1LG4-5s eluted utilizing a 0-1M NaCl gradient. The eluted α 1LG4-5s were then concentrated further and the buffer exchanged at 4°C into TBS50/Ca via centrifugal

filtration utilizing Amicon Ultra-15 centrifugal filters (Millipore). If necessary, especially if manipulating small volumes, the recombinant $\alpha 1\text{LG4-5s}$ were further dialyzed in 2 L of the appropriate buffer at 4°C, with 2 buffer changes over two days, utilizing Slide-A-Lyzer Dialysis Cassettes (Pierce Biotechnology).

De-glycosylation of recombinant $\alpha 1\text{LG4-5}$ protein was accomplished with one of two different methods: by isolating recombinant $\alpha 1\text{LG4-5}$ from the media of stably transfected cell lines grown in 2 $\mu\text{g/ml}$ tunicamycin (Sigma-Aldrich) for 24 hours or by treating 50 μg of purified recombinant $\alpha 1\text{LG4-5}$ with 1,000 u of PNGase F (*N*-glycosidase F [EC 3.5.15.2, *N*-linked-glycopeptide-(*N*-acetyl-beta-D-glucosaminy)-L-asparagine amidohydrolase]; NEB) in TBS50/Ca for 1 hour at 37°C.

Proteolytic cleavage with EK and TEV.

Laminin-111 purified from EHS tumor, the elastase digest proteolytic fragment E3 from the purified laminin-111, recombinant laminin-111, recombinant human $\beta 1$ laminin chain, and recombinant $\alpha 1\text{LG4-5/WT}$ were incubated at 4°C, RT, and 37°C with varying concentrations of Enterokinase (EK; EKMax; Invitrogen) and TEV (Invitrogen) (data not shown). Multiple sets of time and temperature controlled digestion were performed by combining 10ul of 2ug/ml Enterokinase (NEB) or 1ul of 10u/ul TEV (Invitrogen) per 10 ug of $m\alpha 1\text{LG4-5/WT}_{\text{Nf}}$ (with N-terminal FLAG tag) and elastase EHS Lm-111 fragment E3 protein, and molar equivalents of EHS Lm-111, recombinant mouse Lm-111, and purified recombinant human $\beta 1$ Lm (with N-terminal HA tag) in 50mM Tris-HCl, pH7.4 at RT; 150 mM NaCl, 2mM CaCl_2 and the samples incubated at 4°C, RT, and 37°C. 1/8th of the reaction volume was taken at 0 min. x 2, 5 min., 10 min., 30 min., 60 min., 120 min., 180 min., 8 hr., and 24 hr. The EK treated samples were incubated with trypsin inhibitor agarose (Sigma-Aldrich) and centrifuged to remove the EK. Samples incubated

with TEV were treated with Ni-NTA resin (Invitrogen) in order to remove the TEV by binding through its C-terminal His tail. Supernatants, containing the desired proteins were recovered and 4XLSB with 15% B-Mercaptoethanol was immediately added to the supernatant, samples boiled and placed at -20°C till loading. One aliquot was utilized for coomassie blue staining of a 6-12% SDS-PAGE gel. The other aliquots were run on 6-12% SDS-PAGE gels, electrophoretically transferred onto polyvinylidene difluoride membranes (PVDF) using a BioRad TurboBlotter, and blocked with 5% nonfat dried milk and 0.2% Tween-20 in 150mM NaCl, 50mM Tris-HCl; pH 7.4 at 4°C. Bands were visualized either through incubation with the appropriate primary antibodies, rG50 pAb and protein-C mAb (Roche), followed by HRP-conjugated secondary antibodies (Pierce) or directly with HRP linked primary antibodies: HRP-FLAG M2 mAb (Sigma-Aldrich), HRP-HA mAb (clone 3F10; Roche), HRP-c-myc mAb (clone9E10; Roche), HRP-VSV-G mAb (Cell Signalling), mouse anti-VSV-G mAb – HRP conjugated (Cell Signalling), mouse anti-protein C IgG1,k mAb (clone HPC4; Roche), and mouse anti-V5 IgG2a mAb – HRP conjugated (Invitrogen). Blots were developed with ECL reagents (Amersham Biosciences) and band intensities on autoradiographs scanned and quantitated.

Recombinant $\alpha 1\text{LG4-5/WT}_{\text{NF}}$ was also dialyzed into 50mM NaCl, 1mM CaCl_2 , 50mM Tris-HCl; pH8.0 at RT buffer and 12.5 ug of $\alpha 1\text{LG4-5}$ per unit of EK incubated for 12 hours at 4°C, RT, and 37°C with varying concentrations of EK in 50mM NaCl, 1mM CaCl_2 , 50mM Tris-HCl; pH8.0.

Rotary shadow electron microscopy of recombinant $\alpha 1\text{LG4-5}$ proteins.

Recombinant $\alpha 1\text{LG4-5}$ proteins and elastase digest fragment E3 were dialyzed in 0.15M ammonium bicarbonate and adjusted to 60% glycerol. Pt/C rotary shadowing of proteins

was performed by deposition of 0.9 nm metal at an 8° angle as previously described [45] by Dr. Peter Yurchenco.

Heparin binding of laminin α 1LG4-5 (EHS E3 fragment) and recombinant α 1LG4-5 proteins.

The elastase digest α 1LG4-5 fragment E3 isolated from Lm-111 purified from EHS tumor [45], recombinant α 1LG4-5/WT_{Nf}, recombinant α 1LG4-5/WT treated with enterokinase to remove the FLAG tag (“de-FLAGed” recombinant α 1LG4-5/WT), and mutant recombinant α 1LG4-5 proteins were loaded onto a TosoHass Heparin 5PW column in TBS50/Ca at 4°C on a Pharmacia AKTA FPLC, eluted with a 0-1M NaCl salt gradient, and the salt concentration of their elution determined.

Analysis of recombinant α 1LG4-5 proteins binding to α DG.

The ability of the recombinant fragments to bind α -dystroglycan (α DG) was measured both by a gel overlay assay (α DG run into gel and overlaid with 2 μ g of each recombinant α 1LG4-5) and a solid phase binding assay in which the α DG is attached to microtiter plate wells. α DG was purified from rabbit muscle as previously described [293, 294]. Equal aliquots of α DG (1ug) were loaded into the slots of SDS-acrylamide gels and electrophoresed under reducing conditions. The protein bands were then electroeluted onto nitrocellulose membranes and assessed for binding to each α 1LG4-5 protein (1ug/ml) using a previously described overlay assay method [295]. Binding of the α 1LG4-5 proteins was detected with 1.1 ug/ml of horseradish peroxidase coupled to the monoclonal anti-FLAG antibody M2 (SIGMA). The solid phase ELISA assay was performed in 96 well microtiter plates with 0.1 ug/well of α DG bound to the plate and incubated with various concentrations of α 1LG4-5 proteins as previously described

[296], except that HRP-linked monoclonal antibody M2 was used for detection followed by color development with TMB (3,3',5,5'-tetramethylbenzidine; Bio-Rad). Color development was quantitated at 655nm using a Molecular Dynamics Spectramax 340UV/Vis microplate reader [297]. Estimates of half-maximal binding, corresponding to the apparent dissociation constant (K_d), and binding capacity (B_{max}) were determined using the computer program SIGMA PLOT and by curve fitting of the binding data of $\alpha 1LG4-5$ using a single-site binding algorithm (fitted values = $B_{max} * L / (K_d + L)$, where L is the molar ligand concentration), with the calculated B_{max} value used for subsequent determinations of all other half-maximal binding - an approach employed to minimize errors inherent in estimating binding from plots that are very low over the concentration range employed. A constant B_{max} of 3.6 and MW of 43.1 kDa was utilized. All αDG binding experiments were performed by Ariana Combs in the laboratory of Dr. James Ervasti.

Analysis of recombinant $\alpha 1LG4-5$ binding to galactosyl sulfatide and other lipids as well as lipids utilized in other experiments.

The ammonium salt of $HSO_4-3Gal\beta 1-1'Ceramide$ (brain sulfatides mixture; Avanti Polar Lipids = APL) was dissolved in methanol and 10 μg added per immulon-1B microtiter plate well (ThermoLabsystems). The plate was dried at 37°C for 2 hours and the wells washed four times with 200 μl of ELISA Wash Buffer (EWB): 90mM NaCl, 5mM $CaCl_2$, 50mM Tris-HCl; pH7.4 at room temperature and 1% BSA (a specific fatty acid free prep; Sigma-Aldrich; catalog #A-7030). The wells were then blocked for 1 hour at RT with 200 μl of EWB, followed by three 200 μl washes of EWB. Recombinant $Lm\alpha 1LG4-5$ proteins in varying concentrations in EWB were added to each well and incubated for 1.5 hours at room temperature. The wells were then washed four times with 200 μl of EWB

and HRP-linked monoclonal FLAG antibody M2 in EWB added. After 1 hour at room temperature the wells were washed four times with EWB and 150 μ l of substrate solution (4mM O-phenylenediamine, 50mM citric acid, 100mM Na_2HPO_4 , and 0.012% H_2O_2) added. The developing color reaction was then stopped after 2-10 minutes by the addition of 60ul of 2M H_2SO_4 , followed by 50ul of 90% ethanol and the plates read in a TECAN SpectraFluor microtiter plate spectrophotometer at 492nm. If the obtained values were too high for an accurate reading, an appropriate volume of the sample was removed, placed in a new microtiter plate, diluted with substrate solution, read in the spectrophotometer and the resulting values modified accordingly. A calculated molecular weight of 44.3 kDa was utilized to calculate molar concentrations of recombinant α 1LG4-5s. Inhibition studies were performed in the presence of either 10ug/ml low molecular weight heparin (Sigma-Aldrich), 5mM EDTA, or 1-3% Triton X-100. The assay was also performed with several other lipids and lipid mixtures including: ceramide (APL), galactosyl ceramide (APL and Sigma-Aldrich), lactosyl ceramide (APL and sigma aldrich), N-octanoyl-ceramide-1-phosphate (APL), sphingomyelin (APL), phosphatidic acid (APL), L- α -phosphatidylglycerol (APL), L- α -phosphatidylinositol (APL), L- α -phosphatidylethanolamine (APL), L- α -phosphatidylcholine (APL), L- α -phosphatidylserine (APL), D-erythro-sphingosine (APL), sphingosine-1-phosphate (APL), cholesterol (APL and Sigma-Aldrich), cholesterol-3-sulfate (Sigma-Aldrich), GM1 ganglioside (APL), total brain gangliosides (APL), glc-sulfatide (gift from Ineo Ishizuka, Teikyo University, Tokyo, Japan), and BODIPY-gal-sulfatide [298]. Many different ELISA Wash Buffers, microtiter plates, BSA preparations, drying, incubation, washing, and detection methods were tested. The above method gave higher signal, lower data scatter, and better reproducibility of all the tested

variables. Half-maximal binding (K_d) and B_{max} values were estimated in the same manner as described for αDG .

Various attempts to immunoprecipitate $\alpha 1LG4-5/WT_{Nf}$ complexed with sulfatide and quantitate the direct binding of $\alpha 1LG4-5/WT_{Nf}$ failed. Attempts to measure the sulfatide brought down from either a sulfatide containing solution or from sulfatide bound to BSA, via recombinant $\alpha 1LG4-5/WT_{Nf}$ immunoprecipitated with FLAG mAb or FLAG matrix, failed, however, when the recombinant $\alpha 1LG4-5s$ were incubated with MEFs which had been pre-loaded with BODIPY-sulfatide, extracted, and the $\alpha 1LG4-5$ immunoprecipitated via the N-terminal FLAG tag, sulfatide did bind and remained bound to the recombinant $\alpha 1LG4-5s$, and could be measured and compared. MEFs were loaded with sulfatide according to the method described in this Materials & Methods section. Recombinant $\alpha 1LG4-5/WTs$ were then added to the media and the MEFs incubated for 15 minutes at 37°C. The cells were washed extensively with wash buffer (WB): 150mM NaCl, 5mM $CaCl_2$, 1mM $MgCl_2$, 50mM Tris-HCl; pH 7.5. MEFs were removed from the dish by scraping and then resuspended at 4°C for 30 min. in 0.5 ml extraction buffer containing 50mM Tris-HCl, 150mM NaCl, 5mM $CaCl_2$, 1% Triton X-100, 2mM PMSF, 1 μ g/ml pepstatin A, 2 μ g/ml aprotinin, 5 μ g/ml leupeptin, 2mM sodium fluoride, and 2mM sodium vanadate. Lipid raft microdomains were then isolated from the MEFs after the treatment with 1% Triton X-100 at 4°C as detergent-insoluble glycosphingolipid-rich microdomains (DIGs) by density gradient centrifugation at 4°C. To generate the density gradients for centrifugation, the cell lysate was adjusted to 40% OptiPrep (Sigma-Aldrich) and overlaid with solutions of 30% and 10% Optiprep in the extraction buffer. These gradients were centrifuged for 16 hr at 35,000 rpm at 4°C in a SW40Ti rotor (Beckman Instruments). Fractions of equal volume including the DIG (floating fraction, as judged visually by the presence of a band in the density gradient) and non-DIG (bottom fraction) extracts were

collected and analyzed by SDS-PAGE (10%) followed by immunoblotting. The DIG fraction also contains caveolas in addition to noncaveolar membrane microdomains, therefore, the presence of caveolin was utilized by Western blotting to confirm that the DIG fraction had been correctly identified in each experiment. Immunoprecipitations, were performed with the FLAG M2 mAb specific to the N-terminal FLAG epitope tag present on all the recombinant α 1LG4-5s tested. Both the DIG and non-DIG fractions were resuspended in extraction buffer. In order to remove nonspecifically binding proteins, these fractions were then precleared with a mixture of protein A and G sepharose for 30 min at 4°C. They were then incubated with FLAG M2 mAb agarose overnight at 4°C on a rotating platform. After four washes in extraction wash buffer containing 1% NP-40, equal concentrations of the immunoprecipitations were loaded on gels for SDS-PAGE and immunoblotting to verify fraction constituents and estimate protein content. Appropriate volumes were then analyzed in a fluorimeter and the number of sulfatides per mole of α 1LG4-5 determined.

Antibiotics utilized and kill curves generated.

HEK 293 cells were plated at 30% confluence in 6-well tissue culture dishes with DMEM (Invitrogen) supplemented with 10% FBS (Atlanta Biological), 200 mM L-glutamine (Invitrogen), penicillin-streptomycin (1,000 u/ml and 1,000 ug/ml respectively), and with or without one of the following six antibiotics at the six various concentrations given: 0.5, 1, 2, 4, 6, and 8 ug/ml blasticidin S HCl (Invitrogen); 50, 100, 250, 500, 750 1,000 ug/ml G418/geneticin (Sigma-Aldrich/Invitrogen); 10, 40, 60, 80, 100, and 120 ug/ml zeocin (Invitrogen); 0.1, 0.5, 0.75, 1, 2, 4 ug/ml puromycin (Sigma-Aldrich); 0.5, 1, 2, 4, 6, and ug/ml hygromycin-B (Sigma-Aldrich). Media was changed every 3 days and the number

of surviving cells counted every 24 hours for 14 days. “Kill” curves were then generated from the number of surviving cells.

Antibodies.

The following antibodies were utilized in this study: rG50 – a rabbit polyclonal antibody (pAb) which reacts with the LG4-5 domain of the laminin α 1 chain, EHS Lm – a rabbit polyclonal antibody which reacts with the laminin α 1, β 1, and γ 1 chains, α 2LmLG1-5 – a rabbit pAb which reacts with the LG1-5 domain of the laminin α 2 chain, Lm2/4 – a rabbit pAb which reacts with the laminin α 2 and γ 1 chains, placental Lm – a rabbit pAb which reacts with the α 2, β 1, and γ 1 chains of laminin, which were prepared and characterized as described previously [52, 299], and rat Lm γ 1 mAb (Upstate Biotechnology). Other antibodies utilized, include: nidogen-1 pAbs [51, 70], β 1 integrin hamster mAb Ha2/5 (BD PharMingen), α DG mouse monoclonal IgM Ab IIH6 (gift from K. Campbell, University of Iowa, Iowa City, IA), β DG mouse mAb (Novocastra Laboratories), gal-sulfatide mAb Sulfl (gift from P. Fredman; Sahlgrenska University Hospital, Malmö, Sweden) [300], utrophin mAb DRP2 (Novocastra), S100 mAb (Chemicon), S100 rabbit pAb (gift from P. Amenta; UMDNJ, New Brunswick, NJ), rabbit anti-mouse type I collagen antibody (CHEMICON International, Inc.), rabbit anti-mouse type IV collagen pAb (Rockland Immunochemicals), rat anti-mouse perlecan mAb, myelin basic protein mAb (Sternberger Monoclonals), myelin basic protein pAb (gift from P. Amenta; UMDNJ, New Brunswick, NJ), rabbit cSrc pAb (Santa Cruz Biotechnology), rabbit cSrc-pY₄₁₆ pAb which also cross reacts with activated Fyn (Cell Signaling Technology), caveolin-1 pAb (Sigma-Aldrich), caveolin-1-pY₁₄ pAb (BD Biosciences), Fyn mAb (Sigma-Aldrich), rabbit anti-FLAG IgG pAb (Sigma-Aldrich), mouse anti-FLAG M1 IgG_{2b} mAb (Sigma-Aldrich), mouse anti-FLAG M2 IgG₁ mAb (Sigma-Aldrich), mouse anti-FLAG M5 IgG₁ mAb

(Sigma-Aldrich), anti-FLAG M2-Alkaline Phosphate conjugated mAb (Sigma-Aldrich), anti-FLAG M2–HRP conjugated mAb (Sigma-Aldrich), anti-FLAG M2-CY3 conjugated mAb (Sigma-Aldrich), anti FLAG M2–FITC conjugated mAb (Sigma-Aldrich), anti-FLAG M2 mAb affinity gel (agarose; Sigma-Aldrich), mouse anti-c-myc IgG1,k mAb (clone 9E10; Roche), mouse anti-c-myc mAb (clone 9E10) affinity matrix (Roche), mouse anti-c-myc mAb (clone 9E10)–HRP conjugated (Sigma-Aldrich), rat anti-HA IgG1 mAb (clone 3F10; Roche), rat anti-HA mAb (clone 3F10) affinity matrix (Roche), rat anti-HA (clone 3F10) mAb–Fluorescein conjugated (Roche), rat anti-HA (clone 3F10) mAb–HRP conjugated (Roche), mouse anti-HA IgG2b,k mAb (clone 12CA5; Roche), mouse anti-HA (clone 12CA5) mAb–fluorescein conjugated (Roche), anti-HA (clone 12CA5) mAb–rhodamine conjugated (Roche), mouse anti-VSV-G IgG1, κ mAb (clone P5D4; Roche), mouse anti-VSV-G mAb–HRP conjugated (Cell Signalling), mouse anti-protein C IgG1,k mAb (clone HPC4; Roche), mouse anti-V5 IgG2a mAb (Invitrogen), mouse anti-V5 mAb–HRP conjugated (Invitrogen); as well as, FITC-, Cy3- and Cy5-conjugated secondary antibodies specific for mouse IgG, mouse IgM, and rabbit IgG (Jackson ImmunoResearch Laboratories) were used for immunofluorescence detection, HRP-linked antibodies specific for mouse IgG, rat IgG, and rabbit IgG (Amersham Pharmacia Biotech) were used as secondary antibodies for immunoblotting.

Antibodies and immunofluorescence microscopy.

Schwann and MEF cells grown on glass coverslips or plastic in the presence of extracellular proteins were rinsed 3 times with PBS (10 mM sodium phosphate, pH 7.4, 127 mM NaCl) and fixed in 3% paraformaldehyde for 30 minutes. Cultures were blocked with 5% goat serum and then stained with primary and appropriate secondary antibodies conjugated with fluorescent (FITC, Cy3, and Cy5) probes. Rabbit polyclonal antibodies specific for laminin-111 (EHS), laminin fragment E4 (the β 1LN domain obtained from an

elastase digest of EHS laminin-111), laminin α 1LG4-5 (RG50), and nidogen-1 were used as described [70]. EHS-laminin antibody binding to microtiter wells coated with 1 μ g/ml of different recombinant laminins (WTa, β 1 Δ LN, α 1 Δ LN, α 1 Δ LN-L4b, γ 1 Δ LN and α 1 Δ LG1-5) was evaluated by direct ELISA assay with serial two-fold dilutions of antibody. The binding plots were essentially identical for all substrates except for α 1 Δ LN-L4b whose plot lagged by a single two-fold dilution and whose color intensity at saturation (5 μ g/ml) was decreased by <10%. Therefore, this antibody (20ug/ml) against fragment E4 was used to compare the accumulation of different laminins on cell surfaces, except for recombinant Lm-111s containing N-terminal deletions, in which case the laminin α 1LG4-5 antibody was utilized for comparisons. Nidogen-specific rabbit antibody prepared against recombinant nidogen-1 [71] was used at 3 μ g/ml and type IV collagen-specific rabbit antibody (Chemicon) was used at a 5 ug/ml. Detection was accomplished with Alexa Fluor 488 and 647 goat anti-rabbit IgG secondary antibodies (Molecular Probes) at 1:500 and 1:100 respectively, and FITC-conjugated donkey anti-mouse IgM at 1:100 (Jackson Immuno Research). Slides were counterstained with DAPI and imaged as described [70]. Laminin, type IV collagen and nidogen immunofluorescence levels were quantitated from digital images (average of 9, each 1300 x 1030 pixels, 437 x 346 μ m) recorded using a 20x microscope objective with IPLab 3.7 software (Scanalytics). A segmentation range was chosen to subtract background and acellular immunofluorescence. The sum of pixels and their intensities in highlighted cellular areas of fluorescence were measured and normalized by dividing by the number of cells determined from a count of DAPI-stained nuclei for each image. Data were expressed as the mean and standard deviation of normalized summed intensities with the data analyzed by one-way ANOVA with Holm-Sidak comparisons in SigmaPlot v.9.01 and SigmaStat v3.1 (Jandel).

Immunoprecipitation (IP) and immunoblotting (IB).

Cell lysates of adherent cells were prepared by washing the cells with cold PBS. Followed by disruption in lysis buffer: 50mM Tris, pH 7.4, 100mM NaCl, 0.5 mM EDTA, 1% Triton X-100, 1% SDS, and protease and phosphatase inhibitor cocktails (Sigma-Aldrich; diluted 1:10 and 1:100, respectively) and centrifugal sedimentation to get rid of the cellular debris pellet. Immunoprecipitations were performed at 4°C with the addition of protease inhibitor cocktails (Sigma-Aldrich) to all the protein samples and buffers. Conditioned medium or lysates were precleared with 20 µl of an equal mixture of protein A-agarose and protein G-Sepharose bead slurry. Samples were incubated with antibody overnight and precipitated with 40µl protein A-agarose or protein G-Sepharose beads for 2 hours and followed by washing in 50mM Tris-HCl, pH 7.5, 150mM NaCl, 1% NP-40, and 0.1% SDS. After an additional wash, the supernatant was removed and the immunoprecipitates were analyzed by SDS-PAGE. Duplicates of type IV collagen antibody immunoprecipitates were incubated with 5 U bacterial collagenase (CLSPA; Worthington Biochemical Corporation) at 37°C for 1 hour. After collagenase digestion, the immunoprecipitates were washed twice in PBS and analyzed. Epitope tag specific antibodies, matrix, and peptide for elution were utilized when appropriate. Proteins were quantitated and equal amounts of proteins were separated by SDS-PAGE under reducing conditions: 3.5-12% gradient, 6%, 10% and 12.5% for heterotrimeric laminins, 3-12.5% and 6% for laminin LG1-5, LG1-3, and LG4-5 recombinant proteins, 12% for caveolin-1, 8% for Src, and 6% for utrophin. After SDS-PAGE was performed, proteins from the gels were electrophoretically transferred onto polyvinylidene difluoride membranes (PVDF; BioRad) using an electroblotter, blocked with 5% nonfat dried milk and 0.2% Tween 20 in 150mM NaCl, 50mM Tris-HCl; pH 7.4, and incubated with primary antibodies followed by HRP-conjugated secondary antibodies (Pierce) or HRP-FLAG M2 mAb (Sigma-Aldrich). Blots were developed with ECL reagents (Amersham

Biosciences). Band intensities were quantified from the membrane or scanned films using Quantity 1 software (Bio-Rad Laboratories) after data acquisition with a gel documentation system (ChemiDoc XRS; Bio-Rad Laboratories) as described previously [45, 51].

Protein visualizations and quantifications.

Protein concentrations were determined by absorbance at 280nm, Bradford assay (BioRad Laboratories), amino acid analysis, and comparison against known standards in Coomassie blue-stained gels as described [51, 74, 301]. Proteins were solubilized in Laemmli sample buffer and evaluated by SDS-PAGE under reducing conditions on 3.5-12% linear gradient, 6%, or 10% acrylamide gels. Electrophoresed gels were stained with Coomassie Brilliant Blue R-250, imaged with a BioRad Gel Doc 2000 in brightfield mode, and analyzed with Quantity One software (BioRad).

Polymerization assays with laminin, collagen, and nidogen.

Aliquots (50ul) of laminin in polymerization buffer (TBS, 1mM CaCl₂, 0.1% Triton X-100) at various concentrations were incubated at 37°C in 0.5ml Eppendorf tubes for one hour. Samples were centrifuged at 11,000xg, followed by solubilization of supernatant and pelleted fractions in Laemmli sample buffer and analysis by SDS-PAGE as described above.

Sulfatide (and other lipids) loading of cells.

The sulfatide-BSA complex was prepared as previously described [70, 71]. Gal-sulfatide, glc-sulfatide, BODIPY-gal-sulfatide and other lipids were dissolved under a stream of argon, reconstituted in DMSO, and heated at 60°C for 10 minutes. Lipids were then mixed with an equal molar ratio of de-lipidated BSA (Sigma-Aldrich) in PBS, PH

7.4, and incubated at 37°C for 20 minutes. The lipid-BSA complex was diluted with serum-free DMEM and added to cells for 30 minutes at a final concentration of 10mM. Cells were then rinsed three times with PBS and used immediately for experiments.

Flourescence microscopy of Schwann and fibroblast cells.

Cells that were grown on glass coverslips were rinsed with PBS, fixed in 3% PFA for 30 minutes, and then washed again in PBS. Suspended cell aggregates were collected by sedimentation, washed with PBS, fixed in 3% PFA, embedded in optimal cutting temperature compound (OCT; Tissue-Tek), and sectioned on a cryostat. When intracellular epitopes needed to be stained, the cells were permeabilized with 0.1% Triton X-100 in PBS on ice for 5 minutes. Slides were blocked with 5% goat serum and stained with primary and appropriate secondary antibodies conjugated with FITC, Cy3, or Cy5 (Jackson ImmunoResearch Laboratories). Control staining was achieved using the appropriate IgG or IgM. Nuclear staining was accomplished with DAPI. Immunofluorescence and phase microscopy were performed on an inverted microscope (model IX70; Olympus) with IX-FLA fluorescence and CCD camera, and the data collected and analyzed utilizing IPLab v.3.52 (Scanalytics) as described previously [70].

Electron microscopy.

(a) *Rotary shadow Pt/C replicas* - Laminin (25-50µg/ml in 0.15M ammonium bicarbonate, 60% glycerol) was sprayed onto mica discs, evacuated in a Balzers BAF500K unit, rotary shadowed with 0.9 nm Pt/C at an 8° angle, backed with 8 nm carbon at a 90° angle, and viewed in an electron microscope as otherwise described [301]. Electron micrograph images are shown contrast-reversed.

(b) *Thin sections of cell layers* - Schwann cells were plated in 60-mm Permanox dishes (Nalgene Nunc) 2 days before the experiment. The next day the media was changed. A day later, laminins (20-50 $\mu\text{g/ml}$) were added to freshly replaced medium and incubated for one hour at 37°C. H. promelia arylsulfatase (Sigma-Aldrich) or bacterial collagenase (CLS; Worthington) were added to cell cultures 30 minutes before the addition of Lm-111 when called for. The media was removed and the adherent cells washed once in PBS. The cells were fixed in 0.5% glutaraldehyde and 0.2% tannic acid in PBS for 1 hour at room temperature, and then transferred to modified Karnovsky's fixative (4 % formaldehyde and 2.5 % glutaraldehyde containing 8 mM CaCl_2 in 0.1 M sodium cacodylate buffer, pH 7.4). Samples were washed with PBS and post-fixed in 1% osmium tetroxide in 0.1 M sodium cacodylate buffer, pH 7.4 for 1 hour to produce osmium black. Samples were then dehydrated through a graded series of ethanol and embedded in Epon/SPURR resin (EM Science) that was polymerized at 65°C overnight. Sections (~90 nm) were cut with a diamond knife and stained with saturated uranyl acetate (20 min) followed by 0.2% lead citrate (2.5 min). Images were photographed with a Jeol JEM-1200EX electron microscope (JEOL) as described previously (Tsiper et al., 2002). The percentage of BM coverage was determined as the ratio of measured length of continuous ECM present on the cell surface divided by the total measured length of exposed cell surface in random cross sections cut at different depths within the Epon block.

Schwann cell culturing.

Schwann cells isolated from sciatic nerves from newborn Sprague Dawley rats were the kind gift of Dr. James Salzer (New York University). These cells were expanded in culture for 5-10 passages and maintained in DMEM, 10% fetal calf serum (Gemini Bio

Products), neuroregulin (0.5 µg/ml, Sigma), forskalin (0.2 µg/ml, Sigma), 1% glutamine and penicillin-streptomycin. Schwann cells were then switched to DMEM media supplemented with 10% fetal calf serum, 2% pituitary extract, and 4uM (0.2ug/ml) forskalin. Cells between passage 11 and 17 were utilized for binding experiments and plated at half-confluent densities onto 24-well tissue culture treated dishes (Costar), 22-mm² glass coverslips in 6-well dishes, or 16-well glass chamber slides (Nalgene). The following day, the media were changed and the cells were incubated with 20-40 ug/ml laminin, 10-20 ug/ml type IV collagen, and/or 2-8 ug/ml nidogen-1 at 37° in DMEM/F12 (Invitrogen) containing 10% FBS for one hour, followed by washing and fixation.

Mouse embryonic lung fibroblasts.

Day E12 embryonic lungs from C57BL6 mice were removed and transferred to a bacteriological treated petri dish, where they were dissected and cut into fine pieces and treated with 10% trypsin-versene for 20 minutes, centrifuged and the supernatant plated on tissue culture treated petri dishes, the supernatant was removed 30 minutes later, the adherent cells removed with trypsin-versene again and panned twice more. The adherent cells which remained were greatly enriched for embryonic fibroblasts, any cells not displaying fibroblast like morphology were ignored during the subsequent analyses. These cells were maintained in culture with DMEM and 10% FBS and used in experiments for 4 passages before they were disposed of.

Lipid raft visualization in MEFs.

MEFs were exposed to 20ug/ml recombinant Lm-111_{Nm/Nh/Cf} for 40 minutes, washed twice with groth medium, incubated for 10 minutes with the appropriate Alexa fluorescently conjugated cholera toxin subunit B (CT-B; Vybrant Lipid Raft Labeling Kit;

Molecular Probes), washed four times with 1XTBS containing 5 mM CaCl_2 , incubated with the anti-CT-B antibody for 15 minutes to crosslink the GM1, washed four times with 1XTBS containing 5 mM CaCl_2 , fixed in 4% formaldehyde for 15 minutes, then immunostained with appropriate antibodies (rG50 for laminin and IIH6 for αDG) and reagents (DAPI for nuclear staining).

Culturing of embryonic stem cells and embryoid bodies.

Wild-type R1 and laminin $\gamma 1$ null [31] ES cells were grown on feeder layers of mitomycin treated (10ug/ml for 2 hours) SNL STO cells in ES medium (MEM α -medium; Invitrogen) supplemented with 15% ES-grade FCS (Invitrogen), 0.1 mM nonessential amino acids, 0.1 mM β -mercaptoethanol, 1 mM sodium pyruvate, 100 $\mu\text{g}/\text{ml}$ penicillin, 100 $\mu\text{g}/\text{ml}$ streptomycin, and 1,000 U/ml leukemia inhibitory factor (LIF; Invitrogen). $\beta 1$ -Integrin–null (clone G201) ES cells [302, 303] were cultured directly on Falcon tissue culture dishes (Becton Dickinson) in ES medium. ES cells were subcultured at semi-confluence, and the medium was changed every day to maintain the cells in an undifferentiated state. To culture EBs, subconfluent ES cells were dispersed with 0.25% trypsin-0.53 mM EDTA and plated onto gelatin-coated dishes for 3 hours to allow feeder cells to selectively attach. Nonadherent ES cell aggregates were then dispersed and cultured on bacteriological petri dishes in ES medium without LIF.

Preparation of EBs for immunofluorescence:

EBs were collected into 10ml tubes and allowed to sediment by gravity. After washing in PBS with 0.5% BSA, the EBs were fixed with 3% paraformaldehyde in PBS, followed by incubation in 7.5% sucrose-PBS at room temperature for 3 hours, and then overnight at 4°C in 15% sucrose-PBS. The EBs were embedded in OCT (Tissue-Tek) and 4 μm thick frozen sections were prepared. Nonspecific binding sites were blocked with 5%

goat serum. FITC-, Cy3-, and Cy5-conjugated antibodies were used as secondary reagents and nuclei were counterstained with DAPI.

Microscopy of EB sections:

Slides were viewed by indirect immunofluorescence using an inverted microscope (model IX70; Olympus) fitted with an IX-FLA fluorescence observation attachment and a MicroMax 5-mHz CCD camera (Princeton Instruments) controlled by IP Lab (Scanalytics).

Other proteins utilized in this study.

Several proteins utilized in this study were prepared by the laboratory, gifts, or purchased.

Lm-111:

Laminin-111 was extracted in EDTA from lathyrotic mouse Engelbreth-Holm-Swarm (EHS) tumor and purified as previously described [45].

Recombinant human heterotrimeric laminin-211:

Expressed and purified as described previously [296].

Recombinant nidogen:

A pCIS vector encoding full length mouse nidogen-1 (gift from Dr. Rupert Timpl, MPI for Biochemistry, Martinsried, Germany) was used to stably transfect 293 cells. Secreted protein was purified from medium by metal chelating chromatography as previously described [59].

Type IV collagen:

Was prepared from EHS tumor as previously described [45].

Proteolytic fragments of Lm-111:

Defined proteolytic fragments were prepared after digestion of purified Laminin-111 with either elastase or cathepsin G. Elastase fragments E1' (containing the N-terminal short

arms of $\alpha 1$ and $\gamma 1$ and containing a nidogen fragment), E8 (containing the lower half of the coiled-coil and LG1-3 of $\alpha 1$ chain), E4 (containing the N-terminal LN and LEa of the $\beta 1$ chain), and E3 (containing the C-terminal LG4-5 of the $\alpha 1$ chain) were generated by elastase digest and purified by Sepharose CL-6B gel filtration (Pharmacia) and HPLC DEAE-5PW ion exchange (Toso-Haas) as previously described [48]. Fragment C1-4 (containing all three N-terminal short arms) was prepared and solubilized as previously described [45].

AEBSF Lm-111, AEBSF Lm-111 fragment E1', and AEBSF $\alpha 1$ LG4-5/WT:

Preparation of AEBSF Lm-111 and AEBSF E1' were previously described [304]. 5 mM serine protease inhibitor AEBSF (p-aminoethylbenzenesulfonyl fluoride, HCl) in 50mM Tris-HCl and 90mM NaCl, pH7.4 was incubated overnight on ice with laminin-111 in order to inactivate laminin self-assembly. AEBSF-treated laminin was dialyzed to remove free AEBSF, and then cycled through two rounds of polymerization conditions (37°C, 3 hours) to remove any potentially active laminins. AEBSF-E1' (nonpolymerization inhibition control) was prepared by incubation of E1' under the same conditions as Lm-111, followed by dialysis to remove the AEBSF. AEBSF recombinant $\alpha 1$ LG4-5 was prepared the same way as the other AEBSF treated proteins except the treated material was purified via FLAG chromatography to remove any residual AEBSF.

Recombinant Lm-111 proteins:

Human embryonic kidney cells (HEK293 cells) were cultured in DMEM (Invitrogen) supplemented with 10% Fetal Bovine Serum (Atlanta Biological), 200mM L-Glutamine and Penicillin-Streptomycin (1,000 u/ml Penicillin and 1,000 μ g/ml Streptomycin; Invitrogen). Plasmids containing laminin constructs were linearized and stably transfected into HEK293 cells utilizing Lipofectamine 2000 (Invitrogen). Stable cell lines expressing recombinant laminins were supplemented with 1 μ g/ml puromycin ($\alpha 1$

chains), 80-100 ug/ml Zeocin (β 1 chains), and 500 ug/ml G418 (γ 1 chains) unless otherwise specified. SDS-PAGE, chain specific immunoprecipitation, and western blot analysis of secreted protein was used to confirm expression of trimeric Laminin in the stable cell lines. The α 1, β 1, and γ 1 laminin chains were detected with anti-myc (Roche), anti-hemagglutinin (HA; Roche), and anti-Flag M2 (Sigma) antibodies, respectively, unless otherwise specified. Recombinant laminin was purified from media on a heparin-agarose (Sigma) column and eluted with 500 mM NaCl (in 50mM Tris pH 7.4, 1mM EDTA). The heparin elute containing the recombinant laminin-111 was then bound to a FLAG M2-agarose (Sigma-Aldrich) gravity column and eluted with 100ug/ml FLAG peptide (Sigma-Aldrich) in wash buffer (150mM NaCl, 1mM EDTA, 50mM Tris-HCl; pH 7.4). The dilute protein was concentrated in an Amicon Ultra-15 filter (100K MWCO, Millipore), FLAG peptide recovered for reuse, and the recombinant protein dialyzed in TBS50 (90mM NaCl, 0.125mM EDTA, 50mM Tris-HCl; pH 7.4). Some recombinant proteins were first purified on a heparin 5PW column via an AKTA FPLC system and then FLAG purified in a purification protocol identical to that utilized to purify the recombinant α 1LG4-5 proteins except for the substitution of 1 mM EDTA for CaCl_2 in the buffers utilized.

Expression Constructs

Multiple series of laminin expression constructs were synthesized and can be classified into four main categories (and multiple subcategories) based upon the chain, species, and region of each chain utilized: α 1LG4-5 based (tables 2, 3, and 4), α 1 based (tables 5 and 6), β 1 based (tables 7 and 8), and γ 1 based (tables 9 and 10).

PlatPfx (Invitrogen) and a PTC-100 thermal cycler (MJ Research) were utilized in the PCR reactions. All PCR reactions were cleaned via use of a microcentrifuge tube spin filter (UltraClean PCR Clean-Up Kit; MoBio). Restriction Enzymes were supplied by New England BioLab and Fermentase. When necessary restriction fragments and PCR products were separated on agarose (FMC) gels, stained with Ethidium Bromide, the appropriate band excised, and purified utilizing either an UltraClean 15 DNA Purification kit (MoBio) or a UltraClean GelSpin DNA Extraction kit (MoBio). DNA fragments were ligated with T4 DNA ligase (NEB) and DH5 α (Invitrogen) bacterial cells transformed with the plasmids, plated onto LB-agar plates containing 10ug/ml ampicillin (Sigma-Aldrich), grown O/N at 37°C, bacterial colonies picked and grown in LB media containing 10ug/ml ampicillin, and plasmid DNA purified via the standard alkaline lysis technique utilizing MoBio UltraClean Standard Mini Plasmid Prep kits. All generated plasmids were checked via restriction endonuclease digestion and both the ligation junctions and PCR products of all selected clones were completely sequenced.

Construction of recombinant α 1LG4-5 constructs:

An expression construct containing the mouse laminin α 1 LG4-5 (rE3) WT coding sequence was created by amplifying the WT DNA from the mouse laminin alpha-1 pCIS [299] construct utilizing 3 successive PCR reactions (table 2). Three overlapping upstream 5' sense primers were used to place a 5' terminal Nhe I RE site followed by a

specifically designed 5' UTR, BM40 signal sequence, FLAG epitope tag, and an Enterokinase (Invitrogen) cleavage signal sequence, while the 3' primer placed a Kpn I RE site downstream of the STOP codon on the 3' terminus of the amplified product (see table 2 for diagram of procedure and list of oligonucleotide primers utilized). These sites were used to clone the PCR product into the analogous sites in the pcDNA3.1+/zeo vector (Invitrogen). The mutated recombinant α 1LG4-5s were constructed in a similar manner using the same three 5' upstream sense primers and downstream 3' antisense oligo (table 3). However, first 2 PCR fragments which overlapped at the site of mutation were generated using the first 5' upstream sense primer and a 3' antisense oligo unique to each desired mutated nucleotide sequence and the same downstream 3' terminal primer but with a 5' sense primer unique to each desired mutated nucleotide sequence. The second upstream 5' sense primer and the downstream 3' antisense terminal primer from the downstream fragment, were used in a PCR reaction to sow the two pieces together and generate each mutant recombinant α 1LG4-5 construct. A list and diagram of the actual oligos utilized to construct α 1LG4-5/WT can be found in table 2; while table 3, provides the analogous information for the mutant recombinant mouse α 1 LG4-5. A comprehensive list of the α 1 LG4-5 recombinant proteins and their designations can be found in table 4:

1. α 1LG4-5/WT-pRCX3_{Nf} - An expression construct expressing mouse α 1 LG4-5 with a BM40 signal sequence, followed by an N-terminal FLAG tag, under control of the CMV promoter in the pRCX3 expression vector.
2. m α 1LG4-5/WT-RSV_{Nf} - An expression construct expressing mouse α 1 LG4-5 with a BM40 signal sequence, followed by an N-terminal FLAG tag, under control of the RSV promoter in the pRCX3 expression vector.

3. m α 1LG4-5/WT-m β 1_{Nf} - An expression construct expressing mouse α 1 LG4-5 with a BM40 signal sequence, followed by an N-terminal FLAG tag, under control of the mouse β 1 laminin promoter in the pRCX3 expression vector.
4. m α 1LG4-5/WT_(α 1LG4-5/WT_{Nf}) - An expression construct expressing mouse α 1 LG4-5 with a BM40 signal sequence, followed by an N-terminal FLAG tag, under control of the CMV promoter in the pcDNA3.1/zeo vector and utilizing the "con1" 5' UTR sequence.
5. m α 1LG4-5/WT_{Cf} - An expression construct expressing mouse α 1 LG4-5 with a BM40 signal sequence and a C-terminal FLAG tag, under control of the CMV promoter in the pcDNA3.1/zeo vector and utilizing the "con1" 5' UTR sequence.
6. α 1LG4-5/WTcon2_{Nf} - An expression construct expressing mouse α 1 LG4-5 with a BM40 signal sequence, followed by an N-terminal FLAG tag, under control of the CMV promoter in the pcDNA3.1/zeo vector and utilizing the "con2" 5' UTR sequence.
7. α 1LG4-5/WTh2b_{Nf} - An expression construct expressing mouse α 1 LG4-5 with a BM40 signal sequence, followed by an N-terminal FLAG tag, under control of the CMV promoter in the pcDNA3.1/zeo vector and utilizing the "h2b" 5' UTR sequence.
8. α 1LG4-5/WTtomm7_{Nf} - An expression construct expressing mouse α 1 LG4-5 with a BM40 signal sequence, followed by an N-terminal FLAG tag, under control of the CMV promoter in the pcDNA3.1/zeo vector and utilizing the "tomm7" 5' UTR sequence.
9. α 1LG4-5/WTiars_{Nf} - An expression construct expressing mouse α 1 LG4-5 with a BM40 signal sequence, followed by an N-terminal FLAG tag, under control of the CMV promoter in the pcDNA3.1/zeo vector and utilizing the "iars" 5' UTR sequence.
10. α 1LG4-5/WTfdft1_{Nf} - An expression construct expressing mouse α 1 LG4-5 with a BM40 signal sequence, followed by an N-terminal FLAG tag, under control of the CMV promoter in the pcDNA3.1/zeo vector and utilizing the "fdft1" 5' UTR sequence.

11. α 1LG4-5/WTube2s_{Nf} - An expression construct expressing mouse α 1 LG4-5 with a BM40 signal sequence, followed by an N-terminal FLAG tag, under control of the CMV promoter in the pcDNA3.1/zeo vector and utilizing the "ube2" 5' UTR sequence.
12. α 1LG4-5/WTeif4a1_{Nf} - An expression construct expressing mouse α 1 LG4-5 with a BM40 signal sequence, followed by an N-terminal FLAG tag, under control of the CMV promoter in the pcDNA3.1/zeo vector and utilizing the "eif4a1" 5' UTR sequence.
13. m α 1LG4-5/WT_(-f) - An expression construct expressing mouse α 1 LG4-5 with a BM40 signal sequence and no epitope tag, under control of the CMV promoter in the pcDNA3.1/zeo vector and utilizing the "con1" 5' UTR sequence.
14. α 1LG4-5/WT-IgK_{Nf} - An expression construct expressing mouse α 1 LG4-5 with a Igk signal sequence, followed by an N-terminal FLAG tag, under control of the CMV promoter in the pcDNA3.1/zeo vector and utilizing the "con1" 5' UTR sequence.
15. α 1LG4-5/WT-m α 1_{Nf} - An expression construct expressing mouse α 1 LG4-5 with a mouse α 1 laminin signal sequence, followed by an N-terminal FLAG tag, under control of the CMV promoter in the pcDNA3.1/zeo vector and utilizing the "con1" 5' UTR sequence.
16. α 1LG4-5/WT_{Nm} - An expression construct expressing mouse α 1 LG4-5 with a BM40 signal sequence, followed by an N-terminal myc tag, under control of the CMV promoter in the pcDNA3.1/zeo vector and utilizing the "con1" 5' UTR sequence.
17. α 1LG4-5/WT_{Nm3} - An expression construct expressing mouse α 1 LG4-5 with a BM40 signal sequence, followed by an N-terminal triple myc tag, under control of the CMV promoter in the pcDNA3.1/zeo vector and utilizing the "con1" 5' UTR sequence.
18. α 1LG4-5/WT_{Nh} - An expression construct expressing mouse α 1 LG4-5 with a BM40 signal sequence, followed by an N-terminal HA tag, under control of the CMV promoter in the pcDNA3.1/zeo vector and utilizing the "con1" 5' UTR sequence.

19. α 1LG4-5/WT_{Nv} - An expression construct expressing mouse α 1 LG4-5 with a BM40 signal sequence, followed by an N-terminal VSV-G tag, under control of the CMV promoter in the pcDNA3.1/zeo vector and utilizing the "con1" 5' UTR sequence.

20. α 1LG4-5/WT_{Np} - An expression construct expressing mouse α 1 LG4-5 with a BM40 signal sequence, followed by an N-terminal protein-C epitope tag, under control of the CMV promoter in the pcDNA3.1/zeo vector and utilizing the "con1" 5' UTR sequence.

21. α 1LG4-5/WT_{Nv5} - An expression construct expressing mouse α 1 LG4-5 with a BM40 signal sequence, followed by an N-terminal V5 tag, under control of the CMV promoter in the pcDNA3.1/zeo vector and utilizing the "con1" 5' UTR sequence.

22-65. various α 1LG4-5/WT point mutations- A series of expression constructs expressing mouse α 1 LG4-5 with a BM40 signal sequence, followed by an N-terminal FLAG tag, under control of the CMV promoter in the pcDNA3.1/zeo vector and utilizing the "con1" 5' UTR sequence are described in Table 4. Since the construction of all 44 of these constructs differ only in the two overlapping oligonucleotide primers utilized to substitute Alanines in place of key amino acid residues, they shall not be described here, only listed here and in Table 4:

- | | | |
|---|---|---|
| 22. α 1LG4-5/ <u>RKR</u> ₂₇₂₁ | 23. α 1LG4-5/ <u>RKR</u> ₂₇₂₁ | 24. α 1LG4-5/ <u>RKR</u> ₂₇₂₁ |
| 25. α 1LG4-5/ <u>RKR</u> ₂₇₂₁ | 26. α 1LG4-5/ <u>RKR</u> ₂₇₂₁ | 27. α 1LG4-5/ <u>RKR</u> ₂₇₂₁ |
| 28. α 1LG4-5/ <u>R</u> ₂₇₂₉ | 29. α 1LG4-5/ <u>R</u> ₂₇₅₇ | 30. α 1LG4-5/ <u>KGRTK</u> ₂₇₇₀ |
| 31. α 1LG4-5/ <u>KGRTK</u> ₂₇₇₀ | 32. α 1LG4-5/ <u>KGRTK</u> ₂₇₇₀ | 33. α 1LG4-5/ <u>KGRTK</u> ₂₇₇₀ |
| 34. α 1LG4-5/ <u>K</u> ₂₇₈₁ | 35. α 1LG4-5/ <u>K</u> ₂₇₈₆ | 36. α 1LG4-5/ <u>KRK</u> ₂₇₉₃ |
| 37. α 1LG4-5/ <u>KRK</u> ₂₇₉₃ | 38. α 1LG4-5/ <u>KRK</u> ₂₇₉₃ | 39. α 1LG4-5/ <u>KRK</u> ₂₇₉₃ |
| 40. α 1LG4-5/ <u>KRK</u> ₂₇₉₃ | 41. α 1LG4-5/ <u>RK</u> ₂₈₂₀ | 42. α 1LG4-5/ <u>RK</u> ₂₈₂₀ |
| 43. α 1LG4-5/ <u>RK</u> ₂₈₂₀ | 44. α 1LG4-5/ <u>RAR</u> ₂₈₃₃ | 45. α 1LG4-5/ <u>RAR</u> ₂₈₃₃ |
| 46. α 1LG4-5/ <u>RAR</u> ₂₈₃₃ | 47. α 1LG4-5/ <u>KDR</u> ₂₈₆₀ | 48. α 1LG4-5/ <u>KDR</u> ₂₈₆₀ |

- | | | |
|---|---|---|
| 49. $\alpha 1\text{LG4-5/KDR}_{2860}$ | 50. $\alpha 1\text{LG4-5/R}_{2869}$ | 51. $\alpha 1\text{LG4-5/RKR}_{2721}+\text{KRK}_{2793}$ |
| 52. $\alpha 1\text{LG4-5/RKR}_{2721}+\text{KRK}_{2793}$ | | 53. $\alpha 1\text{LG4-5/N}_{2714}$ |
| 54. $\alpha 1\text{LG4-5/N}_{2811}$ | 55. $\alpha 1\text{LG4-5/N}_{2900}$ | 56. $\alpha 1\text{LG4-5/N}_{2714}+\text{N}_{2811}$ |
| 57. $\alpha 1\text{LG4-5/N}_{2714}+\text{N}_{2900}$ | 58. $\alpha 1\text{LG4-5/N}_{2811}+\text{N}_{2900}$ | 59. $\alpha 1\text{LG4-5/N}_{2714}+\text{N}_{2811}+\text{N}_{2900}$ |
| 60. $\alpha 1\text{LG4-5/D}_{2747}$ | 61. $\alpha 1\text{LG4-5/D}_{2816}$ | 62. $\alpha 1\text{LG4-5/D}_{2747}+\text{D}_{2816}$ |
| 63. $\alpha 1\text{LG4-5/D}_{2923}$ | 64. $\alpha 1\text{LG4-5/D}_{2996}$ | 65. $\alpha 1\text{LG4-5/D}_{2923}+\text{D}_{2996}$ |

Construction of mouse $\alpha 1$ based expression constructs other than $\alpha 1\text{LG4-5}$:

The wild-type cDNAs for mouse laminin $\alpha 1$ in a pCIS vector ($m\alpha 1$ -pCIS), human $\beta 1$ in both the pCEP4 ($h\beta 1$ -pCEP4) and pCIS ($h\beta 1$ -pCIS) vector, and human $\gamma 1$ in a pRc/CMV2 vector ($h\gamma 1$ -pRc/CMV2) have been previously described [296, 299]. A comprehensive list of laminin $\alpha 1$ based expression constructs can be found in Table 5. Table 6 provides diagrams of all $\alpha 1$ laminin constructs, details of their construction, nucleotide sequences of oligonucleotide primers utilized, and amino acid sequences of interest coded for by said constructs:

1. $\alpha 1\text{WT}_{\text{Nm}}$ – A 0.660Kb DNA fragment representing the 5' end of the mature mouse $\alpha 1$ polypeptide (minus signal sequence) was amplified from the mouse $\alpha 1$ cDNA gene in an earlier construct, $m\alpha 1$ -pCIS [27, 133] utilizing 2 oligonucleotide primers, the upstream $ma1p4$ and downstream $ma1F21$ (Table 6.1.), PlatPfx (Invitrogen) and a PTC-100 thermal cycler (MJ Research, Inc.). Three subsequent overlapping PCRs with additional upstream oligonucleotide primers ($ha1p8$, $ha1p9$, and $ha1p6$) were utilized to synthesize a 5' fragment that contained a Not I RE site followed by a 5'UTR, BM40 signal sequence, c-myc epitope tag, Enterokinase cleavage site, and the 5' terminal region of mouse $\alpha 1$. A 0.829Kb 3' terminal section of the mouse $\alpha 1$ cDNA was amplified with primers $ma1F20$ and $ma1F25$. Both the 5' and 3' terminal PCR products were digested

with RE NotI and BspHI. $m\alpha 1$ -pCIS was also digested with BspHI and a 7.719Kb restriction fragment gel purified (MoBio UltraClean 15 DNA Purification Kit). A vector which imparts puromycin resistance was created (DHpuro) and linearized with NotI and treated with CIP. Every PCR and restriction digest reaction was cleaned utilizing MoBio's UltraClean PCR Clean-up kit. T4 DNA ligase was used to ligate the 5' PCR product, 3' PCR product, and large mouse $\alpha 1$ RE fragment into the prepared puromycin based vector. The ligated material was transformed into DH5 α bacteria, plated onto LB-agar plates containing 10ug/ml ampicillin and resistant clones isolated, grown in LB media O/N, and DNA minipreps performed using MoBio's UltraClean Miniplasmid Prep kit. The obtained clones were checked by RE digestions and DNA sequencing of all PCR generated sections and ligation junctions was performed.

2. $\alpha 1$ WT – the DHpuro vector was digested with NotI and treated with CIP (Table 6.2.).

$\alpha 1$ -wt_{Nm} was digested with BspHI and a 7.72Kb fragment of mouse $\alpha 1$ was gel purified. Five sequential overlapping PCRs utilizing five different overlapping upstream primers (ma1F29, ma1F28, ma1F5, ma1F6, ma1F26) and a single downstream primer (ma1F21) were utilized to synthesize a .77Kb 5' fragment that contained a NotI RE site followed by a 5'UTR, BM40 signal sequence, and the 5' terminal region of mouse $\alpha 1$. A second PCR product was generated utilizing primers ma1F20 and ma1F25 to amplify the C-terminal region of $m\alpha 1$ and place two C-terminal STOP signals followed by a NotI RE site downstream of the mouse $\alpha 1$ sequence. Both PCR products were digested with NotI and BspHI. The RE digested PCR products and purified gel fragment were then ligated together, processed, and analyzed same as above.

3. $\alpha 1$ -WT_{Nf} – The DHpuro vector was digested with NotI and treated with CIP (table 6.3.). $\alpha 1$ -wt_{Nm} was digested with BspHI and BstEII. A 6.88Kb fragment of mouse $\alpha 1$ was gel purified. Two sequential overlapping PCRs utilizing two different overlapping

upstream primers (ma1F39 and ma1F30) and a single downstream primer (ma1F22) were utilized to synthesize a 1.60Kb 5' fragment that contained a 5' NotI RE site followed by a 5'UTR, BM40 signal sequence, FLAG epitope tag, Enterokinase cleavage sequence, the 5' terminal region of $\alpha 1$, and a 3' BstEII RE site. This upstream PCR fragment was then digested with NotI and BstEII. A second PCR utilizing primers ma1F20 and ma1F25 was performed to amplify the C-terminal region of mouse $\alpha 1$ and place two C-terminal STOP signals followed by a NotI RE site downstream of the mouse $\alpha 1$ sequence. This downstream PCR fragment was then digested with BspHI and NotI. The RE digested PCR products and purified gel fragment were then ligated together, processed, and analyzed same as above.

4. $\alpha 1$ WT_{Nc} - The DHpuro vector was digested with NotI and treated with CIP (table 6.4.). $\alpha 1$ -wt_{Nm} was digested with BspHI and BstEII. A 6.88Kb fragment of mouse $\alpha 1$ was gel purified. Three sequential overlapping PCRs utilizing three different overlapping upstream primers (ma1F32, ma1F31, and ma1F30) and a single downstream primer (ma1F22) were utilized to synthesize a 1.60Kb 5' fragment that contained a 5' NotI RE site followed by a 5'UTR, BM40 signal sequence, protein C epitope tag, Enterokinase cleavage sequence, the 5' terminal region of mouse $\alpha 1$, and a 3' BstEII RE site. This upstream PCR fragment was then digested with NotI and BstEII. A second PCR utilizing primers ma1F20 and ma1F25 was performed to amplify the C-terminal region of $\alpha 1$ and place two C-terminal STOP signals followed by a NotI RE site downstream of the mouse $\alpha 1$ sequence. This downstream PCR fragment was then digested with BspHI and NotI. The RE digested PCR products and purified gel fragment were then ligated together, processed, and analyzed same as above.

5. $\alpha 1$ WT_{Nv} - The DHpuro vector was digested with NotI and treated with CIP (table 6.5.). $\alpha 1$ -wt_{Nm} was digested with BspHI and BstEII. A 6.88Kb fragment of mouse $\alpha 1$

was gel purified. Three sequential overlapping PCRs utilizing three different overlapping upstream primers (ma1F34, ma1F33, and ma1F30) and a single downstream primer (ma1F22) were utilized to synthesize a 1.60Kb 5' fragment that contained a 5' NotI RE site followed by a 5'UTR, BM40 signal sequence, VSV-G epitope tag, Enterokinase cleavage sequence, the 5' terminal region of mouse $\alpha 1$, and a 3' BstEII RE site. This upstream PCR fragment was then digested with NotI and BstEII. A second PCR utilizing primers ma1F20 and ma1F25 was performed to amplify the C-terminal region of mouse $\alpha 1$ and place two C-terminal STOP signals followed by a NotI RE site downstream of the mouse $\alpha 1$ sequence. This downstream PCR fragment was then digested with BspHI and NotI. The RE digested PCR products and purified gel fragment were then ligated together, processed, and analyzed same as above.

6. $\alpha 1$ WT_{Nh} - The DHpuro vector was digested with NotI and treated with CIP (table 6.6.). $\alpha 1$ -wt_{Nm} was digested with BspHI and BstEII. A 6.88Kb fragment of mouse $\alpha 1$ was gel purified. Three sequential overlapping PCRs utilizing three different overlapping upstream primers (ma1F100, ma1F111, and ma1F30) and a single downstream primer (ma1F22) were utilized to synthesize a 1.60Kb 5' fragment that contained a 5' NotI RE site followed by a 5'UTR, BM40 signal sequence, HA epitope tag, Enterokinase cleavage sequence, the 5' terminal region of mouse $\alpha 1$, and a 3' BstEII RE site. This upstream PCR fragment was then digested with NotI and BstEII. A second PCR utilizing primers ma1F20 and ma1F25 was performed to amplify the C-terminal region of mouse $\alpha 1$ and place two C-terminal STOP signals followed by a NotI RE site downstream of the $\alpha 1$ sequence. This downstream PCR fragment was then digested with BspHI and NotI. The RE digested PCR products and purified gel fragment were then ligated together, processed, and analyzed same as above.

7. $\alpha 1$ WT_{Nm3} - The DHpuro vector was digested with NotI and treated with CIP (table 6.7.). $\alpha 1$ -wt_{Nm} was digested with BspHI and BstEII. A 6.88Kb fragment of mouse $\alpha 1$ was gel purified. Four sequential overlapping PCRs utilizing four different overlapping upstream primers (ma1F36, ma1F38, ma1F37, and ma1F30) and a single downstream primer (ma1F22) were utilized to synthesize a 1.70Kb 5' fragment that contained a 5' NotI RE site followed by a 5'UTR, BM40 signal sequence, three consecutive c-myc epitope tags, Enterokinase cleavage sequence, the 5' terminal region of mouse $\alpha 1$, and a 3' BstEII RE site. This upstream PCR fragment was then digested with NotI and BstEII. A second PCR utilizing primers ma1F20 and ma1F25 was performed to amplify the C-terminal region of $\alpha 1$ and place two C-terminal STOP signals followed by a NotI RE site downstream of the mouse $\alpha 1$ sequence. This downstream PCR fragment was then digested with BspHI and NotI. The RE digested PCR products and purified gel fragment were then ligated together, processed, and analyzed same as above.
8. $\alpha 1\Delta$ LN_{Nm} - The $\alpha 1$ -wt_{Nm} construct was digested with NheI and the 6,881bp fragment containing mostly vector backbone and some C-terminal ma1 was gel purified and CIP treated (table 6.8.). BM40-myc-EK-ma1-puro was also digested with NheI and BstEII and a 3,353bp fragment of mouse $\alpha 1$ was gel purified. As in the construction of BM40-myc-EK-ma1-puro, three sequential overlapping PCRs utilizing different upstream oligonucleotide primers (ma1F90, ma1F35, and 050604-11) and a single downstream primer (050604-13) were utilized to synthesize a 750bp 5' fragment that contained a NheI RE site followed by a 5'UTR, BM40 signal sequence, c-myc epitope tag, Enterokinase cleavage site, and the 5' terminal region of domain V of the mature mouse $\alpha 1$ polypeptide. The PCR product was digested with NheI and BstEII. All three fragments were then ligated and treated as earlier constructs.

9. $\alpha 1 \Delta \text{LN-LEa(A)}_{\text{Nm}}$ - The $\alpha 1\text{-wt}_{\text{Nm}}$ construct was digested with BamHI (NEB) and the 12.598Kb fragment containing the vector backbone and most of the $m\alpha 1$ cDNA, minus the N-terminal section, was gel purified and CIP treated (table 6.9.). As in the construction of $\alpha 1\text{-wt}_{\text{Nm}}$, three sequential PCRs utilizing different upstream oligonucleotide primers and a single downstream primer were utilized to synthesize a 5' fragment that contained a BamHI RE site followed by a 5'UTR, BM40 signal sequence, c-myc epitope tag, Enterokinase cleavage site, and mouse $\alpha 1$ polypeptide. Primers ma1F-duh and 050604-10 were used in a PCR of $m\alpha 1\text{-pCIS}$ to generate a .97Kb fragment. This PCR product was then subsequently amplified with ma1F35 and 050604-10 and then 050604-9 and 050604-10, digested with BamHI, and ligated into the BamHI prepared $\alpha 1\text{-wt}_{\text{Nm}}$.

10. $\alpha 1 \Delta \text{LN-LEa(B)}_{\text{Nm}}$ - The $\alpha 1\text{-wt}_{\text{Nm}}$ construct was digested with BamHI (NEB) and the 12.598Kb fragment containing the vector backbone and most of the $m\alpha 1$ cDNA, minus the N-terminal section, was gel purified and CIP treated (table 6.10.). As in the construction of $\alpha 1\text{-wt}_{\text{Nm}}$, three sequential PCRs utilizing different upstream oligonucleotide primers and a single downstream primer were utilized to synthesize a 5' fragment that contained a BamHI RE site followed by a 5'UTR, BM40 signal sequence, c-myc epitope tag, Enterokinase cleavage site, and mouse $\alpha 1$ polypeptide. Primers ma1F-duh2 and 050604-10 were used in a PCR of $m\alpha 1\text{-pCIS}$ to generate a .61Kb fragment. This PCR product was then subsequently amplified with ma1F35 and 050604-10 and then 050604-9 and 050604-10, digested with BamHI, and ligated into the BamHI prepared $\alpha 1\text{-wt}_{\text{Nm}}$.

11. $\alpha 1 \Delta \text{LN-LEa(C)}_{\text{Nm}}$ - The $\alpha 1\text{-wt}_{\text{Nm}}$ construct was digested with BamHI (NEB) and the 12.598Kb fragment containing the vector backbone and most of the $m\alpha 1$ cDNA, minus the N-terminal section, was gel purified and CIP treated (table 6.11.). Unlike the

construction of $\alpha 1\text{-wt}_{\text{Nm}}$, two separate fragments had to be first generated and then sewn together prior to the series of sequential PCRs utilizing different upstream oligonucleotide primers and a single downstream primer to synthesize a 5' fragment that contained a BamHI RE site followed by a 5'UTR, BM40 signal sequence, c-myc epitope tag, Enterokinase cleavage site, and mouse $\alpha 1$ polypeptide. Primers ma1F-duh and ma1F35 with ma1f-duh3 were used in a PCR of $m\alpha 1\text{-pCIS}$ to generate a .608Kb fragment as well as ma1f-duh4 and 050604-10 to generate a .300Kb fragment which were combined together and amplified with 050604-9 and 050604-10 to create a single .900Kb fragment. All PCR generated fragments were digested with BamHI (NEB) and ligated into the BamHI (NEB) prepared $\alpha 1\text{-wt}_{\text{Nm}}$ and treated as earlier constructs.

12. $\alpha 1\triangle\text{LN-L4b(C)}_{\text{Nm}}$ - The $\alpha 1\text{-wt}_{\text{Nm}}$ construct was digested with AflIII (NEB) and BamHI (NEB). The 5.41 Kb fragment was replaced with an AflIII and BamHI digested PCR synthesized fragment. The 1.2 Kb PCR fragment was synthesized with three sequential PCRs using sense primers ma1f-da2, ma1f35, 050604-9 and antisense primer da2-10. (table 6.12.). Both fragments were ligated together, processed, and analyzed same as above.

13. $\alpha 1\triangle\text{LG1-5(A)}_{\text{Nm}}$ - The $\alpha 1\text{-wt}_{\text{Nm}}$ construct was digested with AflIII (NEB) and AgeI (NEB) to generate a 9.143Kb and 5.059Kb fragment (table 6.13.). The 9.143Kb fragment was treated with CIP and gel purified. The excised 5.059Kb fragment was replaced with a 2.145Kb PCR fragment generated from the PCR sewing of 2 smaller PCR fragments. A 1.046Kb PCR fragment was obtained using primers dg1 and dg2. A second PCR fragment of 1.135Kb was obtained using primers dg3 and dg4. The two fragments, which overlapped, were then sewn together via PCR with dg1 and dg4 to generate a C-terminal 2.145Kb $m\alpha 1$ laminin fragment in which LG1-5 had been

removed, digested with AflIII and AgeI, ligated with the 9.143Kb fragment, processed, and analyzed same as above.

14. $\alpha 1 \Delta LG1-5(B)_{Nm}$ – A second approach to creating a full length mouse $\alpha 1$ laminin chain construct missing its C-terminal LG1-5 domain was also undertaken in which the $\alpha 1$ -wt_{Nm} construct was digested with XhoI (NEB) to generate two RE fragments: a 9.454 Kb fragment, representing the vector backbone and the N-terminal half of m $\alpha 1$, and a 4.748Kb fragment containing the C-terminal fragment of m $\alpha 1$ which was replaced with a 1.866Kb PCR fragment generated using PCR oligos dG5 and dG6 to place a STOP codon immediately following the end of the coiled-coil domain (table 6.14.).

15. $\alpha 1 \Delta LG1-3_{Nm}$ – The $\alpha 1$ -wt_{Nm} expression construct created earlier, was digested with XhoI (NEB) to generate two RE fragments: a 9.454 Kb fragment, representing the vector backbone and the N-terminal half of m $\alpha 1$, and a 4.748Kb fragment containing the C-terminal fragment of m $\alpha 1$ which was replaced with a 3.041 Kb PCR fragment generated from the PCR sewing of two PCR products. The C-terminal fragment was generated by first amplifying two separate PCR products from the $\alpha 1$ -wt_{Nm} construct: a 1.843 Kb PCR using PCR oligos 050604-1 and 050604-4 and a 1.198 Kb PCR using PCR oligos 050604-5 and 050604-6. These two PCR products were then combined and sewn together utilizing PCR with the 050604-1 and 050604-6 PCR primers. This synthesized PCR product was then digested with XhoI and ligated into the 9.454 Kb restriction fragment generated earlier (table 6.15.).

16. $\alpha 1 \Delta LG4-5_{Nm}$ – The $\alpha 1$ -wt_{Nm} construct created earlier, was digested with XhoI (NEB) to generate two RE fragments: a 9.454 Kb fragment, representing the vector backbone and the N-terminal half of m $\alpha 1$, and a 4.748Kb fragment containing the C-terminal fragment of m $\alpha 1$ which was replaced with a 3.6 Kb PCR fragment utilizing PCR primers 050604-1 and 050604-2 (which placed two STOP codons immediately after LG3 and an

XhoI site immediately downstream of the engineered STOP codons). The PCR product was then digested with XhoI and ligated into the 9.454 Kb restriction fragment generated earlier (table 6.16.).

17. $\alpha 1$ /RKR_{2721Nm} – The $\alpha 1$ -wt_{Nm} construct created earlier, was digested with Not I and a 4.930 Kb RE fragment representing most of the vector backbone was purified (RE fragment 1). A second aliquot of the $\alpha 1$ -wt_{Nm} construct, was digested with Not I and Nhe I to generate a 7.258 Kb RE fragment representing the first $\frac{3}{4}$ of the mouse $\alpha 1$ chain (RE fragment 2). A 2.035 Kb PCR fragment digested with NotI and NheI was created by first synthesizing two separate PCR products (1st fragment with primers 051206-1 and XREV; 2nd fragment with primers XFOR and X3) and then using PCR to sew the two pieces together (with primers 051206-1 and X3). The overlapping primers XREV and XFOR were utilized to alter the native DNA sequence and introduce the Alanine substitutions. The two restriction endonuclease purified fragments and the digested sewn PCR product were ligated together (table 6.17.).

18. $\alpha 1$ /KRK_{2793Nm} – The $\alpha 1$ -wt_{Nm} construct created earlier, was digested with Not I and a 4.930 Kb RE fragment representing most of the vector backbone was purified (RE fragment 1). A second aliquot of the $\alpha 1$ -wt_{Nm} construct, was digested with Not I and Nhe I to generate a 7.258 Kb RE fragment representing the first $\frac{3}{4}$ of the mouse $\alpha 1$ chain (RE fragment 2). A 2.035 Kb PCR fragment digested with NotI and NheI was created by first synthesizing two separate PCR products (1st fragment with primers 051206-1 and YREV; 2nd fragment with primers YFOR and X3) and then using PCR to sew the two pieces together (with primers 051206-1 and X3). The overlapping primers YREV and YFOR were utilized to alter the native DNA sequence and introduce the Alanine substitutions. The two restriction endonuclease purified fragments and the digested sewn PCR product were ligated together (table 6.18.).

19. $\alpha 1$ /RAR_{2833Nm} – The $\alpha 1$ -wt_{Nm} construct created earlier, was digested with Not I and a 4.930 Kb RE fragment representing most of the vector backbone was purified (RE fragment 1). A second aliquot of the $\alpha 1$ -wt_{Nm} construct, was digested with Not I and Nhe I to generate a 7.258 Kb RE fragment representing the first $\frac{3}{4}$ of the mouse $\alpha 1$ chain (RE fragment 2). A 2.035 Kb PCR fragment digested with NotI and NheI was created by first synthesizing two separate PCR products (1st fragment with primers 051206-1 and ZREV; 2nd fragment with primers ZFOR and X3) and then using PCR to sew the two pieces together (with primers 051206-1 and X3). The overlapping primers ZREV and ZFOR were utilized to alter the native DNA sequence and introduce the Alanine substitutions. The two restriction endonuclease purified fragments and the digested sewn PCR product were ligated together (table 6.19.).

20. $\alpha 1$ _{Cf} – The DHpuro vector was digested with NotI and treated with CIP (table 6.20.). $\alpha 1$ -wt_{Nm} was digested with BspHI and BstEII. A 6.88Kb fragment of mouse $\alpha 1$ was gel purified. Four sequential overlapping PCRs utilizing four different overlapping upstream primers (ma1p4, halp8, ha1p9, and ha1p6) and a single downstream primer (ma1F21) were utilized to synthesize a 1.60Kb 5' fragment that contained a 5' NotI RE site followed by a 5'UTR, BM40 signal sequence, Enterokinase cleavage sequence, the 5' terminal region of mouse $\alpha 1$, and a 3' BspHI RE site. This upstream PCR fragment was then digested with NotI and BspHI. A second PCR utilizing primers ma1F20 and ma1F25 was performed to amplify the C-terminal region of m $\alpha 1$ and place two C-terminal STOP signals followed by a NotI RE site downstream of the mouse $\alpha 1$ sequence. This downstream PCR fragment was then digested with BspHI and NotI. The RE digested PCR products and purified gel fragment were then ligated together, processed, and analyzed same as above.

21. $\alpha 1 \triangle LG1-5_{Nf}$ – The $m\alpha 1$ -pRCX3 construct [14] was digested with AflII and SacII and the 4.2 Kb fragment, representing all of LG1-5 and $\frac{1}{4}$ of the coiled-coil domain was replaced with a 1.917Kb PCR fragment generated from the same construct but utilizing a PCR primer (da3-10) to introduce a new Sac II site and TWO STOP codons after the end of the coiled-coil (table 6.21.).

22. $\alpha 1 \triangle LG1-5(A)_{Cf}$ – The $\alpha 1$ -wt_{Nm} construct was digested with NotI and BstEII and the N-terminal $m\alpha 1$ fragment replaced with a PCR fragment generated by four sequential overlapping PCRs utilizing four different overlapping upstream primers (ma1p-1, ma1p-2, ma1p-3, and ha1p-6) and a single downstream primer (ma1F22) to synthesize a 1.6 Kb 5' fragment that contained a 5' NotI RE site followed by a 5'UTR, a BM40 signal sequence, the 5' terminal region of $m\alpha 1$, and a 3' BstEII RE site (table 6.22.). This upstream PCR fragment was then digested with NotI and BstEII. Digestion of the $\alpha 1$ -wt_{Nm} construct with AflII and NotI yielded a 4.2 Kb fragment that was replaced with a much shorter PCR fragment generated by using primers da4-1 and da5-11 to amplify a 1.9 Kb PCR fragment and introduce a C-terminal FLAG tag followed by two STOP codons and a Not I RE site immediately proceeding the coiled-coil region of the $m\alpha 1$ sequence. The RE digested PCR products and purified gel fragment were then ligated together, processed, and analyzed same as above.

23. $\alpha 1 \triangle LG1-5(B)_{Cf}$ – The $m\alpha 1$ -pRCX3 construct [14] was digested with AflII and SacII and the 4.2 Kb fragment, representing all of LG1-5 and $\frac{1}{4}$ of the coiled-coil domain was replaced with a 1.9 Kb PCR fragment generated from the same construct but utilizing a PCR primer (da3-11) to introduce a C-terminal FLAG tag followed by two STOP codons and a SacII RE site after the end of the coiled-coil region (table 6.23.). The $m\alpha 1$ -pRCX3 construct was also digested with NotI and BstEII and that N-terminal $m\alpha 1$ fragment replaced with a PCR fragment generated by four sequential overlapping PCRs utilizing

four different overlapping upstream primers (ma1p-1, ma1p-2, ma1p-3, and ha1p-6) and a single downstream primer (ma1F22) to synthesize a 1.6 Kb 5' fragment that contained a 5' NotI RE site followed by a 5'UTR, a BM40 signal sequence, the 5' terminal region of $m\alpha 1$, and a 3' BstEII RE site. This upstream PCR fragment was then digested with NotI and BstEII. The RE digested PCR products and purified gel fragment were then ligated together, processed, and analyzed same as above.

24. $\alpha 1\Delta LN-L4a(A)_{Nm}$ – The $\alpha 1-wt_{Nm}$ construct was digested with BamHI generating three fragments: a 1.1 Kb, 1.5 Kb, and 11.6 Kb RE fragment. The 11.6 Kb fragment was purified and CIP treated, while the remaining 2 fragments were discarded. The $m\alpha 1pCIS$ construct was utilized along with three successive rounds of PCR to synthesize a .4 Kb fragment (sense primers: 050604-40, ma1F35, 050604-9 and antisense primer 050604-10) which was digested with BamHI (table 6.24.). The RE digested PCR product and purified gel fragment were then ligated together, processed, and analyzed same as above.

25. $\alpha 1\Delta LN-L4a(B)_{Nm}$ – The $\alpha 1-wt_{Nm}$ construct was digested with BamHI generating three fragments: a 1.1 Kb, 1.5 Kb, and 11.6 Kb RE fragment. The 11.6 Kb fragment was purified and CIP treated, while the remaining 2 fragments were discarded. The $m\alpha 1pCIS$ construct was utilized along with three successive rounds of PCR to synthesize a .4 Kb fragment (sense primers: 050604-41, ma1F35, 050604-9 and antisense primer 050604-10) which was digested with BamHI (table 6.25.). The RE digested PCR product and purified gel fragment were then ligated together, processed, and analyzed same as above.

26. $\alpha 1\Delta LN-L4a(C)_{Nm}$ – The $\alpha 1-wt_{Nm}$ construct was digested with BamHI generating three fragments: a 1.1 Kb, 1.5 Kb, and 11.6 Kb RE fragment. The 11.6 Kb fragment was purified and CIP treated, while the remaining 2 fragments were discarded. The

m α 1pCIS construct was utilized along with three successive rounds of PCR to synthesize a .4 Kb fragment (sense primers: 050604-42, ma1F35, 050604-9 and antisense primer 050604-10) which was digested with BamHI (table 6.26.). The RE digested PCR product and purified gel fragment were then ligated together, processed, and analyzed same as above.

27. α 1 Δ LN-LEb(A)_{Nm} – The α 1-wt_{Nm} construct was digested with AflII generating two fragments: a 8.8 Kb and 5.4 Kb RE fragment. The 8.8 Kb fragment was purified and CIP treated, while the remaining RE fragment was discarded. The m α 1pCIS construct was utilized along with three successive rounds of PCR to synthesize a 1.9 Kb fragment (sense primers: 050604-43, ma1F35, 050604-60 and antisense primer 050604-50) which was digested with AflII (table 6.27.). The RE digested PCR product and purified gel fragment were then ligated together, processed, and analyzed same as above.

28. α 1 Δ LN-LEb(B)_{Nm} – The α 1-wt_{Nm} construct was digested with AflII generating two fragments: a 8.8 Kb and 5.4 Kb RE fragment. The 8.8 Kb fragment was purified and CIP treated, while the remaining RE fragment was discarded. The m α 1pCIS construct was utilized along with three successive rounds of PCR to synthesize a 1.8 Kb fragment (sense primers: 050604-44, ma1F35, 050604-60 and antisense primer 050604-50) which was digested with AflII (table 6.28.). The RE digested PCR product and purified gel fragment were then ligated together, processed, and analyzed same as above.

29. α 1 Δ LN-LEb(C)_{Nm} – The α 1-wt_{Nm} construct was digested with AflII generating two fragments: a 8.8 Kb and 5.4 Kb RE fragment. The 8.8 Kb fragment was purified and CIP treated, while the remaining RE fragment was discarded. The m α 1pCIS construct was utilized in two separate PCRs which overlapped; the N-terminal fragment with primers 050604-44 and 050604-51 and the C-terminal fragment with primers 050604-48 and 050604-50. PCR with the two distant primers 050604-44 and 050604-50 was then

utilized to “sew” the two fragments together. The “sewn” fragment was then subjected to two more rounds of PCR with sense primers ma1F35 and 050604-60 and antisense primer 050604-50, in order to place a 5’ AflII site, 5’UTR, BM40 signal sequence, myc tag, and EK site onto the 5’ end of the fragment which was digested with AflII (table 6.29.). The RE digested PCR product and purified gel fragment were then ligated together, processed, and analyzed same as above.

30. $\alpha 1 \triangle \text{LN-L4b(A)}_{\text{Nm}}$ – The $\alpha 1\text{-wt}_{\text{Nm}}$ construct was digested with AflII generating two fragments: a 8.8 Kb and 5.4 Kb RE fragment. The 8.8 Kb fragment was purified and CIP treated, while the remaining RE fragment was discarded. The $m\alpha 1\text{pCIS}$ construct was utilized in two separate PCRs which overlapped; the N-terminal fragment with primers 050604-57 and 050604-52 and the C-terminal fragment with primers 050604-49 and 050604-50. PCR with the two distant primers 050604-57 and 050604-50 was then utilized to “sew” the two fragments together. The “sewn” fragment was then subjected to two more rounds of PCR with sense primers ma1F35 and 050604-60 and antisense primer 050604-50, in order to place a 5’ AflII site, 5’UTR, BM40 signal sequence, myc tag, and EK site onto the 5’ end of the fragment which was digested with AflII (table 6.30.). The RE digested PCR product and purified gel fragment were then ligated together, processed, and analyzed same as above.

31. $\alpha 1 \triangle \text{LN-L4b(B)}_{\text{Nm}}$ – The $\alpha 1\text{-wt}_{\text{Nm}}$ construct was digested with AflII generating two fragments: a 8.8 Kb and 5.4 Kb RE fragment. The 8.8 Kb fragment was purified and CIP treated, while the remaining RE fragment was discarded. The $m\alpha 1\text{pCIS}$ construct was utilized in three overlapping PCRs with the sense primers 050604-66, ma1F35, and 050604-60 and the anti-sense primer 050604-50 to generate a 1.2 Kb PCR fragment with a 5’ AflII site, 5’UTR, BM40 signal sequence, myc tag, and EK site on the 5’ end of the PCR fragment which was digested with AflII (table 6.31.). The RE digested PCR

product and purified gel fragment were then ligated together, processed, and analyzed same as above.

32. $\alpha 1(A)_{Nf}$ – Invitrogen's pcDNA3.1/hygro expression vector was digested with NotI and treated with CIP (table 6.32.). The construct $m\alpha 1pCIS$, which contains the mouse $\alpha 1$ laminin cDNA was digested with BspHI and BstEII. The resulting 6.88 Kb RE fragment representing the majority of the mouse $\alpha 1$ cDNA was gel purified. Two sequential overlapping PCRs utilizing two different overlapping upstream primers (ma1F39 and ma1F30) and a single downstream primer (ma1F22) were utilized to synthesize a 1.60Kb 5' fragment that contained a 5' NotI RE site followed by a 5'UTR, BM40 signal sequence, FLAG epitope tag, Enterokinase cleavage sequence, the 5' terminal region of $m\alpha 1$, and a 3' BstEII RE site. This upstream PCR fragment was then digested with NotI and BstEII. A second PCR utilizing primers ma1F20 and ma1F25 was performed to amplify the C-terminal region of mouse $\alpha 1$ and place two C-terminal STOP signals followed by a NotI RE site downstream of the mouse $\alpha 1$ sequence. This downstream PCR fragment was then digested with BspHI and NotI. The RE digested PCR products and purified RE gel fragment were then ligated together, processed, and analyzed same as above.

33. $\alpha 1(B)_{Nf}$ - In order to easily identify and purify both secreted recombinant mouse $\alpha 1$ laminin and trimeric recombinant Lm-111 containing recombinant mouse $\alpha 1$, the cDNA coding for the $\alpha 1$ chain was removed from $m\alpha 1-pCIS$ [27, 133] and placed into a plasmid under a CMV promoter. The endogenous $\alpha 1$ signal sequence was replaced with the BM40 signal sequence followed by an N-terminal FLAG epitope tag. The vector also contains the neomycin selectable marker in order to allow selection of positive stable permanent mouse $\alpha 1$ expressing clones via the use of G418. A 1.5 Kb DNA fragment from the 5' end of the $m\alpha 1$ gene was prepared by PCR with primers ma1F85

and ma1F22 (table 6.33.). The PCR product was digested with NheI and BstEII REs. A 3.7 Kb DNA fragment containing most of the upstream sequence of the $\alpha 1$ cDNA, except for a short region at the 5' end, was isolated by complete digestion of $\alpha 1$ -pCIS with BstEII and AflII. A 4.2 Kb DNA fragment containing most of the downstream sequence of the $\alpha 1$ cDNA was isolated by complete digestion of $\alpha 1$ -pCIS with AflII and SacII. A plasmid derived from pRc/CMV (InVitrogen) containing the BM40 (SPARC) signal peptide and FLAG sequence (generously provided by Dr. Billy Hudson, Vanderbilt University, Nashville, TN) was digested with NheI and SacII REs, treated with CIP, and the 5.6 Kb vector DNA fragment isolated. The 3 fragments (1 generated via PCR and two by RE digestion of $\alpha 1$ -pCIS) were then ligated into the prepared vector and transformed into DH5 α bacteria, processed, and analyzed same as above.

Construction of $\beta 1$ laminin based expression constructs:

A comprehensive list of laminin $\beta 1$ based expression constructs can be found in Table 7. Table 8 provides diagrams of all $\beta 1$ laminin constructs, details of their construction, nucleotide sequences of oligonucleotide primers utilized, and amino acid sequences of interest coded for by said constructs:

1. $\beta 1$ WT - The same general approach used to generate $\alpha 1$ -wt_{Nm} was utilized to construct $\beta 1$ WT (table 8.1.). A short .436Kb N-terminal segment was generated from the construct h $\beta 1$ -pCIS containing the cDNA of human $\beta 1$ using two successive rounds of PCR with two sense oligos (hb1-20 and then hb1-2) and the same anti-sense oligo (hb1-re1) and the final PCR product digested with NheI (NEB) and EcoRI (NEB). A short .469Kb C-terminal segment was also generated via PCR with hb1-re4 and hb1-10 from h $\beta 1$ -pCIS and digested with MluI (NEB) and KpnI (NEB). A large 4.546Kb RE fragment, representing most of the h $\beta 1$ cDNA was gel purified from an EcoRI (NEB) and

MluI (NEB) digestion of h β 1-pCIS. The expression vector pcDNA3.1/zeo+ (Invitrogen) was digested with NheI (NEB) and KpnI (NEB) and treated with CIP (Invitrogen). The 3 fragments and vector were ligated together, processed, and analyzed same as above.

2. β 1WT_{Nh} - The same approach used to generate α 1-wt_{Nm} was utilized to construct β 1WT_{Nh}, except for the substitution of the hemagglutinin epitope tag (HA; Roche) for the myc tag (table 8.2.). A short .436Kb N-terminal segment was generated from the construct h β 1-pCIS containing the cDNA of human β 1 using four successive rounds of PCR with four sense oligos (hb1-1, hb1-2, hb1-3, and hb1-4) and the same anti-sense oligo (hb1-re1) and the final PCR product digested with NheI (NEB) and EcoRI (NEB). A short .469Kb C-terminal segment was also generated via PCR with hb1-re4 and hb1-10 from h β 1-pCIS and digested with MluI (NEB) and KpnI (NEB). A large 4.546Kb RE fragment, representing most of the h β 1 cDNA was gel purified from an EcoRI (NEB) and MluI (NEB) digestion of h β 1-pCIS. The expression vector pcDNA3.1/zeo+ (Invitrogen) was digested with NheI (NEB) and KpnI (NEB) and treated with CIP (Invitrogen). The 3 fragments and vector were ligated together, processed, and analyzed same as above.

3. β 1 Δ LN_{Nh} - The same approach used to generate β 1-wt_{Nh} was employed, except hb1-23, hb1-25, hb1-3, hb1-4, and hb1-re5 were employed to generate the .919Kb N-terminal segment which was digested with NheI (NEB) and AatII (NEB) (table 8.3.). Also, a 3.314Kb RE fragment, representing most of the h β 1 cDNA was gel purified from an AatII (NEB) and MluI (NEB) digestion of h β 1-pCIS.

4. β 1 Δ LN-LEa_{Nh} - The same approach used to generate β 1-wt_{Nh} was employed, except hb1-28, hb1-30, hb1-3, hb1-4, and hb1-re7 were employed to generate the .663Kb N-terminal segment which was digested with NheI (NEB) and BstEII (NEB) (table 8.4.). Also, a 2.753Kb RE fragment, representing most of the h β 1 cDNA was gel purified from a BstEII (NEB) and MluI (NEB) digestion of h β 1-pCIS.

5. β 1WT_{NV} - The same approach used to generate α 1-wt_{Nm} was utilized to construct β 1WT_{Nh}, except for the substitution of the VSV-G epitope tag (Roche) for the myc tag (table 8.5.). A short .44 Kb N-terminal segment was generated from the construct h β 1-pCIS containing the cDNA of human β 1 using four successive rounds of PCR with four sense oligos (hb1-1, hb1-5, hb1-6, and hb1-4) and the same anti-sense oligo (hb1-re1) and the final PCR product digested with NheI (NEB) and EcoRI (NEB). A short .47 Kb C-terminal segment was also generated via PCR with hb1-re4 and hb1-10 from h β 1-pCIS and digested with MluI (NEB) and KpnI (NEB). A large 4.55 Kb RE fragment, representing most of the h β 1 cDNA was gel purified from an EcoRI (NEB) and MluI (NEB) digestion of h β 1-pCIS. The expression vector pcDNA3.1/zeo+ (Invitrogen) was digested with NheI (NEB) and KpnI (NEB) and treated with CIP (Invitrogen). The 3 fragments and vector were ligated together, processed, and analyzed same as above.
6. β 1 Δ LN_{NV} - The same approach used to generate β 1-wt_{Nh} was employed, except hb1-50, hb1-25, hb1-51, hb1-4, and hb1-re5 were employed to generate the .92 Kb N-terminal segment which was digested with NheI (NEB) and AatII (NEB) (table 8.6.). Also, a 3.31 Kb RE fragment, representing most of the h β 1 cDNA was gel purified from an AatII (NEB) and MluI (NEB) digestion of h β 1-pCIS.
7. β 1 Δ LN-LEa_{NV} - The same approach used to generate β 1-wt_{Nh} was employed, except hb1-60, hb1-61, hb1-3, hb1-4, and hb1-re7 were employed to generate the .66 Kb N-terminal segment which was digested with NheI (NEB) and BstEII (NEB) (table 8.7.). Also, a 2.75 Kb RE fragment, representing most of the h β 1 cDNA was gel purified from a BstEII (NEB) and MluI (NEB) digestion of h β 1-pCIS.
8. β 1WT-Ig κ - The same general approach used to generate α 1-wt_{Nm} was utilized to construct β 1WT (table 8.8.) utilizing a Ig κ signal sequence instead of BM40. Successive rounds of PCR with sense primers hb1-12 and hb1-8 were utilized with anti-sense primer

hb1-re1 to generate the .44 Kb N-terminal fragment which was digested with NheI and EcoRI. Primers hb1-re4 and hb1-10 were utilized to amplify a .47 Kb C-terminal fragment which was digested with MluI and KpnI. Both digested PCR fragments were ligated with a 4.55 Kb EcoRI and MluI restriction fragment purified from h β 1-pCIS and expression vector pcDNA3.1/zeo+ (Invitrogen) which had been digested with NheI (NEB) and KpnI (NEB) and treated with CIP (Invitrogen).

9. β 1WT_{Nh}-Ig κ - The same general approach used to generate α 1-wt_{Nm} was utilized to construct β 1WT_{Nh}-Ig κ (table 8.9.) with an N-terminal HA tag utilizing a Ig κ singal sequence instead of BM40. Four consecutive rounds of PCR with sense primers hb1-1, hb1-2, hb1-7, and hb1-8 along with anti-sense primer hb1-re1 were used to generate the .44 Kb N-terminal fragment which was digested with NheI and EcoRI. Primers hb1-re4 and hb1-10 were utilized to amplify a .47 Kb C-terminal fragment which was digested with MluI and KpnI. Both digested PCR fragments were ligated with a 4.55 Kb EcoRI and MluI restriction fragment purified from h β 1-pCIS and expression vector pcDNA3.1/zeo+ (Invitrogen) which had been digested with NheI (NEB) and KpnI (NEB) and treated with CIP (Invitrogen).

10. β 1WT_{Nv}-Ig κ - The same general approach used to generate α 1-wt_{Nm} was utilized to construct β 1WT_{Nh}-Ig κ (table 8.10.) with an N-terminal VSV-G tag utilizing a Ig κ singal sequence instead of BM40. Four consecutive rounds of PCR with sense primers hb1-1, hb1-5, hb1-9, and hb1-8 along with anti-sense primer hb1-re1 were used to generate the .44 Kb N-terminal fragment which was digested with NheI and EcoRI. Primers hb1-re4 and hb1-10 were utilized to amplify a .47 Kb C-terminal fragment which was digested with MluI and KpnI. Both digested PCR fragments were ligated with a 4.55 Kb EcoRI and MluI restriction fragment purified from h β 1-pCIS and expression vector

pcDNA3.1/zeo+ (Invitrogen) which had been digested with NheI (NEB) and KpnI (NEB) and treated with CIP (Invitrogen).

Construction of γ 1 laminin based expression constructs:

A comprehensive list of laminin γ 1 based expression constructs can be found in Table 9. Table 10 provides diagrams of all γ 1 laminin constructs, details of their construction, nucleotide sequences of oligonucleotide primers utilized, and amino acid sequences of interest coded for by said constructs.

1. γ 1WT_{Cf} - The human full length WT γ 1-chain construct with its endogeneous signal sequence and C-terminal FLAG epitope tag under neomycin resistance was constructed as previously described [296] (table 10.1.).
2. γ 1WT - The human full length WT γ 1-chain construct with its endogeneous signal sequence and no epitope tag under neomycin resistance was constructed as previously described [296] (table 10.2.).
3. γ 1 Δ LN_{Cf} - The human full length WT γ 1-chain construct, γ 1WT_{Cf}, was digested with NotI (NEB), generating 3 fragments (table 10.3.). The largest fragment, 6.867Kb, was gel purified and CIPed. γ 1-wt_{Cf} was also digested with ApaLI (NEB) and NotI (NEB) and the 4.817Kb fragment representing the C-terminal half of the human γ 1 chain was gel purified. The N-terminal 1.014Kb fragment was generated by 2 overlapping PCRs with GG1, GG3, and GG6 followed by digestion with NotI (NEB) and ApaLI (NEB). The 2 fragments and vector were ligated together, processed, and analyzed same as above.
4. γ 1 Δ LN-LEa_{Cf} - The human full length WT γ 1-chain construct, γ 1WT_{Cf}, was digested with NotI (NEB), generating 3 fragments (table 10.4.). The largest fragment, 6.867Kb, was gel purified and CIPed. γ 1-wt_{Cf} was also digested with AflIII (NEB) and NotI (NEB) and the 3.131Kb fragment representing the C-terminal half of the human γ 1 chain was gel

purified. The N-terminal 334bp fragment was generated by 2 overlapping PCRs with GG9, GG4, and GG5 followed by digestion with NotI (NEB) and AflII (NEB). The 2 fragments and vector were ligated together, processed, and analyzed same as above.

DHpuro – a vector encoding for puromycin resistance, and the vector backbone in most of the $\alpha 1$ puromycin based constructs, was constructed by replacing the AvrI-PciI 1.730Kb fragment of pcDNA3.1/Hygro (Invitrogen) which contained part of the SV40 promoter and origin, hygromycin resistance, and SV40 polyadenylation signal sequence with a PCR fragment synthesized from the puromycin resistance containing vector pPUR (Clontech), containing the removed SV40 promoter sequence, puromycin resistance gene, a SV40 polyadenylation signal sequence, and a PCR introduced C-terminal PciI site.

Transfection and Establishment of Heterotrimeric Recombinant Lm-111s:

The expression constructs described earlier were linearized by treatment with REs, transfected individually and sequentially into the HEK 293 cell line with Lipofectamine 2000 (Invitrogen), successfully transfected clones selected for using the antibiotic specific for each expression construct, and 12 stable clones from each step isolated and tested for expression of the transfected recombinant proteins. The cells were grown in media containing: 1X DMEM (Invitrogen) + 10% Fetal Bovine Serum (FBS; Atlanta Biologicals) + 1X P/S (1,000 u/ml Penicillin and 1,000ug/ml Streptomycin; Invitrogen) + appropriate antibiotic. The appropriate antibiotic was: 500ug/ml G418 for neomycin (Sigma-Aldrich), 80-100 ug/ml for zeocin (Invitrogen), and 1 ug/ml for puromycin (Sigma-Aldrich). Media from cells were harvested, the cells from the dish isolated, and a portion of the media from each clone, normalized based upon cell number, solubilized in Laemmli sample buffer, reduced with β -mercaptoethanol and boiling, then loaded and

run on a 6-12% gradient SDS-PAGE gels. Proteins were either stained with Coomassie Brilliant Blue R-250 for direct visualization or blotted onto PVDF membranes (BioRad) using a BioRad electroblotter for Western detection. Bound protein was detected with Lm-111 and antibodies specific for the epitope tag present on each of the expressed recombinant proteins. Autoradiographs were scanned and band intensity correlating to expression level of recombinant protein determined by imaging with a BioRad Gel Doc 2000, analyzed, and quantitated with Quantity One software (BioRad). A comprehensive list of the established recombinant heterotrimeric laminin-111s and the individual expression constructs utilized to produce the three chains the recombinant heterotrimeric protein is composed of can be found in Table 11. The designation format of Lm-111"**N**"_{"X"/"Y"/"Z"} is utilized to refer to the heterotrimeric Lm-111s; where "**N**" denotes any alteration to the native sequence of the chain, "X" denotes the α chain tag, "Y" denotes the β chain tag, and "Z" denotes the γ chain tag.

EXPERIMENTAL RESULTS NOTE

One must keep in mind that the generation of expression constructs and production of the expressed recombinant proteins encoded for by the given constructs, was and still is an ongoing effort, therefore, though some experiments would have benefited from the use of certain recombinant proteins that were not tested at the time, those that were most appropriate and available at the time of the experiments were utilized when possible.

Chapter 3. Production and Characterization of recombinant $\alpha 1$ LG4-5s.

Laminin-111 ($\alpha 1\beta 1\gamma 1$; formerly Laminin-1) possesses both architecture-building and cell-interactive activities. Work done by our lab and others, have demonstrated that these activities are required for laminin's proper function in many cell systems examined. We have also demonstrated the ability to inhibit proper laminin function via the use of proteolytic fragments of laminin, therefore, I decided to further map, identify, and characterize the residues that are involved in these activities. Identification of key residues specific to certain binding activities, which I could then mutate in recombinant heterotrimeric Lm-111, in conjunction with null cell lines for these binding partners (i.e. $\gamma 1$ laminin $-/-$, $\beta 1$ integrin $-/-$, and DG $-/-$ cell lines) and cell lines with differential expression of laminin receptors, would enable us to further dissect laminin functions and the role of these laminin binding partners. However, due to technical, temporal, and fiscal realities along with our own data showing the necessity of LG4+5 for laminin's proper function, I first focused on the elastase proteolytic fragment E3 from the 956 residue $\alpha 1$ C-terminal G domain (figure 11). The 372 residue E3 fragment and constructs we created to mimic it, contain a short C-terminal section of LG3 through to the *de novo* termination site at the C-terminus of LG5 (figure 12). Constructs containing these sequences are referred to as $\alpha 1$ LG4-5. In order to understand sequence contributions of LG4 activities, I substituted specific amino acid residues with Alanine. LG4 contains many charged residues which are good candidates for identifying binding interactions; including those previously identified by Andac et al. [162]. I also made use of the coordinates from Tisi et al.'s [305] crystal structure of mouse $\alpha 2$ LG4-5 to homology model mouse $\alpha 1$ LG4-5 and identify potential candidates to mutate. The generated mutants showed wide

differences in their ability to bind heparin, sulfatide, and dystroglycan; as well as their ability to block laminin accumulation and basement membrane formation in Schwann cells, fibroblast, and embryo bodies derived from ES cell lines.

Section I. Recombinant mouse α 1LG4-5s.

An expression system for efficient production of recombinant α 1LG4-5s and larger laminin chains was created by testing a wide assortment of expression factors in order to design an optimum expression construct platform. The recombinant α 1LG4-5 was utilized to test and perfect much of the system employed in generating the larger more complicated and labor intensive laminin chain constructs designed for recombinant heterotrimeric laminin-111 production. Different promoters, 5' UTR sequences, signal sequences, epitope tags, and engineered proteolytic recognition and cleavage sequences were tested, these included: P_{CMV} , P_{RSV} , P_{SV40} , and the mouse β 1 laminin promoter for driving expression of the recombinant proteins and obtaining maximum transcriptional production; several different 5' UTR sequences to increase translational yields; the signal sequences of BM40, IG κ , and the endogeneous mouse α 1 Lm signal sequence for processing and secretion of the expressed recombinant proteins; the epitope tags FLAG, myc, mycX3, HA, VSV-G, protein-C, V5, and inclusion of no tag for purification and identification purposes; engineered proteolytic cleavage sequences for EK and TEV in order to retain the capability to remove the epitope tags from mature recombinant proteins; and development not only of individual selectable markers, but also, combinations of all three for recombinant heterotrimeric laminin production, these included neomycin (neo/G418), zeocin (zeo), hygromycin (hygro), puromycin (puro), and blasticidin (blstd) (figure 13A). These many parts of the expression construct needed to be determined, tested, selected, and optimized since their function/efficiency are affected by the cellular environment, each other, and other elements of the construct.

Section IA. Promoter selection.

Both the viral promoters CMV and RSV, as well as the endogeneous mouse $\beta 1$ laminin promoter were evaluated not only for their ability to drive recombinant mouse $\alpha 1$ LG4-5 expression in the 293 fibroblast cell line but whether other segments of the construct, such as the SV40 promoter, may interfere with expression of the recombinant proteins under a CMV promoter. The m $\alpha 1$ LG4-5/WT-pRCX3_{Nf} expression construct contains a BM40 signal sequence followed by the FLAG epitope tag which is attached to the N-terminus of mouse $\alpha 1$ LG4-5. Two other constructs were derived from this construct in which the CMV promoter was replaced with either the RSV or mouse $\beta 1$ laminin promoter. Quantitation of the recombinant $\alpha 1$ LG4-5 purified from the media of HEK 293 cells stably transfected with these three constructs, revealed that the CMV promoter produced a 3 fold increase in expression over RSV and approximately 50 fold over the $\beta 1$ Lm promoter (figure 13B). Furthermore, the addition of retinoic acid (RA) to the cell lines stably transfect with constructs under the mouse $\beta 1$ Lm promoter, resulted in a four fold increase in expression. Therefore, the CMV promoter was selected to drive recombinant protein expression of later expression constructs.

Section IB. 5' UTR sequence selection.

Nine 5' UTR sequences were tested to see if any would increase expression levels of an N-terminaly FLAG tagged $\alpha 1$ LG4-5 sequence under a CMV promoter (figure 13D). One UTR was that which was already present in the $\alpha 1$ LG4-5/WT-pRCX3_{Nf} construct, two were chosen by generating consensus 5' UTRs from collating the data collected by Kozak [306], and six were the 5' UTR of genes shown to be highly expressed in fibroblast cell lines and found by analyzing NCBI's gene chip array expression profiles database [22]. A single new construct, $\alpha 1$ LG4-5/WT_{Nf}, was constructed in which the

CMV promoter drove the expression of a BM40-FLAG-EK-mouse α 1LG4-5 recombinant protein in a pCDNA/zeo 3.1 + vector backbone utilizing the “consensus-1” 5’ UTR. Further PCR mutagenesis of this new construct was utilized to generate seven other constructs in which the “consensus-1” 5’ UTR was replaced with the other selected 5’ UTRs. Thus the nine 5’ UTRs tested were: “consensus-1” (construct α 1LG4-5/WT_{Nf}) and “consensus-2” (construct α 1LG4-5/WTcon2_{Nf}) derived from Kozak’s data and others [307, 308], the 5’UTR in α 1LG4-5/WT-pRCX3_{Nf}, the 5’ UTRs from human histone H2B (H2B; construct α 1LG4-5/WTh2b_{Nf}) [309, 310], human translocase of outer mitochondrial membrane 7 homolog (TOMM7; construct α 1LG4-5/WTtomm7_{Nf}) [311-313], human isoleucyl-tRNA synthetase (IARS; construct α 1LG4-5/WTiars_{Nf}) [314, 315], human farnesyl-diphosphate farnesyltransferase 1 (FDFT1; construct α 1LG4-5/WTfdft1_{Nf}) [316], human ubiquitin-conjugating enzyme E2S (UBE2S; construct α 1LG4-5/WTube2s_{Nf}) [317, 318], and human eukaryotic translation initiation factor 4A (EIF4A1; construct α 1LG4-5/WTeif4a1_{Nf}) [311-313, 319]. The eight new constructs were transfected into 293 cells, stable clones isolated, media harvested, and recombinant α 1LG4-5/WT expression levels compared (figure 13E). Clones transfected with the construct utilizing the “consensus-1” 5’ UTR (construct α 1LG4-5/WT_{Nf}) consistently demonstrated a 3-4 fold higher expression of the recombinant α 1LG4-5 than any other construct. Therefore, future expression constructs were designed utilizing the “consensus-1” 5’ UTR sequence.

Section IC. Signal sequence selection.

An approach similar to the one utilized to generate the expression constructs for testing in the “promoter selection” section was utilized to replace the existing BM40 signal sequence with either the IG κ signal sequence or the endogenous mouse α 1 laminin

signal sequence. Harvested media from stably transfected clone isolates of the three expression constructs, revealed a 55% increase in expression of $\alpha 1$ LG4-5 recombinant proteins with a BM40 signal sequence over that of those having an IGk signal sequence and 65% over those containing a mouse $\alpha 1$ laminin signal sequence (figure 13C). SDS-PAGE analysis and use of a FLAG epitope tag antibody, FLAG M1, which only recognizes N-terminal FLAG tags demonstrated that all signal sequences were properly cleaved, leaving a free N-terminal FLAG moiety (figure 22D) (data shown only for BM40 signal sequence).

The cleavage of the signal sequence is governed by many factors, one of which is that sequences immediately after the C-terminal c-region of the signal sequence may affect the cleavage site. Neural network software programs ACN, SignalP, Signal-NN, and SignalP-HMM were used on all proposed constructs prior to their construction, in order to make sure that there were no potential alterations in the signal sequence cleavage site which may lead to improper cleavage, improper transport, failure to secrete, loss of N-terminal epitope tag, or proteolysis. Figure 14 shows the representative results from the analysis of an untagged human $\beta 1$ laminin chain with its endogenous signal sequence in place. More than 50 constructs were vetted through this process prior to their construction (data not shown).

Section ID. Epitope tag selection

After an exhaustive search, seven epitope tags for which there was antibody, peptide, and antibody coupled matrix, commercially available, were chosen for further study: FLAG, myc, mycX3, HA, VSV-G, protein-C, and V5 (figure 15A). Since there was no way to predict what effect any tag may have on stability or activity of the $\alpha 1$ LG4-5 (or other potential recombinant protein) and we had no experience with regards to the

behaviour or effectiveness of any of these tags in detection or purification, other than FLAG, expression constructs containing all tags were made, transfected, purified, and simultaneously tested and compared to determine the best epitope tags for $\alpha 1$ LG4-5 production and which tags to test for individual chains in establishment of the recombinant heterotrimeric laminin projects. Individual P_{CMV} driven BM40 signal sequence containing expression constructs were created which contained recombinant $\alpha 1$ LG4-5 with a FLAG (construct $\alpha 1LG4-5/WT_{Nf}$), myc (construct $\alpha 1LG4-5/WT_{Nm}$), mycX3 (construct $\alpha 1LG4-5/WT_{Nm3}$), HA (construct $\alpha 1LG4-5/WT_{Nh}$), VSV-G (construct $\alpha 1LG4-5/WT_{Nv}$), or protein-C (construct $\alpha 1LG4-5/WT_{Np}$) epitope tag on the N-terminus, separated by an EK cleavage sequence from recombinant mouse $\alpha 1LG4-5$. The epitope tags were also tested on the N-terminus of full length mouse $\alpha 1$ laminin and human $\beta 1$ laminin recombinant proteins.

Media was harvested from isolated HEK 293 clones of stably transfected cells producing these various tagged Lm expression constructs. Coomassie blue stained PAGE of the affinity purified recombinant $\alpha 1LG4-5$ s revealed no proteolytic degradation, aberrant migration or apparent size changes (figure 15B). Western analysis revealed detection of all epitope tags, no cross-reactivity issues, nor any proteolytic degradation (figure 15C). The observed immunoreactivity on blots with VSV-G and protein-C was less than the others. Furthermore, treatment with enterokinase was confirmed by SDS-PAGE coomassie blue stained gels and Western analysis, to remove all N-terminal tags with no apparent non-specific proteolysis (figure 15C and 22D).

Section IE. Engineered proteolytic cleavage sequence.

There was a concern that the addition of a non-native signal sequence and an N-terminal epitope tag may result in improper cleavage, instability, or affect binding

activities of the recombinant proteins produced. Many of the amino acid residues which comprise these tags are charged and/or carry bulky side chains. The FLAG epitope tag for instance, is comprised of eight amino acids: N-Asp-Tyr-Lys-Asp-Asp-Asp-Asp-Lys. The charged groups of the epitope tags could potentially affect binding activities such as multimerization or binding to heparin or sulfatide which are thought to bind mainly through a generalized charged interaction. Furthermore, the N-terminal LN globular domains of the individual chains contain the polymerization domains, as well as, heparin and integrin binding sites. Therefore, artificial proteolytic cleavage sites were designed into the expression constructs in order to provide a means of removing any N-terminal sequence upstream of the cleavage recognition site. Both Enterokinase (EK) and tobacco etch virus protease (TEV) were tested in incubations with EHS Lm-111, recombinant Lm-111, and elastase fragment E3 from EHS Lm-111 (data not shown). The EHS Lm-111 showed less degradation than the recombinant Lm-111 and TEV digested samples demonstrated much more proteolysis than those similarly treated with EK. Incubations at RT and at 4°C dramatically reduced proteolysis, however, it then became difficult to completely remove all of the epitope tags from the proteins. The EHS purified elastase proteolytic fragment E3 (α 1LG4-5) did not show any degradation with EK or TEV. Therefore, all N-terminally epitope tagged recombinant proteins were designed with an enterokinase recognition and cleavage sequence placed between the epitope tag and the recombinant laminin protein so that the tag could be removed from the recombinant protein post synthesis and purification. Figure 22D shows the successful removal of the N-terminal FLAG tag from recombinant mouse α 1LG4-5/WT_{NF} after digestion with Enterokinase. Enterokinase removal of N-terminal epitope tags was also demonstrated with recombinant m α 1LG4-5/WT proteins bearing N-terminal epitope tags: myc, mycX3, HA, VSV-G, protein-C, and FLAG (figure 15C).

Section IF. Selection of selectable markers, antibiotics, and expression vectors.

The decision to include a unique antibiotic selection with each transfected recombinant laminin chain in order to increase expression stability required finding three antibiotics which could be used together and the optimal concentrations of each to use when used in combinations with the other antibiotics. Furthermore, the corresponding expression constructs containing the selectable resistance genes had to be amenable to our system and the very large full length laminin chains which were to be manipulated.

Five antibiotics were examined for their suitability as selectable markers in the HEK 293 cell line. "Kill curves" were generated for the five antibiotics and the optimal concentration at which to use each, determined: 500ug/ml G418 for neomycin, 80-100 ug/ml for zeocin, 5 ug/ml for hygromycin, 1 ug/ml for puromycin, and 5ug/ml for blasticidin. Furthermore, all potential combinations of three of the five antibiotics were tested utilizing either 100%, 80%, or 60% of each individual antibiotic's optimum concentration. The combination of either neomycin, zeocin, and puromycin or blasticidin, zeocin, and puromycin were the most effective, followed by neomycin-blasticidin-zeocin and neomycin-blasticidin-puromycin. Combinations involving neomycin and hygromycin were too lethal for the cells.

Despite the determination of puromycin as a desirable selectable marker in the expression system being constructed, there was no commercially available expression construct with puromycin resistance which was suitable for our purposes. Therefore, a puromycin based expression vector, DHPuro, was created (figure 16). The constructed expression vector provides for CMV promoter driven expression of recombinant genes placed in a unique MCS which is followed by the bovine growth hormone polyadenylation sequence (BGH pA) for high efficiency expression and polyadenylation of recombinant mRNA. The construct also contains the *Streptomyces alboniger* puromycin-N-acetyl-transferase (pac, puromycin, PuroR) gene under the control of the

SV40 early promoter and followed by the SV40 poly adenylation sequence, allowing for simultaneous puromycin resistance selection. There is also a pBR322 origin of replication and ampicillin resistance gene for propagation and selection in *E. coli*. The majority of the mouse $\alpha 1$ chain constructs for recombinant heterotrimeric Lm-111 production were expressed from this expression vector. Figure 16B depicts the insertion of full length mouse $\alpha 1$ laminin chain into the DHpuro expression vector.

Section IG. Creation of a three dimensional model for $\alpha 1$ LG4-5 and selection of amino acid residues to examine.

Since there exists a high degree of sequence conservation between mouse $\alpha 1$ and $\alpha 2$ LG4-5, 41.4% identity and 56.8% homology (figure 17A and B respectively), the two sequences were analyzed using 12 different secondary structure prediction programs, the results compiled and compared (figure 18). The NPS@ analysis suite hosted by the IBCP (Institut de Biologie et Chimie des Proteines) in Lyon, France as part of their contribution to the PBIL (Pole BioInformatique Lyonnais) was utilized for this analysis. The NPS@ server performed the following secondary structure prediction programs: DPM, DSC, GOR IV, HNN, PHD, PREDATOR, SIMPA96, SOPM, SOPMA, MLRC, GOR I, and GOR III. Once the results from these analyses were compiled and compared among themselves and between $\alpha 1$ and $\alpha 2$, it became apparent that a high degree of similarity in the predicted secondary structure between the two alpha chains existed and that the predicted $\alpha 2$ secondary structure correlated well with what was observed in the generated $\alpha 2$ LG4-5 crystal structure and with the crystal structure for $\alpha 1$ LG4-5 which we elucidated later. The tabulated data was then enhanced further with inclusion of the characteristics of the individual amino acids and other data as it became available (figure 18).

The crystal structure of the homologous mouse $\alpha 2$ LG4-5 was elucidated by Tisi et al., in 2000 [305]. Therefore, the data generated by the secondary structure prediction programs, as well as other amino acid characteristics, were utilized along with the laminin mouse $\alpha 2$ crystal structure coordinates [305] to homology model mouse $\alpha 1$ LG4-5 using both Swiss-Model in conjunction with Swiss-Pdb Viewer/DeepView on the ExPASy (Expert Protein Analysis System; <http://www.expasy.org>) proteomics server of the Swiss Institute of Bioinformatics (SIB) [320] and MODELLER provided by the lab of Andrej Sali at Rockefeller Institute (now at UCSF, USA). Further refinement of the proposed structure was accomplished by utilization of energy minimization [321, 322] programs CHARMM, AMBER, GROMOS96, ENCAD, and the secondary structure program MEAD, as well as the other data already tabulated (figure 18). WHAT IF and WHAT_CHECK at EMBL [323] were also utilized to check both for minor alterations to the three dimensional structure when resolving conflicts and suggesting potential consequences of Ala substitutions of key residues we wished to mutate. This homology model, along with tabulated data and afore mentioned programs were used not only to generate the final homology model of $\alpha 1$ LG4-5 (figure 19), but also, identify likely amino acid residue candidates for mutational analysis and the potential consequences of the proposed substitutions on the overall structure of $\alpha 1$ LG4-5.

Two of the known anchors for Lm-111 involve the negatively charged sulfate moieties found in heparin and sulfatide, therefore, it was decided to first focus and mutate residues most likely to affect these binding sites by mutating positively charged amino acid residues. Despite the high degree of primary and predicted secondary structure homology and the fact that both heparin and sulfatide were known to bind the LG4-5 of both $\alpha 1$ and $\alpha 2$, when the positively charge amino acid residues, Arg, Lys, and

His, were mapped onto the two structures, their locations only occasionally coincided in the primary, secondary, or tertiary structures of the two homologs (figure 20).

The homology modeled $\alpha 1$ LG4-5 (residues Ser₂₆₆₅ - Pro₃₀₆₀; comprising the C-terminal residues from LG3, the LG3-LG4 linker, and LG4 through to the C-terminus of LG5) revealed 61 potentially solvent exposed Arg, Lys, and His residues (figures 19-20). However, earlier work [162, 324] suggested that the heparin and sulfatide binding sites of $\alpha 1$ laminin resided in LG4 of mouse $\alpha 1$ laminin and not LG5; which could potentially involve any of the 28 Arg, Lys, or His residues which compose LG4. This was still an overwhelming number of potential candidates to mutate, therefore, a decision was made not to mutate any of the His residues due to their restricted torsional constraints and proclivity for being involved in demarcation of secondary structure. This still left a total of 20 Arg and Lys residues in LG4 to examine via Ala substitution. This number was further reduced by grouping charged residues together which were in close proximity to one another and making constructs which contained multiply mutated residues. Mutation of 1-3 residues per construct, however, still left 34 potential combinations. Eventually, after consulting the homology model, the previously referenced computer analysis programs, tabulated data represented in Figure 18, and earlier results; eight mutational combinations were chosen for recombinant protein production and inclusion in the initial screen: $\alpha 1$ LG4-5/**RKR**₂₇₂₁ (formerly rE3-A), $\alpha 1$ LG4-5/**RKR**₂₇₂₁ (formerly rE3-A2), $\alpha 1$ LG4-5/**KGR****TK**₂₇₇₀ (formerly rE3-D), $\alpha 1$ LG4-5/**KRK**₂₇₉₃ (formerly rE3-G), $\alpha 1$ LG4-5/**RK**₂₈₂₀ (formerly rE3-H), $\alpha 1$ LG4-5/**RAR**₂₈₃₃ (formerly rE3-I), $\alpha 1$ LG4-5/**KDR**₂₈₆₀ (formerly rE3-J), and mutant $\alpha 1$ LG4-5/**RKR**₂₇₂₁+**KRK**₂₇₉₃ a “double mutant” which was comprised of two separate stretches of Ala substituted residues (figure 21). The bolded and underlined characters represent the single letter amino acid code of an amino acid substituted with an Ala residue. None of the proposed Ala substitutions were predicted

via the utilized modeling programs to cause folding changes or major structural changes such as alterations in β -sheets.

Section IH. Generation and expression of recombinant mouse α 1LG4-5s.

Expression constructs of the α 1 laminin LG4-5s described earlier, were transfected into HEK 293 cells and permanent stable lines established under zeocin selection. Media harvested from recombinant α 1LG4-5/WT_{Nf} producing 293 cells was crudely purified through a gravity heparin column and then the entire heparin bound material was passed through a heparin-5PW column and eluted with a 0-1M NaCl gradient on an AKTA FPLC system (figure 22A). The Coomassie blue stained SDS-PAGE gel (figure 22B), and subsequent Westerns, of the material revealed several proteins that eluted with the recombinant α 1LG4-5/WT_{Nf}. Unfortunately, all attempts to obtain significant amounts of purified α 1LG4-5 free of all other contaminating proteins via further charge, hydrophobicity, and sizing chromatography failed (data not shown). Furthermore, since the subsequent recombinant mutant α 1LG4-5 proteins would potentially demonstrate differences in heparin, charge, and hydrophobicity, any attempts to perfect an untagged purely chromatographic means for purification of the recombinant proteins would likely be futile as a general method. Instead the recombinant α 1LG4-5s were constructed with an N-terminal Enterokinase cleavable epitope tag. The epitope tag enabled the recombinant protein to be purified in a single day from harvested media and the tag could be easily and efficiently removed with Enterokinase treatment. Collected media was concentrated by centrifugal filtration (Amicon spin filters), passed through a FLAG M2 mAb matrix packed gravity column, the recombinant protein eluted with FLAG peptide and the elute was then passed through a heparin-5PW column on an AKTA FPLC system. Thus, the FLAG peptide was recovered for re-use and the recombinant

α 1LG4-5 obtained in the NaCl elute (further concentrating the recombinant protein), was exchanged into the buffer of choice through centrifugal filtration (still further concentrating the recombinant protein). The purified recombinant protein obtained was completely pure, intact, and demonstrated binding activities similar to the analogous EHS purified E3 (figure 22C). Furthermore, the FLAG epitope tag could be quickly and completely removed with Enterokinase treatment (figure 22D).

A system of overlapping PCRs, with the internal overlapping oligonucleotide primers encoding for the Ala substitution of targeted residues, followed by subsequent PCRs with oligonucleotide primers designed to synthesize the 5'/upstream restriction site, 5' UTR, BM40 signal sequence, FLAG epitope tag, and EK cleavage site was utilized (figure 22E) to generate the subsequent recombinant mutant α 1LG4-5 proteins which were purified to homogeneity as previously described (figure 22F). Recombinant α 1LG4-5/KDR₂₈₆₀ demonstrated a slightly slower migration on SDS-PAGE analysis than the other recombinant α 1LG4-5s, however, when the recombinant protein was harvested from 293 cells grown in the presence of tunicamycin, the recombinant protein was observed to migrate at the same position/size as the other recombinant α 1LG4-5s (data not shown); implying it contained a post-translational glycosylation difference when compared to the other recombinant α 1LG4-5 and that it was this difference which was responsible for the observed difference in size compared to the other α 1LG4-5s.

The different recombinant α 1LG4-5s demonstrated no differences in stability, proteolytic sensitivity, or multimeric state when examined over time post purification as judged by their behaviour when examined by SDS-PAGE, heparin affinity, sulfatide ELISA, and sizing columns (data not shown). Rotary shadow electron microscopy, performed by Dr. Peter Yurchenco, of elastase digest fragment E3, recombinant α 1LG4-5/WT, mutant α 1LG4-5/KRK₂₇₉₃, and mutant α 1LG4-5/RKR₂₇₂₁ revealed α 1LG4-5s

which all appeared to be morphologically identical: monomeric proteins with two bifurcated domains separated by a short linker (figure 22G).

Section II. Characterization of recombinant α 1LG4-5s.

Stable cell lines were kept under zeocin selection and recombinant α 1LG4-5 proteins purified from collected media by FLAG chromatography, followed by heparin FPLC, to very high homogeneity (figure 22F). The typical yield of recombinant α 1LG4-5s was greater than 6.0 μ g/ml of harvested culture media from a 3 day incubation once the recombinant protein producing cells had reached 80% confluency. There was no observable degradation or contaminating proteins and the FLAG tag was completely cleavable by Enterokinase treatment, with no observable adverse affect to the recombinant α 1LG4-5s (figure 22D). All recombinant α 1LG4-5s were observed to migrate at their expected MW, except for α 1LG4-5/KDR₂₈₆₀, which ran slightly larger than the other recombinant α 1LG4-5s (figure 22F). However, when both α 1LG4-5/KDR₂₈₆₀ and α 1LG4-5/WT_{Nf} were harvested from cells under tunnicamycin treatment they migrated at the same MW, suggesting that the increase in apparent size of α 1LG4-5/KDR₂₈₆₀ is due to a difference in post translational glycosylation of α 1LG4-5/KDR₂₈₆₀ as compared to the other α 1LG4-5s. The tunnicamycin derived α 1LG4-5 also demonstrated that recombinant α 1LG4-5 possess N-linked glycosylation. Rotary shadow electron microscopy of elastase fragment E3 (LG4-5) derived from EHS Lm-111, recombinant α 1LG4-5/WT_{Nf}, α 1LG4-5/RKR₂₇₂₁, and α 1LG4-5/KRK₂₇₉₃ all showed a similar monomeric appearance with two bifurcated globular domains linked together by a small linker region (figure 22G). Gel filtration of these recombinant proteins on a Superose 6 column demonstrated a single peak co-eluting with EHS E3 (data not shown). Both acetylation and non-reducing gel studies of the α 1LG4-5/WT_{Nf} and mutant α 1LG4-5s showed no differences when compared to E3, the analogous α 1LG4-5 proteolytically prepared from Lm-111 isolated from EHS tumor (EHS E3; data not shown).

Section IIA. Heparin binding affinity of recombinant α 1LG4-5s.

Because heparin affinity of a protein can be directly correlated with the salt concentration necessary to elute it from a heparin column or off a heparin coated microtiter plate well, the NaCl elution behavior of the different recombinant α 1LG4-5 proteins was evaluated to determine their relative binding affinities for heparin and thereby the implied relative heparin affinity of the amino acid residues mutated in the recombinant proteins. Elastase derived EHS fragment E3 (LG4-5), recombinant α 1LG4-5/WT_{Nf}, enterokinase treated α 1LG4-5/WT_{Nf}, and PNGaseF treated α 1LG4-5/WT_{Nf} all eluted at 0.252 M NaCl (figure 23A). All mutant α 1LG4-5s eluted at salt concentrations lower than WT, with the following order of elution from highest to lowest: α 1LG4-5/WT_{Nf} > α 1LG4-5/KDR₂₈₆₀ > α 1LG4-5/RAR₂₈₃₃ > α 1LG4-5/KGRTK₂₇₇₀ > α 1LG4-5/RKR₂₇₂₁ \cong α 1LG4-5/KRK₂₇₉₃ > α 1LG4-5/RKR₂₇₂₁ > α 1LG4-5/RKR₂₇₂₁+KRK₂₇₉₃. The actual salt molarities required for elution can be found in the binding data summation table 12. The location of these residues on the surface of α 1 LG4 are shown in figure 23B. The spatial location on the surface of α 1LG4-5 and relative degree of contribution to heparin binding of individual amino acid residues based upon affinities derived from the salt elution behaviours of the various recombinant α 1LG4-5s are represented in figure 23B as well as a plot (figure 23C) of the change in charge of the recombinant mutants in relation to their salt elution showing a direct correlation between reduction in charge represented in the mutant α 1LG4-5s and observed decrease in heparin binding.

Section IIB. α -dystroglycan binding affinity of recombinant α 1LG4-5s.

The affinity of the recombinant α 1LG4-5 proteins for α DG was evaluated by both a gel overlay assay (figure 24A and B) and a solid phase ELISA assay (figure 24C and D) in which the recombinant α 1LG4-5 proteins were incubated and tested for their ability to

bind α DG present either transferred onto nitrocellulose filters (gel assay) or immobilized in a microtiter plate well (ELISA), respectively. The recombinant α 1LG4-5 proteins were provided to Dr. James Ervasti (University of Minnesota) and the α DG binding assays performed by Ariana Combs, a technician in his laboratory. The observed binding affinities and relationships between the recombinant α 1LG4-5s were consistent between the two assays employed. All mutant recombinant α 1LG4-5s showed a decrease in α DG binding, with mutant α 1LG4-5/RKR₂₇₂₁, α 1LG4-5/KDR₂₈₆₀, and α 1LG4-5/RAR₂₈₃₃ demonstrating particularly low α DG binding affinity. The order of binding activity was α 1LG4-5/WT_{Nf} > α 1LG4-5/RKR₂₇₂₁ + KRK₂₇₉₃ > α 1LG4-5/KRK₂₇₉₃ \cong α 1LG4-5/RKR₂₇₂₁ > α 1LG4-5/KGRTK₂₇₇₀ > α 1LG4-5/RAR₂₈₃₃ > α 1LG4-5/KDR₂₈₆₀ \cong α 1LG4-5/RKR₂₇₂₁. Two surprises were the finding that α 1LG4-5/RKR₂₇₂₁ bound α DG with higher affinity than α 1LG4-5/RKR₂₇₂₁ and that the recombinant double mutant α 1LG4-5/RKR₂₇₂₁+KRK₂₇₉₃, bound α DG nearly as well as WT and much better than either of the binding activities observed for the individual mutants which were combined in this recombinant protein. Both recombinant α 1LG4-5/WT_{Nf} and EHS purified E3 were shown in a gel overlay experiment to bind α DG with equal affinity (data not shown). Also, α 1LG4-5/WT_{Nf} which had been enzymatically deglycosylated with PNGaseF demonstrated little if any binding to α DG (figure 24D). The generated binding data for the recombinant α 1LG4-5s were fitted to a single-site binding curve and apparent dissociation constants calculated. The values obtained for the recombinant α 1LG4-5s can be found in the binding data summation table 12. The spatial location on the surface of α 1LG4-5 and relative degree of contribution to α DG binding of individual amino acid residues based upon affinities derived from the two assays of the various recombinant α 1LG4-5s, are represented in figure 24E.

Section IIC. Sulfatide binding affinity of recombinant α 1LG4-5s.

Binding of α 1LG4-5 proteins to immobilized galactosyl sulfatide was also examined. The interaction appeared to be specific for lipids bearing a sulfated carbohydrate moiety, since no binding was detected with: the non-sulfated galactosyl-ceramide, ceramide, a lipid bearing a sulfated charge in the absence of a carbohydrate moiety (sulfated cholesterol), lipids bearing phosphate (e.g. phosphatidyl serine, phosphatidyl choline, phosphatidyl ethanolamine, phosphatidyl inositol, phosphatidyl glycerol, phosphatidic acid), or sialic acid (GM1 ganglioside) (figure 25A and B).

Binding of recombinant α 1LG4-5/WT_{Nf} was blocked by heparin (figure 25B), partially blocked by EDTA (figure 23C), and not affected by 1-2% Triton. However, the treatment of α 1LG4-5/WT_{Nf} or the EHS derived E3 (α 1 LG4-5) with AEBSF did result in a complete abolishment of their ability to bind sulfatide (figure 25C). This was an unexpected finding since we previously believed that AEBSF treatment only inactivated laminin's polymerization activity. Holly Colognato, from our lab, had previously demonstrated, through reaction of Lm with labeled AEBSF, elastase digestion, and fragment purifications, that the vast majority of the AEBSF bound the N-terminal domains of the individual laminin chains, however, there was some AEBSF which appeared to bind E3. Apparently, this low level of reactivity was sufficient to inhibit the sulfatide binding activity of laminin. The N-terminal FLAG tag was removed from recombinant α 1LG4-5/WT_{Nf} and the "FLAGless" recombinant α 1LG4-5/WT compared against recombinant α 1LG4-5/WT which retained its FLAG tag, and proteolytically derived EHS E3. Detection performed both with a Lm-111 polyclonal antibody and the α 1 LG1-5 domain specific polyclonal antibody rG50 (at low concentration), revealed similar binding affinities for all three proteins (data not shown). The monoclonal HRP-linked antibody M2 (SIGMA) derived against the N-terminal FLAG tag common to all recombinant α 1LG4-5s and utilized for

detection in these assays was compared against the popular rG50 polyclonal Ab directed against the $\alpha 1$ LG1-5 domains, and other laminin specific antibodies (data not shown). The polyclonal rG50 antibody appeared to be an effective inhibitor of recombinant $\alpha 1$ LG4-5 binding to sulfatide.

The $\alpha 1$ LG4-5 recombinant proteins bound to immobilized sulfatide with different half-maximal binding values, reflecting differences in affinities (figure 26A). The demonstrated affinities were $\alpha 1$ LG4-5/RKR₂₇₂₁ \cong $\alpha 1$ LG4-5/RKR₂₇₂₁+KRK₂₇₉₃ \cong $\alpha 1$ LG4-5/WT_{Nf} > $\alpha 1$ LG4-5/KRK₂₇₉₃ \cong $\alpha 1$ LG4-5/KDR₂₈₆₀ \cong $\alpha 1$ LG4-5/RKR₂₇₂₁ > $\alpha 1$ LG4-5/KGRTK₂₇₇₀ > $\alpha 1$ LG4-5/RAR₂₈₃₃. Recombinant mutant $\alpha 1$ LG4-5/RAR₂₈₃₃ interaction with sulfatide was greatly reduced. The generated binding data for the recombinant $\alpha 1$ LG4-5s were fitted to a single-site binding curve and apparent dissociation constants calculated. The values obtained for the recombinant $\alpha 1$ LG4-5s can be found in the binding data summation table 12. The spatial location on the surface of $\alpha 1$ LG4-5 and relative degree of contribution to sulfatide binding of individual amino acid residues based upon affinities derived from the solid phase binding assay of the various recombinant $\alpha 1$ LG4-5s, are represented in figure 26B.

When the recombinant $\alpha 1$ LG4-5s were incubated with MEFs which had been loaded with BODIPY-sulfatide, extracted, and the $\alpha 1$ LG4-5 immunoprecipitated via the N-terminal FLAG tag, sulfatide bound to the recombinant $\alpha 1$ LG4-5s could be measured and compared. The results compared favorably with those obtained in the solid phase binding experiments in which the sulfatide had been immobilized on the surface of microtiter plate wells. Recombinant $\alpha 1$ LG4-5/RKR₂₇₂₁, $\alpha 1$ LG4-5/RKR₂₇₂₁+KRK₂₇₉₃, and $\alpha 1$ LG4-5/WT_{Nf} each bound approximately 2 (2.2 +/- .4) moles of sulfatide per mole of recombinant $\alpha 1$ LG4-5. Recombinant $\alpha 1$ LG4-5/KRK₂₇₉₃, $\alpha 1$ LG4-5/KDR₂₈₆₀, and $\alpha 1$ LG4-5/RKR₂₇₂₁ each bound less than 2 moles of sulfatide, while $\alpha 1$ LG4-5/KGRTK₂₇₇₀ bound

approximately 1 mole and α 1LG4-5/RAR₂₈₃₃ almost no sulfatide (figure 26C). The values obtained for the recombinant α 1LG4-5s can be found in the binding data summation table 12.

Section IID. Ability of recombinant α 1LG4-5s to inhibit binding of Lm-111 to sulfatide.

The recombinant α 1LG4-5 proteins demonstrated different abilities to inhibit binding of Lm-111 to sulfatide coated microtiter plate wells. The total amount of α 1LG4-5 necessary to effect an efficient inhibition was higher than expected, however, inhibition was achieved in the following order, from highest to lowest: α 1LG4-5/WT > α 1LG4-5/KDR₂₈₆₀ > α 1LG4-5/RKR₂₇₂₁ > α 1LG4-5/KRK₂₇₉₃ >> α 1LG4-5/RAR₂₈₃₃. The analysis was complicated by the observation that at very low molar concentrations, all of the recombinant α 1LG4-5s actually increased the observed binding of Lm-111 prior to exerting inhibition at higher concentrations. This could be explained by the hypothesis that there is also a weak association between recombinant α 1LG4-5 and the rest of laminin, creating a ternary complex. There was effectively no inhibition of Lm-111 binding observed by the simultaneous addition of recombinant α 1LG4-5/RAR₂₈₃₃ (figure 26D), implying that this mutant had lost all ability to bind sulfatide and thereby the ability to block Lm-111 binding to the sulfatide coated microtiter plate wells. Therefore, the RAR₂₈₃₃ sequence of α 1 LG4 must be required for sulfatide binding.

Section IIE. Crystalization and structure determination of mouse laminin α 1 LG4-5.

A collaborative effort was undertaken with Dr. Erhard Hohenester (Imperial College London, UK) in order to crystalize and determine the three dimensional structure of

mouse $\alpha 1$ LG4-5. I provided assorted laminin expression constructs and over 80 mg of various purified recombinant proteins to the Hohenester laboratory. Eventually, after many attempts, Erhard Hohenester and Sadaf-Ahmahni Hussain were able to crystallize and generate the structure of mouse $\alpha 1$ LG4-5, however, only after altering the expressed recombinant protein to contain a quadruple mutation, N₂₇₁₄Q / N₂₈₁₁K / N₂₉₀₀Q / C₃₀₁₄S, in which the unpaired Cys₃₀₁₄ and all three N-linked carbohydrate sites were removed.

Unlike the other alpha laminin chains, the C-terminal LG4-5 domain pair of the laminin $\alpha 1$ chain ($\alpha 1$ LG4-5) contains an unpaired cysteine, Cys₃₀₁₄ (figure 27A, C, and E). Homology modeling and comparison with the crystal structure of the $\alpha 2$ chain homolog, lead us to predict that Cys₂₆₈₆ of the linker arm preceding LG4 would bind to Cys₂₉₅₈ of LG5, Cys₂₈₄₅ of LG4 would bind to Cys₂₈₇₀ in the linker arm between LG4-5, Cys₃₀₂₄ of LG5 would bind to Cys₃₀₅₅, analogous to the arrangement in LG4 and in LG4 and LG5 of the $\alpha 2$ chain, and the third Cysteine in LG5, Cys₃₀₁₄, not found in LG4 or the other α chains (figure 27B, D, and F), would remain unpaired and be buried within the LG5 globular domain rather than be solvent/surface accessible for potential disulfide bridge formation. Later, solution of the crystal structure of $\alpha 1$ LG4-5 would prove us correct in our predictions [297]. However, since we found that wild-type $\alpha 1$ LG4-5 preparations always contained a small fraction of disulfide-linked dimers (data not shown) and in higher salt often formed a dimer or higher order multimers, we mutated Cys₃₀₁₄ to Ser. Unfortunately, a recombinant $\alpha 1$ LG4-5/C₃₀₁₄S_{Nhis} construct, replacing Cys₃₀₁₄ with Ser and containing an N-terminal His-tag failed to crystallize, even when the His tag was removed. Furthermore, recombinant $\alpha 1$ LG4-5/WT with or without an N-terminal FLAG tag also failed to crystallize (data not shown).

Since $\alpha 1$ LG4-5 contains three predicted potential N-linked glycosylation sites (Asn₂₇₁₄, Asn₂₈₁₁, and Asn₂₉₀₀), both PNGaseF and tunicamycin treatments of $\alpha 1$ LG4-5/WT had demonstrated heteroglycosylation of $\alpha 1$ LG4-5, and glycosylation can cause failure of crystal formation, several combinations of mutants were constructed which removed the potential N-linked glycosylation Asn. However, all recombinant proteins from these mutant constructs still failed to result in a recombinant $\alpha 1$ LG4-5 which would crystallize until a construct was generated which removed the N-terminal His tag and consisted of a quadruple mutation, N₂₇₁₄Q / N₂₈₁₁K / N₂₉₀₀Q / C₃₀₁₄S (construct $\alpha 1$ LG4-5/N₂₇₁₄Q+N₂₈₁₁K+N₂₉₀₀Q+C₃₀₁₄S, devoid of any N-linked carbohydrate or unpaired Cys. The crystal structure of this mutant, was refined at 1.9 Å resolution to $R_{\text{free}} = 0.261$. The crystallographic statistics associated with the determination of this structure can be found in Appendix Table 1.

The obtained crystals contained two crystallographically independent $\alpha 1$ LG4-5 molecules, termed A and B. Clear electron density were observed for both molecules, with the exception of residues 2987-2990, 3032-3034 and 3060 of molecule A, and residues 2682-2684 and 3060 of molecule B. Molecules A and B are very similar in their LG4 and LG5 domain structures (r.m.s. deviation 0.36 Å and 0.58 Å, respectively, for all C α atoms), but differ substantially in their respective domain arrangements. When the molecules are superimposed on their LG4 domains, a rotation by 14.5° is required to bring their LG5 domains into superposition. The pivot point of this rotation is in the linker separating LG4 and LG5 from each other, near Tyr₂₈₇₁ ("Y₂₈₇₁") (figure 28A).

Since there is more complete structure data for molecule B, the following detailed structure description shall focus on molecule B and data generated from it (figure 28B and 28C). The $\alpha 1$ LG4-5 structure consists of two globular LG domains, LG4 and LG5, connected by a short linker and interacting through a small interface near the domain

termini (figures 27 and 28). Each LG domain folds into a curved β -sandwich built from two antiparallel sheets and contains a single disulfide bond near the C-terminus (figures 27 and 28). A third disulfide bond tethers the segment preceding LG4 to an α -helical turn in LG5. The interface between LG4 and LG5 is water-filled and predominantly polar, and the different conformations of molecules A and B are likely to be due to the paucity of specific interactions in the LG4-LG5 interface. Each of the domains contain one bound metal ion, located on the rim of the β -sandwich opposite the interdomain linker. These ions have been modelled as magnesium, given their coordination geometry and the high magnesium concentration in the crystals, however, *in vivo* these ions are most likely calcium. Magnesium ion 1, located in LG4, is coordinated octahedrally by the side chains of both Asp₂₇₄₇ and Asp₂₈₁₆, the main chain carbonyl oxygens of residues Leu₂₇₆₄ and Thr₂₈₁₄, and two water molecules; the average metal-ligand distance is 2.17 Å. Magnesium ion 2, located in LG5, is coordinated octahedrally by the side chains of both Asp₂₉₂₃ and Asp₂₉₉₆, the main chain carbonyl oxygens of residues Asn₂₉₄₀ and Ser₂₉₉₄, and two water molecules; the average metal-ligand distance is 2.15 Å. The unpaired cysteine of α 1LG5, Cys₃₀₁₄, is located in the convoluted loop that occupies most of the concave face of LG5. Two predicted N-linked glycosylation sites are located in LG4, Asn₂₇₁₄ and Asn₂₈₁₁, and one in LG5, Asn₂₉₀₀. Asn₂₈₁₁ in LG4 is close to the metal ion binding site and putative receptor/anchorage molecules whose binding affinities are affected in the mutated recombinant mouse α 1LG4-5s.

Section IIF. Structural comparison of α 1LG4-5 and α 2LG4-5, as well as, identification of the similarities and differences between the two proteins in the spatial location of key amino acid residues.

Mouse laminin $\alpha 1$ LG4-5 exhibits 41% sequence identity and 57% homology when compared to the corresponding homologous region of the mouse $\alpha 2$ chain (figure 17A and B respectively), whereas, the sequence identity to the $\alpha 3$ - $\alpha 5$ chains is substantially lower (less than 30%). Despite the significant differences in primary sequence, both $\alpha 1$ and $\alpha 2$ LG4-5 show a high degree of similarity when it comes to secondary structure, according to their determined crystal structures (figure 29A and B). A structural comparison of $\alpha 1$ LG4-5 and $\alpha 2$ LG4-5 [305] reveals only a few notable differences at the secondary, tertiary, and quaternary level. LG4 of laminin $\alpha 1$ and $\alpha 2$ can be superimposed with an r.m.s. deviation of 0.91 Å for 148 C α atoms (figure 29C). The major differences between $\alpha 1$ and $\alpha 2$ LG4 are concentrated in the spatially adjacent B-C and L-M loops, and in the edge β -strand J, which is irregular in $\alpha 1$ LG4-5. The end of the B-C loop and start of the C strand, is the location of KRK₂₇₂₁ – one of the crucial sequences for α DG and heparin binding in $\alpha 1$ LG4. The LG5 domains of $\alpha 1$ and $\alpha 2$ are more conserved and can be superimposed with an r.m.s. deviation of 0.59 Å for 153 C α atoms (figure 29D). Just like LG4, the major differences are again concentrated in the B-C and L-M loops.

The relative arrangement of LG4 and LG5 in both $\alpha 1$ LG4-5 and $\alpha 2$ LG4-5 is also similar, with the arrangement in $\alpha 2$ LG4-5 more closely resembling molecule B rather than molecule A of $\alpha 1$ LG4-5. However, only a few of the contacts in the LG4-LG5 interface are conserved between the two laminin isoforms (figure 30A and B). In $\alpha 1$, near the pivot point of interdomain flexibility between LG4 and LG5, an aromatic side chain from Tyr₂₈₇₁ in the linker region between LG4 and LG5 stacks against Pro₃₀₅₆ near the C-terminus of $\alpha 1$ LG5. Further away from the hinge, a conserved leucine in LG4, Leu₂₇₀₃ in $\alpha 1$ LG4, makes a van der Waals contact with a proline in LG5, Pro₃₀₅₂ in $\alpha 1$

LG5. Finally, a conserved Gln, Gln₂₇₀₀ in $\alpha 1$ LG4, points its side chain into the water-filled cavity within the inter-domain interface (figure 30C). Conservation of secondary structure between $\alpha 1$ and $\alpha 2$ LG4-5 is also quite evident when examining the ribbon diagram of figure 30C and D with its depicted β -sheet (grey arrows) and random coil/loops (green tubes). Figure 30E is an enlargement of the discussed area in $\alpha 1$ LG4-5 with the residues mentioned indicated on the ribbon diagram.

The location of Cys residues and disulfide linkage arrangements are also conserved between $\alpha 1$ and $\alpha 2$ LG4-5, except for the Cys₃₀₁₄ present in the LG5 domain of mouse $\alpha 1$ (figure 27A and B). The Cys₂₆₈₆ of the $\alpha 1$ LG3-LG4 linker forms a disulfide bond with Cys₂₉₅₈ of LG5 just like Cys₂₇₄₇ does to Cys₃₀₁₇ of $\alpha 2$ (figure 27). The intradomain disulfide linkage between Cys₂₈₄₅ and Cys₂₈₇₀ of $\alpha 1$ LG4 is also represented by the Cys₂₉₀₅ and Cys₂₇₄₇ disulfide bond in $\alpha 2$ LG4. The analogous intradomain disulfide linkage between Cys₃₀₂₄ and Cys₃₀₅₅ of $\alpha 1$ LG5 and Cys₃₀₈₃ and Cys₃₁₁₅ of $\alpha 2$ LG5 are also present. The unpaired Cys₃₀₁₄ of $\alpha 1$ LG5 is not present in LG4-5 of $\alpha 2$, $\alpha 3$, $\alpha 4$, or $\alpha 5$. Homology modeling correctly predicted, and the crystal structure determination confirmed, that Cys₃₀₁₄ would not be present on the surface of the folded state.

The homology model also correctly predicted the location of the bound Ca²⁺ ion in both LG4 and LG5 of the $\alpha 1$ chain. The Asp residues involved and location of the Ca²⁺ binding sites are highly conserved between $\alpha 1$ and $\alpha 2$ LG4-5. All residues and binding arrangements involved in Ca²⁺ binding are perfectly conserved between $\alpha 1$ and $\alpha 2$, with two exceptions: Thr₂₈₁₄ of $\alpha 1$ LG4 and Ile₂₈₇₄ of $\alpha 2$ LG4, and the replacement of water molecules in $\alpha 2$ LG5 with Asp₂₈₆₁. Both Asp₂₇₄₇ and Asp₂₈₁₆, together with the main chain carbonyl oxygens of Leu₂₇₆₄ and Thr₂₈₁₄, along with two water molecules form the octahedral binding arrangement for Ca²⁺ in LG4 of $\alpha 1$. The analogous site in LG4 of $\alpha 2$

is formed by: Asp₂₈₀₈, Asp₂₈₇₆, Leu₂₈₂₅, Ile₂₈₇₄, and two water molecules. The LG5 Ca²⁺ co-ordination site in α 1 is formed by Asp₂₉₂₃, Asp₂₉₉₆, Asn₂₉₄₀, Ser₂₉₉₄, and two water molecules. While the α 2 LG5 site, is formed by Asp₂₉₈₂, Asp₃₀₅₅, Asn₂₉₉₉, Ser₃₀₅₃, and Asp₂₈₆₁; instead of water molecules as in α 1.

Post translational N-linked glycosylation of LG4-5 is not conserved between α 1 and α 2 laminin. Laminin α 1 LG4-5 contains three N-linked glycosylation sites: Asn₂₇₁₄ and Asn₂₈₁₁ in LG4 and Asn₂₉₀₀ in LG5. There is just a single N-linked glycosylation site in α 2 LG4-5, Asn₂₈₈₉ of LG4 and it's location is not homologous to any of the α 1 N-linked sites. SDS-PAGE of purified recombinant proteins both mutant and WT, with or without tunicamycin treatment, as well as the crystal structure data for both the α 1 and α 2 LG4-5 demonstrate that all four glycosylation sites are utilized and surface accessible. Furthermore, in α 1 LG4, the Asn₂₇₁₄ glycosylation site can be found in the B-C loop and the Asn₂₈₁₁ glycosylation site is located in the loop between the J and K β -strands adjacent to the Ca²⁺ binding site and on the rim of a grouping of positively charged amino acid residues which encircle the calcium binding site and are crucial for α DG and heparin binding.

The Ca²⁺ binding sites in LG4-5 are highly conserved between α 1 and α 2, however, the N-linked glycosylation sites are not and α 1 contains an extra unpaired Cys residue. Furthermore, despite α 1 and α 2 also binding many of the same ligands within LG4-5, the location of the residues involved and spatial location of the binding sites differ drastically between the two chains. These differences also explain both proteins Ca²⁺ requirements in both sulfatide and α DG binding, as well as the ability of heparin to block the binding of α 1, but not α 2, LG4-5 to α DG.

The location of amino acid residues which carry a charge, either positive (Arg, Lys, or His) or negative (Asp and Glu) under physiological pH conditions were mapped to both $\alpha 1$ and $\alpha 2$ LG4-5 and compared. There does not appear to be any general conservation of charges in the primary sequence or in tertiary structure locations and very few specific conservations outside of those incurred by disulfide linkages and Ca^{2+} coordination. Electrostatic surface representations of $\alpha 1$ and $\alpha 2$ LG4-5 demonstrate patches of positive and negative potential on both LG4 and LG5 of both $\alpha 1$ and $\alpha 2$.

Overlay of the $\text{C}\alpha$ atoms of the proposed mouse $\alpha 1$ LG4-5 homology model with the determined crystal structure of $\alpha 1$ LG4-5 resulted in a r.m.s. deviation of $.29 \text{ \AA}$, once the pivot at Tyr₂₈₇₁ between the two domains of the homology modeled LG4-5 was altered to better align with the two LG domains of the crystal structure. Furthermore, once the residues in the immediate vicinity of the amino acid sequences mutated to enable crystalization (Asn₂₇₁₄, Asn₂₈₁₁, Asn₂₉₀₀, and Cys₃₀₁₄) were removed from the analysis, the remaining 123 $\text{C}\alpha$ of LG4 superimposed with a r.m.s. deviation of $.13 \text{ \AA}$ and the remaining 142 $\text{C}\alpha$ of LG5 with a r.m.s. deviation of $.11 \text{ \AA}$. The extremely minor deviations between the homology model and the $\alpha 1$ LG4-5 we were able to eventually crystalize demonstrates that the predictive homology model of $\alpha 1$ LG4-5 was extremely accurate. Despite the differences in primary sequence and lack of conservation of charged residues, $\alpha 1$ and $\alpha 2$ LG4-5 share a high degree of secondary and tertiary structure homology, as first proposed by the predictive programs and homology model, then determined/confirmed via crystalization of $\alpha 1$ LG4-5. Thus, both vindicating the use of the $\alpha 2$ crystal structure coordinates to homology model $\alpha 1$ LG4-5 and demonstrating the accuracy of the proposed homology model.

Section III. Summary

Mouse Lm-111 is composed of three different chains totaling over 800,000 kDa and composed of approximately 6,300 amino acid residues. The average eukaryotic protein, on the other hand, is monomeric and 21 times as small, composed of approximately 300 amino acids (figure 7). The manipulation of Lm-111 is further complicated by its heterotrimeric nature. The mouse $\alpha 1$ laminin chain is 3,084 amino acids long with the majority of cell anchorage sites found in the 950 amino acids of the five globular domains (LG1-5) which collectively comprise the C-terminal G domain of the α chain (figure 7 and 11). While LG1-3 contains the $\alpha 6\beta 1$, $\alpha 6\beta 4$, and $\alpha 7\beta 1$ integrin binding sites as well as the HNK-1 binding site, the LG4-5 domains contained within the 372 residue elastase digest fragment E3 (which contains the C-terminal section of LG3, the LG3-LG4 linker, LG4, and LG5), has been shown to contain heparin, sulfatide, and α DG binding sites (figure 7 and 12). In order to better understand these activities, an attempt was made to map crucial residues required for binding of these macromolecules, so that we could then examine how loss of these functions would affect laminin-111's role in basement membrane formation, differentiation, and cell signaling.

Section IIIA. Expression of recombinant $\alpha 1$ LG4-5 proteins.

An expression system was established that would efficiently produce the highest yield, quality, and purity of recombinant $\alpha 1$ LG4-5s and much larger laminin chains. The recombinant $\alpha 1$ LG4-5 was utilized to test and perfect much of the system employed in generating the larger laminin chain constructs. Its smaller size and monomeric nature made it much more easier to manipulate and manage than the much larger heterotrimeric laminin. The expression vectors utilized contain many parts, many of which had several candidates for utilization: promoters - P_{CMV} , P_{RSV} , P_{SV40} , and the

mouse $\beta 1$ Lm promoter; various 5' UTR sequences; signal sequences – endogeneous, BM40, IG κ , and the mouse $\alpha 1$ Lm signal sequence; epitope tags and their location – inclusion of an N-terminal, C-terminal, or internal FLAG, myc, mycX3, HA, VSV-G, protein-C, V5, or no tag; engineered proteolytic recognition and cleavage sequence – EK, TEV, or no cleavage sequence; and selectable marker – neomycin (neo/G418), zeocin (zeo), hygromycin (hygro), puromycin (puro), and blasticidin (blstd) (figure 13A). These many parts of the expression construct needed to be determined, tested, selected, and optimized since their function/efficiency are affected by the cellular environment and other parts of the construct.

The viral promoters CMV, RSV, and SV40 demonstrate, not only, different levels of expression, but also, each individual promoter can exhibit tissue, including both temporal and spatial, and cell line specific differences in expression [325-332]. Furthermore, consideration had to be given to such things as promoter interactions, for example: SV40's observed inhibition or enhancement of expression from CMV and RSV promoters depending upon the cell line. Furthermore, since multiple SV40 promoters have been shown to decrease expression in some cases, SV40 was not utilized to drive expression of the recombinant proteins, because the SV40 promoter was already being utilized to drive expression of the selectable marker in the constructs. The same promoter eventually chosen for generation of the recombinant $\alpha 1$ LG4-5s and other laminins was the CMV promoter, however, the RSV and mouse $\beta 1$ Lm promoter were also tested in HEK 293 cells using an $\alpha 1$ LG4-5/WT_{Nf} construct which contains mouse $\alpha 1$ LG4-5 expressed under the CMV promoter. The same CMV based construct was utilized to create two other constructs in which the CMV promoter was replaced with either the RSV or mouse $\beta 1$ Lm promoter [333, 334] and all three constructs were stably transfected into the HEK 293 cell line. The CMV promoter demonstrated a threefold

expression level increase over RSV and approximately 50 times that of the mouse $\beta 1$ Lm promoter (figure 13B). The addition of retinoic acid (RA) to the cell lines stably transfected with constructs under the mouse $\beta 1$ Lm promoter, resulted in a four fold increase in expression, however, N6,O2'-dibutyryl adenosine 3',5'-cyclic monophosphate (Bt2cAMP) which is also reported in conjunction with RA to further increase expression [335] was not tested.

The 5' UTR of eukaryotic mRNAs have been shown to affect gene expression through both stimulatory [336-341] and inhibitory [342, 343] mechanisms. Furthermore, the 5'UTR has been demonstrated to contain sequence elements that not only influence RNA transcription [344-346], but also, post-transcriptional gene regulation and expression, through posttranscriptional modification of RNA via secondary structure and mRNA stability [339, 345, 347-351], nucleo-cytoplasmic mRNA transport [352, 353], subcellular localization [354, 355] translation efficiency [337, 341-343, 356-366], and other factors [362-366]. Several different 5'UTR sequences, initially identified by examining the data of Kozak [306, 367] were further refined via a BLAST [368-373] search of GENE BANK together with an examination of NCBI's gene chip array expression profiles databases utilizing NCBI's Gene Expression Omnibus (GEO) [22, 374] to identify potential candidate 5'UTR from genes shown to be highly expressed in fibroblast cells. Two 5'UTR sequences were chosen from a 5'UTR consensus sequence derived from the data of Kozak [306, 367] and six other 5'UTRs were chosen from genes shown to be highly expressed in fibroblasts (figure 13D). Each of the eight 5'UTRs were placed under the control of a CMV promoter in a vector designed to express an N-terminal FLAG tagged mouse $\alpha 1$ LG4-5, HEK 293 cells transfected, stable clones isolated, and their yields of recombinant protein compared (figure 13E). The ninth 5'UTR examined was that which is present in the expression construct $\alpha 1$ LG4-5/WT-

pRCX3, constructed earlier and tested previously. The “consensus-1” 5' UTR of 5'-CCCGCCGCCACCATGG clearly and consistently demonstrated the highest yield; 3-4 fold higher than any other 5'UTR and was, therefore, used in the design of subsequent expression constructs.

Secreted proteins are synthesized with a 15-25 amino acid long N-terminal signal sequence required for its proper transport, cleavage, and secretion [375-377]. In eukaryotes this short peptide mediates the interaction between the ribosome and the signal recognition particle (SRP) [378], release of SRP from the ribosome [379-381], and its own cleavage from the mature polypeptide. There is no concrete consensus sequence for signal sequence, but rather a three region structure each with particular characteristics [382, 383]. The positive net charge of the N-terminal “n-region” has been shown to influence both the level of translation and efficiency of export [375, 376, 380, 384, 385], the hydrophobic “h-region” binds the SRP [378], and the neutral but polar C-terminal “c-region” defines the site of cleavage between the signal sequence and the mature protein [375, 377, 382-384, 386, 387] (figure 14). There is also a strong bias for neutral small side chain amino acid residues at positions -1 and -3 of the signal sequence for proper cleavage to occur [377, 387]. The m α 1LG4-5/WT-pRCX3 expression construct contains the signal sequence for BM40 under the CMV promoter. Much like the promoter testing, the BM40 signal sequence was also replaced with either the IG κ or endogeneous mouse α 1 Lm signal sequence and all three expression constructs stably transfected into HEK 293 cells. The BM40 signal sequence gave approximately twice the expression of the recombinant α 1 LG4-5 than that observed from the IG κ signal sequence and 65% more than the mouse α 1 Lm signal sequence (figure 13C). Both the IG κ and BM40 signal sequence were also used to make a series of full length human β 1 laminin chain expression constructs. Again, the constructs

containing the BM40 signal sequence demonstrated higher recombinant protein yields than IG κ .

A further complication when dealing with signal sequences is that the sequences placed immediately downstream of them may have drastic effects, resulting in either improper cleavage or folding, leading to proteolytic degradation, potential loss or gain of N-terminal amino acids, potential loss of N-terminal epitope tags or binding activities, or improper intracellular trafficking, post-translational modification, and export. Therefore, all recombinant proteins made were first analyzed and vetted utilizing the adaptive encoding artificial neural network programs ACN [388], SignalP, SignalP-NN, and SignalP-HMM [389, 390]. These programs were primarily utilized to make sure that cleavage occurred where it was designed to and did not remove the epitope tags. Figure 14 depicts the computer programs analysis results of just one example from the many (more than 50) recombinant proteins evaluated and expressed. The figure includes the signal sequence and analysis results for human β 1 laminin without any N-terminal epitope tag. This sort of analysis was of particular interest during the construction of the trimeric recombinant laminins. The human β 1 Lm chain which normally was not exported outside of the cell, even with a BM40 signal sequence, was secreted once an N-terminal HA epitope tag was placed on it but not if a VSV-G epitope tag was utilized.

An epitope tag was placed on the N-terminus of the recombinant proteins in order to aid in both their purification and detection. Seven different tags were chosen to be tested based upon their commercial availability as antibody, matrix linked for purification purposes, and ability to be eluted under gentle non-denaturing conditions from the matrix whether through peptide elution or other mechanism. All of these tags were expressed on the N-terminus of recombinant α 1LG4-5s as well as full length

mouse $\alpha 1$ recombinant proteins and other laminin chain constructs. Eight constructs were made which contained the mouse $\alpha 1$ LG4-5 under a CMV promoter, the “consensus-1” 5'UTR, a BM40 signal sequence, and one of seven different epitope tags or no tag, and an EK cleavage signal immediately upstream of the $\alpha 1$ LG4-5 sequence. HEK 293 cells were stably transfected with the constructs, stable lines isolated, media collected, and tested. There was no discernable difference in protein yields between the resulting eight different cell lines, nor was there any difference in the quality of the recombinant $\alpha 1$ LG4-5. All seven epitope tagged recombinant proteins reacted specifically only with their epitope specific antibody (figure 15). All recombinant proteins were of the correct size, none of the recombinant proteins demonstrated degradation of any kind nor inappropriate behavior during purification. The 14 amino acid V5 epitope tag (N-Gly-Lys-Pro-Ile-Pro-Asn-Pro-Leu-Leu-Gly-Leu-Asp-Ser-Thr-C; Invitrogen) derived from the P and V proteins of the paramyxovirus SV5 [391] was dropped due to its length and because the peptide and matrix for it became commercially unavailable. The 12 amino acid protein-C epitope tag (N-Glu-Asp-Gln-Val-Asp-Pro-Arg-Leu-Ile-Asp-Gly-Lys-C) derived from the human plasma protein Protein C [392-394] was held for other projects (use and suitability as an epitope tag: 395-401). The calcium binding dependency for activity of the protein C antibody would be a convenient method for elution from matrix [402], however, it was foreseen that some of the future purifications and experiments would have to be performed in the absence of calcium – either to test the role of calcium in certain activities and/or inhibit polymerization of recombinant trimeric laminin during purification or experimentation. Both the 11 amino acid VSV-G epitope tag (N-Tyr-Thr-Asp-Ile-Glu-Met-Asn-Arg-Leu-Gly-Lys-C) derived from the vesicular stomatitis virus glycoprotein [403; use and suitability as an epitope tag: 404-408] and the 9 amino acid HA epitope tag (N-Tyr-Pro-Tyr-Asp-Val-Pro-Asp-Tyr-Ala-C) derived from

the influenza hemagglutinin protein [409; [use and suitability as an epitope tag: 410-424](#)] were held for other projects; including the epitope tagging of human β 1 laminin recombinant proteins. There were two different monoclonal antibodies utilized to detect the HA epitope tag, eventhough, the mouse IgG_{2b,k} mAb 12CA5 (Roche) was not as specific as the rat IgG₁ mAb 3F10 [425, 426], the species difference enabled double labeling experiments with other antibodies. Both the 10 amino acid myc (N-Glu-Gln-Lys-Leu-Ile-Ser-Glu-Glu-Asp-Leu-C) and 30 amino acid triple myc epitope tag (mycX3; same 10 amino acid residues repeated three times) derived from the human c-myc protein [427] were held for other projects; including the epitope tagging of larger mouse α 1 laminin recombinant proteins [[use and suitability as an epitope tag: 428-430](#)]. The eight amino acid FLAG epitope tag (N-Asp-Tyr-Lys-Asp-Asp-Asp-Asp-Lys-C; SIGMA) was chosen as the epitope tag for expression of recombinant mouse α 1LG4-5 proteins. The short nature and inclusion of the enterokinase cleavage sequence within the FLAG epitope sequence, along with multiple commercially available epitope specific antibodies with different binding characteristics [431-436] made it an ideal epitope tag. Unfortunately, the FLAG binding antibodies have often demonstrated unacceptably high background binding when used in most immunohistochemical staining procedures. This binding was thought to be non-specific, however, it may be related to a recently discovered splicing isoform of Mg²⁺ dependent protein phosphatase beta (MPP beta) [437]. Not only do the FLAG epitope and MPP beta share five of the eight residues which comprise the FLAG epitope sequence but the FLAG M2 mAb recognizes MPP beta recombinant protein in Westerns and immunohistochemical staining.

The N-terminally epitope tagged recombinant proteins were designed with an Enterokinase recognition and cleavage sequence placed between the epitope tag and the recombinant laminin protein so that the tag could be removed from the recombinant

protein post synthesis. Therefore, if it was found that the tag interfered with processing, trafficking, post-translational modification, secretion, or any activity of the recombinant protein, or increased its proteolytic sensitivity, it could then be removed post synthesis. This was a concern for three reasons: the heparin binding activity observed in $\alpha 1$ LG4 was thought to be a simple general charge interaction and the FLAG epitope contains five Asp and two Lys residues which could potentially interact or interfere with binding, the N-terminal LN domains of the individual laminin chains contain unmapped polymerization activities, and the $\alpha 1$ LN domain also contains integrin and heparin binding sites. Two serine proteases were chosen for testing: the 31 kDa serine protease enterokinase (EK) [438] whose recognition sequence is N-Asp-Asp-Asp-Asp-Lys-C [439, 440] which EK cleaves after the C-terminal Lys residue of the recognition sequence and the serine-like proteolytic 27 kDa catalytic domain of the Nuclear Inclusion a (Nla) protein encoded by the tobacco etch virus (TEV) [441-444] whose recognition sequence we were lead to believe was Glu-Asn-Leu-Tyr-Phe-Gln-Gly, however, experiments by others revealed a more permissive recognition sequence of N- Glu-X_{aa}-X_{aa}-Tyr-X_{aa}-Gln-Gly/Ser-C (with some restrictions on Xaa) [445-447] with cleavage occurring between the Gln and Gly/Ser residues. Furthermore, there are now recombinant variants of TEV which are more stable, i.e. no self cleavage [448, 449], however, they were not available at the time of testing. The two protease were tested on purified EHS derived Lm-111, recombinant mouse Lm-111, purified recombinant human $\beta 1$ Lm, EHS derived E3, and recombinant mouse $\alpha 1$ LG4-5/WT_{Nf} (data not shown). Initially, only the recombinant $\beta 1$ Lm showed any degradation by the two proteases. Later experiments showed degradation of the EHS Lm-111, recombinant Lm-111, and purified recombinant human $\beta 1$ Lm, though this degradation could be almost completely suppressed in the case of the EHS Lm-111 and recombinant Lm-111 if kept at 4°C, however, efficiency of the

designed cleavage site also decreased. In both cases EHS-111 was the least sensitive to degradation, not surprising considering the protection derived from its hyperglycosylated state, followed by mouse recombinant Lm-111, and then human $\beta 1$ Lm, which again was no surprise given the exposure of the unpaired “coiled-coil” region of $\beta 1$ without the α and γ chains being present. Furthermore, TEV protease treated samples did demonstrate slightly more degradation than their EK treated counterparts and less efficient designed cleavage of epitope tags. Treatment with either TEV or EK, revealed no degradation of either EHS E3 or recombinant mouse $\alpha 1$ LG4-5, except for the planned removal of the N-terminal FLAG tag from mouse $\alpha 1$ LG4-5. TEV protease did have a HIS tag which would have aided in its separation from recombinant proteins after its use, however, inactivation of TEV by autoproteolysis was an issue, until later variants became available; as was its “soft” recognition sequence and observed higher proteolysis of laminins when compared to EK. EK could be cleared from recombinant laminins when necessary based upon its size, inability to bind heparin, and a commercially available EK binding resin. Ultimately, EK was chosen because it would require less non-laminin sequence on the N-terminus of the generated recombinant proteins and the concern that any “extra” sequence could potentially lead to proteolysis or interfere with native activities; such as the polymerization activity mapped to the N-terminal LN domains when examining full length laminin chains or interfere with binding assays due to its charged nature or through steric hindrance. Furthermore, the last 5 amino acid residues of the eight amino acid FLAG epitope tag, N-Asp-Tyr-Lys-**Asp-Asp-Asp-Asp-Lys**-C, are the recognition sequence for EK so there is no extra sequence necessary when utilizing an N-terminal FLAG tag and the cleavage occurs immediately following the C-terminal Lys, therefore, the epitope tag and cleavage recognition sequences are as short as possible and after EK cleavage there are no extraneous

amino acid residues left on the N-terminus of the recombinant protein. Figure 22D shows the detection of α 1LG4-5 with FLAG epitope monoclonal antibody M2 and α 1LG4-5 polyclonal antibody rG50, pre and post incubation with Enterokinase. A downshift in size is observable when the FLAG tag is removed and its immunoreactivity to FLAG antibody lost with no further discernable proteolysis. Furthermore, recombinant α 1LG4-5 with the FLAG epitope tag removed via Enterokinase treatment or construct design, demonstrated no difference when compared to α 1LG4-5 with an N-terminal FLAG tag in either heparin binding, sulfatide binding, or gel filtration. Clearly, the inclusion of the FLAG epitope tag does not appear to alter any of the observed activities of recombinant α 1LG4-5.

While individually expressed recombinant proteins such as the mouse α 1LG4-5 only require a single selectable marker, the decision was made to utilize three selectable markers which could be simultaneously expressed together and have each assigned to a laminin chain type so that when heterotrimeric recombinant laminins were produced each chain would be under a unique selectable marker. Furthermore, all markers would be on the same expression construct as the laminin chain to which it was assigned in order to minimize loss of recombinant expression during transfection and with time during passage of the cells. Each marker was placed under the SV40 promoter in order to normalize any effects of promoter differences or interactions. The hope was to greatly reduce the observed rate of recombinant protein loss observed with passage of stable cell lines. Five unique selectable markers were tested: neomycin, zeocin, hygromycin, puromycin, and blasticidin. Neomycin resistance is conferred by the aminoglycoside phosphotransferase gene product Tn5 and Tn601 which will inactivate the G418/neomycin/geneticin that blocks protein synthesis through interference with ribosomal function by binding the 30S and sometimes 50S subunit causing miscoding

and inhibiting initiation and elongation during protein synthesis [450-453]. Zeocin resistance is conferred by the Sh ble gene product that binds zeocin and inactivates it, thereby preventing it from binding and cleaving the cellular DNA [454, 455]. Hygromycin resistance is conferred by the hygromycin-B-phosphotransferase (HPH) gene product that phosphorylates and inactivates hygromycin-B, which binds a single site within the 30S subunit region that contains the A, P, and E sites of tRNA and distorts the ribosomal A site, preventing it from inhibiting protein synthesis by disrupting translocation and promoting mistranslation [456, 457]. Puromycin resistance is conferred by the puromycin-N-acetyl transferase (PAC, Puro) gene product which inactivates puromycin by acetylation and prevents its inhibition of protein synthesis, causing premature chain termination by acting as an analog of the 3' terminal end of aminoacyl-tRNA [458-460]. Blasticidin resistance is conferred by the blasticidin S deaminase (BSD) gene product which inactivates blasticidin by deamination, thereby preventing its inhibition of translation by inhibiting peptide bond formation [461-465]. "Kill curves" were established for each selectable marker individually in the HEK 293 cell line and then in various combinations of three markers with each antibiotic at 100%, 80%, and 60% of its optimal kill concentration. The following concentrations for antibiotic usage in HEK 293 cells were derived from the kill curves for the individual antibiotics: 500ug/ml for G418 (neomycin), 80-100 ug/ml for zeocin, 5 ug/ml for hygromycin, 1 ug/ml for puromycin, and 5ug/ml for blasticidin. Puromycin was the most efficient killer of cells, in means of time and amount of antibiotic necessary; followed shortly by zeocin. Eventhough blasticidin's effect is quicker and less is required than G418/neomycin, there was not a suitable blasticidin based expression vector available at the time, therefore, neomycin was chosen over blasticidin. The combinations of neomycin, zeocin, and puromycin as well as blasticidin, zeocin, and puromycin were observed to be the most effective, probably because all three antibiotics exert their activity via different modes of action, while the

combinations of neomycin-blasticidin-zeocin and neomycin-blasticidin-puromycin were nearly as effective. Interestingly, any triple combination that involved neomycin, hygromycin, and one of the other markers was too toxic for the cells. The targeting of the 30S subunit by both antibiotics may have been too much for the cells to accommodate/survive. Therefore, zeocin (80-100 ug/ml) was selected for recombinant α 1LG4-5 and laminin β 1 constructs which were placed into a pcDNA3.1/zeo(+) expression vector (Invitrogen), neomycin (500 ug/ml G418) was reserved for laminin γ 1 constructs which were placed into a pcDNA3.1/neo(+) expression vector (Invitrogen), and puromycin (1 ug/ml) utilized for laminin α 1 constructs. Furthermore, there were no acceptable commercially available puromycin based expression vectors, therefore, a unique puromycin based expression vector was constructed and used for α 1 expression constructs: DHpuro.

In order to effectively test and compare recombinant α 1LG4-5 proteins, a method was devised to obtain the recombinant protein in large amounts, efficiently (time and money), relatively pure, and without a reduction or alteration in activity. Despite α 1LG4-5s heparin binding activity, even the combination of heparin affinity and sizing chromatography did not produce completely pure α 1LG4-5/WT_{Nf} protein (figure 22A and B). Furthermore, since the subsequent recombinant mutant α 1LG4-5 proteins would potentially demonstrate differences in heparin affinity, charge, and hydrophobicity, any attempts to perfect a purely chromatographic means for purification of the recombinant proteins would be futile since it would need to be constantly refined for each unique recombinant protein. Instead the recombinant α 1LG4-5s were constructed with an N-terminal Enterokinase cleavable FLAG epitope tag which enabled quick and convenient purification and detection of the recombinant proteins. Furthermore, the expression constructs were optimized for the best promoter, 5'UTR, and signal sequence in order to

produce recombinant levels up to 8 fold higher than anything we had previously observed. The epitope tags in conjunction with heparin affinity chromatography enabled the recombinant protein to be purified in a single day from harvested media, easy detection, and improved assay performance.

Section IIIB. Generation of a homology model for $\alpha 1$ LG4-5 and selection of amino acid residues to mutate.

It was the conservation of secondary structure, more than primary structure, which was responsible for, what would turn out to be a remarkably accurate, homology modeling of mouse $\alpha 1$ LG4-5 based upon the crystal structure of mouse $\alpha 2$ LG4-5. The LG4-5 sequence from $\alpha 1$ and $\alpha 2$ are only 41% identical and share 57% homology (figure 17), however, the summation of twelve secondary structure prediction programs showed an extremely high degree of secondary structure conservation between the two divergent chains (figure 18). This allowed generation of a highly accurate homology model for $\alpha 1$ LG4-5, through the use of the $\alpha 2$ LG4-5 crystal coordinates, secondary prediction programs, homology modeling programs, and energy minimization programs. The subsequent determination of the actual crystal structure for $\alpha 1$ LG4-5 by us and it's comparison to the predicted homology model structure reveals that our derived model for $\alpha 1$ LG4-5 was very accurate. This model allowed for the highly focused mutagenesis of just a few key residues from almost 400 potential candidates. Furthermore, the vast majority of chosen residues had dramatic effects on the very binding interactions we were attempting to disrupt. Also, further evidence of the accuracy and reliability of our system was the dramatic differences in some of the determined binding affinities we observed with our recombinant proteins from those obtained by another group which produced

only an untagged LG4 for analysis and our identification of novel critical sites for certain LG4 activities.

Section IIIC. Characterization of recombinant α 1LG4-5s.

The various generated recombinant α 1LG4-5 were tested and compared with regards to their binding affinity for: heparin, α DG, and sulfatide. Furthermore, the crystal structure of α 1 LG4-5 was determined, analyzed, and compared against α 2 LG4-5.

Section IIIC1. Heparin affinity.

Laminin mouse α 1LG4-5 elastase digest fragment (E3) isolated by heparin chromatography of elastase digested Lm-111 purified from EHS tumor, recombinant α 1LG4-5/WT_{Nf}, recombinant α 1LG4-5/WT in which the FLAG tag had been removed by enterokinase treatment, recombinant α 1LG4-5/WT with no epitope tag, and PNGaseF treated recombinant α 1LG4-5/WT_{Nf}, all eluted at the same salt concentration (figure 23A). The FLAG epitope tag had no affect upon heparin affinity. PNGase F treated α 1 LG4-5 material demonstrated observable shifts in size based upon SDS-PAGE, indicating removal of N-linked glycosylation and no changes in it's salt elution behavior in heparin FPLC. PNGase F is an amidase that cleaves the glycosidic bond between the modified Asp residue and the first GlcNAc moiety. However, recombinant α 1LG4-5/WT purified from cells grown in the presence of tunicamycin, an inhibitor of N-acetylglucosamine transferase, not only, demonstrated a decrease in size, but also, a dramatic increase in heparin affinity. Several other heparin binding proteins have demonstrated increases in heparin binding when N-linked glycosylation moieties were removed, including FGF and midkine. The lack of an observed change in heparin binding of the PNGase F treated α 1LG4-5 may be a direct result of the enzymatic

reaction which removed the glycosylation moiety from the Asn residue. The process results in the carbohydrate linked Asn being converted into an Asp residue after removal of the carbohydrate moiety. The change in charge as a result of the substitution of Asn for Asp, coupled with the strange decrease and then increase in the observed mobility/size of α 1LG4-5 being digested with PNGase F (perhaps indicating the removal of a large charged moiety; data not shown), or potential disruption of the positively charged grouping of amino acid residues implicated in heparin binding surrounding the glycosylated Asn₂₈₁₁, or potential disruption of the adjacent Ca²⁺ coordination site, may be contributing causes to why the PNGase F treated α 1 LG4-5 did not exhibit an increase in heparin affinity. All mutant recombinant α 1LG4-5s eluted at a lower salt concentration than WT and their decrease in binding seemed to follow in direct relation to the number of positively charged residues (Arg or Lys) removed, i.e. the more charged groups removed the larger the decrease in heparin binding (figure 23C). We found elution behavior for heparin binding similar to those mutants in common evaluated by Andac et. al [162]. Hozumi et. al [466] used an energy minimized homology model of α 1LG4-5 to gain insight into the interactions of LG4 with heparin/heparin sulfate proteoglycan syndecan. They found heparin binding to α 1 LG4 dependent upon contributions from RKR₂₇₂₁, KRK₂₇₉₃, and, to a lesser extent, KGRTK₂₇₇₀; in full agreement with out heparin binding data.

Section IIIC2. α DG affinity.

The ability of the recombinant α 1LG4-5s to bind α DG was measured via a gel overlay assay (figure 24A and B) and an ELISA assay from which binding curves were generated and dissociation constants determined (figure 24 C and D). The results observed from both assays were in general agreement with one another. All mutant

recombinant α 1LG4-5s show some decrease in α DG binding. Recombinant laminin α 1LG4-5 mutants representing sequences RAR₂₈₃₃, KDR₂₈₆₀, and RKR₂₇₂₁ show the largest decrease in α DG binding. The finding that RKR₂₇₂₁ bound α DG with higher affinity than RKR₂₇₂₁ was surprising given the greater loss of charge of the former compared to the latter. The sequences of RKR₂₇₂₁ and RKR₂₇₂₁, as well as all other recombinant proteins, were confirmed by PCR and direct sequencing of genomic DNA isolated from the very cells the recombinant proteins were harvested from. The unusual behavior demonstrated may be due to the Lys₂₇₂₀ residue of RKR₂₇₂₁ forming a salt bridge with Asp₂₇₁₇ or alterations in either of the adjacent Ca²⁺ binding site or N-linked glycosylation site of Asn₂₈₁₁. A similar observation could potentially explain the α DG binding activity of the double recombinant mutant α 1LG4-5/RKR₂₇₂₁+KRK₂₇₉₃, which binds α DG nearly as well as WT and better than either of the binding activities observed for the individual mutants which were combined in this recombinant protein.

The observation that recombinant α 1LG4-5/WT_{Nf} which had been enzymatically deglycosylated with PNGaseF demonstrated little if any binding to α DG must be analyzed with two other observations taken into account: the strange mobility shifts observed during the time course digestion of α 1LG4-5/WT_{Nf}, and that the enzymatic reaction results in the Asn residue being converted into a negatively charged Asp residue after the deglycosylation reaction has been completed.

Furthermore, there are some notable discrepancies between our data and those of a previously published study by another group [162]. Our α DG assays demonstrated only moderately reduced binding for mutants α 1LG4-5/KGRTK₂₇₇₀ (145 vs. >3500 nM) and α 1LG4-5/KRK₂₇₉₃, whereas, the same mutations led to a complete loss of α DG binding for the other group. Furthermore, our α 1LG4-5/RAR₂₈₃₃ (2250 vs. 19 nM) and α 1LG4-5/KDR₂₈₆₀ (438 vs 37 nM) also demonstrated significant differences with Andac

et al.'s [162] analogous LG4 recombinant proteins. Several potential reasons exist for these discrepancies. We expressed $\alpha 1$ LG4-5, mimicking the elaste digest fragment E3, whereas, the other group expressed their mutants as $\alpha 1$ LG4 only. The disulfide bond observed between the hinge region preceding LG4 (on the N-terminal side of LG4) that bonds with another cysteine within the downstream LG5 linking the two domains together, as well as, the analogous production of E3 ($\alpha 1$ LG4-5) via elastase digestion suggest perhaps our recombinant proteins may have been more structurally and proteolytically stable. There were also methodological differences which may have contributed to the observed differences. We discovered that the drying and rehydrating that the other group employed, led to loss of activity. Also, there are distinct advantages to utilizing a unique epitope tag placed far away from the residues of interest. We demonstrated that the popular polyclonal $\alpha 1$ G domain antibody rG-50 is capable of blocking recombinant $\alpha 1$ LG4-5 binding to sulfatide. The charged amino acid residues being replaced in these studies are prime antigenic determinants and often the epitopes from which many antibodies are derived. This could make the use of polyclonal antibodies unreliable because there exists a high potential that the binding events being measured with polyclonal antibodies are not measuring differences in binding but instead are actually measuring differences in antigenic determinants which are present or absent. Furthermore, the unique tag enabled us to employ a monoclonal antibody directly linked with HRP so that all recombinant proteins were measured equally no matter what their state and simultaneously avoiding amplification issues arising from use of a secondary HRP linked antibody for detection as the other group did. Finally, we utilized a different α DG preparation in our study compared to theirs. We utilized α DG purified from a rabbit skeletal muscle preparation, whereas, the other group utilized a chick lung preparation. It has been well established that α DG demonstrates tissue and

temporal specific differences in post-translational modifications and laminin binding activity.

Section IIIC3. Sulfatide affinity.

Binding of recombinant α 1LG4-5s to sulfatide (SM4) was examined utilizing an O-phenylenediamine based colorimetric ELISA assay in which lipids were bound to microtiter plate wells, recombinant proteins added in solution, and binding detected in most cases by use of an HRP conjugated FLAG M2 monoclonal antibody. Many different microtiter plates from several different manufacturers were tested; as were plating, drying, washing, incubation, BSA preparations, chromagrapic substrates, and buffer conditions in order to optimize the assay and provide consistent reproducible results (data not shown).

The binding of α 1 LG4-5 to sulfatide involves the sulfate moiety found on position 3 of the carbohydrate. The assays demonstrate that α 1LG4-5 binds sulfatide (3'-sulfogalactosylceramide; SM4) and 3'-sulfoglucosylceramide, quite well, however, it does not bind galactosylceramide (the "de-sulfated" analog and precursor of sulfatide), glucosylceramide (the "de-sulfated" analog of 3'-sulfoglucosylceramide), lactosylceramide, or ceramide (figure 25A). Furthermore, α 1LG4-5 does not bind the sulfate moiety present on cholesterol-3-sulfate or the sulfated HNK-1 moiety present on SGGL-1 or SGGL-2. The observed binding is not just a non-specific charge interaction either since similar lipids possessing various types of charges do not bind α 1G4-5, including: N-octanoyl-ceramide-1-phosphate, sphingomyelin, phosphatidic acid, phosphatidylglycerol, L- α -phosphatidylinositol, L- α -phosphatidylethanolamine, L- α -phosphatidylcholine, L- α -phosphatidylserine, sphingosine-1-phosphate, GM1

ganglioside, and a total brain ganglioside preparation. Mixture of sulfatide with other lipids resulted in a corresponding decrease in observed $\alpha 1$ LG4-5 binding.

Furthermore, immunoprecipitations directed against the FLAG epitope tag present on recombinant $\alpha 1$ LG4-5s, of cellular extracts from Schwann cells loaded with sulfatide and incubated with recombinant $\alpha 1$ LG4-5s, were positive for sulfatide and immunohistochemical staining revealed co-localization of Lm-111 and sulfatide; neither of which occurred if the sulfatide was first desulfated with ASA treatment. Furthermore, co-localization of the Lm-111 and sulfatide on the cell surface could then be re-established by sulfatide loading of the Schwann cells after ASA treatment.

The binding of sulfatide by $\alpha 1$ LG4-5 was blocked by the addition of heparin and partially blocked by EDTA (figure 25), whereas, 1-2% Triton X-100 had no affect upon binding. The heparin blockage is not unexpected given the close proximity of critical residues for both heparin and sulfatide affinity on mouse $\alpha 1$ LG4. Mapping of the apparent sites on the crystal structure of $\alpha 1$ LG4-5, reveals that the major heparin and sulfatide sites may be separated on LG4, however, the long heparin chain would most likely sterically block access of sulfatide to at least one of its binding sites on LG4. It is interesting to note how this may explain $\alpha 1$ containing Lm-111's sensitivity to heparin in binding experiments and $\alpha 2$ containing Lm-211's lack of sensitivity. The partial inhibition by EDTA is also expected as experimental data has suggested that more than one sulfatide molecule binds Lm-111 and at least one of the major sulfatide binding sites is clustered around the Ca^{2+} binding site on LG4. The EDTA driven decrease in sulfatide binding by $\alpha 1$ LG4-5 could also be due to a divalent cation being necessary for proper sulfatide packing (Ca^{2+} has been shown to be involved in packing of the carbohydrate moiety of the polar heads of sulfatide by interactions between Ca^{2+} and the sulfate of the carbohydrate), proper maintenance of $\alpha 1$ LG4-5 structure, or involvement in a direct

binding interaction between $\alpha 1$ LG4-5 and sulfatide. Furthermore, AEBSF treatment of either EHS E3 or $\alpha 1$ LG4-5/WT_{Nf} resulted in a complete abolishment of their ability to bind sulfatide, therefore, treatment of laminin-111 with AEBSF not only abolishes its polymerization activity, but also, its $\alpha 1$ LG4 mediated anchorage through sulfatide.

Recombinant $\alpha 1$ LG4-5s, in which select Arg and Lys residues were substituted with Ala, were tested and compared for their ability to bind sulfatide in a solid phase ELISA assay (figure 26A). Most mutant $\alpha 1$ LG4-5s showed some degree of binding to sulfatide, however, mutant $\alpha 1$ LG4-5/RAR₂₈₃₃ demonstrated the greatest decrease in binding followed by $\alpha 1$ LG4-5/KGRTK₂₇₇₀. The general affinity to sulfatide was $\alpha 1$ LG4-5/WT similar to $\alpha 1$ LG4-5/RKR₂₇₂₁ similar to $\alpha 1$ LG4-5/RKR₂₇₂₁+KRK₂₇₉₃ > $\alpha 1$ LG4-5/KRK₂₇₉₃ > $\alpha 1$ LG4-5/KDR₂₈₆₀ > $\alpha 1$ LG4-5/RKR₂₇₂₁ >> $\alpha 1$ LG4-5/KGRTK₂₇₇₀ >> $\alpha 1$ LG4-5/RAR₂₈₃₃. Unlike Andac et al. (1999), we observed mutation of RAR₂₈₃₃ ($\alpha 1$ LG4-5/RAR₂₈₃₃) and KDR₂₈₆₀ ($\alpha 1$ LG4-5/KDR₂₈₆₀) to have strong effects upon sulfatide binding. The binding activity of $\alpha 1$ LG4-5/RKR₂₇₂₁+KRK₂₇₉₃ was unexpected, since it seems to bind sulfatide just as well if not better than WT despite consisting of two different clusters of substitutions, either of which individually demonstrated a decrease in sulfatide affinity. Again, examination of the structure of $\alpha 1$ LG4-5 may provide some clues to this apparently aberrant behavior. The first Arg residue of RKR₂₇₂₁, found at the start of β -strand C, is involved with a salt bridge to Asp₂₇₁₇ in another β -sheet and its Ala substitution may be affecting not only local secondary structure but distant binding sites by affecting adjacent secondary structures involved in binding activities. Furthermore, the middle Arg residue of KRK₂₇₉₃ is surface-exposed in the H-I turn of the crystal structure and makes two hydrogen bonds with the main chain carbonyl groups in the loop between the J and K β -strands. The J-K loop appears to make contact with the body of the domain, with four internal water molecules located between the H-I loop in

the front and the F-G loop in the back. This loop is comprised of residues 2808-2815, which are part of the calcium binding site (figure 30).

The solid phase ELISA assay in which the recombinant α 1LG4-5s were used to block Lm-111 binding to sulfatide demonstrated that very high concentrations of recombinant α 1 LG4-5 were necessary to inhibit Lm-111 binding. This both reflects and stresses the contribution of Lm-111's polymerization activity. The sulfatide-laminin binding interaction is a relatively weak one, however, once laminin begins to polymerize and a nucleation propagation event is initiated it would be extremely difficult to compete off any polymerized Lm-111 with monomeric α 1LG4-5. Every laminin which joins the polymerizing conglomerate would add at least two more sulfatide binding events to the collective and once anchored many of those bonds with sulfatide would have to be broken by a competing α 1LG4-5 to displace the entire conglomerate. That may explain why so much α 1LG4-5 was necessary to achieve an effective inhibition. It should be noted that even at the extremely high concentrations, α 1LG4-5/RAR₂₈₃₃ was unable to affect any inhibition of Lm-111 binding to the sulfatide coated microtiter plate wells. This result is in agreement with both the cell lysate IP data that LG4 contains 2 sulfatide binding sites and the sulfatide ELISA showing that the substitutions in α 1LG4-5/RAR₂₈₃₃ had the greatest effect upon sulfatide binding (almost a complete loss). Furthermore, the individual recombinant α 1LG4-5 sulfatide ELISA data were fitted using a single site algorithm, however, the recombinant proteins demonstrating the highest affinity for sulfatide (α 1LG4-5/WT, α 1LG4-5/RKR₂₇₂₁+KRK₂₇₉₃, α 1LG4-5/RKR₂₇₂₁, and α 1LG4-5/KRK₂₇₉₃) did not fit very well. Re-fitting utilizing a two-site model did improve the fits for some of these recombinant proteins (data not shown). This along with the other recombinant mutants and their mapping to the crystal structure further suggests not only

that LG4 contains 2 sulfatide binding sites but that mutation of both Arg₂₈₃₁ and Arg₂₈₃₃ represented in $\alpha 1$ LG4-5/RAR₂₈₃₃ will abolish both binding sites.

Furthermore, closer examination of the location of Arg₂₈₃₁ and Arg₂₈₃₃ in the crystal structure reveals that the reactive amine for both residues are relatively distant from one another and their side chains are oriented away from each other. Examination of the crystal structure and the mutated sequences also reveals that one of the proposed sulfatide sites is adjacent to the Ca²⁺ binding site, while the other is more distant. Since EDTA inhibition of $\alpha 1$ LG4-5/WT shows ½ maximal binding, it may be that one of the sulfatide binding sites involves the co-ordinated Ca²⁺ bound to $\alpha 1$ LG4. Future sulfatide binding experiments with individual Ala substitutions of the identified sites involved, in conjunction with or without Ca²⁺, could reveal if some sites are more affected than others. CD spectral analysis of the recombinants may also be informative in examining if any mutations resulted in gross secondary structure alterations or if removal of the Ca²⁺ from $\alpha 1$ LG4 via treatment with EDTA does.

Unfortunately, the assays with $\alpha 1$ LG4-5/RAR₂₈₃₃, $\alpha 1$ LG4-5/RAR₂₈₃₃, and $\alpha 1$ LG4-5/RAR₂₈₃₃ could not be repeated in time. It would also be very informative to repeat these inhibition experiments replacing Lm-111 with a polymerization deficient recombinant laminin, $\alpha 1$ LG1-5, or an $\alpha 1$ LG4-5/WT containing an epitope tag different from the FLAG tag on the competing $\alpha 1$ LG4-5s, in order to avoid the polymerization contribution of Lm-111 which needs to be overcome in order to better analyze the competition experiments.

Section IIID. The three dimensional structure of mouse $\alpha 1$ LG4-5 and its implications for amino acid residues identified to interact with heparin, sulfatide, and α -dystroglycan.

Despite significant differences in primary sequence, secondary and tertiary structure is highly conserved between $\alpha 1$ and $\alpha 2$ LG4-5. Furthermore, laminin $\alpha 1$ LG4-5 binds to the same cell surface molecules as $\alpha 2$ LG4-5, but to different residues present in different locations on LG4-5 and in some cases in different domains entirely. Using a similar approach as in the present study, Wizemann et al. [467] found that heparin and sulfatide binding to $\alpha 2$ LG4-5 were most strongly affected by mutation of KK_{2871} in LG4 and KLTKGTGK_{3095} in LG5, whereas α -DG binding was particularly dependent upon residues Arg_{2803} and KK_{2871} , as well as upon the calcium ion in LG4. Remarkably, neither of these critical sequences correspond to the binding sites identified in $\alpha 1$ LG4-5. The lack of conservation of functionally important residues in two such closely related proteins is unusual. Perhaps the preponderance of electrostatic interactions available for ligand binding by the laminin LG4-5 accounts for the poor conservation of binding sites. It may simply be sufficient to maintain the general basic character of the binding surfaces for interaction with some of LG4-5's ligands.

An electrostatic surface representation of $\alpha 1$ LG4-5 reveals a large, contiguous surface area of positive potential extending over both LG domains, however, the greatest concentration and intensity by far is focused in LG4 (figure 29 and 31C). Basic residues implicated in receptor binding [162] are clustered around the metal ion, presumptive Ca^{2+} , binding site in LG4. A particularly striking feature is the spatial proximity of two basic sequences implicated in several binding activities, RKR_{2721} and KRK_{2793} , which are located, respectively, at the start of β -strand C and in the H-I turn (figure 31B). The B-C loop contains Asn_{2714} , one of LG4's two glycosylation sites. Five of the six basic side chains of RKR_{2721} and KRK_{2793} are fully surface-exposed and available for receptor binding. The only exception is Arg_{2792} , which makes two hydrogen bonds with main chain carbonyl groups in the long J-K loop which contains Asn_{2811} , the

other glycosylation sites in LG4. Furthermore, the J-K loop in this region appears to make loose contacts with the body of the domain, with four internal water molecules located between the H-I loop, which contains KRK₂₇₉₃, in the front, and the F-G loop KGRTK₂₇₇₀ in the back (figure 30).

Two asparagine residues in laminin α 1 LG4, Asn₂₇₁₄ and Asn₂₈₁₁, carry bulky glycan modifications, are found near clusters of charged amino acid residues implicated in binding several ligands, and the N-linked glycosylation status of these residues directly influences ligand binding. Asn₂₇₁₄ has KDR₂₈₆₀ on one side and RK₂₈₂₀ on the other. The second glycosylation site, Asn₂₈₁₁, is also surrounded by a cluster of charge residues. It is lined on one side by KGRTK₂₇₇₀ and on the other by KRK₂₇₉₃. Furthermore, both RKR₂₇₂₁ and the Ca²⁺ ion can be found on the charged rim below it.

With the aid of the new crystal structure for mouse laminin α 1 LG4-5 that we have generated, the heparin/heparan sulfate binding site of laminin α 1 LG4 can be assigned to the basic patch made up of RKR₂₇₂₁ and KRK₂₇₉₃. Only the side chain of Lys₂₇₆₆ from the KGRTK₂₇₇₀ sequence is positioned to contribute to heparin binding. The α -DG binding site appears to be formed by a larger, semi-circular arrangement of basic side chains, with RAR₂₈₃₃ and KDR₂₈₆₀, located away from the heparin binding site, playing a key role as well as RKR₂₇₂₁. The metal ion bound to LG4 (expected to be calcium under physiological conditions) is likely to be essential for α DG, given that mutation of calcium ligands in LG4 of the related laminin α 2 chain abolished α -DG binding [467] and that equivalent calcium sites in the LG domains of neuexin and agrin are critical for biological function. Sulfatide binding is most strongly affected by mutations of basic residues on the upper face of LG4: RAR₂₈₃₃ and KGRTK₂₇₇₀. The LG4 domain of laminin α 1 likely posses binding sites for two suflatide molecules, one of which requires Ca²⁺

and both of which are inactivated by the simultaneous mutation of both Arg₂₈₃₁ and Arg₂₈₃₃.

Our earlier findings do not support a role of heparin/heparan sulfates in basement membrane anchorage, but instead argue for a prominent role of sulfated glycolipids with a signaling and perhaps also an anchorage contribution arising from α -DG [71]. Analysis of general and tissue-specific DG knockouts has revealed an essential role of DG for Reichert's membrane, but not basement membrane formation in muscle, peripheral nerve, embryo bodies, and other basement membranes where it may function primarily as a signaling receptor. A recent analysis of cultured breast epithelial cells revealed an anchoring activity for DG, raising the possibility that some cells may employ DG as an anchor in a manner similar to sulfatide or other sulfated glycolipids.

Chapter 4. Production, Characterization, and Biological Activity of Heterotrimeric Recombinant Laminin-111s.

Analysis of recombinant fragments of laminin, such as the $\alpha 1$ LG4-5s, are not just easier to manipulate and study, but necessary in order to keep separate the polymerization and anchorage activities of full length heterotrimeric laminins, so that individual contributions to basement membrane formation can be studied. However, the multiple activities and multivariate binding nature of laminin, also makes it necessary to examine mutations in the context of the heterotrimeric laminin. An understanding of these activities and binding contributions is required not only because of the importance of basement membranes in embryonic development and the pathogenesis of several diseases, but also because the insights gained into the process of basement membrane formation would provide invaluable data for developing therapeutic approaches to several diseases. Schwann cells, embryonic stem (ES) cells / embryoid bodies (EBs), C2C12 myotubes, and mouse embryonic fibroblasts (MEFs) provided platforms on which to test the various recombinant laminin-111 heterotrimeric proteins generated in human embryonic kidney fibroblast cell line HEK 293, and evaluate their ability to polymerize, interact with nidogen and type IV collagen, bind on cell surfaces, accumulate, condense, form basement membranes, and induce both differentiation and cell signaling events.

Section I. Establishment of a mixed species strategy for reliable production of recombinant heterotrimeric Lm-111s.

Several different approaches were attempted in HEK 293 fibroblasts in order to produce sufficient levels, purity, and activity of recombinant laminin-111s. Approaches utilizing all mouse chains and all human chains of laminin-111 failed. Eventually, an approach utilizing the mouse $\alpha 1$, human $\beta 1$, and human $\gamma 1$ chain each with its unique epitope tag and selective antibiotic resistance residing on the same expression construct as the recombinant chain to which it had been assigned, was developed and utilized for further evaluation.

Section IA. Establishment of an all mouse recombinant heterotrimeric Lm-111.

Our laboratory's 1997 PNAS article [\[299\]](#) described the first production of recombinant trimeric laminin-111. The mouse $\alpha 1$, $\beta 1$, and $\gamma 1$ chains were expressed in the human embryonic kidney 293 cell line, individually and in combinations. The $\alpha 1$ chain when expressed by itself was expressed with either an N-terminal or C-terminal FLAG tag, was mostly secreted, and appeared to be the only chain secreted into the media by itself, however, the majority of the $\alpha 1$ was proteolytically degraded (experiment performed by Holly Colognato and Todd Mathus). The major proteolytic fragments were 275 kDa, 175 kDa, and 150 kDa. Use of the FLAG epitope tag, N or C terminally, allowed the determination that the cleavage site for all three products was within the coiled-coil region of the $\alpha 1$ chain. The $\beta 1$ and $\gamma 1$ chains were not secreted when expressed individually or together, however, when all three chains were expressed together, they formed a heterotrimeric molecule and were secreted together and with very little degradation of the α chain observed.

The media from the HEK 293 cells was tested for expression of endogenous Lm-111 chains prior to and during expression of the recombinant chains, however, the species cross-reactivity of the antibodies (except for the FLAG tagged $\alpha 1$ chain) made it impossible to definitively prove the trimeric laminin was composed entirely of recombinant chains. This necessitated utilizing RT-PCR not only to verify which laminin chain mRNA species were present prior to and post transfection and expression, but also, delineate between the potential endogenous human chains and the transfected mouse chains. RT-PCR verified transfection identity and mRNA expression of the recombinant laminin chains and that there was no endogenous mRNA detected for mouse $\alpha 1$, $\alpha 2$, $\beta 1$, $\beta 2$, or $\gamma 1$, nor was there any detectable increase in endogenous mRNA expression of any of these endogenous chains after transfections (figure 32) [299].

Unfortunately, with time the transfected cell lines consistently became unstable and the expression of recombinant heterotrimeric Lm-111 was repeatedly lost. The progressive loss of recombinant chain expression with passage of stable cell lines was observed repeatedly. In order to help keep stable lines expressing all three chains, it was decided that from that point on, each individual laminin chain would have a unique selectable marker assigned to it and that each laminin chain expression construct would include that selectable marker as part of the construct. Both mouse $\alpha 1$ and $\alpha 2$ with either an N-terminal FLAG tag or no tag were placed into the G418 based expression vector pRCX3 (constructs: $m\alpha 1WT-g$, $m\alpha 1WT-g_{Nf}$, $m\alpha 2WT-g$, $m\alpha 2WT-g_{Nf}$, and $m\alpha 2-12bp-g_{Nf}$), mouse $\beta 1$ into the hygromycin based expression vector pcDNA3.1/hygro ($m\beta 1WT-h$), and mouse $\gamma 1$ either with or without a C-terminal FLAG tag into the puromycin based expression vector pCEP4 ($m\gamma 1WT-p$ and $m\gamma 1WT-p_{Ct}$) (figure 33). Just as in earlier published results [299], mouse $\alpha 1$ was secreted and proteolytically

degraded, however, no detectable heterotrimeric laminin was secreted (data not shown). The recombinant laminin retained in the cell was highly degraded. The same RT-PCR primers and methods utilized in the 1997 article [299] were repeated and demonstrated that the expression constructs were intact and integrated into the transfected cell line genomic DNA. Further attempts to re-establish a permanent recombinant heterotrimeric mouse Lm-111 failed. Eventually, even the actual chain identity of the earlier recombinant Lm-111 came under suspicion. There is the distinct possibility that the individual chains which constituted the heterotrimeric Lm-111 may not have all been authentic transfected chains and/or a cloning error in which an endogeneous chain had replaced a transfected chain may have occurred. Furthermore, it was discovered later (we were notified via personal communication from Takako Sasaki) that the mouse $\gamma 1$ cDNA used to make all of the expression construct contained an error within one of the EGF repeats and that this sequence error may have been a major contributing factor to the failure to re-establish the permanent cell lines.

Section IB. Establishment of an all human recombinant heterotrimeric Lm-111.

After the failure to establish an all mouse recombinant heterotrimeric Lm-111, a similar attempt was made using all human laminin chains. Like the later generation mouse constructs just discussed, each laminin chain had a unique selectable marker included in its expression construct, however, unlike the mouse constructs, each expressed chain also contained a unique epitope tag. The epitope tags enabled both chain specific detection and purification, creating artificial abilities especially critical with a heterotrimeric molecule with potential proteolysis and chain contamination/identity issues. The human $\alpha 1$ chain without any epitope tag, with an N-terminal FLAG epitope tag, or a C-terminal FLAG tag were placed into hygromycin (pcDNA3.1/hygro) and G418

(pRc/CMV2) selection based expression constructs (figure 34). Human $\alpha 1$ was also expressed in a hygromycin based vector with either its endogeneous signal sequence or the BM40 signal sequence and with or without an N-terminal FLAG tag. Human $\beta 1$ was expressed in a puromycin based vector, with an N-terminal HIS tag or with out a tag. Human $\gamma 1$ was expressed in a G418 based vector with and without a C-terminal FLAG tag. Repeated transfections of multiple combinations of the individual chains, all resulted in production of recombinant heterotrimeric Lm-111 in which most of the $\alpha 1$ chain appeared to be processed into 2 smaller fragments: the same 275 KDa and 150 KDa sized fragments that were observed previously when attempting to make an all mouse Lm-111. Western blot analysis with chain and domain specific antibodies revealed that the cleavage site appeared to be approximately one-third of the way into the coiled-coil domain of the $\alpha 1$ chain.

A final attempt was made at establishing an all human heterotrimeric recombinant laminin-111 by placing human $\alpha 1$ without an epitope tag into a puromycin based vector, placing human $\beta 1$ into a zeocin based vector without an epitope tag, and using the already established human $\gamma 1$ either with a C-terminal FLAG epitope tag or no tag in a G418 based expression construct. As in the previous attempts the linearized expression construct DNA successfully integrated into the host cell's genomic DNA and the correct full length mRNA was expressed, however, all produced heterotrimeric laminin demonstrated a high level of proteolytic cleavage and degradation.

The $\alpha 1$ chain was expressed in several different versions and purified via different strategies in an attempt to avoid this proteolytic cleavage, including: $\alpha 1$ chains without a tag, an N-terminal FLAG tag, a C-terminal FLAG tag, and $\alpha 1$ with its endogeneous signal sequence instead of the BM40 signal sequence. Furthermore, complete sequencing of the $\alpha 1$, $\beta 1$, and $\gamma 1$ expression cDNAs and corresponding mRNAs purified

from the transfected cell lines, as well as the entire mRNA transcript via RT-PCR amplification of mRNA harvested from laboratory personnel as controls, revealed no errors in the expressed recombinant mRNAs for the transfected chains which may have suggested why the $\alpha 1$ chain was being proteolytically cleaved. Despite all the effort to the contrary, there was no apparent means of easily purifying significant amounts of all human recombinant heterotrimeric Lm-111 in which the $\alpha 1$ chain had not been proteolytically processed.

Section IC. Adoption of a recombinant mouse $\alpha 1$ / human $\beta 1$ / human $\gamma 1$ containing Lm-111 strategy.

Since the $\alpha 1$ chain demonstrated proteolytic processing issues in all attempts of establishing an all human recombinant Lm-111, the all mouse recombinant Lm-111 demonstrated secretion and extensive proteolysis issues, an extensive panel of expression constructs had been created for both the human and mouse $\alpha 1$, $\beta 1$, and $\gamma 1$ laminin chains, and a human $\beta 1$ / human $\gamma 1$ laminin stable cell line had been established; a mixed species heterotrimeric recombinant Lm-111 was created by transfection of the mouse $\alpha 1$ expression construct into a stable human $\beta 1$ / human $\gamma 1$ cell line. The resulting stable cell line appeared to produce full length heterotrimeric Lm-111 with no apparent degradation associated with it and became the model system for producing future recombinant heterotrimeric laminin-111s.

Several expression constructs containing the mouse $\alpha 1$, human $\beta 1$, and human $\gamma 1$ laminin chains were made. Figures 35-37 depict the mouse $\alpha 1$ recombinant proteins expressed from the mouse $\alpha 1$ expression constructs made and listed in Table 5. Table 6 provides the details concerning the construction of the $\alpha 1$ chain expression constructs. Figure 38 depicts the human $\beta 1$ recombinant proteins, Table 7 a summation of the

individual $\beta 1$ constructs, and Table 8 the details of the $\beta 1$ constructs' construction. The human $\gamma 1$ recombinant proteins expressed are depicted in Figure 39, with Table 9 and 10 providing the summation of constructs and their construction details. The expression constructs were stably transfected into the fibroblast HEK 293 cell line to produce the resulting modified recombinant protein sequences for the $\alpha 1$, $\beta 1$ and $\gamma 1$ chains of laminin depicted in Figures 35-37 (mouse $\alpha 1$ based constructs), 38 (human $\beta 1$ based constructs), and 39 (human $\gamma 1$ based constructs). The individual constructs were transfected in sequential order and a unique antibiotic selection employed for each chain. Epitope tags were placed either at the amino or carboxyl terminus of the subunits to aid in selection of 293 cell clones expressing one, two, or three subunits, with both the Flag tag and heparin affinity used for purification of the recombinant trimeric laminins. Stable clones expressing laminin heterotrimers consisting of appropriate appearing $\alpha 1$, $\beta 1$ and $\gamma 1$ chains were selected and expanded. Table 11 contains a partial list of the recombinant heterotrimeric Lm-111s generated, their designation, and expression construct composition. Wild-type laminins containing either an N-terminal Flag tag on the α chain and no $\gamma 1$ tag (WTa; Lm-111_{Nf/Nh/0}), or containing an N-terminal myc tag on the α chain with a $\gamma 1$ C-terminal Flag tag (WTb; Lm-111_{Nm/Nh/Cf}), or with an N-terminal Flag tag on the α chain with a $\gamma 1$ C-terminal Flag tag (WTc; Lm-111_{Nf/Nh/Cf}) were created. There were no appreciable differences observed between the three laminins in stability, polymerization, or ability to assemble BMs on Schwann cells (SCs). Lm-111_{Nm/Nh/Cf} was used for subsequent studies unless otherwise indicated. Figure 40 shows the coomassie blue stained PAGE gels of some of the recombinant Lm-111s produced. Protein yields were typically about 10 to 20 $\mu\text{g/ml}$ of recombinant heterotrimeric laminin per three day harvest from conditioned medium of confluent stable clones.

When it came time to place epitope tags on the N-terminus of the individual laminin chains for creation of recombinant heterotrimeric laminin-111s the same concerns as with the $\alpha 1$ LG4-5 constructs existed: the potential for improper transport, processing, secretion, clipping, instability, and degradation due to the non-native signal sequence and N-terminal epitope tag. An added concern was that several binding activities as well as laminin's polymerization activity were located in the N-terminal LN domain. Epitope tag interference with any of these activities was a major concern, therefore, several different epitope tags were examined by placement on the N- and C-termini of full length laminin chains in order to gauge, not only, their usefulness in detection and purification, but also, any affect they may have upon laminin's normal functions. N-terminal FLAG, myc, HA, VSV-G, and protein-C epitope tags and a C-terminal FLAG tag on the $\alpha 1$ chain had no detrimental effects upon the resulting recombinant laminin's synthesis, secretion, processing, ability to polymerize, or accumulation on the surface of Schwann cells (figure 41). However, an N-terminal triple myc tag (myc₃) blocked Lm polymerization and prohibited effective accumulation of Lm on Schwann cells. Furthermore, the recombinant laminins demonstrated no proteolytic degradation and all N-terminal epitope tags were recognizable with their corresponding antibody in both Westerns of collected media and immunoprecipitations utilizing the epitope tag (figure 41B and C). Subsequent $\alpha 1$ chain expression constructs were synthesized with an N-terminal myc epitope tag.

Three full length human $\beta 1$ expression construct were made: one with no tag, one with a N-terminal VSV-G epitope tag, and a third with a N-terminal HA tag. Both the untagged and VSV-G tagged $\beta 1$ recombinant heterotrimeric proteins had no detectable proteolytic degradation. The HA tagged $\beta 1$ producing cells did produce a small amount of proteolytically processed material; this was probably due to the fact that the HA

tagged $\beta 1$ protein demonstrated the ability to be secreted without any accompanying $\alpha 1$ and $\gamma 1$ laminin chains (data not shown). Both the VSV-G and HA tagged $\beta 1$ proteins were immunoreactive when the appropriate epitope specific antibodies were utilized and neither showed any inhibition to binding on Schwann cell surfaces (data not shown). Subsequent $\beta 1$ chain expression constructs utilized a N-terminal HA tag for the $\beta 1$ laminin chain.

Laminin $\gamma 1$ chain expression constructs were designed to contain a $\gamma 1$ chain with either a C-terminal FLAG tag or no tag.

Each laminin chain was also assigned a unique selectable marker. The testing of various antibiotic combinations and dosage requirements in order to obtain three which could be used simultaneously was previously described in the $\alpha 1$ LG4-5 section of this thesis. In most cases, puromycin (at 1ug/ml) was assigned to $\alpha 1$ chain expression constructs, zeocin (at 80-100ug/ml) to $\beta 1$ constructs, and neomycin (at 500ug/ml of G418) to $\gamma 1$ constructs. Furthermore, most expression constructs contained the 5'UTR "consensus-1", as well as the BM40 signal sequence and an EK cleavage site immediately downstream of any N-terminal epitope tags which were utilized in the expression constructs.

Section II. Characterization of recombinant Lm-111s.

Purified recombinant heterotrimeric laminins were analyzed by SDS-PAGE, immunoprecipitation, and Western analysis. All three chains were detected with epitope-specific and laminin specific antibodies after the recombinant laminins were immunoprecipitated with a subunit-tag specific antibody. Wild type protein exhibited a typical Coomassie blue stained pattern of three bands corresponding to the α 1, β 1 and γ 1 subunits. Deletion of different domains resulted in the expected observation of increased migration with no discernable proteolytic degradation (figure 40). Deletion of the β 1 LN domain resulted in a superimposition of the normally faster migrating γ 1 band by the shortened β 1 band and deletion of almost the entire α 1 short arm (domains LN – L4b) resulted in superimposition of the α 1 band on the β 1 band.

Rotary showed Pt/C replicas were prepared and examined for many of the recombinant laminins, including: Lm-111_{Nf/Nh/O} (WTa), Lm-111_{Nm/Nh/Cf} (WTb), Lm-111 $\beta\Delta$ LN-LEa_{0/Nh/Cf}, Lm-111 $\gamma\Delta$ LN-LEa_{Nm/Nh/Cf}, Lm-111 $\gamma\Delta$ LN_{Nm/Nh/Cf}, Lm-111 $\alpha\Delta$ LN-L4b_{Nm/Nh/Cf}, Lm-111 $\alpha\Delta$ LN_{Nm/Nh/Cf}, and Lm-111 $\alpha\Delta$ LG1-5_{Nm/Nh/Cf} (appendix figures 2 and 3) (rotary shadow photographs taken by Peter Yurchenco). All samples examined revealed a population of monomeric heterotrimers. Loss of the expected LN domains, LG domains, or larger N-terminal deletions of the short arms could be detected in well-spread laminins. Several of the recombinant laminins depicted in the appendix figures clearly show the “short arms” (N-terminal sequence prior to coiled-coil) of α 1, β 1, and γ 1, the coiled-coil, the C-terminal α 1 LG domains, and the lack of N-terminal domains and C-terminal LG1-5 in three of the recombinant deletion mutants.

Section IIA. Polymerization of recombinant Lm-111s.

A standard assay of laminin polymerization was employed to evaluate the recombinant laminins. The assay consists of incubating small aliquots of laminin at different concentrations in neutral salt buffer (TBS) containing 1mM calcium chloride at 37°C, followed by centrifugation to separate the pellet containing the polymer fraction from the supernatant containing the free non-polymerized laminin, and analysis by SDS-PAGE with quantitation of Coomassie blue stained and scanned gel bands by densitometry [51]. This assay was used to evaluate polymerization of the different heterotrimeric recombinant laminins (appendix figure 4). Most polymerization assays and quantifications, as well as protein purifications of the heterotrimeric laminins for the polymerization assays, were performed by Karen McKee. Wild type laminin polymerized in a concentration dependent fashion. Plots of polymer concentration vs. total concentration revealed a slope of 0.81 ± 0.21 and an x-axis intercept of 0.091 ± 0.03 mg/ml (average \pm S.D., $n = 7$), the latter corresponding to the apparent critical concentration of polymerization ($0.13 \mu\text{M}$; appendix figure 5). EHS-laminin typically has a slope of 0.9 to 0.95 and a similar ($0.14 \mu\text{M}$) critical concentration. Polymerization was prevented, as typically seen with EHS laminin, by incubating the recombinant laminin in TBS containing 1 mM EDTA instead of calcium. Laminins with deletions of the LG domains (Lm-111 $\alpha\Delta\text{LG1-5}_{\text{Nm/Nh/Cf}}$, Lm-111 $\alpha\Delta\text{LG1-3}_{\text{Nm/Nh/Cf}}$, and Lm-111 $\alpha\Delta\text{LG4-5}_{\text{Nm/Nh/Cf}}$) or point mutations in LG4 (Lm-111 $\alpha\text{RKR}_{2721\text{Nm/Nh/Cf}}$, Lm-111 $\alpha\text{KRK}_{2793\text{Nm/Nh/Cf}}$, and Lm-111 $\alpha\text{RAR}_{2833\text{Nm/Nh/Cf}}$), also polymerized in a manner similar to WT laminin. However, all recombinant laminins with deletions of N-terminal LN domains did not polymerize: $\alpha 1\Delta\text{LN}$ showed very little aggregation and only at concentrations above 0.4 mg/ml, while $\beta 1\Delta\text{LN}$ and $\gamma 1\Delta\text{LN}$ did not polymerize in the concentration range analyzed. Furthermore, any recombinant laminins containing deletion of the LN domain

and additional downstream domains: Lm-111 $\alpha\Delta$ LN-LEa_{Nm/Nh/Cf}, Lm-111 $\alpha\Delta$ LN-L4a_{Nm/Nh/Cf}, Lm-111 $\beta\Delta$ LN-LEa_{0/Nh/Cf}, and Lm-111 $\gamma\Delta$ LN-LEa_{Nm/Nh/Cf}; also failed to polymerize. The heterotrimeric laminin, Lm-111 $\alpha\Delta$ LN-L4b_{Nm/Nh/Cf}, lacking almost the entire α -subunit short arm (α 1 Δ LN-L4b), a model for the truncated laminins-3A11, -3A21, -411 and -421 found in a variety of tissues, also did not polymerize.

Two recombinant Lm-111s were generated to further test the LN requirements for laminin polymerization (cloning and polymerization assays performed by Karen McKee). If laminin polymer formation is a consequence of a ternary complex requiring three different LN domains, one from each laminin subfamily (i.e. one α chain, one β chain, and one γ chain), then substitution of the γ 1 chain's LN domain with the LN domain from the β 1 or α 1 chain should result in loss of polymerization capability for that recombinant laminin. If on the other hand, the individual LN domains can bind themselves or other members within or outside their family and three separate LNs from three separate chain family members is not required as reported by Odenthal et. al [468], then replacement of the γ 1 LN by the α 1 LN, construct Lm-111 γ 1 $\Sigma\alpha$ 1LN_{Nm/Nh/Cf}, should not result in a loss of polymerization. Furthermore, if Odenthal was correct in reporting α 1 LN to α 1 LN binding, deletion of the N-terminal LN domain of the β 1 or γ 1 chain should not completely abrogate polymerization. Our observed results were that any domain substitution or N-terminal LN domain deletion was associated with an inability of the resulting recombinant laminin to polymerize, supporting the prediction that the three different domains, one from each family subfamily, are required for polymerization.

This hypothesis was further supported by direct binding assays utilizing individual recombinant LN-LEb α 1, β 1, and γ 1 proteins, derived from just three expression constructs, in various combinations. The α 1LN-LEb_{v/m} expression construct secretes a mouse α 1 recombinant protein containing the N-terminal LN-LEb5 of mouse α 1 with a

C-terminal TEV protease cleavage site, followed by a FLAG epitope tag and Enterokinase cleavage site, and a terminal myc epitope tag (figure 42A). The recombinant protein was purified with FLAG matrix and some purified protein processed with EK to yield $\alpha 1\text{LN-LEb}_{\text{tf}}$ which possesses a C-terminal FLAG epitope tag and no myc tag (figure 42B). The recombinant protein could also be processed with TEV to yield $\alpha 1\text{LN-LEb}_t$ which contains no epitope tags. The $\beta 1\text{LN-LEb}_{\text{tf/h}}$ expression construct produces mouse $\beta 1\text{LN}$ through LEb_5 , with a C-terminal TEV site, followed by the FLAG epitope tag and accompanying EK cleavage signal sequence, with a terminal HA epitope tag. EK treatment of purified $\beta 1\text{LN-LEb}_{\text{tf/h}}$ produced $\beta 1\text{LN-LEb}_{\text{tf}}$ with no HA epitope tag. A similar process was utilized with mouse $\gamma 1$ to produce $\gamma 1\text{LN-LEb}_{\text{tf/h}}$ and $\gamma 1\text{LN-LEb}_{\text{tf}}$. Both EK processed and unprocessed recombinant LN-LEb proteins were then evaluated in a solid phase ELISA assay in which $\alpha 1\text{LN-LEb}_{\text{tf/m}}$ was bound to anti-myc Ab coated microtiter plate wells and various combinations of the recombinant LN-LEb proteins tested for binding to $\alpha 1$ via the C-terminal HA epitope tag on the added recombinant proteins (figure 42C). The $\alpha 1$ chain construct did not demonstrate significant self-binding in the assay, nor was $\alpha 1$ observed to significantly bind to $\beta 1$ or $\gamma 1$ without all three chains being present. The only significant binding observed was when all three laminin chains, $\alpha 1$, $\beta 1$, and $\gamma 1$, were present together.

Section IIB. Heparin affinity of recombinant laminin-111s and laminin-211s.

Heparin FPLC of various recombinant laminin-111s and laminin-211s, revealed that Lm-111 binds heparin with a slightly higher affinity than Lm-211. The deletion heterotrimeric recombinant Lm-111s and recombinant $\alpha 1\text{LG4-5s}$, demonstrated that the majority of heparin binding activity possessed by laminin-111 was contributed from LG4, with some from LG1-3 (figure 43A). In contrast, LG4-5 provided very little heparin binding activity in

laminin-211 (figure 43B). The vast majority of heparin binding activity in Lm-211 was derived from LG3 contributions. Both Lm-111 and Lm-211 demonstrated a small degree of heparin binding from outside LG1-5; most likely contributed from the N-terminal LN domains of $\alpha 1$ and $\alpha 2$ laminin.

The various recombinant Lm-211 proteins tested were obtained from stable cell lines provided by Dr. Sergei Smirnov [296] of our laboratory.

Section IIC. Sulfatide affinity of recombinant laminin-111s and laminins-211s.

Domain deletion containing recombinant heterotrimeric laminins reveal that the sulfatide binding of recombinant Lm-111 largely depends upon sulfatide contributions from the LG4-5 domain of the $\alpha 1$ chain. There may be minor contributions from the $\alpha 1$ LN and LG1-3 domains, however, the majority of the sulfatide binding activity resides in LG4 (figure 44A). This binding activity is completely abolished with AEBSF treatment, greatly reduced in the presence of heparin, partially EDTA sensitive, but not Triton (1-2%) sensitive (figure 44B and C). Furthermore, while recombinant Lm-111 can bind more sulfatide than Lm-211, both proteins exhibit similar K_d values (figure 44D). The proteolytically processed form of Lm-211, in which cleavage has occurred in the LG3 domain but the cleaved C-terminal fragment maintains non-covalently attached to the laminin, demonstrates a significant reduction in sulfatide affinity.

Furthermore, recombinant Lm-111_{Nm/Nh/Cf} was shown to specifically bind sulfatide albumin complexes which had been allowed to settle in DMEM media onto tissue culture treated plastic (figure 45). No binding was observed between Lm-111 and galactosyl ceramide, the non-sulfated analog of sulfatide, complexes. Furthermore, Lm-111 binding to the sulfatide albumin complexes was partially inhibited with EDTA and greatly

inhibited by heparin. The observed binding behaviour of Lm-111 was in agreement with similar experiments performed with Lm-111 in the solid phase sulfatide ELISA experiments.

Section III. The role of laminin-111 and its receptors in Schwann cells.

Laminin-111 possesses both α DG and sulfatide binding capabilities via its α 1 LG4 domain. Schwann cells not only express both α DG and sulfatide, but also, form a basement membrane (BM) *in vivo* which incorporates laminin, therefore, they were a natural choice for study.

Section IIIA. Individual domain and amino acid residue requirements of Lm-111 for BM formation on the surface of cultured Schwann cells.

Earlier work in our laboratory had shown that AEBSF treatment of Lm-111 not only eliminated its ability to polymerize, but also, negated its ability to accumulate on SC surfaces. It was believed that the lack of measurable laminin binding to the Schwann cell surface was due primarily to AEBSF's inhibition of laminin's ability to polymerize. However, sulfatide binding assays revealed that AEBSF treatment of both Lm-111 and α 1 LG4-5 also completely inhibited their ability to bind sulfatide. Therefore, AEBSF treatment destroyed not only laminin's polymerization activity centered in the N-terminal LN domains of the individual laminin chains, but also, its C-terminal α 1 LG4 anchorage activity through sulfatide binding, thereby, explaining why AEBSF treated heterotrimeric Lm-111 bound Schwann cells and sulfatide even less than recombinant Lm-111s with defunct polymerization capabilities due to N-terminal LN deletion (figure 46). Laminin-111 accumulation on the surface of cultured Schwann cells was also severely inhibited by the polymerization inhibiting fragments C1-4, E1' and E4, as well as the anchorage inhibiting fragment E3 analog, recombinant α 1LG4-5/WT_{Nf}, but not fragment E8 (figure 46). The inhibitory effect of C1-4, E4, E1', and α 1LG4-5/WT_{Nf} were reversible if the fragments and recombinant protein were first treated with AEBSF.

Mutant α 1LG4-5 proteins were tested for their ability to block Lm-111 accumulation on the Schwann cell surface (figure 47). Lm-111(U) (20ug/ml) was mixed with increasing amounts (1, 10, 20, 50, 100, 200, 300, and 400ug/ml) of the recombinant α 1LG4-5 proteins and incubated for 30 minutes at 37°C in cultures of confluent Schwann cells. The amount of Lm-111 which bound to the surface of the Schwann cells was measured and thus the ability of the α 1LG4-5s to inhibit the Lm-111 binding compared. Recombinant α 1LG4-5/KDR₂₈₆₀ was the most effective inhibitor of Lm-111 binding followed closely by α 1LG4-5/WT. After WT the order of inhibition was α 1LG4-5/RAR₂₈₃₃ > α 1LG4-5/KRK₂₇₉₃ > α 1LG4-5/RKR₂₇₂₁ > α 1LG4-5/RKR₂₇₂₁ which were all much greater than no treatment with α 1LG4-5, except for the double mutant. Mixture of Lm-111 with the recombinant double mutant α 1LG4-5/RKR₂₇₂₁+KRK₂₇₉₃ actually resulted in an observed persistent increase in Lm-111 binding to the Schwann cell surface.

Our laboratory has previously shown that incubation of Schwann cells with exogenous laminin-111 results in the formation of a basement membrane like ECM on the exposed, previously free cell surface, resulting in accumulation of Lm-111, nidogen-1 and type IV collagen [71, 469] (appendix figures 6-9). The cells express no detectable endogenous laminin, but do express low levels of nidogen-1 and type IV collagen which are not retained on the cell surface (appendix figure 10). If laminin-111 is exogeneously added to the media of a 12 hour culture of Schwann cells and allowed to incubate at 37°C for one hour; the laminin, nidogen, collagen and other components will accumulate and form a BM on the Schwann cell surface. However, if the cells are washed prior to addition of laminin, no appreciable detectable nidogen or collagen will accumulate. This cell surface assembly process depends upon the presence of galactosyl-sulfatide on the cell surface which provides anchorage to the laminin through its LG4 domain.

To analyze the ability of modified laminins to assemble a BM, SCs were incubated in fresh medium containing 20 $\mu\text{g/ml}$ of recombinant protein for one hour (figure 48). The cells were then washed, fixed, and incubated with laminin-111 specific polyclonal antibody which detects all three laminin subunits or a $\beta 1$ LN domain specific antibody (anti-E4) which will detect all recombinant Lm-111s except for those missing the $\beta 1$ LN domain. Digital microscope images were recorded and then analyzed to determine the relative amount of cell surface bound fluorescence divided by the number of DAPI-stained nuclei to normalize the data to cell number. Lm-111_{Nf/Nh/0} (formerly WTa) and Lm-111_{Nm/Nh/Cf} (formerly WTb) recombinant laminin showed nearly identical levels of fluorescence (data not shown). Lm-111_{Nm/Nh/Cf} laminin fluorescence was then compared to that produced by incubation with equal concentrations of EHS Lm-111(U), EHS Lm-111(B), EHS Lm-111 treated with AEBSF, and recombinant laminins with various alterations, including those with: different epitope tags (Lm-111_{0/0/0}, Lm-111_{0/Nh/0}, Lm-111_{0/Nh/Cf}, Lm-111_{Cf/Nh/0}, Lm-111_{0/Nv/Cf}, Lm-111_{Nm/Nh/0}, Lm-111_{Nm3/Nh/0}, Lm-111_{Nv/Nh/0}, Lm-111_{Nh/Nh/0}, Lm-111_{Nc/Nh/0}, and Lm-111_{Nf/Nh/0}), deletions of N-terminal domains (Lm-111 $\Delta\alpha\text{LN}$ _{Nm/Nh/Cf}, Lm-111 $\Delta\alpha\text{LN-LEa}$ _{Nm/Nh/Cf}, Lm-111 $\Delta\alpha\text{LN-L4a}$ _{Nm/Nh/Cf}, Lm-111 $\Delta\alpha\text{LN-LEb}$ _{Nm/Nh/Cf}, Lm-111 $\Delta\alpha\text{LN-L4b}$ _{Nm/Nh/Cf}, Lm-111 $\Delta\beta\text{LN}$ _{0/Nh/Cf}, Lm-111 $\Delta\beta\text{LN-LEa}$ _{0/Nh/Cf}, Lm-111 $\Delta\gamma\text{LN}$ _{Nm/Nh/Cf}, and Lm-111 $\Delta\gamma\text{LN-LEa}$ _{Nm/Nh/Cf}), chemical modification with AEBSF(Lm-111_{Nm/Nh/Cf-A}), C-terminal deletions of the $\alpha 1$ chain (Lm-111 $\Delta\alpha\text{LG1-5}$ _{Nm/Nh/Cf}, Lm-111 $\Delta\alpha\text{LG1-3}$ _{Nm/Nh/Cf}, and Lm-111 $\Delta\alpha\text{LG4-5}$ _{Nm/Nh/Cf}), and point mutations of the $\alpha 1$ chain's LG4 domain (Lm-111 αRKR _{2721Nm/Nh/Cf}, Lm-111 αKRK _{2793Nm/Nh/Cf}, and Lm-111 αRAR _{2833Nm/Nh/Cf}). Only one variant of the three constructed for each α chain domain deletion of LEa, L4a, L4b, and LEB was included in this analysis, however, it should be noted that all variants were tested and performed similarly (data not shown).

During the purification of Lm-111 from harvested EHS tumor, the unbound peak from the DEAE-Sepharose ion exchange chromatography column consists of Lm-111 without intact nidogen attached (either no nidogen or various proteolytic fragments of nidogen) and is called Lm-111(U), whereas, the bound Lm-111 peak contains intact nidogen bound to it and is called Lm-111(B) [48, 470]. The highest level of fluorescence was observed with EHS Lm-111(U) followed closely by Lm-111(B) and then recombinant WT Lm-111s, irregardless of the N-terminal or C-terminal epitope tags employed, except for the $\alpha 1$ N-terminal triple myc in Lm-111_{Nm3/Nh/0}, which effectively inhibited the ability of the recombinant Lm-111 to polymerize and thereby accumulate on the surface of the Schwann cells. Incubation of SCs with laminins unable to polymerize, either lacking an N-terminal LN domain (or more), triple myc epitope tag, or chemically treated with AEBSF, resulted in very low levels (<10 % of WT) of laminin fluorescence, indicating very low binding of the laminins. All of these polymerization incompetent laminins were unable to polymerize in the standard sedimentation assay employed. Furthermore, any deletion of $\alpha 1$ LG4 or $\alpha 1$ LG4 point mutation recombinant laminin which adversely affected binding to sulfatide or dystroglycan also resulted in a recombinant laminin incapable of appreciable accumulation on the surface of the Schwann cells. Interestingly, the recombinant Lm-111 containing a deletion of $\alpha 1$ LG1-3 resulted in near WT coverage of the Schwann cells. Colocalization of α DG revealed, not only, that the Lm-111(B) fraction containing nidogen bound slightly better than the Lm-111(U) fraction which does not contain intact nidogen, but also, that the α DG signal colocalized better and quicker in the Lm-111(B) treated Schwann cells (figure 49). The addition of exogenous laminin also resulted in a consistently observed increase in α DG signal; indicating some type of upregulation of DG expression or release from intracellular sources. Furthermore, α DG colocalization and condensation with laminin was observed

even if LG1-3 was missing from the laminin, however, if the exogenous laminin did not possess LG4 there was no α DG colocalization nor condensation of the α DG signal observed. Therefore, it is also clear Lm-111s lacking either N-terminal LN domain polymerization activity or anchorage provided through the C-terminal α 1LG4 are unable to accumulate to appreciable levels on the surface of Schwann cells, α DG colocalization and condensation require α 1 LG4, Lm binding to the cell surface is increased in the presence of nidogen, and binding through β 1 integrin is not required for this process.

Recombinant heterotrimeric laminin bearing point mutations in LG4 were also observed to have significantly decreased binding to the Schwann cell surface. Mutagenesis of RKR₂₇₂₁ (Lm-111 α RKR_{2721Nm/Nh/Cf}), KRK₂₇₉₃ (Lm-111 α KRK_{2793Nm/Nh/Cf}), and RAR₂₈₃₃ (Lm-111 α RAR_{2833Nm/Nh/Cf}) resulted in nearly a 90% reduction in laminin binding to the cell surface (figure 50). As predicted by the solid phase assay results of both the recombinant α 1LG4-5 and heterotrimeric recombinant point mutation laminins, the mutation of RAR₂₈₃₃, which practically eliminates the ability of laminin to bind sulfatide through LG4 still colocalizes with the α DG signal and the α DG displays some condensation, however, the mutation which predominately affects α DG binding, RKR₂₇₂₁, displays no colocalization with α DG nor does the α DG exhibit any condensation. Furthermore, the exogenous addition of any of the three heterotrimeric recombinant point mutation Lm-111s, did not result in the increase of α DG previously observed with recombinant Lm-111s which contained α 1 LG4-5.

Since purified Lm-111(B), which contains intact nidogen associated with it, bound to the surface of Schwann cells better than any of the recombinant Lm-111 WTs, which themselves contain no nidogen associated with them because the HEK 293 cells utilized to produce the recombinant proteins does not express nidogen; exogenous nidogen

and type IV collagen were added to the recombinant Lm-111 WT to see if binding could be improved to the level observed with Lm-111(B) and determine what, if any, role nidogen and type IV collagen may play in laminin binding, accumulation, or condensation. The addition of exogenous Lm-111 with the simultaneous equimolar addition of nidogen and collagen or just collagen resulted in a small increase in observed binding of Lm-111 to the Schwann cell surface, however, the simultaneous addition of just nidogen actually resulted in a small decrease in observed laminin binding (figure 50). The contributions of nidogen-1 and type IV collagen to the exogenous Lm-111 driven basement membrane component accumulation on SC surfaces were examined later in further detail by Stephanie Capizzi in a series of experiments utilizing the various recombinant heterotrimeric laminins produced (appendix figure 13) [471].

Section IIIB. Ultrastructure of Schwann cell surfaces with and without the addition of exogenous Lm-111s.

Schwann cells treated with EHS-laminin or recombinant laminins (50 µg/ml) for one hour were washed, fixed, embedded in epon and sectioned perpendicular to the flat surface of the plastic substrate. Metal stained cross sections of adherent cells were observed by electron microscopy. Cells were often located adjacent to each other. Basement membranes in WT laminins appeared as continuous or near-continuous linear densities (lamina densa) separated by a thin lucent line (lamina lucida) and measured 25 to 50 nm in thickness from the edge of the exposed plasma membrane. They were positioned on most of the cell surface but often spared the nuclear region and most peripheral (thin) cell extensions. As expected based upon the immunohistochemical staining results, electron micrographs of Schwann cells treated with polymerization incompetent, Lm-111 $\Delta\beta$ LN-LEa_{Nm/Nh/Cf}, showed barely any BM with very short segments dispersed

throughout the cell surface (figures 51 and 52). Treatment with recombinant Lm-111 $\Delta\alpha$ LG4-5_{Nm/Nh/Cf}, demonstrated even less "coverage", whereas, Lm-111 $\Delta\alpha$ LG1-3_{Nm/Nh/Cf} treatment resulted in a much more consistent but still patchy "coverage", approximately three-quarters of WT coverage. Also, just like the immunohistochemical results, the α 1 LG4 point mutation recombinant proteins, Lm-111 α RKR_{2721Nm/Nh/Cf} and Lm-111 α RAR₂₈₃₃, provided a little more coverage than the complete loss of α 1 LG4 (Lm-111 $\Delta\alpha$ LG4-5_{Nm/Nh/Cf}) and less than, just loss of polymerization activity only, mutant Lm-111 $\Delta\beta$ LN-LEa_{Nm/Nh/Cf}.

The contributions of nidogen-1 and type IV collagen to the exogenous Lm-111 accumulation and basement membrane formation on the surface of Schwann cells was also examined by electron microscopy utilizing the various recombinant heterotrimeric laminins produced (electron microscopy by Peter Yurchenco) (appendix figure 14) [471]. Exogenous recombinant Lm-111_{Nm/Nh/Cf} produced a continual basement membrane, whereas, recombinant Lm-111s missing either the N-terminal α 1 LN domain or C-terminal α 1 LG1-5 failed to; resulting in a few small discrete extracellular aggregates on the cell surface. The simultaneous addition of both collagen and nidogen, which did not accumulate on the Schwann cell surface without contemporaneous addition of laminin, resulted in a much denser and thicker basement membrane on Schwann cells when added simultaneously with Lm-111_{Nm/Nh/Cf}. The contemporaneous addition of type IV collagen, nidogen, and either Lm-111 Δ LG1-5_{Nm/Nh/Cf} or Lm-111 Δ LN_{Nm/Nh/Cf} produce an increase in the number of aggregates observed on the cell surface over that seen without the addition of both type IV collagen and nidogen.

Section IIIC. Comparison of laminin-111 and lamininm-211 accumulation and BM formation on Schwann cell surfaces.

The accumulation and BM formation capabilities of both Lm-111 and Lm-211 on Schwann cells was compared by incubating 20ug/ml of each laminin at 37°C for one hour on sparsely plated Schwann cells and staining with a monoclonal antibody specific to the $\gamma 1$ chain common to both Lm-111 and Lm-211. Overall Lm-111 staining was much more intense than Lm-211, whose signal had to be increased 2 fold for proper analysis (figure 53). There was no endogenous Lm-111 or Lm-211 produced by the Schwann cells. The unbound fraction of Lm-111(U) purified from EHS tumor gave the highest signal level, followed closely by the bound fraction of Lm-111(B), and then recombinant Lm-111/WT_{Nm/Nh/Cf}, with just a 10% decrease in observed binding on Schwann cell surfaces. The unprocessed recombinant Lm-211 binding and accumulation on the Schwann cell surfaces was approximately one-half that of recombinant Lm-111/WT_{Nm/Nh/Cf}. Processed recombinant Lm-211 signal intensity was 85% less than unprocessed Lm-211. Deletion of either $\alpha 1$ or $\alpha 2$ LG1-5 led to a complete loss of binding to Schwann cell surfaces. While deletion of $\alpha 2$ LG1-3 demonstrated a 90% decrease in binding when compared to Lm-211u, the corresponding LG1-3 deletion in $\alpha 1$, resulted in just a 15% reduction in binding. The deletion of $\alpha 2$ LG4-5u led to an 85% decrease in binding, comparable to Lm-211p levels, whereas, the processed deletion of LG4-5 resulted in a complete loss of binding. The comparable deletion of LG4-5 in $\alpha 1$ led to a 95+% reduction in signal intensity. The Schwann cell coverage results are in agreement with the solid phase sulfatide binding affinities of Lm-111 and Lm-211 observed and compared earlier in the recombinant heterotrimeric Lm-111s characterization section. Lm-211 probably only possess a single binding site and it requires sequences in LG5 not LG4 as is the case for $\alpha 1$ (and/or

sequences either within LG3 or other sequences which require a specific orientation of LG5 which processing alters) and a higher affinity for α DG than Lm-111 and, unlike Lm-111, Lm-211 α DG binding also requires a contribution from LG1-3 in α 2 for efficient α DG binding. The contribution from α 2 LG1-3 may involve direct participation of a grouping of charged amino acid residue which constitute the furin cleavage site in LG3. However, it may also involve a structural component and LG1-3's influence on the structure of LG4-5 or orientation of LG4-5 with respect to LG1-3. Examination of the crystal structure of the α 1 and α 2 LG4-5 domains reveals a significant difference in the orientation of their respective LG4 and LG5 domains, as well as, the volume of space between the two domains' facing sides. When coupled with the observed disulfide linkage between the hinge region preceding LG4 and the downstream LG5 domain linking the two domains together, in conjunction with α 2's much longer linker region between LG3 and LG4, and the differences in binding affinities between α 2 processed and unprocessed laminin-211, suggest that perhaps α 2 LG1-3 may exert a structural and/or orientation influence upon LG4-5 and thereby affect specific binding affinities in α 2.

Section IV. The role of laminin-111 in embryonic stem cell differentiation, basement membrane formation, and embryo body formation.

β 1 integrin null, γ 1 laminin null, and dystroglycan null embryonic stem (ES) cells were examined for their ability to differentiate and form an outer endodermal layer, assemble a basement membrane (BM) on the basal side of the endodermal layer, differentiate and form an inner polarized epiblast layer underneath the BM, cavitate, and form a proper embryo body (EB) much as WT ES cells will when properly dispersed in LIF-free medium for several days (appendix figure 15). This developmental progression was

observed in WT ES cells with endoderm appearing in 3-4 days, a BM underneath the outer developing endodermal layer in 4-5 days, epiblast formation under the BM layer in 5-7 days, and cavitation and eventual formation of a central cavity in 6-8 days (71). Aumailley et al. [472] had previously shown that $\beta 1$ integrin null ES cells will form a outer endodermal layer, however, the $\alpha 1$ laminin chain synthesis is rapidly switched off in the derived EBs in a $\beta 1$ integrin dependent/mediated feed-back regulatory mechanism and without the $\alpha 1$ laminin chain, any synthesized $\beta 1$ and $\gamma 1$ laminin chains will fail to form a trimeric laminin and be secreted into the extracellular space. Furthermore, without Lm-111 present, the EBs fail to form a BM on the basal side of the outer endodermal layer and fail to differentiate further, i.e. do not form an inner epiblast layer or cavitate. Similarly, EBs derived from $\gamma 1$ laminin null ES cells, do form an outer endodermal layer, but fail to deposit a BM on the basal side of the endodermal layer, differentiate to form an epiblast layer, or cavitate. The EBs produce no Lm-111 and the small amount of $\alpha 1$ laminin subunit produced undergoes proteolytic degradation resulting in a truncated $\alpha 1$ laminin chain [31]. DG null ES cells were previously reported [172] to aggregate but fail to differentiate and form embryoid bodies.

When Dr. Li, of our laboratory, cultured WT ES cells to form EBs he was able to obtain 72% BM formation and 64% epiblast differentiation [70]. The $\beta 1$ integrin null ES and $\gamma 1$ laminin null ES cell lines did not form a basement membrane or differentiated epiblast layer without the addition of exogenous laminin. With the addition of exogenous laminin-111, 46% and 18% of $\beta 1$ integrin null and 57% and 34% of $\gamma 1$ laminin null EBs, formed basement membranes and a differentiated epiblast layer, respectively. Despite published reports to the contrary, the DG null ES cell line was able to form EBs and a BM was observed to spontaneously develop in 72% of the EBs which formed; of which 64% also possessed a differentiated epiblast layer.

Later, experiments demonstrated increased efficiencies in BM formation and epiblast differentiation, perhaps due to alterations in the preparation of the recombinant laminins or alterations in experimental procedures, but also likely due to a change in the recombinant laminin chain composition; specifically, the removal of the C-terminal FLAG epitope tag from the $\gamma 1$ laminin chain. The inclusion of a FLAG tag on the C-terminus of the laminin $\gamma 1$ chain was later shown to abolish the ability of recombinant heterotrimeric laminins to bind $\beta 1$ integrin (work of Karen McKee; data not shown). Not only did the overall EB formation from cultured ES cells efficiency increase, but approximately 87% of all WT ES cells formed a proper BM on the basal side of an outer endodermal layer and 82% a polarized differentiated epiblast layer underneath that BM (figure 54A); whereas, the $\beta 1$ integrin and $\gamma 1$ laminin null ES cells formed no BM nor showed signs of epiblast formation. When $\beta 1$ integrin null ES cells were cultured in the presence of 25 ug/ml Lm-111, 56 +/-3% of the resulting EBs formed a proper BM and 24 +/-7% an epiblast layer. On the other hand, the addition of exogenous Lm-111 to $\gamma 1$ laminin null ES cells resulted in 77 +/-6% of the EBs forming a BM and 56 +/-5% an epiblast layer (figure 55A and B).

Section IVA. The role of laminin-111 in $\gamma 1$ laminin null ES/EB BM formation and differentiation.

Without the addition of exogenous Lm-111, $\gamma 1$ laminin null EBs were unable to overcome their differentiation blockage, form a BM layer on the basal side of a well defined and differentiated outer endodermal layer, further differentiate to form a distinctive second cell layer consisting of a polarized pseudo-stratified columnar epiblast layer, or cavitate to form a sharply demarcated central cavity. These developmental stages, however, can be reached by $\gamma 1$ laminin null EBs if exogenous Lm-111 is

supplied. Initially the EB cells are polygonal and lack obvious polarity. An endodermal cell layer differentiates, polarizes, and develops prominent rough endoplasmic reticulum (RER). The RER becomes the principal secretory “factory” for Lm-111 and type IV collagen. Lm-111 and type IV collagen begin to accumulate in a basement membrane which forms underneath the endodermal layer and overlying the ICM. The ICM adherent to the BM elongates and polarizes to form the epiblast while non-adherent ICM undergoes apoptosis and cavitation. Figure 55B shows a typical successful rescue of $\gamma 1$ laminin null EBs.

The ability of exogenously added Lm-111 to rescue $\gamma 1$ laminin null EBs was utilized to test the contributions of both laminin polymerization, through the N-terminal LN domains of the individual chains which compose laminin, and anchorage, through the C-terminal LG domains of the $\alpha 1$ laminin chain, in the rescue of $\gamma 1$ null EBs via inhibition of the exogenous Lm-111 rescue with Lm-111 proteolytic fragments, proteolytic laminin fragments and laminins treated with AEBSF (aminoethyl benzene sulfonyl fluoride; which was previously shown to inhibit laminin’s ability to polymerize), and recombinant $\alpha 1$ LG4-5s. Several heterotrimeric recombinant Lm-111 mutants were also utilized. Lm-111 rescue of $\gamma 1$ laminin null EBs was inhibited by polymerization inhibiting fragments E1’ and E4 (figure 55). Lm-111 which was capable of rescuing $\gamma 1$ laminin null EBs lost this ability once it was treated with AEBSF. Furthermore, both fragment E1’ and E4, which were able to inhibit Lm-111’s ability to polymerize and rescue EBs, lost their ability to inhibit Lm-111’s polymerization and failed to block rescue of $\gamma 1$ laminin null EBs by the addition of exogenous Lm-111, if the fragments were treated with AEBSF. Also, fragment C1-4 which includes the short arm of all three chains of Lm-111 failed to accumulate in a BM pattern or rescue the EBs (data not shown). Lm-111 purified from EHS tumor was much more efficient at BM formation and epiblast differentiation than

recombinant Lm-111_{Nf/Nh/Cf}, however, once the FLAG tag was removed from the C-terminus of the γ 1 laminin chain of the construct, recombinant heterotrimeric laminin, Lm-111_{Nm/Nh/0}, made without the γ 1 FLAG tag demonstrated an increase in the efficiency of BM formation and epiblast differentiation observed. Furthermore, three polymerization deficient mutant heterotrimeric recombinant Lm-111s: Lm-111 $\Delta\alpha$ LN_{Nm/Nh/Cf} missing the N-terminal LN domain of the α 1 laminin chain, Lm-111_{Nm3/Nh/0} with a triple myc epitope tag on the N-terminus of the α 1 chain which interfered with polymerization, and Lm-111 $\Delta\beta$ LN-LEa_{0/Nh/Cf} missing the N-terminal LN and LEa domains of the β 1 laminin chain, also failed to form a BM or cause epiblast differentiation to occur (figure 55).

Lm-111 proteolytic fragment E8, which does not inhibit Lm polymerization, failed to inhibit Lm-111 rescue of the γ 1 laminin null EBs, however, EHS derived E3 did unless treated with AEBSF; suggesting that the integrin binding site (α 6 β 1, α 6 β 4, and α 7 β 1) and HNK-1 site in LG1-3 of fragment E8 are not critical anchorage sites, but that LG4-5 represented by fragment E3 are essential for BM formation and epiblast differentiation (figure 55). The addition of exogenous Lm-111 $\Delta\alpha$ LG1-5_{Nm/Nh/Cf} failed to result in formation of a BM or epiblast differentiation. Furthermore, mutant recombinant laminin α 1LG4-5s were tested for their ability to block the rescue of γ 1 laminin null EBs via the addition of exogenous Lm-111. Recombinant α 1LG4-5/RKR₂₇₂₁ which was shown to barely bind, if at all, α DG, while its ability to bind sulfatide approximates WT, was a good inhibitor of Lm-111 rescue of γ 1 laminin null EBs. Whereas, α 1LG4-5/KRK₂₇₉₃ which was shown to have a small decrease in DG binding but a much larger decrease in sulfatide binding, was a poor inhibitor of Lm-111 rescue of γ 1 laminin null EBs. This inhibition pattern, along with the dispensable nature of α DG as evidenced by the DG null ES cells, suggests that the sulfatide binding contribution is more necessary than α DG for BM formation and epiblast differentiation in ES/EB cultures.

Section V. The role of laminin-111 and its receptors in C2C12 myotubes.

Recombinant heterotrimeric Lm-111s were also evaluated for their ability to bind and accumulate on the surface of C2C12 myotubes (figure 56). Recombinant Lm-111_{Nm/Nh/Cf} coverage of the C2C12 myotubes was almost equal to that of EHS Lm-111, whereas, laminin missing the C-terminal LG1-5, Lm-111 $\Delta\alpha$ LG1-5_{Nm/Nh/Cf}, was practically undetectable. Recombinant laminin missing LG1-3, Lm-111 $\Delta\alpha$ LG1-3_{Nm/Nh/Cf}, demonstrated coverage equivalent to WT, however, the binding of laminin missing LG4-5, Lm-111 $\Delta\alpha$ LG4-5_{Nm/Nh/Cf}, was barely detectable. Clearly the binding of laminin-111 to C2C12 myotubes requires the binding activities present in LG4-5 of the α 1 chain.

The β 1 integrin antibody Ha2/5 has been shown to be a potent blocking antibody when it comes to laminin binding of β 1 integrin and α DG antibody IIH6 effectively blocks laminin binding to α DG, however, neither antibody, individually nor in combination, were able to substantially inhibit exogenous laminin-111 coverage of C2C12 myotubes (figure 57). Furthermore, the contemporaneous addition of α 1 LG4-5 was able to reduce the binding of exogenous laminin-111 to the myotube surface.

The recombinant α 1LG4-5 proteins were evaluated for their ability to inhibit the binding of exogenous EHS Lm-111 to the surface of C2C12 myotubes. 10ug/ml of EHS Lm-111 was incubated for one hour at 37°C with 10, 100, 200, and 300 ug/ml of various α 1LG4-5s and binding of Lm-111 detected using the laminin β 1 LN domain specific polyclonal antibody, E4 (figure 58). Recombinant α 1LG4-5/WT was only able to inhibit Lm-111 binding by approximately 70%. While α 1LG4-5/KDR₂₈₆₀ was able to inhibit almost as well as α 1LG4-5/WT, the other mutant α 1LG4-5s were only able to inhibit 30-45% of Lm-111 binding; degree of inhibition: α 1LG4-5/WT > α 1LG4-5/KDR₂₈₆₀ >> α 1LG4-5/RAR₂₈₃₃ > α 1LG4-5/KGRTK₂₇₇₀ > α 1LG4-5/RKR₂₇₂₁ > α 1LG4-5/RKR₂₇₂₁ > α 1LG4-5/KRK₂₇₉₃ > α 1LG4-5/RKR₂₇₂₁. Even larger inhibitions were possible if the

EHS Lm-111 was replaced with recombinant heterotrimeric Lm-111 $\Delta\alpha$ LG1-3_{Nm/Nh/Cf}, however, base line binding was much less. Nonetheless, the same hierarchy of inhibition was observed among the recombinant mutant α 1LG4-5 proteins (data not shown).

Section VI. The role of laminin-111 and its receptors in embryonic fibroblasts.

Fibroblasts are known for being ECM and BM macromolecule factories but normally do not assemble a BM on their own cell surface; rather instead, contributing their production to the BM of adjacent cell types. Even in the presence of laminin, fibroblasts do not form a BM. If this inability to accumulate laminin was due to a complete absence of any anchors for laminin, then this could potentially be exploited to artificially induce and examine just such an event. Therefore, mouse embryonic fibroblasts (MEFs) were examined for their potential to be used as a building platform on which to artificially establish and test BMs and their components.

Section VIA. The accumulation and condensation of exogenous Lm-111 on the cell surfaces of MEFs without the aid of sulfatide loading.

During the course of experiments, it was discovered that if the polyclonal antibodies directed against the elastase digest fragments E4, E1', E8, or E3 of laminin-111 were utilized in immunohistochemical staining of MEFs without sulfatide loading but with the addition of exogenous Lm-111, there appeared to be a distinct observable punctuate laminin pattern on the surface of the MEFs (figure 59A). This pattern was not noticed in the earlier experiments which utilized the laminin γ 1 chain mAb. Furthermore, the observed laminin signal co-localized perfectly with α DG (figure 59B). On Schwann cell surfaces, individual immunohistochemical staining signals for laminin-111 and α DG

signal rarely perfectly coincided, usually they were adjacent and exclusionary when it came to the signal observed in immunohistochemical staining. However, the signals were observed to comigrate and clear from the surface together. The assumption at the time was that the DG antibody (IIH6) could not recognize α DG bound to laminin-111 and/or that they are in the same complex but not necessarily bound to one another.

Cultured mouse embryonic lung fibroblasts do not express the laminin γ 1 chain nor γ 1 containing laminins, such as Lm-111. MEFs express and secrete type IV collagen and nidogen-1, however, neither is retained in appreciable amounts on the cell surface (figure 60). Exogenous Lm-111 will bind to the cell surface and result in a increase in type IV collagen and nidogen-1 observed to be bound and colocalized with the laminin on the cell surface of the MEFs. Furthermore, the α DG which is already present on the cell surface will colocalize with the exogenous Lm-111 bound on the cell surface (figure 61A). There is no endogenous sulfatide present in MEFs, however, if the MEFs are first loaded with sulfatide, via addition sulfatide bound albumin to the media, a very dramatic increase in the exogenous Lm-111, as well as, both the secreted endogenous type IV collagen and nidogen-1, is observed to accumulate on the cell surface.

Much like on Schwann cells, exogenous Lm-111 will bind to the MEF cell surface and with time, accumulate, and condense towards the center of the cell (figure 62). Membrane bound α DG will become co-localized and co-migrate with the exogenous Lm-111, condensing towards the center of the cell, however, without the addition of exogenous Lm-111, the α DG signal remains diffuse. Not only did the exogenous laminin-111, endogenous nidogen-1, and endogenous α DG colocalize, but each component also colocalized with GM1 clusters (figure 61B), suggesting that all three proteins were also present in GM1 containing lipid rafts. Furthermore, contrary to what

is observed in Schwann cells, the Lm-111 signal did not merge into higher order structures. The individual Lm-111 signals remained separate for the most part; forming just a few very dense and intense clusters (figure 63).

This process of condensing exogeneous Lm-111 from the cell periphery was so stable that the MEFs could be exposed to multiple rounds of exogeneous laminin and multiple condensing concentric rings observed (figure 64). Alexa 488 dye labeled recombinant laminin-111 was added to the MEFs, incubated, washed, incubated, a second incubation with Alexa 488-Lm-111 initiated, washed, and allowed to incubate further. The MEFs were removed from the incubator at various times and fluorescent microscopy images taken of isolated individual MEFs over this period of time. At the end of the experiment the MEFs were washed, fixed, and stained with an α DG antibody. The images taken depicted the formation and condensation of a ring of laminin followed by the formation and condensation of a second ring of colocalized laminin and α DG after the second exposure to exogeneous laminin.

The specificity of Lm-111 for sulfatide was further evaluated by testing the ability of Lm-111 to bind MEFs loaded with: glc-sulfatide (HSO_3 -3-glucosyl β -1ceramide), gal-sulfatide (HSO_3 -3-galactosyl-ceramide), cholesterol-3-sulfate, GM1-ganglioside, GT1b-ganglioside, phosphatidic acid, phosphatidyl inositol, and phosphatidylserine (figure 65A). Only glc-sulfatide and gal-sulfatide supported the accumulation and condensation of Lm-111 on the cell surface of lipid loaded MEFs. These results were consistent with the Lm-111 lipid binding specificity determined in previous solid phase assays and in Schwann cells already described in this thesis and by others [65, 70]. Furthermore, after loading MEFs with sulfatide, arylsulfatase treatment resulted in no Lm-111, type IV collagen, or nidogen-1 being detected on the cell surface (figure 65B).

Section VIB. Inhibition of exogenous Lm-111 accumulation on MEF cell surfaces by the simultaneous addition of recombinant α 1LG4-5 proteins.

Exogenous Lm-111 accumulation on MEF cell surfaces was inhibited by the contemporaneous addition of recombinant α 1LG4-5 proteins. MEF cell cultures were incubated with 20 ug/ml of EHS Lm-111 for one hour at 37°C with 1, 10, 20, 50, 100, or 200 ug/ml of various recombinant α 1LG4-5 proteins (figure 66). The detectable bound laminin on MEFs simultaneously exposed to recombinant α 1LG4-5/WT decreased by 85%, however, MEFs treated with mutant α 1LG4-5/KDR₂₈₆₀ exhibited a 95% decrease in bound laminin. Treatment with α 1LG4-5/RKR₂₇₂₁ + KRK₂₇₉₃ resulted in a 15% increase in bound laminin. While mutants α 1LG4-5/KRK₂₇₉₃, α 1LG4-5/RKR₂₇₂₁, and α 1LG4-5/RKR₂₇₂₁, ability to inhibit laminin binding to the cell surface followed their DG affinities exhibited in the heparin and solid phase DG assays (i.e. the stronger the DG binding affinity, α 1LG4-5/RAR₂₈₃₃ = α 1LG4-5/RKR₂₇₂₁ > α 1LG4-5/RKR₂₇₂₁ > α 1LG4-5/KRK₂₇₉₃), the greater the demonstrated laminin binding inhibition on MEFs: α 1LG4-5/RAR₂₈₃₃ = α 1LG4-5/RKR₂₇₂₁ > α 1LG4-5/RKR₂₇₂₁ > α 1LG4-5/KRK₂₇₉₃.

Section VIC. Accumulation of various exogenous recombinant heterotrimeric Lm-111s on the cell surfaces of MEFs.

Lm-111 purified from EHS tumor and several recombinant heterotrimeric laminins were tested for their ability to bind the surface of MEFs which had not been loaded with sulfatide. The Lm-111(U) bound slightly more than Lm-111(B) or recombinant Lm-111_{Nm/Nh/Cf}, however, α DG staining colocalized faster and better with Lm-111(B) than Lm-111(U) or Lm-111_{Nm/Nh/Cf}, perhaps due to the nidogen-1 attached to the laminin in Lm-111(B) (figure 67). Recombinant Lm-111_{Nm/Nh/Cf} coverage of the MEF surface was almost equal that of the two EHS purified Lm-111s, and Lm-111 Δ α LG1-3_{Nm/Nh/Cf}

accumulation was approximately equal to that of the Lm-111_{Nm/Nh/Cf}, while Lm-111 $\Delta\alpha$ LG1-5_{Nm/Nh/Cf} and Lm-111 $\Delta\alpha$ LG4-5_{Nm/Nh/Cf} binding was practically undetectable. The binding of recombinant α 1 LG4 point mutations Lm-111 α RKR_{2721Nm/Nh/Cf} and Lm-111 α RAR_{2833Nm/Nh/Cf} was also very low; with RAR₂₈₃₃ binding slightly more than RKR₂₇₂₁. Two polymerization incompetent recombinant laminins, Lm-111_{Nm3/Nh/0} and Lm-111 $\Delta\beta$ LN-LEa_{0/Nh/Cf}, exhibited a much reduced and finer punctuate coverage. Figure 68 shows two typical examples of the difference in the coverage pattern between polymerization competent Lm-111s with intact LG4-5 anchorage sites, Lm-111_{Nm/Nh/Cf} for instance, and intact LG4-5 anchorage site but polymerization defective recombinant Lm-111s, such as Lm-111 $\Delta\beta$ LN-LEa_{0/Nh/Cf}.

Section VII. Summary

Genetic analyses of mouse development have revealed that knockout of $\gamma 1$ laminin results in a failure of peri-implantation and peripheral nerve Schwann cell BM assembly. In contrast, knockout of nidogens, type IV collagen, perlecan, $\beta 1$ integrins (if laminin is present) and dystroglycan (except for Reichert's membrane) results in various defects of BMs, but not in a general failure of BM assembly. Together, these data argue for a central role of laminin family members in BM assembly.

Similarly, laminins have been found to be a requirement of BM assembly in embryoid bodies, Schwann cells, and C2C12 myotubes. Furthermore, evaluation of the laminin domains required for this assembly, a focus of this thesis research and of the Yurchenco laboratory, has strongly implicated both the N-terminal LN domains of the three individual laminin subunits ($\alpha 1$, $\beta 1$, and $\gamma 1$) and the C-terminal $\alpha 1$ LG4 domain found in laminin-111 as providing crucial binding interactions for assembly. The LN domains have been found to mediate laminin polymerization while the LG4 domain has been found to mediate binding interactions to cell surface sulfatide and dystroglycan. Inactivation of either activity through mutagenesis resulted in a failure to assemble a BM.

Further analysis of the sequences of $\alpha 1$ LG4 involved in sulfatide and α DG binding have revealed partially overlapping Lysine and Arginine patches that interact with the carbohydrates of the mentioned cell surface ligands. Recombinant $\alpha 1$ LG4-5 inhibited laminin accumulation on cell cell surfaces (and to sulfatide), however, fairly high concentrations were required to achieve these inhibitions. This occurred despite an inability to identify another major domain in laminin capable of binding to cell surfaces. While a loss of activity in the recombinant fragment might explain this apparent dilemma, different preparations exhibited this property. A more likely explanation may lie in the "cooperativity" of interactions exhibited by intact laminin in which a series of additional

weak binding interactions may collectively increase the observed overall laminin adherence to the cell surface beyond that provided by LG4 alone. These interactions seem likely to arise from LG1-3 (weak sulfatide and heparin binding), $\alpha 1$ LN (weak sulfatide and heparin binding) and from laminin polymerization which serves to tie together multiple laminins and hence multiple LG domains into a single cell binding unit. Restated, the LG4-5 fragment, while containing the major cell surface binding sites, must nonetheless compete against a complex with multiple binding interactions, including multiple LG4 interactions, when utilized as an inhibitory agent to block heterotrimeric laminin binding. This may also explain why the binding of isolated LG4-5 to a sulfatide layer occurs with an apparent K_d that is weaker than that seen with intact laminin even though deletion of LG4 from heterotrimeric laminin causes a major (but not complete) loss of binding.

Studies of Li et al [71] in this laboratory provided evidence that sulfatide can be a major contributor to laminin anchorage to the cell surface and that dystroglycan may be dispensable (at least in ES cell derivatives). This is further supported by genetic evidence in which laminin containing BMs form in many tissues despite ablation of DG-laminin binding (LARGE-myd mouse studies). Nonetheless, the data of this thesis suggest that dystroglycan can enhance BM assembly, and while not required, may play some role in BM formation. The differential binding detected for α DG and sulfatide with recombinant heterotrimeric laminins Lm-111 α RKR_{2721Nm/Nh/Cf}, Lm-111 α KRK_{2793Nm/Nh/Cf}, and Lm-111 α RAR_{2833Nm/Nh/Cf} should greatly assist with analyses in the future.

Section VIIA. Expression and characterization of recombinant heterotrimeric Lm-111s.

The human embryonic kidney fibroblast HEK 293 cell line was chosen for production of recombinant heterotrimeric laminins for many reasons, including: fibroblasts *in vivo* are often factories for production of ECM proteins (including laminins), they can survive the expression of recombinant proteins under both the CMV and SV40 promoter, exhibit high levels of recombinant protein expression under both promoters, grow well in tissue culture, are adherent to tissue culture plastic, are easily transfected, and appear to have little or no basal endogenous expression of the laminin chains which comprise laminin-111 and laminin-211. Furthermore, it is a human derived cell line and at the time we were working with mouse laminin chains. The hope was to utilize this species difference to help delineate between the transfected mouse chains and any potential endogenous human chains; especially since there was a potential basal level endogenous contribution present or upregulated when the laminin chains were transfected into the cell line. It was discovered that there was no, or barely, detectable levels of endogenous mRNA or protein expression of the $\alpha 1$, $\alpha 2$, $\alpha 5$, $\beta 1$, $\beta 2$, and $\gamma 1$ laminin chains. There was, however, a very low level of $\gamma 2$ present. Neither was there a perceptible increase in expression of the endogenous laminin chains once laminin expression constructs were introduced into the cells.

Despite many attempts to the contrary, it was not possible to obtain a stable cell line which produced all mouse or all human recombinant heterotrimeric laminin-111 without significant proteolytic degradation. The mixed species recombinant heterotrimeric laminin-111 composed of a mouse $\alpha 1$, human $\beta 1$, and human $\gamma 1$ laminin chain, was the only arrangement that produced un-cleaved protein. Various expression constructs of the $\alpha 1$, $\beta 1$, and $\gamma 1$ chain were created and transfected in combinations to produce

recombinant heterotrimeric laminin-111s. The use of N-terminal FLAG, myc, HA, VSV-G, and protein-C epitope tags on the α 1 chain had no deleterious affect upon it's activity when it was a constituent of a recombinant heterotrimeric Lm-111 protein. The use of a N-terminal triple myc tag (myc_{x3}) on α 1 did inhibit polymerization. N-terminal VSV-G and HA tags were also permissible on the β 1 chain constructs; though the HA tag did result in some of the β 1 chain being secreted without being accompanied by the α and γ chain. A system for recombinant heterotrimeric laminin production was established in which the α 1 chains were expressed with a N-terminal myc epitope tag under puromycin selection, β 1 chains with a N-terminal HA epitope tag under zeocin selection, and the γ 1 chains with a C-terminal FLAG epitope tag under neomycin/G418 selection. The recombinant heterotrimeric laminins produced by this system were largely free of proteolytic degradation and were both quickly and easily extractable from the media of stable cell lines to a very high degree of purity and in a fully functional/active and morphologically "normal" state. Furthermore, the rapid purification system developed favored high activity and minimal degradation of the recombinant heterotrimeric laminins.

All recombinant heterotrimeric laminin-111s containing intact N-terminal LN domains displayed normal polymerization activity and ability to bind to the surface of various examined cell lines in a basement membrane like pattern. Any recombinant laminins containing deletion of an LN domain failed to polymerize and accumulate in appreciable amounts on the cell surface of examined cell lines. ELISA results involving combinations of the N-terminal LN domains from the individual α 1, β 1, and γ 1 chains revealed that the only appreciable accumulation of recombinant proteins occurred when all of the individual LN domains from all three chains were present. Furthermore, substitution of LN domains with other LN domains in recombinant heterotrimeric Lm-111s, also resulted in laminins which failed to polymerize or accumulate. All of these

experimental results further support the model that all three LN domains, one from each α , β , and γ chain, are required for proper polymerization activity.

Recombinant laminin-111s containing deletions of the $\alpha 1$ N-terminal LN, C-terminal LG1-5, LG1-3, and LG4-5 reveal that the vast majority of heparin and sulfatide binding activity is derived from LG4-5 with minor contributions to both from the N-terminal LN domain of $\alpha 1$. Furthermore, the binding to sulfatide is very sensitive to heparin and partially to EDTA treatment.

The heparin affinity of laminin-111 is greater than that of laminin-211 and laminin-111 also binds more moles of sulfatide than laminin-211. Furthermore, just like heparin binding, the processed form of laminin-211 binds sulfatide with a much lower affinity than the unprocessed form. Laminin-111 also binds the surface of Schwann cells and C2C12 myotubes more intensely than Laminin-211 and is much more efficient at converting embryonic stem cells into embryoid bodies.

The generated recombinant laminins do not contain nidogen associated with them because the cell line used for their production does not express nidogen. The generation of laminins without associated nidogen (laminin-nidogen complex), not available in purified EHS-tumor extracts where nidogen or its fragments are associated with the purified laminin, afforded the opportunity to ask what roles nidogen's and type IV collagen's interactions with laminin play in laminin's accumulation and basement membrane formation on cell surfaces. First the interaction of nidogen and type IV collagen with laminin was examined by Karen McKee. The assay chosen was one that took advantage of the property of type IV collagen aggregation, in which the complexes that developed did not have to be subsequently diluted so as to be able to detect weak interactions. This sedimentation assay demonstrated that nidogen associates with both laminin and type IV collagen and that it can provide a bridge between the two

polymerizable proteins. Also, the data suggests that there exists a small yet measurable association directly between laminin and type IV collagen [471]. This was followed by a series of experiments, performed by Stephanie Capizzi, utilizing different combinations of laminin, nidogen, and type IV collagen and then analyzing the accumulation of each component on the cell surface of Schwann cells which revealed a small increase in laminin accumulation on the cell surface due to nidogen and type IV collagen interactions (appendix figure 13).

Section VII.B. The role of laminin, its domains, individual amino acid residues, binding activities, and anchors/receptors in binding, accumulation and basement membrane formation on Schwann cell surfaces.

Despite the *in vivo* expression of $\gamma 1$ chain composed laminins by Schwann cells, laminin $\gamma 1$ expression is turned off shortly after culturing of the cells, however, the cells do continue to express type IV collagen, nidogen, perlecan, $\beta 1$ containing integrins, dystroglycan, and sulfatide. The secreted type IV collagen and nidogen are lost to the media without the presence of laminin-111 or laminin-211 to anchor them to the cell surface and form a basement membrane. Exogeneously supplied laminin-111 or laminin-211 will bind to the surface of the Schwann cells and result in deposition of type IV collagen and nidogen in a basement membrane like pattern, however, neither nidogen nor type IV collagen are required for Lm deposition or subsequent BM formation. Furthermore, the increase in laminin binding with the concurrent addition of exogenous nidogen and type IV collagen was minimal. The laminin binding integrins are also not required for this event and those that are present are sequestered to the basal side of the Schwann cells in culture. Both sulfatide and dystroglycan are expressed on the surface of the Schwann cells and are engaged by laminin. Without

laminin's presence, sulfatide and α DG will not colocalize nor condense. Whereas, once exogenous laminin is supplied, laminin, sulfatide, and DG will colocalize, co-migrate and condense together. Furthermore, laminin, sulfatide, and DG can be found both in lipid raft fractions of Schwann cell extracts and co-localized in immunohistochemical identified lipid rafts on the surface of Schwann cells. Enzymatic hydrolysis, inhibition with a sulfatide binding protein, sulfatide loading, immunoprecipitations and solid phase binding experiments all demonstrate the specificity and requirement of laminin-111 for the sulfated glycolipid sulfatide. Schwann cells will not bind laminin-111 without sulfatide, whereas, dystroglycan appears to be dispensable, yet may enhance overall binding (the α DG blocking antibody IIH6 is a carbohydrate specific antibody which is not present on all expressed DGs). Dystroglycan does provide a direct link to the intracellular cytoskeleton through its association with utrophin, a cytoskeleton protein which binds both β DG and F-actin, however, only when both sulfatide and laminin are present. Utrophin is recruited to the sulfatide-laminin- α DG complex through its association with β DG.

BMs have fairly distinct appearances in their ultrastructure. We examined the treated SCs by EM and found that the laminin-treated cells had long continuous thin ECM deposits typical of BMs. This was not observed if the sulfatide on the cell surface was first removed by treatment with arylsulfatase. After removal of sulfatide from the cell surface, the laminin deposition could be restored by then loading the SCs with sulfatide and re-exposing the cells to exogenous Lm-111.

Polymerization and anchorage blocking proteolytic fragments of Lm-111 demonstrated the requirement of both laminin's polymerization and LG4 anchorage activities for proper basement membrane formation. Recombinant heterotrimeric Lm-111s with deletions, chemical modifications (AEBSF), or interfering epitope tags, which

terminated the laminins' polymerization capabilities also severely inhibit the laminin's accumulation on the Schwann cell surface. Furthermore, deletions and point mutagenesis of cell anchorage/receptor sites in LG4 will effectively terminate all binding of Lm-111 to the Schwann cell surface.

Solid phase binding assay results of the recombinant $\alpha 1$ LG4-5s, examined in context of the three dimensional structure of $\alpha 1$ LG4-5, reveal that there are several binding activities in close proximity to one another in LG4 of $\alpha 1$, but that they are physically separated from one another and, therefore, not necessarily competitive; i.e. each $\alpha 1$ LG4-5 can engage more than a single sulfatide molecule at one time and possibly simultaneously also α DG or at least exchange sulfatide(s) for α DG. It also explains $\alpha 1$'s sensitivity to both EDTA and heparin blockage in sulfatide, dystroglycan, and cell binding assays.

When the recombinant $\alpha 1$ LG4-5 were utilized as inhibitors of exogenous Lm-111 binding on Schwann cell surfaces, the inhibitions observed required high competing concentrations of $\alpha 1$ LG4-5. One should not have expected any of the mutant recombinant $\alpha 1$ LG4-5s to completely lose their ability to block unless the mutation(s) had completely wiped out all sites for all anchors/receptors present on the surface of the Schwann cells. The complete inactivation of any single site for one anchor/receptor would still leave others present to which the recombinant $\alpha 1$ LG4-5 would bind and prevent Lm-111 from binding. However, the heterotrimeric Lm-111 possesses multiple anchors/receptors both in LG4 and outside those present in LG4-5 and will, therefore, have a greater total affinity and could potentially displace any blocking $\alpha 1$ LG4-5 (figure 69). Furthermore, once anchored/bound to the cell surface, the Lm-111 with its multiple anchor and binding sites will be more difficult to disassociate than a recombinant $\alpha 1$ LG4-

5 in which one or more sites have been affected. Even if the binding activity of just one site in an $\alpha 1$ LG4-5 molecule had not been reduced, the competing Lm-111's overall affinity will increase dramatically over the $\alpha 1$ LG4-5 once it begins to engage/polymerize with other laminins and adds each of their binding sites to the collective and initiates a nucleation process which will exponentially increase the collective's binding affinity over that of any competing $\alpha 1$ LG4-5. Still further difficulties for the $\alpha 1$ LG4-5 to be effective inhibitors on the cell surface, is the issue of how many of the engaged binding sites of the collective then must be replaced by the blocking $\alpha 1$ LG4-5 in order to displace the collective Lm-111s from the surface of the Schwann cells or microtiter well. In theory, a polymerized cluster of just 10 Lm-111s, each with 10 potential binding activities, could be potentially engaged in over 100 binding interactions, many of which may involve interactions not represented in $\alpha 1$ LG4-5 and therefore, uninhibitable by $\alpha 1$ LG4-5. Furthermore, even an individual laminin which has had all of its anchorage sites with the cell surface interrupted will still remain part of the polymerized collective on the surface of the Schwann cell due to its binding/polymerization with other laminins in the collective. Yet another complication, is the observation that $\alpha 1$ LG4-5 at low molar concentrations apparently increases Lm-111 binding on the cell surface and different mutants exhibit different proclivities with regards to this observed activity. When taken all together, it soon becomes suprising that any inhibition of laminin was observable with $\alpha 1$ LG4-5 on Schwann cell surfaces and that the interpretation of the results is very difficult.

The observed ability of $\alpha 1$ LG4-5/KDR₂₈₆₀ to inhibit Lm-111 binding more effectively than WT may be due to a poor batch of $\alpha 1$ LG4-5/WT_{Nf} or indicate that it binds to an anchor/receptor more strongly than WT. An increase in affinity by the mutation represented in $\alpha 1$ LG4-5/KDR₂₈₆₀ is plausible and may actually be due to its observed glycosylation difference when compared to the other recombinant $\alpha 1$ LG4-5s. Alterations

in glycosylation have been directly correlated to changes in affinities of several proteins, including binding of α DG and midkine to both heparin and sulfatide, as well as, FGF to heparin. Furthermore, and directly relevant was the demonstration that deglycosylation of α 1LG4-5 lead to a significant decrease in α DG binding affinity and a concurrent increase in heparin affinity. The observed increase in inhibition of α 1LG4-5/RAR₂₈₃₃ over α 1LG4-5/RKR₂₇₂₁ and α 1LG4-5/RKR₂₇₂₁ correlates well with binding observed on the Schwann cell surface of point mutation containing heterotrimeric laminins, where Lm-111 α RAR₂₈₃₃Nm/Nh/Cf binds slightly more than Lm-111 α RKR₂₇₂₁Nm/Nh/Cf.

The inability of the mutant recombinant α 1LG4-5s to effectively prevent Lm-111 binding on the cell surface supports the view of multiple anchors/receptors being engaged at the same time and that these interactions involve both DG and sulfatide, otherwise a single point mutation eliminating a single binding site would have been sufficient to eliminate the use of that recombinant α 1LG4-5 as a blocking agent, and no blocking of Lm-111 would have been observed. The fact that all the recombinant α 1LG4-5s were for the most part poor inhibitors, except for α 1LG4-5/KDR₂₈₆₀ (formerly mutant rE3-J), means that there were several sites and anchors/receptors involved in binding to the cell surface. For example, if anchorage was only dependent upon α DG then the α 1LG4-5s which severely hindered α DG binding would not bind the surface of the Schwann cells and would not block binding and accumulation of exogenous Lm-111 at all, however, they did. Therefore, they must have been binding the Schwann cell surface somewhere and through some receptor and sites other than α DG. A similar situation would explain α 1LG4-5s which displayed severely hindered sulfatide binding. Analysis of sulfatide binding site contributions is further complicated by the existence of multiple sulfatide binding sites, within potentially different affinities, within LG4. Since we know α 1LG4-5 does bind both sulfatide and α DG, only a mutation that either killed both

activities or if both activities were interconnected and dependent upon or required one another in Schwann cell anchorage, would a single mutation that does not directly affect both activities result in no observable decrease in Lm-111 binding being observed while using α 1LG4-5 as an inhibitory agent.

In order to analyze the contributions of domains, amino acid residues, and specific activities of laminin in accumulation and basement membrane formation, several classes of modified laminins were incubated with Schwann cells and their accumulation analyzed. The addition of WT laminins (WTa; Lm-111_{Nf/Nh/0}, WTb; Lm-111_{Nm/Nh/Cf}, Lm-111_{Nm/Nh/0}, Lm-111_{Nv/Nh/0}, Lm-111_{Nh/Nh/0}, Lm-111_{Nc/Nh/0}, and Lm-111_{Nf/Nh/0}) resulted in accumulation on the cell surface approaching the level of EHS purified Lm-111. The laminin polymerization deficient, due to deletion of an N-terminal LN domain (Lm-111 α Δ LN_{Nm/Nh/Cf}, Lm-111 α Δ LN-LEa_{Nm/Nh/Cf}, Lm-111 α Δ LN-L4a_{Nm/Nh/Cf}, Lm-111 α Δ LN-L4b_{Nm/Nh/Cf}, Lm-111 β Δ LN_{0/Nh/Cf}, Lm-111 β Δ LN-LEa_{0/Nh/Cf}, Lm-111 γ Δ LN_{Nm/Nh/Cf}, and Lm-111 γ Δ LN-LEa_{Nm/Nh/Cf}) or epitope tag blocking (Lm-111_{Nm3/Nh/0}) recombinant laminins failed to significantly accumulate on the surface of Schwann cells. Recombinant laminins not possessing the anchoring activities provided by the LG4 domain of the α 1 chain (Lm-111 Δ α LG1-5_{Nm/Nh/Cf} and Lm-111 Δ α LG4-5_{Nm/Nh/Cf}) failed to bind the Schwann cell surface at all. The recombinant Lm-111 Δ α LG1-3_{Nm/Nh/Cf} bound the Schwann cell surface with an intensity almost as high as the recombinant WT laminins. The chemically modified, polymerization and sulfatide binding deficient, AEBSF treated Lm-111_{Nm/Nh/Cf}-A did not bind the cell surface, whereas, the recombinant heterotrimeric laminins containing point mutations of specific residues within LG4 of the α 1 chain (Lm-111 α RKR_{2721Nm/Nh/Cf}, Lm-111 α KRK_{2793Nm/Nh/Cf}, and Lm-111 α RAR_{2833Nm/Nh/Cf}) exhibited greatly reduced binding to the Schwann cell surface. Clearly both polymerization and anchorage via α 1 LG4 are required for accumulation and basement formation on the

surface of Schwann cells. Furthermore, both the DG binding site and sulfatide site are required for efficient anchorage, accumulation, and basement membrane formation.

Section VIIC. Interactions of recombinant laminins with type IV collagen and nidogen.

The addition of a mixture of nidogen and type IV collagen to Lm-111WT_{Nm/Nh/Cf} resulted in only a small increase in the deposition of the laminin on the Schwann cell surface (figure 50). The addition of type IV collagen alone resulted in no increase in laminin accumulation, whereas, the addition of nidogen alone actually resulted in a small decrease in laminin accumulation (data not shown). A more detailed examination of the interaction of recombinant laminins with type IV collagen and nidogen in the deposition of all three proteins on the Schwann cell surface was accomplished by Stephanie Capizzi (appendix figure 13). A mixture of collagen, nidogen, and laminin resulted in an increase in type IV collagen deposition, but a mixture of just collagen and laminin did not. The addition of nidogen and type IV collagen with non-polymerizing laminins, Lm-111 $\alpha\Delta$ LN_{Nm/Nh/Cf} and Lm-111 γ 1 Σ α 1LN_{Nm/Nh/Cf}, enabled increased accumulation of the non-polymerizing laminins on the Schwann cell surface. In contrast, the addition of nidogen and type IV collagen with Lm-111 $\alpha\Delta$ LG1-5_{Nm/Nh/Cf}, resulted in a negligible increase in accumulation. Furthermore, when collagen, nidogen, and the nidogen binding mutant, Lm-111 γ 1N₈₀₂S_{Nm/Nh/Cf}, were added together, there was a very low accumulation of type IV collagen observed on the Schwann cell surface. These results further support the conclusion that laminin accumulation and basement membrane formation do not require nidogen or collagen, however, nidogen will act as a bridge between laminin and type IV collagen, enabling accumulation of type IV collagen and a small increase in laminin deposition.

Section VIID. The effect of AEBSF treatment upon laminin-111 activities and ability to form a BM.

AEBSF treated laminin-111's ability to polymerize is greatly reduced, as is its binding to sulfatide as measured in a solid phase sulfatide ELISA. Furthermore, AEBSF treated α 1LG4-5 also fails to bind in solid phase sulfatide ELISAs and fails to inhibit laminin-111 binding both in the sulfatide ELISA and on Schwann cell surfaces. The observed inability of AEBSF treated laminin to accumulate on cell surfaces is not due solely to AEBSF's inactivation of laminin's polymerization activity, as previously thought, but also, AEBSF's selective inactivation of α 1 LG4's sulfatide binding activity leading to abolishment of laminin's anchorage through LG4. Therefore, AEBSF treated laminin can not bind the cell surface and even if it could, it would not appreciably accumulate without the ability to polymerize.

Section VIIE. Implications of potential β 1 integrin inhibition by the C-terminal FLAG epitope tag on the γ 1 chain of recombinant heterotrimeric laminins.

Recent observations from another group, raised the issue if whether the C-terminal FLAG tag present on the γ 1 chain of most recombinant heterotrimeric laminins constructed and utilized by us may interfere with β 1 integrin binding. This issue was not relevant in experiments involving adherent cells (Schwann, C2C12, and MEF) because the vast majority of the β 1 containing integrins are sequestered to the basal side of the cells and are not engaged by the exogeneously supplied laminin which deposits on the apical side of the cells. This potential interference may actually be beneficial by removing any integrin contributions from the analyses. Karen McKee was able to show that the FLAG epitope tag on the C-terminus of the laminin γ 1 chain did inhibit the ability

of heterotrimeric laminin containing such a modification to bind $\beta 1$ integrin (data not shown).

Section VIIF. The role of Lm-111 in ES cell differentiation, BM formation, and embryoid body formation.

Not only do EBs derived from $\gamma 1$ laminin null ES cells fail to synthesize the $\gamma 1$ chain (null) but, they also turn off the expression of the $\alpha 1$ laminin chain. As a result, just like the $\beta 1$ integrin null EBs, $\gamma 1$ laminin null EBs fail to form a BM, epiblast layer, or cavitate unless supplied with exogenous Lm-111; after which they too can proceed through these developmental processes (figure 70). Furthermore, the $\gamma 1$ laminin null EBs continue to secrete perlecan, nidogen, and type IV collagen, however, none of these BM components accumulate in a BM without the exogenous supply of Lm-111.

The use of proteolytic fragments of Lm-111, mutant recombinant heterotrimeric Lm-111s, and mutant recombinant $\alpha 1$ LG4-5s, enabled the determination that both the polymerization activity provided by the N-terminal LN domain of all three laminin chains and the C-terminal LG4 domain of the $\alpha 1$ chain are required for Lm-111 to rescue Lm-111 deficient EBs (figures 71). The anchorage provided by LG4 could be further mapped to specific residues within LG4 and the receptors involved. Polymerization inhibiting fragments E4 and E1', as well as polymerization incompetent rLm-111s missing either the $\alpha 1$ LN domain or $\beta 1$ LN domain or containing an N-terminal epitope tag which blocked polymerization, inhibited Lm-111 rescue or failed themselves to form a BM, differentiate to form an epiblast layer, or to cavitate. The inhibition of polymerization by E1' and its blocking ability in the Lm-111 rescues, could both be reversed by treating E1' with AEBSF. Similarly, Lm-111 treated with AEBSF also failed to rescue Lm-111 null EBs. Lm-111 purified from EHS tumor was more efficient at

inducing epiblast differentiation than recombinant WT Lm-111. This difference could be attributed to differences in post translational modifications; for example, the hyperglycosylation observed in Lm-111 purified from EHS tumors or differential glycosylation specific to the cell line utilized to produce the recombinant proteins. Clearly, it is required that Lm-111 retain its polymerization capability, not just in order for it to function in, but also, for there to be any BM formation, epiblast differentiation, and cavitation in EBs.

Many of the recombinant Lm-111s generated were done with a $\gamma 1$ chain containing a C-terminal FLAG tag. Recent results by others indicated a potential interaction between the C-terminus of the $\gamma 1$ chain and $\alpha 1$ LG1 when engaging $\alpha 6/\beta 1$ and $\alpha 7/\beta 1$ integrins, raising the issue of whether or not our FLAG epitope tag on the C-terminus of the $\gamma 1$ chain may inhibit interaction between $\alpha 1$ and these integrins. There was an observed increase in recombinant Lm-111's ability to rescue $\gamma 1$ laminin null EBs once the FLAG tag was removed from the $\gamma 1$ laminin chain of the construct (Lm-111_{0/Nh/Cf} vs. Lm-111_{Nm/Nh/0}) (figures 55 and 71), lending further credence to these concerns.

The role of anchorage provided by the LG domains of Laminin-111 was tested using a similar approach. Proteolytic fragment E8 containing the $\alpha 6\beta 1$, $\alpha 6\beta 4$, and $\alpha 7\beta 1$ integrin, as well as HNK-1 binding site, failed to inhibit the rescue of $\gamma 1$ laminin null EBs. Taken together with the $\beta 1$ integrin null and DG null EB observations, it becomes apparent that neither integrin binding nor DG binding is absolutely required in order for Lm-111 to function in the proper formation of an endodermal layer, BM formation, epiblast formation, and cavitation of EBs. Treatment of ES cells with recombinant heterotrimeric Lm-111 missing LG1-5 (Lm-111 $\Delta\alpha$ LG1-5_{Nm/Nh/Cf}) resulted in EBs which failed to form both a BM and a differentiated epiblast layer. Furthermore, both proteolytic fragment E3 and recombinant $\alpha 1$ LG4-5/WT_{Nf} both inhibited Lm-111 rescue of $\gamma 1$ laminin

null EBs. Mutation of RKR₂₇₂₁ to AKA₂₇₂₁ in α 1LG4-5/RKR₂₇₂₁ was shown to nearly wipe out all α DG binding while not affecting sulfatide binding activity and inhibited Lm-111 rescue of γ 1 laminin null EBs at levels approximating WT E3. Whereas, mutation of KRK₂₇₉₃ to AAA₂₇₉₃ in α 1LG4-5/KRK₂₇₉₃, which was shown to have a small decrease in DG binding but a much larger decrease in sulfatide binding activity was a poor inhibitor of Lm-111 rescue of γ 1 laminin null EBs. Obviously, just as the results from the solid phase binding assays predicted, α 1LG4-5/RKR₂₇₂₁ could not bind α DG, which is not required anyways as demonstrated by the DG null EBs, however, it still bound other anchors present on the cell surface other than DG, such as sulfatide (or another sulfated macromolecule, thereby blocking Lm-111 binding and its subsequent rescue. The recombinant α 1LG4-5/KRK₂₇₉₃, on the other hand, had only a reduced binding to α DG, which was irrelevant, but had a much larger decrease in sulfatide binding, a required anchor (or at the very least a binding site for another sulfated macromolecule) which it could not bind and therefore block the exogenous Lm-111 from binding to and rescuing the γ 1 null EBs. The use of these mutated recombinant α 1 laminin LG4-5s with demonstrated differences in their affinities for heparin, sulfatide, and α DG revealed, through their ability to block the rescue of γ 1 laminin null EBs via the addition of exogenous Lm-111, that the sulfatide binding contribution is more necessary than α DG binding in Lm-111s ability to rescue Lm-111 deficient EBs. Therefore, both N-terminal LN driven polymerization and C-terminal α 1 LG4 mediated anchorage of laminin-111 are required activities for laminin-111 to form basement membranes and induce epiblast differentiation and polarization in embryoid bodies.

Section VIIG. The role of laminin-111 and its receptors in C2C12 myotubes.

It was surprising that the recombinant $\alpha 1\text{LG4-5/WT}_{\text{Nf}}$ was unable to cause a more complete inhibition of Lm-111 binding on C2C12 myotubes, given that Lm-111 $\Delta\alpha\text{LG1-3}_{\text{Nm/Nh/Cf}}$ binding was equivalent to WT Lm-111 $_{\text{Nm/Nh/Cf}}$ coverage of C2C12 myotubes and that deletion of either LG1-5 or LG4-5 abrogated that coverage (figure 56). Perhaps, the polymerizing activity of laminin or interaction with other macromolecules or receptors is able to compensate or overcome loss of multiple anchorage sites. Once individual laminin molecules begin to polymerize it may become necessary for all or most of the anchorage sites of each laminin molecule in the polymerized collective to be blocked in order to stop or reverse further laminin binding and BM formation. Polymerization per se does not require anchorage, therefore, once a nucleation event of perhaps just a few laminin molecules is initiated, more laminin can bind this collective irregardless of their individual anchorage status. While possibly not the case in this cell system, this problem can be complicated not just by the multiple anchors of LG4-5 but also, LG1-3, the LN domain, and other binding partners (such as agrin, perlecan, nidogen...) which may themselves potentially bind other anchors which may or may not be present. The difference in observed inhibition between the mutant $\alpha 1\text{LG4-5s}$ did not follow the same relationship as that observed for either sulfatide or αDG affinity.

Recombinant WT laminin, Lm-111 $_{\text{Nm/Nh/Cf}}$, bound to the C2C12 myotube surface with the same intensity as EHS purified Lm-111. Recombinant WT laminins tended not to achieve equal binding with EHS Lm-111 when examined with Schwann cells. Furthermore, the Lm-111 $\Delta\alpha\text{LG1-3}_{\text{Nm/Nh/Cf}}$ showed no decrease in C2C12 binding (figure 56). Deletion of LG1-5 or LG4-5 resulted in almost a complete loss of binding, therefore, the critical anchorage site(s) in Lm-111, with regards to binding C2C12 myotubes, must exist in LG4-5. The full length recombinant heterotrimeric laminins containing point

mutations in $\alpha 1$ LG4, Lm-111 α RKR_{2721Nm/Nh/Cf} (similar to mutant $\alpha 1$ LG4-5 mutants RKR₂₇₂₁ which moderately affected α DG binding and sulfatide binding and RAR₂₇₂₁ which severely affected α DG binding but did not affect sulfatide binding) and Lm-111 α RAR_{2833Nm/Nh/Cf}, (similar to mutant $\alpha 1$ LG4-5 RAR₂₈₃₃ which severely affected both α DG and sulfatide binding) both practically abolished laminin binding to the cell surface. When these results are examined along with the observations that the $\beta 1$ integrin blocking antibody Ha2/5 and the α DG blocking antibody IIH6, both failed individually and together to block Lm-111 binding to the C2C12 cell surface (figure 57), and that $\alpha 1$ LG4-5/KDR₂₈₆₀, a mutant with a severe DG binding defect and a moderate sulfatide binding defect, was observed to still inhibit exogenous Lm-111 binding to the C2C12 cell surface; it suggests, not only, that in C2C12 myotubes both laminin polymerization and anchorage through $\alpha 1$ LG4 are required for laminin accumulation, but also, that while the anchorage through $\alpha 1$ LG4 may not require α DG, it definitely requires another anchor in combination or alone, and that anchor is not sulfatide, as in the Schwann cell.

Section VIIH. Insights derived from the role of Lm-111 and its receptors in MEFs.

Much like the Schwann cells, mouse embryonic lung fibroblasts do not express laminin-111, however, unlike the Schwann cells, MEFs also do not express sulfatide. They do synthesize and secrete type IV collagen and nidogen, however, without laminin-111 to anchor them to the cell surface they are secreted out into the media and do not accumulate on the MEF cell surface to any appreciable degree. The multiple anchorage sites present in laminin $\alpha 1$ LG4 make the identification of specific amino acid residues and dissection of their contribution to individual activities difficult. A further complication is not knowing the identity of all the potential receptors nor their distribution in any given cell system. MEFs offer the opportunity to perform analyses with or without one of these

anchoring molecules being present – sulfatide. Sulfatide is absent from MEFs and dystroglycan appears to be the major receptor present for $\alpha 1$ LG4. The absence of sulfatide also allowed for the potential opportunity through sulfatide loading or not loading of WT and DG null MEFs to create a platform for a quasi biological *in vivo* equivalent of the solid phase ELISA assays. Using a dynamic cell membrane as a platform rather than a static solid phase surface has several advantages, including: being able to present fewer receptors/anchors for interaction in a more dispersed format and thereby avoid the packing and steric hindrance issues inherent in coating a solid phase substrate, receptors are correctly orientated for presentation to ligand in biologically relevant surroundings and geometry, receptors are much more likely to be present in their native and true conformation, lateral movements are possible, and the monitoring of downstream events such as migration, condensation, cytoskeletal rearrangement, and cell signaling are possible.

Like the Schwann cells, which do contain sulfatide on their cell surface, if the MEFs have not been loaded with sulfatide (i.e. contain no sulfatide), exogenous laminin will still bind on the cell surface via α DG, the laminin will provide an anchor for the secreted nidogen and type IV collagen, and all four components (Lm, α DG, Nidogen, and type IV collagen) will condense towards the center of the cell. The laminin and α DG both co-localize together and with GM₁ in a classic lipid raft distribution pattern (figure 61B). Unlike the Schwann cells, however, without the presence of sulfatide, the complexes in MEFs will stay as separate small punctate "islands", never joining into continuous structures that constitute a typical basement membrane pattern (figures 59 and 63). However, if the MEFs are first loaded with sulfatide and then incubated with exogenous laminin, the same process will occur, however, the smaller complexes (small lipid rafts), will merge into higher order lipid raft structures as the rafts condense and a basement

membrane will be formed (figure 65). The observed phenomena is very similar in appearance to the *in vitro* lipid rafts created in lipid vesicle and bilayer experiments where raft formation and changes in both size and lipid composition are induced by altering the lipid mixtures. What is not similar, nor typical of behavior normally seen on cell surfaces, is the stability of these observed rafts once exposed to and bound by exogenous laminin-111 (figure 64). The behavior of the sulfatide loaded and non-loaded MEFs clearly demonstrate not only the requirement for sulfatide and laminin, but also, the roles they play in lipid raft and subsequent basement membrane formation.

Furthermore, the addition and accumulation of exogenous laminin on the cell surface of MEFs is insufficient to induce Src phosphorylation unless the cells are also loaded with sulfatide. The observed Src activation does not occur if the laminin is incapable of polymerizing (either through fragment inhibition, chemical modification, or LN domain deletion) or anchoring to the cell surface through $\alpha 1$ LG4 (either through fragment inhibition, chemical modification, LG4 domain deletion, and LG4 point mutations). This activation is prevented by antibody which blocks the binding of Lm-111 to α DG. Laminin $\alpha 1$ LG4 anchorage ligates laminin to α DG but Lm-111 polymerization is required to sufficiently aggregate the α DG and the putative complex it is part of (and thereby indirectly Src), to a point where Src activation will be induced.

While LG4 is required for binding to the surface of MEFs, the polymerization activity of laminin-111 is also required for larger aggregate formation, condensation and basement membrane formation. The polymerization incapable recombinant Lm-111_{Nm3/Nh/0} and Lm-111 $\Delta\beta$ LN-LEa_{0/Nh/Cf} will bind to the MEF cell surface to a much lesser degree and with a much finer punctuate coverage pattern than WT laminin, furthermore, it does not seem to migrate or condense (figure 67and 68). In Figure 68, the exposure is increased threefold in the mutant Lm-111 in order to be able to observe the pattern.

Lm-111 will bind the MEF cell surface as long as it has a functional LG4, however, it requires laminin's polymerization activity to form larger (but still small) aggregates. MEF's then require sulfatide and laminin's polymerization activity to form still larger higher order aggregates (lipid rafts). Both the smaller order and larger higher order aggregates/rafts will both migrate and condense, however, only the larger higher order aggregates/rafts which require sulfatide and laminin polymerization will join into still larger aggregated complexes and form a basement membrane.

A puzzling observation initially was that recombinant WT $\alpha 1$ LG4-5 was generally an “inefficient” inhibitor of Lm-111 binding in both sulfatide and cell surface assays, requiring high molar excess to affect effective inhibition. This may be explainable by assuming the existence of cooperative binding and, when examined in context with the recombinant $\alpha 1$ LG4-5 and heterotrimeric laminin characterizations and cellular deposition results, fits together to describe an elegant solution by nature's design for a complicated problem. Assume for a moment that there are only three binding sites in LG4, there are probably more and this is an intentional oversimplification, indicated in figure 69 and 72 by: “S₁” (1st sulfatide binding site), “S₂” (2nd sulfatide binding site), and “DG” (α DG binding site). Also, for the moment, disregard other potential binding events between laminin and other receptors/anchors or factors which bind to other anchors/receptors on the cell surface and may contribute to laminin accumulation on the cell surface, for example: the heparin, syndecan, perlecan, or fibulin binding activities present in $\alpha 1$ LG4, $\beta 1$ integrin binding activity in $\alpha 1$ LG1-3, integrin and polymerization activities of the N-terminal LN domain of the $\alpha 1$ chain, nidogen, agrin, etc. Mutation and inactivation of site “DG” in a recombinant $\alpha 1$ LG4-5 may be shown via solid phase assay, however, when this recombinant fragment is used in an attempt to block binding and

accumulation of heterotrimeric laminin, it would still act as an effective blocking agent unless the binding of “S₁” and “S₂”, together or individually, were also affected directly or indirectly by mutation of site “DG”, require α DG for binding, or the binding interactions in question are so weak that all three or two are required for anchorage to the cell surface. Despite the specificity, laminin-to-sulfatide affinities are quite weak as are sulfatide-to-sulfatide affinities. These weak affinities are compensated for and require increased numbers of interactions and distant but linked higher affinity interactions. The ability of laminins to polymerize allows for dramatic increases in net affinity by the simple fact that each laminin which joins the bound collective brings with it several binding interactions which it adds to the collective’s overall binding affinity. The cumulative effect, much like the cumulative effect of hydrogen bond contributions in protein folding, structure maintenance, and stability, is the production of a very high overall binding affinity due to the accumulation of large numbers of low affinity bindings which have become linked together. This effect is still further increased through laminin accumulation by laminin polymerization and interaction with other factors which bind laminins together directly or indirectly (nidogen and type IV collagen) and directly or indirectly to other factors, anchors, and receptors (agrin, dystroglycan, integrin, perlecan, etc.) forming large complexes. This process makes for an apparent binding event which is much stronger and more resilient than it would otherwise be if it were just a single isolated binding event. Like the individual grains of sand in cement (with rebar in this case), which individually are held together very weakly (as anyone who has attempted to build sandcastle for their impatient child at the Jersey shore can attest to), but with numbers and increased interactions with other molecules become very strong and resilient.

This process also explains why the accumulation of polymerization defective recombinant heterotrimeric Lm-111 mutants and native non-polymerizing laminin family members on certain cell surfaces is so low and there is no observable basement

membrane formation despite no apparent loss of anchorage/receptor sites in the laminin. Polymerization is necessary in order to increase the number of binding events and overcome the inherent limitation of the individual low affinity binding events. This represents an elegant solution and control mechanism for formation of basement membranes only where all these factors are localized to specific sites, in sufficient numbers, and in the presence of a polymerizable laminin. Furthermore, these anchorage interactions, such as laminin-to-sulfatide as well as sulfatide-to-sulfatide, are out of necessity of low affinity and rely on increases in local concentrations, such as aggregate formation and lipid rafts, to increase their affinity. If these interactions were of high affinity, basement membranes would form in every temporal and spatial location one of these receptors/anchors was present not just at defined spatial and temporal locations (and we would become immobile cement statues not sunburned nimble sandcastle builders chasing our dreams down the beach).

Lm-111 is capable of inducing cytoskeletal rearrangements through dystroglycan. While Lm-111 will assemble, accumulate, and condense on the cell surface of MEFs in the presence of α DG, it will not form a proper BM without the involvement of another one of its anchors - a sulfated glycolipid. Unlike the observed Schwann cells which possess both DG and sulfatide, unless sulfatide is provided to the MEFs, exogenous Lm-111 will accumulate, condense, and move towards the center of the cell, however, it will retain its punctuate appearance and not coalesce into a BM pattern as in the Schwann cell or MEFs loaded with sulfatide. Not only are sulfatide, laminin, and DG often found within lipid rafts, lipid raft complexes containing these molecules are also highly enriched in certain GMs and contain caveolin. Furthermore, the observed aggregation and condensation patterns, including the clearing around the nucleus, are typical of caveolin-1 dependent endocytosis of glycosphingolipids and classic lipid raft

characteristics. Also observed, as is typical of lipid rafts and their constitutive molecules, was association with and influence upon the behavior of cytoskeletal components and induction of cell signaling through Src, FAK, and caveolin-1. The results show that sulfatide loaded MEFs clearly form a BM when supplied with exogenous Lm-111, whereas, the non-sulfatide loaded MEFs will not. Furthermore, Src activation and downstream cell signaling, such as caveolin-1 phosphorylation, induced by laminin requires that the Lm-111 not only possess both its polymerization and LG4 anchorage through both DG and sulfatide, but that both α DG and sulfatide be present and engaged by laminin. β 1 containing Integrins are not required in this process. There is remarkable similarity between the role of sulfatide in laminin-111 anchorage and the role of HSPGs like perlecan and syndecan which, like sulfatide, are low affinity receptors for their ligands, growth factors like FGF and VEGF, and function to both bring and present ligand to receptor complexes and increase ligand concentrations in these complexes in order to favor higher order affinity interactions of the ligands with their other receptors. Furthermore, HSPG and sulfatide are also typically found in lipid rafts and the molecules they weakly bind and bring to complexes are capable of activating the same cell signaling pathways we observed.

Furthermore, the exogenous laminin-111 appears to provide a means to stabilize the otherwise transitory nature of lipid rafts by bringing together and holding in place not just sulfatides and DG, but also, other factors and lipids associated with them into a complex; initially through the anchorage activity of the laminin α 1 LG4 domain and then through laminin polymerization holding them in place, recruiting more factors to the collective, and not allowing them to disperse. Laminin provides a function similar in manner to the crosslinking of GM₁ by treatment with cholera toxin subunit B (CT-B) and antibody to CT-B performed routinely to immobilize lipid rafts and stop them from

dispersing for study [474]. *In vitro*, the binding interactions of laminin with receptors/anchors on the cell surface and its components are "cemented" in place by further interactions on the extracellular side, intracellular side, and within the membrane (lipid raft) itself. The resulting complex and/or lipid raft interactions are bolstered by molecules on the extracellular side which accumulate through laminin and tie the complex on the cell surface to the extracellular matrix through interactions such as nidogen's linkage to a type IV collagen network and directly through laminin to other constituents of the lipid rafts on the cell surface via laminin's interaction with molecules such as agrin, perlecan, integrin, α DG, and syndecan. The glycosphingolipids (GSLs) which compose the raft contribute their attraction to one another [475] and many of the other molecules which compose it [476, 477], as well as interactions between non-lipid components, to also stabilize the complex. The intracellular side of the lipid raft complexes are then stabilized by linkages through complexes to the cytoskeletal F-actin via such means as dystroglycan's interaction with cytosolic dystrophin and utrophin complexes and integrin's interaction with α -actinin and talin (and through both of them vinculin) as well as glycosylphosphatidylinositol (GPI) [475, 478, 479] anchored proteins, caveolins [479] and cell signaling complexes [480, 481]. If not the glue which holds everything together, laminin is, at the very least, both the workhorse through and of which the glue is made.

Chapter 5. Summary and Conclusions

Basement membranes (BMs) are cell surface-associated extracellular matrices (ECMs) composed primarily of an interconnected network of laminin and type IV collagen meshes. A system of producing recombinant heterotrimeric laminin-111 and laminin $\alpha 1$ LG4-5 was devised in order to examine laminin's different activities and their role/contribution to laminin binding, accumulation, and basement membrane formation. Various recombinant laminin proteins were created not only to identify the critical residues pertaining to a given binding interaction, but also, so residues responsible for a given binding interaction could be selectively removed and the role of that binding interaction in BM formation determined. Recombinant proteins were designed with an optimized 5'UTR which increased recombinant production levels by more than 4 fold over previous constructs, followed by the BM40 signal sequence for secretion, an epitope tag for purification and detection, the recognition site for cleavage by Enterokinase in order to cleave off the epitope tag if desired, and the desired laminin sequence. The expression constructs also included a unique antibiotic selectable marker on the expression construct. The kidney fibroblast 293 cell line was chosen for production of the recombinant proteins because it is easily transfected and maintained in culture, can produce large amounts of recombinant protein, and *in vivo* is typically a source of extracellular matrix proteins and therefore deemed most likely to provide post-translational modifications similar to those observed *in vivo*.

Three types of molecules have been described that mediate the interaction of $\alpha 1$ LG4-5 with cell surfaces: heparin/heparan sulfates, sulfated glycolipids (sulfatides), and α -DG. Since the interaction of all three appear to be dominated by electrostatic forces between negatively charged receptor moieties (e.g., sulfate groups) and basic

amino acid side chains (Arg and Lys residues) in the LG4 domain of $\alpha 1$ LG4-5 [162, 305, 324, 297, 482], the positively charged amino acids Lys and Arg were the focus for the mutational analysis of $\alpha 1$ LG4-5. Previous studies had identified residues in LG4, either by site-directed mutagenesis [162] or by systematic peptide mapping [483]. Mouse laminin $\alpha 1$ LG4 contains 19 Lys and Arg residues and 8 His residues. Homology and energy minimization computer modeling programs along with tabulation of secondary structure prediction programs and individual amino acid residue characteristics, enabled the prediction of the three dimensional structure of mouse $\alpha 1$ LG4-5 using the coordinates from the crystal structure of the homologous mouse $\alpha 2$ LG4-5. This generated homology model of mouse $\alpha 1$ LG4-5 and data from the analyses performed were then utilized to identify individual amino acid residues for mutagenesis. Histidine residues were not included in the mutational screen because of their inherent restricted conformational constraints and key roles in secondary structures. Seven mutant $\alpha 1$ LG4-5s were created for the first mutational screen and examined. All analyses revealed that no single basic residue is exclusively associated with one activity. In the case of $\alpha 1$ LG4-5, loss of overall charge affects all three components, but to different degrees. Of the three molecules evaluated, we found that loss of heparin binding correlated best with a decrease in overall basic charge, whereas, loss of dystroglycan correlated least with charge (figures 23C, 24F, and 26E).

Furthermore, when one compares the contributions of different residues to binding and maps these to the surface topography of the domains as shown for the $\alpha 1$ LG4-5 subunit in Figure 73, it becomes evident there are distinct differences in residue contributions such that mutations of residues within a cluster can cause a substantially greater loss of one activity compared to another. Notably, Ala substitution of Arg₂₇₁₉ and

Lys₂₇₂₀ results in an eleven-fold loss of dystroglycan binding compared to a less than two-fold loss of sulfatide binding and modest decrease in heparin affinity elution.

Compared to the earlier study of Andac et al., [162] which evaluated binding interactions of recombinant α 1 LG4, we found similar heparin elution behaviour for those sequences evaluated in common (figure 23). Furthermore, a recent report used an energy minimalization analysis of the laminin α 2 LG4 structure to gain insight into the α 1 LG4 structure and its interaction with syndecans [484]. The syndecan binding activity, reflecting a heparan sulfate contribution, was found with a solid phase binding assay to depend upon contributions from RKR₂₇₂₁ and KRK₂₇₉₃ and is in agreement with both our heparin binding data and crystal structure. However, considerably different interactions for interactions of LG4-5 with dystroglycan and sulfatide were found with our data compared to those of Andac et al., i.e. interactions of dystroglycan to KGRTK₂₇₇₀ (145 vs. > 3500 nM; figure 24), sulfatide to RAR₂₈₃₃ (2250 vs. 19 nM) and sulfatide to KDR₂₈₆₀ (438 vs. 37 nM) were observed (figure 26). Possible reasons for these differences are modulating effects, e.g. those, arising from the adjacent and disulfide-linked LG5 domain and differences in methodology as discussed earlier. Perhaps the most striking contributions came from RKR₂₇₂₁ (mutant protein α 1LG4-5/RKR₂₇₂₁), which was required for dystroglycan binding but not sulfatide binding, and RAR₂₈₃₃ (mutant protein α 1LG4-5/RAR₂₈₃₃), which was required for both. These binding results and their location in the new crystal structure for mouse α 1 LG4-5 that we determined, enabled assignment of the heparin/heparan sulfate binding site of laminin α 1 to the basic patch of LG4 made up of RKR₂₇₂₁ and KRK₂₇₉₃. The α -DG binding site is formed by a larger, semi-circular arrangement of basic side chains with a key role played by residues, RAR₂₈₃₃ and KDR₂₈₆₀, located away from the heparin binding site (figure 73). This binding site also involves both the N-linked glycosylation moiety of Asn₂₈₁₁ located on the rim of this

circular arrangement and the Ca^{2+} found bound in the center of this circular arrangement of basic charges. Laminin $\alpha 1$ LG4 appears to contain two sulfatide binding loci: one site involves the bound Ca^{2+} ion of LG4 and is affected by and situated adjacent to Arg₂₈₃₃ of RAR₂₈₃₃ and the Lys₂₇₆₆ of KGRTK₂₇₇₀. The second site is "around the bend" in LG4 and is both closer in proximity to and affected by the second Arg₂₈₃₁ residue of RAR₂₈₃₃. That is why $\alpha 1\text{LG4-5/RAR}₂₈₃₃ completely abolishes sulfatide binding (it affects both sulfatide sites), $\alpha 1\text{LG4-5/KGRTK}₂₇₇₀ cuts sulfatide binding in half (it affects the site adjacent to the bound Ca^{2+}), and many of the other mutant recombinant $\alpha 1\text{LG4-5s}$ ($\alpha 1\text{LG4-5/RKR}₂₇₂₁, $\alpha 1\text{LG4-5/RKR}₂₇₂₁, and $\alpha 1\text{LG4-5/KRK}₂₇₉₃) situated around the charged ring containing the calcium site indirectly affect sulfatide binding, quite possibly just by affecting the Ca^{2+} or adjacent N-linked glycosylation site of Asn₂₈₁₁. This explanation also fits the sulfatide immunoprecipitation data and would also explain why in the presence of EDTA, sulfatide binding is cut in half, i.e. Ca^{2+} is required for just one of the two sulfatide sites in LG4. Furthermore, a two site fit of the sulfatide ELISA plots works much better for several of the recombinant $\alpha 1\text{LG4-5s}$ than the single site fit did.$$$$$

Despite the conservation in secondary and tertiary sequence, as well as binding ligands, the identity and locations of the residues involved in receptor/anchorage binding activities and their affinities in the respective $\alpha 1$ and $\alpha 2$ LG4-5s differ. This along with identification of the critical residues for these interactions and the mapping of their location onto the crystal structure of $\alpha 1$ LG4-5 that we obtained, explain certain observations, such as the ability of heparin to block αDG binding in $\alpha 1$ but not $\alpha 2$ laminin and the Ca^{2+} requirement for αDG and sulfatide binding. The LG4 domain is the major site of heparin, DG, and sulfatide binding in $\alpha 1$ laminin. It contains just one αDG binding site and also binds both sulfatide and heparin with higher affinity than $\alpha 2$; $\alpha 1$ also possess two sulfatide binding sites as opposed to $\alpha 2$ LG4-5's one site. Laminin $\alpha 2$

contains DG binding site(s) within both LG1-3 and LG4-5, whereas, there is only one α DG binding site within α 1 and it is located in LG4. Proteolytic processing in LG3 of α 2 further complicates the comparison, as the proteolytic processing disrupts a potential binding site and whether or not the released C-terminal fragment remains associated with the G domain also affects several binding activities. The DG site in α 1 LG4 is adjacent to the heparin binding site, whereas, that is not the case in α 2 and that is why heparin can block α DG binding in α 1 but not in α 2. Both α 1 and α 2 α DG binding sites are adjacent to Ca^{2+} binding sites and that is why α DG binding in both α 1 and α 2 can be abolished with EDTA treatment. Furthermore, not all analogous residues have been studied by mutation; for instance, the RKR₂₇₂₁ sequence of α 1 LG4-5 is represented by KNR in α 2 LG4-5, but that sequence was not targeted by Wizemann et al. [482], therefore, there are still more similarities and disparities between α 1 and α 2 to be investigated.

It should be noted that due to the conformational constraints imposed by the disulfide linkages, the location of the identified binding sites are at the distal end of α 1LG4-5 (relative to the LG3-LG4 linker), *i.e.* well positioned for anchorage to cell surfaces.

The α 1 LG4-5 mutagenesis approach enabled identification and determination of key residues involved in specific binding activities and the ability to select just a few residues for inclusion in full length recombinant heterotrimeric laminins for further testing without the monumental effort of generating large numbers of recombinant full length heterotrimeric laminins. Furthermore, since laminin contains several binding interactions, the analysis of the smaller recombinant fragment data aided in the interpretation of the results garnered from the recombinant heterotrimeric laminins and enabled identification and preclusion of those interactions stemming from outside of LG4-5 which would have influenced interpretation of the results.

Laminin-111 requires both its self polymerization activity, mediated by the N-terminal LN domains of the individual $\alpha 1$, $\beta 1$, and $\gamma 1$ subunit chains, as well as its cell anchorage activities, mediated by the C-terminal LG4 module of the $\alpha 1$ chain, for proper basement membrane formation. These activities, the residues in laminin involved, their requirement, and the consequences of their absence were tested in several cell systems, including: Schwann cells, several embryonic stem cell lines and embryoid bodies derived from them, C2C12 myotubes, and mouse embryonic fibroblasts. Consistently in all systems examined, in order for proper laminin accumulation and basement membrane formation to occur, laminin-111 required both polymerization and anchorage activities. Recombinant trimeric Lm-111s missing the N-terminal LN or LN and adjoining EGF repeats from either the $\alpha 1$, $\beta 1$, or $\gamma 1$ chain failed to polymerize and form a BM. Domain swaps, chemical inactivation, and a triple myc epitope tag on the N-terminus of $\alpha 1$ of Lm-111 also resulted in loss of polymerization and the ability to form a BM on Schwann cells, C2C12 myotubes, and MEF (loaded with sulfatide). Recombinant trimeric Lm-111s missing either the C-terminal LG1-5 or LG4-5 also failed to form a BM when tested on Schwann cells or C212 myotubes, whereas, recombinant trimeric Lm-111 missing LG1-3 but retaining LG4-5 did form a BM. Furthermore, the recruitment of type IV collagen to the basement membrane appears to be mediated through a nidogen bridge with laminin. Exogenously added fully functional Lm-111 enables BM formation, proper differentiation, formation of an epiblast layer, and cavitation in embryoid bodies from both $\gamma 1$ laminin null and $\beta 1$ -integrin null embryonic stem cells (figure 54). Any loss of polymerization or $\alpha 1$ LG4 anchorage resulted in a failure to rescue (figure 55). The combination of laminin transport across the outer endodermal layer and its concentration in the relatively small confined space between the endodermal and developing outer epiblast layer of the inner cell mass, lead to a dramatic increase in

localized critical concentration levels which made for ideal inhibition environments. Furthermore, DG null ES cells could differentiate, form a BM and EBs, however, DG is clearly required for continued survival of the differentiated epiblast layer.

In Schwann cells, sulfatide provides a glycolipid anchor for proper laminin accumulation and BM formation. Both solid phase ELISA and Schwann cell experiments, not only, demonstrated the specificity requirement for the sulfate moiety on sulfatide, but also, the location and identity of the residues involved in binding sites in $\alpha 1$ LG4. MEF's lack of sulfatide and ability to be loaded with sulfatide, along with the data collected in the Schwann cell system, provided the opportunity to examine the roles of sulfatide and DG, both individually and in concert, and examine DG's role without the masking contribution of sulfatide to discern from. MEFs isolated from a DG null line contain neither DG nor sulfatide. Dr. Shaohua Li showed [71] the nidogen and type IV collagen the MEFs secrete will not be retained on the cell surface, no basement membrane will form, nor is there Src cell signaling. If exogenous Lm-111 is supplied, it will not bind the cell surface and there is no change in the behavior of the cell, unless the cells are first loaded with sulfatide. In which case, the exogenous Lm-111 will bind on the cell surface, aggregate, condense, and form a BM. Type IV collagen and nidogen will bind and co-localize with the exogenous laminin, however, no Src phosphorylation/activation will occur without the presence of DG. MEF cells containing DG (but no sulfatide) will bind exogenous Lm-111 on the cell surface. Several laminin molecules will aggregate (probably polymerizing) and other extracellular proteins, such as nidogen and type IV collagen, which bind laminin, as well as GM1 will also accumulate in micro lipid raft complexes which form. The laminin stabilizes the normally transitory lipid raft complex and these complexes will migrate and condense, however, they will not join in higher order lipid raft complexes, they will not form a proper basement membrane, nor will Src activation be induced. With the addition of

exogenous Lm-111, the exogenous laminin, endogenous nidogen-1, and endogenous type IV collagen will bind the cell surface, however, without sulfatide they will not migrate, condense, and form higher order lipid raft complexes, form a proper basement membrane, nor induce Src phosphorylation/activation. Polymerization deficient recombinant Lm-111s will bind the cell surface of sulfatide deficient MEFs through α DG, however, they will not form micro lipid complexes, migrate, condense, or form a basement membrane. Deletion of the anchorage sites in domain LG4, represented in recombinant Lm-111 $\Delta\alpha$ LG1-5_{Nm/Nh/Cf} and α LG1-3_{Nm/Nh/Cf}, resulted in laminins not able to bind the cell surface of MEFs, whereas, both heterotrimeric point mutation Lm-111 α RKR_{2721Nm/Nh/Cf} and Lm-111 α RAR_{2833Nm/Nh/Cf} accumulated very poorly on the cell surface. Just like our earlier findings in embryoid bodies and Schwann cells, the MEF results suggest a prominent role of sulfated glycolipids with more of a signalling rather than an anchorage contribution arising from dystroglycan, though dystroglycan is capable of supplying sufficient anchorage for binding of laminin to the cell surface and is required for Src activation.

MEFs and Schwann cells require sulfatide (or sulfated carbohydrate moiety) as an anchor to varying degrees, α DG may be dispensible if a sulfatide anchor is present, but required if sulfatide is absent for anchorage, however, higher order aggregations and basement membrane formation will not occur without the prescence of sulfatide. Laminin bound aggregates in MEFs will migrate and condense, and bind both nidogen and type IV collagen, however, they will not fuse to form higher order aggregates, form a basement membrane, or induce Src activation without sulfatide. Sulfatide is required for laminin's formation of these higher order aggregates, formation of a proper basement membrane, and induction of cell signaling events such as Src activation and

downstream activation of caveolin-1 (both of which are preferentially located in lipid rafts), whereas, laminin induce FAK activation is through $\beta 1$ integrin.

Laminin's many different activities, including their roles in binding to cell surfaces, contribution to basement membrane formation, differentiation, and cell signaling were examined. Basement membrane formation is a progressive process initiated by laminin-111's initial binding to anchors and receptors on the cell surface, followed by deposition of several laminins to form small aggregates and accumulation of other extracellular matrix proteins through laminin and other anchors/receptors in the small aggregates, then migration of these aggregated complexes in lipid rafts and condensation to form higher order rafts and complexes and the eventual establishment of a basement membrane. Proper basement membrane formation and downstream effects of this process, such as cytoskeletal rearrangement and cell signaling, require both laminin-111's polymerization and $\alpha 1$ LG4 anchorage activities. Laminin-111 polymerization requires all three of its constituent individual chains' LN domains and functions to not only bring in more laminins and their binding partners into the resulting complex, but also, plays a role in maintaining the stability of the otherwise transient lipid raft which is an integral part of the complex and serves as a platform itself for anchors and receptors, as well as a means of attaining a cytosolic connection to the cytoskeleton and cell signaling mechanisms. Laminin-111 anchorage to the cell surface requires only binding sites in the LG4 domain of $\alpha 1$. Laminin binding through either the αDG or sulfatide binding sites is sufficient for laminin-111 binding to the cell surface, however, basement membrane formation only requires the sulfatide binding sites and can not occur with just αDG to anchor the laminin-111, whereas, cytoskeletal association and Src signaling require the additional contributions provided by the binding of laminin to

α DG. This arrangement of so many factors allows for exceptional specificity and control which would not be achievable otherwise. The multiple low affinity interactions involved allows for minor alterations in expression patterns of any constituent of the collective to have dramatic effects in laminin binding, accumulation, basement membrane formation, and thereby laminin's induction of downstream events such as cytoskeletal rearrangement, cell signaling, differentiation, and cellular polarization.

Figure Legends

Figure 1. Potential laminin interactions. A diagram of laminin-111 and some of the potential interactions between laminin-111 and other extracellular matrix proteins (α DG, nidogen, type IV collagen, agrin, and perlecan), as well as some cellular receptors. Red lines denote potential interaction between laminin and other molecules. Grey lines denote potential interactions between molecules other than laminin. Legend: grey “N” denotes N-terminal domain; grey “C” denotes C-terminus of protein; red “LN” denotes the N-terminal LN domain of the α 1 chain of laminin; red “LG1-3” denotes the LG1-3 domains of the C-terminal G domain of the α 1 chain of laminin; red “LG4” denotes the LG4 domain of the C-terminal G domain of the α 1 chain of laminin.

Figure 2. The laminin family. **(A)** A representation of heterotrimeric laminin-111. The α chains are colored blue, the β chains red, and the γ chains green. **(B)** Representations of the 5 known α chains, 3 β chains, and 3 γ chains which compose heterotrimeric laminin. **(C)** Phylogenetic tree showing the evolutionary (and homology) relationship between the 11 individual laminin chains. Domains are marked utilizing the nomenclature formalized in Aumailley et al. [3].

Figure 3. The proteolytic fragments of laminin-111. Diagram of the proteolytic fragments of laminin-111 often utilized for inhibition and binding studies. Enzymatic digestion of laminin-111 purified from EHS tumor with cathepsin-G produces fragment C1-4 **(A)**. Digestion with trypsin yields fragments E1', E4, E8, and E3 **(B)**.

Figure 4. The summation of EST expression results for laminin α chains in NCBI's GEO repository. A summation of the EST expression array results held at

NCBI and organized by tissue classification for all laminin α chains. The colored bar represents the theoretical number of transcripts for the given chain per million of transcripts synthesized in the indicated tissue. No bar represents either no transcripts detected for the given laminin chain or that there are no results. Appendix figure 1 list the actual numbers.

Figure 5. The summation of EST expression results for laminin β chains in NCBI's GEO repository. A summation of the EST expression array results held at NCBI and organized by tissue classification for all laminin β chains. The colored bar represents the theoretical number of transcripts for the given chain per million of transcripts synthesized in the indicated tissue. No bar represents either no transcripts detected for the given laminin chain or that there are no results. Appendix figure 1 list the actual numbers.

Figure 6. The summation of EST expression results for laminin γ chains in NCBI's GEO repository. A summation of the EST expression array results held at NCBI and organized by tissue classification for all laminin γ chains. The colored bar represents the theoretical number of transcripts for the given chain per million of transcripts synthesized in the indicated tissue. No bar represents either no transcripts detected for the given laminin chain or that there are no results. Appendix figure 1 list the actual numbers.

Figure 7. The number of amino acid residues composing laminin-111, its constituent α 1, β 1, and γ 1 chains, and other proteins it interacts with, as well as the location in Lm-111 of these binding interactions. (A) Bar graph depicting the number of amino acid residues per average protein (300 residues), laminin-111 (6,300 residues), α 1 laminin chain (3,084 residues), β 1 laminin chain (1,786 residues), γ 1

laminin chain (1,607 residues), and elastase proteolytic fragment recombinant α 1LG4-5 is based upon (372 residues). **(B)** Diagram of laminin-111's known binding activities and their approximate location in laminin-111. **(C)** Bar graph depicting the number of amino acid residues comprising laminin-111 and both ECM components and cellular receptors laminin-111 may interact with.

Figure 8. Extracellular matrix genes and related diseases. Defects in laminin and other extracellular matrix genes are associated with a wide selection of diseases. This represents only a partial list of known ECM genes and the diseases associated with defects in them.

Figure 9. Mouse knockout results of ECM proteins, their receptors, and related BM components. The targeted deletion of genes involved in the ECM and BM are listed along with their associated null phenotype and reference for the appropriate knockout article. Embryonic lethal knockouts are in blue.

Figure 10. Embryoid body development. **(A)** A schematic representation of embryogenesis showing development up to day 5.5 p.c. and formation of BMs, as well as differentiation and development of several cell types. BMs first appear (E3.5-4 in the mouse) after implantation and before the start of gastrulation and can be studied in embryoid bodies which recapitulate early differentiation and BM formation. **(B)** The analogous developmental stages observed in developing embryoid bodies.

Figure 11. Amino acid sequence of mouse laminin α 1LG1-5. The amino acid sequence of α 1 LG1-5 is depicted and individual globular LG domains color coded. The

entire mouse $\alpha 1$ laminin sequence is 3,084 amino acid residues, approximately 956 of those residues are contributed by the five LG domains which comprise the C-terminal G domain of $\alpha 1$.

Figure 12. The amino acid sequence of the elastase proteolytic fragment E3 derived from mouse Lm-111. (A) Diagram of the proteolytic fragments generated by elastase digestion of Lm-111. **(B)** The 372 amino acid sequence of E3 is depicted which also represents the same sequence expressed in the recombinant $\alpha 1$ LG4-5 constructs.

Figure 13. Optimization of recombination protein production – selection of promoter, signal sequence, and 5'UTR for expression constructs. (A) Diagram of mouse $\alpha 1$ LG4-5 expression construct showing the location of the promoters, 5'UTR, signal sequences, epitope tags, engineered proteolytic cleavage sites, and selectable markers tested. **(B)** Tabulated results from Westerns of stably transfected cell lines, showing the relative expression levels of recombinant $\alpha 1$ LG4-5 produced under the CMV, RSV, and mouse $\beta 1$ laminin promoter with and without retinoic acid (RA). **(C)** Tabulated results from Westerns of stably transfected cell lines, showing relative expression levels of recombinant $\alpha 1$ LG4-5 produced under the same CMV promoter and 5'UTR but, with either the BM40, IG κ , or endogeneous mouse $\alpha 1$ signal sequence. **(D)** The upper segment of the table shows the collated data collected by Kozak [394, 462] and the percentage of each nucleotide found at each given position in the 5'UTR. Cells colored red represent a strong bias for that nucleotide at that position, orange a moderate bias for that nucleotide, and green a strong bias against that nucleotide. The ATG coding for the initiating Methionine is colored blue. Below Kozak's data, is the nine different 5'UTRs compared in expression constructs as well as the 5'UTR for mouse $\alpha 1$,

$\beta 1$, and $\gamma 1$ laminin. The compared 5'UTRs include: "consensus-1" and "consensus-2" derived from Kozak's data, the 5'UTR in $\alpha 1$ LG4-5/WT-pRCX3, and the 5'UTRs from human histone H2B (H2B), human translocase of outer mitochondrial membrane 7 homolog (TOMM7), human isoleucyl-tRNA synthetase (IARSB1), human farnesyl-diphosphate farnesyltransferase 1 (FDFT1), human ubiquitin-conjugating enzyme E2S (UBE2S), and human eukaryotic translation initiation factor 4A (EIF4A1). **(E)** Representative direct FLAG Western of media from cell lines stably transfected with the 5'UTRs listed in part D.

Figure 14. Determination of signal sequence cleavage sites. **(A)** Schematic of the characteristics of signal sequences: an N-terminal positively charged region called the n-region, followed by a hydrophobic stretch of residues called the h-region, followed by a series of amino acid residues which possess a neutral charge but are polar in nature, and finally neutral small side chain containing residues at positions -1 and -3 of the cleavage site. **(B)** SignalP-HMM analysis results of human $\beta 1$ laminin with its own endogenous signal sequence and no epitope tag. **(C)** Signal-NN analysis results of human $\beta 1$ laminin with its own endogenous signal sequence and no epitope tag. **(D)** SignalP analysis results of human $\beta 1$ laminin with its own endogenous signal sequence and no epitope tag. **(E)** Compilation of the results from analysis of the human $\beta 1$ laminin with ACN, SignalP, Signal-NN, and SignalP-HMM. The potential cleavage sites are color coded: blue for SignalP-HMM, green for signal-NN, red for SignalP, and black for ACN.

Figure 15. Epitope tagging of recombinant mouse $\alpha 1$ LG4-5 laminins. Six epitope tags were tested by expression on either the N-terminus or C-terminus of recombinant $\alpha 1$ LG4-5/WT. **(A)** A list of the epitope tags examined and their recognition sequence.

Cells were transfected with the corresponding expression construct, stable cell lines expressing the appropriate recombinant protein selected, and the recombinant $\alpha 1$ LG4-5/WTs purified from media by affinity chromatography with matrix appropriate for each epitope tag followed by heparin FPLC. **(B)** Purified recombinant $\alpha 1$ LG4-5/WTs were run on a 6-12% PAGE gel and stained with Coomassie blue. An aliquot of each purified protein was subjected to digestion with EnteroKinase (EK) and loaded adjacent to undigested material. All expressed recombinant proteins appeared to be of correct size and no proteolytic degradation detected. **(C)** Aliquots of recombinant protein, both untreated and EK treated, were also subjected to 6-12% PAGE and blotted to PVDF membranes for Western analysis with various antibodies. Immunoblotting with rG50 demonstrated the correct identity of the recombinant protein as well as the approximate concentration of loaded material. All epitope tags were successfully recognized by the appropriate epitope specific antibody, there was no cross-reactivity detected, and EK successfully removed the N-terminal tags without cleaving within the $\alpha 1$ LG4-5 sequence. The FLAG positive band observed after EK treatment of $\alpha 1$ LG4-5/WT_{Cf} is because the FLAG tag in this recombinant protein is C-terminal and the EK cleavage site, like in the other recombinant proteins, is N-terminal. These results demonstrated the suitability of the six epitope tags examined for inclusion in future expression constructs.

Figure 16. Puromycin based expression construct DHpuro and the mouse $\alpha 1$ laminin construct, $\alpha 1$ _{Nf}, derived from DHpuro. (A) A schematic diagram of the expression construct DHpuro, created with several of the key components shown in the diagram. (B) A diagram of the expression construct, $\alpha 1$ _{NF}, made utilizing the DHpuro vector to express under the CMV promoter the full length mouse $\alpha 1$ laminin chain with

an N-terminal FLAG tag and puromycin selection. Many of the subsequent mouse $\alpha 1$ constructs were made utilizing the Dh puro expression vector.

Figure 17. Conservation of the primary sequence between the LG4-5 of mouse $\alpha 1$ and $\alpha 2$ laminin. The top of the figure depicts the $\alpha 1$ chain of laminin and the location of $\alpha 1$ LG4-5 which is analyzed below. **(A)** Space filling diagram of a representation of the Van der Waal's forces and ribbon diagram both generated using Swiss-Model and Siss-Pdb Viewer/DeepView. The LG4-5 domains of both mouse $\alpha 1$ and $\alpha 2$ share 41.4% identity. This relationship is depicted as identical residues shown in red and non-identical in blue. This color coding scheme is mapped onto both the generated structures as well as an alignment of the two sequences found directly below them. **(B)** The same corresponding sequence of $\alpha 1$ and $\alpha 2$ are 56.8% homologous. The same procedures, programs, and structures were utilized as above, however, the color scheme is changed in order to depict the change in relationships: red represents identity, orange a conservative substitution, and blue non-identity.

Figure 18. Conservation of both primary sequence and predicted potential secondary structure between mouse $\alpha 1$ and $\alpha 2$ LG4-5 of laminin. Despite the differences in primary sequence, the predicted secondary structure of laminin $\alpha 1$ and $\alpha 2$ LG4-5 is conserved between the two chains and the predicted secondary structure for $\alpha 2$ coincides for the most part with the secondary structure observed in the crystal structure of $\alpha 2$ LG4-5. The primary sequence block contains the single character representation for the amino acid residue present at that position. If the block is colored orange it means $\alpha 1$ and $\alpha 2$ contain the identical amino acid residue at this position. If the block is colored grey they do not. Furthermore, the blue arrows and red coil directly

below the primary sequence for $\alpha 2$, represent the secondary structure elements, β -sheet and α -helix respectively, observed in the crystal structure of mouse $\alpha 2$ LG4-5. The β -sheet residues are also lettered according to the crystal structure. Below this data, are the results from nine of the twelve secondary structure prediction programs accessed through the NPS@ server: DPM, DSC, GOR IV, HNN, PHD, PREDATOR, SIMPA96, SOPM, and SOPMA. The results from MLRC, GOR I, and GOR III are not depicted in this figure. Furthermore, the final line of the block of results, marked "2⁰ con" represents the secondary structure consensus implied by the preponderance of results from the prediction programs. An orange block containing the character "c" means the program predicted random coil for this amino acid position, a red block containing " α " represents α -helix, a blue block containing " β " represents β -sheet, a light blue block containing "bt" represents β -turn, and a grey block containing a question mark, "?", represents an unclassified residue.

Figure 19. Homology model of mouse $\alpha 1$ LG4-5 (recombinant E3 analog). The laminin mouse $\alpha 2$ crystal structure coordinates [305] were utilized to homology model the mouse $\alpha 1$ LG4-5. The figure depicts the three dimensional model from five view points in order to gain a better understanding, not only, of the location of key residues on the surface of the protein, but also, their relationship to one another on the static representation rendered.

Figure 20. Comparison of both the spatial and primary location of Arg, Lys, His, and Cys residues in mouse laminin $\alpha 1$ and $\alpha 2$ LG4-5. The location of the Arg, Lys, His, and Cys residues are shown both in the primary sequence of $\alpha 1$ and $\alpha 2$ laminin **(A)** and on the three dimensional model of $\alpha 2$ LG4-5 **(B)**. The $\alpha 1$ residues were mapped

onto the $\alpha 2$ crystal structure rather than the $\alpha 1$ homology model in order to get a better sense of any conservation in the location of these charged residues between the two proteins. Despite the sequence homology, binding partner similarities, and conservation of secondary structure, positively charged residues of the two laminins rarely coincided in the primary or proposed tertiary structures of the two proteins.

Figure 21. Mutational combinations of Arg and Lys residues in initial recombinant $\alpha 1$ LG4-5 screen. Potentially key residues are shown on both a space filled representation of the homology modeled $\alpha 1$ LG4-5 **(A)** and the primary sequence below **(B)**. The spatial and primary location of the mutated residues represented in the recombinant mutant $\alpha 1$ LG4-5s are also depicted. One mutant not directly represented, is the double mutant which combines two different patches of charged residues, mutant $\alpha 1$ LG4-5/RKR₂₇₂₁+KRK₂₇₉₃.

Figure 22. Generation, production, and purification of recombinant mouse $\alpha 1$ LG4-5 laminins. **(A)** Salt elution profile off a heparin-5PW column of media harvested from HEK 293 cell line stably transfected with and secreting $\alpha 1$ LG4-5/WT_{Nf}. **(B)** Corresponding coomassie blue stained gel of collected fractions. There are several contaminating bands from protein(s) other than $\alpha 1$ LG4-5 present in the elution fractions containing $\alpha 1$ LG4-5. **(C)** SDS-PAGE of pre- and post purification of recombinant $\alpha 1$ LG4-5s. The expression level of recombinant $\alpha 1$ LG4-5 produced from the stably transfected cell lines is so high it is visible in a straight media load. Note the observed BSA band from the 10% FBS containing DMEM media in which the cells were grown in relation to the observed $\alpha 1$ LG4-5 recombinant proteins. The post purification recombinant $\alpha 1$ LG4-5 is of very high purity and lacks any obvious proteolytic

degradation. **(D)** SDS-PAGE and Western blot analysis of recombinant $\alpha 1\text{LG4-5/WT}_{\text{NT}}$ and a mutant recombinant $\alpha 1\text{LG4-5}$ treated or not treated (NT) with Enterokinase (EK) reveals decrease in size of recombinant protein after EK treatment with no spurious degradation and the expected loss of FLAG epitope tag. **(E)** Schematic of sequential PCR reactions and cloning procedure, along with agarose gel of sequential PCR products referenced, performed in order to produce the $\alpha 1\text{LG4-5}$ constructs containing a unique 5'UTR, which increased recombinant production levels by 4 fold over previous constructs, followed by the BM40 signal sequence for secretion, a FLAG tag for purification and visualization, the recognition site for cleavage by Enterokinase in order to cleave off the FLAG tag if desired, and the laminin $\alpha 1\text{LG4-5}$ sequence. **(F)** Coomassie blue stained SDS-PAGE of purified recombinant $\alpha 1\text{LG4-5s}$. Note the increased size observed for $\alpha 1\text{LG4-5/KDR}_{2860}$ when compared to the other recombinant proteins – this difference in migration was shown to be due to a difference in post-translational glycosylation of this mutant. **(G)** Rotary shadow electron microscopy of recombinant $\alpha 1\text{LG4-5s}$ reveal monomeric bifurcated dual domains ("WT" refers to recombinant $\alpha 1\text{LG4-5/WT}$, "G" to recombinant $\alpha 1\text{LG4-5/KRK}_{2793}$, and "A" to $\alpha 1\text{LG4-5/RKR}_{2721}$. Furthermore, gel filtration, acetylation, and non-reducing gel studies (data not shown) of the mutant recombinant $\alpha 1\text{LG4-5s}$ showed no differences when compared to $\alpha 1\text{LG4-5/WT}$.

Figure 23. Heparin affinity of recombinant mouse $\alpha 1\text{LG4-5}$ laminins. (A) The NaCl elution profile of various recombinant $\alpha 1\text{LG4-5s}$ from a heparin-5PW column run on an AKTA FPLC. **(B)** The spatial location on the surface of $\alpha 1\text{LG4-5}$ and relative degree of contribution to heparin binding of individual amino acid residues based upon affinities derived from the salt elution behaviours of the various recombinant $\alpha 1\text{LG4-5s}$. **(C)** A

plot of the change in charge of the recombinant mutants in relation to their salt elution. There is a very good correlation between reduction in charge and observed decrease in heparin binding. The individual amino acids represented in the recombinant mutants are shown mapped to the surface of $\alpha 1\text{LG4-5}$ and the residues color coded to indicate the level of heparin affinity contribution of the individual residues, implied from the observed behaviour of their respective recombinant $\alpha 1\text{LG4-5}$ in the heparin elution assay. Mutated residues have been both color coded and lettered to make identifying them easier.

Figure 24. αDG affinity of recombinant mouse $\alpha 1\text{ LG4-5}$ laminins. The affinity of the recombinant $\alpha 1\text{LG4-5}$ proteins for αDG was evaluated with both a gel overlay assay and a solid phase ELISA assay. **(A)** αDG was run on a gel and transferred onto nitrocellulose filters, overlaid with recombinant $\alpha 1\text{LG4-5}$ s, washed, and the bound $\alpha 1\text{LG4-5}$ detected through its N-terminal FLAG epitope tag with an HRP linked monoclonal antibody. **(B)** The amount of bound $\alpha 1\text{LG4-5}$ in the overlay experiment was quantitated and graphed. **(C)** Recombinant $\alpha 1\text{LG4-5}$ s were also examined for their ability to bind αDG immobilized in a microtiter plate well (ELISA). **(D)** The binding was repeated with varying concentrations of recombinant $\alpha 1\text{LG4-5}$ s, quantitated with use of the HRP-FLAG monoclonal antibody directed against the N-terminal FLAG epitope common to all the recombinant $\alpha 1\text{LG4-5}$ s. The results were fitted to a single-site binding curve, apparent dissociation constants calculated, and reported in table 12. **(E)** The individual amino acids represented in the recombinant mutants are shown mapped to the surface of $\alpha 1\text{LG4-5}$ and the residues color coded to indicate the level of αDG affinity contributed by the individual residues, as implied from the observed behaviour of their respective recombinant $\alpha 1\text{LG4-5}$ in the two αDG binding assays. Mutated residues

have been both color coded and lettered to make identifying them easier. **(F)** A plot of the change in charge of the recombinant mutants in relation to their derived α -dystroglycan dissociation constants. There does not appear to be any correlation between reduction in charge and observed decrease in α -dystroglycan binding.

Figure 25. Sulfatide specificity and affinity of recombinant mouse α 1 LG4-5 laminins. **(A)** Binding of α 1LG4-5/WT_{Nf} (0.4 mg/ml) to microtiter wells containing 10ug/ml of the indicated lipids was tested. Recombinant α 1LG4-5/WT_{Nf} bound only to gal-sulfatide. **(B)** Binding of α 1LG4-5/WT_{Nf} to sulfatide was inhibited by heparin. Furthermore, α 1LG4-5/WT_{Nf} bound sulfatide and not the "desulfated" version of sulfatide, galactosyl ceramide (GalCer). **(C)** Binding of α 1LG4-5/WT_{Nf} to sulfatide was partially inhibitable, 50% reduction, in the presence of EDTA and completely inhibited if the α 1LG4-5/WT_{Nf} had been treated with AEBSF prior to its use in the binding assays.

Figure 26. Sulfatide affinity of mutant recombinant mouse α 1 LG4-5 laminins. **(A)** The various recombinant α 1LG4-5s were analyzed in a solid phase binding assay in which sulfatide was bound to the wells of microtiter plates and incubated with various concentrations of the recombinant α 1LG4-5s. Binding was detected with the HRP-FLAG antibody which recognized the N-terminal FLAG epitope tag common to all recombinant α 1LG4-5s. The results were fitted to a single-site binding curve, apparent dissociation constants calculated, and reported in table 12. **(B)** The individual amino acids represented in the recombinant mutants are shown mapped to the surface of α 1LG4-5 and the residues color coded to indicate the level of sulfatide affinity contributed by the individual residues, as implied from the observed behaviour of their respective recombinant α 1LG4-5 in the sulfatide solid phase binding assay. Mutated residues have

been both color coded and lettered to make identifying them easier. **(C)** MEFs were loaded with BODIPY-sulfatide, incubated with the various recombinant $\alpha 1$ LG4-5s, collected, lysed, the $\alpha 1$ LG4-5/s complexed with BODIPY sulfatide immunoprecipitated via FLAG matrix, the samples read in a fluorimeter, the approximate moles of BODIPY-sulfatide bound per mole of $\alpha 1$ LG4-5 calculated. **(D)** The sulfatide affinity of the mutated amino acid residues represented in the recombinant $\alpha 1$ LG4-5s was also examined by testing the ability of the mutants to block the binding of Lm-111 to sulfatide coated microtiter plate wells. Recombinant mutant $\alpha 1$ LG4-5/RAR₂₈₃₃ ("I") failed to inhibit binding of Lm-111 at all, even at extremely high concentrations of the mutant, implying that it completely failed to bind the sulfatide and thereby block the Lm-111 from binding to the sulfatide. Therefore, the residues mutated in $\alpha 1$ LG4-5/RAR₂₈₃₃ ("I") must be critical for sulfatide binding. **(E)** A plot of the change in charge of the recombinant mutants in relation to their derived sulfatide dissociation constants. There does not appear to be any correlation between reduction in charge and observed decrease in sulfatide binding.

Figure 27. Comparing the three dimensional crystal structure, Cys residues, and disulfide linkages of $\alpha 1$ and $\alpha 2$ LG4-5. The primary sequence of both $\alpha 1$ **(A)** and $\alpha 2$ **(B)** laminin LG4-5 with the Cys residues marked and disulfide linkages depicted. Both **(C)** and **(E)** and **(D)** and **(F)** are ribbon diagram representations generated using Swiss-Pdb Viewer of $\alpha 1$ and $\alpha 2$ laminin LG4-5, respectively. Grey arrows represent β -sheet, red and blue stick representations of Cys residue side chains are colored using the same color scheme utilized in figure A and B, and the unpaired Cys in $\alpha 1$ LG5 is colored purple and its side chain represented with a purple space filling representation. Note the conservation in secondary structure, Cys spatial location, and disulfide linkages between

$\alpha 1$ and $\alpha 2$; including the disulfide linkage connecting the globular domains of LG4 and LG5. Furthermore, the unpaired Cys in $\alpha 1$ LG5 is not surface exposed.

Figure 28. Crystal structure of mouse laminin $\alpha 1$ LG4-5. **(A)** Superposition of the two asymmetric crystal units of $\alpha 1$ LG4-5; superimposed on their LG4 domains. Molecule A (mol A) is light brown and molecule B (mol B) is blue. Note the “shift” in the overlay of $\alpha 1$ and $\alpha 2$ LG5 representing a difference in the orientation of the two domains respective to one another between the two chains **(B)** Schematic ribbon diagram of mouse $\alpha 1$ LG4-5 molecule B (LG4 is cyan and LG5 is green). The N and C-termini are labeled. Disulfide bonds are shown as yellow ball and stick models. Metal ions are shown as purple spheres. **(C)** Space filled diagram of $\alpha 1$ LG4-5 molecule B. LG5 is colored light grey, LG4 is dark grey, Arg and Lys residues are dark blue, His residues are light neon blue, Cys residues are yellow, Ca^{2+} ion is represented as a red sphere, and the amino acid residues of the linker between LG3 and LG4 are colored brown.

Figure 29. Comparing the crystal structure of the individual LG4 and LG5 domains of mouse $\alpha 1$ and $\alpha 2$ laminin. Sequence alignment of $\alpha 1$ LG4-5 **(A)** and $\alpha 2$ LG4-5 **(B)**. The β sheet secondary structure observed in the crystal structure of LG4 is shown in blue above the primary sequence it is associated with. Individual stretches of β -sheet are designated A through N. **(C)** Superposition of $\alpha 1$ LG4 and $\alpha 2$ LG4. A total of 148 $\text{C}\alpha$ atoms were superimposed with a root mean square deviation of 0.91 \AA . **(D)** Superposition of $\alpha 1$ LG5 and $\alpha 2$ LG5. A total of 153 $\text{C}\alpha$ atoms were superimposed with a root mean square deviation of 0.59 \AA .

Figure 30. Comparing the three dimensional crystal structure, domain separation, and domain interface interactions of $\alpha 1$ and $\alpha 2$ LG4-5. Sequence alignment of $\alpha 1$ LG4-5 **(A)** and $\alpha 2$ LG4-5 **(B)**. Several residues involved in the interface of $\alpha 1$ LG4 and LG5 are highlighted. **(C)** Ribbon diagram of $\alpha 1$ LG4-5. **(D)** Ribbon diagram of $\alpha 2$ LG4-5. **(E)** A closer examination of the residues involved in interface interactions between the LG4 and LG5 domains of $\alpha 1$ laminin.

Figure 31. Secondary structure, charge distribution, and spatial location of mutated amino acid residues on the surface of the crystal derived three dimensional structure of $\alpha 1$ LG4-5. **(A)** Full length mouse $\alpha 1$ chain. **(B)** Location of β sheet secondary structure and identity of amino acid residues which comprise the β sheets based upon the crystal structure of $\alpha 1$ LG4-5. Several residues involved in the interface of $\alpha 1$ LG4 and LG5 are highlighted. **(C)** Electrostatic surface representation of the $\alpha 1$ LG4-5 structure. Positive and negative potential are indicated by *blue* and *red* coloring, respectively. **(D)** Space filling representation of $\alpha 1$ LG4-5. The amino acid residues which were mutated in this study are marked, as is their relative contribution to α DG ("DG"), heparin ("H"), and sulfatide ("S") binding.

Figure 32. Characterization of endogeneous and transfected laminin mRNA expression in HEK 293 cells. **(A)** RT-PCR amplification products from the ORF(dark gray bars) of mouse $\alpha 1$, $\beta 1$, and $\gamma 1$ cDNAs, from pCIS extending into the ORFs (light gray bars), and from corresponding human $\alpha 1$, $\beta 1$, and $\gamma 1$ chains (white bars) were prepared from $\alpha\beta\gamma$, $\alpha\beta$, and wild-type (wt) cells, using either total RNA (DNase-treated) or genomic DNA (D) as template. The human primers amplified the expected products from human placental RNA but not from midterm mouse embryo RNA. Conversely, the

mouse primers amplified the expected products from mouse RNA but not from human RNA (data not shown). **(B)** The 293 cell products were electrophoresed on agarose gels to analyze recombinant and endogenous chain-specific mRNA expression (coded bars matched to map; standards were 2.0, 1.2, 0.8, 0.4, and 0.2 Kb). The pCIS-specific products revealed that recombinant DNAs are present and that the RNA was not contaminated with these DNAs. As expected, recombinant mouse chains were expressed in the $\alpha\gamma$ and $\alpha\beta\gamma$ clones and not in wild-type cells.

Figure 33. Recombinant heterotrimeric laminin-111 and laminin-211 composed entirely of all mouse derived α , β , and γ chains. Diagram of the mouse $\alpha 1$, $\alpha 2$, $\beta 1$, and $\gamma 1$ chain expression constructs made and transfected in various combinations in order to express recombinant heterotrimeric laminin-111 and laminin-211 proteins.

Figure 34. Recombinant heterotrimeric laminin-111 composed entirely of all human derived α , β , and γ chains. Diagram of the human $\alpha 1$, $\beta 1$, and $\gamma 1$ chain expression constructs made and transfected in various combinations in order to express recombinant heterotrimeric laminin-111 proteins.

Figure 35. Recombinant full length $\alpha 1$ laminin chains constructed and utilized to make rLm-111s. Diagram of the mouse $\alpha 1$ chain expression constructs made and transfected in various combinations in order to express mixed species recombinant heterotrimeric laminin-111 proteins.

Figure 36. Recombinant α 1 laminin N-terminal deletions constructed and utilized to make rLm-111s. Diagram of the mouse α 1 chain expression constructs made and transfected in various combinations in order to express mixed species recombinant heterotrimeric laminin-111 proteins.

Figure 37. Recombinant α 1 laminin G domain manipulated constructs utilized to make rLm-111s. Diagram of the mouse α 1 chain expression constructs made and transfected in various combinations in order to express mixed species recombinant heterotrimeric laminin-111 proteins.

Figure 38. Recombinant β 1 laminins constructed and utilized to make rLm-111s. Diagram of the mouse β 1 chain expression constructs made and transfected in various combinations in order to express mixed species recombinant heterotrimeric laminin-111 proteins.

Figure 39. Recombinant γ 1 laminin chains constructed and utilized to make rLm-111s . Diagram of the mouse γ 1 chain expression constructs made and transfected in various combinations in order to express mixed species recombinant heterotrimeric laminin-111 proteins.

Figure 40. Coomassie blue stained SDS-PAGE gels of various recombinant heterotrimeric Lm-111s. Coomassie blue stained SDS-PAGE gel of several of the recombinant heterotrimeric Lm-111s after heparin and FLAG purification from media of stably transfected HEK 293 fibroblast cells producing the recombinant proteins shown. Above each sample load is the designation for each heterotrimeric recombinant protein.

Below each designation for the heterotrimeric recombinant protein are the designations for each of the three individual recombinant chains which comprise the heterotrimeric recombinant protein listed above them.

Figure 41. Examination of different N-terminal epitope tags on the N-terminus of full length mouse α 1 laminin chains in recombinant heterotrimeric laminin-111s.

The ability to be expressed on the N-terminus of the mouse α 1 chain as well as any potential effects of the N-terminal epitope tag were examined. **(A)** Cells were transfected with the corresponding expression constructs, stable cell lines expressing the appropriate heterotrimeric recombinant proteins selected, the recombinant heterotrimeric Lm-111s immunoprecipitated with the β 1 LN chain specific polyclonal antibody anti-E4, run reduced on a 6-12% PAGE gel and Silver stained. All expressed heterotrimeric recombinant proteins appeared to be of the correct size with very little if any proteolytic degradation detected. **(B)** Aliquots of the immunoprecipitated material were also run on 6-12% PAGE gel, blotted to a PVDF membrane, and subjected to Western analysis utilizing the α 1 chain C-terminal LG4-5 specific polyclonal antibody rG50. The immunoblotting results demonstrated the correct identity of the recombinant protein, very little degradation of the α chain, and the approximate concentration of the loaded material. **(C)** More aliquots of anti-E4 immunoprecipitated material were run, blotted, and analyzed by Western analysis utilizing epitope tag specific antibodies. All expressed recombinant proteins appeared to be of correct size with little or no proteolytic degradation, and were recognized with the appropriate epitope specific antibody for that chain with no cross-reactivity. All epitope tags examined, appeared to be expressable on the N-terminus of the α 1 chain with no deleterious effects. However, polymerization assays conducted on these purified recombinant proteins revealed that the

heterotrimeric laminin containing the triple myc epitope tag on the N-terminus of the $\alpha 1$ chain failed to polymerize in our standard polymerization assay (data not shown). **(D)** Heterotrimeric recombinant protein was purified from media utilizing the appropriate antibody linked matrix followed by heparin FPLC. 20 ug/ml of each protein was added to sparsely plated Schwann cells and incubated at 37°C for 45 minutes. The cells were then washed, fixed, and immunohistochemical staining performed with polyclonal antibody rG50 and DAPI. All heterotrimeric Lm-111s, with the exception of the one containing the triple myc epitope tag on the N-terminus of the $\alpha 1$ chain, accumulated and condensed on the surface of the Schwann cells. These results demonstrated the suitability of the myc, HA, VSV-G, and protein-C epitope tags for inclusion as N-terminal tags in mouse $\alpha 1$ expression constructs, as well as, the potential use of the triple myc epitope tag on the $\alpha 1$ chain as means to construct and produce a full length polymerization deficient heterotrimeric Lm-111.

Figure 42. Accumulation of recombinant LN-LEb constructs in a solid phase association assay. **(A)** An expression construct which contained the N-terminal LN through LEb domains, along with various C-terminal epitope tags and engineered proteolytic cleavage sequences, was made for each of the individual chains which compose laminin-111. The constructs were stably transfected into HEK 293 cells, permanent cell lines established, and the recombinant proteins purified from media by absorption to FLAG affinity matrix and FLAG peptide elution, followed by salt elution from a heparin FPLC column. Treatment of the purified recombinant proteins with either Enterokinase (EK) or tobacco etch virus protease (TEV) was utilized to generate variants of the expressed recombinant proteins with different C-terminal epitope tag combinations. **(B)** Western analysis (12% PAGE) with epitope specific antibodies of

purified recombinant proteins pre and post treatment with EK. All recombinant proteins expressed the appropriate C-terminal epitope tags, demonstrated appropriate cleavage with EK treatment, and were recognized with the appropriate epitope specific antibody.

(C) Ability of purified recombinant proteins to associate and accumulate. The purified recombinant proteins diagramed in figure A were incubated in various combinations for 1 hour in EWB buffer in myc antibody coated microtiter wells then washed and binding determined with HA-HRP or FLAG-HRP antibody, OPD, and a microtiter plate reader. The results for each incubation are as follows (the recombinant protein being detected in each is color coded in the legend entry for that result): (1) all values were normalized against the binding of $\alpha 1\text{LN-C}_{\text{v/f/m}}$ which bound the myc antibody coated microtiter wells through its C-terminal myc epitope tag and helped orientate the recombinant protein so that its N-terminal LN domain projected up from the surface of the microtiter plate well; (2) demonstrated that there was no cross-reactivity observed between the HA antibody and $\alpha 1\text{LN-C}_{\text{v/f/m}}$, as well as provided a basal level for any HA background staining; (3) and (4) neither the $\beta 1$ nor $\gamma 1$ recombinant proteins demonstrated adhesion to the surface of the microtiter plate well by themselves; (5) and (6) demonstrated that there was no observed increase in $\alpha 1$ binding due to additional $\alpha 1$ unless that $\alpha 1$ possessed a C-terminal myc tag which would enable it to bind the microtiter plate well directly since the $\alpha 1$ is plated at suboptimal coverage to avoid steric accessibility issues; the lack of an observed increase in FLAG staining in (5) suggests no detectable $\alpha 1$ to $\alpha 1$ interaction; (7) and (8) revealed very little association of $\alpha 1$ with either the $\beta 1$ or $\gamma 1$ chain separately but (9) and (10) demonstrated significant accumulation of both the $\beta 1$ and $\gamma 1$ chain when all three chains are present; (11) as expected the incubation with both the $\beta 1$ and $\gamma 1$ chain being simultaneously detected with the same epitope tag demonstrated a doubling in the signal over that observed when the $\beta 1$ and $\gamma 1$ chain were assayed

individually in (9) and (10). It seems quite clear from these association experiments that laminin polymerization requires the interaction of the LN domains from each of the $\alpha 1$, $\beta 1$, and $\gamma 1$ chains.

Figure 43. Heparin binding affinities of recombinant Lm-111s and Lm-211s. The elution profile and corresponding molar salt concentration required to elute the shown recombinant Lm-111 and Lm-211 proteins from a heparin-5PW column on an AKTA FPLC. The majority of Lm-111's heparin binding affinity resides within the LG4-5 subdomains of the $\alpha 1$ chain (as demonstrated by the observed binding of rLm-111 Δ LG1-3) with a significant contribution from LG1-3 (as demonstrated by the observed binding of rLm-111 Δ LG4-5) and very minor heparin binding outside of the LG1-5 domains of the $\alpha 1$ chain (as demonstrated by the observed binding of rLm-111 Δ LG1-5). Unprocessed Lm-211 has a heparin affinity approaching that of Lm-111, however, heparin affinity is greatly reduced by proteolytic processing of the Lm-211 (Lm-111 vs. Lm-211 WTu vs. Lm-211WTP).

Figure 44. Sulfatide binding affinities of recombinant Lm-111s and Lm-211s. Sulfatide binding ELISA results for various recombinant heterotrimeric Lm-111 and Lm-211 proteins. **(A)** Sulfatide ELISA results of Lm-111s with deletion of C-terminal LG domains and a $\beta 1$ LN deletion mutant. The results demonstrate that the majority of the sulfatide binding activity in Lm-111 comes from the $\alpha 1$ LG4-5 domains. Also, the LN deletion mutant suggests that laminin polymerization is a factor in the observed signal (previous fragment binding studies suggested that the $\beta 1$ chain itself does not bind sulfatide). **(B)** The binding of laminin-111 to sulfatide is not affected by 1% Triton, partially inhibited with EDTA, and almost completely inhibited by heparin. Furthermore,

AEBSF treatment of laminin-111 completely abolishes, not only, its ability to polymerize (data not shown), but also, its ability to bind sulfatide. **(C)** Lm-111 binds sulfatide with a higher affinity than Lm-211 and the binding of Lm-211 (Lm-211 WTu) dramatically decreases after proteolytic processing (Lm-211 WTP).

Figure 45. Laminin-111 binding to sulfatide albumin complexes. Sulfatide:BSA and GalCer:BSA complexes were allowed to settle in media onto tissue cultured plastic and then incubated for 45 minutes with recombinant heterotrimeric Lm-111_{Nf/Nh/Cf} in the presence or absence of EDTA and/or heparin. The samples were washed and immunostained for laminin-111. The binding of Lm-111 to the sulfatide albumin complexes was observed to be partially inhibited with EDTA and almost completely inhibited in the presence of heparin. Furthermore, the Lm-111 did not bind the GalCer albumin complexes. All observed results were in agreement with the sulfatide ELISA results.

Figure 46. Inhibition of Lm-111 binding to Schwann cell surfaces. Densely plated, nearly confluent, Schwann cells were incubated with 20ug/ml of Lm-111_{Nf/Nh/Cf} and 20 fold molar excess of proteolytic fragments where indicated, as well as other laminins, also at 20ug/ml, for 30 minutes, then immunostained for laminin, total signal intensity normalized based upon cell number (counted via DAPI staining of nuclei), and graphed. Laminins incapable of polymerizing either through chemical modification or LN domain deletion, as well as, laminin incubated with polymerization inhibiting fragments, resulted in an 85-98% reduction in laminin binding to the surface of the Schwann cells. The anchorage inhibiting fragment, E3, also resulted in an 85% reduction in laminin binding. Fragment E8 containing the β 1 integrin binding sites of LG1-3 and AEBSF treated fragments failed to block laminin accumulation.

Figure 47. Inhibition of Lm-111 binding to the cell surface of Schwann cells via contemporary addition of recombinant α 1LG4-5 proteins. Confluent Schwann cells were incubated with 20ug/ml of EHS laminin-111 and various concentrations of recombinant α 1LG4-5 proteins for 30 minutes. The cells were then washed, fixed, immunostained, and photographed. Laminin was detected using anti-E4. A β 1 N-terminal LN domain specific polyclonal antibody which will recognize the exogenous laminin-111 but not react with the α 1LG4-5 proteins was utilized. Laminin total signal intensity was normalized based upon cell number (counted via DAPI staining of nuclei), and graphed. The α 1 LG4-5s were assayed to determine the effect each mutated amino acid residue in each given recombinant α 1LG4-5 had upon its ability to block laminin-111 binding to the surface of the Schwann cells. The rationale was that if the sequence mutated in the α 1LG4-5 was critical to a binding activity it would not bind the cell surface as efficiently and therefore be less efficient at blocking laminin-111 binding to the cell surface; i.e. the higher the laminin signal observed the more important the residue mutated in the blocking α 1LG4-5 is to binding on the cell surface. The converse is also true: the less laminin signal observed, the less important the mutated sequence in the α 1LG4-5, utilized to block, is to binding on the cell surface of Schwann cells. Unfortunately, extremely high molar excesses of recombinant α 1LG4-5 were required to observe significant reduction in laminin binding. The results did suggest that the sequence represented by α 1LG4-5/KDR₂₈₆₀ (rE3-J) was not required and that those represented by α 1LG4-5/RKR₂₇₂₁ (rE3-A), α 1LG4-5/KRK₂₇₉₃ (rE3-G), and α 1LG4-5/RAK₂₈₃₃ (rE3-I) did have an effect.

Figure 48. Assembly of heterotrimeric recombinant Lm-111s on the surface of Schwann cells. Schwann cells were incubated with 20ug/ml of the indicated laminins

for 60 min., washed, fixed, incubated with laminin specific antibody, and prepared for immunofluorescence microscopy. The images are representative samples from the Schwann cells incubated with each laminin indicated above the image. The bar graph is a quantitative representation of the laminin specific fluorescence observed divided by the number of DAPI stained nuclei in the image quantitated (average \pm standard deviation, $n = 7-14$ for each condition). The gold trimmed images and text represent recombinant laminins which demonstrate loss of polymerization activity, blue trimmed images and text laminins with defective $\alpha 1$ LG4 anchorage, and the red trimmed images and text AEBSF treated laminins which demonstrate a loss of both polymerization and anchorage activity. Recombinant laminins which have lost either polymerization or anchorage through $\alpha 1$ LG4 demonstrate a profound loss in their ability to bind and accumulate on the cell surface of Schwann cells.

Figure 49. The binding of recombinant heterotrimeric laminins to the cell surface of Schwann cells. Schwann cells were incubated with 20ug/ml of the indicated laminins for 60 min., washed, fixed, incubated with laminin specific antibody, α DG specific antibody, DAPI, and prepared for immunofluorescence microscopy. The images are representative samples from the Schwann cells incubated with each laminin indicated above the image. Lm-111 (B) which contains intact nidogen bound to a higher degree than any other laminin, followed closely by Lm-111 (U), and then recombinant Lm-111 WT. Polymerization null laminin lost 85% of its binding signal, while deletion of $\alpha 1$ LG4 resulted in an almost complete loss of binding. Deletion of $\alpha 1$ LG1-3 had little affect upon binding and accumulation of laminin. Furthermore, the addition of laminin resulted in a corresponding increase in α DG signal on the surface of the Schwann cells.

Figure 50. The binding of heterotrimeric $\alpha 1$ LG4 point mutations Lm-111s, as well as, the effect of concurrent addition of exogenous Nd-1 and Coll IV, to the cell surface of Schwann cells. Schwann cells were incubated with 10ug/ml of the indicated laminins for 60 min., washed, fixed, incubated with laminin specific antibody, α DG specific antibody, DAPI, and prepared for immunofluorescence microscopy. The images are representative samples from the Schwann cells incubated with each laminin indicated above the image. All three Lm-111 point mutations (only RKR₂₇₂₁ and RAR₂₈₃₃ are shown) in $\alpha 1$ LG4 demonstrated a drastically reduced ability to bind and accumulate on the cell surface. Furthermore, the simultaneous addition of nidogen-1 and type IV collagen to the incubation with the exogenous recombinant Lm-111 WT resulted in an increase in Lm-111 signal on the cell surface.

Figure 51. Electron microscopy images depicting the accumulation of recombinant heterotrimeric Lm-111s and BM formation on the cell surface of Schwann cells (1 of 2). Schwann cells were incubated with recombinant laminins depicted (40ug/ml) for one hour, fixed, stained for basement membrane (BM), embedded, sectioned, and examined utilizing electron microscopy (EM). Cells treated with WT laminin exhibited a thin continuous electron dense line. Scattered small extracellular aggregates were observed on the cell surface of Schwann cells incubated with polymerization deficient Lm-111 $\Delta\beta 1$ LN-LEa_{Nm/Nh/Cf}, however, deletion of the LG1-3 domain of $\alpha 1$, represented by recombinant protein Lm-111 $\Delta\alpha$ LG1-3_{Nm/Nh/Cf}, resulted in only a 20% decrease in coverage and formation of a slightly discontinuous BM.

Figure 52. Electron microscopy images depicting the accumulation of recombinant heterotrimeric Lm-111s and BM formation on the cell surface of Schwann cells (2

of 2). Schwann cells were incubated with recombinant laminins depicted (40ug/ml) for one hour, fixed, stained for basement membrane (BM), embedded, sectioned, and examined utilizing electron microscopy (EM). Cells treated with WT laminin exhibited a thin continuous electron dense line. Even fewer scattered small extracellular aggregates were observed on the cell surface of Schwann cells incubated with polymerization deficient $\alpha 1$ LG4 point mutation recombinant proteins, Lm-111 α RKR_{2721Nm/Nh/Cf} and RAR₂₈₃₃Lm-111 $\Delta\beta 1$ LN-LEa_{Nm/Nh/Cf}, than those observed with the polymerization deficient laminin, and practically no aggregates were observed on the surfaces of Schwann cells incubated with $\alpha 1$ LG4 anchorage deficient Lm-111 $\Delta\alpha 1$ LG4-5_{Nm/Nh/Cf}. Clearly both polymerization and $\alpha 1$ LG4 anchorage activities are necessary for efficient binding, aggregation, accumulation, and basement membrane formation. Of course, anchorage is more critical because even if a laminin polymer could form it will not bind to the cell surface without anchorage activity.

Figure 53. Comparison of recombinant Lm-111 and Lm-211 BM formation on Schwann cell surfaces. Schwann cells were incubated for one hour with 20ug/ml of the indicated laminins. The cells were then washed, fixed, and immunostained for laminin-111, laminin-211, α DG, and DAPI. Quantitation of immunofluorescence was accomplished by averaging several photographs and dividing each by the number of DAPI stained nuclei present. Lm-111 and Lm-211 immunofluorescence was detected by use of the anti-E4 polyclonal antibody which recognizes the N-terminal LN domain of the $\beta 1$ chain of laminin common to both Lm-111 and Lm-211. Lm-111 WT immunofluorescence was three times higher than Lm-211 WT and images from Lm-211 incubations were adjusted accordingly to increase signal intensity in order for measurements to be taken and proper analysis to be performed. Deletion of LG1-5 or

LG4-5 of the $\alpha 1$ chain in Lm-111 resulted in a severe reduction in Lm-111 signal on the surface of Schwann cells, whereas, deletion of $\alpha 1$ LG1-3 had little effect on Lm-111 binding. Conversely, the processed form of Lm-211 or deletion of LG1-3 or LG4-5 resulted in a severe reduction in Lm-211 signal. Clearly, unlike Lm-111, Lm-211 requires some binding contribution from LG1-3 in conjunction with that found in LG4-5 for efficient binding to the Schwann cell surface.

Figure 54. Basement membrane formation and epiblast differentiation in wild-type, $\beta 1$ integrin null and $\gamma 1$ laminin null embryo bodies. Both $\beta 1$ integrin and $\gamma 1$ laminin null ES cells were incubated with or without exogenous laminin-111 and encouraged to form EBs. The EBs were collected, fixed, embedded, sectioned, and immunostained. The percentage of EBs possessing at least 30% basement membrane between an outer endodermal layer and inner epiblast layer and a defined epiblast layer were recorded.

Figure 55. Exogenous Lm-111 induced BM formation and epiblast differentiation in $\gamma 1$ laminin null EBs. Laminin $\gamma 1$ null ES cells were cultured for 6 days in the presence of 25 $\mu\text{g/ml}$ Lm-111 and where indicated, 30 fold molar excess of Lm-111 proteolytic fragment or recombinant $\alpha 1\text{LG4-5}$. EBs and ES cell aggregates were collected, fixed, embedded, sectioned and stained with an anti-E1' antibody for Lm-111 detection, a type IV collagen antibody, and DAPI. **(A)** Diagrams of recombinant Lm-111s utilized as well as Lm-111 proteolytic fragments. **(B)** Representative image of a $\gamma 1$ null EB rescued with the addition of exogenous recombinant Lm-111_{Nm/Nh/0}. There is clear co-localization of both Lm-111 (Lm) and type IV collagen (Coll) in a BM pattern on the basal side of an outer endodermal cell layer and a polarized elongated epiblast layer below with obvious central cavitation. **(C)** Representative image of a $\gamma 1$ null EB Lm-111

rescue image showing two EBs in the section side by side, which are utilized to demonstrate the selection criteria for scoring formation of a BM and epiblast differentiation. In order for an EB to be scored positive for BM formation, Lm-111 and type IV collagen must be co-localized and present in a circular distribution pattern surrounding at least 40% of the cell aggregate and be between a clearly defined outer endodermal cell layer and inner epiblast layer. In order for an EB to be scored positive for epiblast differentiation there must be significant central apoptosis and cavitation, as well as, a 1-3 cell thick layer of cells clearly adjacent to the inner side of the BM demonstrating elongated nuclei under DAPI staining along at least 40% of the circumference of the EB. Under these criteria, even though the EB on the right is clearly positive for both BM formation and epiblast differentiation, and the EB on the left is probably just slightly behind in development to the one on the right and is in the process of BM formation and epiblast differentiation, the EB on the left would be scored as no BM formation since the Lm staining has yet to reach the 40% circumferential threshold and no epiblast differentiation since the developing epiblast layer has also yet to reach the threshold level for circumferential percentage of elongated nuclei. **(D)** Tabulation and graphing of BM formation and epiblast differentiation observed in Lm-111 rescue of $\gamma 1$ laminin null EBs utilizing the addition of various recombinant laminins and laminin fragments to inhibit the rescue of the exogenous Lm. Exogenous Lm-111 added concurrently with proteolytic fragments and recombinant proteins which inhibit Lm polymerization, as well as recombinant Lm-111 unable to polymerize due to chemical modification, blocking epitope tag, or LN domain deletion, effectively inhibited or failed to induce BM formation and epiblast differentiation. Treatment of proteolytic fragments with AEBSF effectively abolished their ability to inhibit Lm rescue of the $\gamma 1$ null EBs. Recombinant Lm-111 with deletion of the LG1-5 anchorage domains or ES cells treated

concurrently with both WT Lm-111 and $\alpha 1\text{LG4-5}/\text{WT}_{\text{Nf}}$ failed to form BMs or undergo epiblast differentiation. Inhibition with mutant $\alpha 1\text{LG4-5s}$ also showed a role for the KRK_{2793} sequence in $\alpha 1$ LG4 in BM formation.

Figure 56. Binding of various recombinant heterotrimeric Lm-111s on the surface of C2C12 myotubes. C2C12 myotubes were incubated with 20ug/ml of various laminin-111s for 30 minutes, washed, fixed, and immunostained. There was no endogeneous Lm-111 staining. Recombinant heterotrimeric laminin-111 bound almost as efficiently as EHS purified Lm-111. Furthermore, recombinant Lm-111 missing LG1-3 but retaining the anchorage of LG4-5 bound almost as well as WT recombinant laminin-111, whereas, deletion of LG4-5 or point mutations of the LG4 domain which affect anchorage (Lm-111 αRKR_{2721} Nm/Nh/Cf (mutant A) and $\alpha 1\text{Lm-111}\alpha\text{RAK}_{2833}$ Nm/Nh/Cf (mutant I)) resulted in almost no laminin binding to the cell surface of C2C12 myotubes.

Figure 57. Inhibition of Lm-111 binding to C2C12 myotube surfaces via laminin receptor blocking antibodies and recombinant $\alpha 1\text{LG4-5}$. C2C12 myotubes were incubated with 20ug/ml of EHS laminin-111s for 30 minutes, washed, fixed, and immunostained. The laminin binding was inhibited by the addition of $\alpha 1\text{LG4-5}$ but barely at all with antibodies which block laminin binding to αDG or $\beta 1$ integrin. αDG and $\beta 1$ integrin blocking antibodies failed to inhibit laminin binding when used separately or in combination with one another.

Figure 58. Inhibition of EHS Lm-111 binding to C2C12 myotubes by various recombinant $\alpha 1\text{LG4-5s}$. C2C12 myotubes were incubated with 20ug/ml of EHS laminin-111 and various concentrations of recombinant $\alpha 1\text{LG4-5}$ proteins for 30 minutes.

The cells were then washed, fixed, immunostained, and photographed. The $\alpha 1$ LG4-5s were assayed to determine the effect each mutated amino acid residue in each given recombinant $\alpha 1$ LG4-5 had upon its ability to block laminin-111 binding to the surface of the C2C12 myotubes. The rationale was that if the sequence mutated in the $\alpha 1$ LG4-5 was critical to a binding activity it would not bind the cell surface as efficiently and therefore be less efficient at blocking laminin-111 binding to the cell surface; i.e. the higher the laminin signal observed the more important the residue mutated in the blocking $\alpha 1$ LG4-5 is to binding on the cell surface. The converse is also true: the less laminin signal observed, the less important the mutated sequence in the $\alpha 1$ LG4-5, utilized to block, is to binding on the cell surface of C2C12 myotubes. Very high molar excesses of recombinant $\alpha 1$ LG4-5 were required to observe significant reduction in laminin binding. The results did suggest that the sequence represented by rE3-J (KDR₂₈₆₀) was not essential and that those represented by rE3-A (RKR₂₇₂₁) and rE3-G (KRK₂₇₉₃) were more important than those represented by rE3-I (RAK₂₈₃₃).

Figure 59. Accumulation of exogenous Lm-111 on cell surfaces of MEFs without sulfatide loading. Sparsely plated MEFs were incubated with 10ug/ml of EHS Lm-111 for 30 minutes, washed, fixed, and immunostained. The laminin coverage pattern was punctate, however, the aggregates of laminin signal were of uniform size and did not appear to condense into higher order aggregates **(A)**. Furthermore, the laminin and α DG signal perfectly co-localized **(B)**.

Figure 60. Accumulation of exogenous Lm-111 and other macromolecules on the surface of MEFs in the absence of sulfatide (1 of 2). MEFs were either incubated with 5 ug/ml of Lm-111_{Nm/Nh/Cf} for 30 minutes at 37°C or not treated with Lm-111. Cells

were washed, fixed, and co-stained with both rG50 to detect bound laminin and an antibody to detect either nidogen-1 or type IV collagen. Cultured MEFs do not secrete Lm-111 nor retain appreciable amounts of the type IV collagen and nidogen they do secrete on their cell surface. However, once exposed to exogenous Lm-111 which does bind the cell surface and aggregates, both type IV collagen and nidogen appear to accumulate and co-localize with the laminin signal on the cell surface of the MEFs.

Figure 61. Accumulation of exogenous Lm-111 and other macromolecules on the surface of MEFs in the absence of sulfatide (2 of 2). (A) MEFs were incubated with either 10 ug/ml of Lm-111_{Nm/Nh/Cf} or 10 ug/ml of Alexa 488 labelled Lm-111_{Nm/Nh/Cf} for 30 minutes at 37°C or not treated with Lm-111. Cells were washed, fixed, and co-stained with both rG50 (except for the Lm-111 Alexa labeled sample) to detect bound laminin and an antibody to α DG, sulfatide, or perlecan. Cultured MEFs express α DG. In the absence of exogenous Lm-111, the α DG signal remained diffuse and did not condense. However, in the presence of exogenous Lm-111, the α DG is observed to co-localize and condense with the laminin signal. Furthermore, just like in the Schwann cells, the addition of exogenous laminin appeared to increase surface expression of α DG. The MEFs did not express sulfatide, nor was sulfatide expression induced by addition of exogenous Lm-111. The MEFs were observed to express and retain perlecan on their cell surface, however, most of the signal appeared to be on the basal side of the cells. Some of the perlecan signal appeared to co-localize with the exogenous Lm-111 on the apical cell surface. (B) A similar approach was utilized with Molecular Probes Vybrant Lipid Raft Labeling Kit to visualize GM1 rich clusters or “lipid rafts” through use of the cholera toxin B subunit. Exogenous Lm-111 was observed to

co-localize and condense with these GM1 rich domains, as was nidogen-1 and α DG after the MEFs were incubated with 10 μ g/ml of Lm-111_{Nm/Nh/Cf} for 45 minutes at 37°C.

Figure 62. Accumulation and condensation of exogenous Lm-111 on MEF cell surfaces over time, in the absence of suflatide. Near confluent MEFs were incubated with 20 μ g/ml of EHS Lm-111(B) at 37°C and samples removed, washed, fixed and co-stained with antibodies to Lm-111 and α DG at 0, 15, 45, 60, and 90 minutes. The Lm-111 was observed binding, accumulating, aggregating, and condensing on the cell surface of the MEFs. The originally diffuse endogeneous α DG signal was observed not only increasing in intensity, but also, aggregating and condensing along with the Lm-111 signal.

Figure 63. Inability to form higher order aggregates and a BM on the surface of MEFs without the presence of sulfatide. Sparsely plated MEFs were incubated with 20 μ g/ml of EHS Lm-111(B) at 37°C for 45 minutes, washed, fixed and co-stained with the rG50 antibody to the G domain of the α 1 chain of Lm-111. Exogenous Lm on the cell surface of sparsely plated MEFs is slow to show any signs of condensing and when the laminin does aggregate it does so in small patches, never forming the higher order aggregates and BM like coverage observed in Schwann cells and C2C12 myotubes.

Figure 64. Time course of multiple loadings of Alexa 488 labeled Lm-111 onto the surface of MEFs in the absence of sulfatide. MEFs were plated and a single isolated MEF identified and followed over time through a series of incubations. The MEFs were incubated with 20 μ g/ml of Alexa 488 labeled Lm-111_{Nm/Nh/Cf} for 10 minutes, then the media was removed, the cells washed, fresh non-laminin containing media added, the

cells photographed, and allowed to continue incubating with further pictures at 20 minutes and 30 minutes. The cells were then exposed to a second addition of Alexa labeled laminin, incubated for 10 minutes, the media removed, the cells washed, fresh non-laminin containing media added, cells photographed, and allowed to continue incubating with further pictures at 10, 30 and 45 minutes post the 2nd addition of exogenous Lm. The cells were fixed and also co-stained for α DG for the last time point picture. The multiple separated additions of exogenous Alexa 488 labeled Lm-111_{Nm/Nh/Cf} resulted in formation of two concentric rings of laminin condensing around the central nuclei of the MEF. This experiment was utilized to demonstrate both the stability and nature of the exogenous Lm-111 as it bound, accumulated, aggregated, and condensed towards the center of the cell. This process is a continually regenerating one which the individual MEF can repeatedly undergo.

Figure 65. Sulfated glycolipid specificity of Lm-111 binding to the surface of MEFs.

(A) Nearly confluent cultures of MEFs were loaded with various lipids via transfer from BSA loaded with same exogenous lipids, then incubated with 10 ug/ml of Lm-111_{Nm/Nh/Cf} for 45 minutes, washed, fixed, and Lm-111 signal detected with anti-rG50 antibody to the C-terminal LG4-5 of the Lm-111. **(B)** Total bound Lm signal intensity was determined, normalized based upon cell number (via DAPI co-staining) per field examined, and plotted relative to the signal observed in MEFs loaded with Gal-sulfatide and exposed to Lm-111. MEFs loaded with Gal-sulfatide or Glc-sulfatide demonstrated a 5 fold increase in total laminin accumulation over that observed in MEFs with no sulfatide present. The coverage observed was also quite different between MEFs loaded with sulfatide from those without sulfatide. Non-sulfatide loaded cells demonstrated a much more disperse Lm binding pattern. The bound Lm migrated, aggregated and condensed, however, it never formed the higher order aggregates observed in Schwann cells or sulfatide loaded

MEFs. Furthermore, the Lm coverage in the sulfatide loaded MEFs was much more dense than that observed in the non-sulfatide loaded MEFs. In addition, both the amount of Lm-111 which bound the cell surface and overall Lm coverage could be increased by increasing the amount of sulfatide loaded onto the MEFs. Also, the observed Lm binding was specific for the sulfate moiety found on the sugar moiety of the glycolipid. Loading of MEFs with galactosyl ceramide, a glycolipid with the exact same structure as Gal-sulfatide except for the absence of the sulfate moiety, resulted in no increase in Lm binding or coverage. Loading of MEFs with cholesterol-3-sulfate resulted in minimal increase in laminin binding and no migration/condensation of the Lm signal. MEFs loaded with Gal-sulfatide and then treated with ASA, which removes the sulfated moiety from the sulfated glycolipid, demonstrated no increase in Lm binding or coverage.

Figure 66. Inhibition of exogenous Lm-111 accumulation on MEF cell surfaces (in the absence of sulfatide) by contemporaneous addition of recombinant α 1LG4-5 proteins. Cultures of nearly confluent MEFs were incubated with 20 μ g/ml of EHS Lm-111 and 100 μ g/ml of various recombinant α 1LG4-5 proteins for 45 minutes at 37°C, washed, fixed, stained with anti-rG50 antibody, and Lm-111 binding to the cell surface of the MEFs measured. **(A)** Representative images of the inhibitions are depicted. **(B)** The total Lm-111 signal in each image was measured, equilibrated based on cell number (determined by counting DAPI stained nuclei), and values plotted relative to the binding observed in the presence of exogenous Lm-111 and the absence of competing α 1LG4-5. The theory behind this inhibition is that if a mutation in the competing mutant recombinant α 1LG4-5 is deleterious to the binding activity responsible for binding of the LG4-5 to the cell surface then the competing α 1LG4-5 will not efficiently bind to the cell surface nor be an efficient competitor for binding of the Lm-111

and the resulting Lm-111 signal will not decrease. Conversely, competing α 1LG4-5 recombinant proteins bearing mutations which result in an observed decrease in Lm-111 binding must be binding the cell surface and, therefore, contain mutations which do not affect the binding activity responsible for Lm binding to the cell surface of MEFs. Accordingly, the binding results suggest that KDR₂₈₆₀ (rE3-J) does not represent a sequence involved in binding to the cell surface of Schwann cells, whereas, RKR₂₇₂₁ (rE3-A), KRK₂₇₉₃ (rE3-G), and RAR₂₈₃₃ (rE3-I) are involved to varying degree in the binding of Lm to the MEF cell surface.

Figure 67. Accumulation of various exogenous recombinant heterotrimeric laminins on the cell surface of MEFs in the absence of sulfatide. Cultures of nearly confluent MEFs were incubated with 20 ug/ml of EHS Lm-111 and various recombinant heterotrimeric Lm-111s for 45 minutes at 37°C, washed, fixed, stained with anti E1' antibody, and Lm-111 binding to the cell surface of the MEFs measured. **(A)** Representative images of the laminin binding observed. **(B)** The total Lm-111 signal in each image was measured, equilibrated based on cell number (determined by counting DAPI stained nuclei), and values plotted relative to the binding observed in the MEFs incubated with Lm-111_{Nm/Nh/Cf}. Recombinant heterotrimeric WT laminin, Lm-111_{Nm/Nh/Cf}, bound to the MEF cell surface with a signal intensity similar to EHS purified Lm-111. Recombinant laminins unable to polymerize, both Lm-111_{Nm3/Nh/Cf} and Lm-111 $\beta\Delta$ 6-5_{N0/Nh/Cf}, or not possessing anchorage through deletion of the α 1 chain's LG4 domain, both Lm-111 $\alpha\Delta$ LG1-5_{Nm/Nh/Cf} and Lm-111 $\alpha\Delta$ LG4-5_{Nm/Nh/Cf}, demonstrated a severe reduction in their ability to bind the cell surface of MEFs. Furthermore, both α 1 LG4 point mutation heterotrimeric Lm-111s, Lm-111 α RKR_{2721Nm/Nh/Cf} (rE3-A) and Lm-111 α RAR_{2833Nm/Nh/Cf} (rE3-I), also revealed a severe reduction in binding.

Figure 68. Differences in accumulation patterns on MEF cell surfaces (sulfatide not present) between recombinant heterotrimeric laminins, as a consequence of their polymerization capability. 20 ug/ml of exogenous WT Lm-111_{Nm/Nh/Cf} and polymerization incapable Lm-111 $\Delta\beta$ LN-LEa_{0/Nh/Cf} were incubated with MEFs for 45 min. at 37°C. The exposure is increased threefold in the mutant Lm in order to be able to observe the pattern. The accumulation of polymerization incompetent Lm-111 on the cell surface of MEFs is much less than that observed with WT laminins. Furthermore, the polymerization incompetent Lm-111 appears to bind the surface in a much finer punctate pattern, perhaps indicative of its inability to bind other laminins and form larger aggregates.

Figure 69. Recombinant α 1G4-5 inhibition of Lm-111 binding. Diagram representing a theoretical explanation as to why the various recombinant α 1LG4-5s were not more efficient inhibitory reagents with regards to blocking heterotrimeric laminin binding. First of, the α 1LG4-5s contain multiple binding sites and only some are effected by mutation, whereas, the full length laminins possess multiple binding activities not present in LG4-5 which may provide added anchorage, stability, or affinity of the heterotrimer over the LG4-5 fragment. Furthermore, the ability of the heterotrimer to bind other laminins and bring them into a complex may quickly generate an aggregate which the LG4-5 can not effectively compete against. The combined overall number of binding sites in a laminin aggregate may be too much for LG4-5 to displace. There are also potential post-translational glycosylation, stability, activity, and LG1-3 contributing factors which may also be affecting the system.

Figure 70. Embryoid body summary. Both laminin $\gamma 1$ null and $\beta 1$ integrin null EBs will develop an outer endodermal layer of cells, however, neither will progress further in development without the addition of exogenous laminin. The addition of exogenous Lm-111 will enable the EBs to pass this differentiation blockage and form a BM underneath the outer endodermal layer, undergo apoptosis to form a central cavity and differentiate to form an epiblast layer underneath the formed BM.

Figure 71. Basement membrane formation and epiblast differentiation in $\gamma 1$ laminin null embryoid bodies treated with Lm-111, modified Lm-111, Lm-111 fragments, and recombinant Lm-111s. Laminin $\gamma 1$ null EBs were grown in the absence or presence of various laminins and laminin fragments and the percentage of EBs to form a BM and develop a differentiated epiblast layer recorded. Any deficiency in laminin polymerization (chemical modification, domain deletion, fragment inhibition) or LG4 anchorage (domain deletion and fragment inhibition) resulted in no to very low BM formation and epiblast differentiation.

Figure 72. Lm-111 binding, accumulation, condensation, formation of higher order complexes, BM formation, and cell signaling. MEFs do not contain sulfatide, however, they do contain α DG. **(A)** In DG null MEFs, with no DG and no sulfatide, ganglioside GM₁ containing transitory micro lipid rafts will form, they may migrate, but will not condense, and will not form higher order lipid rafts, nor will a basement membrane assemble. Exogenous laminin-111 will not bind the cell surface and there is no change in the behavior of the cell. **(B)** In WT MEFs, with α DG present but no sulfatide, DG will associate in GM₁ positive micro lipid rafts of a very transitory state, however, the complex micro lipid raft will not condense, form higher order lipid rafts, or

assemble a basement membrane. Exogenous laminin-111 will bind α DG in the micro lipid rafts, laminin binding proteins will also accumulate on the surface of the micro lipid rafts, the micro lipid raft complex will migrate and condense, however, there is no formation of higher order lipid rafts or basement membrane formation. **(C)** In DG null MEFs, with no DG and sulfatide, once the cells have been loaded with sulfatide, exogenous laminin-111 will bind and accumulate in micro lipid rafts, as well as laminin binding proteins, such as nidogen and type IV collagen, these rafts will migrate, condense, and form both higher order complexes and a basement membrane, however, there is no induction of Src phosphorylation/activation. **(D)** In WT MEFs, with DG but no sulfatide, once the cells have been loaded with sulfatide, the addition of exogenous laminin-111 results in a process identical to that observed in (C), however, Src phosphorylation/activation is induced by the addition of the exogenous laminin-111.

Figure 73. Spatial location of binding activities in mouse α 1 LG4. The spatial location of heparin, α DG, and sulfatide binding activities were mapped onto three dimensional representations of the mouse α 1 LG4-5 crystal structure. The sites overlap to varying degrees and explain the observed binding behaviours. The major heparin site involves residues Arg₂₇₁₉, Arg₂₇₂₁, Lys₂₇₉₀, and Lys₂₇₉₁ of LG4. There is also a combination minor heparin site and major α DG site containing residues Lys₂₇₆₆ and Arg₂₇₆₈. A second major α DG site is comprised by Lys₂₈₂₀, Arg₂₈₃₁, and Arg₂₈₃₃.

Figures

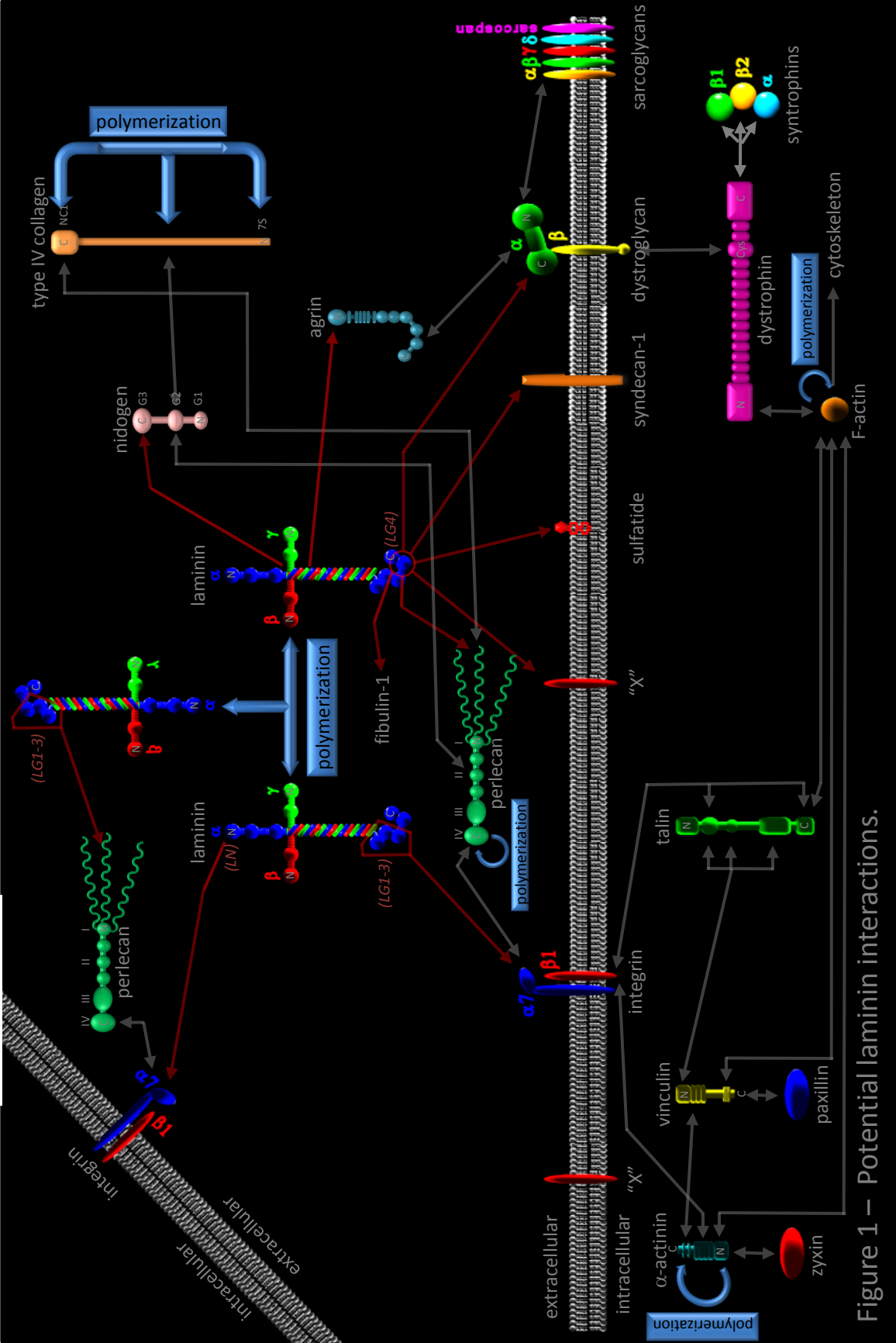


Figure 1 – Potential laminin interactions.

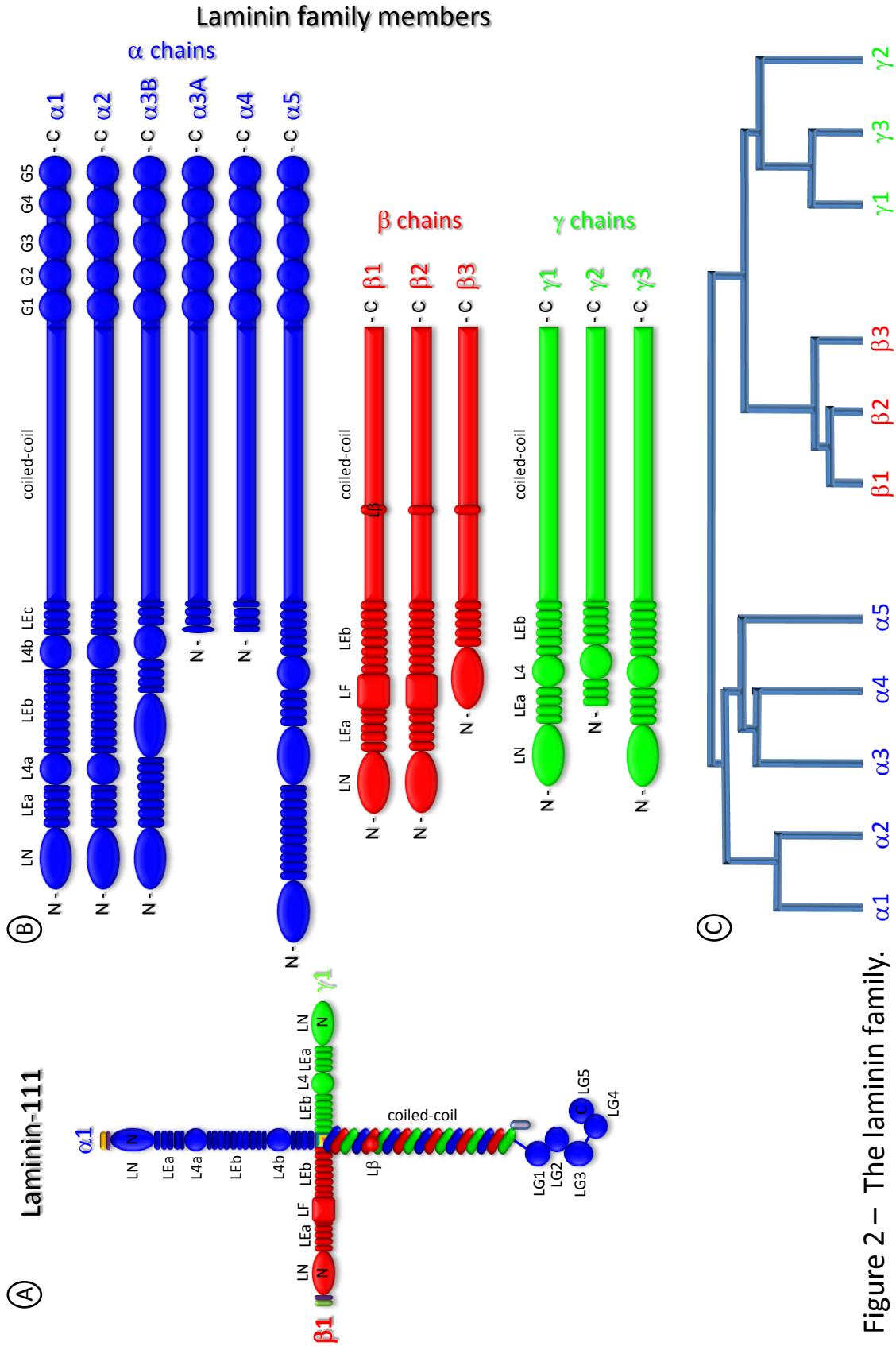


Figure 2 – The laminin family.

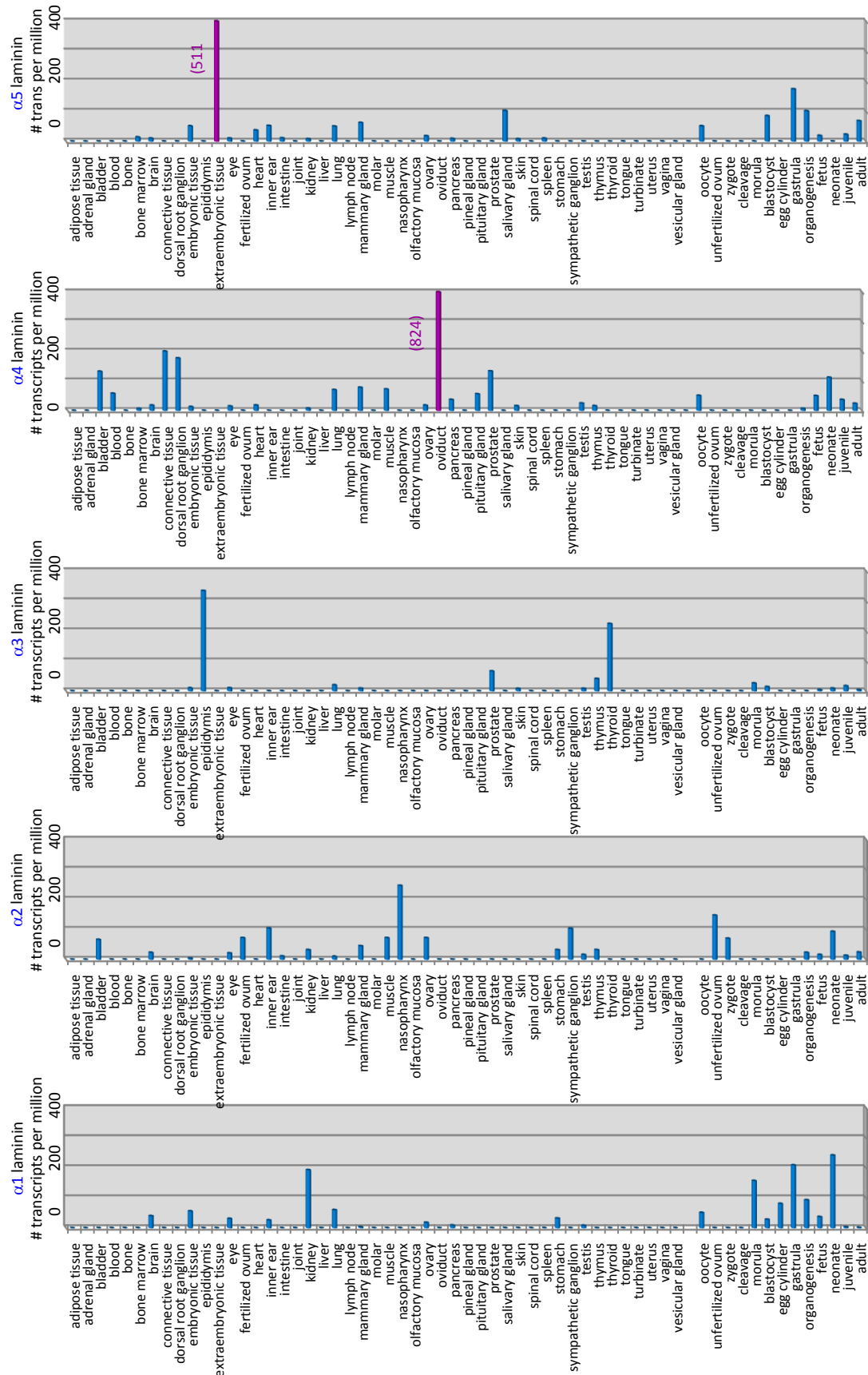


Figure 4 - The summation of EST expression results for laminin α chains in NCBI's GEO repository.

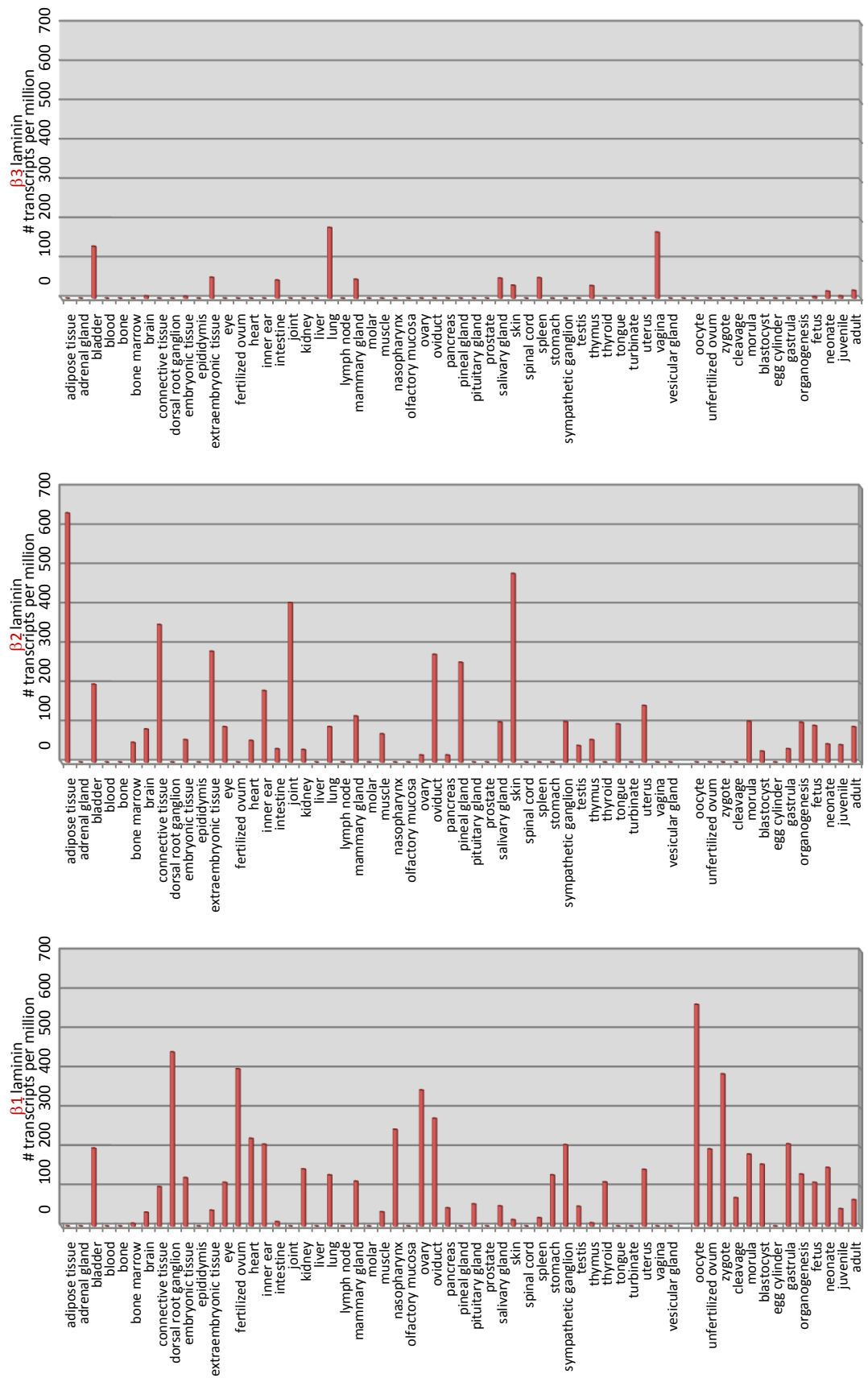


Figure 5 - The summation of EST expression results for laminin β chains in NCBI's GEO repository.

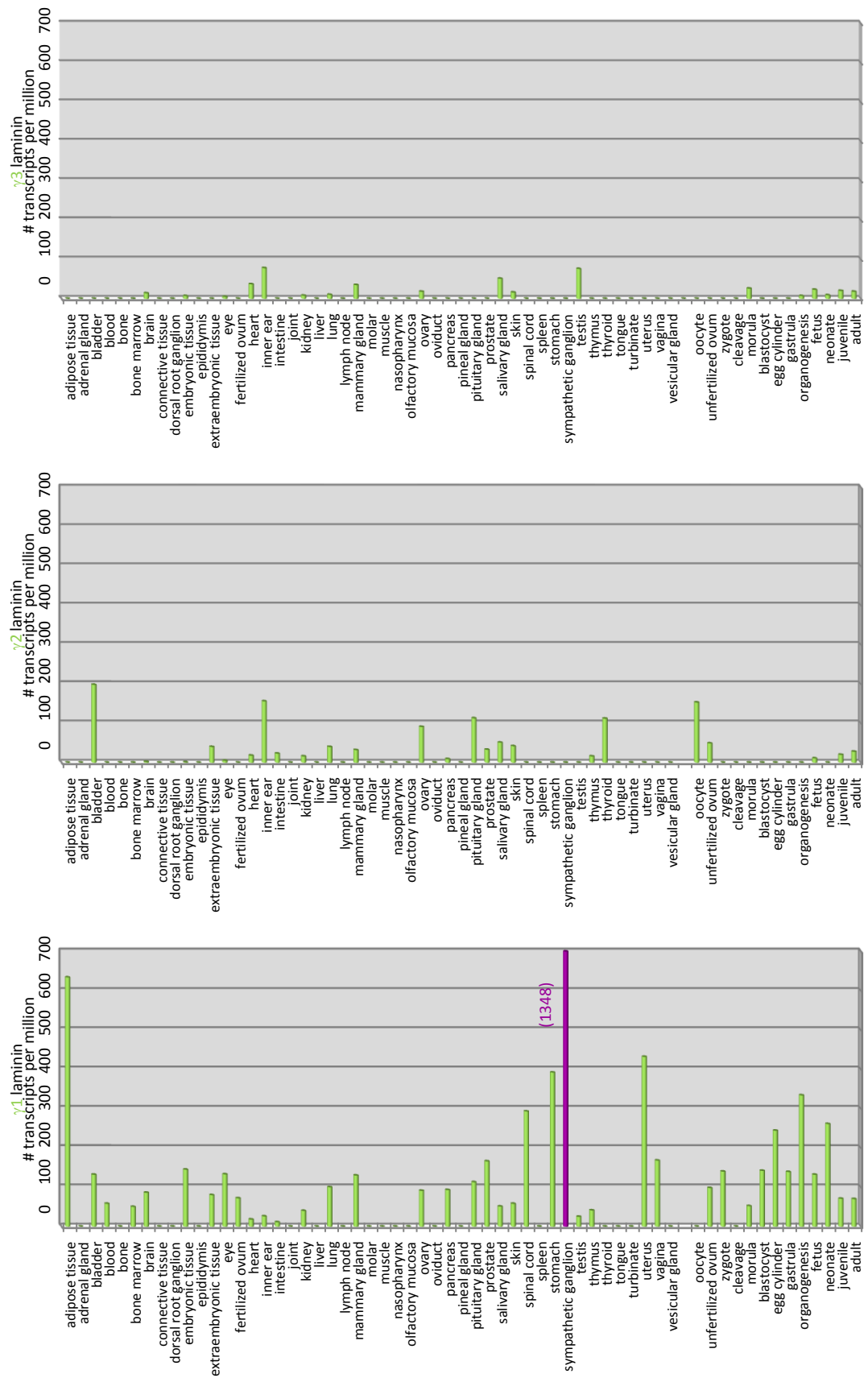


Figure 6 - The summation of EST expression results for laminin γ chains in NCBI's GEO repository.

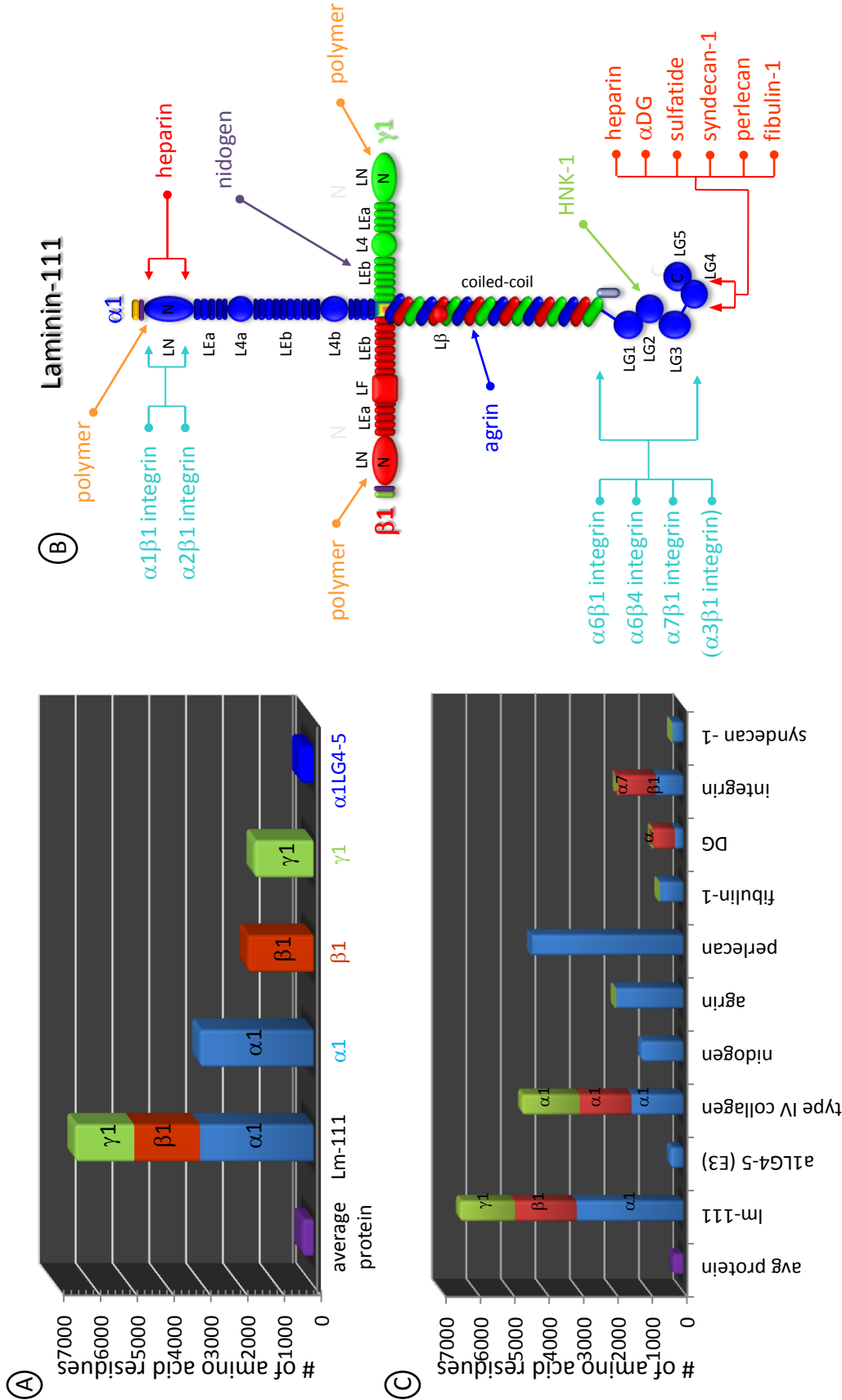


Figure 7 – The number of amino acid residues composing laminin-111, its constituent $\alpha 1$, $\beta 1$, and $\gamma 1$ chains, and other proteins it interacts with, as well as the location in Lm-111 of these binding interactions.

<u>gene family</u>	<u>gene</u>	<u>disease caused by mutation of gene</u>	<u>collagen family</u>	<u>gene</u>	<u>disease caused by mutation of gene</u>
laminin	$\alpha 2$	congenital muscular dystrophy (CMD)	type I	$\alpha 1$	osteogenesis imperfecta (OI) osteoporosis (OP)
	$\alpha 3$	Herlitz junctional epidermolysis bullosa (JEB)			
	$\beta 1$	neonatal cutis laxa with marfanoid phenotype	type I	$\alpha 2$	Ehlers-Danlos syndrome (EDS) Marfan syndrome (MFS), atypical osteogenesis imperfecta (OI)
	$\beta 3$	Herlitz junctional epidermolysis bullosa			
	$\gamma 2$	generalized atrophic benign epidermolysis bullosa (GABEB) Herlitz junctional epidermolysis bullosa	type II	$\alpha 2$	Stickler/Wagner syndrome Ehlers-Danlos syndrome osteoarthritis chondrodysplasias
elastin	elastin	Marfan syndrome (MFS) Buschke-Ollendorf syndrome (BOS) Williams-Beuren syndrome (WBS) pseudoxanthoma elasticum (PXE) supravalvular aortic stenosis (SVAS) cutis laxa, congenital	type III	$\alpha 1$	Ehlers-Danlos syndrome arterial aneurysms (aortic and cerebral)
fibrillin	fibrillin	"true" Marfan syndrome Shprintzen-Goldberg syndrome	type IV	$\alpha 3$	Alport syndrome
fibronectin	FN	Ehlers-Danlos syndrome	type IV	$\alpha 4$	Alport syndrome benign familial hematuria (BFH)
	TN-C TN-X	AV canal and conotruncal defects in infants Ehlers-Danlos-like syndrome	type IV	$\alpha 5$	Alport syndrome
perlecan	perlecan	Schwartz-Jampel Syndrome Type 1 (SJS1) Silverman-Handmaker type of dyssegmental dysplasia (DDSH)	type VI	$\alpha 1$	Bethlem myopathy with contractures
	GPC3	Simpson-Golabi-Beihmel syndrome (SGBS) Type I SGBS is also called Simpson dysmorphia syndrome (SDYS) somatic Wilms tumor development	type VI	$\alpha 2$	Bethlem myopathy
glypican-3	GPC3		type VI	$\alpha 3$	Bethlem myopathy with contractures
			type VII	$\alpha 1$	epidermolysis bullosa (EB) bullous systemic lupus erythematosus (BSLE)
			type X	$\alpha 1$	Schmid type metaphyseal chondrodysplasia Japanese type spondylometaphyseal dysplasia (SMD)

Figure 8 – Extracellular matrix genes and related diseases.

BM components	Null phenotype	References
α1 laminin	~E5.5/6.5 embryonic lethal (Reichert's membrane and defective epiblast polarization)	[239, 240]
α1ΔLG4-5	~E6.5 embryonic lethal	[488]
α2 laminin	postnatal lethal muscular dystrophy; peripheral and central neuropathy	[489]
α3 laminin	~P0 lethal = JEB (junctional epidermolysis bullosa; skin and esophageal blistering)	[490]
α4 laminin	viable (vascular defects)	[491, 492]
α5 laminin	~E14-17 lethal (anterior neural tube closure, placental vasculature, syndactyly, kidney and limb development)	[493, 494]
β1 laminin	ND	[240]
β2 laminin	post-natal lethal, defects in NMJ and renal glomerulus	[495-497]
β3 laminin	~P0 lethal ; JEB	[448]
γ1 laminin	~E5.5 embryonic lethal (peri-implantation lethal with failure of blastocyst differentiation)	[31]
γ1 Lm-Nd site	neonatal lethal (is mutation of the nidogen binding site in g1 chain, domain III4, of laminin)	[499, 500]
γ2 laminin	~P0 lethal = JEB	[501]
γ3 laminin	viable	
α1α2[IV] collagen	E10.5-E11 embryonic lethal , rupture of Reichert's membrane (unpublished)	[502, 503]
α3[IV] collagen	adult lethal from Alport's-like syndrome of kidney	[504, 505]
perlecan	~E10 lethal (hemopericardium), defects of brain and cartilage	[506, 507]
nidogen-1	viable	[508]
nidogen-2	viable	[509]
Nd-1+Nd-2	~P0 lethal - lung development and maintenance and/or integrity of cardiac tissue	[125, 510]
agrin	~P0 lethal - defective neuromuscular junctions	
Receptors	Null phenotype	References
β1-integrin	~E5.5 embryonic lethal (Schwann cell tissue-specific; resembles muscular dystrophy)	[302, 303, 511]
β4-integrin	P0 lethal (skin = JEB)	[512]
α1-integrin	viable (no obvious abnormal phenotype)	[513]
α2-integrin	viable	[514, 515]
α3-integrin	neonatal lethal (lung and kidney organogenesis, epidermal blistering)	[516, 517]
α6-integrin	P0 lethal (skin = JEB, brain)	[149, 150]
α7-integrin	viable (skeletal myopathy)	[518]
dysglycan	~E6.5 embryonic lethal (disruption of Reichert's membrane)	[170, 171]
syndecan-1	viable/fertile	[519]
syndecan-3	viable/fertile	[520, 521]
syndecan-4	viable/healthy	[522, 523]
		[521, 524]
glypican-2	viable/fertile	[525]
glypican-3	perinatal death (lung and kidney defects)	[526]
EXT-1 (HS synth)	~E8.5 embryonic lethal (failure of mesoderm formation during gastrulation)	[527]
sulfatide	viable - Cst-/-; paranodal junction formation and spermatogenesis defects	[528, 529]
LAR (RTPase)	viable (mammary gland, brain, insulin defects)	[530, 531]

Figure 9 – Mouse knockout results of ECM proteins, their receptors, and related BM components.

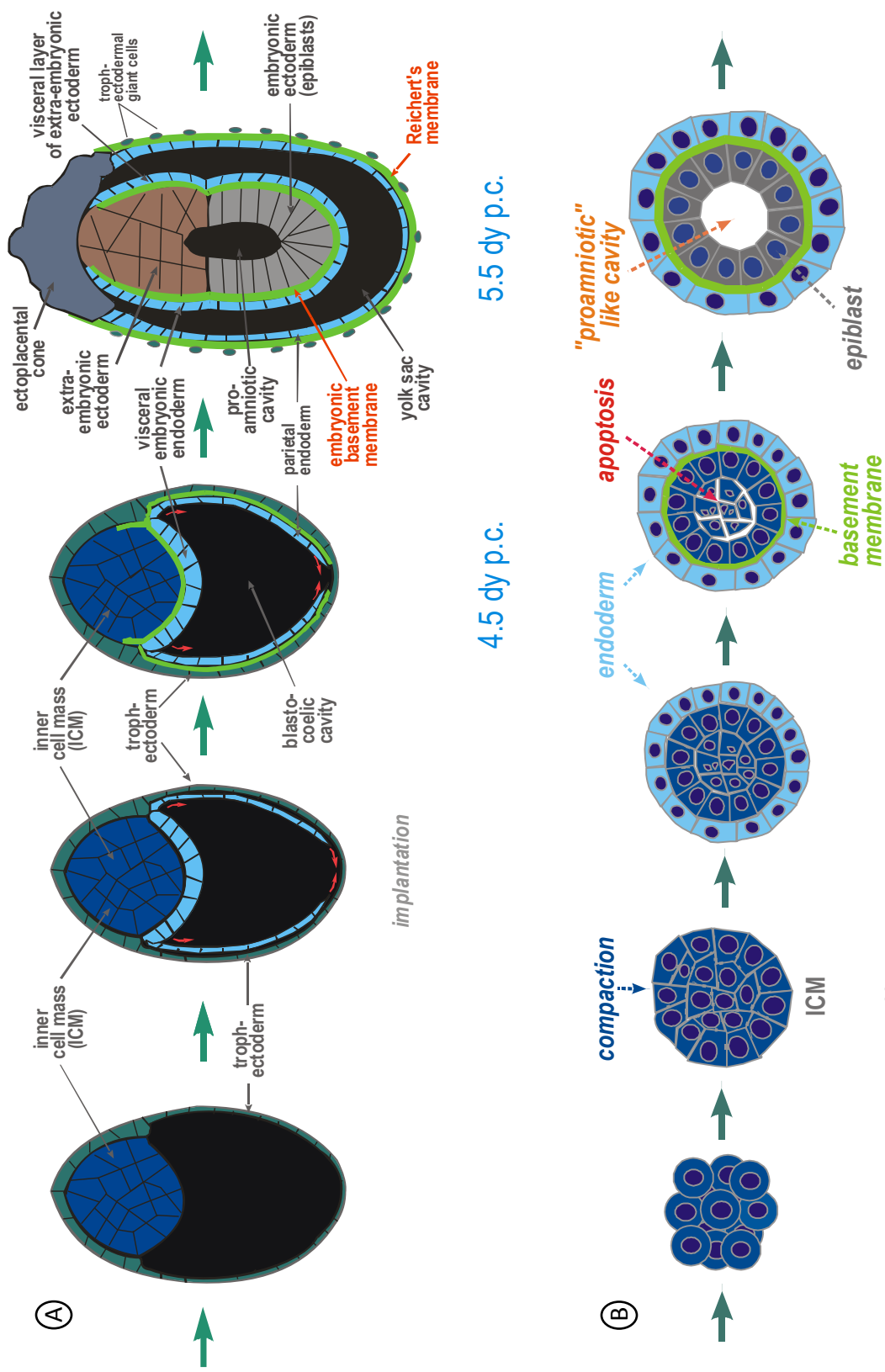


Figure 10 – Embryoid body differentiation.

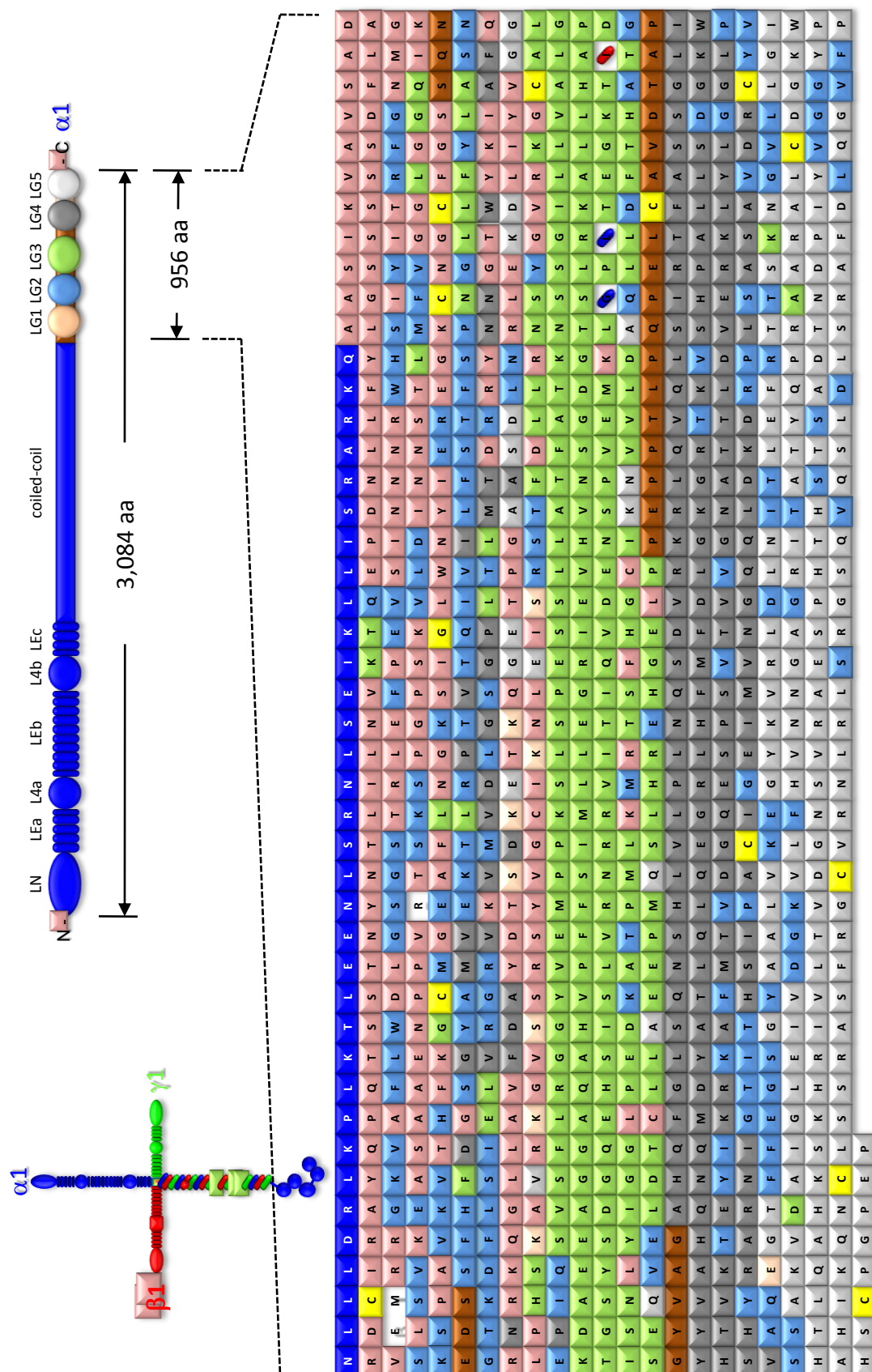


Figure 11 – Amino acid sequence of mouse laminin $\alpha 1$ LG1-5.

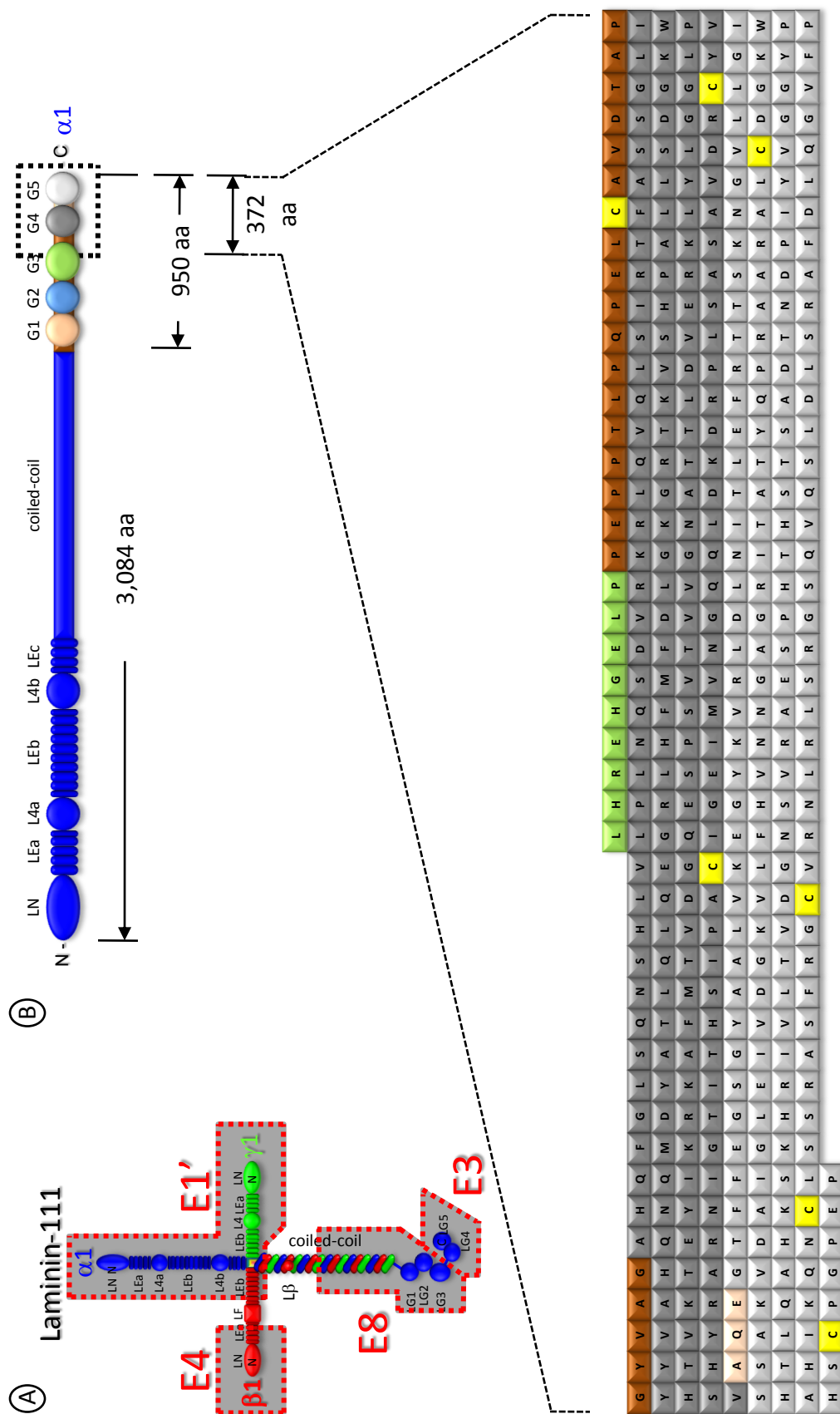
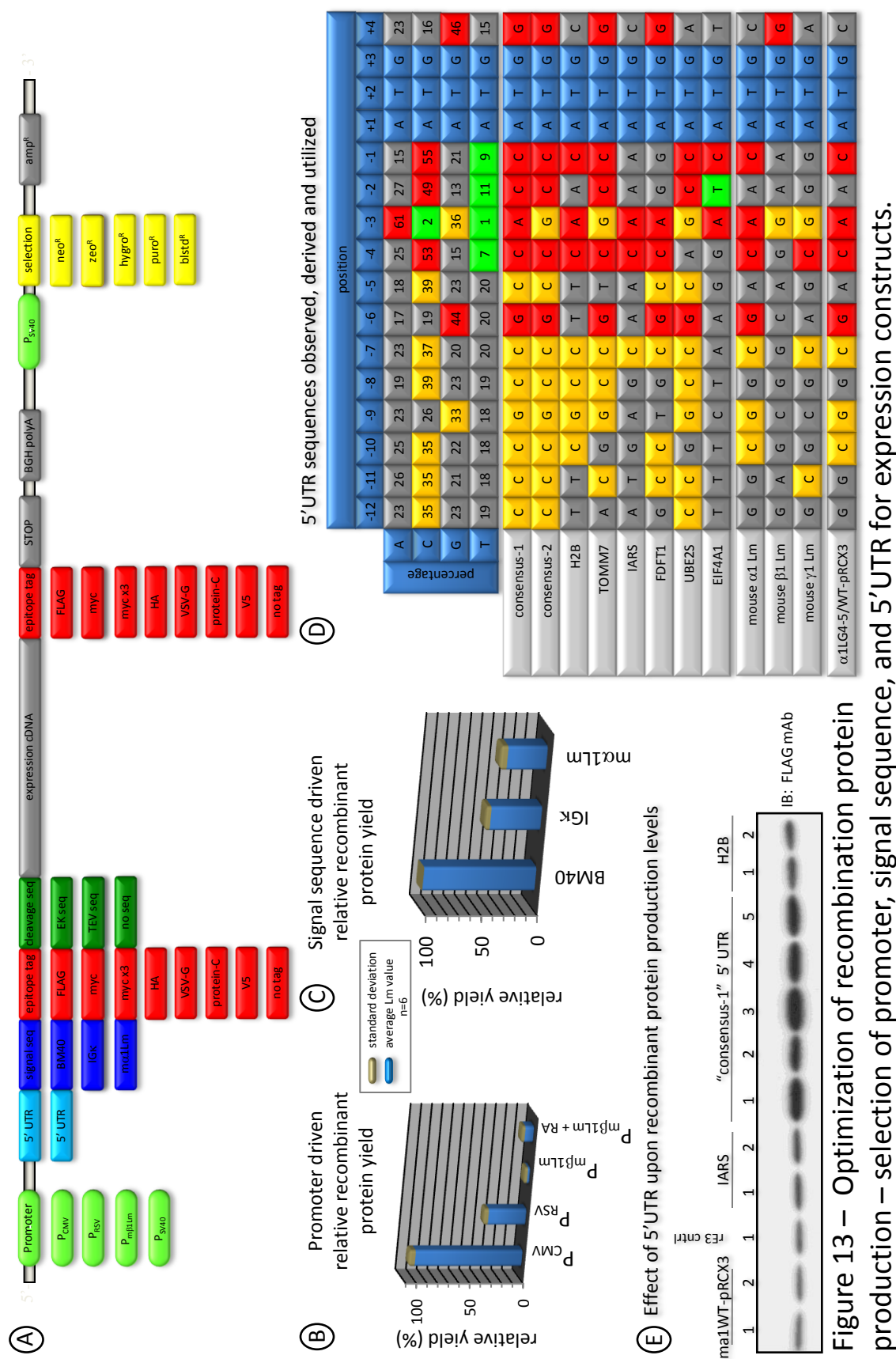


Figure 12 – The amino acid sequence of the elastase proteolytic fragment E3 derived from mouse Lm-111.



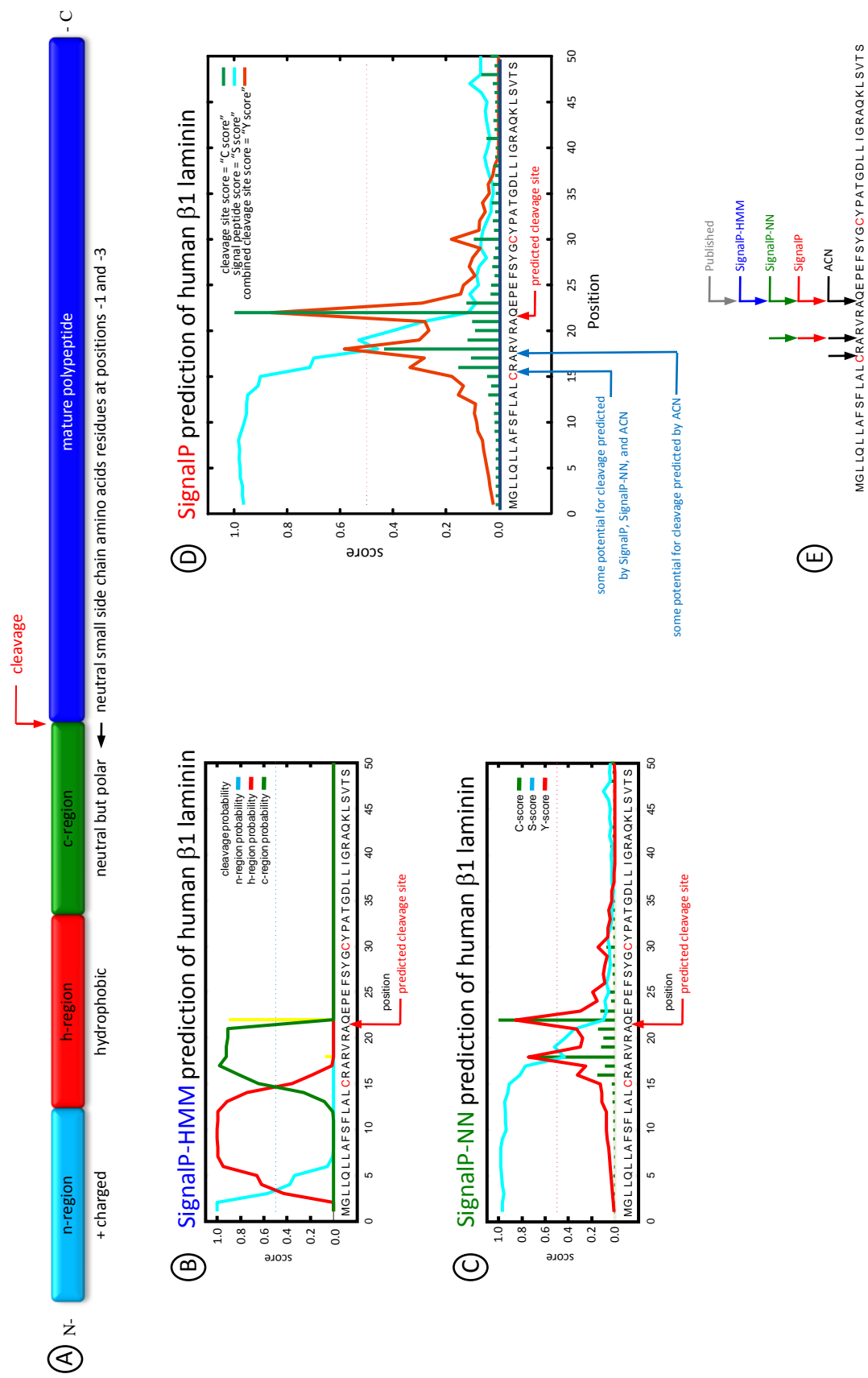


Figure 14 – Determination of signal sequence cleavage sites.

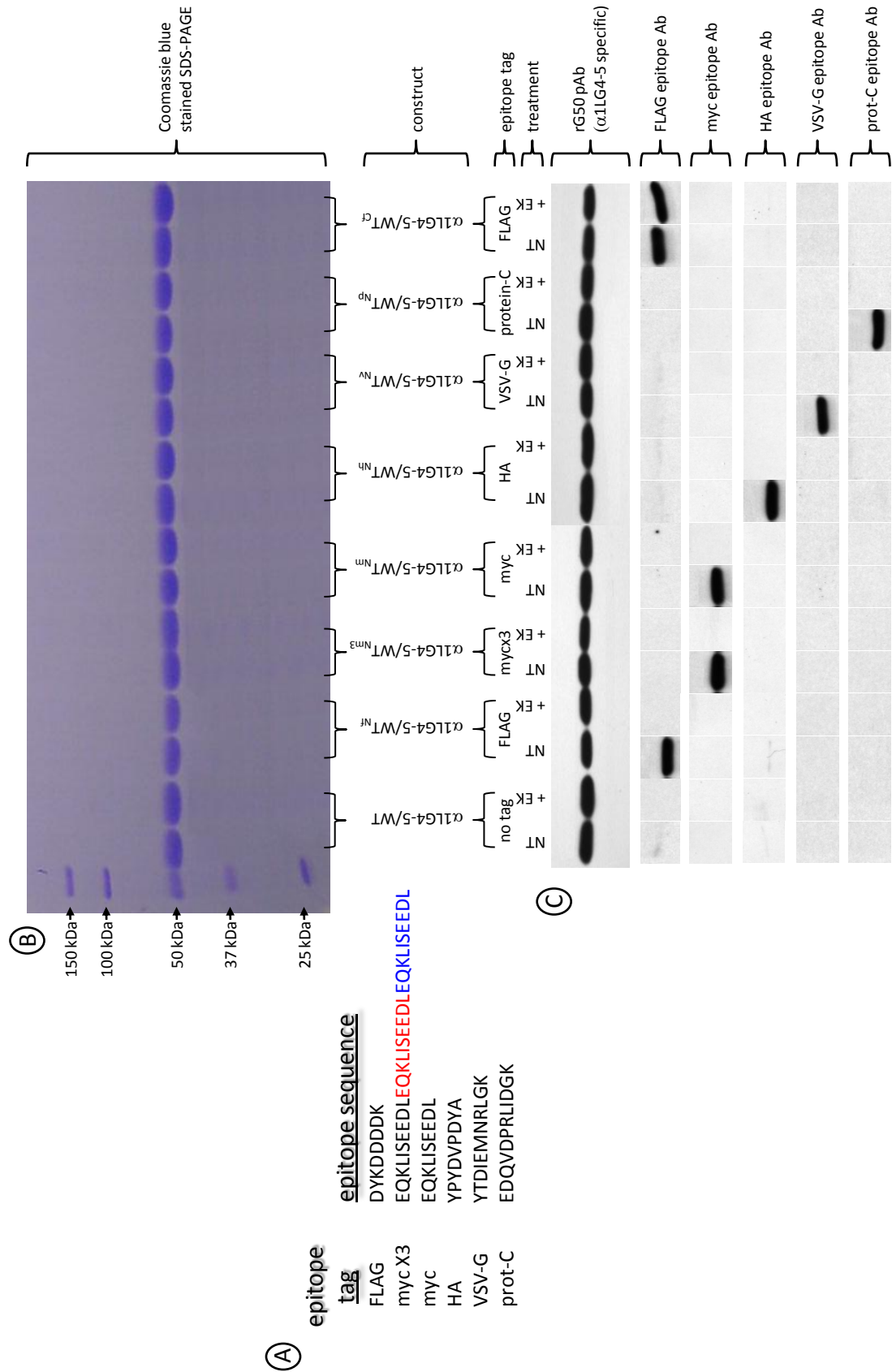


Figure 15 – Epitope tagging of recombinant mouse α1 LG4-5 laminins.

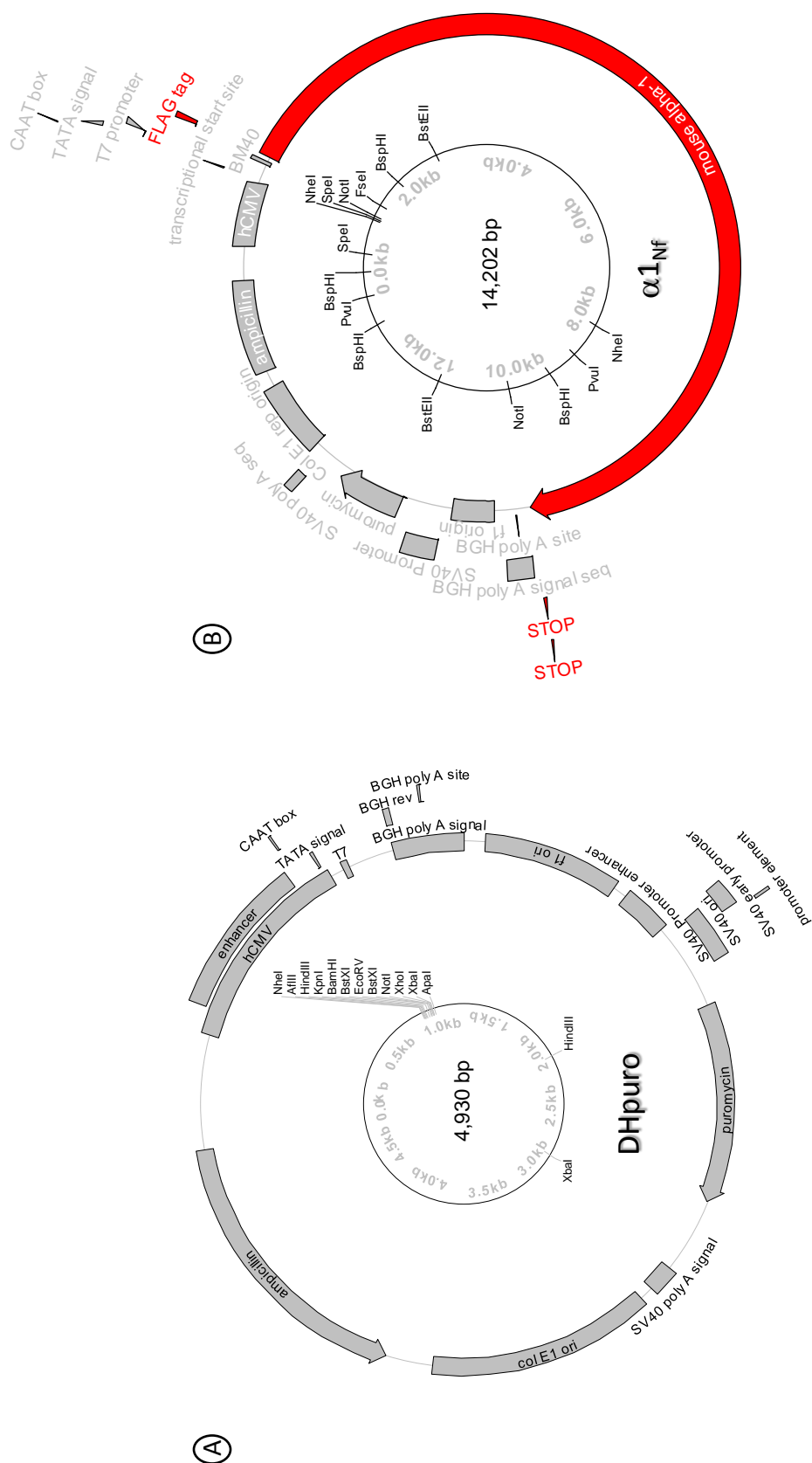


Figure 16 – Puromycin based expression construct DHpuro and the mouse $\alpha 1$ laminin construct, $\alpha 1_{Nf}$ derived from DHpuro.

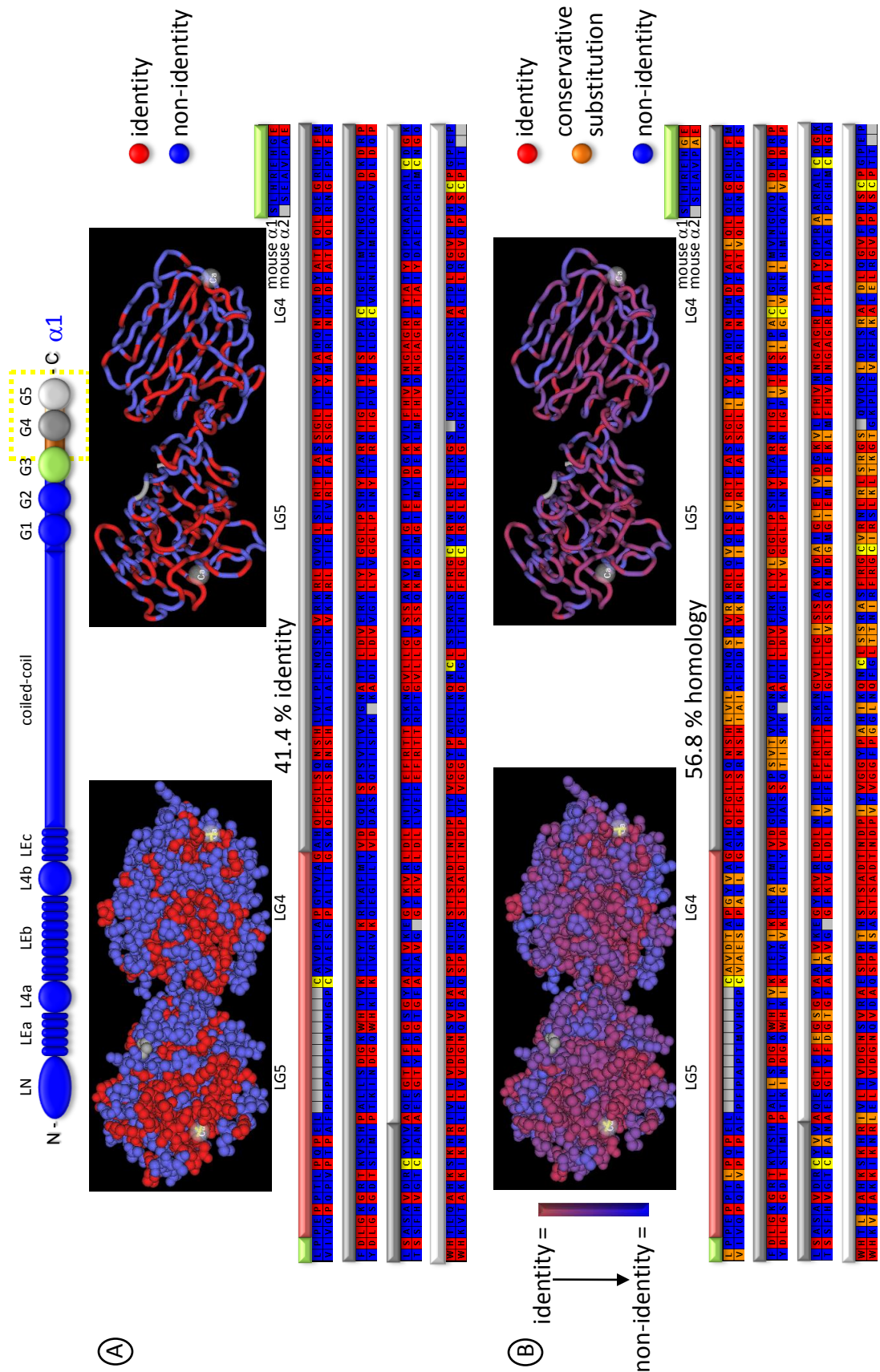


Figure 17 – Conservation of the primary sequence between the LG4-5 of mouse $\alpha 1$ and $\alpha 2$ laminin.

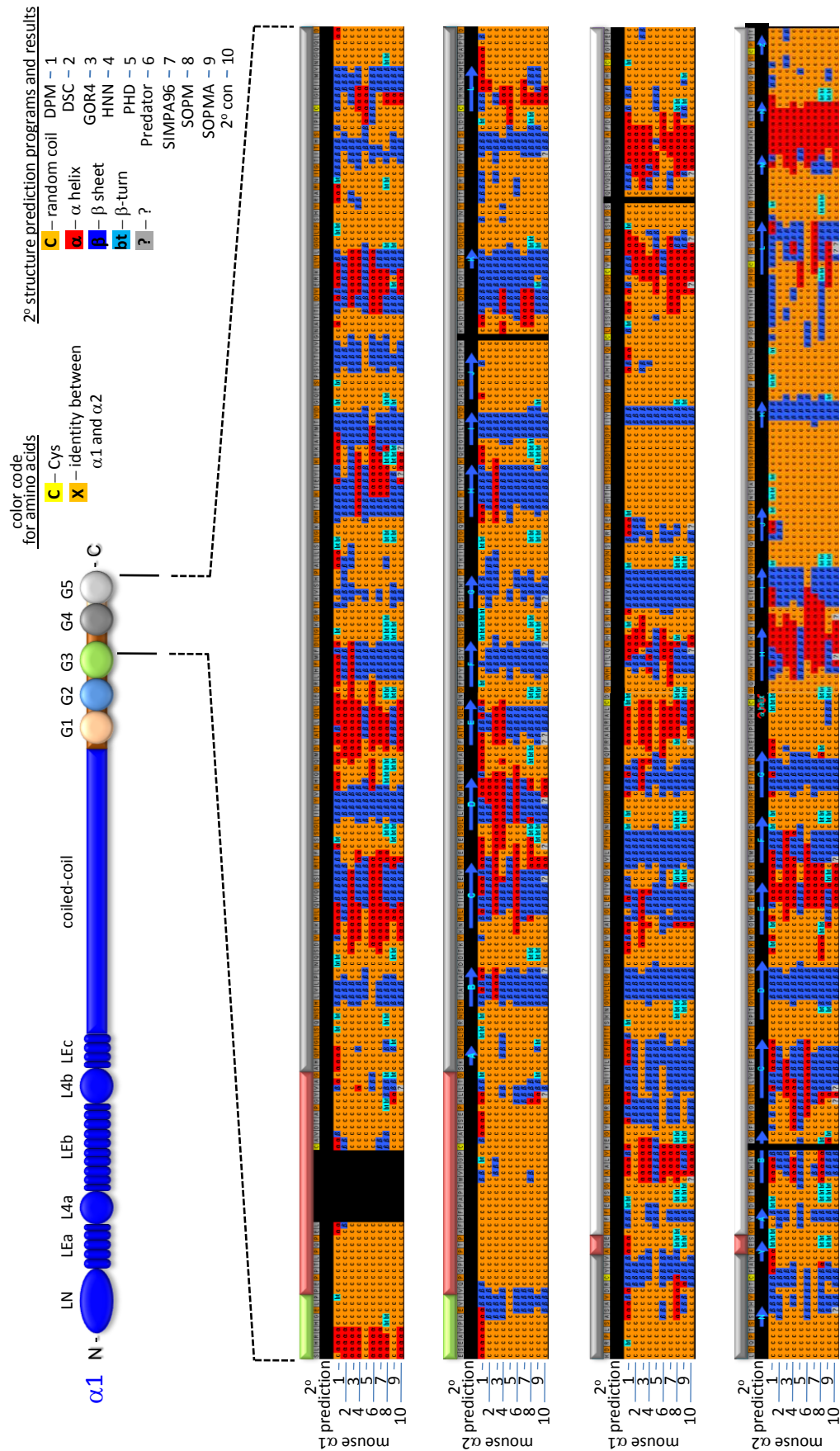


Figure 18 – Conservation of both primary sequence and predicted potential secondary structure between mouse $\alpha 1$ and $\alpha 2$ LG4-5 of laminin.

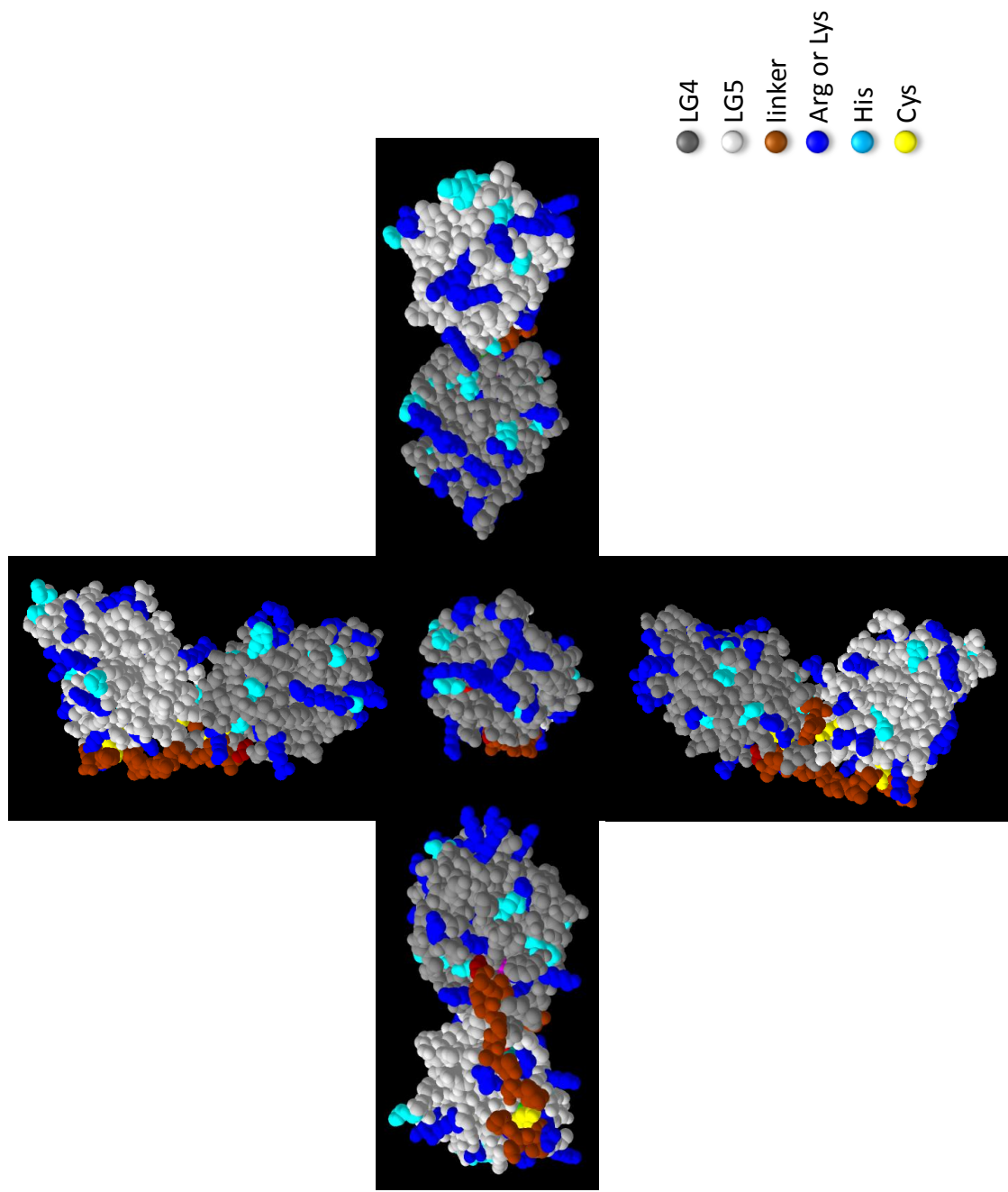
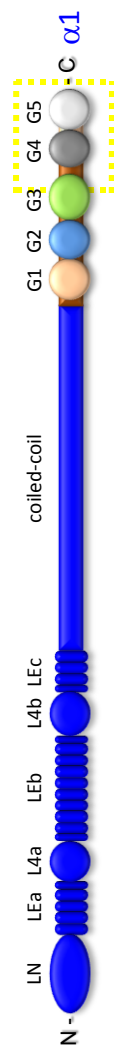
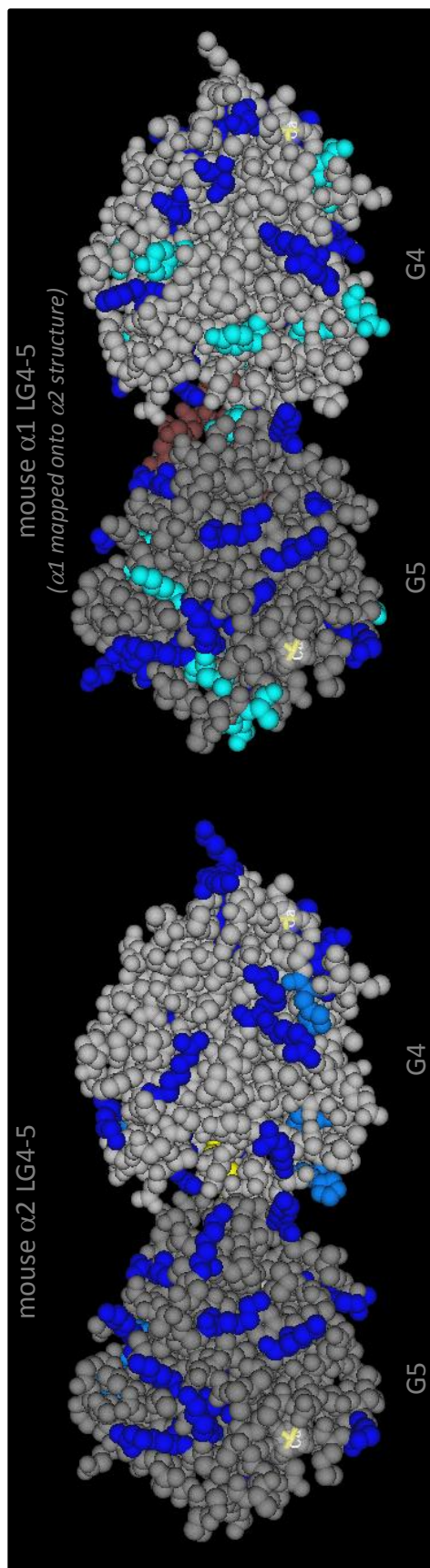


Figure 19 – Homology model of mouse $\alpha 1\text{LG4-5}$ (recombinant E3 analog).



A



ⓑ

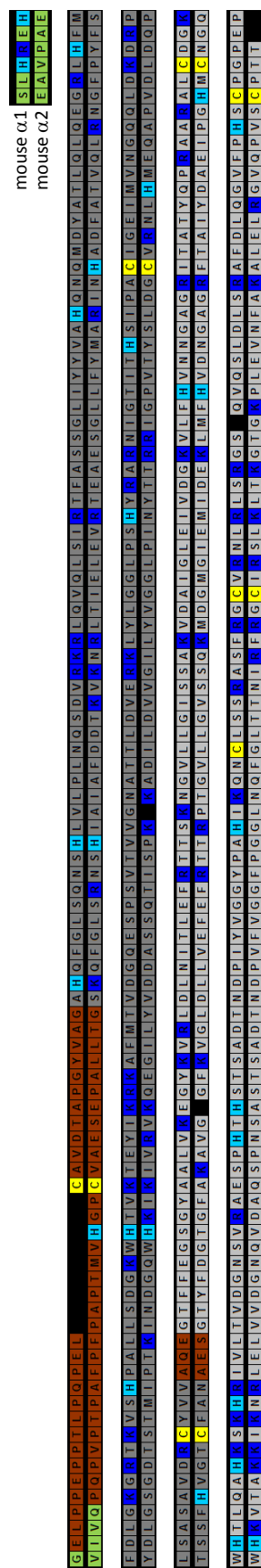


Figure 20 – Comparison of both the spatial and primary location of Arg, Lys, His, and Cys residues in mouse laminin $\alpha 1$ and $\alpha 2$ LG4-5.

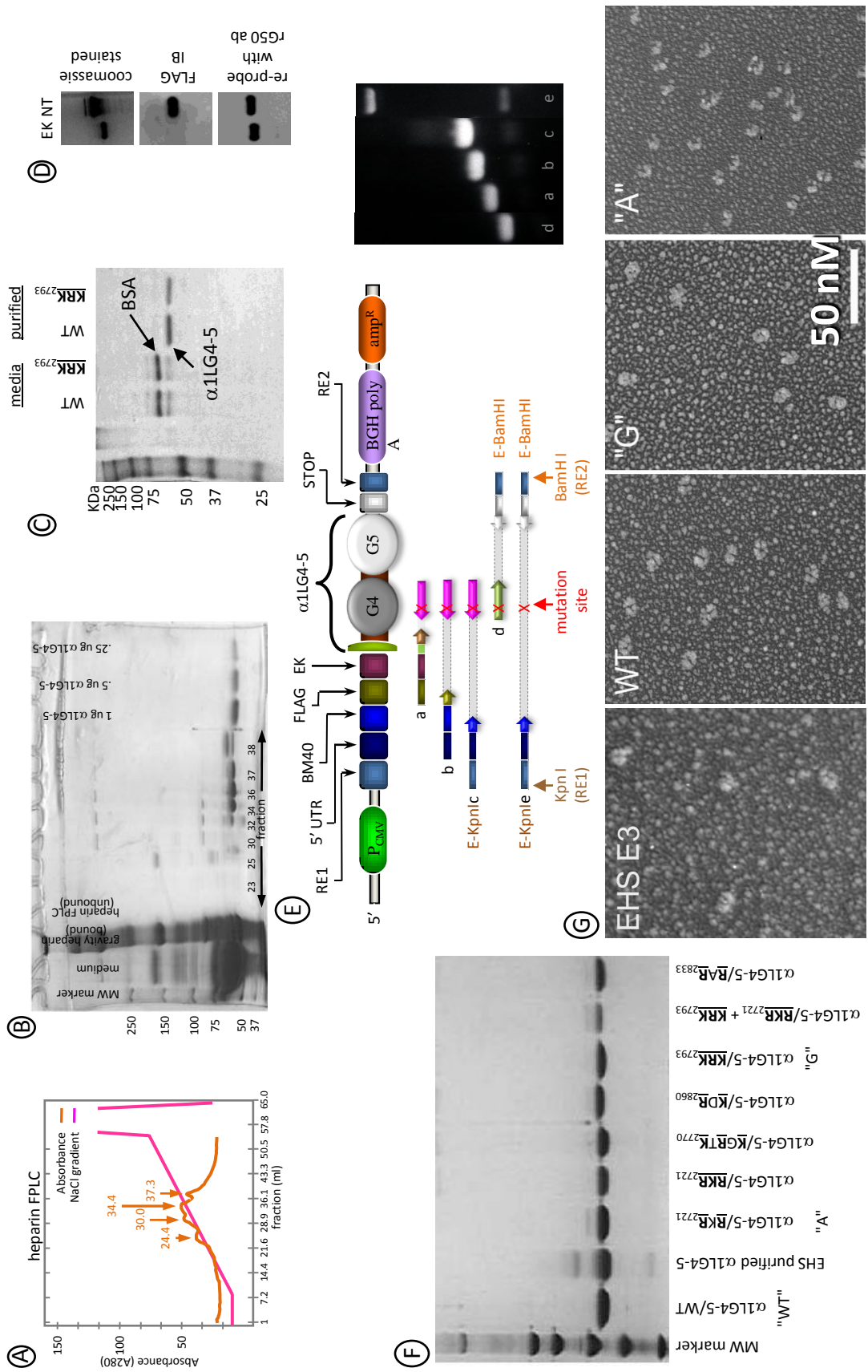


Figure 22 – Generation, production, and purification of recombinant mouse α1 LG4-5 laminins.

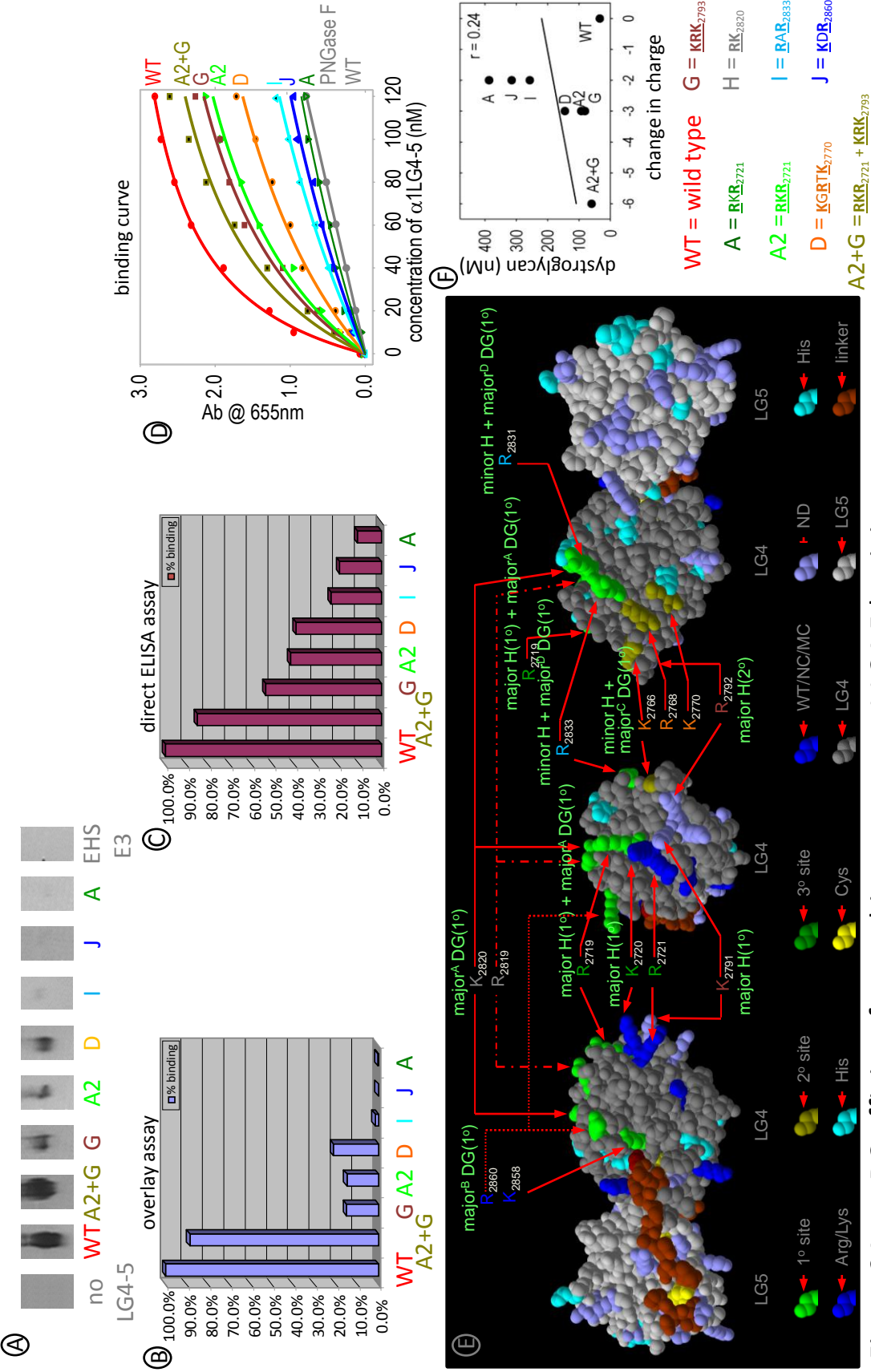


Figure 24 – α DG affinity of recombinant mouse α 1 LG4-5 laminins.

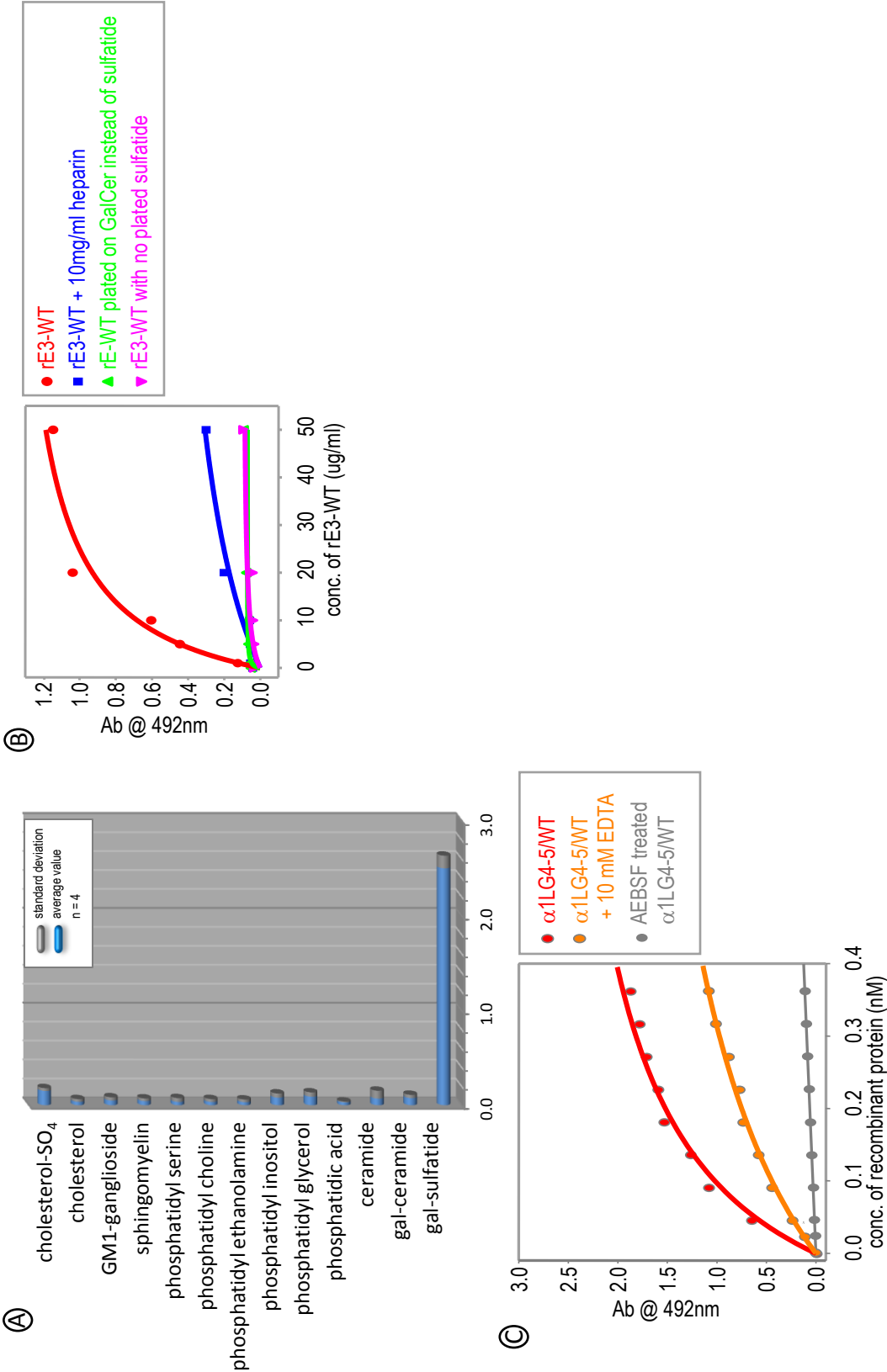


Figure 25 – Sulfatide specificity and affinity of recombinant mouse $\alpha 1$ LG4-5 laminins.

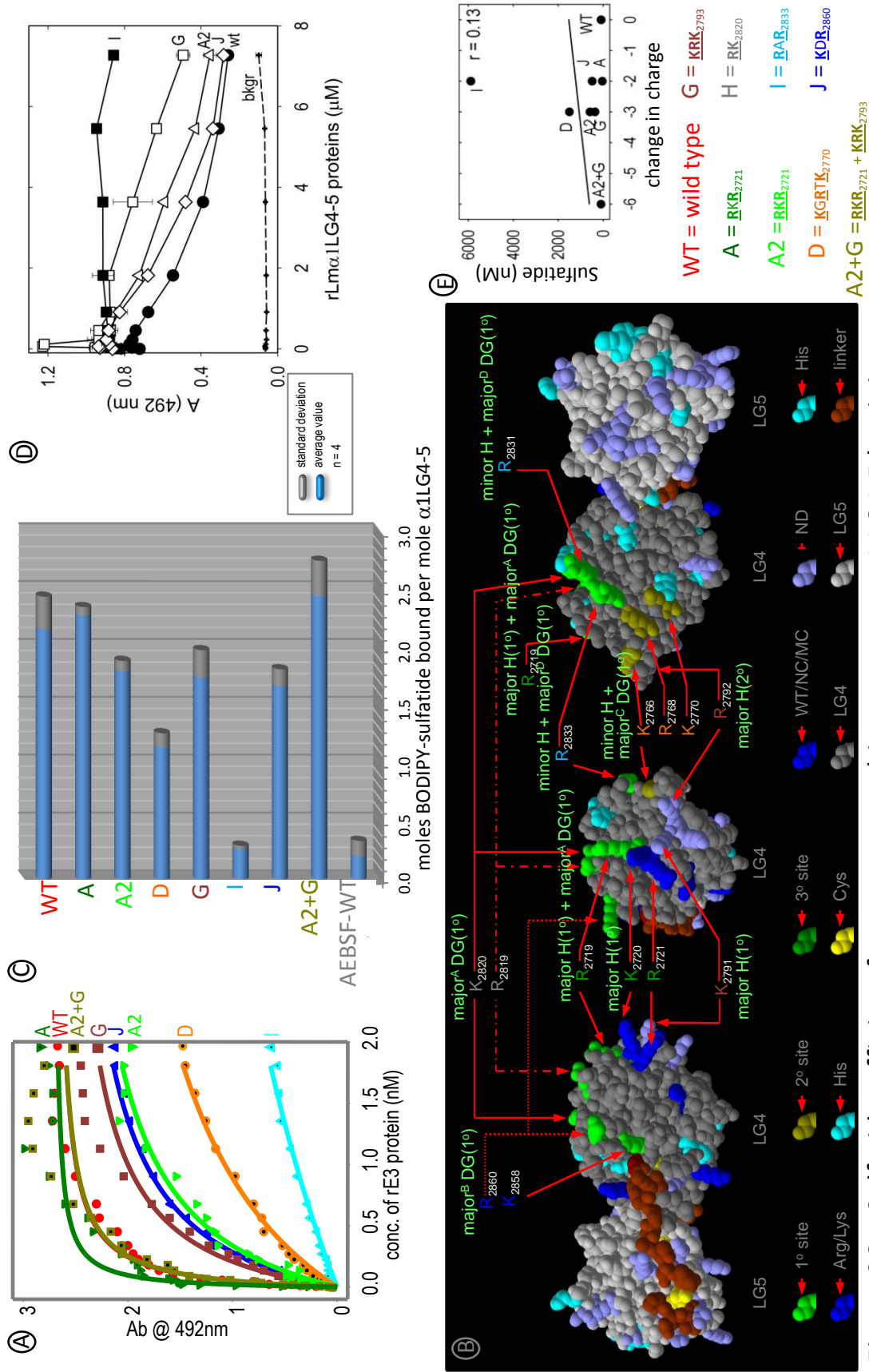


Figure 26– Sulfate affinity of mutant recombinant mouse α1 LG4-5 laminins.

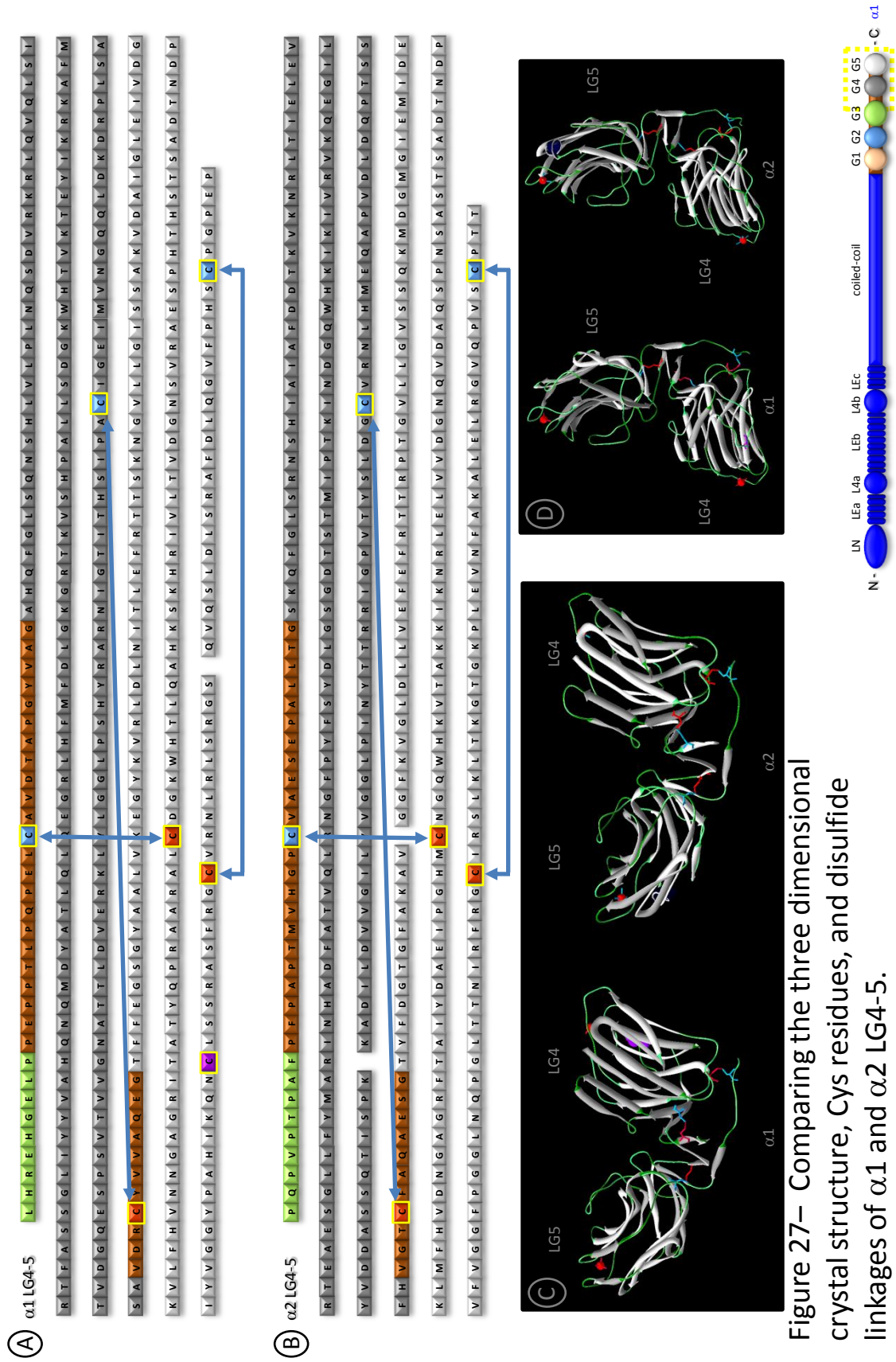


Figure 27– Comparing the three dimensional crystal structure, Cys residues, and disulfide linkages of $\alpha 1$ and $\alpha 2$ LG4-5.

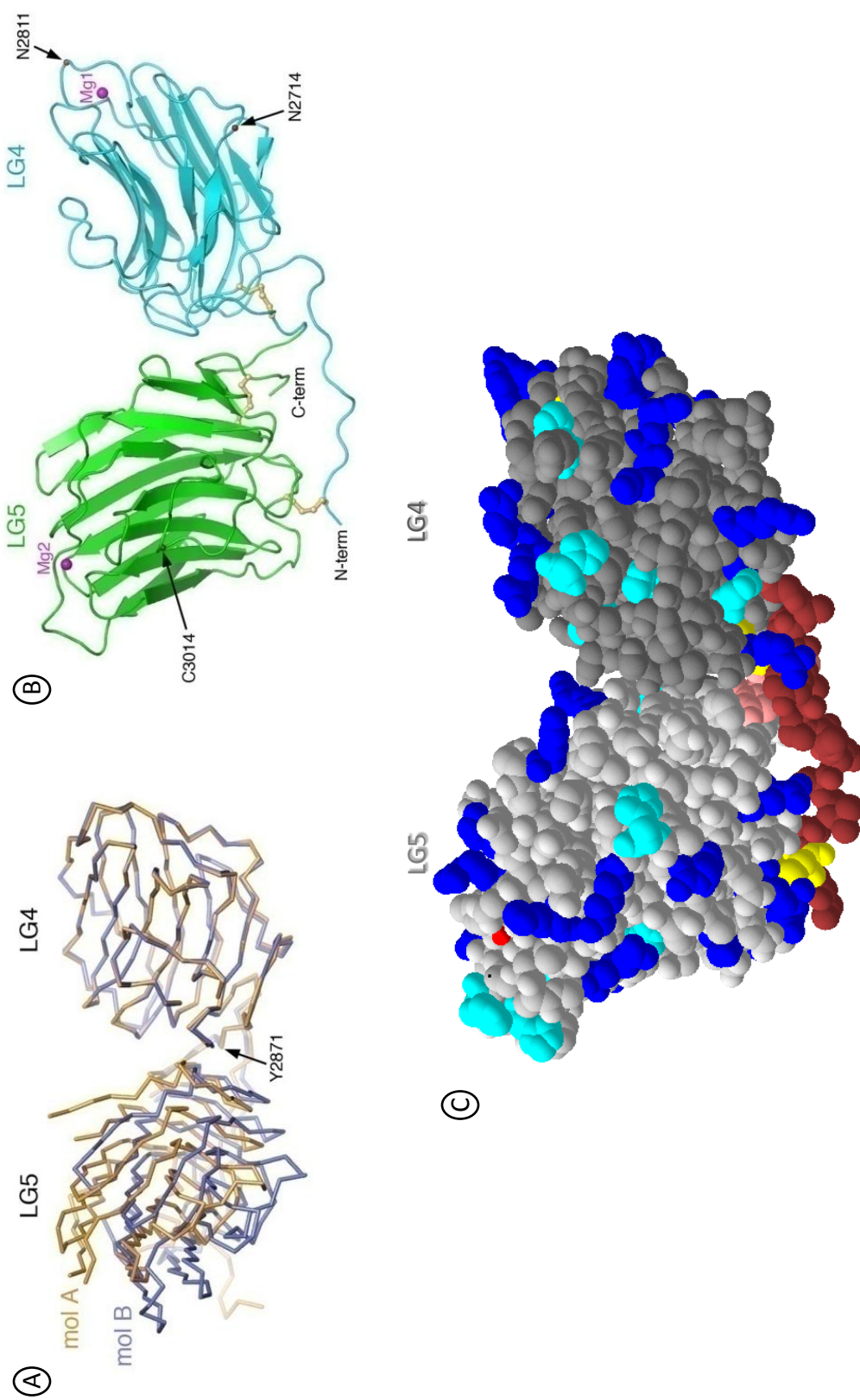


Figure 28 – Crystal structure of mouse laminin $\alpha 1$ LG4-5.

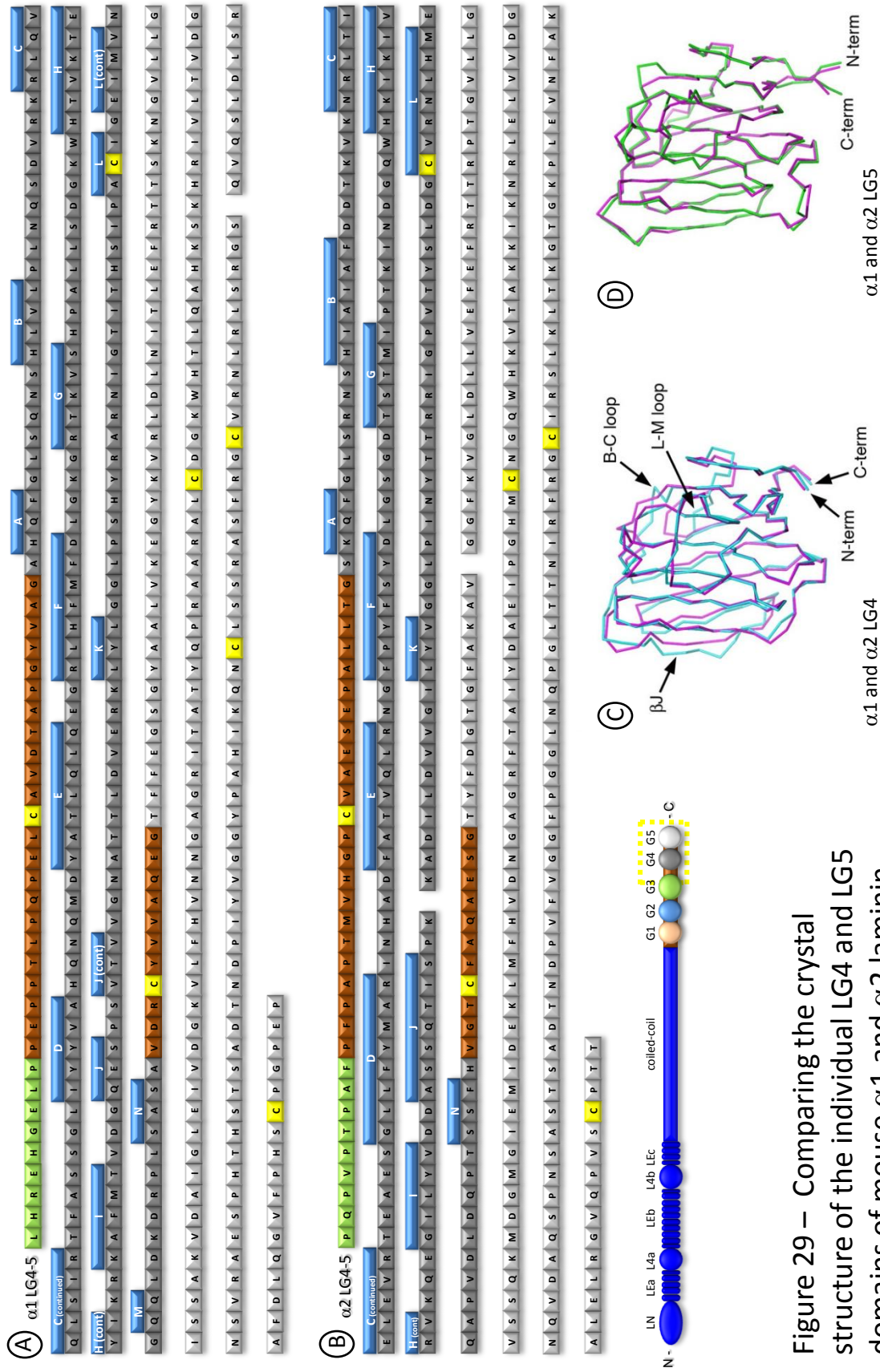


Figure 29 – Comparing the crystal structure of the individual LG4 and LG5 domains of mouse $\alpha 1$ and $\alpha 2$ laminin.

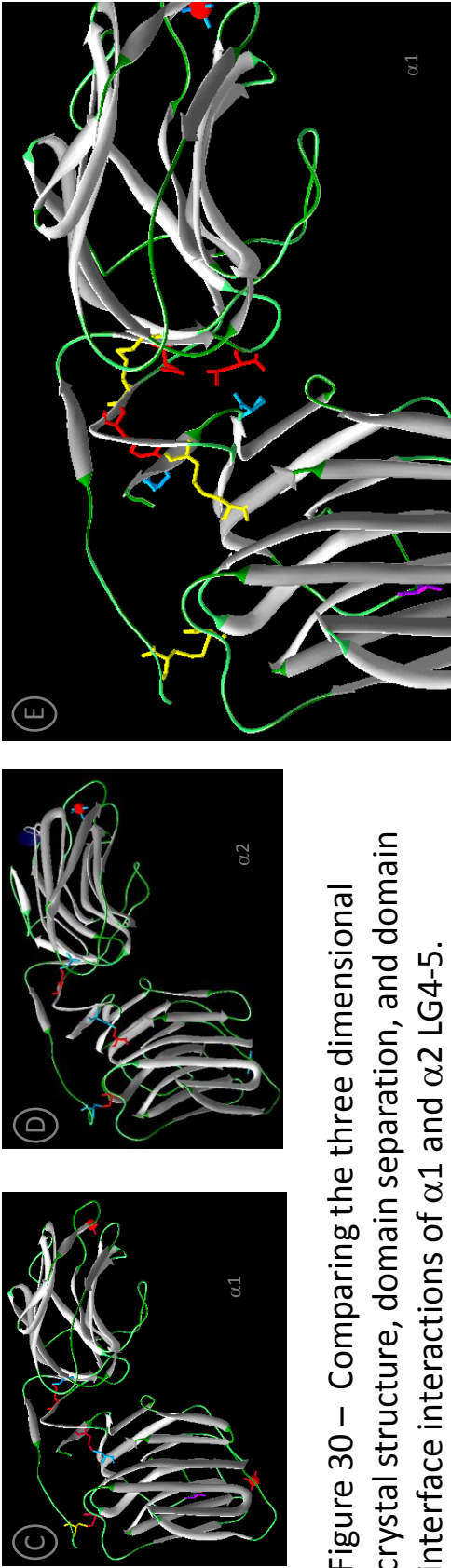
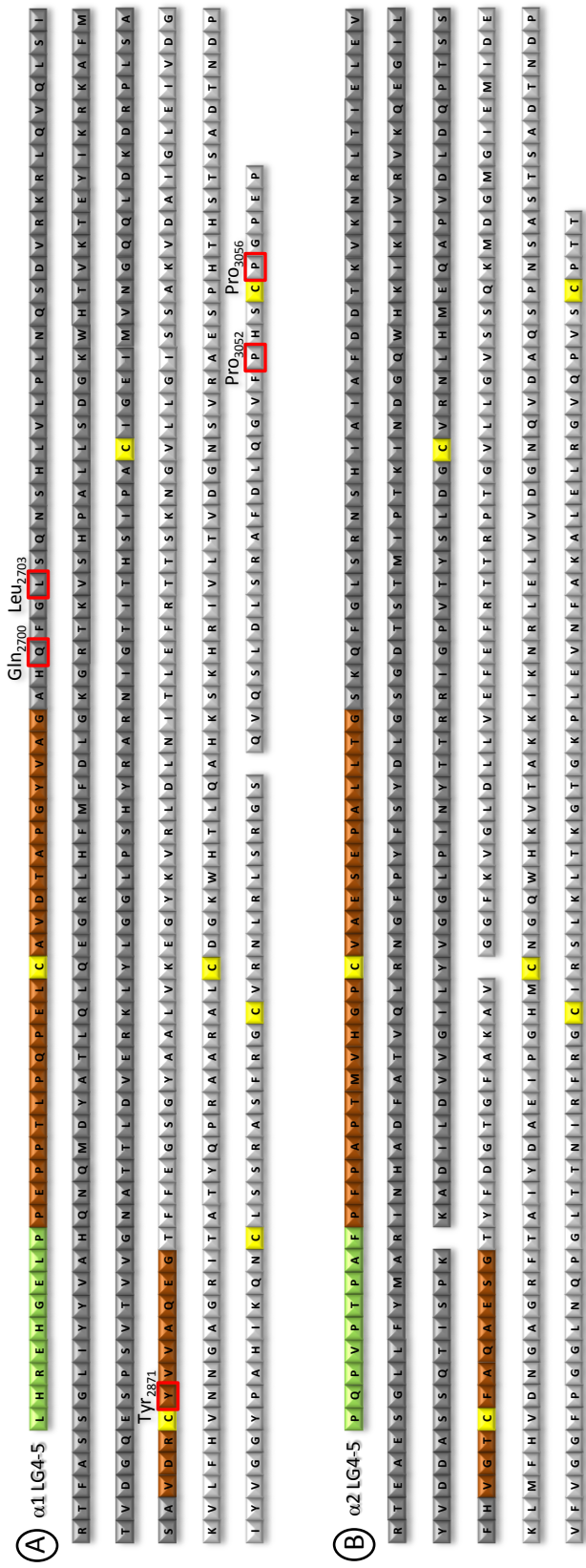


Figure 30 – Comparing the three dimensional crystal structure, domain separation, and domain interface interactions of $\alpha 1$ and $\alpha 2$ LG4-5.

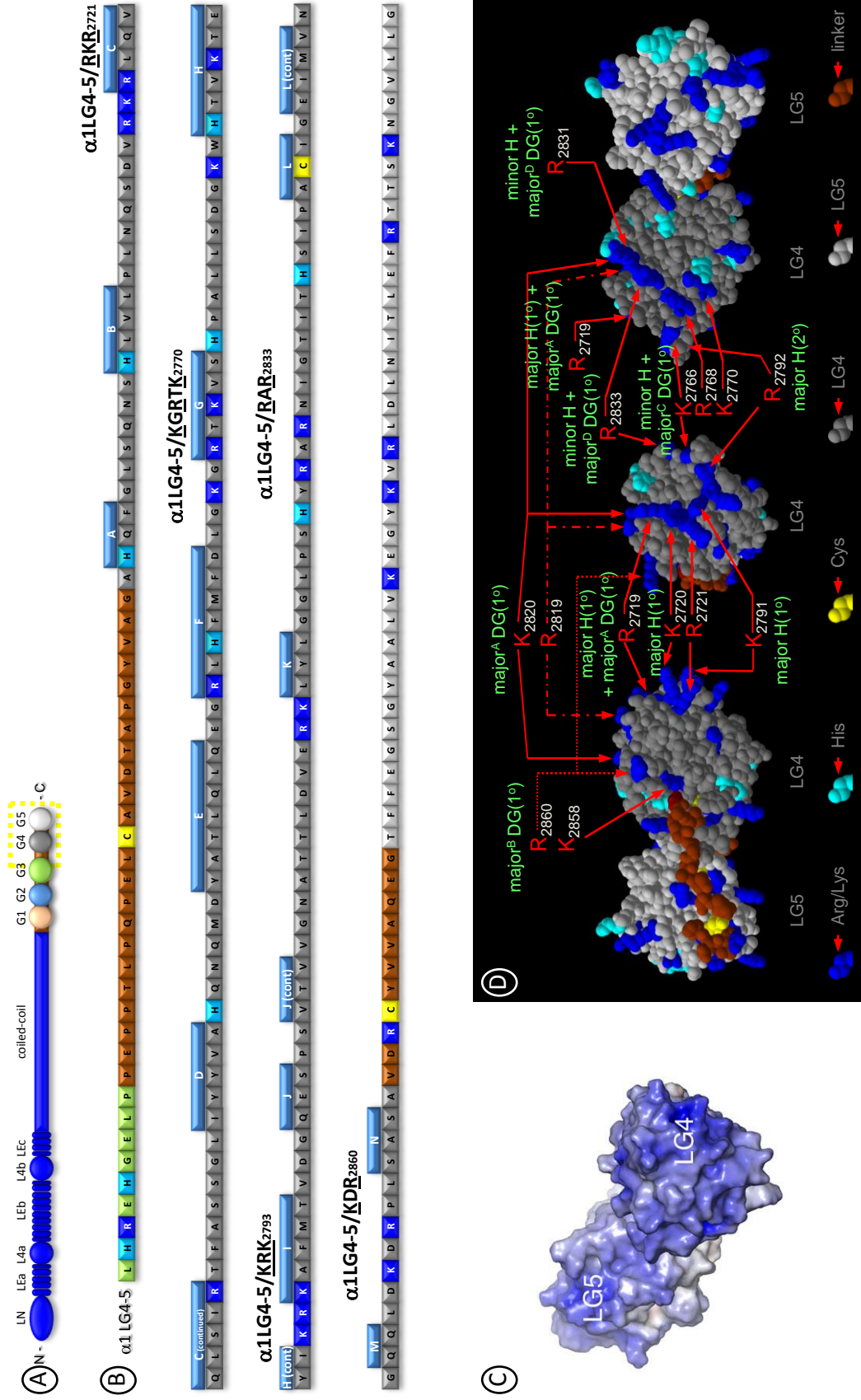


Figure 31 – Recombinant full length $\alpha 1$ laminin chains constructed and utilized to make rLm-111s.

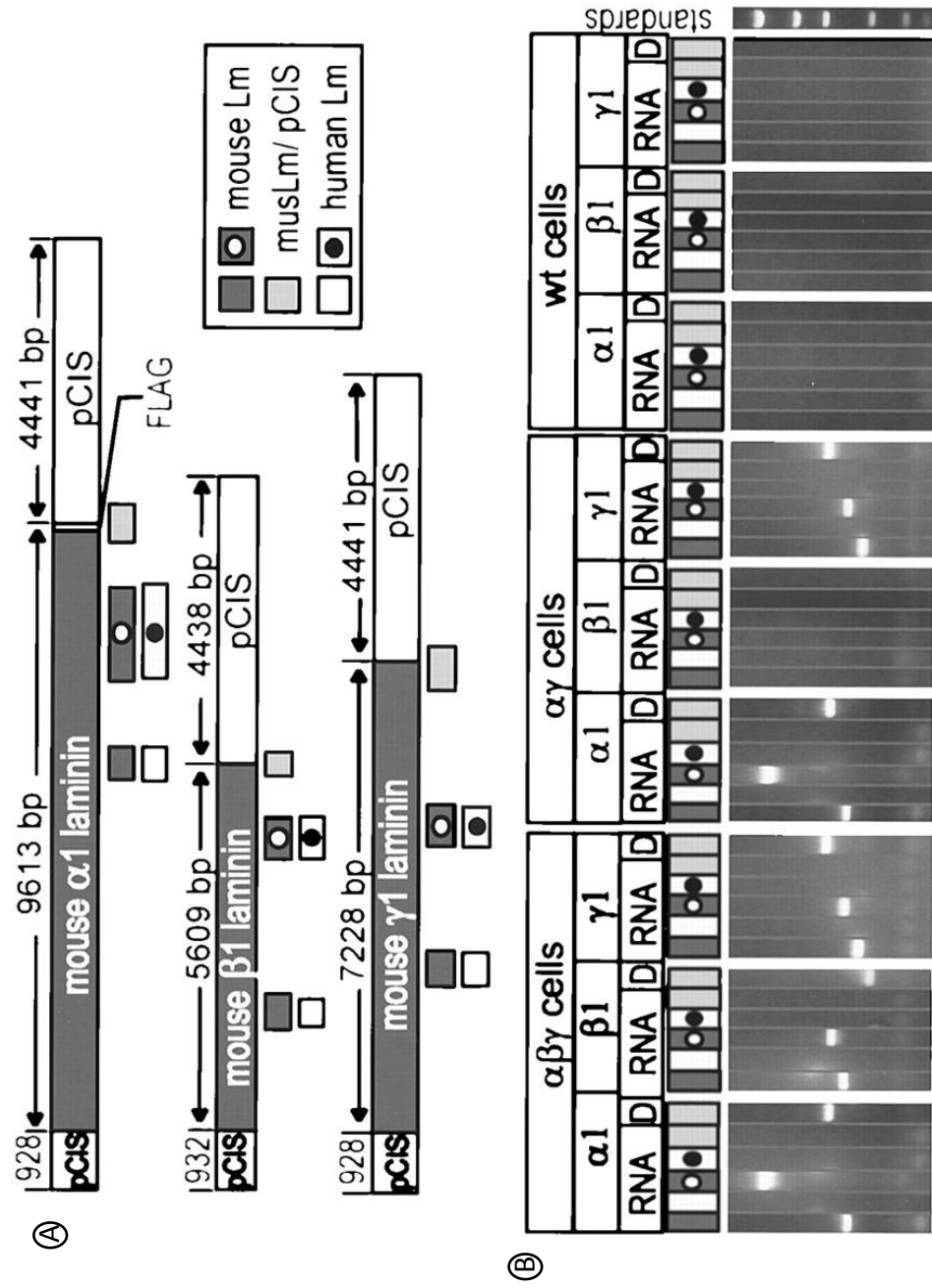


Figure 32 – Characterization of endogeneous and transfected laminin mRNA expression in HEK 293 cells

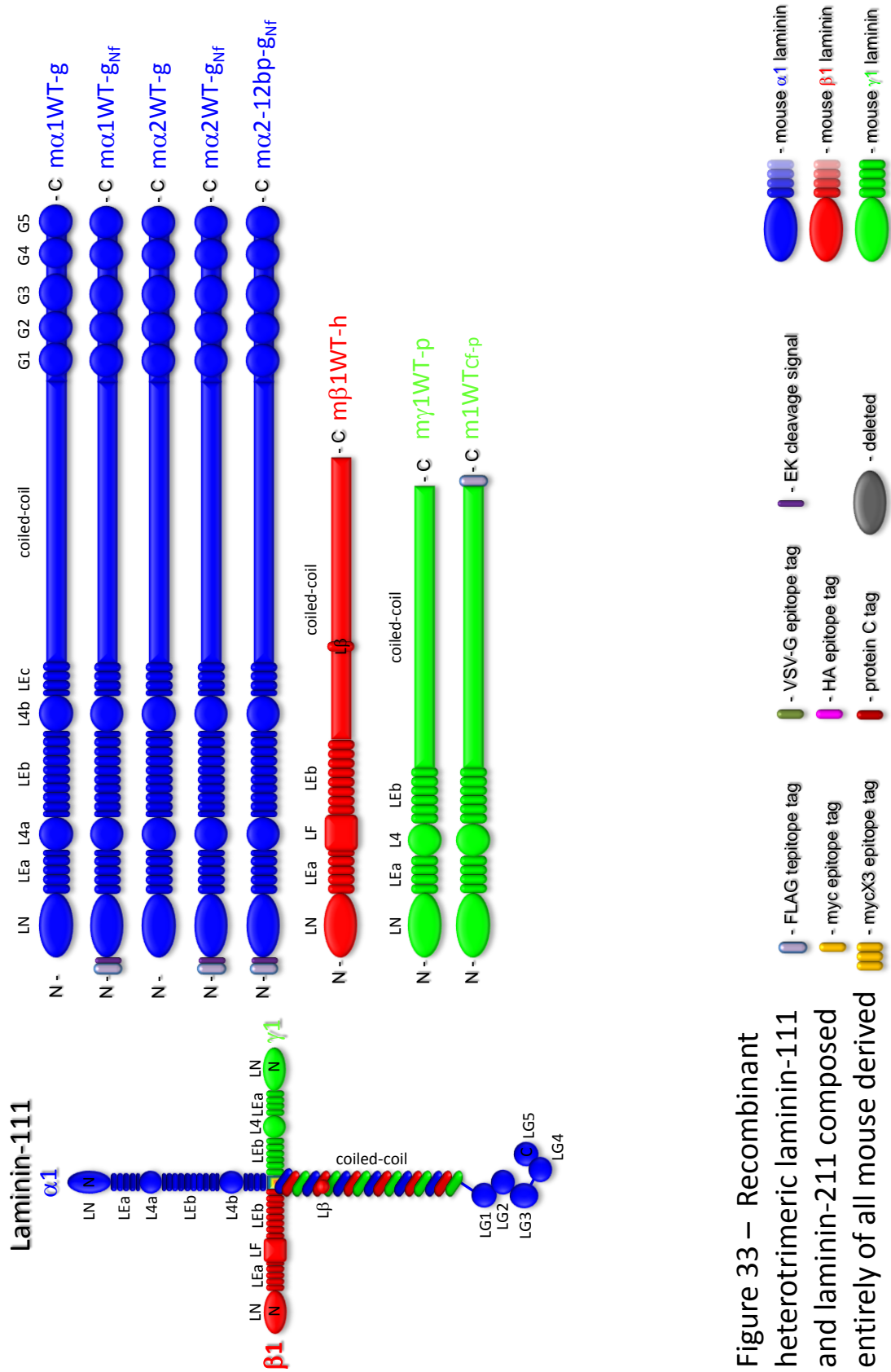


Figure 33 – Recombinant heterotrimeric laminin-111 and laminin-211 composed entirely of all mouse derived α , β , and γ chains.

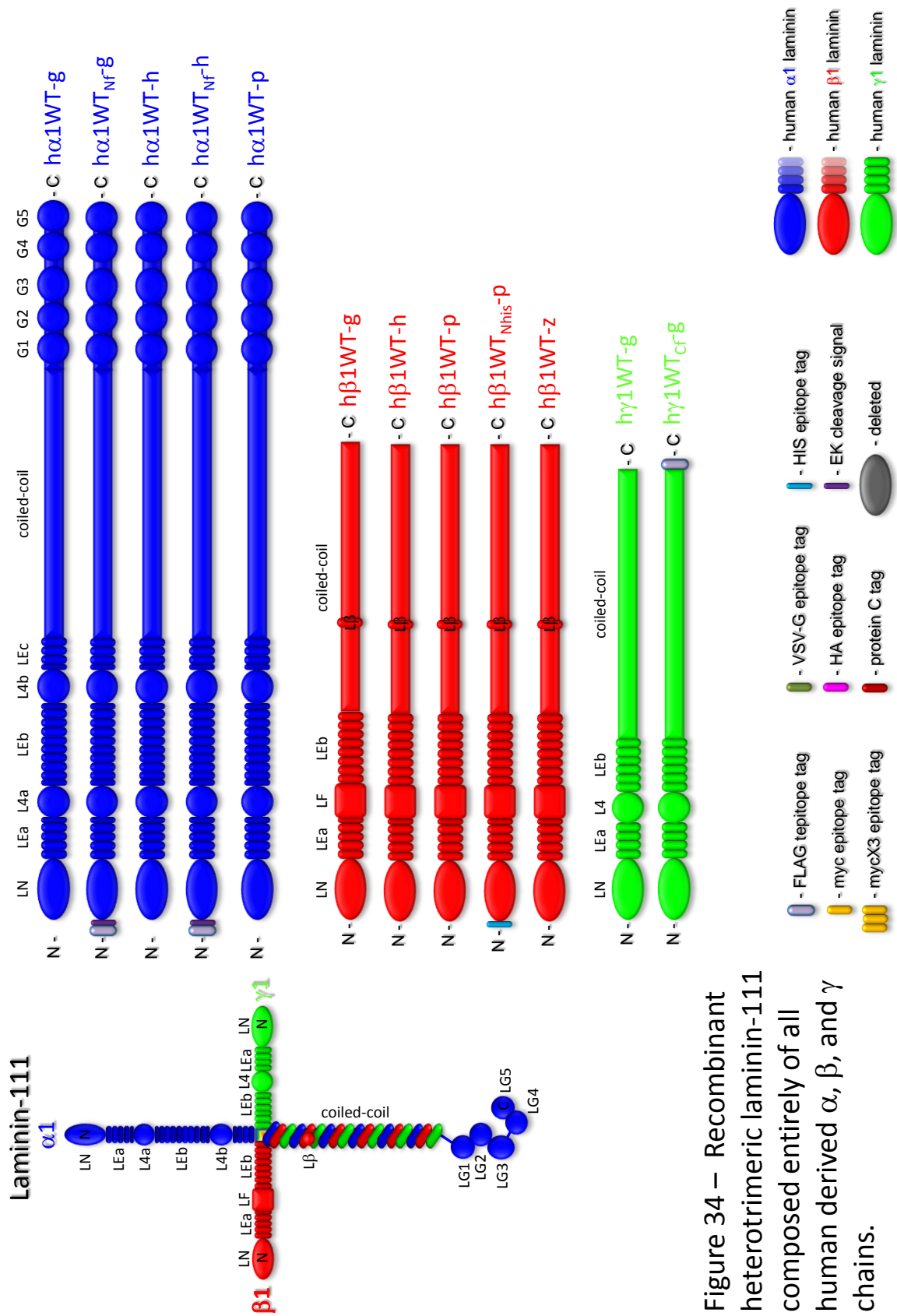


Figure 34 – Recombinant heterotrimeric laminin-111 composed entirely of all human derived α , β , and γ chains.

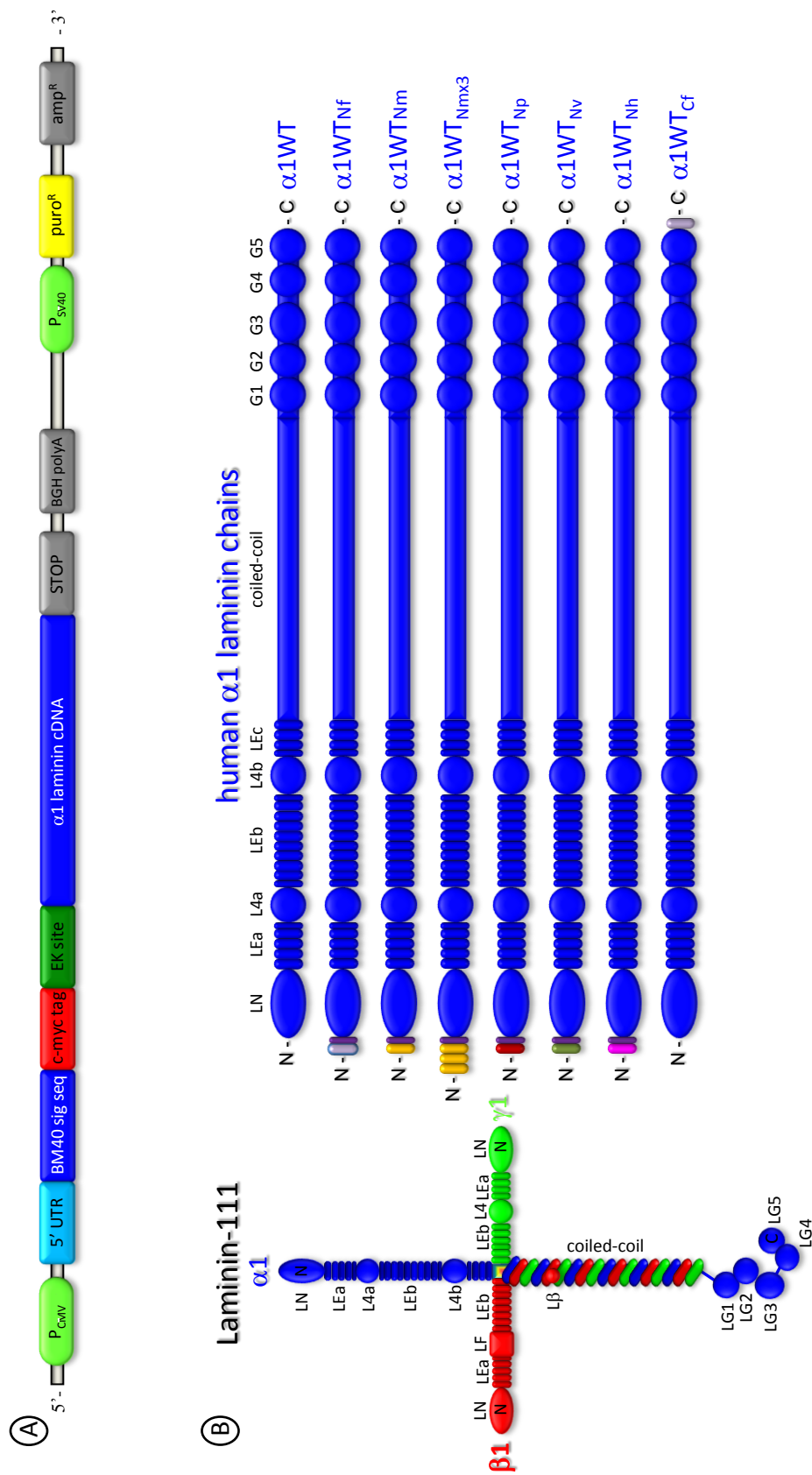
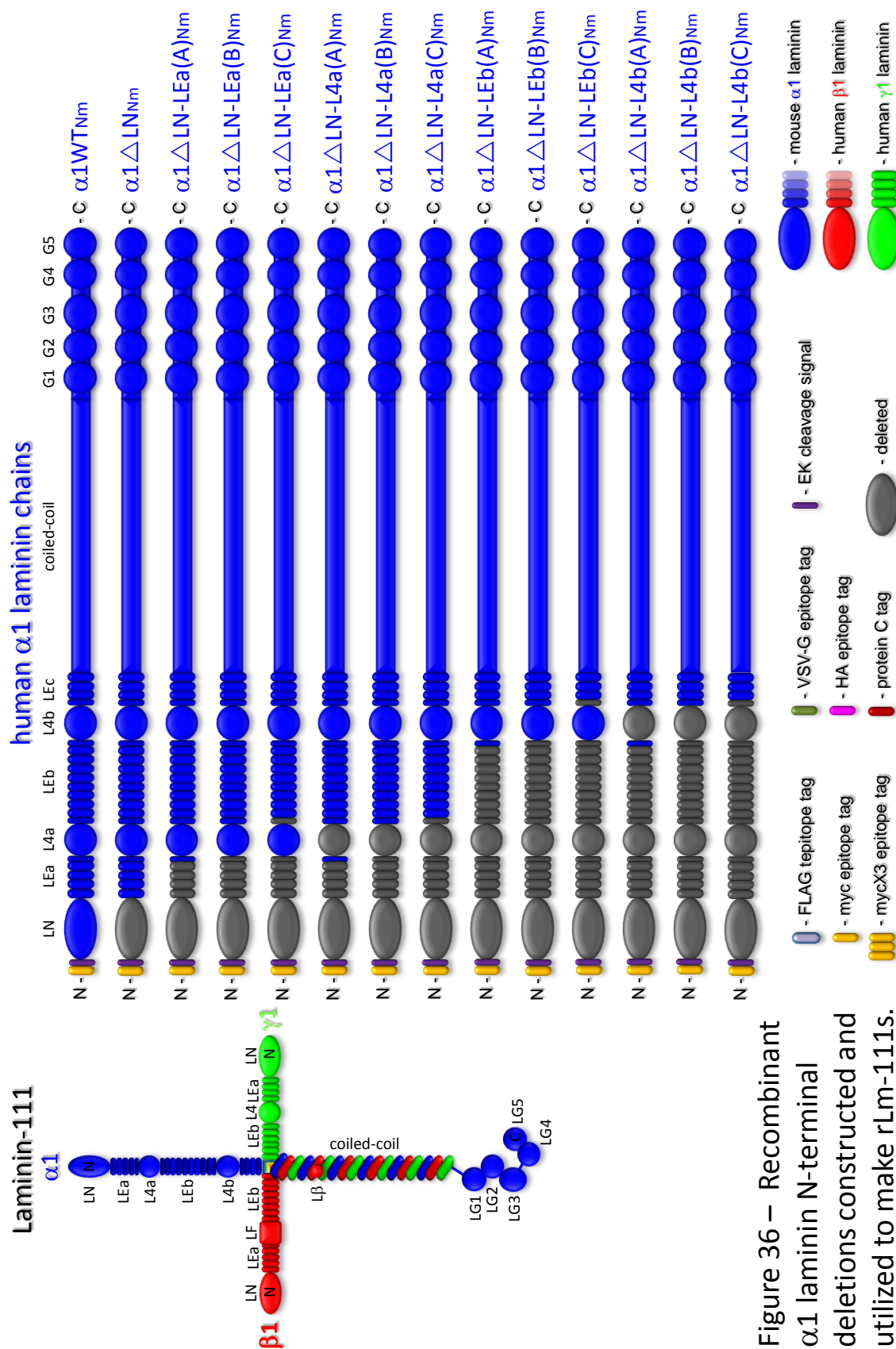


Figure 35 – Recombinant full length α1 laminin chains constructed and utilized to make rLm-111s.



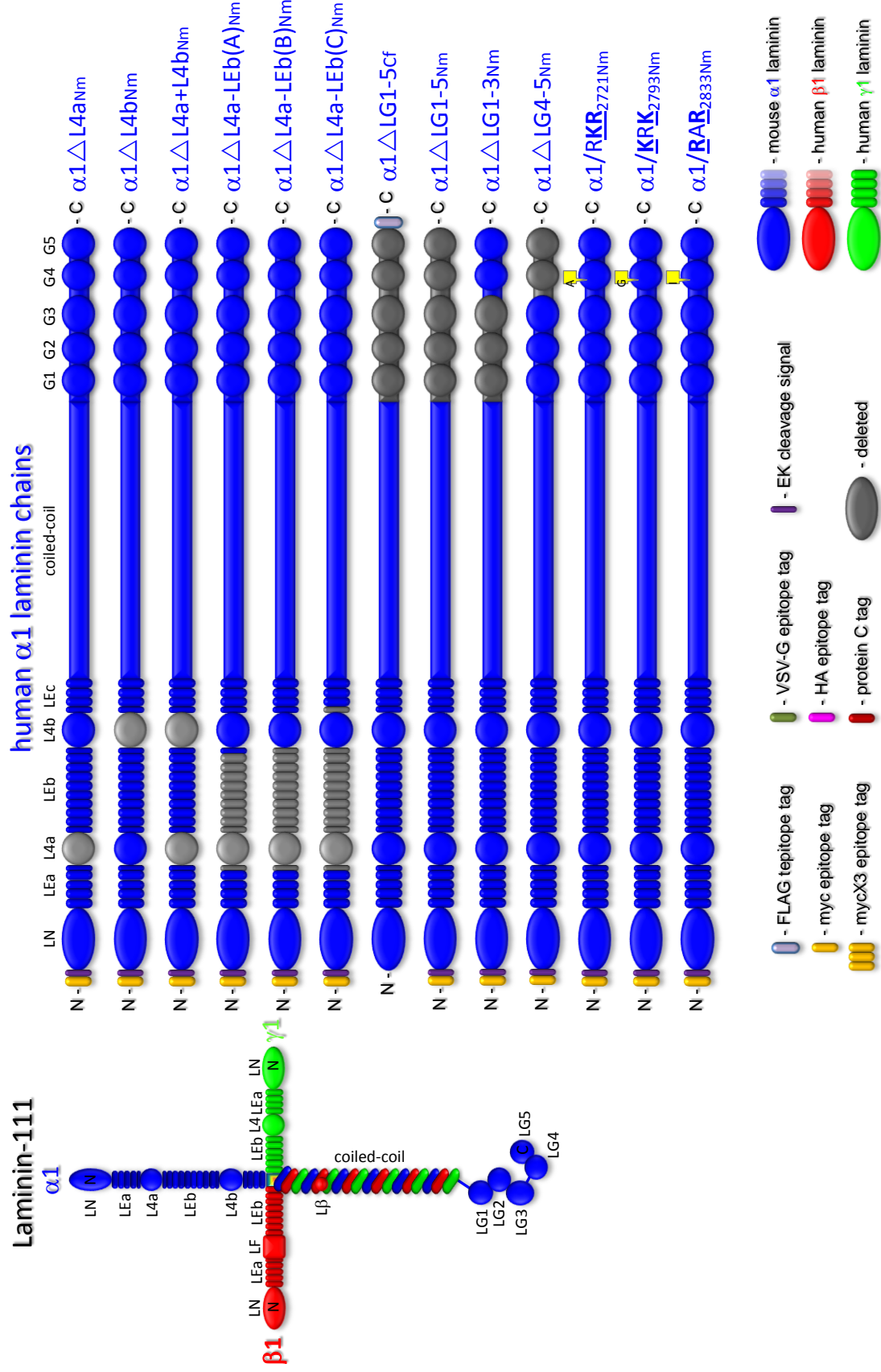


Figure 37 – Recombinant $\alpha 1$ laminin G domain manipulated constructs utilized to make rLm-111s.

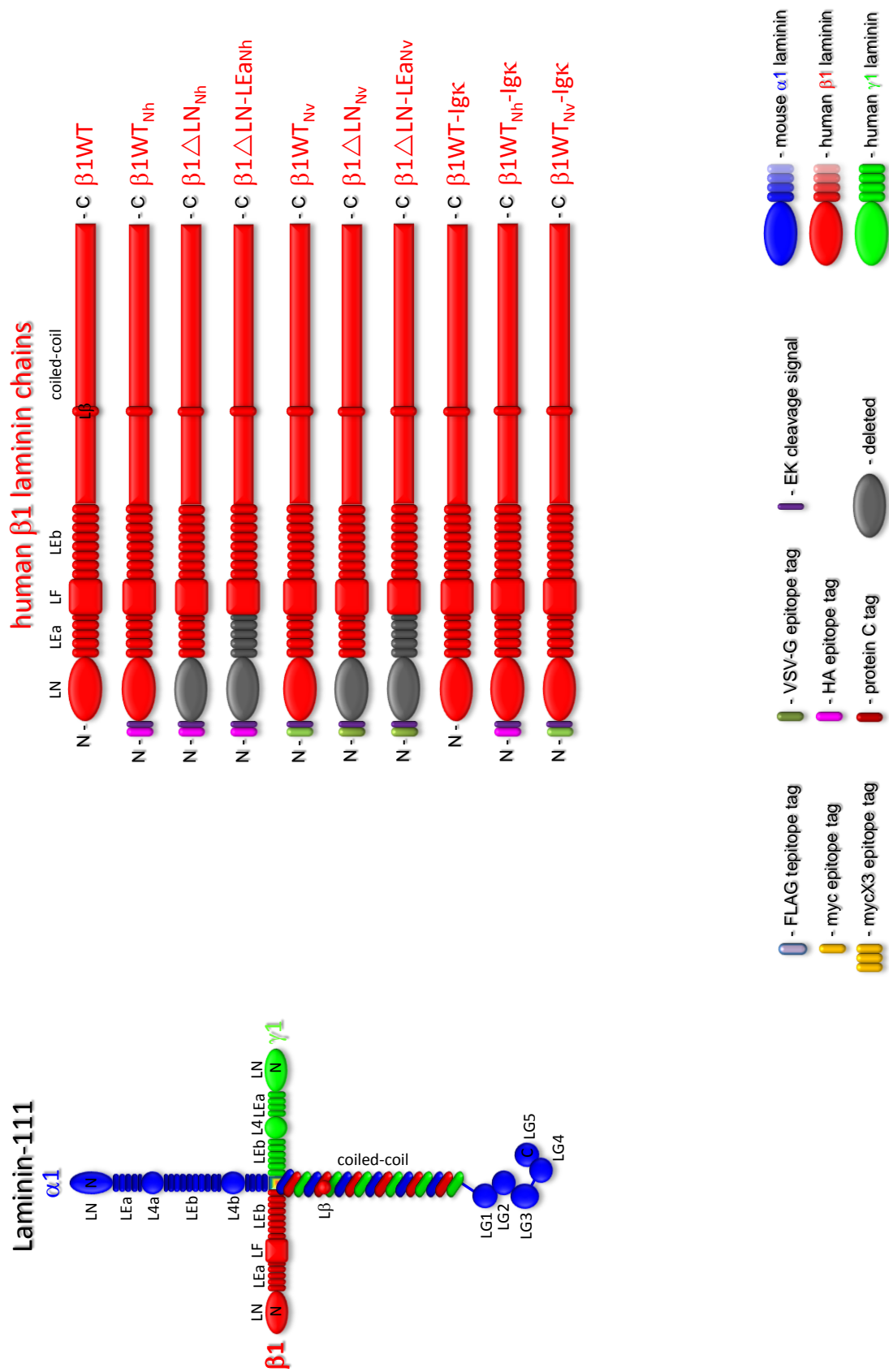


Figure 38 – Recombinant $\beta 1$ laminins constructed and utilized to make rLm-111s.

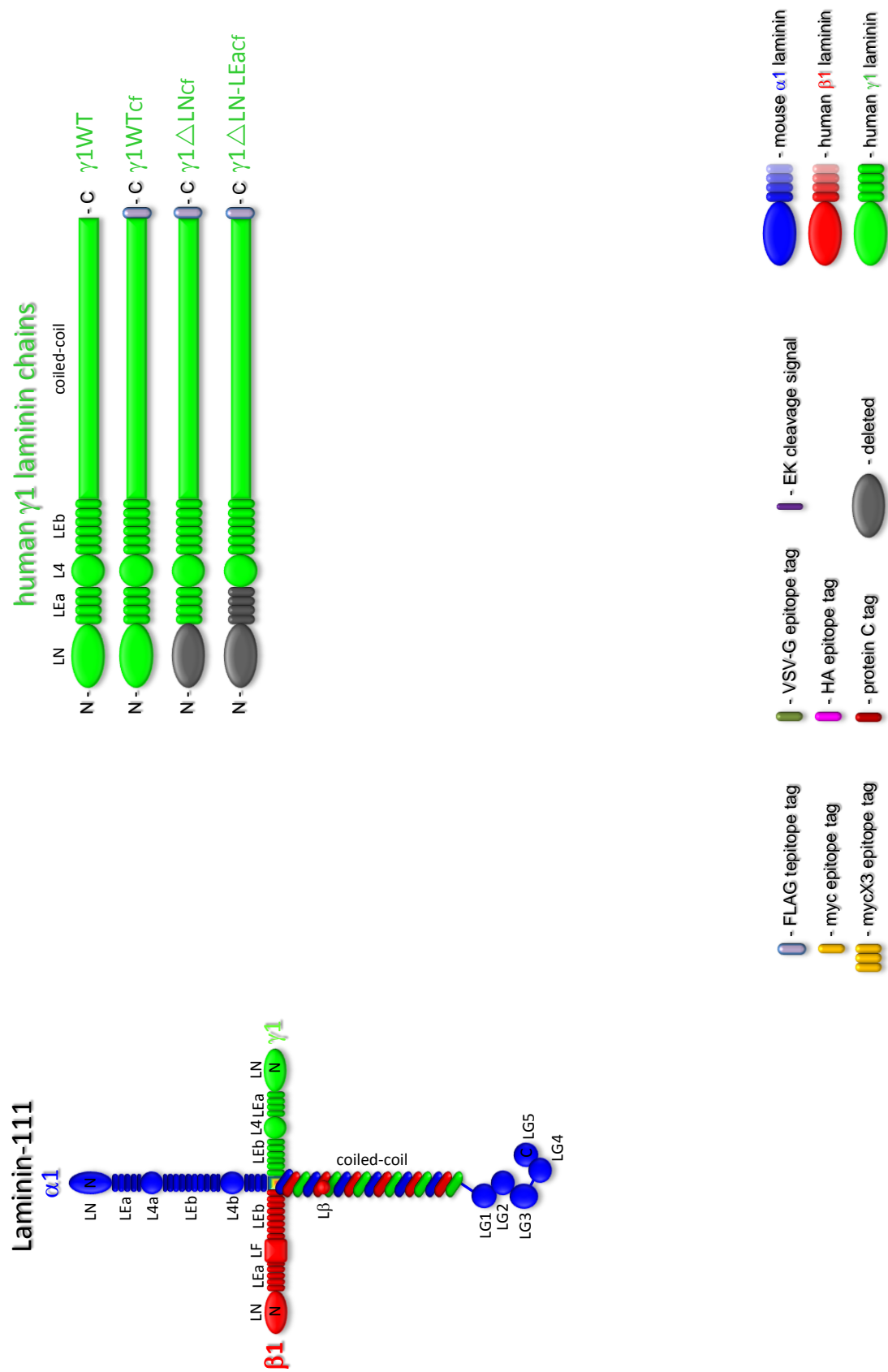


Figure 39 – Recombinant $\gamma 1$ laminin chains constructed and utilized to make rLm-111s.

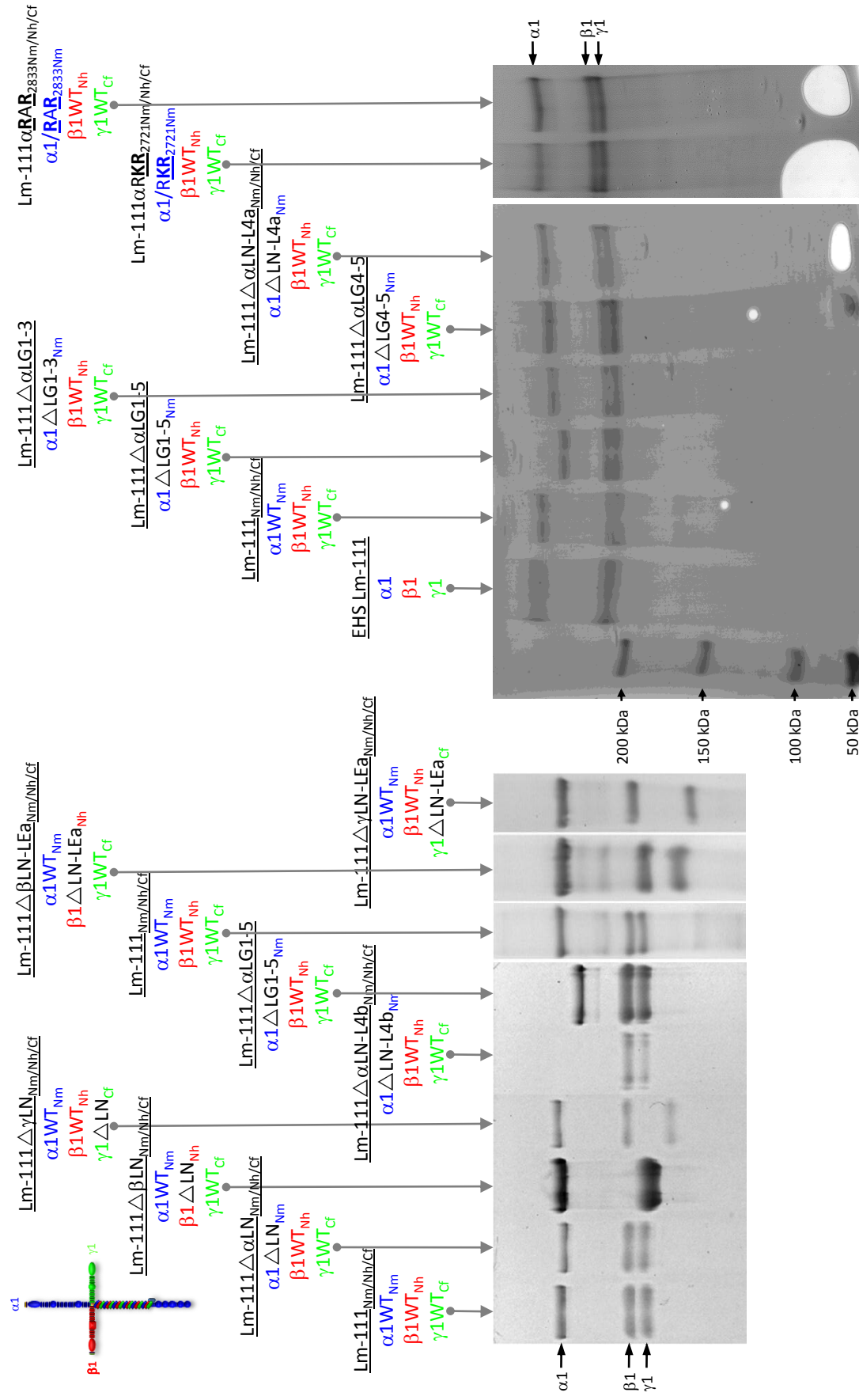
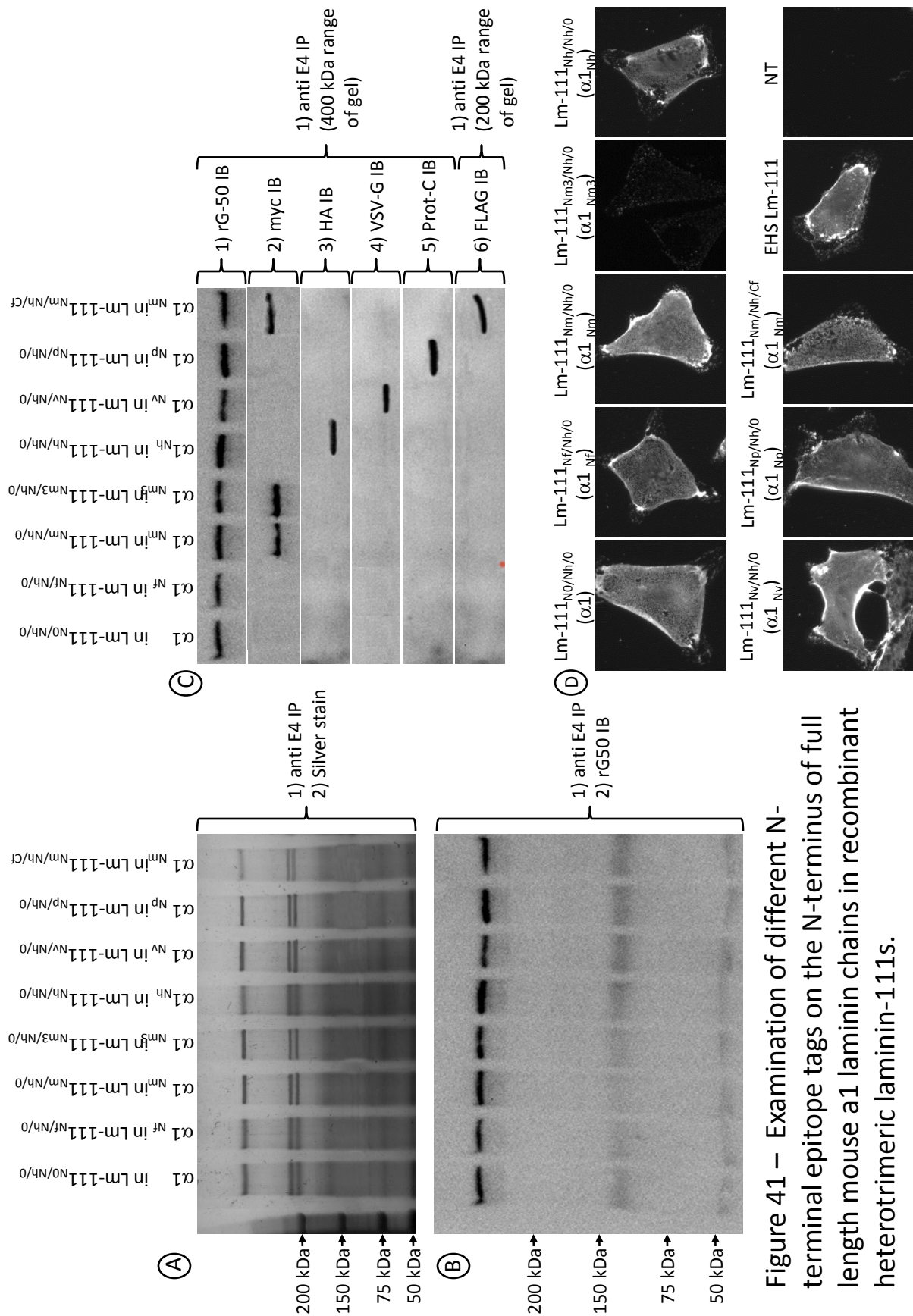


Figure 40 – Coomassie blue stained SDS-PAGE gels of various recombinant heterotrimeric Lm-111s.



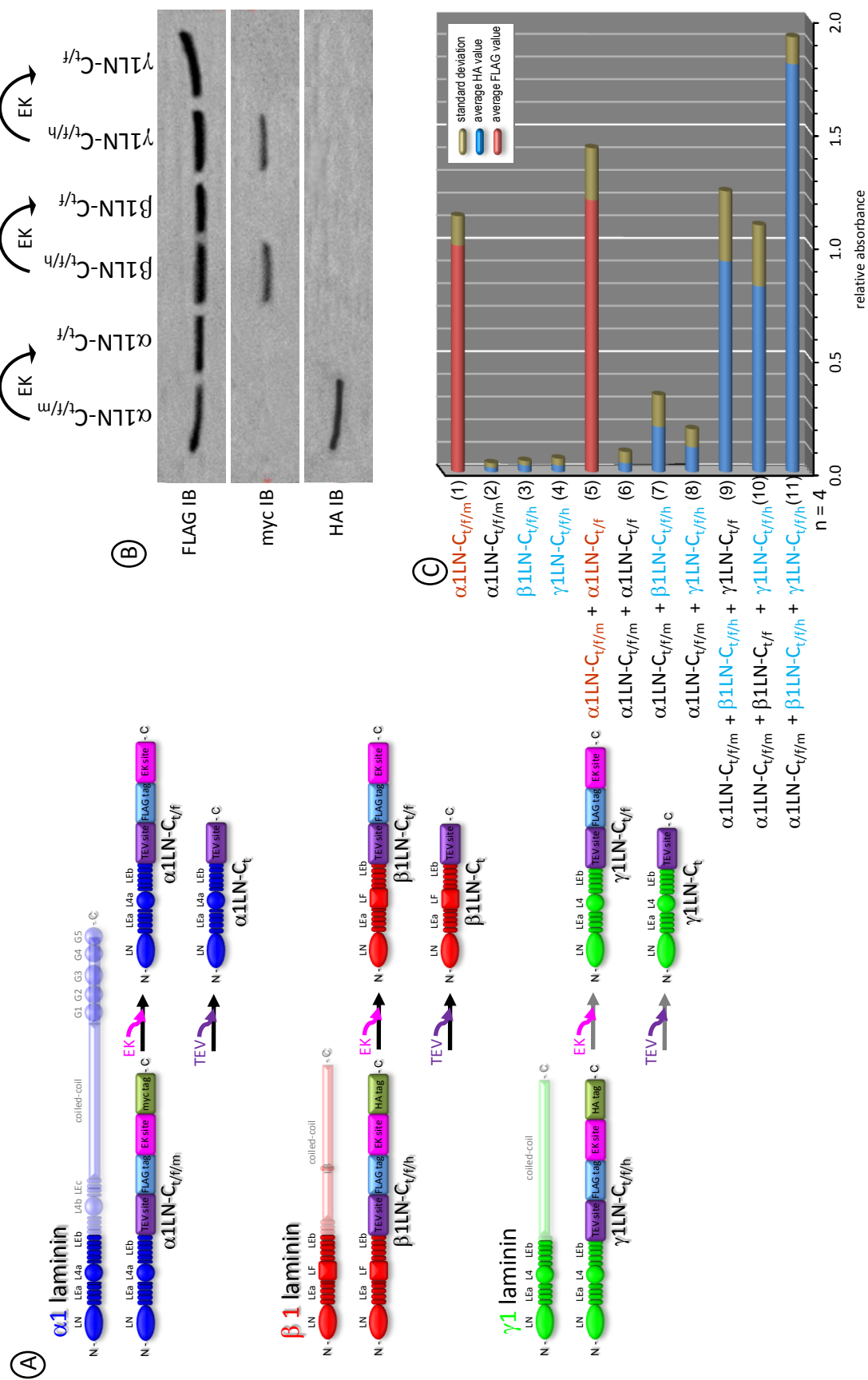


Figure 42 – Accumulation of recombinant LN-LEb constructs in a solid phase association assay.

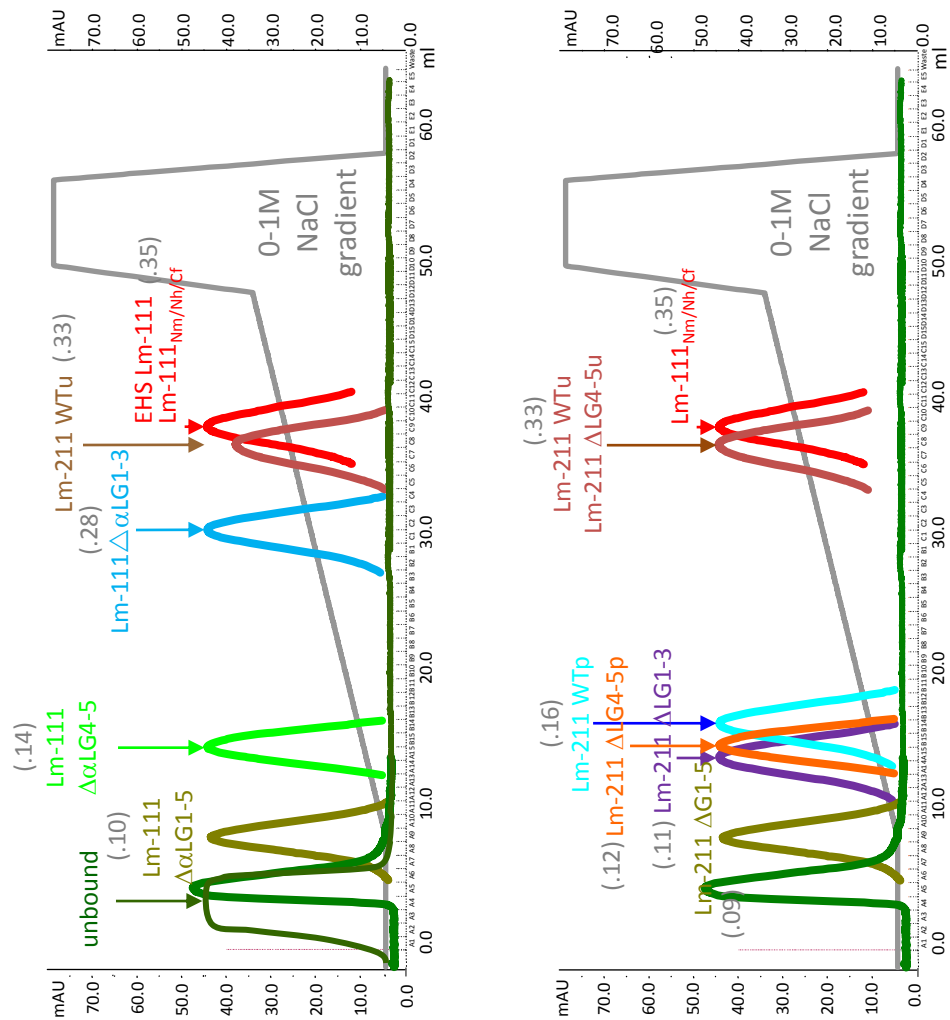
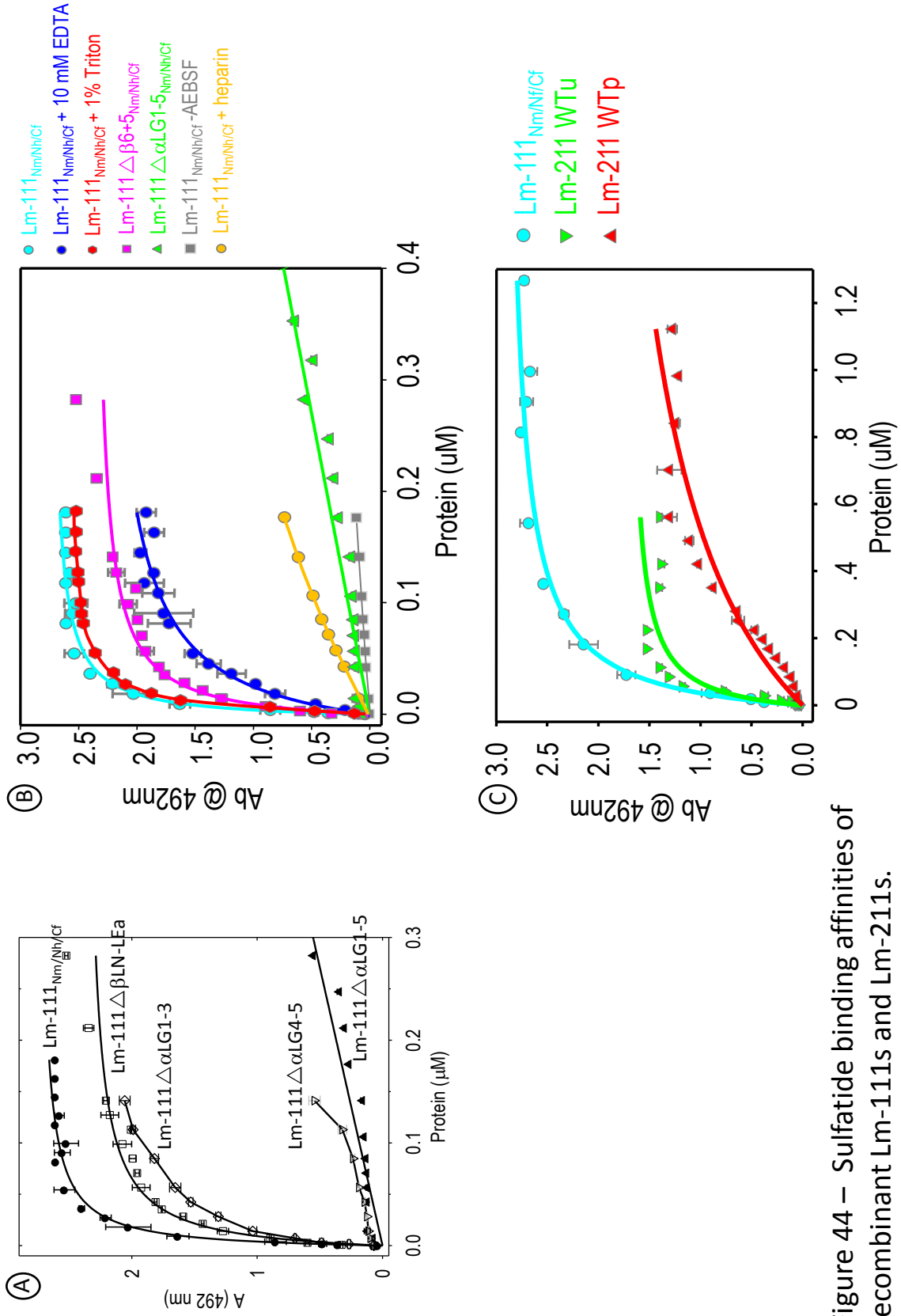


Figure 43 – Heparin binding affinities of recombinant Lm-111s and Lm-211s.



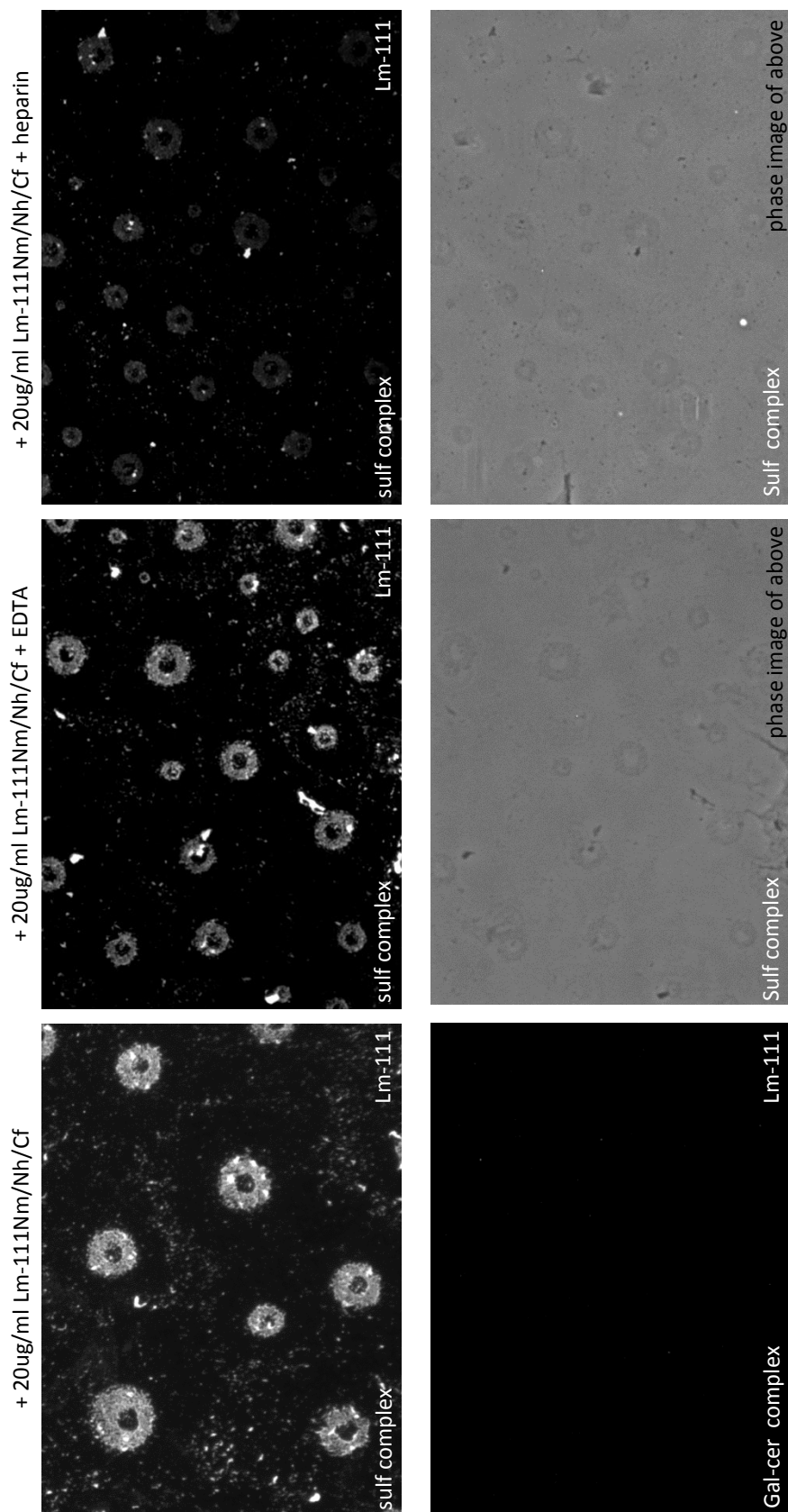


Figure 45 – Laminin-111 binding to sulfatide albumin complexes.

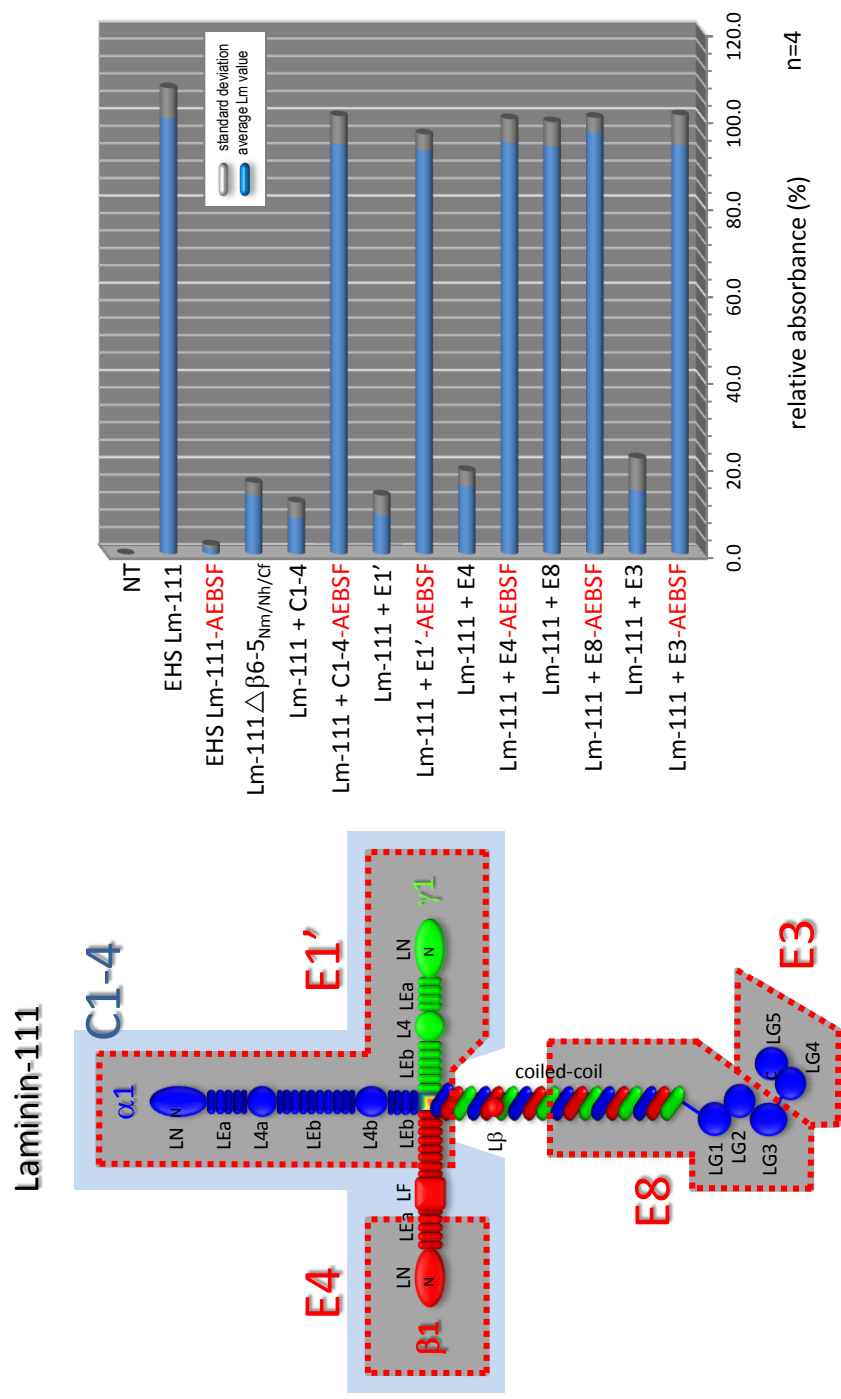


Figure 46 – Inhibition of Lm-111 binding to Schwann cell surfaces.

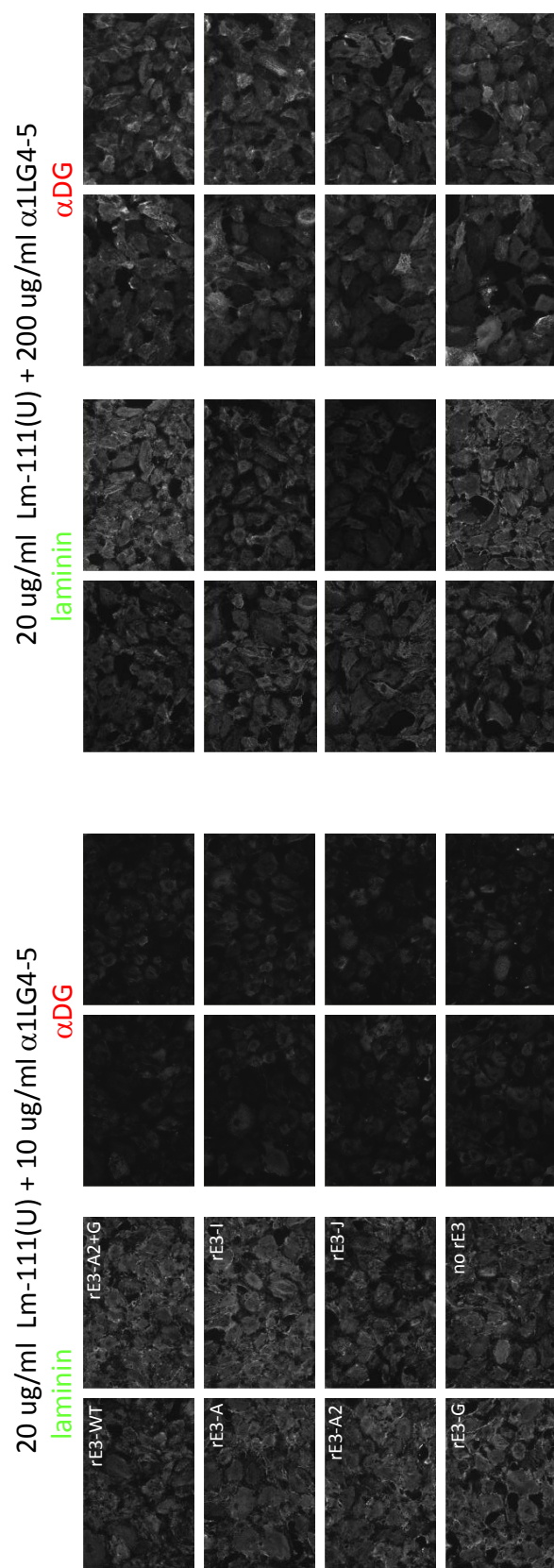
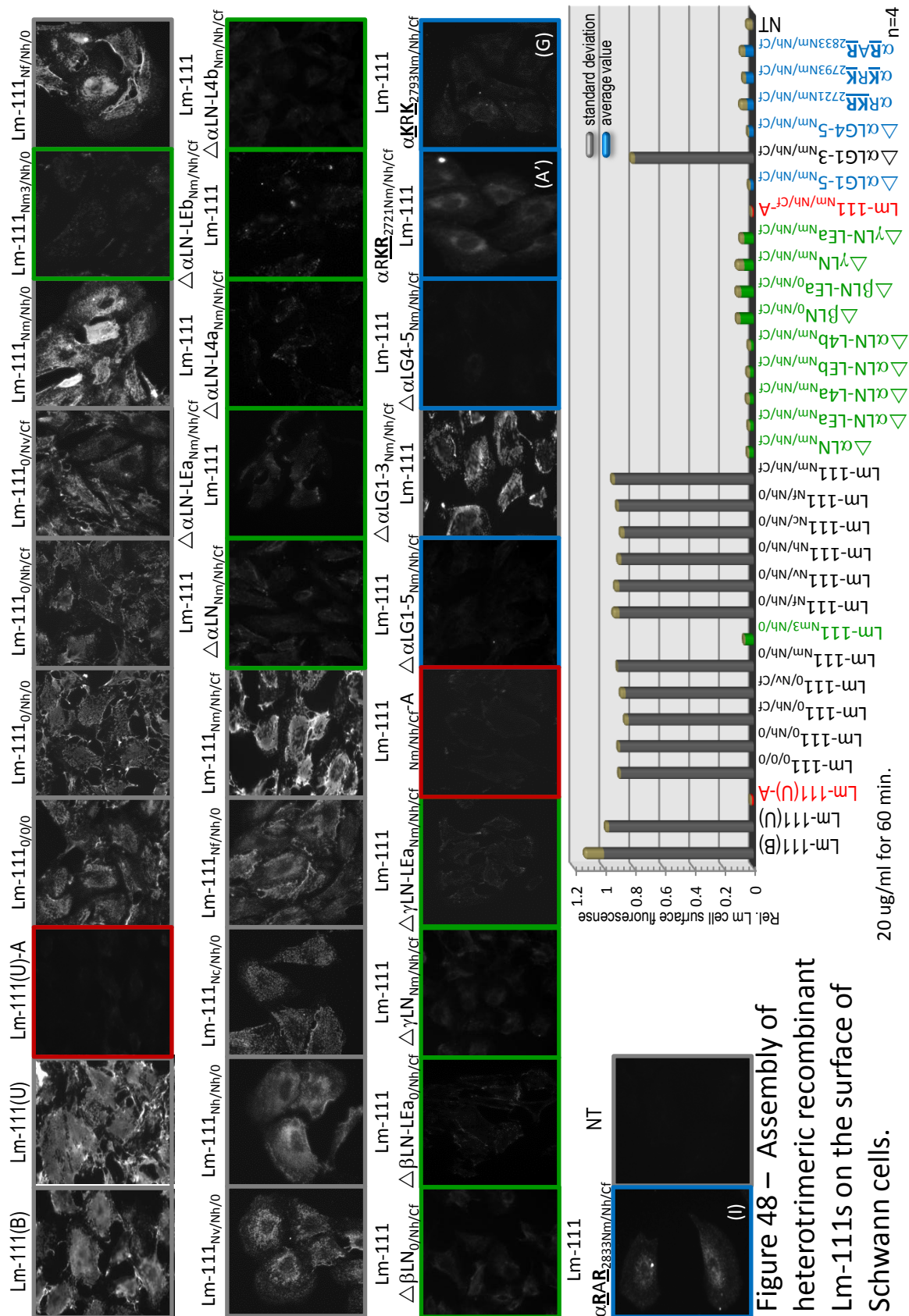


Figure 47 – Inhibition of Lm-111 binding to the cell surface of Schwann cells via contemporary addition of recombinant α 1LG4-5 proteins.



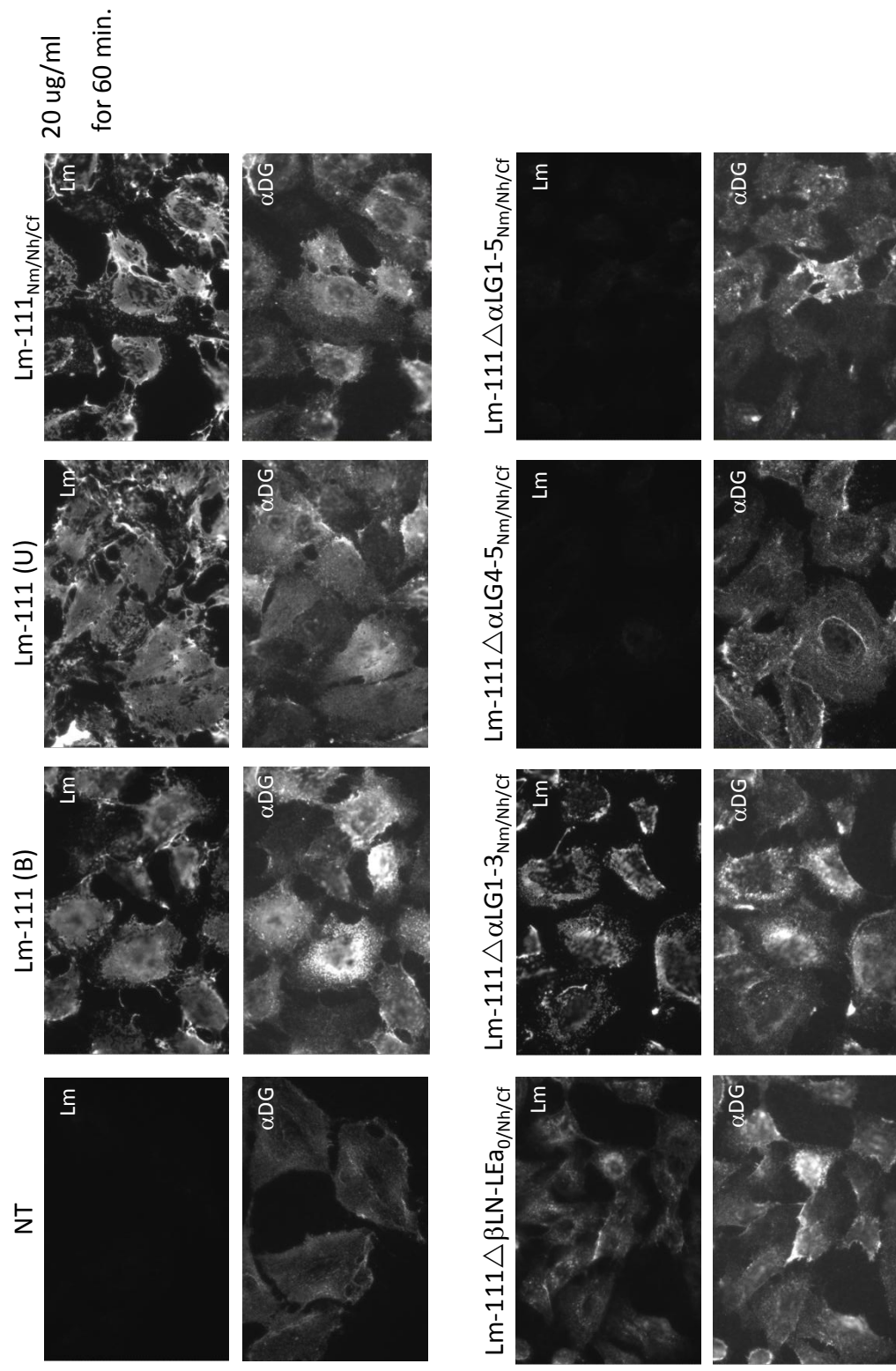
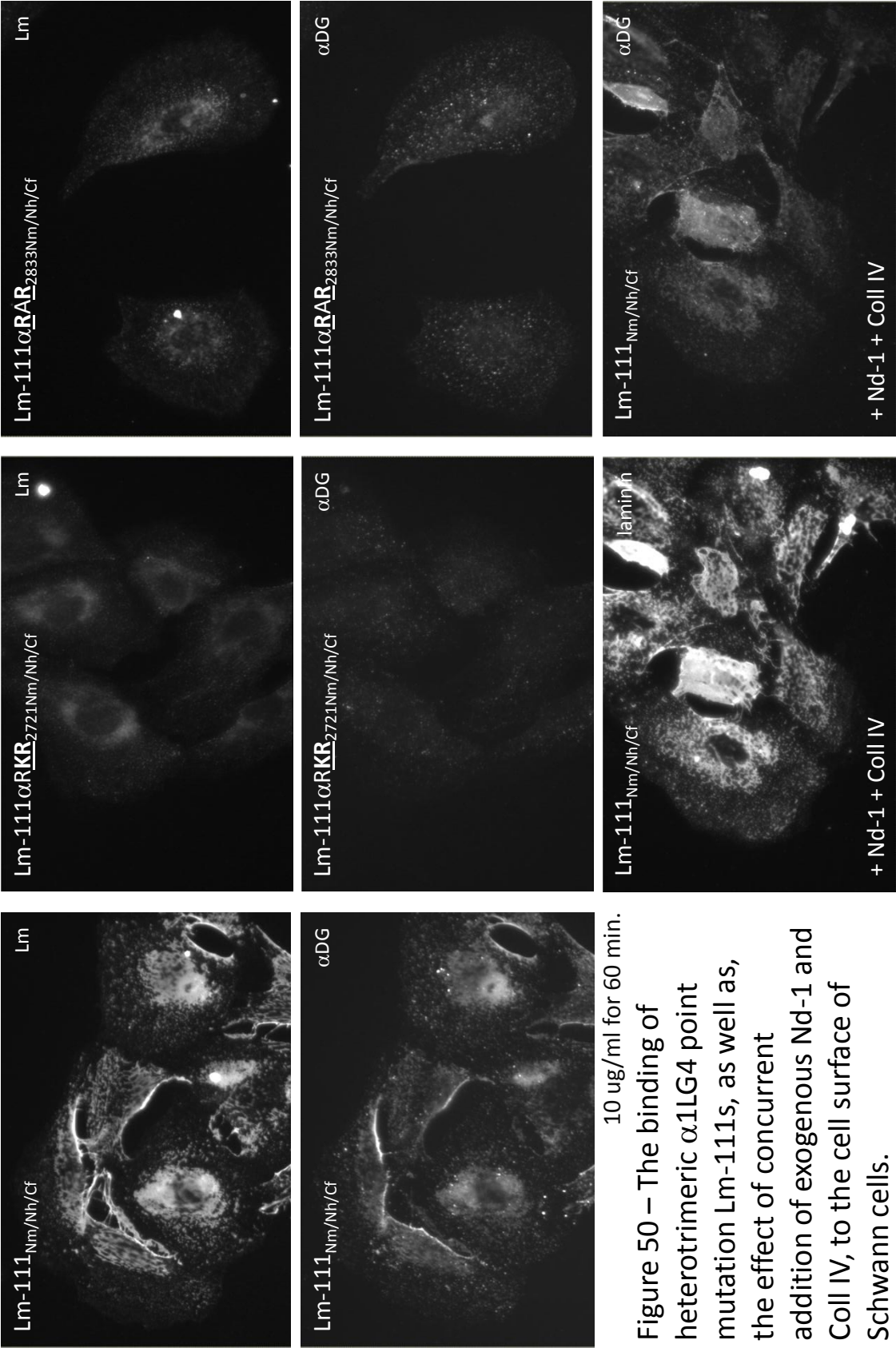


Figure 49 – The binding of recombinant heterotrimeric laminins to the cell surface of Schwann cells.



10 μ g/ml for 60 min.

Figure 50 – The binding of heterotrimeric α 1LG4 point mutation Lm-111s, as well as, the effect of concurrent addition of exogenous Nd-1 and Coll IV, to the cell surface of Schwann cells.



Figure 51 – Electron microscopy images depicting the accumulation of recombinant heterotrimeric Lm-111s and BM formation on the cell surface of Schwann cells (1 of 2).

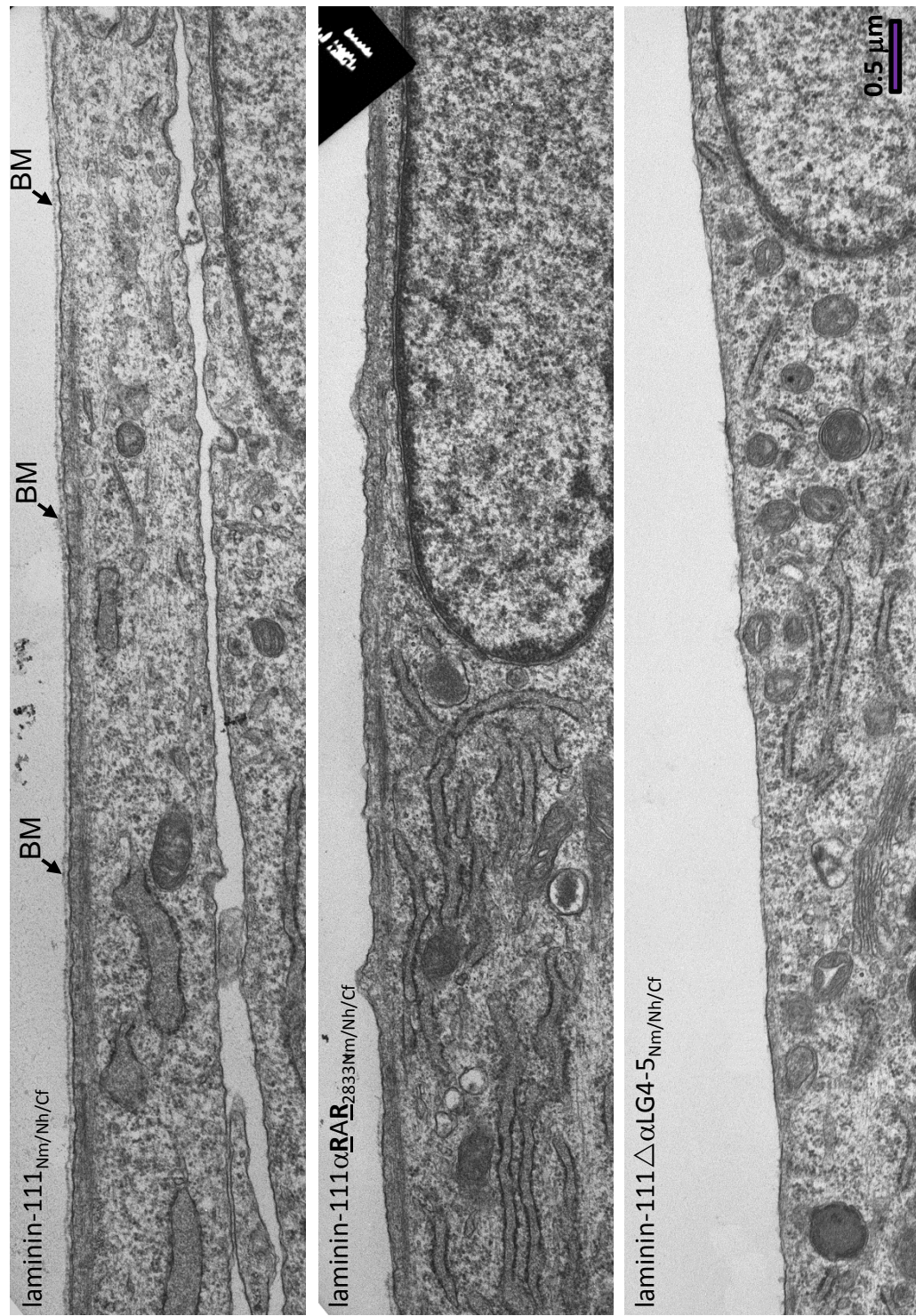


Figure 52 – Electron microscopy images depicting the accumulation of recombinant heterotrimeric Lm-111s and BM formation on the cell surface of Schwann cells (2 of 2).

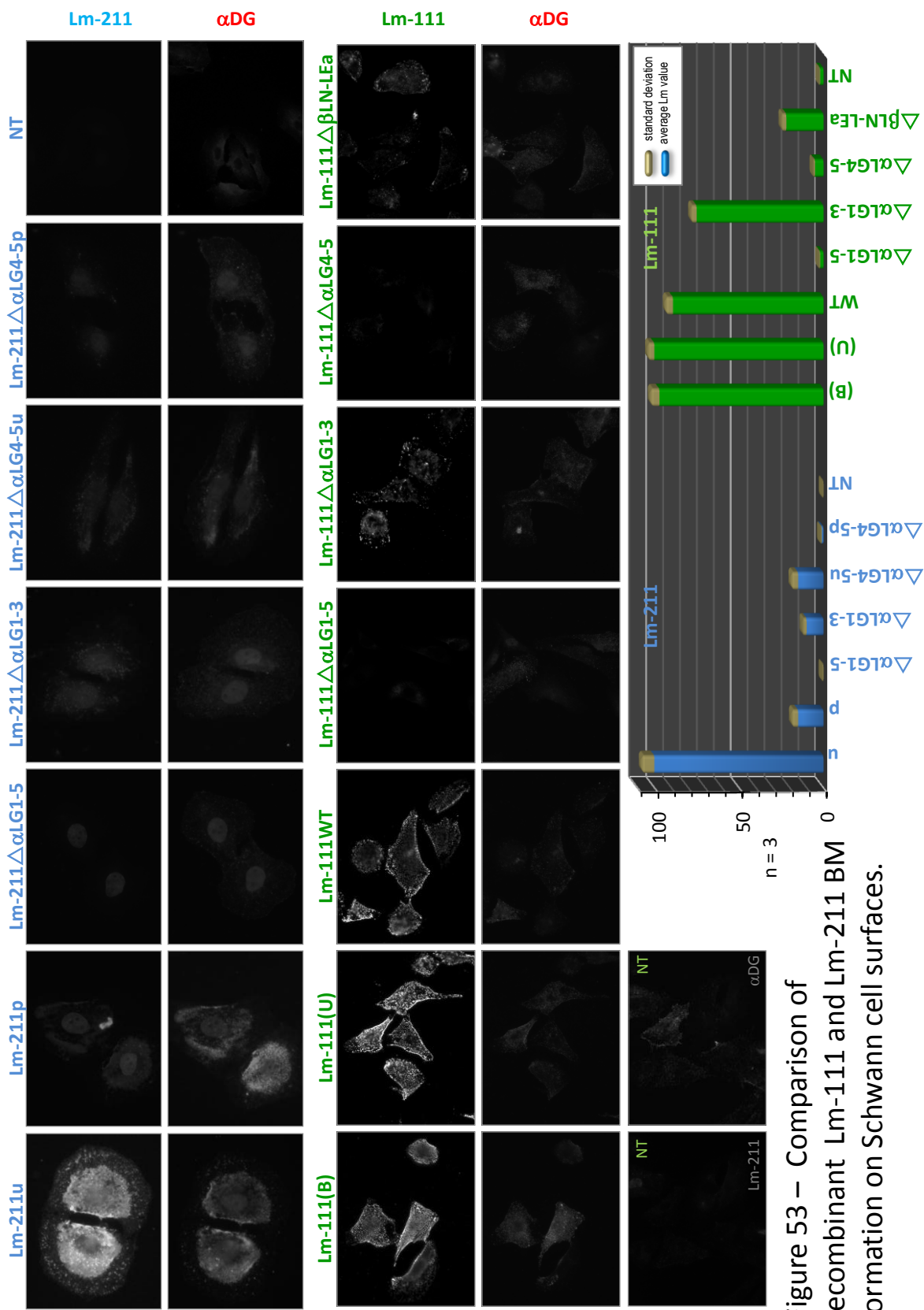


Figure 53 – Comparison of recombinant Lm-111 and Lm-211 BM formation on Schwann cell surfaces.

(A)

EBs	Treatment	BM formation	Epiblast differentiation	Number counted
WT	none	87 +/- 4 %	82 +/- 6 %	153
β1 integrin null	none	0 %	0 %	29
β1 integrin null	+ Lm-111	56 +/- 3 %	24 +/- 7 %	63
γ1 laminin null	none	0 %	0 %	403
EP ¹ laminin null body; BM = basement membrane; WT = wild-type; DG = dystroglycan Data obtained from 3-12 separate experiments for each group			56 +/- 5 %	521

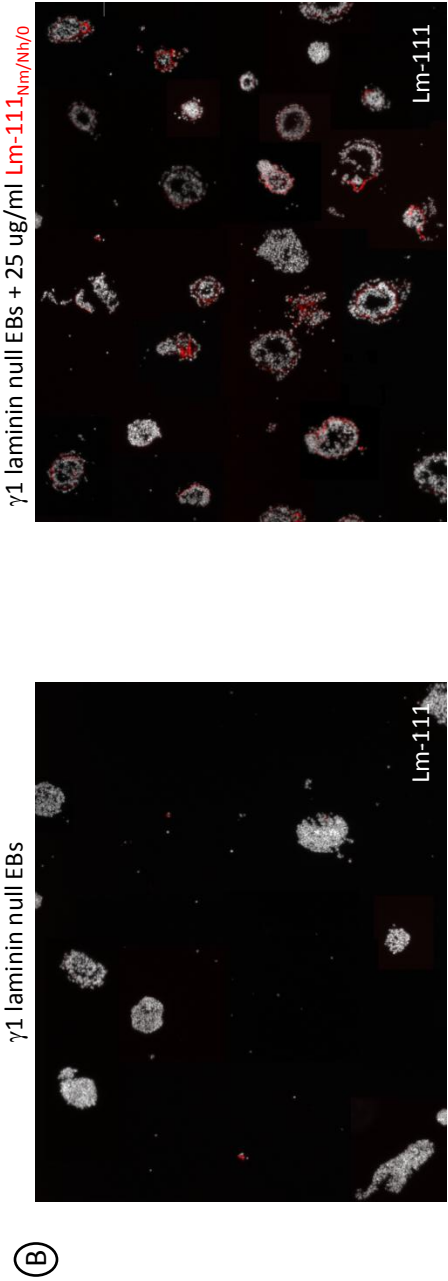


Figure 54 – Basement membrane formation and epiblast differentiation in wild-type, β1 integrin null, γ1 laminin null, and DG null embryoid bodies.

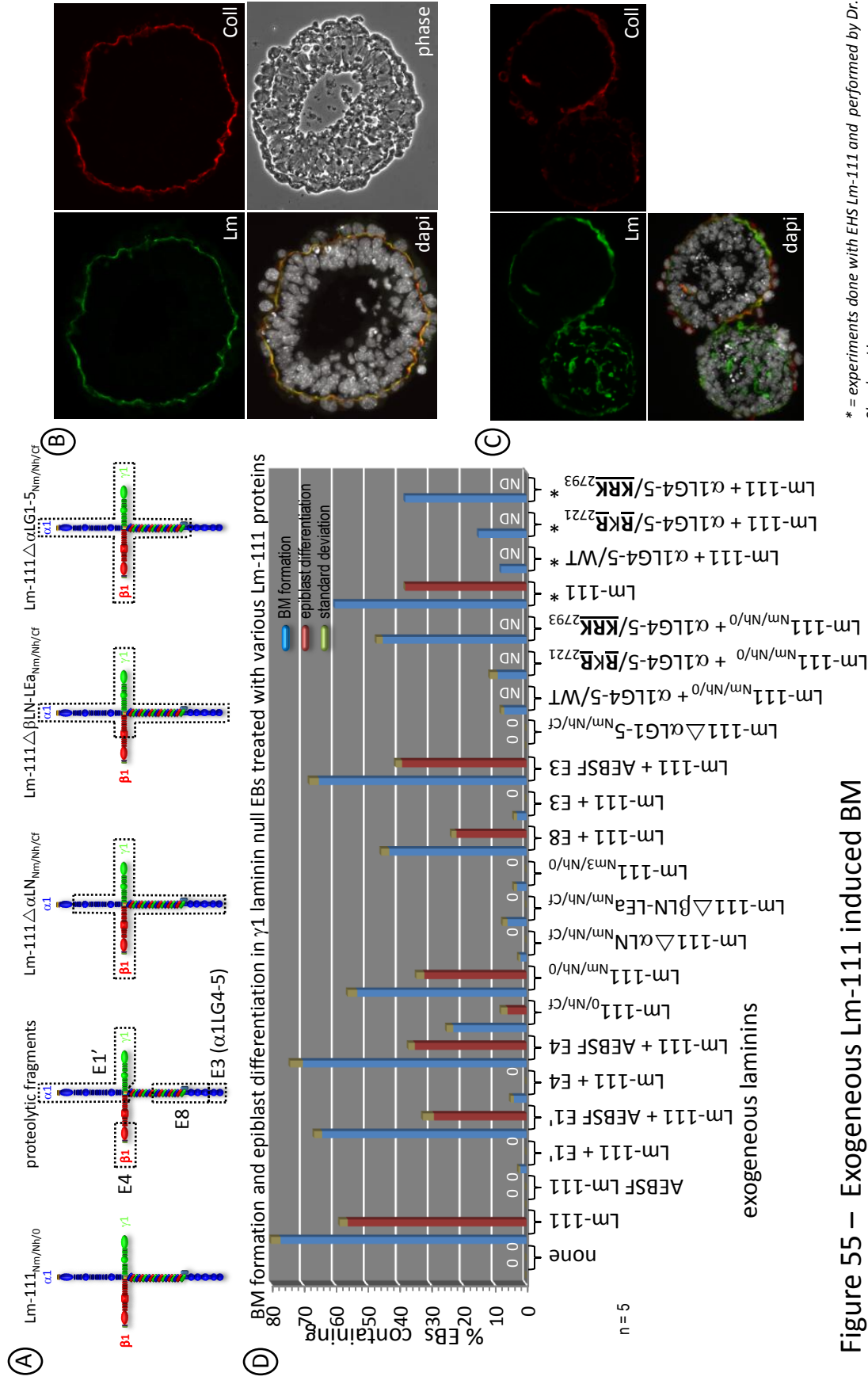


Figure 55 – Exogeneous Lm-111 induced BM formation and epiblast differentiation in $\gamma 1$ laminin null EBs.

* = experiments done with EHS Lm-111 and performed by Dr. Shaohua Li.

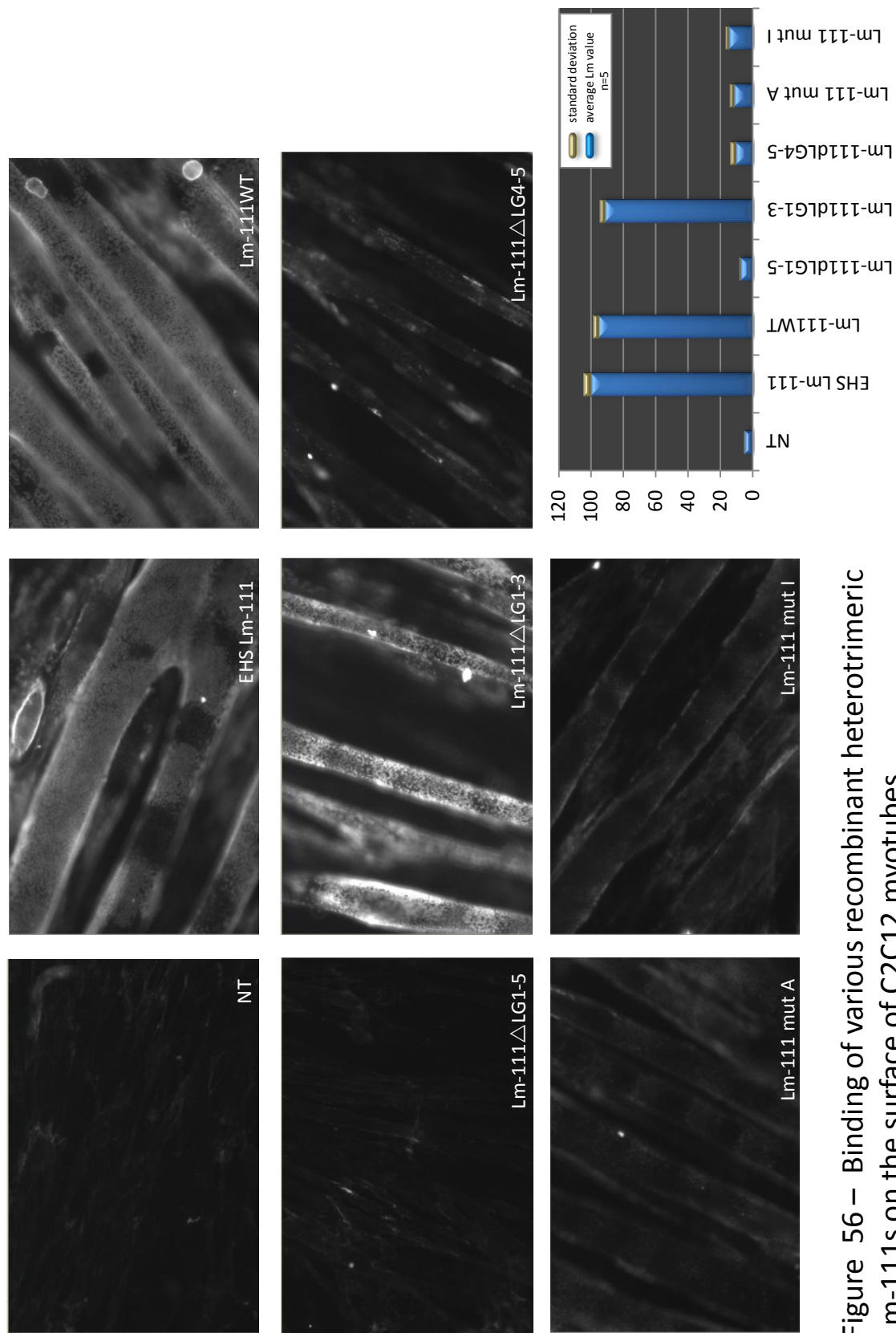


Figure 56 – Binding of various recombinant heterotrimeric Lm-111s on the surface of C2C12 myotubes.

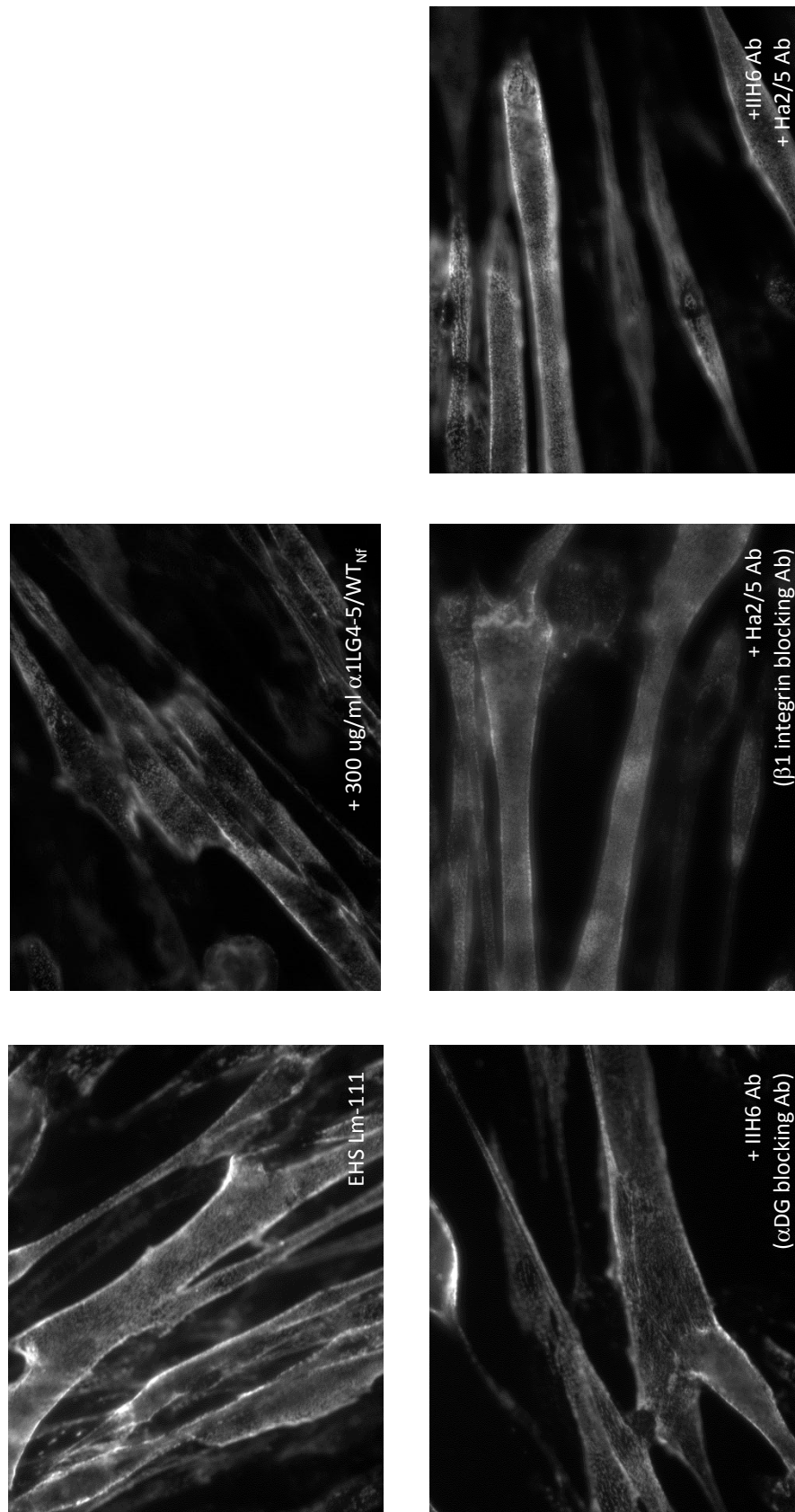


Figure 57 – Inhibition of Lm-111 binding to C2C12 myotube surfaces via laminin receptor blocking antibodies and recombinant α 1LG4-5.

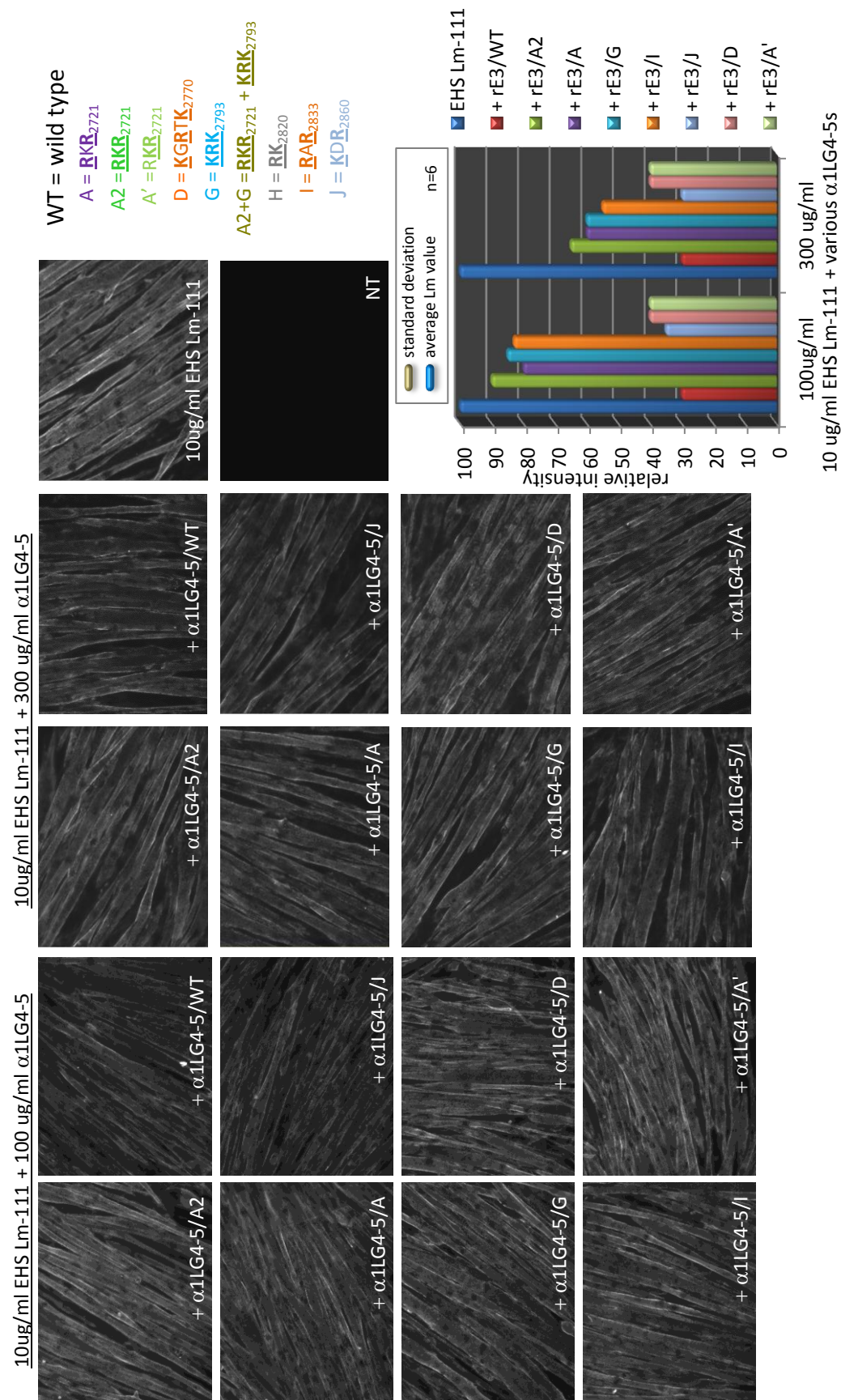


Figure 58 – Inhibition of EHS Lm-111 binding to C2C12 myotubes by various recombinant α 1LG4-5s.

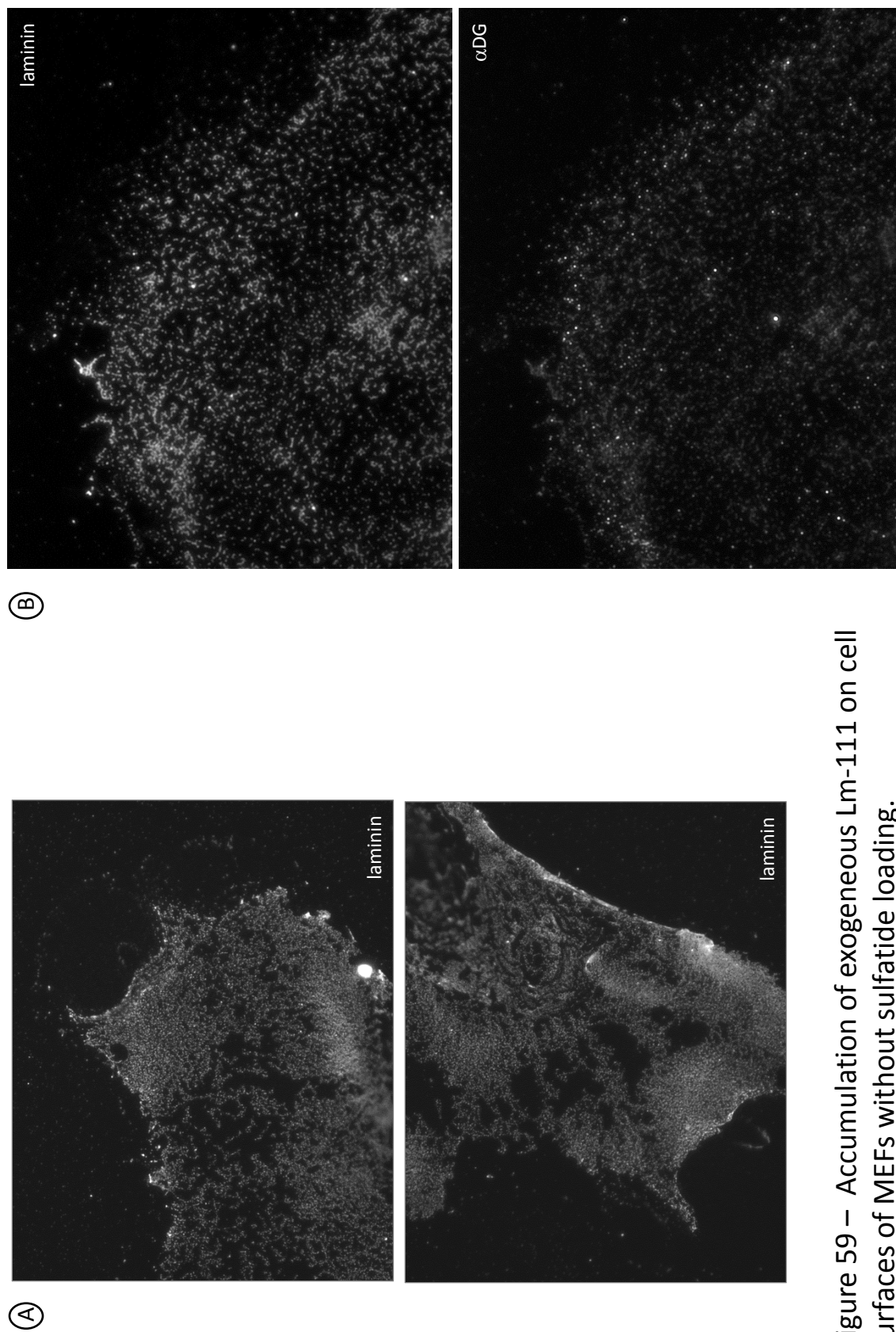


Figure 59 – Accumulation of exogenous Lm-111 on cell surfaces of MEFs without sulfatide loading.

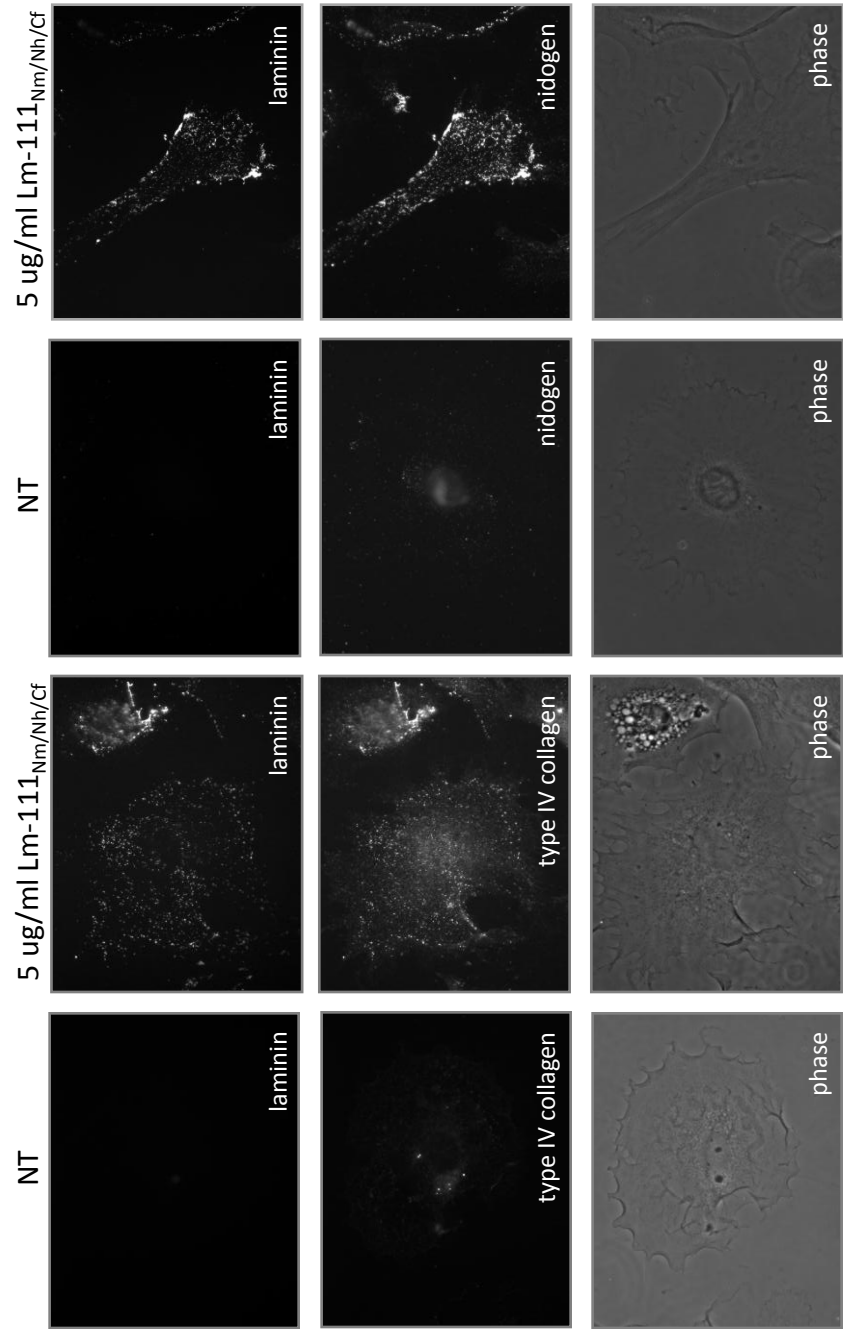


Figure 60 – Accumulation of exogenous Lm-111 and other macromolecules on the surface of MEFs in the absence of sulfatide (1 of 2).

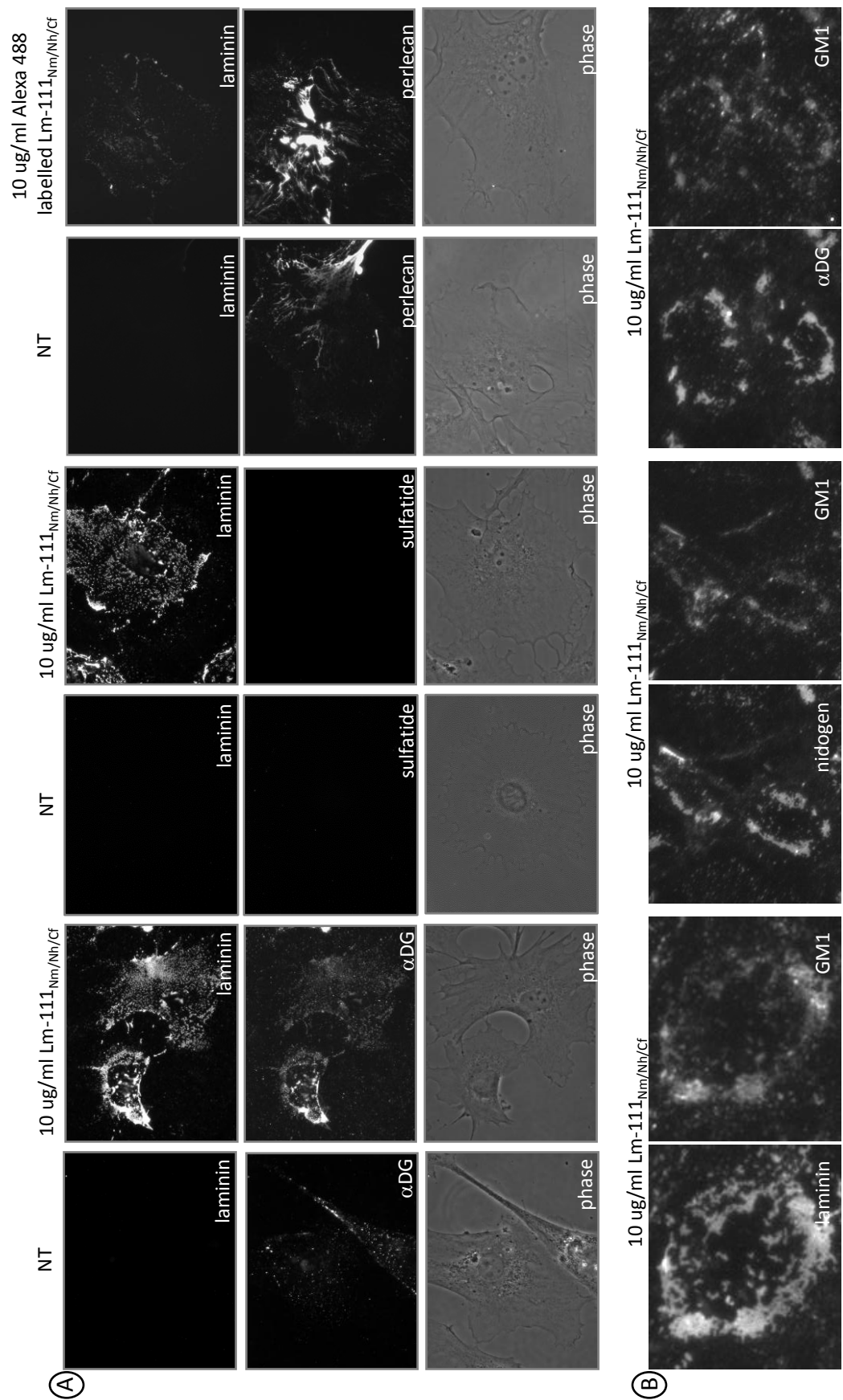


Figure 61 – Accumulation of exogenous Lm-111 and other macromolecules on the surface of MEFs in the absence of sulfatide (2 of 2).

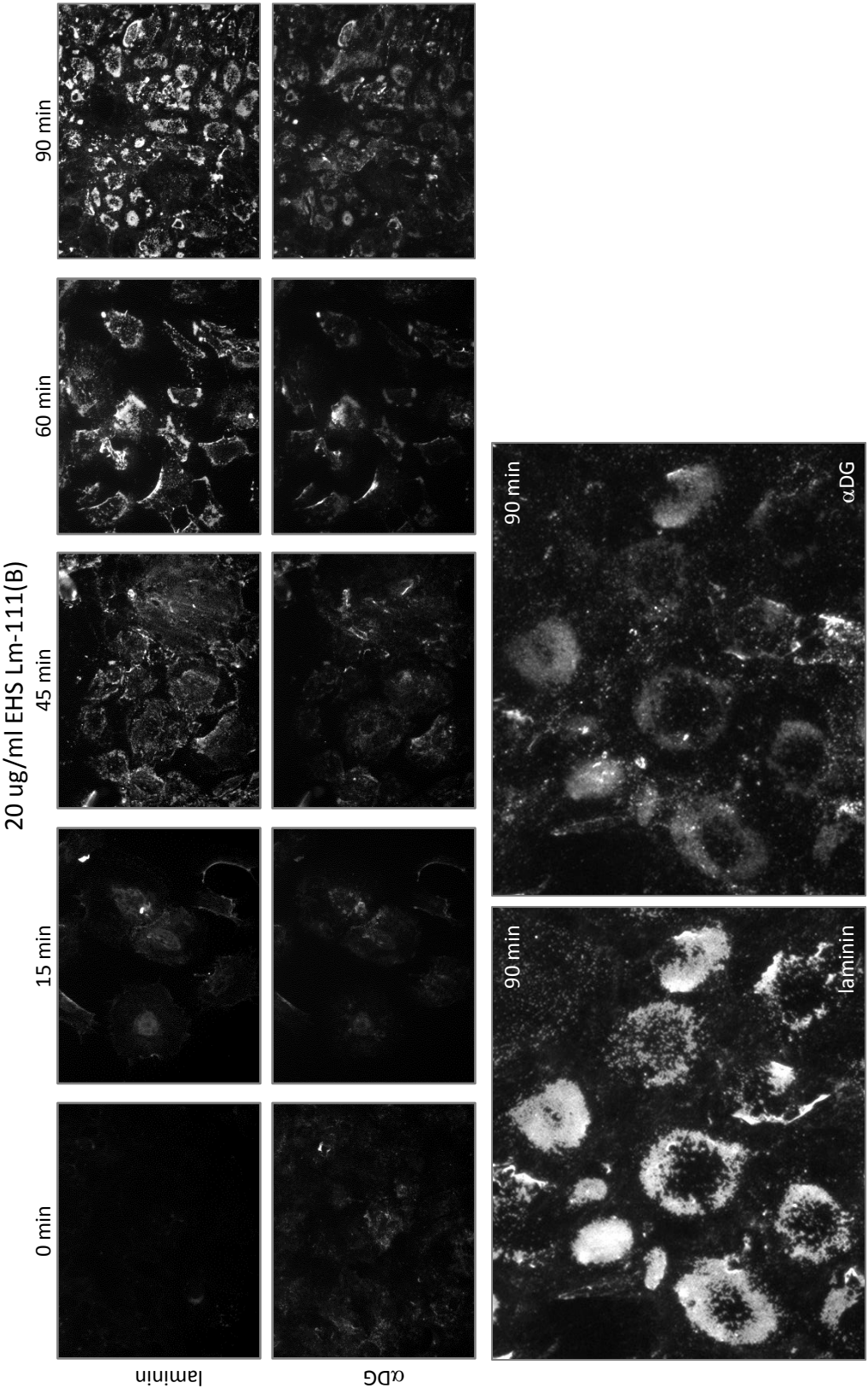


Figure 62 – Accumulation and condensation of exogenous Lm-111 on MEF cell surfaces over time, in the absence of suflatide.

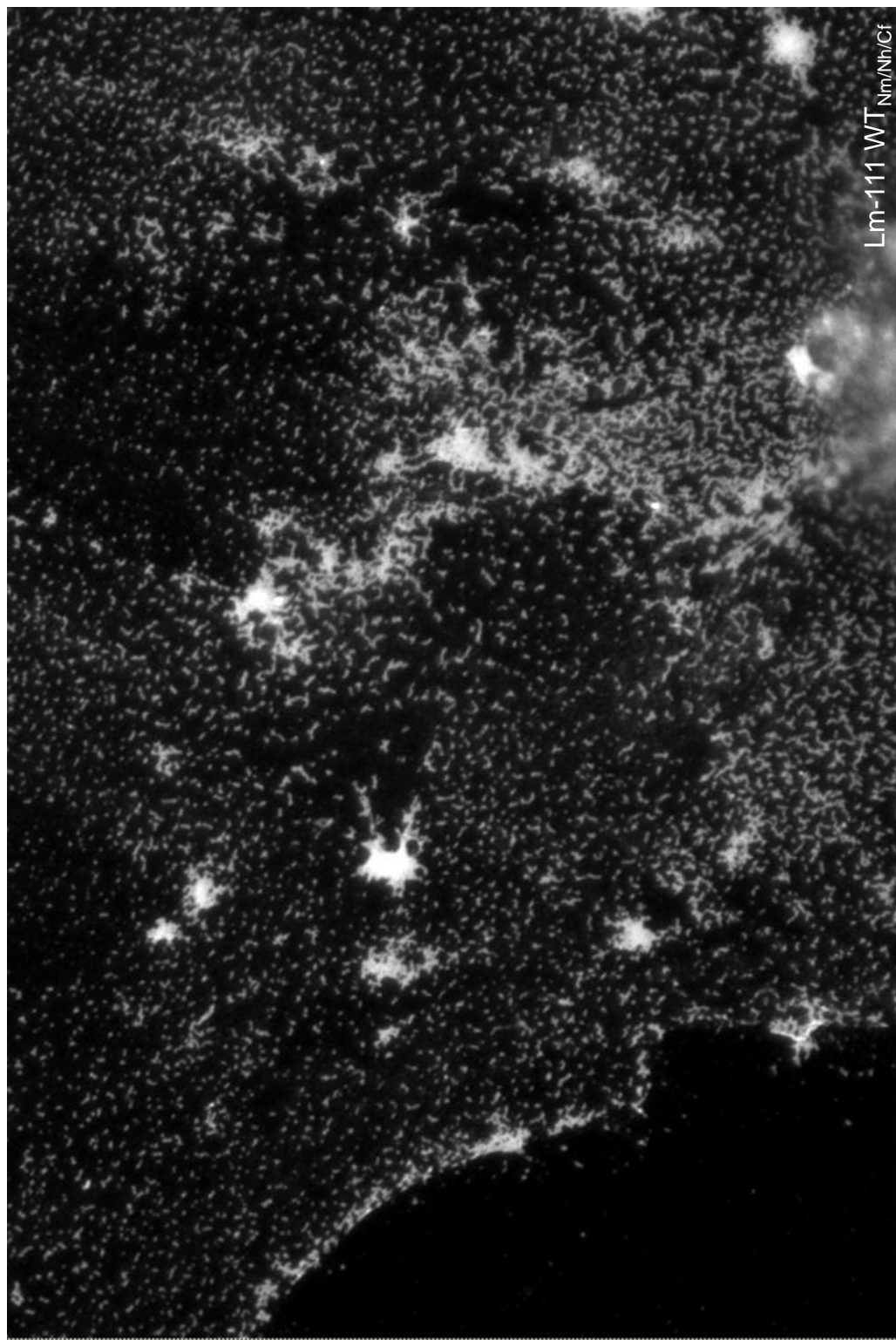


Figure 63 – Inability to form higher order aggregates and a BM on the surface of MEFs without the presence of sulfatide.

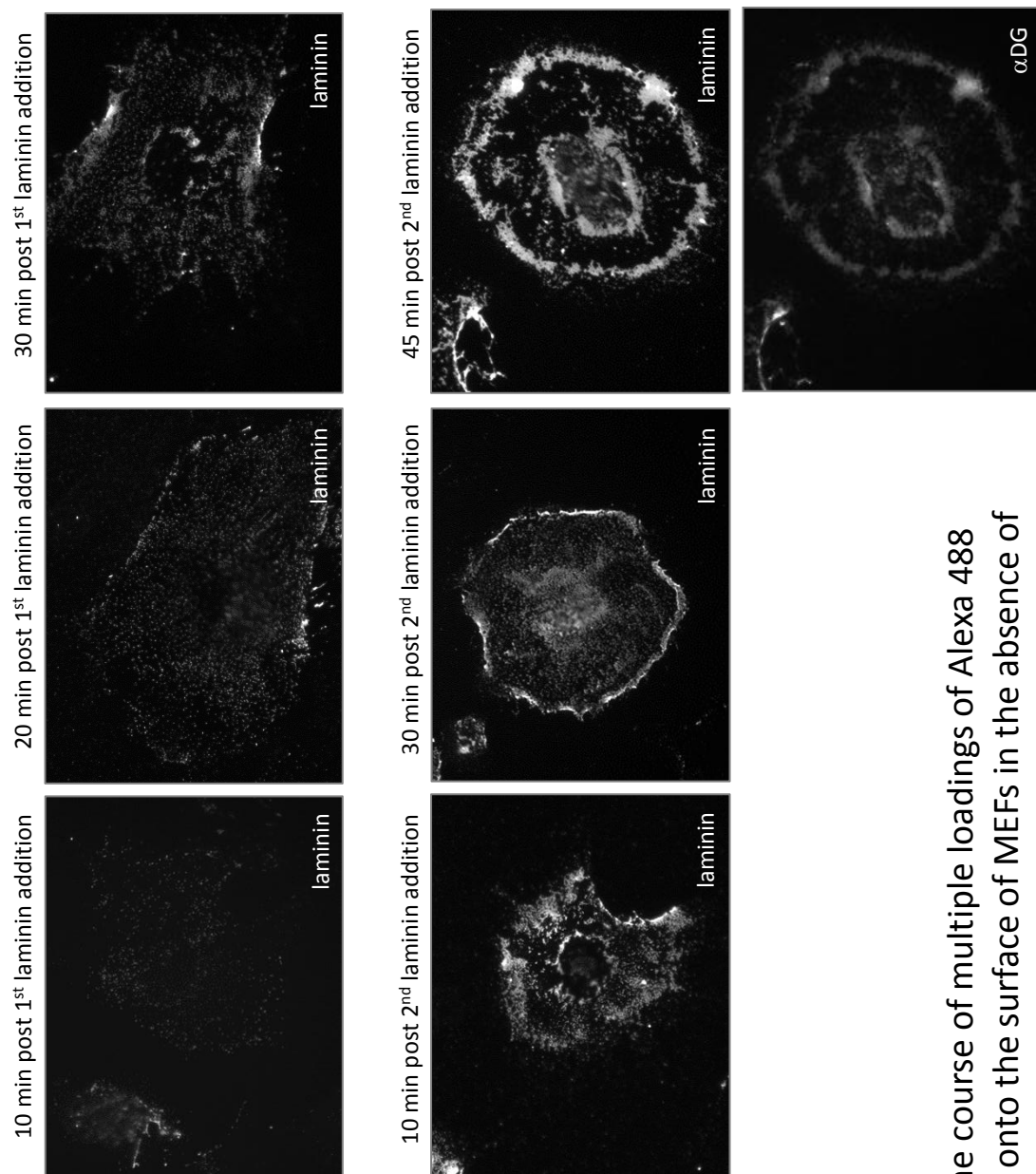


Figure 64 – Time course of multiple loadings of Alexa 488 labeled Lm-111 onto the surface of MEFs in the absence of sulfatide.

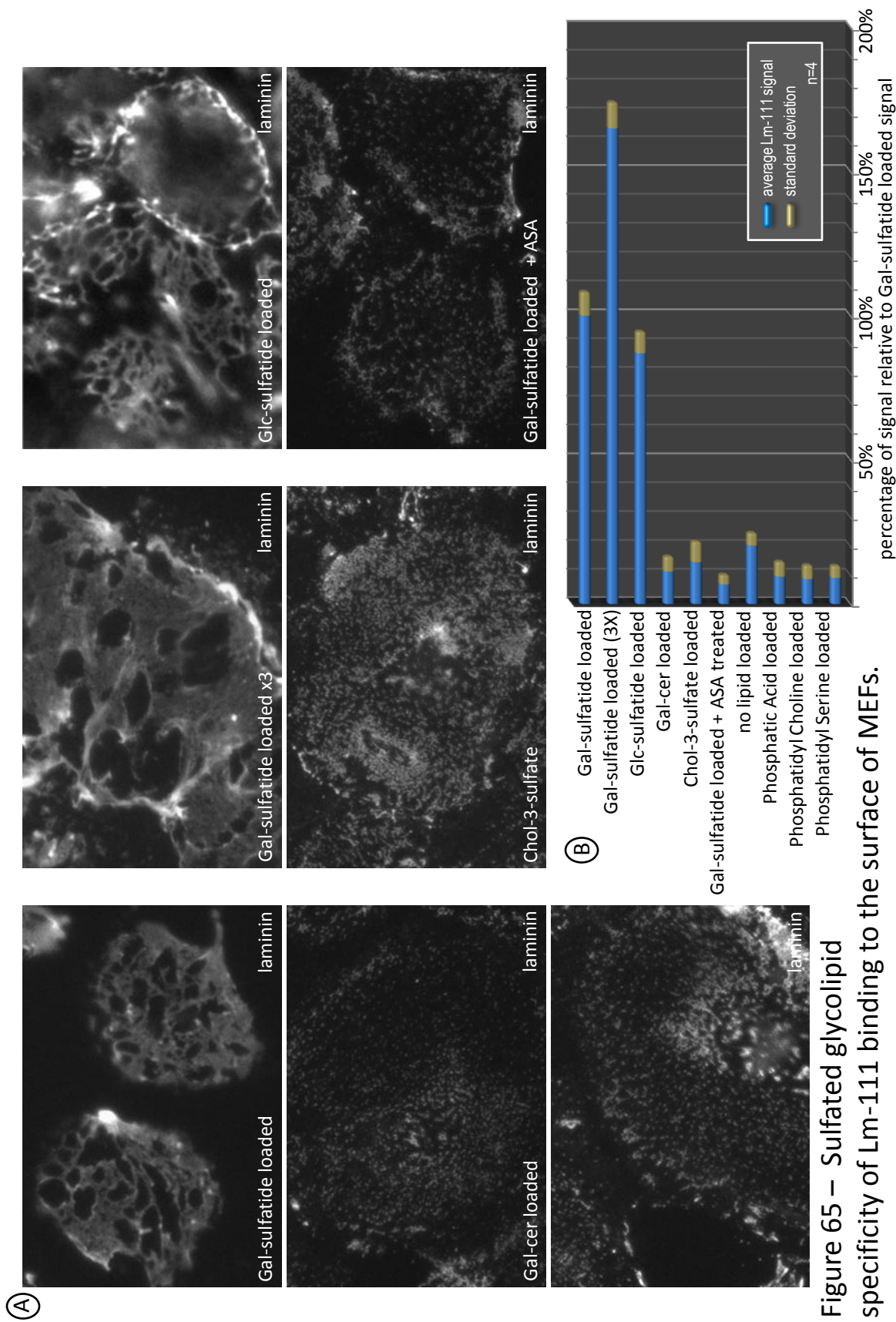


Figure 65 – Sulfated glycolipid specificity of Lm-111 binding to the surface of MEFs.

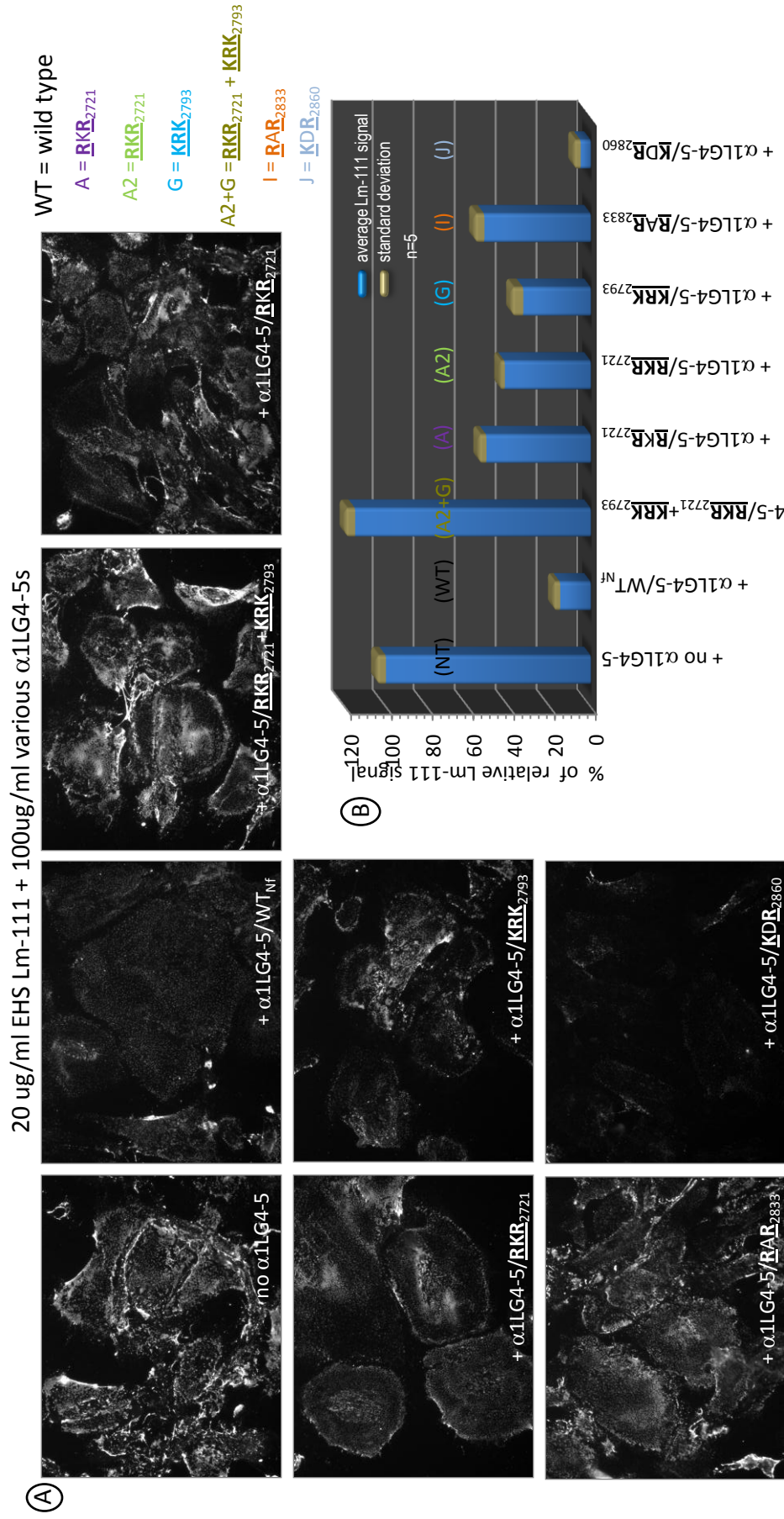


Figure 66 – Inhibition of exogenous Lm-111 accumulation on MEF cell surfaces (in the absence of sulfatide) by contemporaneous addition of recombinant α 1LG4-5 proteins.

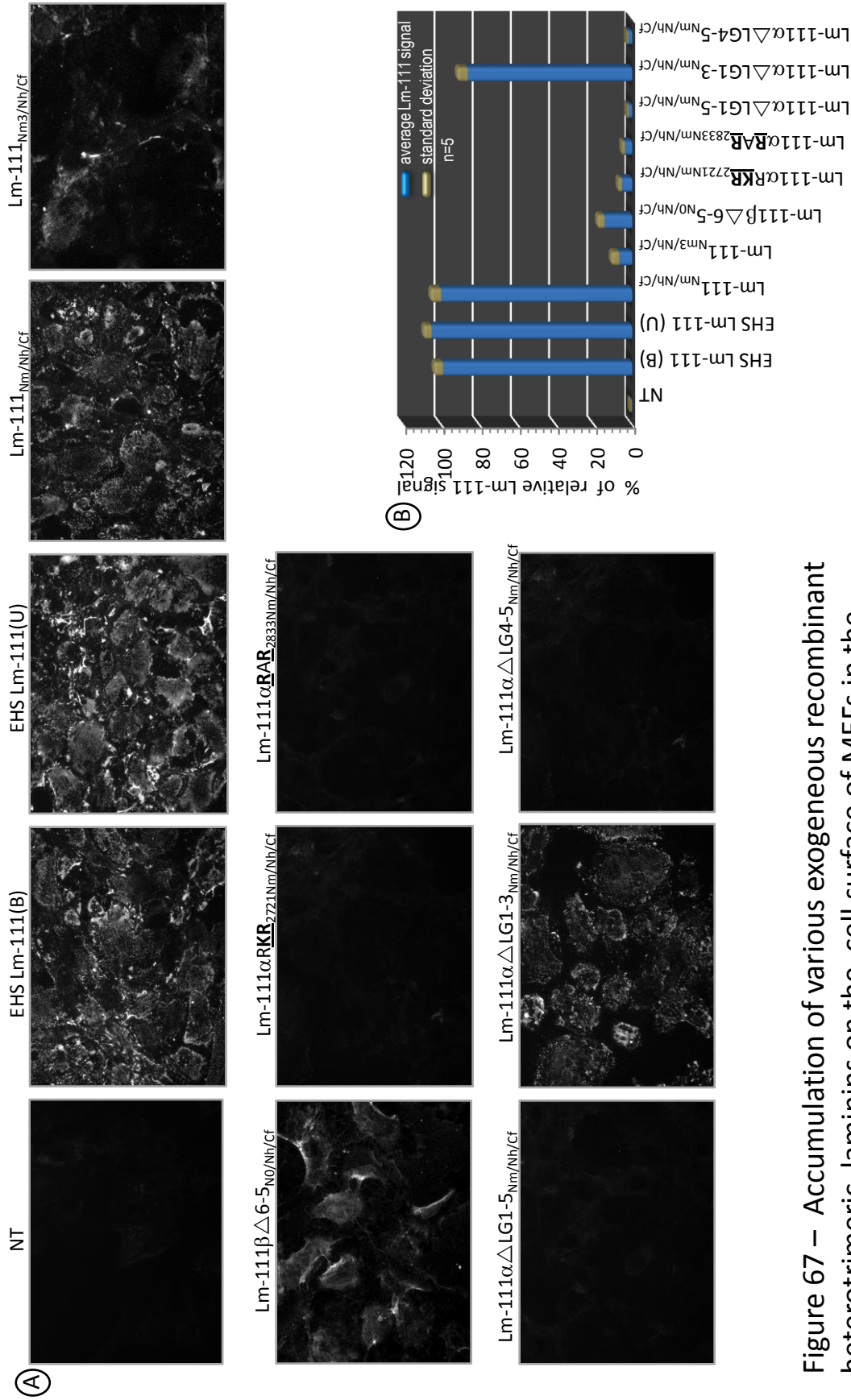


Figure 67 – Accumulation of various exogenous recombinant heterotrimeric laminins on the cell surface of MEFs in the absence of sulfate.

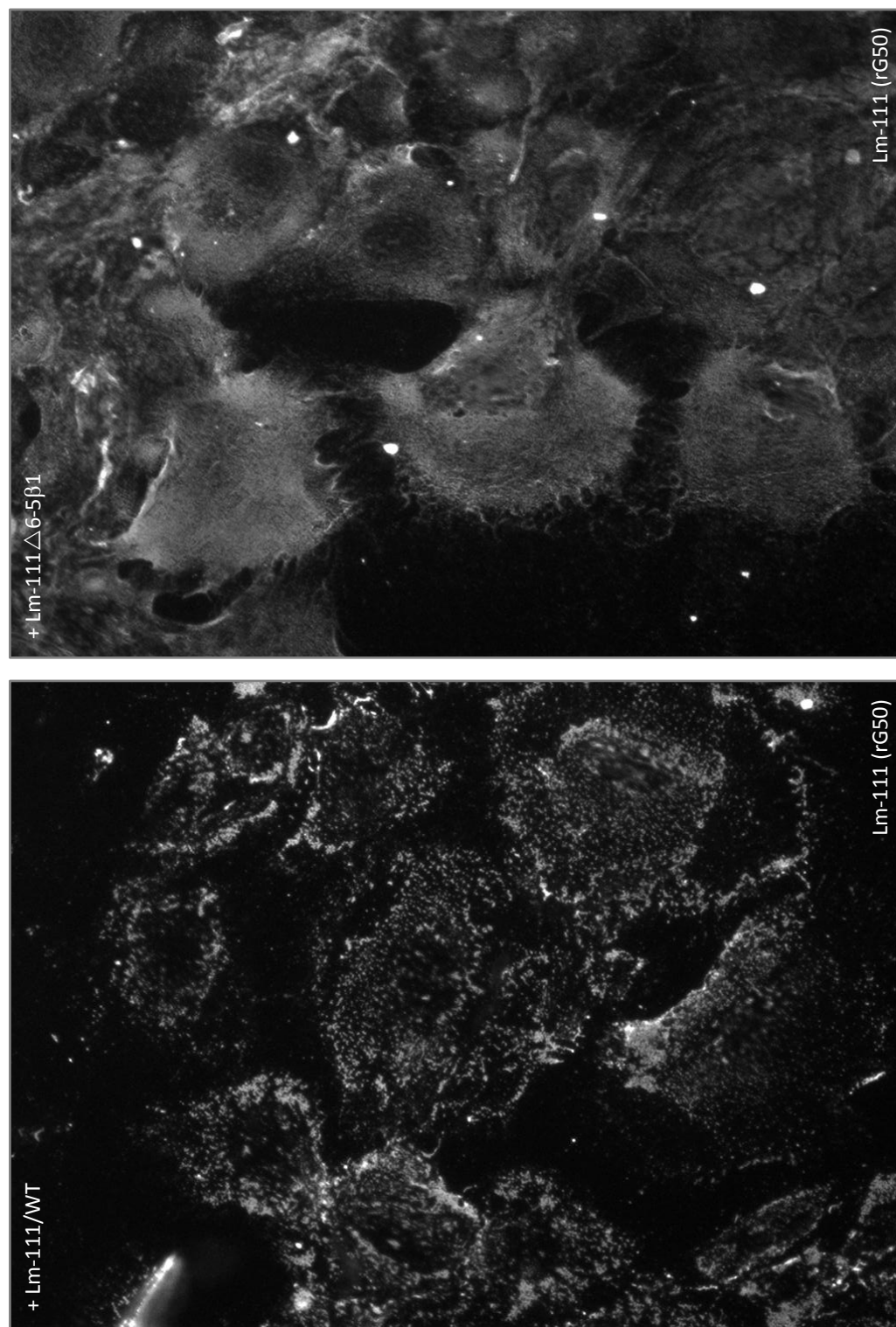


Figure 68 – Differences in accumulation patterns on MEF cell surfaces (sulfatide not present) between recombinant heterotrimeric laminins, as a consequence of their polymerization capability.

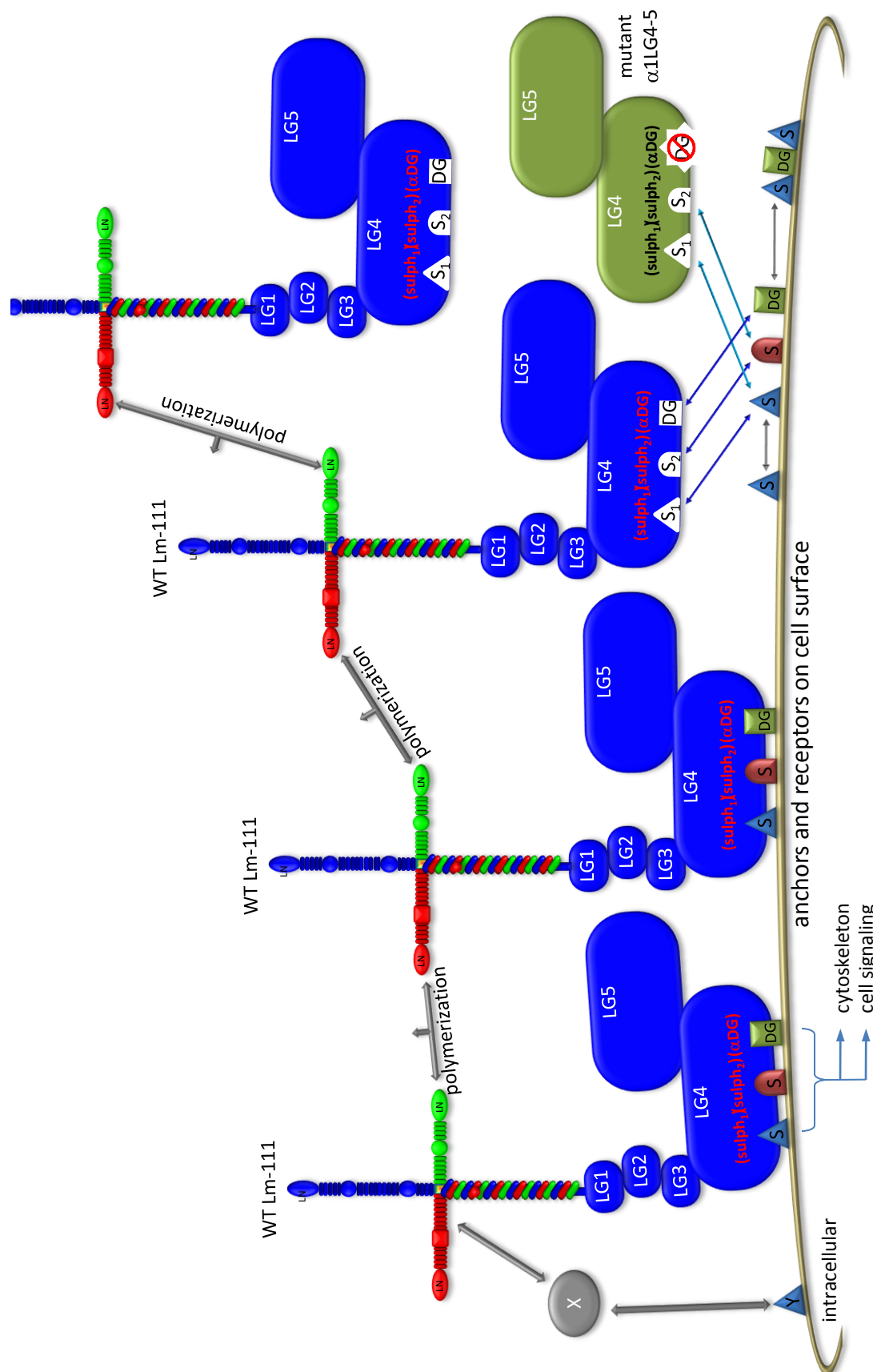


Figure 69 – Recombinant α 1G4-5 inhibition of Lm-111 binding.

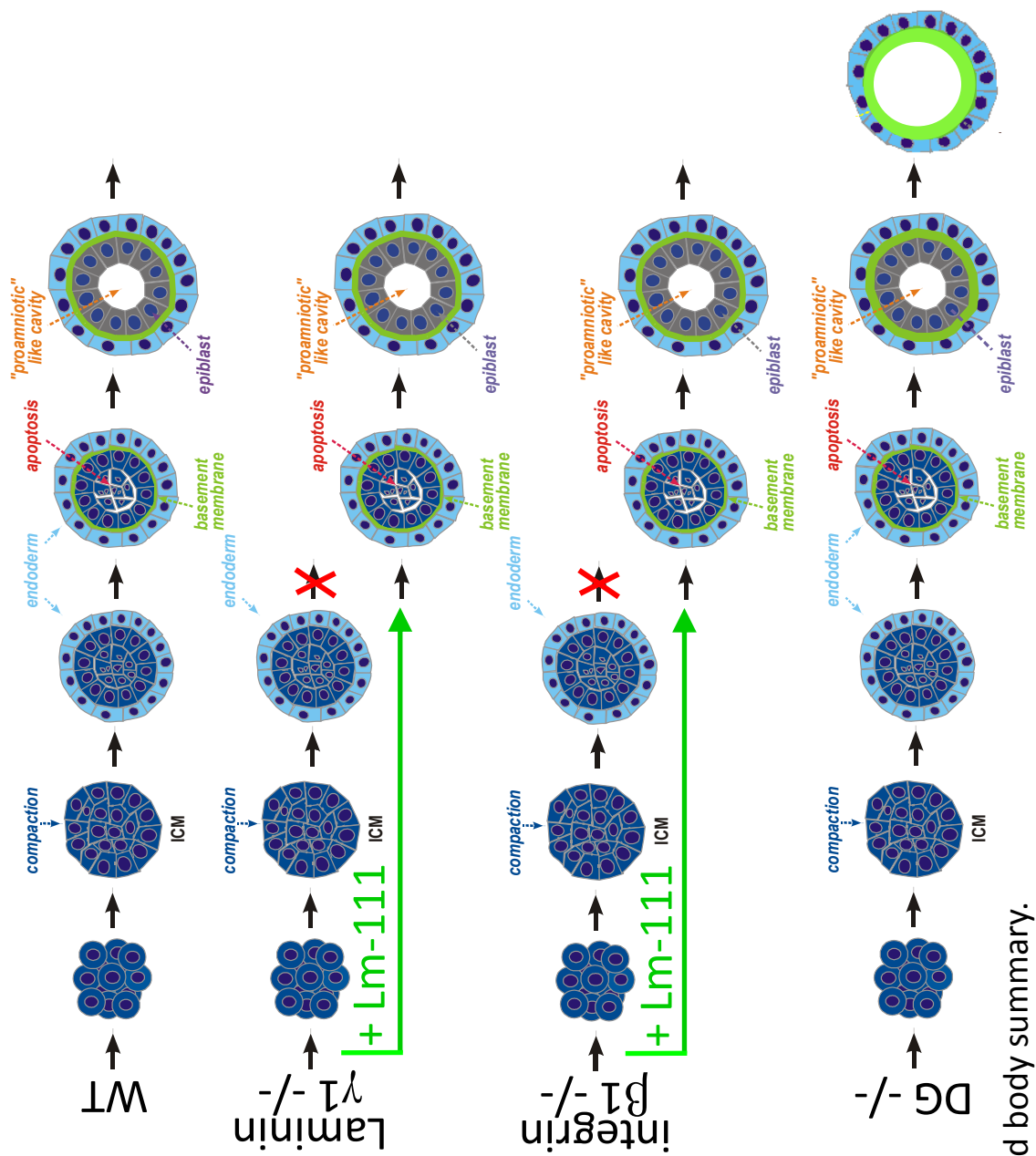


Figure 70 – Embryoid body summary.

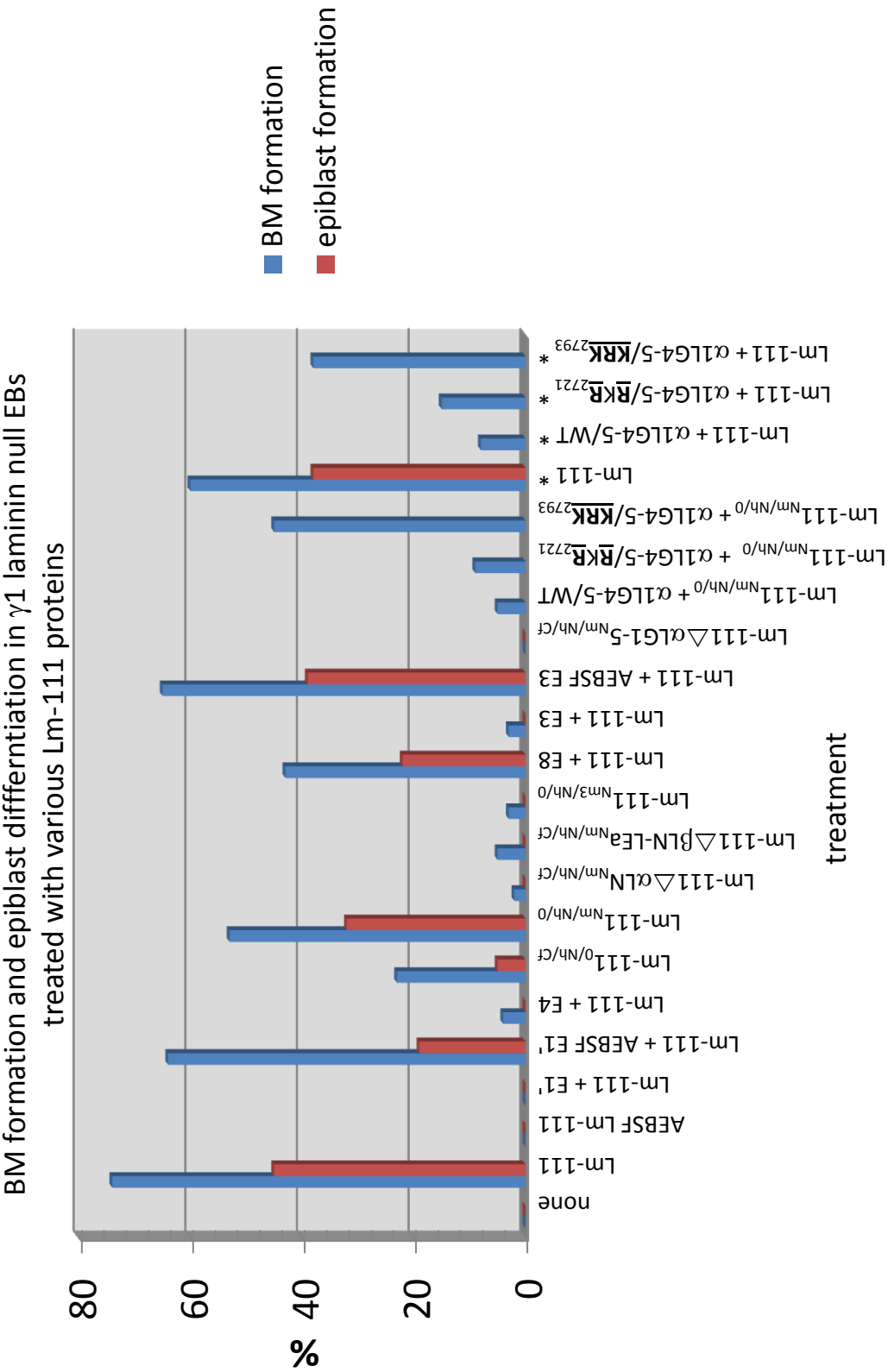


Figure 71 – Basement membrane formation and epiblast differentiation in $\gamma 1$ laminin null embryoid bodies treated with Lm-111, modified Lm-111, Lm-111 fragments, and recombinant Lm-111s.

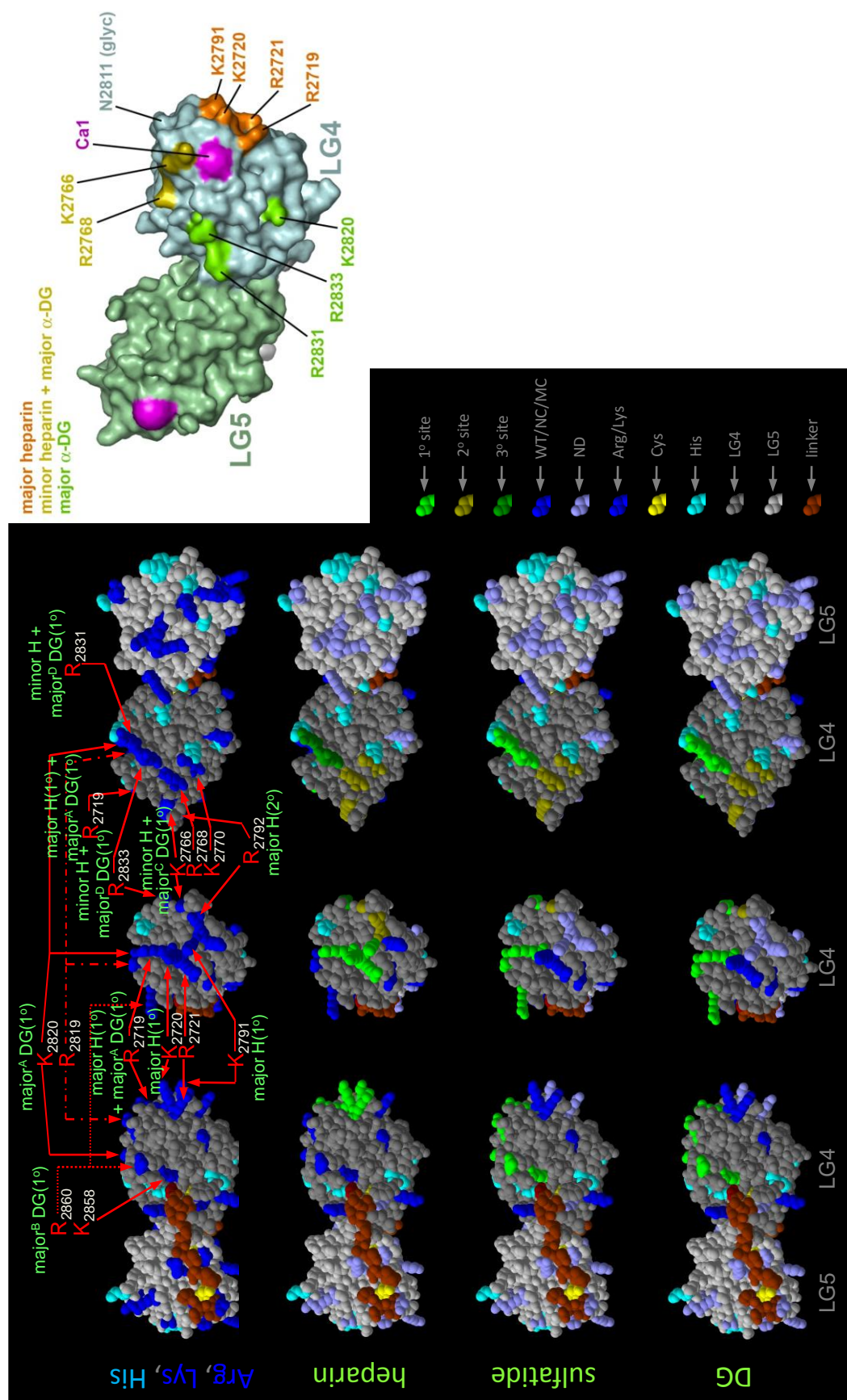


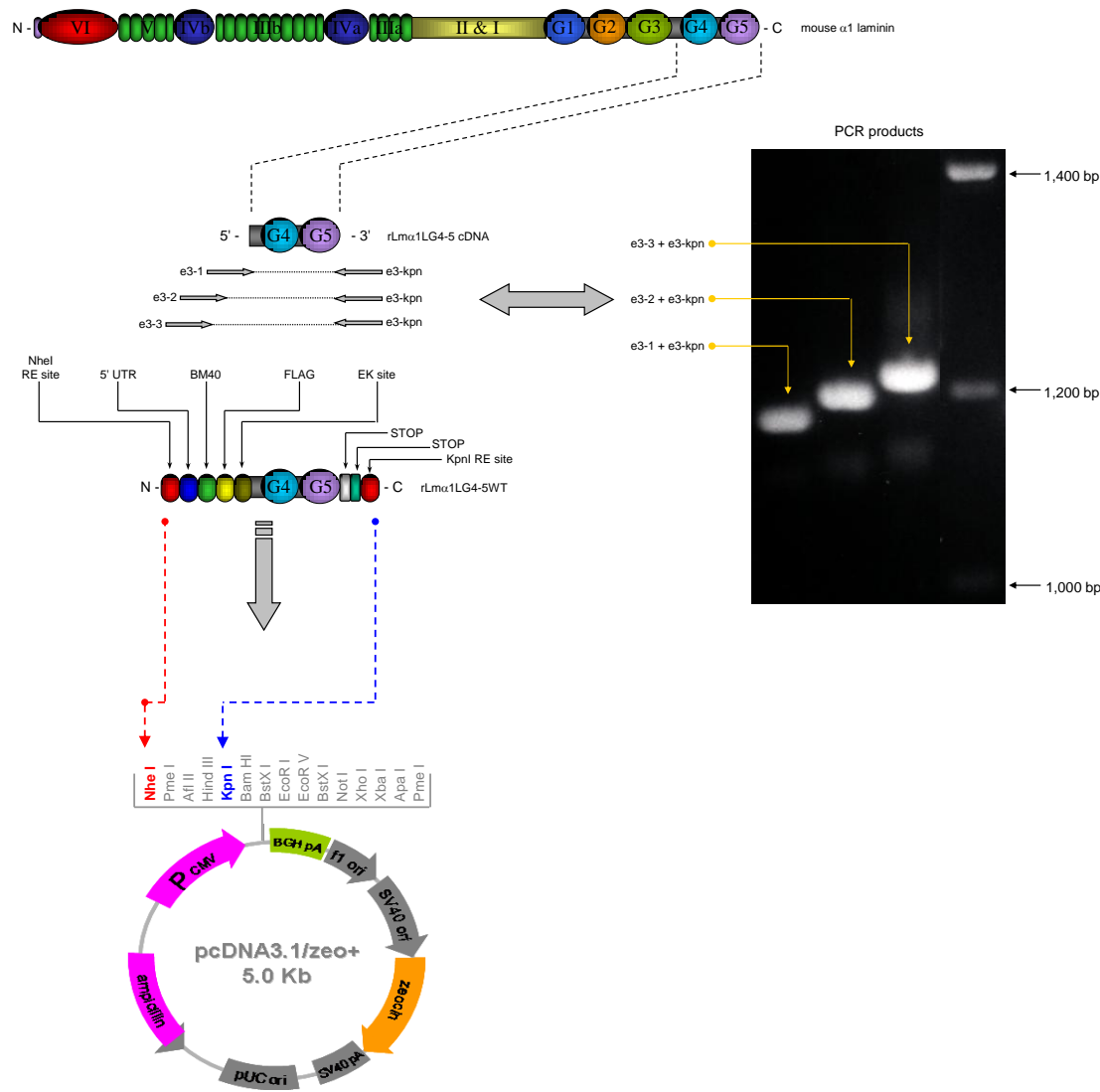
Figure 73 – Spatial location of amino acid residues involved in heparin, α DG, and sulfatide binding activities in mouse α 1 LG4-5.

Tables

Table 1. Temporal and spatial expression patterns of individual laminin chains. The temporal and spatial expression patterns of the individual laminin chains along with references for the observations.

Laminin Chain	Tissue Expression	Selected References
$\alpha 1$	BM of epithelial tissues during embryogenesis; placenta, fetal and new born kidney, brain, neuroretina, placenta, a few adult tissues	[27, 31, 240, 488, 532, 533]
$\alpha 2$	BM of skeletal and cardiac muscle, peripheral nerve, brain, capillaries, placenta	[244-246, 248, 532, 534, 535]
$\alpha 3$	BM of stratified epithelial; skin and other	[490, 536-538]
$\alpha 4$	Vascular BMs (mesenchymal); adult muscle, lung, nerve, blood vessel	[43, 539-544]
$\alpha 5$	BM of epithelial tissues; widespread expression; developing muscle and nerve, synaptic BM, kidney	[11, 493, 494, 543, 544]
$\beta 1$	Ubiquitous; most tissues - embryogenesis, fetal, and adult	[26, 240]
$\beta 2$	Wide expression pattern; Neuromuscular junction (NMJ), glomerulus	[2, 495, 496, 545, 546]
$\beta 3$	BM of stratified epithelial; skin and other	[547, 548]
$\gamma 1$	Ubiquitous; most tissues - embryogenesis, fetal, and adult	[28, 31]
$\gamma 2$	BM of stratified epithelial; skin and other	[549, 550]
$\gamma 3$	Non BM distribution in nerve, brain, epithelia	[551]

Table 2. Primer table and diagram for construction of recombinant α1LG4-5/WT.



primer designation	oligonucleotide primer sequence (5'-3')
e3-1	GCTCTGGCAGACTACAAGGACGACGATGACAAGCTGCACAGAGAACACGGGGAATC
e3-2	CTGGATCTTCTTTCTCTTTGCCTGGCCGGGAGGGCTCTGGCAGACTACAAGGACGAC
e3-3	GCCTAGGCTAGCCCGCCGCCACCATGAGGGCCTGGATCTTCTTTCTCTCTTTGCCTG
e3-kpn	GGGCAGAGGGGTACCTCATTAGGGCTCAGGCCCGGGCAGGAATG

Table 4. Individual recombinant laminin constructs - mouse $\alpha 1$ LG4-5s.

mouse $\alpha 1$ LG4-5 based constructs			
construct designation	description	epitope tag	selectable marker
1 $\alpha 1$ LG4-5/WT-pRCX3	WT sequence with BM40, N-FLAG, under P _{CMV}	N-terminal FLAG	neomycin
2 $\alpha 1$ LG4-5/WT-PRSV	WT sequence with BM40, N-FLAG, under P _{RSV}	N-terminal FLAG	neomycin
3 $\alpha 1$ LG4-5/WT-Pm β 1Lm	WT sequence with BM40, N-FLAG, under P _{mβ1Lm}	N-terminal FLAG	neomycin
4 $\alpha 1$LG4-5/WT_{Nf}	WT sequence with 5'UTR "consensus-1"	N-terminal FLAG	zeocin
5 $\alpha 1$ LG4-5/WT _{Cf}	WT sequence with 5'UTR "consensus-1"	C-terminal FLAG	zeocin
6 $\alpha 1$ LG4-5/WTcon2 _{Nf}	WT sequence with 5'UTR "consensus-2"	N-terminal FLAG	zeocin
7 $\alpha 1$ LG4-5/WT _{H2b} Nf	WT sequence with 5'UTR "H2B"	N-terminal FLAG	zeocin
8 $\alpha 1$ LG4-5/WT _{tom7} Nf	WT sequence with 5'UTR "TOMM7"	N-terminal FLAG	zeocin
9 $\alpha 1$ LG4-5/WT _{Iars} Nf	WT sequence with 5'UTR "IARS"	N-terminal FLAG	zeocin
10 $\alpha 1$ LG4-5/WT _{fdft1} Nf	WT sequence with 5'UTR "FDFT1"	N-terminal FLAG	zeocin
11 $\alpha 1$ LG4-5/WT _{ube2s} Nf	WT sequence with 5'UTR "UBE2S"	N-terminal FLAG	zeocin
12 $\alpha 1$ LG4-5/WT _{ef4a1} Nf	WT sequence with 5'UTR "EIF4A1"	N-terminal FLAG	zeocin
13 $\alpha 1$ LG4-5/WT(-f)	WT sequence with 5'UTR "consensus-1"; FLAG removed	no tag	zeocin
14 $\alpha 1$ LG4-5/WT-IG _{kNf}	WT sequence with IG κ signal sequence	N-terminal FLAG	zeocin
15 $\alpha 1$ LG4-5/WT-m α 1 _{Nf}	WT sequence with mouse $\alpha 1$ laminin signal sequence	N-terminal FLAG	zeocin
16 $\alpha 1$ LG4-5/WT _{Nm}	WT sequence with N-terminal myc tag	N-terminal myc	zeocin
17 $\alpha 1$ LG4-5/WT _{Nm3}	WT sequence with N-terminal myc X3 tag	N-terminal mycX3	zeocin
18 $\alpha 1$ LG4-5/WT _{Nh}	WT sequence with N-terminal HA tag	N-terminal HA	zeocin
19 $\alpha 1$ LG4-5/WT _{Nv}	WT sequence with N-terminal VSV-G tag	N-terminal VSV-G	zeocin
20 $\alpha 1$ LG4-5/WT _{Np}	WT sequence with N-terminal protein C tag	N-terminal protein C	zeocin
21 $\alpha 1$ LG4-5/WT _{Nv5}	WT sequence with V5 tag	N-terminal V5	zeocin
22 $\alpha 1$ LG4-5/ RKR ₂₇₂₁	mutated sequence reads AKA ₂₇₂₁ ; formerly rE3-A	N-terminal FLAG	zeocin
23 $\alpha 1$ LG4-5/ RKR ₂₇₂₁	mutated sequence reads AAA ₂₇₂₁ ; formerly rE3-A2	N-terminal FLAG	zeocin
24 $\alpha 1$ LG4-5/ RKR ₂₇₂₁	mutated sequence reads RAA ₂₇₂₁ ; formerly rE3-A'	N-terminal FLAG	zeocin
25 $\alpha 1$ LG4-5/ RKR ₂₇₂₁	mutated sequence reads AKR ₂₇₂₁	N-terminal FLAG	zeocin
26 $\alpha 1$ LG4-5/ RKR ₂₇₂₁	mutated sequence reads RAR ₂₇₂₁	N-terminal FLAG	zeocin
27 $\alpha 1$ LG4-5/ RKR ₂₇₂₁	mutated sequence reads RKA ₂₇₂₁	N-terminal FLAG	zeocin
28 $\alpha 1$ LG4-5/ R ₂₇₂₉	mutated sequence reads A ₂₇₂₉ ; formerly rE3-B	N-terminal FLAG	zeocin
29 $\alpha 1$ LG4-5/ R ₂₇₅₇	mutated sequence reads A ₂₇₅₇ ; formerly rE3-C	N-terminal FLAG	zeocin
30 $\alpha 1$ LG4-5/ KGRTK ₂₇₇₀	mutated sequence reads AGATA ₂₇₇₁ ; formerly rE3-D	N-terminal FLAG	zeocin
31 $\alpha 1$ LG4-5/ KGRTK ₂₇₇₀	mutated sequence reads AGRTK ₂₇₇₁	N-terminal FLAG	zeocin
32 $\alpha 1$ LG4-5/ KGRTK ₂₇₇₀	mutated sequence reads KGATK ₂₇₇₁	N-terminal FLAG	zeocin
33 $\alpha 1$ LG4-5/ KGRTK ₂₇₇₀	mutated sequence reads KGRTA ₂₇₇₁	N-terminal FLAG	zeocin
34 $\alpha 1$ LG4-5/ K ₂₇₈₁	mutated sequence reads A ₂₇₈₁ ; formerly rE3-E	N-terminal FLAG	zeocin
35 $\alpha 1$ LG4-5/ K ₂₇₈₆	mutated sequence reads A ₂₇₈₆ ; formerly rE3-F	N-terminal FLAG	zeocin
36 $\alpha 1$ LG4-5/ KRK ₂₇₉₃	mutated sequence reads AAA ₂₇₉₃ ; formerly rE3-G	N-terminal FLAG	zeocin
37 $\alpha 1$ LG4-5/ KRK ₂₇₉₃	mutated sequence reads ARA ₂₇₉₃ ; formerly rE3-G'	N-terminal FLAG	zeocin
38 $\alpha 1$ LG4-5/ KRK ₂₇₉₃	mutated sequence reads ARK ₂₇₉₃	N-terminal FLAG	zeocin
39 $\alpha 1$ LG4-5/ KRK ₂₇₉₃	mutated sequence reads KAK ₂₇₉₃	N-terminal FLAG	zeocin
40 $\alpha 1$ LG4-5/ KRK ₂₇₉₃	mutated sequence reads KRA ₂₇₉₃	N-terminal FLAG	zeocin

Table 4. Individual recombinant laminin constructs - mouse α 1 LG4-5s.
(continued)

mouse α 1LG4-5 based constructs			
construct designation	description	epitope tag	selectable marker
41 α 1LG4-5/ <u>RK</u> ₂₈₂₀	mutated sequence reads AA ₂₈₂₀ ; formerly rE3-H	N-terminal FLAG	zeocin
42 α 1LG4-5/ <u>RK</u> ₂₈₂₀	mutated sequence reads AK ₂₈₂₀	N-terminal FLAG	zeocin
43 α 1LG4-5/ <u>RK</u> ₂₈₂₀	mutated sequence reads RA ₂₈₂₀	N-terminal FLAG	zeocin
44 α 1LG4-5/ <u>RAR</u> ₂₈₃₃	mutated sequence reads AAA ₂₈₃₃ ; formerly rE3-I	N-terminal FLAG	zeocin
45 α 1LG4-5/ <u>RAR</u> ₂₈₃₃	mutated sequence reads AAR ₂₈₃₃	N-terminal FLAG	zeocin
46 α 1LG4-5/ <u>RAR</u> ₂₈₃₃	mutated sequence reads RAA ₂₈₃₃	N-terminal FLAG	zeocin
47 α 1LG4-5/ <u>KDR</u> ₂₈₆₀	mutated sequence reads ADA ₂₈₆₀ ; formerly rE3-J	N-terminal FLAG	zeocin
48 α 1LG4-5/ <u>KDR</u> ₂₈₆₀	mutated sequence reads ADR ₂₈₆₀	N-terminal FLAG	zeocin
49 α 1LG4-5/ <u>KDR</u> ₂₈₆₀	mutated sequence reads KDA ₂₈₆₀	N-terminal FLAG	zeocin
50 α 1LG4-5/ <u>R</u> ₂₈₆₉	mutated sequence reads A ₂₈₆₉ ; formerly rE3-K	N-terminal FLAG	zeocin
51 α 1LG4-5/ <u>RKR</u> ₂₇₂₁ + <u>KRK</u> ₂₇₉₃	mutated sequence reads AAA ₂₇₂₁ and AAA ₂₇₉₃ ; formerly rE3-A2+G	N-terminal FLAG	zeocin
52 α 1LG4-5/ <u>RKR</u> ₂₇₂₁ + <u>KRK</u> ₂₇₉₃	mutated sequence reads RAA ₂₇₂₁ and ARA ₂₇₉₃ ; formerly rE3-A'+G'	N-terminal FLAG	zeocin
53 α 1LG4-5/ <u>C</u> ₃₀₁₄ S ^{Nhis}	quadruple mutant utilized in crystal structure determination	N-terminal His tag	puromycin
54 α 1LG4-5/ <u>C</u> ₃₀₁₄ S	quadruple mutant utilized in crystal structure determination	no tag	puromycin
55 α 1LG4-5/ <u>N</u> ₂₇₁₄ Q+ <u>N</u> ₂₈₁₁ K+ <u>N</u> ₂₉₀₀ Q+ <u>C</u> ₃₀₁₄ S	quadruple mutant utilized in crystal structure determination	no tag	puromycin
56 α 1LG4-5/ <u>N</u> ₂₇₁₄	mutated sequence reads A ₂₇₁₄ ; mutant of N-link site 1 in LG4	N-terminal FLAG	zeocin
57 α 1LG4-5/ <u>N</u> ₂₈₁₁	mutated sequence reads A ₂₈₁₁ ; mutant of N-link site 2 in LG4	N-terminal FLAG	zeocin
58 α 1LG4-5/ <u>N</u> ₂₉₀₀	mutated sequence reads A ₂₉₀₀ ; mutant of N-link site 3 in LG4	N-terminal FLAG	zeocin
59 α 1LG4-5/ <u>N</u> ₂₇₁₄ + <u>N</u> ₂₈₁₁	mutated sequence reads A ₂₇₁₄ + A ₂₈₁₁ ; N-link site 1 + 2	N-terminal FLAG	zeocin
60 α 1LG4-5/ <u>N</u> ₂₇₁₄ + <u>N</u> ₂₉₀₀	mutated sequence reads A ₂₇₁₄ + A ₂₉₀₀ ; N-link site 1 + 3	N-terminal FLAG	zeocin
61 α 1LG4-5/ <u>N</u> ₂₈₁₁ + <u>N</u> ₂₉₀₀	mutated sequence reads A ₂₈₁₁ + A ₂₉₀₀ ; N-link site 2 + 3	N-terminal FLAG	zeocin
62 α 1LG4-5/ <u>N</u> ₂₇₁₄ + <u>N</u> ₂₈₁₁ + <u>N</u> ₂₉₀₀	mutated sequence reads A ₂₇₁₄ + A ₂₈₁₁ + A ₂₉₀₀ ; N-link site 1+2+3	N-terminal FLAG	zeocin
63 α 1LG4-5/ <u>D</u> ₂₇₄₇	mutated sequence reads A ₂₇₄₇ ; 1st Asp of Ca2+ site in LG4	N-terminal FLAG	zeocin
64 α 1LG4-5/ <u>D</u> ₂₈₁₆	mutated sequence reads A ₂₈₁₆ ; 2nd Asp of Ca2+ site in LG4	N-terminal FLAG	zeocin
65 α 1LG4-5/ <u>D</u> ₂₇₄₇ + <u>D</u> ₂₈₁₆	mutated sequence reads A ₂₇₄₇ + A ₂₈₁₆ ; 1st and 2nd Asp of Ca2+ site in LG4	N-terminal FLAG	zeocin
66 α 1LG4-5/ <u>D</u> ₂₉₂₃	mutated sequence reads A ₂₉₂₃ ; 1st Asp of Ca2+ site in LG4	N-terminal FLAG	zeocin
67 α 1LG4-5/ <u>D</u> ₂₉₉₆	mutated sequence reads A ₂₉₉₆ ; 2nd Asp of Ca2+ site in LG4	N-terminal FLAG	zeocin
68 α 1LG4-5/ <u>D</u> ₂₉₂₃ + <u>D</u> ₂₉₉₆	mutated sequence reads A ₂₉₂₃ + A ₂₉₉₆ ; 1st and 2nd Asp of Ca2+ site in LG5	N-terminal FLAG	zeocin

Table 5. Individual recombinant laminin chain constructs.

- $\alpha 1$ based constructs

mouse $\alpha 1$ laminin based constructs			
construct designation	description	epitope tag	selectable marker
1 $\alpha 1 \text{WT}_{\text{Nm}}$	$\alpha 1$ full length WT	N-terminal c-myc	puromycin
2 $\alpha 1 \text{WT}$	$\alpha 1$ full length WT	none	puromycin
3 $\alpha 1 \text{WT}_{\text{Nf}}$	$\alpha 1$ full length WT	N-terminal FLAG	puromycin
4 $\alpha 1 \text{WT}_{\text{Nc}}$	$\alpha 1$ full length WT	N-terminal protein-C	puromycin
5 $\alpha 1 \text{WT}_{\text{Nv}}$	$\alpha 1$ full length WT	N-terminal VSV-G	puromycin
6 $\alpha 1 \text{WT}_{\text{Nh}}$	$\alpha 1$ full length WT	N-terminal HA	puromycin
7 $\alpha 1 \text{WT}_{\text{Nm3}}$	$\alpha 1$ full length WT	N-terminal c-myc x3	puromycin
8 $\alpha 1 \Delta \text{LN}_{\text{Nm}}$	$\alpha 1$ with deletion of the LN domain	N-terminal c-myc	puromycin
9 $\alpha 1 \Delta \text{LN-LEa(A)}_{\text{Nm}}$	$\alpha 1$ with deletion of the LN-LEa domains; leaves partial EGF in LEa	N-terminal c-myc	puromycin
10 $\alpha 1 \Delta \text{LN-LEa(B)}_{\text{Nm}}$	$\alpha 1$ with deletion of the LN-LEa domains; leaves partial EGF in LEb	N-terminal c-myc	puromycin
11 $\alpha 1 \Delta \text{LN-LEa(C)}_{\text{Nm}}$	$\alpha 1$ with deletion of the LN-LEa domains; removes partial EGF from LEb	N-terminal c-myc	puromycin
12 $\alpha 1 \Delta \text{LN-L4b(C)}_{\text{Nm}}$	$\alpha 1$ with deletion of the LN-L4b domains; removes partial EGF in LEc	N-terminal c-myc	puromycin
13 $\alpha 1 \Delta \text{LG1-5 (A)}_{\text{Nm}}$	$\alpha 1$ with deletion of the LG1-5 domains	N-terminal c-myc	puromycin
14 $\alpha 1 \Delta \text{LG1-5(B)}_{\text{Nm}}$	$\alpha 1$ with deletion of the LG1-5 domains	N-terminal c-myc	puromycin
15 $\alpha 1 \Delta \text{LG1-3}_{\text{Nm}}$	$\alpha 1$ with deletion of the LG1-3 domains	N-terminal c-myc	puromycin
16 $\alpha 1 \Delta \text{LG4-5}_{\text{Nm}}$	$\alpha 1$ with deletion of the LG4-5 domains	N-terminal c-myc	puromycin
17 $\alpha 1/\text{RKR}_{2721\text{Nm}}$	$\alpha 1$ full length with 2 point mutations; mutated RKR_{2721} to RAA	N-terminal c-myc	puromycin
18 $\alpha 1/\text{KRK}_{2793\text{Nm}}$	$\alpha 1$ full length with 2 point mutations; mutated KRK_{2793} to ARA	N-terminal c-myc	puromycin
19 $\alpha 1/\text{RAR}_{2833\text{Nm}}$	$\alpha 1$ full length with 2 point mutations; mutated RAR_{2833} to AAA	N-terminal c-myc	puromycin
20 $\alpha 1 \text{WT}_{\text{Cf}}$	$\alpha 1$ full length WT	C-terminal FLAG	puromycin
21 $\alpha 1 \Delta \text{LG1-5}_{\text{Nf}}$	$\alpha 1$ with deletion of the LG1-5 domains	N-terminal FLAG	G418
22 $\alpha 1 \Delta \text{LG1-5(A)}_{\text{Cf}}$	$\alpha 1$ with deletion of the LG1-5 domains	C-terminal FLAG	puromycin
23 $\alpha 1 \Delta \text{LG1-5(B)}_{\text{Cf}}$	$\alpha 1$ with deletion of the LG1-5 domains	C-terminal FLAG	G418
24 $\alpha 1 \Delta \text{LN-L4a(A)}_{\text{Nm}}$	$\alpha 1$ with deletion of the LN-L4a domains; leaves partial EGF in LEa	N-terminal c-myc	puromycin
25 $\alpha 1 \Delta \text{LN-L4a(B)}_{\text{Nm}}$	$\alpha 1$ with deletion of the LN-L4a domains; leaves partial EGF in LEb	N-terminal c-myc	puromycin
26 $\alpha 1 \Delta \text{LN-L4a(C)}_{\text{Nm}}$	$\alpha 1$ with deletion of the LN-L4a domains; removes partial EGF in LEb	N-terminal c-myc	puromycin
27 $\alpha 1 \Delta \text{LN-LEb(A)}_{\text{Nm}}$	$\alpha 1$ with deletion of the LN-LEb domains; leaves partial EGF in LEb	N-terminal c-myc	puromycin
28 $\alpha 1 \Delta \text{LN-LEb(B)}_{\text{Nm}}$	$\alpha 1$ with deletion of the LN-LEb domains; leaves partial EGF in LEc	N-terminal c-myc	puromycin
29 $\alpha 1 \Delta \text{LN-LEb(C)}_{\text{Nm}}$	$\alpha 1$ with deletion of the LN-LEb domains; removes partial EGF in LEc	N-terminal c-myc	puromycin
30 $\alpha 1 \Delta \text{LN-L4b(A)}_{\text{Nm}}$	$\alpha 1$ with deletion of the LN-L4b domains; leaves partial EGF in LEb	N-terminal c-myc	puromycin
31 $\alpha 1 \Delta \text{LN-L4b(B)}_{\text{Nm}}$	$\alpha 1$ with deletion of the LN-L4b domains; leaves partial EGF in LEc	N-terminal c-myc	puromycin
32 $\alpha 1 \text{(A)}_{\text{Nf}}$	$\alpha 1$ full length WT	N-terminal FLAG	hygro
33 $\alpha 1 \text{(B)}_{\text{Nf}}$	$\alpha 1$ full length WT	N-terminal FLAG	G418

Table 6. Construction of mouse laminin α chain expression constructs and other assorted information.

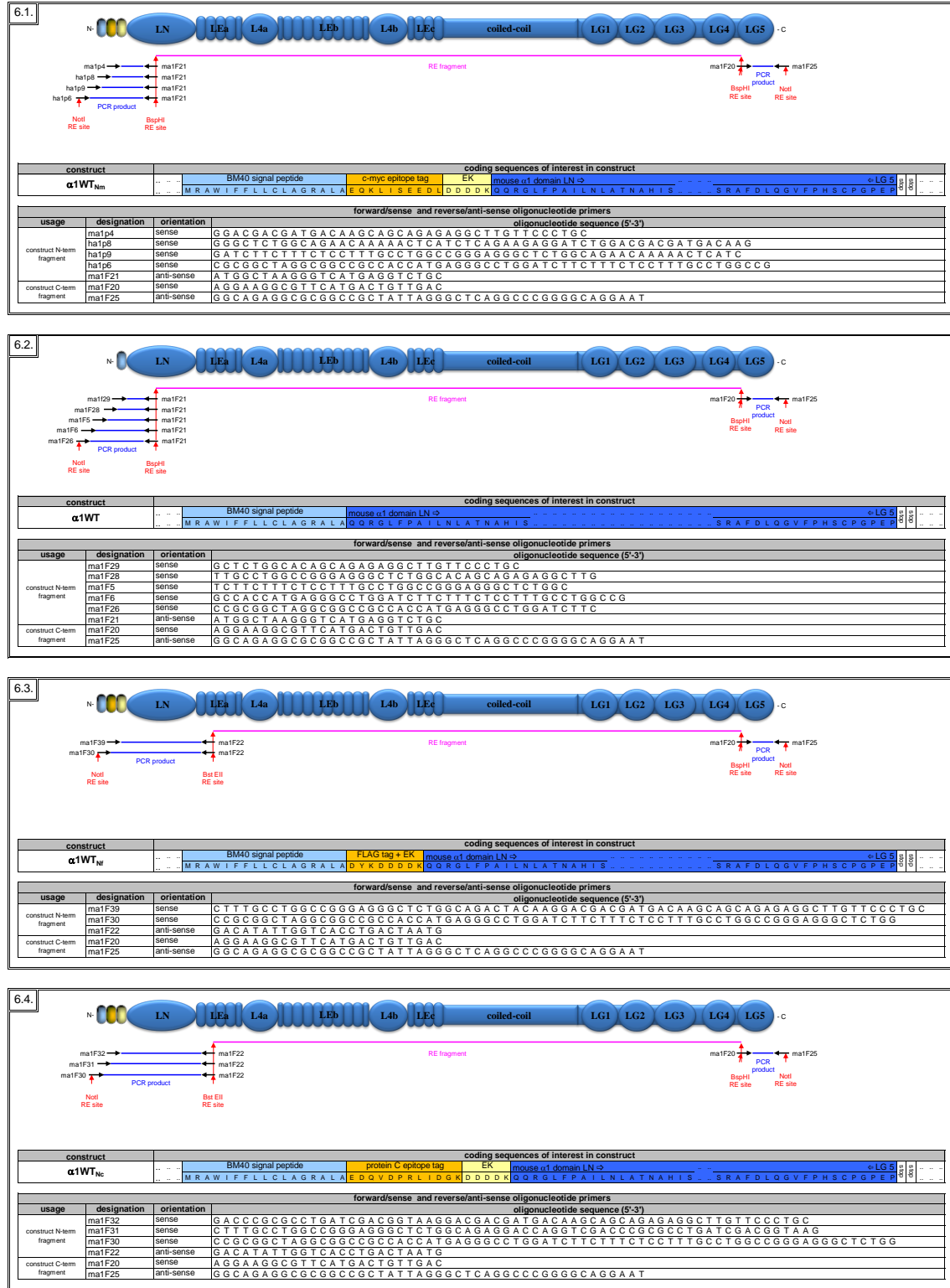


Table 6. Construction of mouse laminin α chain expression constructs and other assorted information. (continued)

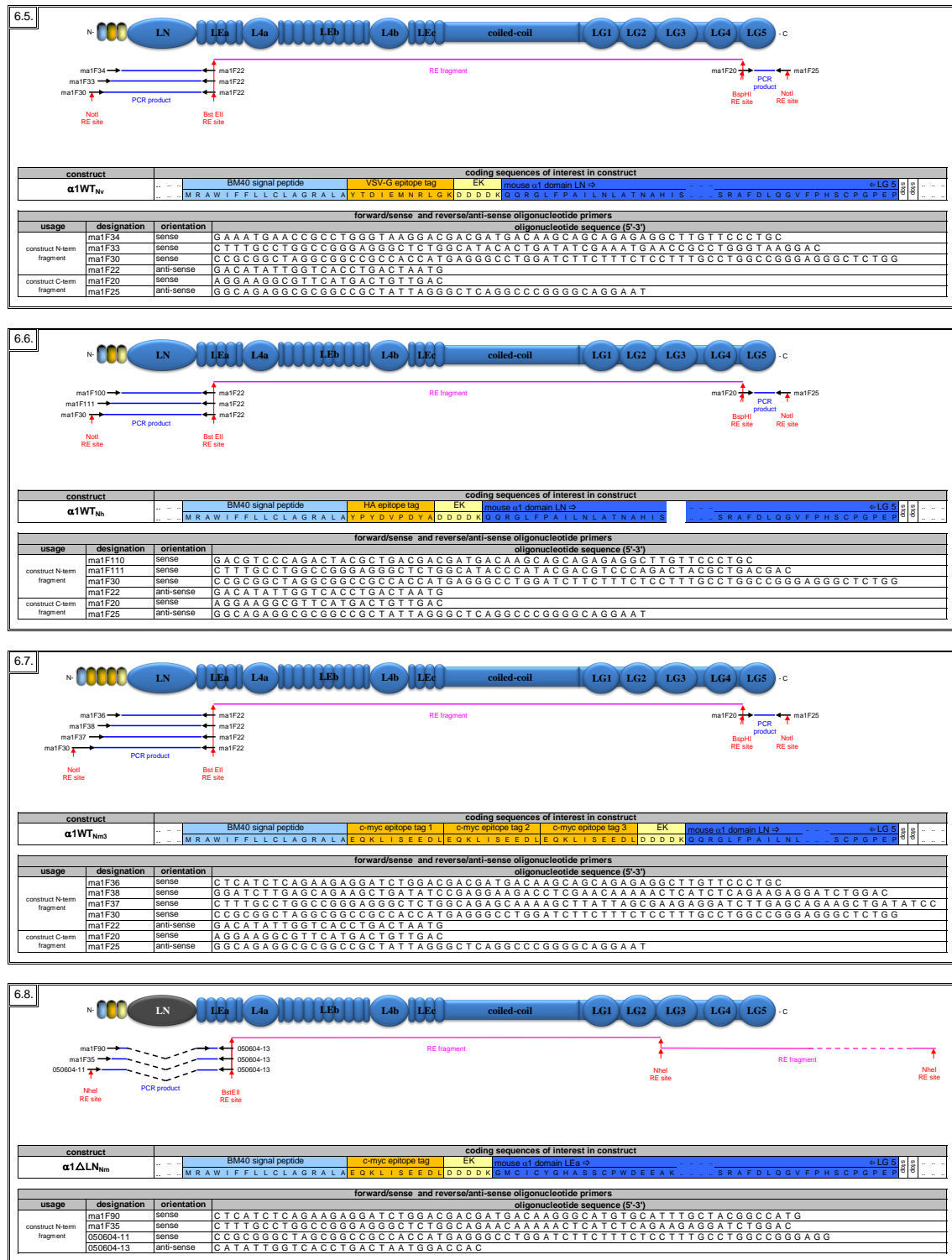


Table 6. Construction of mouse laminin α chain expression constructs and other assorted information. (continued)

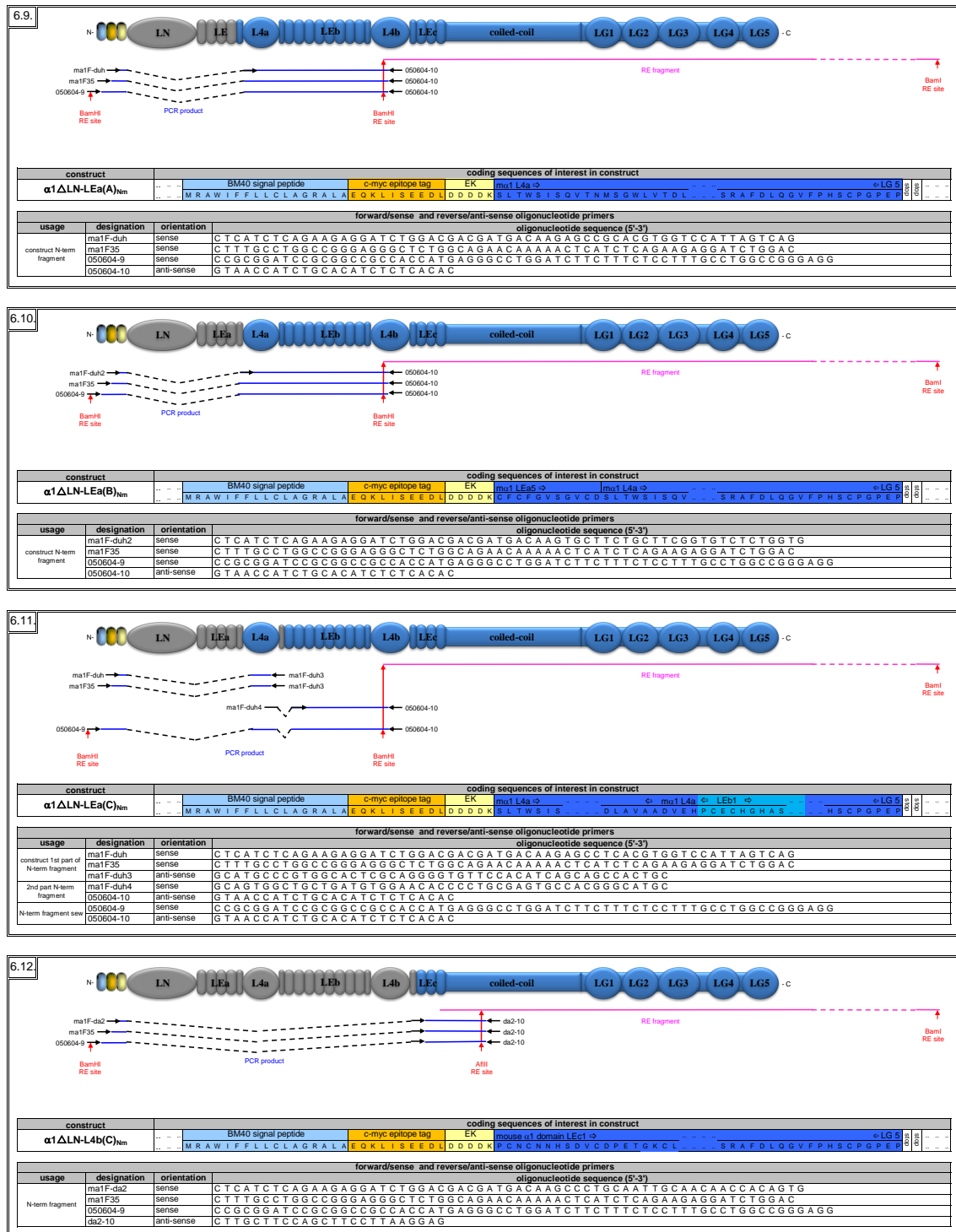


Table 6. Construction of mouse laminin α chain expression constructs and other assorted information. (continued)

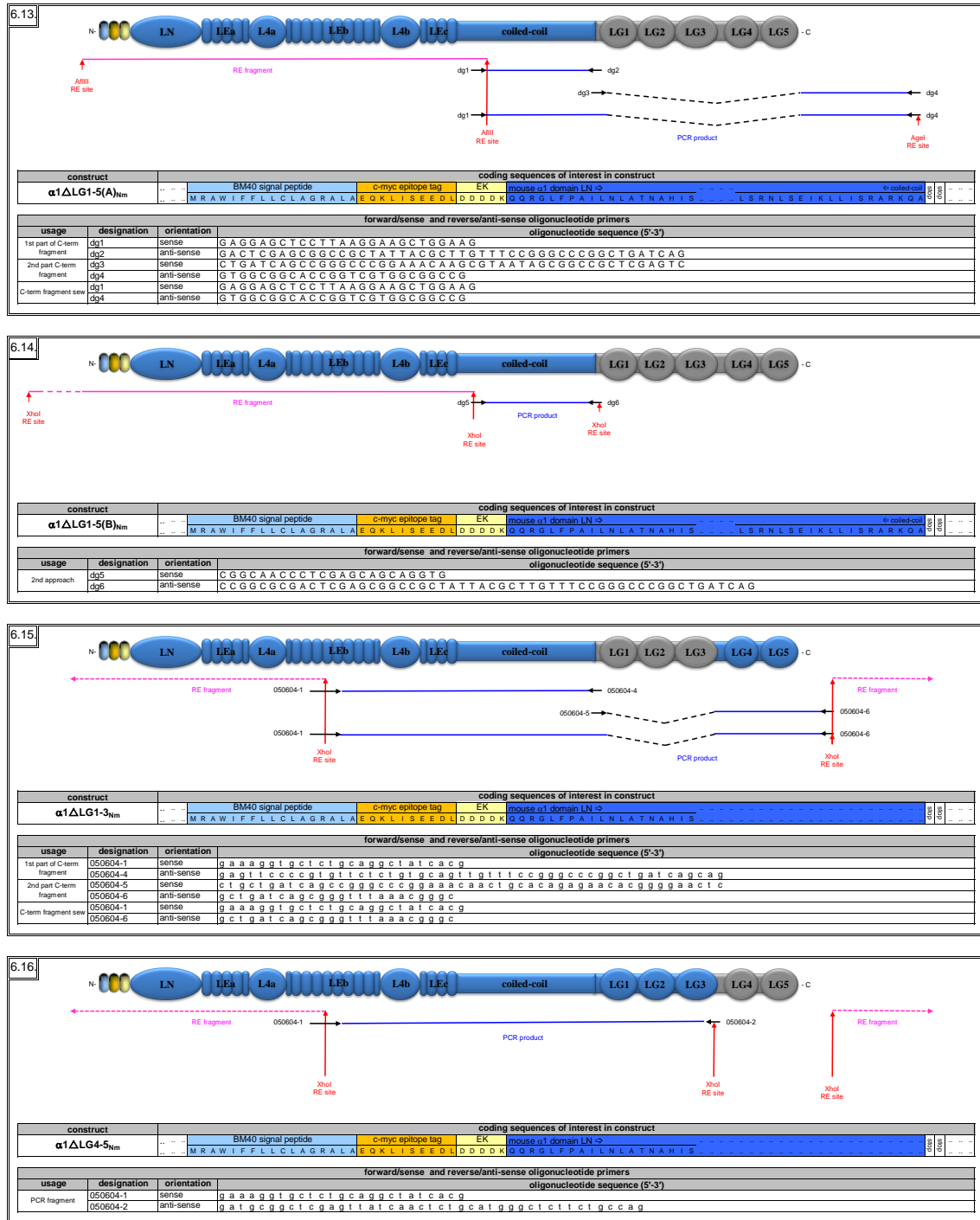


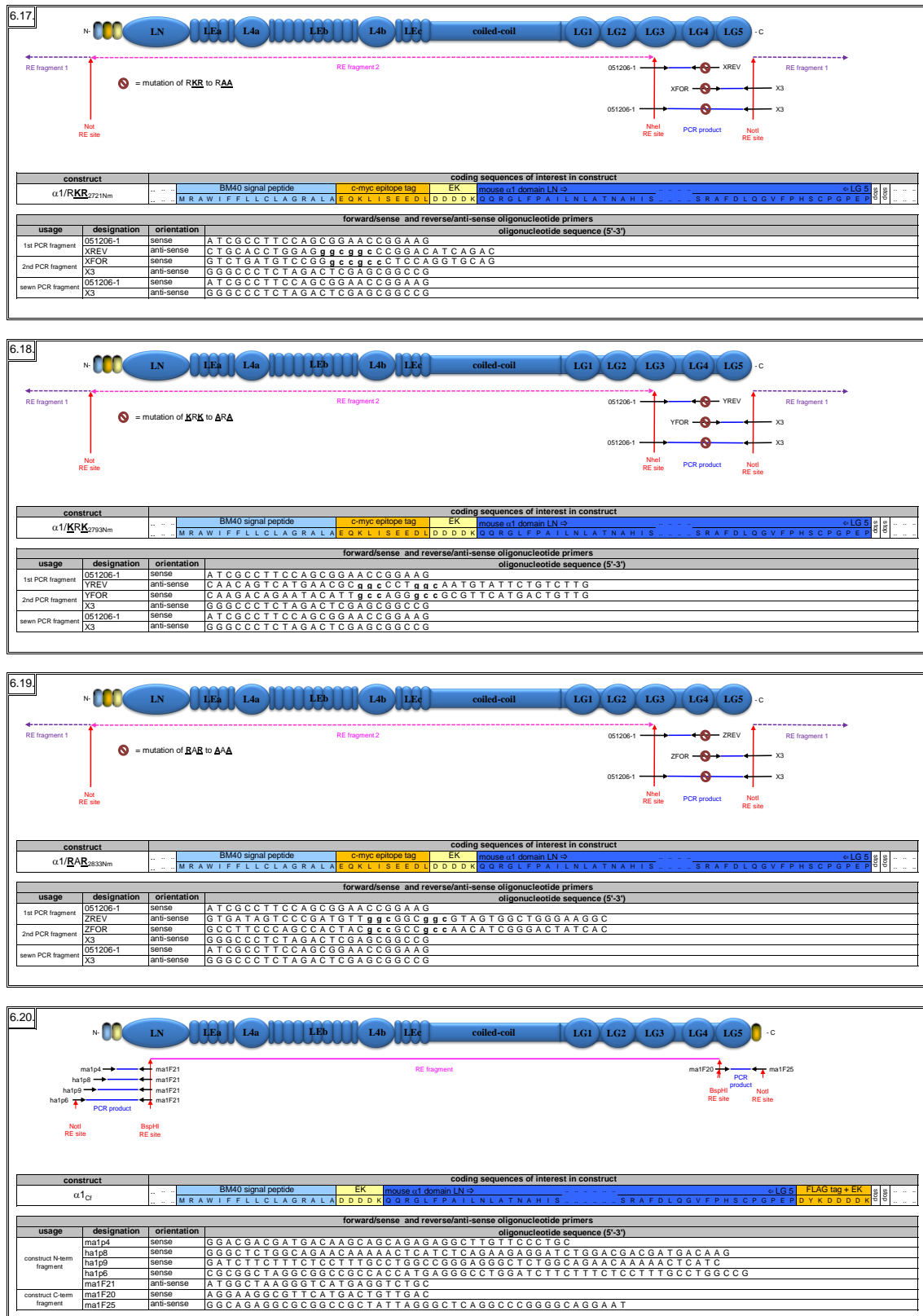
Table 6. Construction of mouse laminin α chain expression constructs and other

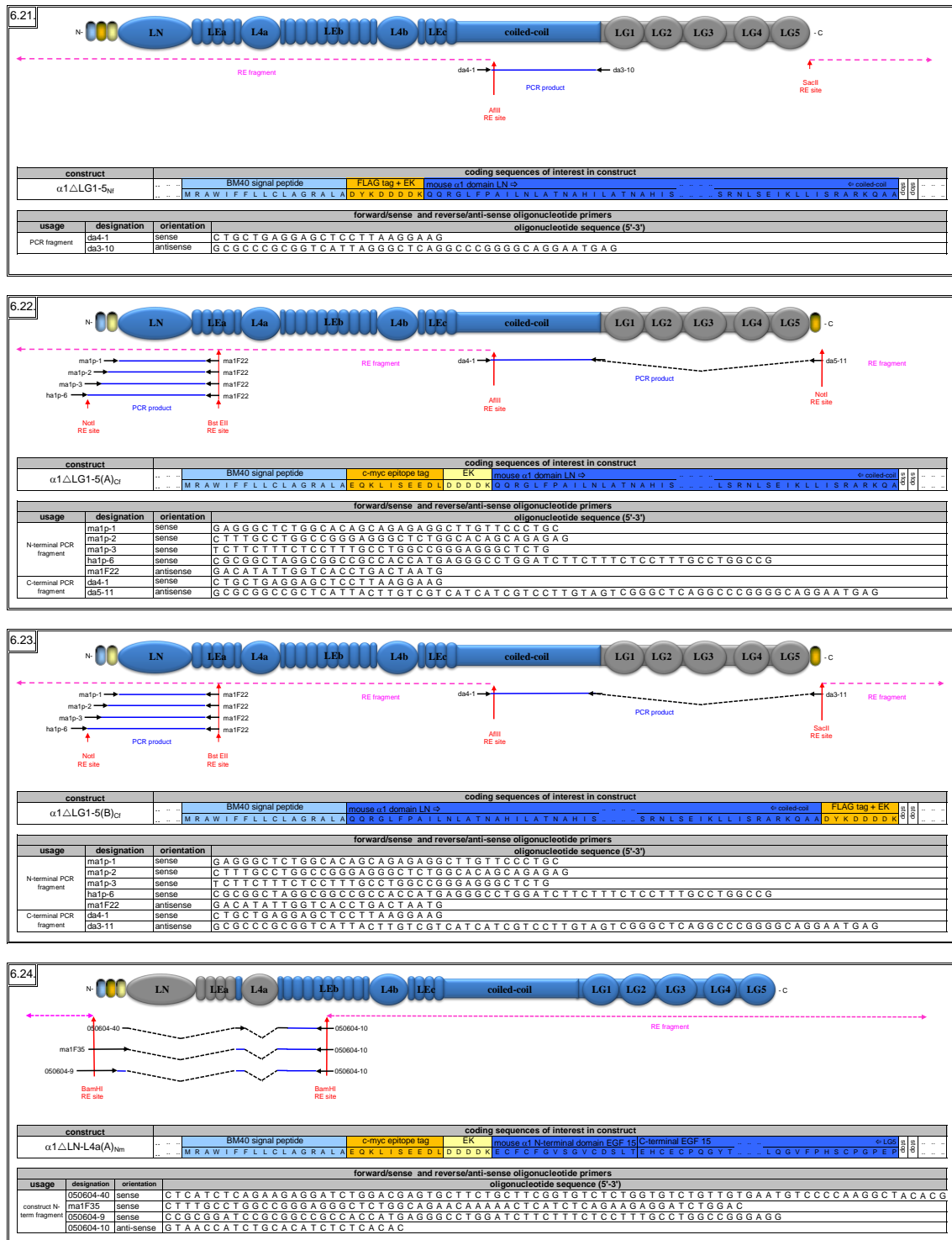
Table 6. Construction of mouse laminin α chain expression constructs and other

Table 6. Construction of mouse laminin α chain expression constructs and other

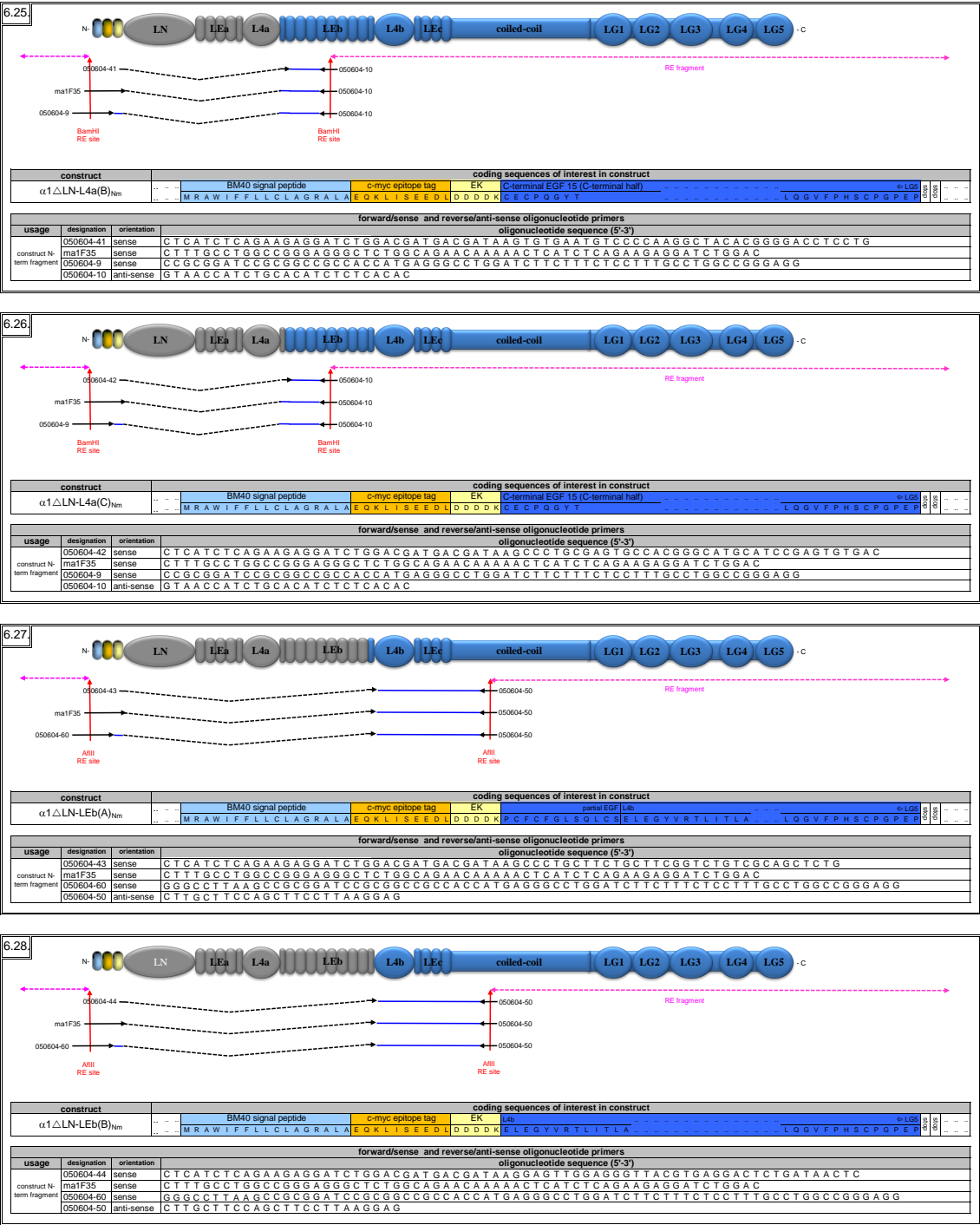


Table 6. Construction of mouse laminin α chain expression constructs and other

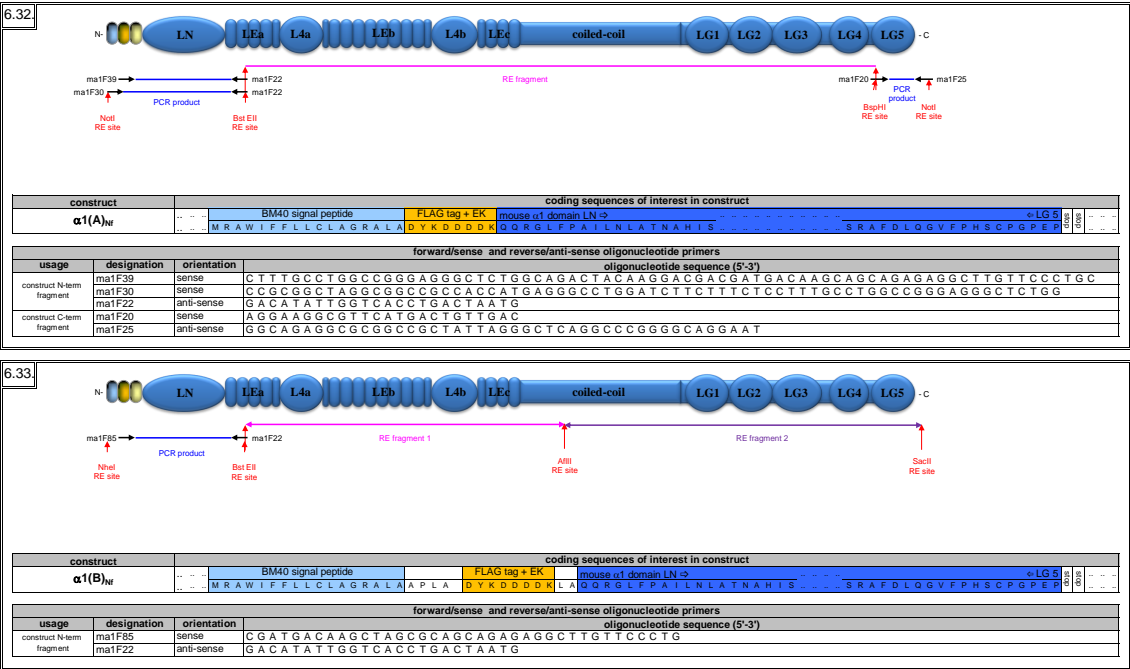


Table 7. Individual recombinant laminin chain constructs.

- β 1 based constructs

human β 1 laminin based constructs			
construct designation	description	epitope tag	selectable marker
1 β 1WT	β 1 WT with no tag	no tag	zeocin
2 β 1WT _{Nh}	β 1 WT	N-terminal HA	zeocin
3 β 1 Δ LN _{Nh}	β 1 with deletion of the LN domain	N-terminal HA	zeocin
4 β 1 Δ LN-LEa _{Nh}	β 1 with deletion of LN-LEa	N-terminal HA	zeocin
5 β 1WTN _v	β 1 WT	N-terminal VSV-G	zeocin
6 β 1 Δ LN _{Nv}	β 1 with deletion of the LN domain	N-terminal VSV-G	zeocin
7 β 1 Δ LN-LEa _{Nv}	β 1 with deletion of LN-LEa	N-terminal VSV-G	zeocin
8 β 1WT-Igk	β 1 WT with IgK signal sequence	no tag	zeocin
9 β 1WT _{Nh} -Igk	β 1 WT with IgK signal sequence	N-terminal HA	zeocin
10 β 1WT _{Nv} -Igk	β 1 WT with IgK signal sequence	N-terminal VSV-G	zeocin

Table 8. Construction of human laminin β chain expression constructs and other assorted information

8.1.

construct

construct	coding sequences of interest in construct
$\beta 1WT$	BM40 signal peptide M R A W I F F L L C L A G R A L A human $\beta 1$ domain LN \rightarrow G E F E F S Y G C A E G S C Y P A T G D L human $\beta 1$ domain LN \rightarrow S E V R S L L K D I S G K V A Y Y S T C L C-terminus h101

usage

usage	designation	orientation	oligonucleotide sequence (5'-3')
construct N-term fragment	hb1-20	sense	C T T T G C C T G G C C G G G A G G G C T C T G G C A C A G G A A C C C G A G T T C A G C T A C G G C T G
	hb1-2	sense	C G C G G C T A G C C C G C C C C A C C A T G A G G C C T G G A T C T T T C T C T T T G C C T G G C C G G G A G G G C T C T G
	hb1-re1	anti-sense	G A A A G T C A T T A T G A G A T G A G T A A A T G
	hb1-re4	sense	G C T T C T G A G G A A A C C T T G T T C A A C
construct C-term fragment	hb1-re4	sense	G C T T C T G A G G A A A C C T T G T T C A A C
	hb1-10	anti-sense	G C G G G T A C C T G T T A C A A G C A T G T G C T A T A C A C A G

8.2.

construct

construct	coding sequences of interest in construct
$\beta 1WT_{NH}$	BM40 signal peptide M R A W I F F L L C L A G R A L A HA epitope tag Y P D V P D Y A D D D D K human $\beta 1$ domain LN \rightarrow G E F E F S Y G C A E G S C Y P A T G D L human $\beta 1$ domain LN \rightarrow S E V R S L L K D I S G K V A Y Y S T C L C-terminus h101

usage

usage	designation	orientation	oligonucleotide sequence (5'-3')
construct N-term fragment	hb1-1	sense	C G C G A C G A C G A T G A C A A G C A G G A A C C C G A G T T C A G C T A C G G C T G
	hb1-2	sense	C G C T A C C C A T A C G A C G T C C C A G A C T A C G C T G A C G A C G A T G A C A A G C A G G A A C C C G
	hb1-3	sense	C G C C T T T G C C T G G C C G G G A G G G C T C T G G C A T A C C C A T A C G A C G T C C C A G A C T A C
	hb1-4	sense	C G C G G C T A G C C C G C C G C C A C C A T G A G G C C T G G A T C T T C T T T C C T T T G C C T G G C C G G G A G G G C T C T G
construct C-term fragment	hb1-re1	anti-sense	G A A A G T C A T T A T G A G A T G A G T A A A T G
	hb1-re4	sense	G C T T C T G A G G A A A C C T T G T T C A A C
	hb1-re4	sense	G C T T C T G A G G A A A C C T T G T T C A A C
	hb1-10	anti-sense	G C G G G T A C C T G T T A C A A G C A T G T G C T A T A C A C A G

8.3.

construct

construct	coding sequences of interest in construct
$\beta 1ALN_{NH}$	BM40 signal peptide M R A W I F F L L C L A G R A L A HA epitope tag Y P D V P D Y A D D D D K human $\beta 1$ domain LEa \rightarrow G N C T C Y G H A S E C A Y V D G F N E E human $\beta 1$ domain LEa \rightarrow S E V R S L L K D I S G K V A Y Y S T C L C-terminus h101

usage

usage	designation	orientation	oligonucleotide sequence (5'-3')
construct N-term fragment	hb1-23	sense	G A C G A C G A T G A C A A G G G A A A T T G C T T C T G C T A T G G T C A T G
	hb1-25	sense	T A C C C A T A C G A C G T C C C A G A C T A C G C T G A C G A C G A T G A C A A G G G A A A T T G C
	hb1-3	sense	C G C C T T T G C C T G G C C G G G A G G G C T C T G G C A T A C C C A T A C G A C G T C C C A G A C T A C
	hb1-4	sense	C G C G G C T A G C C C G C C G C C A C C A T G A G G C C T G G A T C T T C T T T C C T T T G C C T G G C C G G G A G G G C T C T G
construct C-term fragment	hb1-re5	anti-sense	C C A G G T T C C A C T T C G T T G C A C T G A C
	hb1-re4	sense	G C T T C T G A G G A A A C C T T G T T C A A C
	hb1-re4	sense	G C T T C T G A G G A A A C C T T G T T C A A C
	hb1-10	anti-sense	G C G G G T A C C T G T T A C A A G C A T G T G C T A T A C A C A G

8.4.

construct

construct	coding sequences of interest in construct
$\beta 1ALN-LEa_{NH}$	BM40 signal peptide M R A W I F F L L C L A G R A L A HA epitope tag Y P D V P D Y A D D D D K human $\beta 1$ domain LF \rightarrow G E R S Y P A T L D H Y L Y E A E A N human $\beta 1$ domain LF \rightarrow S E V R S L L K D I S G K V A Y Y S T C L C-terminus h101

usage

usage	designation	orientation	oligonucleotide sequence (5'-3')
construct N-term fragment	hb1-28	sense	G A C G A C G A T G A C A A G G T G G A A C C T G G T T A C T A C T T T G C C A C
	hb1-30	sense	T A C C C A T A C G A C G T C C C A G A C T A C G C T G A C G A C G A T G A C A A G G G A A A T T G C
	hb1-3	sense	C G C C T T T G C C T G G C C G G G A G G G C T C T G G C A T A C C C A T A C G A C G T C C C A G A C T A C
	hb1-4	sense	C C C G G C T A G C C C G C C G C C A C C A T G A G G C C T G G A T C T T C T T T C C T T T G C C T G G C C G G G A G G G C T C T G
construct C-term fragment	hb1-re7	anti-sense	G T T T C C C A G G C A C T T T G G T G A C
	hb1-re7	anti-sense	G T T T C C C A G G C A C T T T G G T G A C
	hb1-re4	sense	G C T T C T G A G G A A A C C T T G T T C A A C
	hb1-10	anti-sense	G C G G G T A C C T G T T A C A A G C A T G T G C T A T A C A C A G

Table 8. Construction of human laminin β chain expression constructs and other assorted information

8.5.																																	
construct		<table border="1"> <thead> <tr> <th>construct</th><th>BM40 signal peptide</th><th>VSV-G epitope tag</th><th>coding sequences of interest in construct</th></tr> </thead> <tbody> <tr> <td>$\beta 1WT_Nv$</td><td>M R A W I F F L L C L A G R A L A</td><td>Y T D I G M N R L G K</td><td>D D D D K G N C F Y S Y G A E G S C Y P A T G D L V R S L L K D I S G K Y A Y T S T C</td></tr> </tbody> </table>		construct	BM40 signal peptide	VSV-G epitope tag	coding sequences of interest in construct	$\beta 1WT_Nv$	M R A W I F F L L C L A G R A L A	Y T D I G M N R L G K	D D D D K G N C F Y S Y G A E G S C Y P A T G D L V R S L L K D I S G K Y A Y T S T C																						
construct	BM40 signal peptide	VSV-G epitope tag	coding sequences of interest in construct																														
$\beta 1WT_Nv$	M R A W I F F L L C L A G R A L A	Y T D I G M N R L G K	D D D D K G N C F Y S Y G A E G S C Y P A T G D L V R S L L K D I S G K Y A Y T S T C																														
usage		<table border="1"> <thead> <tr> <th>usage</th><th>designation</th><th>orientation</th><th>oligonucleotide sequence (5'-3')</th></tr> </thead> <tbody> <tr> <td rowspan="4">construct N-term fragment</td><td>hb1-1</td><td>sense</td><td>C G C G A C G A C G A T G A C A A G C A G G A A C C C G A G T T C A G C T A C G G C T G</td></tr> <tr> <td>hb1-5</td><td>sense</td><td>T A C A C T G A T A T C G A A A T G A A C C G C T G G G T A A G G A C G A C G A T G A C A A G C A G G A A C C C G</td></tr> <tr> <td>hb1-6</td><td>sense</td><td>C T T T G C C T G G C C G G G A G G G C T C T G G C A T A C A C T G A T A T C G A A A T G A A C C C G</td></tr> <tr> <td>hb1-4</td><td>sense</td><td>C G C G G C T A G C C C G C G C C A C C A T G A G G G C C T G G A T C T T T C T C T T T G C C T T G C C T G G C C G G G A G G G C T C T G</td></tr> <tr> <td rowspan="4">construct C-term fragment</td><td>hb1-re1</td><td>anti-sense</td><td>G A A A G T C A T T A T G A G A T G A G T A A A T G</td></tr> <tr> <td>hb1-re4</td><td>sense</td><td>G C T T C T G A G G A A A C C T T G T T C A A C</td></tr> <tr> <td>hb1-10</td><td>anti-sense</td><td>G C G G G T A C C T G T T A C A A G C A T G T G C T A T A C A G</td></tr> <tr> <td>hb1-10</td><td>anti-sense</td><td>G C G G G T A C C T G T T A C A A G C A T G T G C T A T A C A G</td></tr> </tbody> </table>		usage	designation	orientation	oligonucleotide sequence (5'-3')	construct N-term fragment	hb1-1	sense	C G C G A C G A C G A T G A C A A G C A G G A A C C C G A G T T C A G C T A C G G C T G	hb1-5	sense	T A C A C T G A T A T C G A A A T G A A C C G C T G G G T A A G G A C G A C G A T G A C A A G C A G G A A C C C G	hb1-6	sense	C T T T G C C T G G C C G G G A G G G C T C T G G C A T A C A C T G A T A T C G A A A T G A A C C C G	hb1-4	sense	C G C G G C T A G C C C G C G C C A C C A T G A G G G C C T G G A T C T T T C T C T T T G C C T T G C C T G G C C G G G A G G G C T C T G	construct C-term fragment	hb1-re1	anti-sense	G A A A G T C A T T A T G A G A T G A G T A A A T G	hb1-re4	sense	G C T T C T G A G G A A A C C T T G T T C A A C	hb1-10	anti-sense	G C G G G T A C C T G T T A C A A G C A T G T G C T A T A C A G	hb1-10	anti-sense	G C G G G T A C C T G T T A C A A G C A T G T G C T A T A C A G
usage	designation	orientation	oligonucleotide sequence (5'-3')																														
construct N-term fragment	hb1-1	sense	C G C G A C G A C G A T G A C A A G C A G G A A C C C G A G T T C A G C T A C G G C T G																														
	hb1-5	sense	T A C A C T G A T A T C G A A A T G A A C C G C T G G G T A A G G A C G A C G A T G A C A A G C A G G A A C C C G																														
	hb1-6	sense	C T T T G C C T G G C C G G G A G G G C T C T G G C A T A C A C T G A T A T C G A A A T G A A C C C G																														
	hb1-4	sense	C G C G G C T A G C C C G C G C C A C C A T G A G G G C C T G G A T C T T T C T C T T T G C C T T G C C T G G C C G G G A G G G C T C T G																														
construct C-term fragment	hb1-re1	anti-sense	G A A A G T C A T T A T G A G A T G A G T A A A T G																														
	hb1-re4	sense	G C T T C T G A G G A A A C C T T G T T C A A C																														
	hb1-10	anti-sense	G C G G G T A C C T G T T A C A A G C A T G T G C T A T A C A G																														
	hb1-10	anti-sense	G C G G G T A C C T G T T A C A A G C A T G T G C T A T A C A G																														
8.6.																																	
construct		<table border="1"> <thead> <tr> <th>construct</th><th>BM40 signal peptide</th><th>VSV-G epitope tag</th><th>coding sequences of interest in construct</th></tr> </thead> <tbody> <tr> <td>$\beta 1\Delta LN_Nh$</td><td>M R A W I F F L L C L A G R A L A</td><td>Y T D I G M N R L G K</td><td>D D D D K G N C F Y G H A S E C A P V D G F N E E V R S L L K D I S G K Y A Y T S T C</td></tr> </tbody> </table>		construct	BM40 signal peptide	VSV-G epitope tag	coding sequences of interest in construct	$\beta 1\Delta LN_Nh$	M R A W I F F L L C L A G R A L A	Y T D I G M N R L G K	D D D D K G N C F Y G H A S E C A P V D G F N E E V R S L L K D I S G K Y A Y T S T C																						
construct	BM40 signal peptide	VSV-G epitope tag	coding sequences of interest in construct																														
$\beta 1\Delta LN_Nh$	M R A W I F F L L C L A G R A L A	Y T D I G M N R L G K	D D D D K G N C F Y G H A S E C A P V D G F N E E V R S L L K D I S G K Y A Y T S T C																														
usage		<table border="1"> <thead> <tr> <th>usage</th><th>designation</th><th>orientation</th><th>oligonucleotide sequence (5'-3')</th></tr> </thead> <tbody> <tr> <td rowspan="4">construct N-term fragment</td><td>hb1-50</td><td>sense</td><td>G A C G A C G A T G A C A A G G G A A A T T G C T T C T G C T A T G G T C A T G C C A G</td></tr> <tr> <td>hb1-51</td><td>sense</td><td>T A C C C A T A C G A C G T C C C A G A C T A C G T G A C G A C G A T G A C A A G G G A A T T G</td></tr> <tr> <td>hb1-3</td><td>sense</td><td>C G C C T T T G C C T G G C C G G G A G G G C T C T G G C A T A C C C A T A C G A C G T C C C A G A C T A C</td></tr> <tr> <td>hb1-4</td><td>sense</td><td>C G C G G C T A G C C C G C G C C A C C A T G A G G G C C T G G A T C T T C T T T C C T T T G C C T G G C C G G G A G G G C T C T G</td></tr> <tr> <td rowspan="4">construct C-term fragment</td><td>hb1-re5</td><td>anti-sense</td><td>C A G G T T C C A C T T C G T T G C A C T G A C</td></tr> <tr> <td>hb1-re4</td><td>sense</td><td>G C T T C T G A G G A A A C C T T G T T C A A C</td></tr> <tr> <td>hb1-10</td><td>anti-sense</td><td>G C G G G T A C C T G T T A C A A G C A T G T G C T A T A C A G</td></tr> <tr> <td>hb1-10</td><td>anti-sense</td><td>G C G G G T A C C T G T T A C A A G C A T G T G C T A T A C A G</td></tr> </tbody> </table>		usage	designation	orientation	oligonucleotide sequence (5'-3')	construct N-term fragment	hb1-50	sense	G A C G A C G A T G A C A A G G G A A A T T G C T T C T G C T A T G G T C A T G C C A G	hb1-51	sense	T A C C C A T A C G A C G T C C C A G A C T A C G T G A C G A C G A T G A C A A G G G A A T T G	hb1-3	sense	C G C C T T T G C C T G G C C G G G A G G G C T C T G G C A T A C C C A T A C G A C G T C C C A G A C T A C	hb1-4	sense	C G C G G C T A G C C C G C G C C A C C A T G A G G G C C T G G A T C T T C T T T C C T T T G C C T G G C C G G G A G G G C T C T G	construct C-term fragment	hb1-re5	anti-sense	C A G G T T C C A C T T C G T T G C A C T G A C	hb1-re4	sense	G C T T C T G A G G A A A C C T T G T T C A A C	hb1-10	anti-sense	G C G G G T A C C T G T T A C A A G C A T G T G C T A T A C A G	hb1-10	anti-sense	G C G G G T A C C T G T T A C A A G C A T G T G C T A T A C A G
usage	designation	orientation	oligonucleotide sequence (5'-3')																														
construct N-term fragment	hb1-50	sense	G A C G A C G A T G A C A A G G G A A A T T G C T T C T G C T A T G G T C A T G C C A G																														
	hb1-51	sense	T A C C C A T A C G A C G T C C C A G A C T A C G T G A C G A C G A T G A C A A G G G A A T T G																														
	hb1-3	sense	C G C C T T T G C C T G G C C G G G A G G G C T C T G G C A T A C C C A T A C G A C G T C C C A G A C T A C																														
	hb1-4	sense	C G C G G C T A G C C C G C G C C A C C A T G A G G G C C T G G A T C T T C T T T C C T T T G C C T G G C C G G G A G G G C T C T G																														
construct C-term fragment	hb1-re5	anti-sense	C A G G T T C C A C T T C G T T G C A C T G A C																														
	hb1-re4	sense	G C T T C T G A G G A A A C C T T G T T C A A C																														
	hb1-10	anti-sense	G C G G G T A C C T G T T A C A A G C A T G T G C T A T A C A G																														
	hb1-10	anti-sense	G C G G G T A C C T G T T A C A A G C A T G T G C T A T A C A G																														
8.7.																																	
construct		<table border="1"> <thead> <tr> <th>construct</th><th>BM40 signal peptide</th><th>VSV-G epitope tag</th><th>coding sequences of interest in construct</th></tr> </thead> <tbody> <tr> <td>$\beta 1\Delta LN-LEa_Nh$</td><td>M R A W I F F L L C L A G R A L A</td><td>Y T D I G M N R L G K</td><td>D D D D K V E P S Y T A T L D N Y L Y A E E A N V R S L L K D I S G K Y A Y T S T C</td></tr> </tbody> </table>		construct	BM40 signal peptide	VSV-G epitope tag	coding sequences of interest in construct	$\beta 1\Delta LN-LEa_Nh$	M R A W I F F L L C L A G R A L A	Y T D I G M N R L G K	D D D D K V E P S Y T A T L D N Y L Y A E E A N V R S L L K D I S G K Y A Y T S T C																						
construct	BM40 signal peptide	VSV-G epitope tag	coding sequences of interest in construct																														
$\beta 1\Delta LN-LEa_Nh$	M R A W I F F L L C L A G R A L A	Y T D I G M N R L G K	D D D D K V E P S Y T A T L D N Y L Y A E E A N V R S L L K D I S G K Y A Y T S T C																														
usage		<table border="1"> <thead> <tr> <th>usage</th><th>designation</th><th>orientation</th><th>oligonucleotide sequence (5'-3')</th></tr> </thead> <tbody> <tr> <td rowspan="4">construct N-term fragment</td><td>hb1-60</td><td>sense</td><td>G A C G A C G A T G A C A A G G T G G A A C C T G G T T A C T A C T T T G C C A C C C T G</td></tr> <tr> <td>hb1-61</td><td>sense</td><td>T A C C C A T A C G A C G T C C C A G A C T A C G T G A C G A C G A T G A C A A G G T G G A A C</td></tr> <tr> <td>hb1-3</td><td>sense</td><td>C G C G C T A G C C C G C G C C A C C A T G G A G A C A C A C A C A C T C T G C T A T A C C C A T A C G A C G T C C C A G A C T A C</td></tr> <tr> <td>hb1-4</td><td>sense</td><td>C G C G G C T A G C C C G C G C C A C C A T G A G G G C C T G G A T C T T C T T T C C T T T G C C T G G C C G G G A G G G C T C T G</td></tr> <tr> <td rowspan="4">construct C-term fragment</td><td>hb1-re7</td><td>anti-sense</td><td>G G T T T C C C A G G C A C T G T T G G T G A C</td></tr> <tr> <td>hb1-re4</td><td>sense</td><td>G C T T C T G A G G A A A C C T T G T T C A A C</td></tr> <tr> <td>hb1-10</td><td>anti-sense</td><td>G C G G G T A C C T G T T A C A A G C A T G T G C T A T A C A G</td></tr> <tr> <td>hb1-10</td><td>anti-sense</td><td>G C G G G T A C C T G T T A C A A G C A T G T G C T A T A C A G</td></tr> </tbody> </table>		usage	designation	orientation	oligonucleotide sequence (5'-3')	construct N-term fragment	hb1-60	sense	G A C G A C G A T G A C A A G G T G G A A C C T G G T T A C T A C T T T G C C A C C C T G	hb1-61	sense	T A C C C A T A C G A C G T C C C A G A C T A C G T G A C G A C G A T G A C A A G G T G G A A C	hb1-3	sense	C G C G C T A G C C C G C G C C A C C A T G G A G A C A C A C A C A C T C T G C T A T A C C C A T A C G A C G T C C C A G A C T A C	hb1-4	sense	C G C G G C T A G C C C G C G C C A C C A T G A G G G C C T G G A T C T T C T T T C C T T T G C C T G G C C G G G A G G G C T C T G	construct C-term fragment	hb1-re7	anti-sense	G G T T T C C C A G G C A C T G T T G G T G A C	hb1-re4	sense	G C T T C T G A G G A A A C C T T G T T C A A C	hb1-10	anti-sense	G C G G G T A C C T G T T A C A A G C A T G T G C T A T A C A G	hb1-10	anti-sense	G C G G G T A C C T G T T A C A A G C A T G T G C T A T A C A G
usage	designation	orientation	oligonucleotide sequence (5'-3')																														
construct N-term fragment	hb1-60	sense	G A C G A C G A T G A C A A G G T G G A A C C T G G T T A C T A C T T T G C C A C C C T G																														
	hb1-61	sense	T A C C C A T A C G A C G T C C C A G A C T A C G T G A C G A C G A T G A C A A G G T G G A A C																														
	hb1-3	sense	C G C G C T A G C C C G C G C C A C C A T G G A G A C A C A C A C A C T C T G C T A T A C C C A T A C G A C G T C C C A G A C T A C																														
	hb1-4	sense	C G C G G C T A G C C C G C G C C A C C A T G A G G G C C T G G A T C T T C T T T C C T T T G C C T G G C C G G G A G G G C T C T G																														
construct C-term fragment	hb1-re7	anti-sense	G G T T T C C C A G G C A C T G T T G G T G A C																														
	hb1-re4	sense	G C T T C T G A G G A A A C C T T G T T C A A C																														
	hb1-10	anti-sense	G C G G G T A C C T G T T A C A A G C A T G T G C T A T A C A G																														
	hb1-10	anti-sense	G C G G G T A C C T G T T A C A A G C A T G T G C T A T A C A G																														
8.8.																																	
construct		<table border="1"> <thead> <tr> <th>construct</th><th>Igc signal peptide</th><th>human $\beta 1$ domain LN \rightarrow</th><th>coding sequences of interest in construct</th></tr> </thead> <tbody> <tr> <td>$\beta 1WT-Igc$</td><td>M E T D T L L L W L L L W V P G S T G D</td><td></td><td>D E P E S Y S G A E G S C Y P A T G D L V R S L L K D I S G K Y A Y T S T C</td></tr> </tbody> </table>		construct	Igc signal peptide	human $\beta 1$ domain LN \rightarrow	coding sequences of interest in construct	$\beta 1WT-Igc$	M E T D T L L L W L L L W V P G S T G D		D E P E S Y S G A E G S C Y P A T G D L V R S L L K D I S G K Y A Y T S T C																						
construct	Igc signal peptide	human $\beta 1$ domain LN \rightarrow	coding sequences of interest in construct																														
$\beta 1WT-Igc$	M E T D T L L L W L L L W V P G S T G D		D E P E S Y S G A E G S C Y P A T G D L V R S L L K D I S G K Y A Y T S T C																														
usage		<table border="1"> <thead> <tr> <th>usage</th><th>designation</th><th>orientation</th><th>oligonucleotide sequence (5'-3')</th></tr> </thead> <tbody> <tr> <td rowspan="4">construct N-term fragment</td><td>hb1-21</td><td>sense</td><td>C T G C T C T G G T T C C A G G T T C C A C T G G T G A C C A G G A A C C C G A G T T C A G C T A C G G C T G</td></tr> <tr> <td>hb1-8</td><td>sense</td><td>C G C G C T A G C C C G C G C C A C C A T G G A G A C A C A C A C A C T C T G C T A T G G G T A C T G C T G C T G G G T T C C A G G T T C C A C T G</td></tr> <tr> <td>hb1-re1</td><td>anti-sense</td><td>G A A A G T C A T T A T G A G A T G A G T A A A T G</td></tr> <tr> <td>hb1-re4</td><td>sense</td><td>G C T T C T G A G G A A A C C T T G T T C A A C</td></tr> <tr> <td rowspan="2">construct C-term fragment</td><td>hb1-10</td><td>anti-sense</td><td>G C G G G T A C C T G T T A C A A G C A T G T G C T A T A C A G</td></tr> <tr> <td>hb1-10</td><td>anti-sense</td><td>G C G G G T A C C T G T T A C A A G C A T G T G C T A T A C A G</td></tr> </tbody> </table>		usage	designation	orientation	oligonucleotide sequence (5'-3')	construct N-term fragment	hb1-21	sense	C T G C T C T G G T T C C A G G T T C C A C T G G T G A C C A G G A A C C C G A G T T C A G C T A C G G C T G	hb1-8	sense	C G C G C T A G C C C G C G C C A C C A T G G A G A C A C A C A C A C T C T G C T A T G G G T A C T G C T G C T G G G T T C C A G G T T C C A C T G	hb1-re1	anti-sense	G A A A G T C A T T A T G A G A T G A G T A A A T G	hb1-re4	sense	G C T T C T G A G G A A A C C T T G T T C A A C	construct C-term fragment	hb1-10	anti-sense	G C G G G T A C C T G T T A C A A G C A T G T G C T A T A C A G	hb1-10	anti-sense	G C G G G T A C C T G T T A C A A G C A T G T G C T A T A C A G						
usage	designation	orientation	oligonucleotide sequence (5'-3')																														
construct N-term fragment	hb1-21	sense	C T G C T C T G G T T C C A G G T T C C A C T G G T G A C C A G G A A C C C G A G T T C A G C T A C G G C T G																														
	hb1-8	sense	C G C G C T A G C C C G C G C C A C C A T G G A G A C A C A C A C A C T C T G C T A T G G G T A C T G C T G C T G G G T T C C A G G T T C C A C T G																														
	hb1-re1	anti-sense	G A A A G T C A T T A T G A G A T G A G T A A A T G																														
	hb1-re4	sense	G C T T C T G A G G A A A C C T T G T T C A A C																														
construct C-term fragment	hb1-10	anti-sense	G C G G G T A C C T G T T A C A A G C A T G T G C T A T A C A G																														
	hb1-10	anti-sense	G C G G G T A C C T G T T A C A A G C A T G T G C T A T A C A G																														

Table 8. Construction of human laminin β chain expression constructs and other assorted information

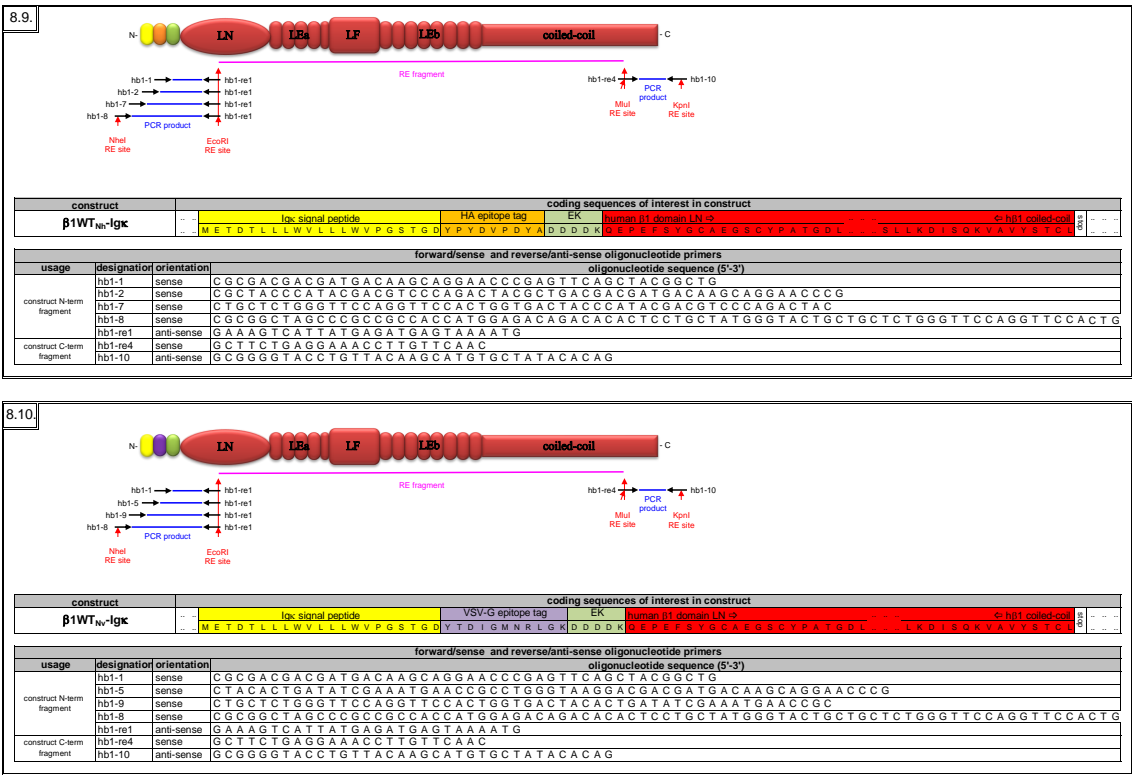


Table 9 . Individual recombinant laminin chain constructs.

- γ 1 based constructs

human γ 1 laminin based constructs			
construct designation	description	epitope tag	selectable marker
1 γ 1WT _{Ct}	γ 1 WT with C-terminal FLAG tag	C-terminal FLAG	G418
2 γ 1WT	γ 1 WT with no tag	no tag	G418
3 γ 1 Δ LN _{Ct}	γ 1 with deletion of the LN domain	C-terminal FLAG	G418
4 γ 1 Δ LN-LEa _{Ct}	γ 1 with deletion of the LN-LEa domain	C-terminal FLAG	G418

Table 10. Construction of human laminin γ chain expression constructs and other assorted information

10.1.

construct

coding sequences of interest in construct	
human v1 signal peptide	human v1 domain LN \rightarrow
MRGSHRAAPALRPGRGLWPVLAVALAAAAAGCAQAA	MD ECTDEGG

usage

designation	orientation	oligonucleotide sequence (5'-3')
construct 1st N-term fragment		
construct 2nd N-term fragment		
new N-term fragment		

[see reference 296]

10.2.

construct

coding sequences of interest in construct	
human v1 signal peptide	human v1 domain LN \rightarrow
MRGSHRAAPALRPGRGLWPVLAVALAAAAAGCAQAA	MD ECTDEGG

usage

designation	orientation	oligonucleotide sequence (5'-3')
construct 1st N-term fragment		
construct 2nd N-term fragment		
new N-term fragment		

[see reference 296]

10.3.

construct

coding sequences of interest in construct	
human v1 signal peptide	human v1 domain LEa \rightarrow
MRGSHRAAPALRPGRGLWPVLAVALAAAAAGCAQAA	MD ECTDEGG

usage

designation	orientation	oligonucleotide sequence (5'-3')
construct N-term fragment		
gg1	sense	GCCCAGGCAGCCGGCAGATGTAAATGTAAATGGACACG
gg3	sense	GCTGGCCGTGCTGGCGCGCCGCCCGCGGGCTGTGCCAGGCAGCCGGCAGATGTAAATG
gg5	anti-sense	CTCCAAAGTAGCCATCATCACAGAG

10.4.

construct

coding sequences of interest in construct	
human v1 signal peptide	human v1 domain L4 \rightarrow
MRGSHRAAPALRPGRGLWPVLAVALAAAAAGCAQAA	MD ECTDEGG

usage

designation	orientation	oligonucleotide sequence (5'-3')
construct N-term fragment		
gg0	sense	GGCTGTGCCAGGCAGCCGGCTACAGTGTTTATCTATCTCTCTAC
gg4	sense	GCTGGCCGTGCTGGCGCGCCGCCCGCGGGCTGTGCCAGGCAGCCGGCTACAGT
gg5	anti-sense	CAC TTGGATAGGAATTGCCCTGAGC

Table 11. Recombinant heterotrimeric laminin - construct composition

	recombinant heterotrimeric laminin designation	chain construct composition			additional comments
		α (mouse)	β (human)	γ (human)	
1	Lm-111 _{o/o}	α 1WT	β 1WT	γ 1WT	
2	Lm-111 _{Nm/Nh/Cf}	α 1WT _{Nm}	β 1WT _{Nh}	γ 1WT _{Cf}	formerly WTb
3	Lm-111 _{Nm3/Nh/Cf}	α 1WT _{Nm3}	β 1WT _{Nh}	γ 1WT _{Cf}	
4	Lm-111 _{Ni/Nh/Cf}	α 1WT _{Ni}	β 1WT _{Nh}	γ 1WT _{Cf}	
5	Lm-111 _{Nv/Nh/Cf}	α 1WT _{Nv}	β 1WT _{Nh}	γ 1WT _{Cf}	
6	Lm-111 _{Nh/Nh/Cf}	α 1WT _{Nh}	β 1WT _{Nh}	γ 1WT _{Cf}	
7	Lm-111 _{Nc/Nh/Cf}	α 1WT _{Nc}	β 1WT _{Nh}	γ 1WT _{Cf}	
8	Lm-111 _{Cf/Nh/Cf}	α 1WT _{Cf}	β 1WT _{Nh}	γ 1WT _{Cf}	
9	Lm-111 _{Nm/Nh/o}	α 1WT _{Nm}	β 1WT _{Nh}	γ 1WT	formerly WTa
10	Lm-111 _{Nm3/Nh/o}	α 1WT _{Nm3}	β 1WT _{Nh}	γ 1WT	
11	Lm-111 _{Ni/Nh/o}	α 1WT _{Ni}	β 1WT _{Nh}	γ 1WT	
12	Lm-111 _{Nv/Nh/o}	α 1WT _{Nv}	β 1WT _{Nh}	γ 1WT	
13	Lm-111 _{Nh/Nh/o}	α 1WT _{Nh}	β 1WT _{Nh}	γ 1WT	
14	Lm-111 _{Nc/Nh/o}	α 1WT _{Nc}	β 1WT _{Nh}	γ 1WT	
15	Lm-111 _{Cf/Nh/o}	α 1WT _{Cf}	β 1WT _{Nh}	γ 1WT	
16	Lm-111 α Δ LN _{Nm/Nh/Cf}	α 1 Δ LN _{Nm}	β 1WT _{Nh}	γ 1WT _{Cf}	
17	Lm-111 α Δ LN-LEa _{Nm/Nh/Cf}	α 1 Δ LN-LEa(A) _{Nm}	β 1WT _{Nh}	γ 1WT _{Cf}	
18	Lm-111 α Δ LN-LEa(B) _{Nm/Nh/Cf}	α 1 Δ LN-LEa(B) _{Nm}	β 1WT _{Nh}	γ 1WT _{Cf}	
19	Lm-111 α Δ LN-LEa(C) _{Nm/Nh/Cf}	α 1 Δ LN-LEa(C) _{Nm}	β 1WT _{Nh}	γ 1WT _{Cf}	
20	Lm-111 α Δ LN-L4b(C) _{Nm/Nh/Cf}	α 1 Δ LN-L4b(C) _{Nm}	β 1WT _{Nh}	γ 1WT _{Cf}	
21	Lm-111 α Δ LG1-5 (A) _{Nm/Nh/Cf}	α 1 Δ LG1-5 (A) _{Nm}	β 1WT _{Nh}	γ 1WT _{Cf}	
22	Lm-111 α Δ LG1-5(B) _{Nm/Nh/Cf}	α 1 Δ LG1-5(B) _{Nm}	β 1WT _{Nh}	γ 1WT _{Cf}	
23	Lm-111 α Δ LG1-3 _{Nm/Nh/Cf}	α 1 Δ LG1-3 _{Nm}	β 1WT _{Nh}	γ 1WT _{Cf}	
24	Lm-111 α Δ LG4-5 _{Nm/Nh/Cf}	α 1 Δ LG4-5 _{Nm}	β 1WT _{Nh}	γ 1WT _{Cf}	
25	Lm-111 α Δ LG1-5(A) _{Cf/Nh/Cf}	α 1 Δ LG1-5(A) _{Cf}	β 1WT _{Nh}	γ 1WT _{Cf}	
26	Lm-111 α Δ LN-L4a(A) _{Nm/Nh/Cf}	α 1 Δ LN-L4a(A) _{Nm}	β 1WT _{Nh}	γ 1WT _{Cf}	
27	Lm-111 α Δ LN-L4a(B) _{Nm/Nh/Cf}	α 1 Δ LN-L4a(B) _{Nm}	β 1WT _{Nh}	γ 1WT _{Cf}	
28	Lm-111 α Δ LN-L4a(C) _{Nm/Nh/Cf}	α 1 Δ LN-L4a(C) _{Nm}	β 1WT _{Nh}	γ 1WT _{Cf}	
29	Lm-111 α Δ LN-LEb(A) _{Nm/Nh/Cf}	α 1 Δ LN-LEb(A) _{Nm}	β 1WT _{Nh}	γ 1WT _{Cf}	
30	Lm-111 α Δ LN-LEb(B) _{Nm/Nh/Cf}	α 1 Δ LN-LEb(B) _{Nm}	β 1WT _{Nh}	γ 1WT _{Cf}	
31	Lm-111 α Δ LN-LEb(C) _{Nm/Nh/Cf}	α 1 Δ LN-LEb(C) _{Nm}	β 1WT _{Nh}	γ 1WT _{Cf}	
32	Lm-111 α Δ LN-L4b(A) _{Nm/Nh/Cf}	α 1 Δ LN-L4b(A) _{Nm}	β 1WT _{Nh}	γ 1WT _{Cf}	
33	Lm-111 α Δ LN-L4b(B) _{Nm/Nh/Cf}	α 1 Δ LN-L4b(B) _{Nm}	β 1WT _{Nh}	γ 1WT _{Cf}	
34	Lm-111 α Δ LN _{Nm/Nh/o}	α 1 Δ LN _{Nm}	β 1WT _{Nh}	γ 1WT	
35	Lm-111 α Δ LN-LEa _{Nm/Nh/o}	α 1 Δ LN-LEa(A) _{Nm}	β 1WT _{Nh}	γ 1WT	
36	Lm-111 α Δ LN-LEa(B) _{Nm/Nh/o}	α 1 Δ LN-LEa(B) _{Nm}	β 1WT _{Nh}	γ 1WT	
37	Lm-111 α Δ LN-LEa(C) _{Nm/Nh/o}	α 1 Δ LN-LEa(C) _{Nm}	β 1WT _{Nh}	γ 1WT	
38	Lm-111 α Δ LN-L4b(C) _{Nm/Nh/o}	α 1 Δ LN-L4b(C) _{Nm}	β 1WT _{Nh}	γ 1WT	
39	Lm-111 α Δ LG1-5 (A) _{Nm/Nh/o}	α 1 Δ LG1-5 (A) _{Nm}	β 1WT _{Nh}	γ 1WT	
40	Lm-111 α Δ LG1-5(B) _{Nm/Nh/o}	α 1 Δ LG1-5(B) _{Nm}	β 1WT _{Nh}	γ 1WT	
41	Lm-111 α Δ LG1-3 _{Nm/Nh/o}	α 1 Δ LG1-3 _{Nm}	β 1WT _{Nh}	γ 1WT	
42	Lm-111 α Δ LG4-5 _{Nm/Nh/o}	α 1 Δ LG4-5 _{Nm}	β 1WT _{Nh}	γ 1WT	
43	Lm-111 α /RKR _{2721Nm/Nh/Cf}	α 1/RKR _{2721Nm}	β 1WT _{Nh}	γ 1WT _{Cf}	formerly A'
44	Lm-111 α /KRK _{2793Nm/Nh/Cf}	α 1/KRK _{2793Nm}	β 1WT _{Nh}	γ 1WT _{Cf}	formerly G'
45	Lm-111 α /RAR _{2833Nm/Nh/Cf}	α 1/RAR _{2833Nm}	β 1WT _{Nh}	γ 1WT _{Cf}	formerly I
46	Lm-111 α /RKR _{2721Nm/Nh/o}	α 1/RKR _{2721Nm}	β 1WT _{Nh}	γ 1WT	
47	Lm-111 α /KRK _{2793Nm/Nh/o}	α 1/KRK _{2793Nm}	β 1WT _{Nh}	γ 1WT	
48	Lm-111 α /RAR _{2833Nm/Nh/o}	α 1/RAR _{2833Nm}	β 1WT _{Nh}	γ 1WT	
8	Lm-111 _{Cf/Nh/Cf}	α 1WT _{Cf}	β 1WT _{Nh}	γ 1WT _{Cf}	
15	Lm-111 _{Cf/Nh/o}	α 1WT _{Cf}	β 1WT _{Nh}	γ 1WT	
49	Lm-111 _{Cf/o/Cf}	α 1WT _{Cf}	β 1WT	γ 1WT _{Cf}	
50	Lm-111 _{Cf/o/o}	α 1WT _{Cf}	β 1WT	γ 1WT	

The designation format of Lm-111"**N**" "**x**" / "**y**" / "**z**" is utilized to refer to the heterotrimeric Lm-111s; where "**N**" denotes any alteration to the native sequence of the chain, "**x**" denotes the α chain tag, "**y**" denotes the β chain tag, and "**z**" denotes the γ chain tag.

♻ and no color fill of the row = denotes a combination already described in the table but shown again in order to provide a reference

Table 11. Recombinant heterotrimeric laminin - construct composition (continued)

	recombinant heterotrimeric laminin	chain construct composition			additional comments
		α	β	γ	
1	Lm-111 _{0/0/0}	α 1WT	β 1WT	γ 1WT	U
51	Lm-111 _{0/Nh/0}	α 1WT	β 1WT _{Nh}	γ 1WT	
52	Lm-111 $\beta\Delta$ LN _{0/Nh/0}	α 1WT	β 1 Δ LN _{Nh}	γ 1WT	
53	Lm-111 $\beta\Delta$ LN-LEa _{0/Nh/0}	α 1WT	β 1 Δ LN-LEa _{Nh}	γ 1WT	U
54	Lm-111 _{0/Nh/Cf}	α 1WT	β 1WT _{Nh}	γ 1WT _{Cf}	
55	Lm-111 $\beta\Delta$ LN _{0/Nh/Cf}	α 1WT	β 1 Δ LN _{Nh}	γ 1WT _{Cf}	
56	Lm-111 $\beta\Delta$ LN-LEa _{0/Nh/Cf}	α 1WT	β 1 Δ LN-LEa _{Nh}	γ 1WT _{Cf}	U
57	Lm-111 _{0/Nv/0}	α 1WT	β 1WT _{Nv}	γ 1WT	
58	Lm-111 $\beta\Delta$ LN _{0/Nv/0}	α 1WT	β 1 Δ LN _{Nv}	γ 1WT	
59	Lm-111 $\beta\Delta$ LN-LEa _{0/Nv/0}	α 1WT	β 1 Δ LN-LEa _{Nv}	γ 1WT	U
60	Lm-111 _{0/Nv/Cf}	α 1WT	β 1WT _{Nv}	γ 1WT _{Cf}	
61	Lm-111 $\beta\Delta$ LN _{0/Nv/Cf}	α 1WT	β 1 Δ LN _{Nv}	γ 1WT _{Cf}	
62	Lm-111 $\beta\Delta$ LN-LEa _{0/Nv/Cf}	α 1WT	β 1 Δ LN-LEa _{Nv}	γ 1WT _{Cf}	U
63	Lm-111 β -IgK _{0/0/0}	α 1WT	β 1WT-IgK	γ 1WT _{Cf}	
64	Lm-111 β -IgK _{0/Nh/0}	α 1WT	β 1WT _{Nh} -IgK	γ 1WT _{Cf}	
65	Lm-111 β -IgK _{0/Nv/0}	α 1WT	β 1WT _{Nv} -IgK	γ 1WT _{Cf}	U
2	Lm-111 _{Nm/Nh/Cf}	α 1WT _{Nm}	β 1WT _{Nh}	γ 1WT _{Cf}	
66	Lm-111 $\beta\Delta$ LN _{Nm/Nh/Cf}	α 1WT _{Nm}	β 1 Δ LN _{Nh}	γ 1WT _{Cf}	U
67	Lm-111 $\beta\Delta$ LN-LEa _{Nm/Nh/Cf}	α 1WT _{Nm}	β 1 Δ LN-LEa _{Nh}	γ 1WT _{Cf}	
9	Lm-111 _{Nm/Nh/0}	α 1WT _{Nm}	β 1WT _{Nh}	γ 1WT	U
68	Lm-111 $\beta\Delta$ LN _{Nm/Nh/0}	α 1WT _{Nm}	β 1 Δ LN _{Nh}	γ 1WT	
69	Lm-111 $\beta\Delta$ LN-LEa _{Nm/Nh/0}	α 1WT _{Nm}	β 1 Δ LN-LEa _{Nh}	γ 1WT	
2	Lm-111 _{Nm/Nh/Cf}	α 1WT _{Nm}	β 1WT _{Nh}	γ 1WT _{Cf}	U
70	Lm-111 $\gamma\Delta$ LN _{Nm/Nh/Cf}	α 1WT _{Nm}	β 1WT _{Nh}	γ 1 Δ LN _{Cf}	
71	Lm-111 $\gamma\Delta$ LN-LEa _{Nm/Nh/Cf}	α 1WT _{Nm}	β 1WT _{Nh}	γ 1 Δ LN-LEa _{Cf}	
72	Lm-111 _{Nm/Nh/Cf} -A	α 1WT _{Nm}	β 1WT _{Nh}	γ 1WT _{Cf}	Lm-111 _{Nm/Nh/Cf} treated with AEBSF
73	Lm-111 _{Nm/Nh/0} -A	α 1WT _{Nm}	β 1WT _{Nh}	γ 1WT	

The designation format of Lm-111"**N**" "**x**" "**y**" "**z**" is utilized to refer to the heterotrimeric Lm-111s; where "**N**" denotes any alteration to the native sequence of the chain, "**x**" denotes the α chain tag, "**y**" denotes the β chain tag, and "**z**" denotes the γ chain tag.

U and no color fill of the row = denotes a combination already described in the table but shown again in order to provide a reference

Table 12. Summary of recombinant mouse α 1 LG4-5 binding data.

	construct designation	mutations	former symbol	Heparin (M) NaCl	α DG (nM)	sulfatide (nM)	sulfatide bound (A_{492})
1	α 1LG4-5/WT	none; WT	WT	0.252	34 +/- 3.4	93 +/- 6.7	2.16 +/- .29
2	α 1LG4-5/ <u>RKR</u> ₂₇₂₁	<u>RKR</u> ₂₇₂₁ to <u>AKA</u>	A	0.154	387 +/- 357	38 +/- 6.5	2.28 +/- .08
3	α 1LG4-5/ <u>RKR</u> ₂₇₂₁	<u>RKR</u> ₂₇₂₁ to <u>AAA</u>	A2	0.137	93 +/- 15	382 +/- 53	1.8 +/- .09
4	α 1LG4-5/ <u>KGRTK</u> ₂₇₇₀	<u>KGRTK</u> ₂₇₇₀ to <u>AGATA</u>	D	0.199	145 +/- 164	1627 +/- 147	1.14 +/- .13
5	α 1LG4-5/ <u>KRK</u> ₂₇₉₃	<u>KRK</u> ₂₇₉₃ to <u>AAA</u>	G	0.150	81 +/- 18	382 +/- 43	1.74 +/- .24
6	α 1LG4-5/ <u>RAR</u> ₂₈₃₃	<u>RAR</u> ₂₈₃₃ to <u>AAA</u>	I	0.216	257 +/- 33	6729 +/- 2377	0.26 +/- .03
7	α 1LG4-5/ <u>KDR</u> ₂₈₆₀	<u>KDR</u> ₂₈₆₀ to <u>ADA</u>	J	0.234	315 +/- 35	512 +/- 28	1.67 +/- .15
8	α 1LG4-5/ <u>RKR</u> ₂₇₂₁ + <u>KRK</u> ₂₇₉₃	<u>RKR</u> ₂₇₂₁ + <u>KRK</u> ₂₇₉₃ to <u>AAA</u> + <u>AAA</u>	A2 + G	0.080	60 +/- 20	62 +/- 6.8	2.45 +/- .31

The construct designation and mutations of the mouse α 1 LG4-5 sequence they represent are listed, as well as the former symbol utilized to reference them in Harrison, et al., 2007 [325]. Heparin binding is expressed as the molar NaCl concentration required for elution of the recombinant α 1LG4-5 protein from a heparin affinity column. Both the α DG and sulfatide binding is expressed as the apparent dissociation constant +/- standard error obtained from a single-site binding curve fit of the experimental data.

Appendix

Section I. NCBI's GEO EST expression data.

EST results from gene chip arrays which were submitted to NCBI, were tabulated. The actual numbers of transcripts and relative numbers from NCBI's GEO EST expression repository utilized to generate figures 4-6 are listed both as a number and a graphical representation (oval) whose shading intensity is directly proportional to the number of transcripts in each tissue source (appendix figure 1).

Section II. Rotary Shadow EM of recombinant heterotrimeric Lm-111s.

Rotary shadow EM was performed by Dr. Peter Yurchenco. Appendix Figure 2 depicts several of the recombinant heterotrimeric Lm-111s constructed, expressed, and purified. A higher magnification image can be seen in Appendix Figure 3.

Section III. Recombinant heterotrimeric Lm-111 polymerization assays.

Appendix Figure 4 depicts representative SDS-PAGE gels of polymerization assays of several of the recombinant Lm-111s, which were digitized and relative yields/intensities plotted in Appendix Figure 5.

Section IV. Laminin accumulation on the surface of cultured Schwann cells.

Schwann cells cultured from rat sciatic nerve, lose their ability to express $\gamma 1$ chain containing laminins; i.e. there is no detectable Lm-111 or Lm-211 secreted into the media or associated with the SC surface. Cell lysates and immunohistochemical staining of both sciatic nerve and cultured SC demonstrate continued expression of sulfatide, $\beta 1$ integrin, dystroglycan, nidogen-1, and type IV collagen by the SCs. Cultured SCs continue to secrete nidogen-1 and type IV collagen, however, it is not

retained on the cell surface of the SCs unless exogenous laminin (Lm-111 or Lm-211) is supplied. In which case, the exogenously supplied laminin will accumulate along with the endogenous nidogen-1, type IV collagen, and membrane bound α DG, migrate, and condense in a BM pattern on the surface of the SCs (appendix figure 10) [71, 469]. The addition of exogenous Lm-111 results in an increased expression of α DG on the cell surface, furthermore, without the addition of exogenous Lm-111, the α DG will remain in a dispersed punctate pattern and not condense. Sulfatide, perlecan, syndecan-1, syndecan-3, and β 1 integrin are also present on the cell surface in the absence of exogenous Lm-111 (appendix figures 11 and 12). The sulfatide signal remains dispersed and punctate, however, it will co-localize and condense with exogenous Lm-111. In the absence of exogenous laminin, most of the perlecan is found on the basal side of the cell, however, some will begin to co-localize on the apical side of the cell with exogenous laminin. Despite the presence of both syndecan-1 and syndecan-3 prior to the addition of laminin, neither will co-localize with the exogenous laminin signal. Furthermore, β 1 integrin is expressed in cultured SCs, however, it is sequestered to the basal side of the Schwann cells and does not colocalize with exogenous laminin which binds predominately on the apical side.

Experiments with Schwann cells were performed with Schwann cells either at a very low density or near confluency depending on what experiment was being conducted. Sparsely plated Schwann cells were very efficient binders of exogenous Lm-111, however, their active growth state resulted in high basal Src phosphorylation levels. Furthermore, they were difficult to use for scoring and comparing mutant recombinant Lm accumulation levels with since the Lm which bound quickly condense and began to clear, skewing numbers, and the difficulty in equilibrating signal intensity with both highly variable number of cells and high levels of “dead” space between the cells. Further

complicating their use was that sparsely plated Schwann were very difficult to efficiently load and perform sulfatide experiments with. Confluent cultures of Schwann cells had the benefit of no free plastic surfaces in sulfatide loading experiments which would bind the added sulfatide, they were slow to condense and process the exogeneous Lm which bound their surface, and the number of cells per field was more uniform from sample to sample making equilibrations and comparisons in binding of different recombinant Lms not just easier, but also, more accurate.

When 20ug/ml of Lm-111 was added to subconfluent SCs, the Lm-111 initially bound diffusely on the cell surface, however, over 30 minutes this binding began to accumulate and condense into a much less random distribution (appendix figure 6). The Lm-111 retracted from the cell's peripheral edges and migrated towards the center of the cell, as did the nidogen-1, type IV collagen, and α DG. When exogeneous Lm-111 (20ug/ml) was added to near confluent SCs, there was an accumulation of Lm but little condensation. Furthermore, the Lm began to clear from the surface of the confluent Schwann cells at a much slower rate and the Lm coverage took on the appearance of the exogeneous Lm coverage observed in C2C12 myotubes (appendix figure 7). A similar binding, though much less than that observed for Lm-111, and redistribution was observed with exogeneous Lm-211 (data not shown). A process similar to that observed with the low density Schwann cells, was also observed when recombinant Lm-111 labeled with fluorescent dye Alexa 488 was added to Schwann cell cultures (appendix figure 8 and 9). The modification of the Lm with the fluorescent dye did not appear to hinder the ability of the Lm to bind, aggregate, and condense.

Section V. The role of sulfatide and Lm-111 in BM formation on cultured Schwann cells.

SCs in the absence of laminin treatment, revealed (via detection with the sulf-I antibody) a diffuse distribution of sulfatide, however, after addition and incubation with 10ug/ml of Lm-111 or Lm-211, the sulfatide condensed and colocalized with the cell surface anchored Laminin. Sulfatide migration was also observed by use of sulfatide in which the acyl chain had been chemical linked to BODIPY [71]. Previous laboratories [485] had shown that sulfatides can be intercalated into the outer leaflet of the plasma membrane in the presence of defatted albumin to which sulfatide can be loosely bound. When this was done with BODIPY-labeled sulfatide and cultured SCs, it was apparent that the sulfatide was uniformly distributed on the surface of the SCs, however, with addition of exogenous Lm-111, the sulfatide co-migrated and condensed in the same pattern as the Lm-111. Furthermore, Lm-111 accumulation was blocked by treatment of the SCs with malarial circumsporozoite protein, which binds sulfatides and cholesterol sulfate, but not by treatment with a mixture of heparitinase and heparanase, chondroitinase ABC, or neuraminidase (data not shown).

Shaohua Li of our laboratory also demonstrated [71] that if SCs were treated with arylsulfatase (from *Helix pomatia*; EC 3.1.6.1), an enzyme that hydrolyzes the sulfate from sulfatides and seminolipid but not glycosaminoglycans [486, 487], prior to addition of exogenous Lm-111, then the sulfatide epitope detected by the sulf-I antibody was lost and Lm-111 did not accumulate on the surface of the SCs. Furthermore, positive sulfatide staining, Lm-111 accumulation, co-localization and co-condensing of both the sulfatide and Lm-111 staining could be restored after arylsulfatase treatment by loading the cells with sulfatide absorbed onto de-lipidated albumin.

The binding of sulfatide by Lm-111 was further examined by Shaohua Li [71] via loading delipidated BSA with BODIPY tagged gal-sulfatide, loading SCs by lipid

exchange with 10uM BODIPY-sulfatide:BSA complex, and then incubating the SCs with 10ug/ml of either Lm-111 or AEBSF treated Lm-111 for one hour. The SCs were then extracted with 1% Triton X-100, centrifuged, and the lysate immunoprecipitated with a Lm-111 E1' specific polyclonal antibody. There was virtually no fluorescence detected in the BSA control nor the polymerization incompetent AEBSF treated Lm-111, however, there was considerable fluorescence detected in the exogenous Lm-111 sample.

Furthermore, sulfatide based ELISAs demonstrated that both Lm-111 and Lm-211, as well as $\alpha 1$ LG4-5, bound sulfatide in a measurable manner; that Lm-111 demonstrated a higher capacity for the number of molecules of sulfatide it could bind than Lm-211, Lm-211 unprocessed bound with a much higher affinity than the processed Lm-211, and that Lm-111's binding was not impeded by the addition of 1% Triton X-100 (figure 43).

Shaohua Li also showed [71] that cultured SCs have a diffuse DG and utrophin base staining pattern, however, after 1 hour incubation with 10ug/ml of exogenous Lm-111, both proteins exhibited an induced condensation pattern similar to Lm-111. If the SCs are also treated with arylsulfatase in addition to the exogenous Lm-111, then there was no accumulation of Lm-111, nor condensation of DG or utrophin observed. However, if the SCs are replenished with sulfatide via sulfatide loaded delipidated BSA post arylsulfatase treatment and then incubated with Lm-111, the Lm-111 accumulation and condensation, as well as condensation of DG and utrophin are re-established.

SCs incubated with 10ug/ml of Lm-111 for 1 hour, were collected, detergent extracted and immunoprecipitated with β -DG antibody and utrophin antibody, then immunoblotted with Lm-111, β -DG, and utrophin antibody to determine the presence or absence of above mentioned proteins in a precipitable complex. As expected, there was no detectable Lm-111 in the untreated SCs and Lm-111 was pulled down with the anti-

β DG antibody. Furthermore, there was no detectable increase in DG observed upon addition of the exogenous Lm-111. Anti-utrophin antibody only pulled down β DG in SCs which had been treated with exogenous Lm-111, and like β DG showed no increase in expression upon addition of the exogenous Lm-111. The exogenous Lm-111 induced β DG–utrophin association was blocked in the presence of the DG antibody IIH6, which blocks Lm-111 binding to α DG. Therefore, it became apparent that utrophin was recruited to a sulfatide associated Lm-111- α DG complex through its association with β DG.

Section VI. Interactions of recombinant laminins with nidogen and type IV collagen.

When Type IV collagen is mixed with nidogen-1 and allowed to polymerize, a fraction of the nidogen is found in the polymer pellet associated with the collagen (appendix figure 13E) [74]. Purified type IV collagen, $\alpha 1_2\alpha 2$ [IV], which polymerizes when incubated in PBS at 37°C, was incubated at increasing concentrations with 0.1 mg/ml (a concentration at which even polymerization capable laminins will not polymerize and pellet) recombinant wild-type laminin Lm-111_{Nf/Nh/O} (WTa), non-polymerizing laminin Lm-111 $\alpha\Delta$ LN_{Nm/Nh/Cf1} and nidogen binding mutant Lm-111 $\gamma 1$ N₈₀₂S_{Nm/Nh/Cf1} in the absence or presence of 0.02 mg/ml nidogen-1; followed by sedimentation. The supernatant and pelleted fraction were analyzed by SDS-PAGE (appendix figure 4 and 5) [471], scanned, and quantitation performed based on the intensity of the Coomassie blue stained laminin $\beta 1$ band, which migrates slower than the collagen $\alpha 2$ band when co-electrophoresed. The fraction of WT or $\alpha 1\Delta$ LN laminins in the collagen pellets increased with increasing collagen concentration, however, the highest fractions of laminin in the pellet were achieved in the presence of equimolar nidogen-1. Lower, but substantial, fractions of

laminin were detected in the collagen pellet in the absence of nidogen. A similar relationship was observed between WT and $\alpha 1\Delta\text{LN}$ laminin, however, there was less $\alpha 1\Delta\text{LN}$ laminin detected in the pellet than that observed with WT laminin. The recombinant laminin containing the $\gamma 1$ chain nidogen binding mutant, $\gamma 1\text{N}_{802}\text{S}$, also was recoverable in the collagen pellet, however, there was even less than that achieved with the $\alpha 1\Delta\text{LN}$ laminin. Therefore, nidogen must mediate a laminin association with type IV collagen.

Section VII. Collagen and nidogen contributions to the accumulation of exogenous laminin on Schwann cells.

The contributions of nidogen-1 and type IV collagen to the exogenous Lm-111 driven basement membrane component accumulation on the surface of Schwann cells were examined in further detail in a series of experiments performed by Stephanie Capizzi [471]. Representative immunohistochemical stained SCs are shown for some of the recombinant laminins and conditions (appendix figure 13A) whose results are shown in panels B-E. The highest laminin immunofluorescence observed resulted from treatment of cells with a mixture of recombinant WT laminin with or without nidogen-1 and type IV collagen (appendix figure 13B). Although a small increase of laminin immunofluorescence appeared to be present in several experimental sets due to co-incubation with nidogen and collagen (compared to laminin treatment alone), the differences were not found to be significant within data sets (appendix figure 13B and data not shown). The highest nidogen immunofluorescence level (appendix figure 13C) was observed when nidogen was incubated with laminin and collagen ($P < 0.001$, compared to other conditions). Nidogen immunofluorescence was reduced to an intermediate level if only laminin and nidogen were present ($32 \pm 6\%$ compared to WT

laminin + nidogen + collagen, $P < 0.001$), and essentially absent ($0.2 \pm 0.1\%$, $P < 0.001$) if N_{802}S laminin was incubated in place of WT laminin with nidogen and type IV collagen. Type IV collagen levels were highest (appendix figure 13D) when incubated with WT laminin and nidogen ($P < 0.001$, compared to other conditions). Collagen levels were reduced if the collagen was incubated with $\text{Lm-111}\gamma 1\text{N}_{802}\text{S}_{\text{Nm/Nh/Cf}}$ and nidogen ($33\% \pm 4\%$ compared to WT laminin + nidogen + collagen, $P < 0.001$) or if incubated with WT laminin in the absence of nidogen ($25 \pm 11\%$ compared to WT-laminin + nidogen + collagen, $P < 0.001$). Collagen immunofluorescence was further reduced if the collagen was incubated with $\text{Lm-111}\alpha\Delta\text{LG1-5}_{\text{Nm/Nh/Cf}}$ and nidogen ($12 \pm 4\%$ compared to WT-laminin + nidogen + collagen, $P < 0.001$), a level not significantly different from the baseline values observed with collagen + nidogen ($7 \pm 3\%$). Type IV collagen levels were also low when the collagen was incubated with nidogen and the non-polymerizing $\text{Lm-111}\alpha\Delta\text{LN}_{\text{Nm/Nh/Cf}}$, but higher than that observed when the collagen was incubated with nidogen and $\text{Lm-111}\alpha\Delta\text{LG1-5}_{\text{Nm/Nh/Cf}}$ ($40 \pm 9\%$ vs. $12 \pm 4\%$, $P < 0.002$). If polymerization incompetent $\text{Lm-111}\alpha\Delta\text{LN}_{\text{Nm/Nh/Cf}}$ and type IV collagen were kept at a fixed concentration, 40ug/ml and 20ug/ml respectively, and the nidogen concentration allowed to increase, a very small laminin immunofluorescence and a moderate collagen immunofluorescence were observed (appendix figure 13E).

The increase in exogenous laminin accumulation and basement membrane formation on the Schwann cell surface with contemporaneous addition of both type IV collagen and nidogen was observed in electron micrographs (images taken by Peter Yurchenco) (appendix figure 14) [471]. Continual basement membranes were observed in electron micrographs only following treatment with EHS purified laminin-111, recombinant $\text{Lm-111}_{\text{Nf/Nh/O}}$, and recombinant $\text{Lm-111}_{\text{Nm/Nh/Cf}}$. A few small discrete extracellular aggregates (asterisks in Appendix Figure 14) in the absence of basement

membranes were present on exposed cell surfaces of cells treated with Lm-111 $\alpha\Delta$ LN_{Nm/Nh/Cf}, Lm-111 $\alpha\Delta$ LG1-5_{Nm/Nh/Cf}, or if untreated. The contemporaneous addition of type IV collagen and nidogen-1 to the recombinant laminins resulted in increased deposition of basement membrane or aggregates on the surface of the Schwann cells.

VIII. Ultrastructure of MEF cell surfaces with and without the addition of exogenous Lm-111.

The determination of the ultrastructural characteristics of Schwann cells and MEFs are a necessity for proper examination of the cells and BM formation because the light and fluorescent microscopy levels of magnification are insufficient to properly identify cellular structures and characteristics. MEFs were grown in culture till they reached a confluent state and then treated either with exogenous Lm-111 (40ug/ml for 1 hour), loaded with gal-sulfatide and then treated with Lm-111, or loaded with gal-sulfatide + Lm-111 + arylsulfatase and examined by transmission electron microscopy.

There was no detectable BM in non-treated (data not shown) nor Lm-111 only exposed MEFs. A continuous BM was observed in MEFs first loaded with sulfatide then given Lm-111, however, there was no observable BM if the MEFs were also treated with arylsulfatase.

APPENDIX FIGURE LEGENDS

Appendix Figure 1. **Laminin chain expression profiles suggested by analysis of EST counts.** The actual numbers of transcripts and relative numbers from NCBI's GEO EST expression repository utilized to generate figures 4-6 listed both as a number and a graphical representation (oval) whose shading intensity is directly proportional to the number of transcripts.

Appendix Figure 2. **Rotary shadow EM of heterotrimeric Lm-111s.** Rotary shadow EM was performed by Dr. Peter Yurchenco.

Appendix Figure 3. **Higher magnification rotary shadow EM of heterotrimeric Lm-111s.** Rotary Shadow EM was performed by Dr. Peter Yurchenco.

Appendix Figure 4. **Polymerization ability of recombinant heterotrimeric Lm-111s – SDS-PAGE results.** Coomassie blue stained SDS-PAGE gels from polymerization assays of various recombinant Lm-111s performed by Karen McKee.

Appendix Figure 5. **Polymerization ability of recombinant heterotrimeric Lm-111s – plotted results.** The gels from appendix figure 4 were scanned, density of individual bands determined, and plotted in order to generate polymerization curves and determine the critical concentrations for polymerization (performed by Karen McKee).

Appendix Figure 6. Accumulation, aggregation, and condensation of exogeneous Lm-111 on cell surfaces of sparsely plated Schwann cell cultures. Sparsely plated Schwann cells were incubated with 20ug/ml of Lm-111_{Nm/Nh/Cf} and samples removed at specific time intervals and immunostained. The laminin signal is observed to be initially light and punctate, accumulating with time, increasing in coverage, and condensing from the periphery towards the center of the cell, where it begins to take on a typical BM like appearance, and eventually begins to be cleared from the cell surface. Neither the recombinant nature nor N-terminal myc tag on the $\alpha 1$ chain, N-terminal HA tag on the $\beta 1$ chain, and C-terminal FLAG tag on the $\gamma 1$ chain of the exogeneous recombinant Lm-111_{Nm/Nh/Cf} appear to adversely affect Lm-111 binding to the surface, accumulation, aggregation, and condensation on the surface of Schwann cells.

Appendix Figure 7. Accumulation, aggregation, and condensation of exogeneous Lm-111 on cell surfaces of near confluent Schwann cell cultures. Densely plated, nearly confluent, Schwann cells were incubated with 20ug/ml of Lm-111_{Nf/Nh/Cf} and samples removed at specific time intervals and immunostained. The laminin signal is observed to be initially light and punctate, accumulating with time, increasing in coverage, however, unlike the sparsely plated Schwann cells there is much less migration and condensation of the signal, however, it does with time take on a typical BM like appearance, and eventually begins to be cleared from the cell surface.

Appendix Figure 8. Accumulation, aggregation, and condensation of exogeneous Alexa-488 labeled Lm-111 on Schwann cell surfaces. Sparsely plated Schwann cells were incubated with 20ug/ml of Alexa-488 labeled Lm-111_{Nf/Nh/Cf} and samples removed at specific time intervals and immunostained. In a manner similar to the Schwann cells

incubated with non-labeled Lm-111, the laminin signal is observed to be initially light and punctate, accumulating with time, increasing in coverage, and condensing from the periphery towards the center of the cell, where it begins to take on a typical BM like appearance though not as efficient as unlabelled laminin, and eventually begins to be cleared from the cell surface. There were approximately 21 moles of dye per mole of laminin. It appears that the fluorescent labelling of the laminin through its primary amines did not interfere with laminin activities (polymerization or anchorage) required for BM formation. This is a concern since we had shown that mutation of Arg and Lys residues (primary amine containing amino acids) in $\alpha 1$ LG4-5 recombinant proteins affected specific binding activities of laminin to heparin, α DG, and sulfatide.

Appendix Figure 9. Accumulation, aggregation, and condensation of exogenous Alexa-488 labeled Lm-111 on Schwann cell surfaces – single cell. Enlargement of individual cells incubated with Alexa-488 labeled Lm-111 depicted in Appendix Figure 11. Note the increase in α DG signal with time upon addition of laminin as well as “co-condensation” with the exogenous laminin.

Appendix Figure 10. α -Dystroglycan, nidogen-1, and type IV collagen expression in cultured Schwann cells. Schwann cells were incubated with either 20 ug/ml of EHS laminin-111 and BSA or BSA alone containing media for 45 minutes, washed, and immunostained in order to detect the expression of: Lm-111, α DG, nidogen-1, and type IV collagen. Schwann cells express α DG on the cell surface, however, the amount observed on the surface with the IIH6 α DG antibody increases upon addition of exogenous Lm-111 and the α DG signal is observed to co-localize and condense with the laminin signal on the cell surface of the Schwann cells. Both type IV collagen and

nidogen-1 are expressed and secreted by the Schwann cells, however, very little is retained on the cells surface unless exogeneous laminin is also supplied, after which, both type IV collagen and nidogen accumulate on the surface, co-localize, and condense with the exogeneous laminin.

Appendix Figure 11. Perlecan, syndecan-1, and syndecan-3 expression in cultured Schwann cells. Schwann cells were incubated either with 20 ug/ml of Alexa-488 labeled EHS laminin-111 and BSA or BSA alone containing media for 45 minutes, washed, and immunostained for perlecan, syndecan-1, and syndecan-3. Perlecan was observed on the basal side of the Schwann cells prior to addition of the exogeneous laminin and some did colocalize with the laminin signal on the apical side after incubation with the exogeneous laminin, however, most still appeared to be associated with the basal side of the cell. The HNK-1 epitope antibody revealed staining levels barely above background and did not appear to colocalize with the exogeneous Lm-111. Both syndecan-1 and syndecan-3 were expressed prior and post laminin addition, however, neither co-localized with the exogeneous laminin signal.

Appendix Figure 12. β 1 integrin, sulfatide, and agrin expression in cultured Schwann cells. Schwann cells were incubated with either 20 ug/ml of Alexa-488 labeled EHS laminin-111 and BSA or BSA alone containing media for 45 minutes, washed, and immunostained for β 1 integrin, sulfatide, and agrin. The β 1 integrin, as expected, was observed on the basal side of the Schwann cells prior to addition of the exogeneous laminin and remained sequestered on the basal side even after incubation with exogenous Lm-111. No β 1 signal was observed to colocalize with the exogeneous

laminin on the apical side. Sulfatide was present and did colocalize and condense with the exogenous laminin signal. Agrin was not present or barely detectable.

Appendix Figure 13. Contributions of type IV collagen and nidogen to ECM assembly. Stephanie Capizzi incubated Schwann cells for one hour with mixtures of various laminins (20ug/ml), and/or nidogen-1 (4ug/ml; Nd), and/or type IV collagen (10ug/ml; Coll). She then washed, fixed, immunostained, and analyzed the cells for either laminin-111, nidogen-1, or type IV collagen signal. **(A)** Images representative of the cell immunofluorescence observed are shown. Quantitation of immunofluorescence (both the average and standard deviation of the sums of pixel intensities divided by the number of DAPI stained nuclei) of cells treated with the indicated combinations of laminin, nidogen, and collagen, then immunostained for either **(B)** laminin-111, **(C)** nidogen, or **(D)** type IV collagen are depicted. The average (+/- S.D.) immunofluorescence per cell is represented as grey bars; n = 5-9. Recombinant heterotrimeric laminins possessing defective polymerization or $\alpha 1$ LG4 anchorage do not significantly accumulate on the Schwann cell surface, however, all laminins, even those with reductions in binding due to loss of afore mentioned activities, will demonstrate increased binding in the prescence of collagen, or nidogen and collagen. Treatment of cells with either just nidogen and laminin or nidogen and collagen results in a decrease in observed laminin or collagen binding to the cell surface.

Appendix Figure 14. Electron microscopy images depicting the accumulation of recombinant heterotrimeric Lm-111s and BM formation on the cell surface of Schwann cells in the prescence or absence of type IV collagen and nidogen-1. Schwann cells were incubated with recombinant laminins (40ug/ml) alone or in the prescence of type IV collagen (Col; 20ug/ml) and/or nidogen (Nd; 4ug/ml) for one hour.

Cells treated with WT laminin, Lm-111_{Nm/Nh/Cf}, exhibited a thin continuous electron dense line (BM; lamina densa, upper arrowheads) adjacent to the plasma membrane (lower arrowheads). Scattered small extracellular aggregates instead of continuous BM were observed on the Schwann cell surface with treatments utilizing the polymerization deficient Lm-111 $\Delta\alpha1$ LN_{Nm/Nh/Cf} and LG1-5 anchorage deficient Lm-111 $\Delta\alpha1$ LG1-5_{Nm/Nh/Cf}. The ECM deposition of all three laminin improved with the addition of type IV collagen and nidogen-1, however, the ECM deposition of Lm-111 $\Delta\alpha1$ LN_{Nm/Nh/Cf} and Lm-111 $\Delta\alpha1$ LG1-5_{Nm/Nh/Cf} treated Schwann cells still remained discontinuous. Electron microscopy was performed by Dr. Peter Yurchenco.

Appendix Figure 15. The different stages of differentiation and development WT ES cells undergo during embryoid body development. Phase and DAPI stained EBs depicting the development stages diagrammed below them (performed by Shaohua Li).

Appendix Figure 16. Immunofluorescence and electron microscopy of exogenous Laminin-111 induction of BM formation, epiblast differentiation, and cavitation in $\gamma1$ laminin null EBs: aggregation and condensation.

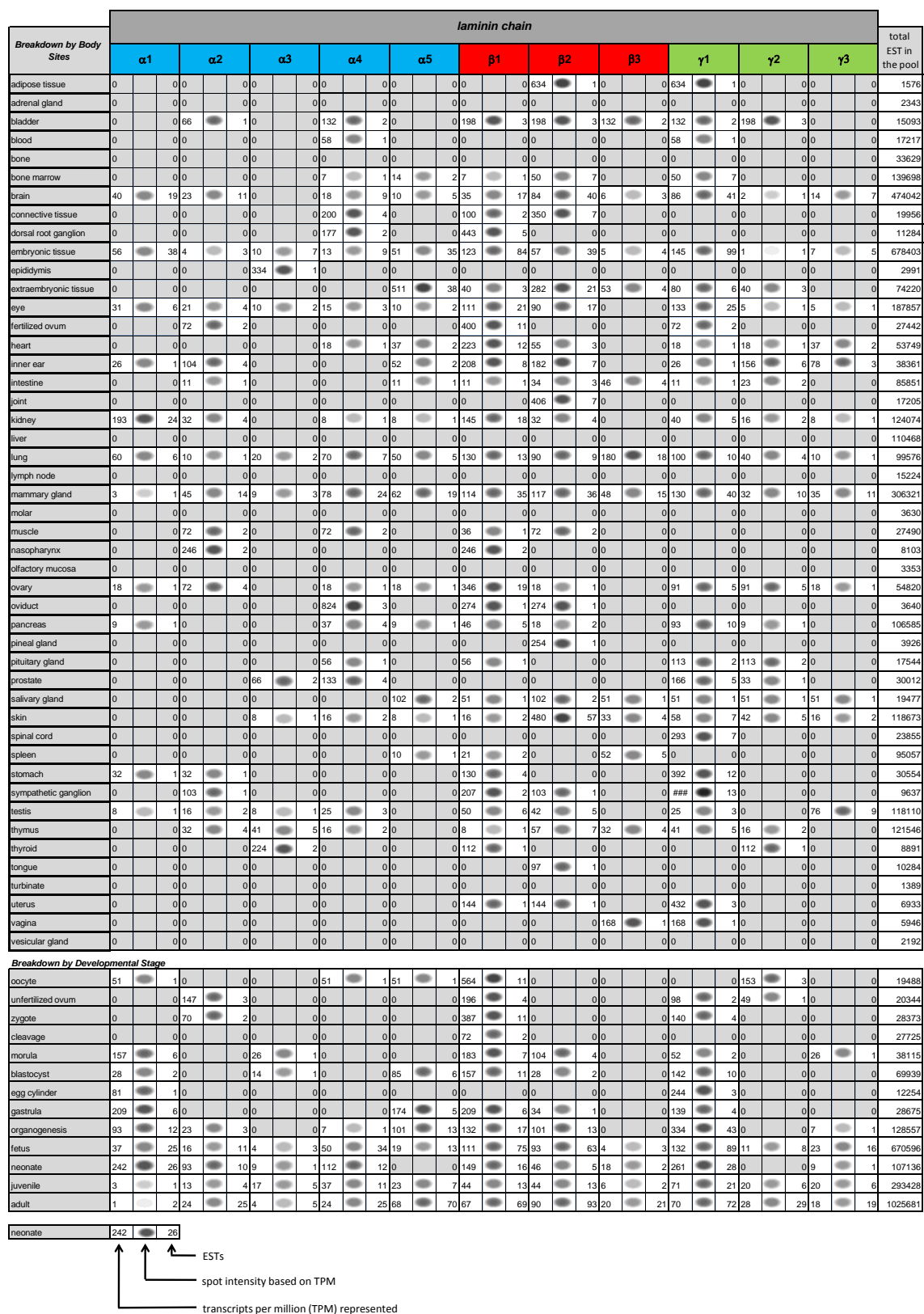
Appendix Figure 17. Immunofluorescence and electron microscopy of exogenous Laminin-111 induction of BM formation, epiblast differentiation, and cavitation in $\gamma1$ laminin null EBs: BM formation, formation and elongation of epiblast layer.

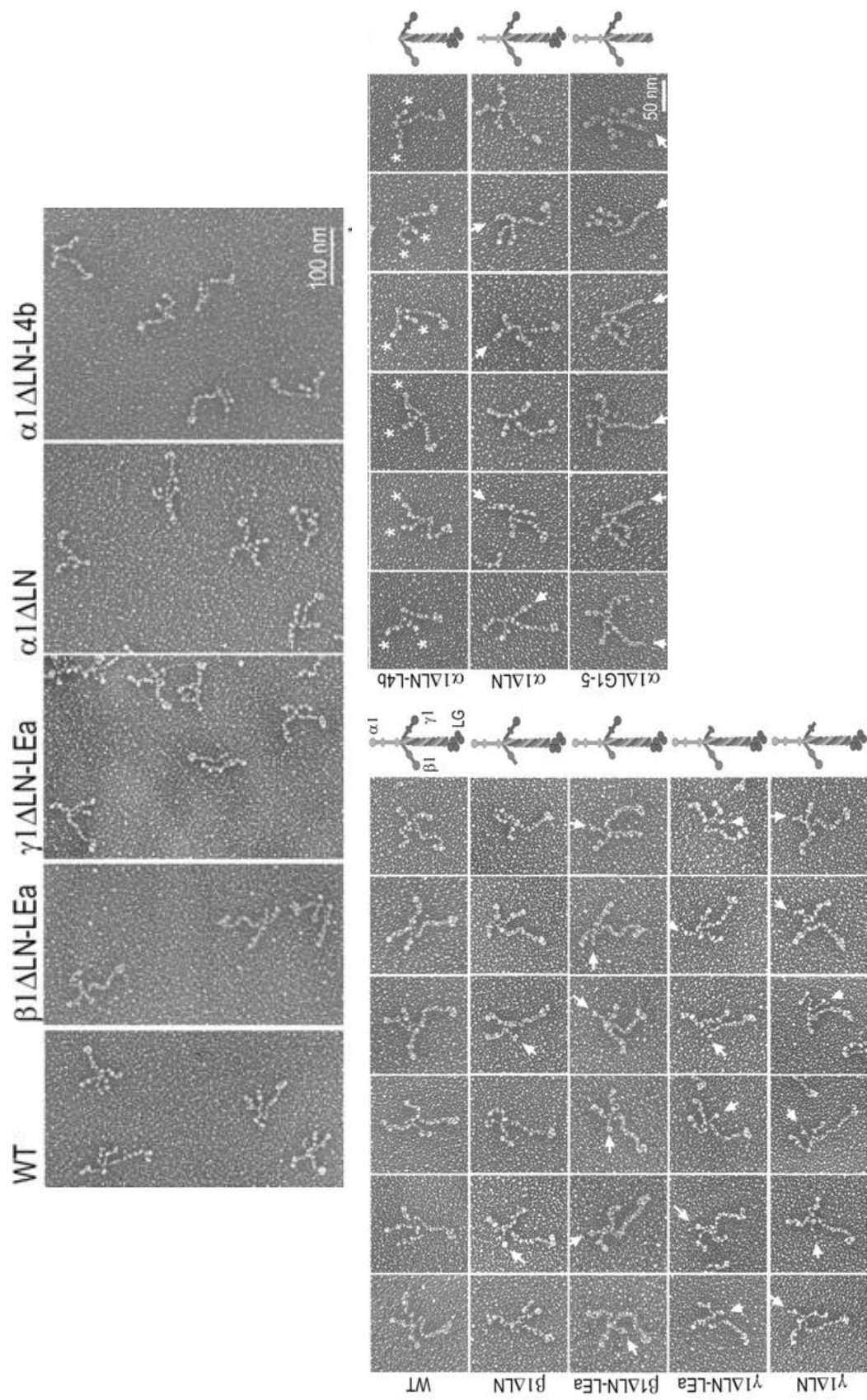
Appendix Figure 18. **Immunofluorescence and electron microscopy of exogenous Laminin-111 induction of BM formation, epiblast differentiation, and cavitation in $\gamma 1$ laminin null EBs: cavitation.**

Appendix Figure 19. **Basement membrane formation and epiblast differentiation in $\gamma 1$ laminin null embryoid bodies treated with Lm-111, modified Lm-111, Lm-111 fragments, and recombinant Lm-111s.** The number of EBs counted and actual numbers generated for BM and epiblast formation.

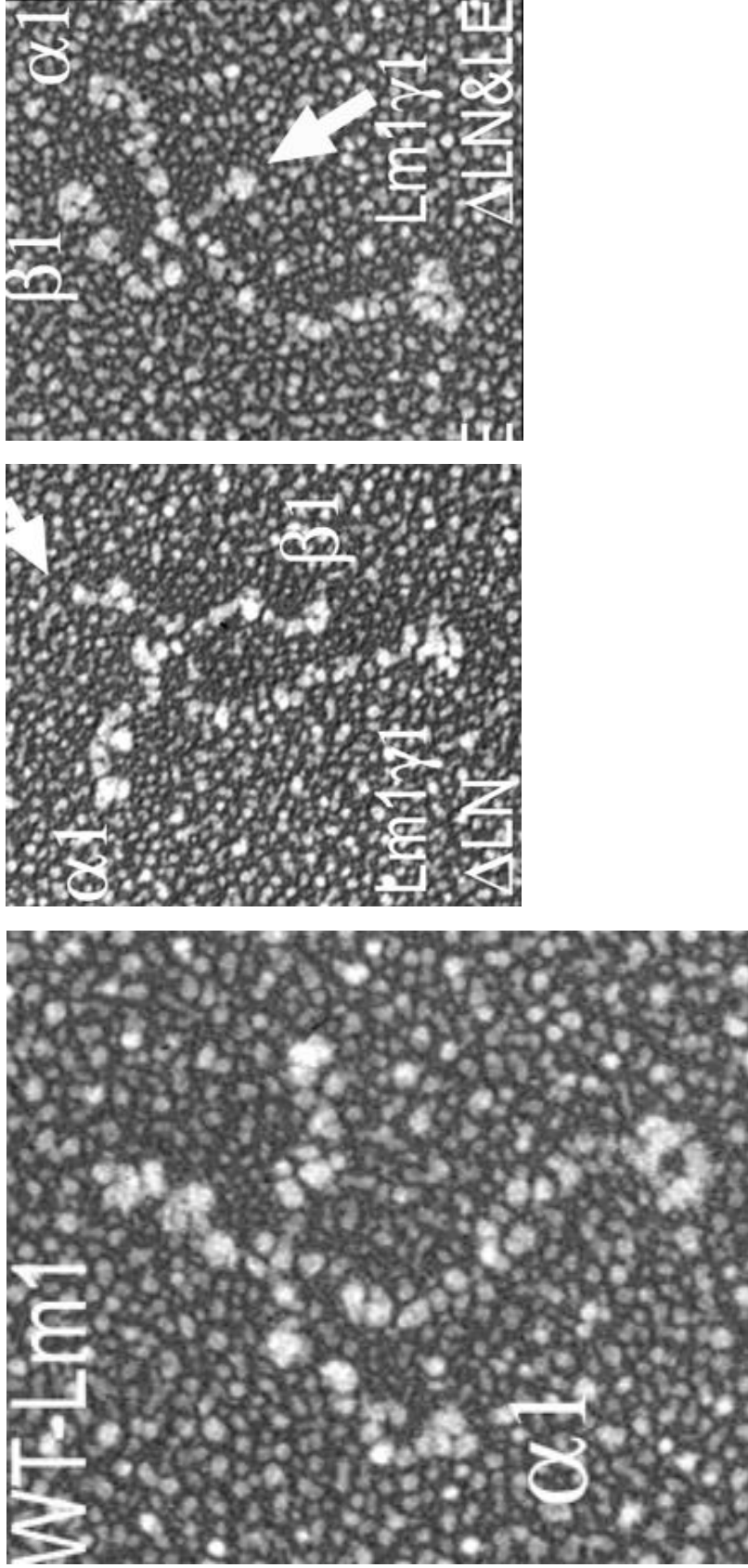
Appendix Table 1. **Crystallographic statistics for recombinant mouse $\alpha 1$ LG4-5.**
The crystallographic statistics for recombinant mouse $\alpha 1$ LG4-5 generated by Erhard Hohenester.

Appendix figure 1. Laminin chain expression profiles suggested by analysis of EST counts.

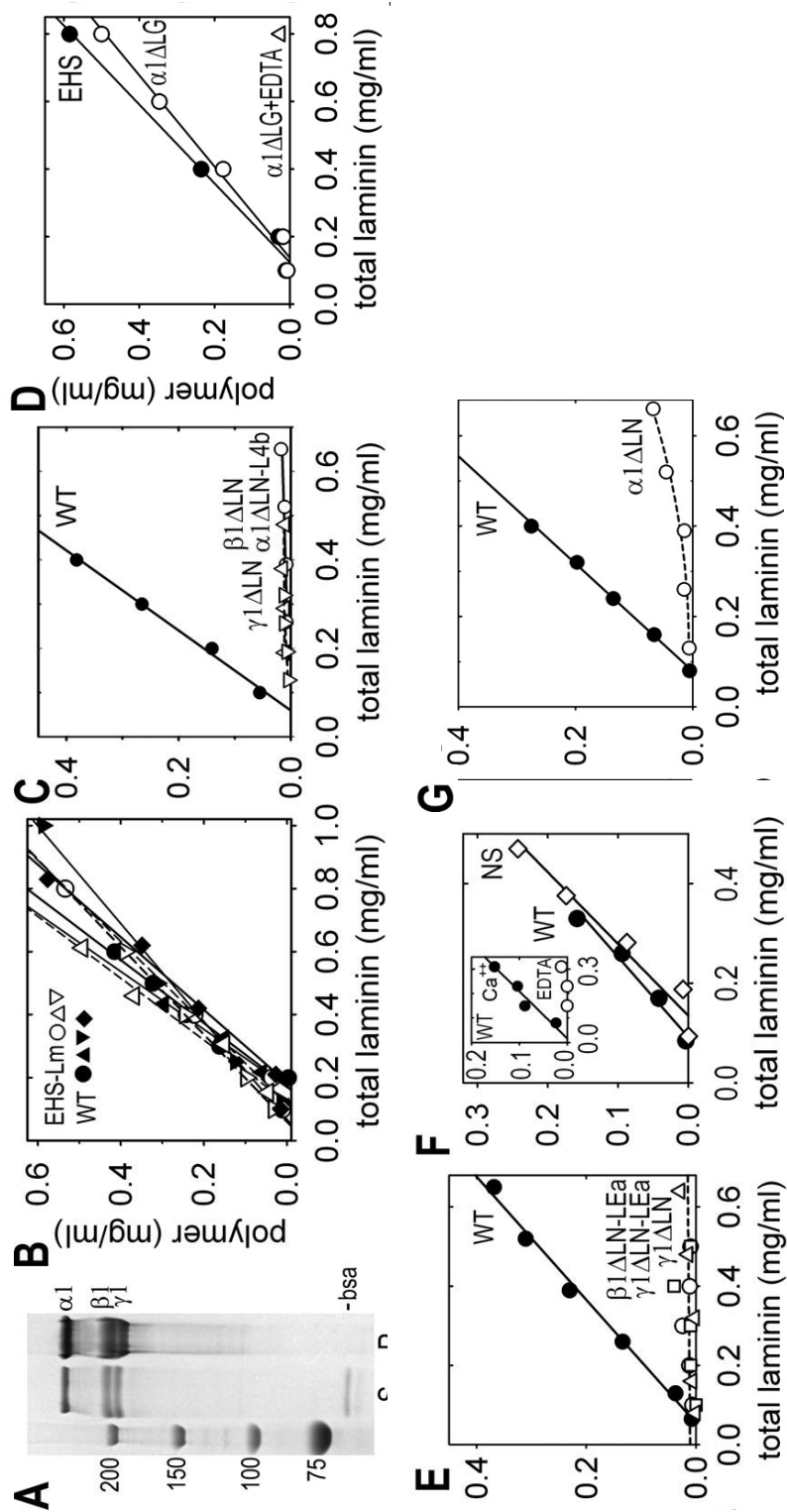




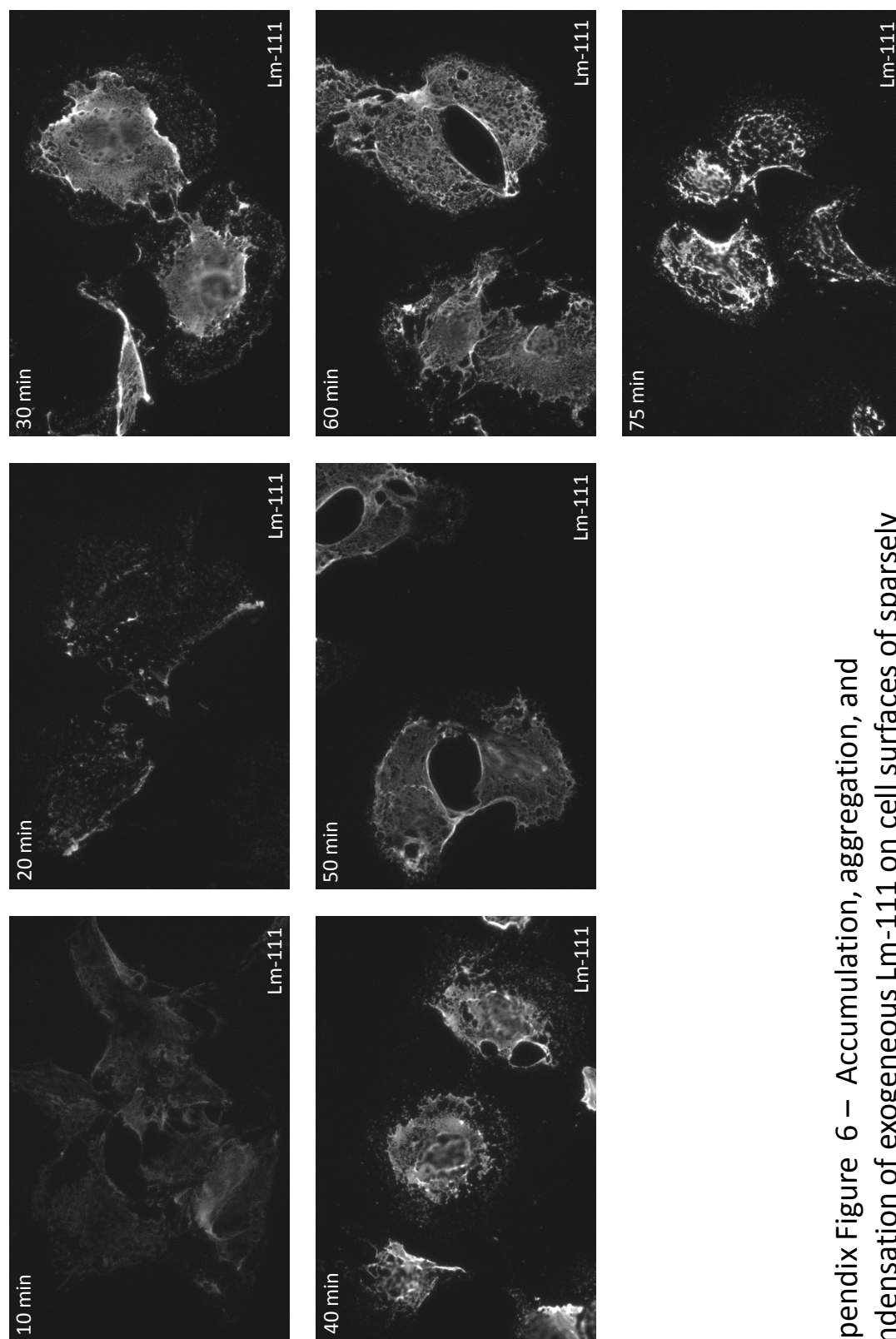
Appendix figure 2 – Rotary shadow EM of heterotrimeric Lm-111s.



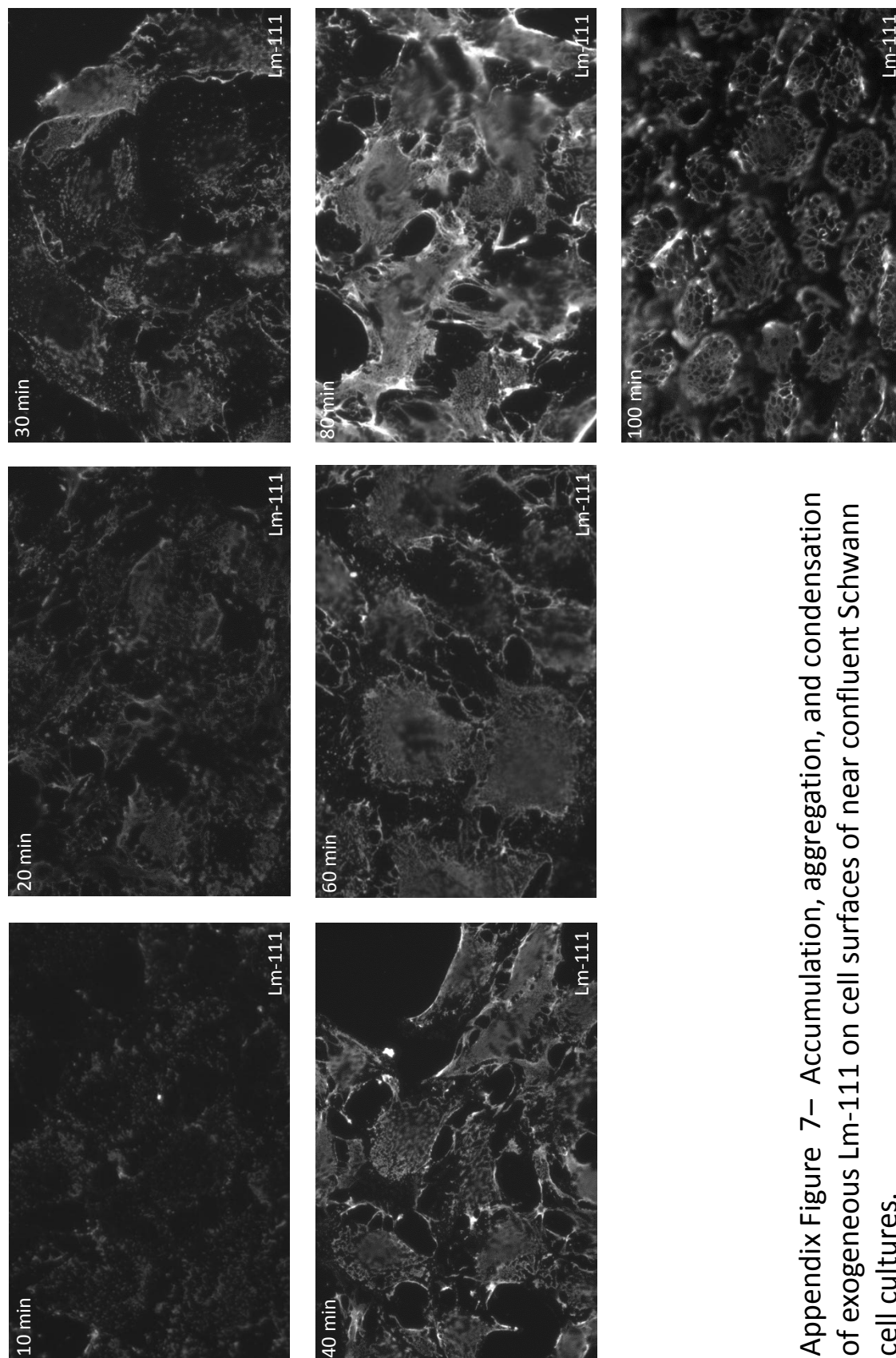
Appendix figure 3 – Higher magnification rotary shadow EM of heterotrimeric Lm-111s.



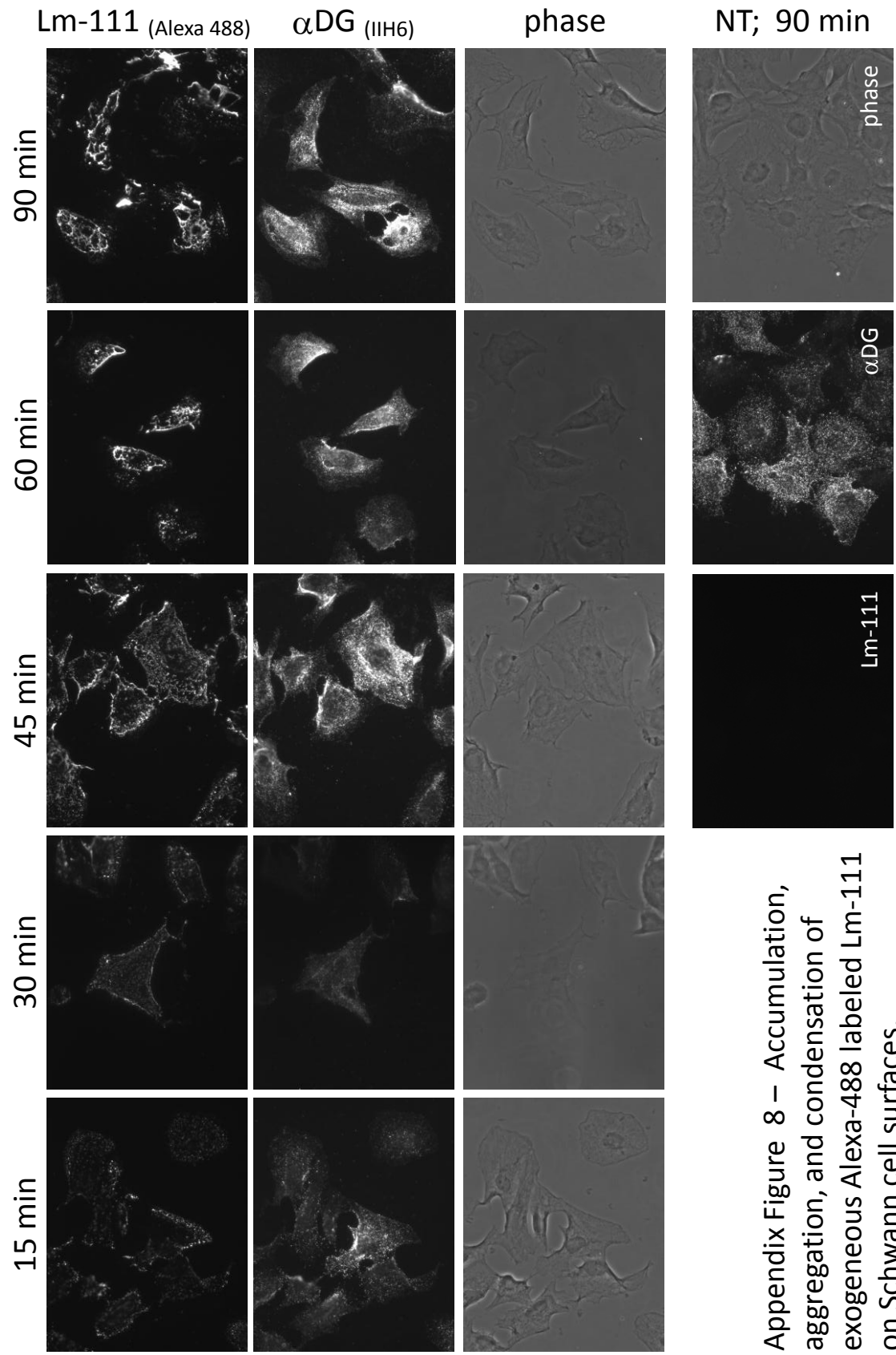
Appendix figure 5 – Polymerization ability of recombinant heterotrimeric Lm-111s – plotted results.



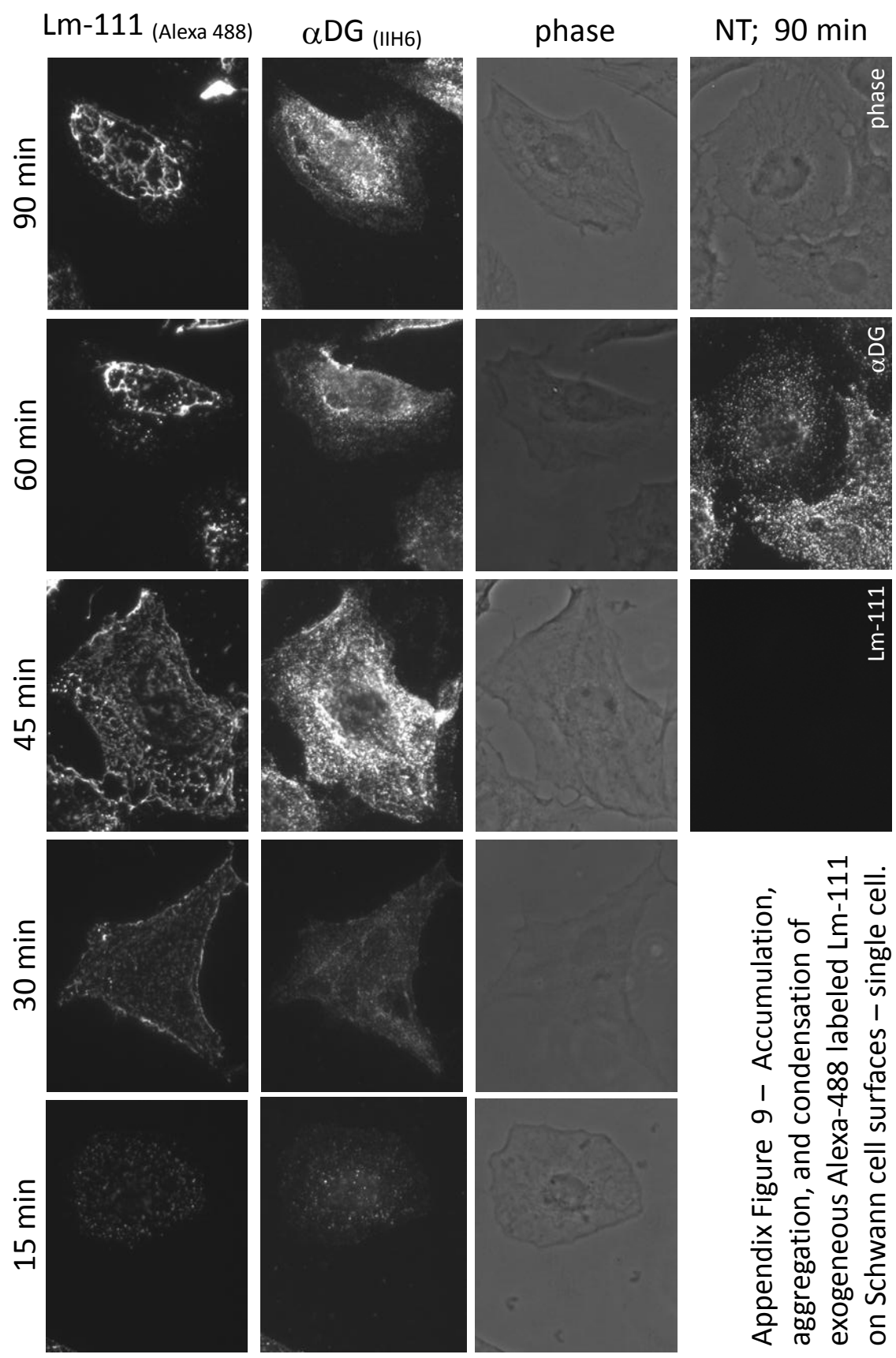
Appendix Figure 6 – Accumulation, aggregation, and condensation of exogenous Lm-111 on cell surfaces of sparsely plated Schwann cell cultures.



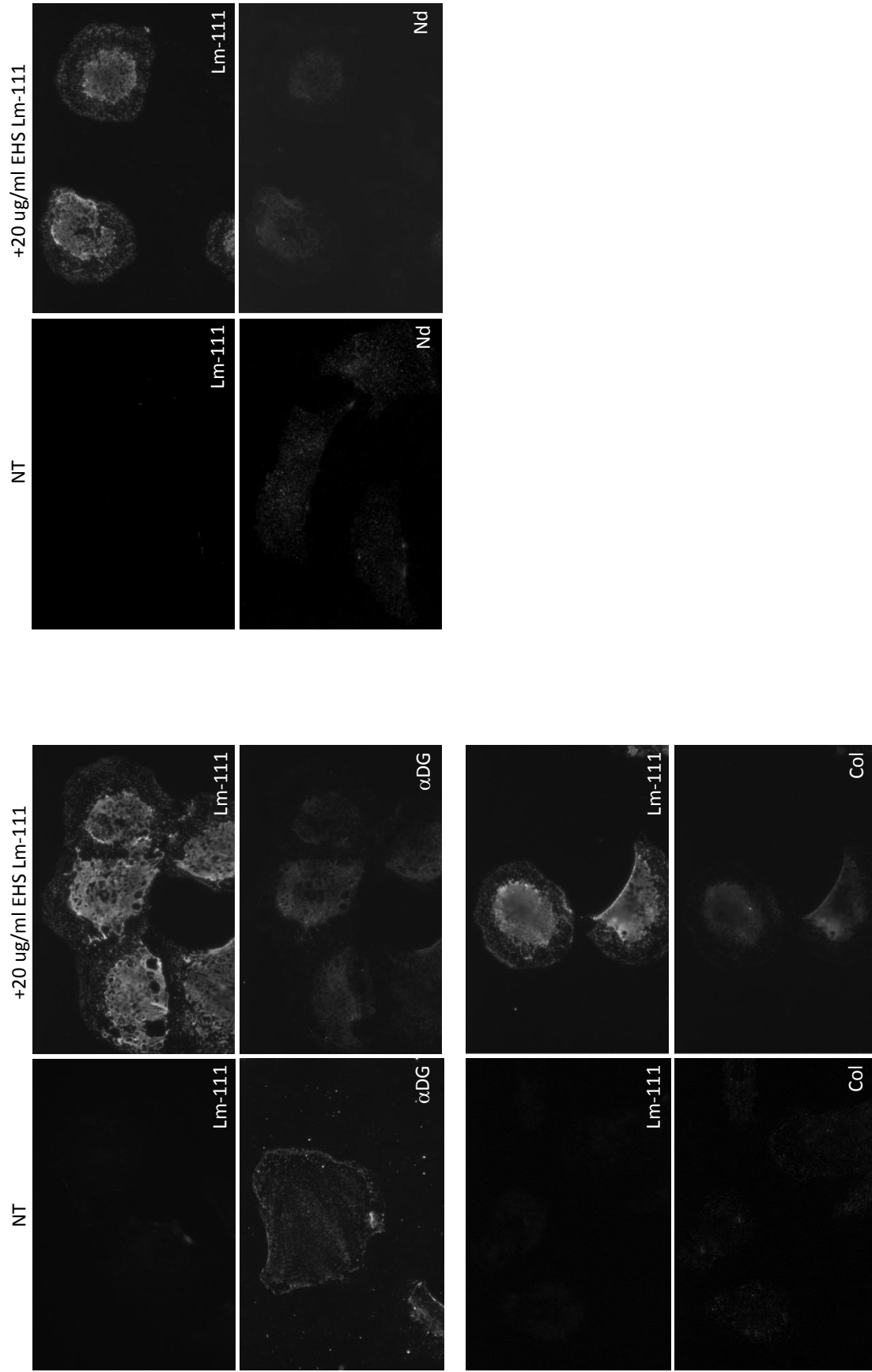
Appendix Figure 7– Accumulation, aggregation, and condensation of exogenous Lm-111 on cell surfaces of near confluent Schwann cell cultures.



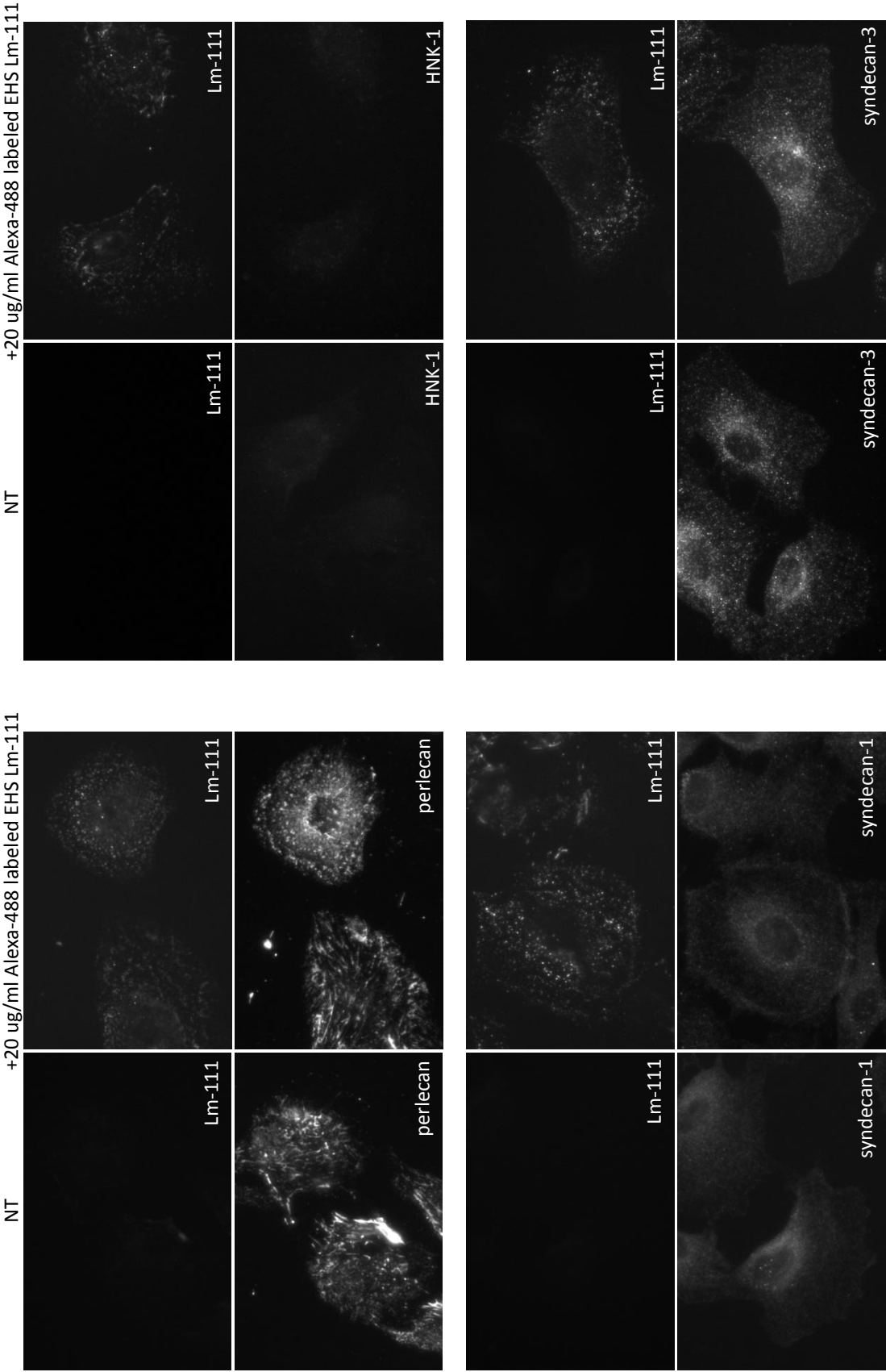
Appendix Figure 8 – Accumulation, aggregation, and condensation of exogenous Alexa-488 labeled Lm-111 on Schwann cell surfaces.



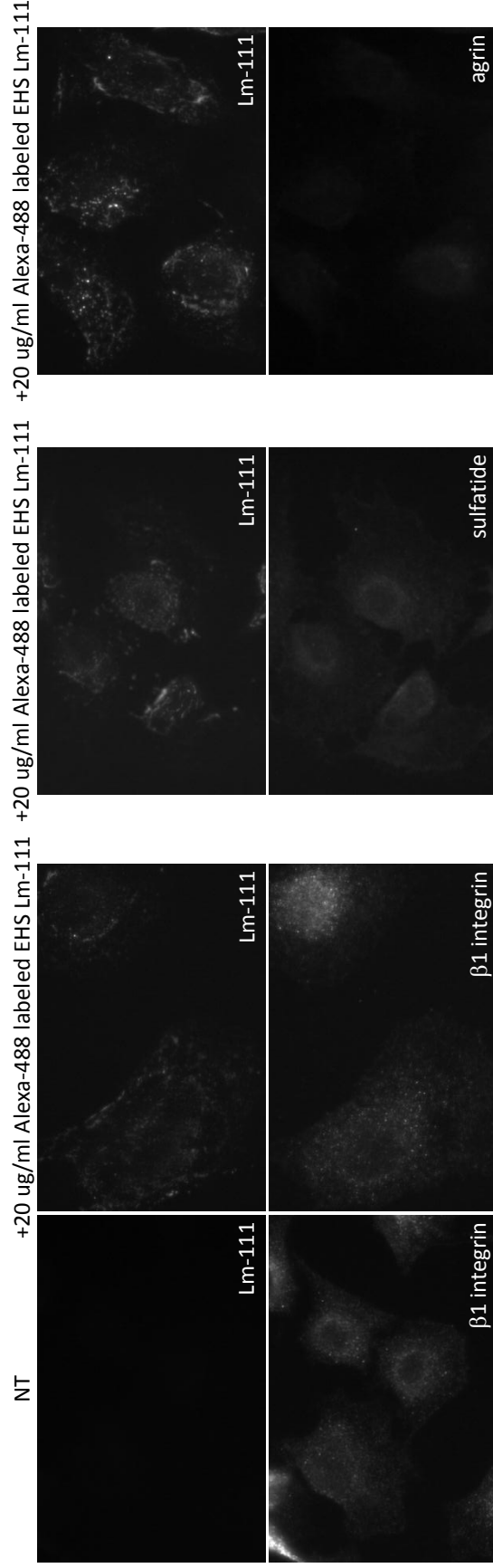
Appendix Figure 9 – Accumulation, aggregation, and condensation of exogenous Alexa-488 labeled Lm-111 on Schwann cell surfaces – single cell.



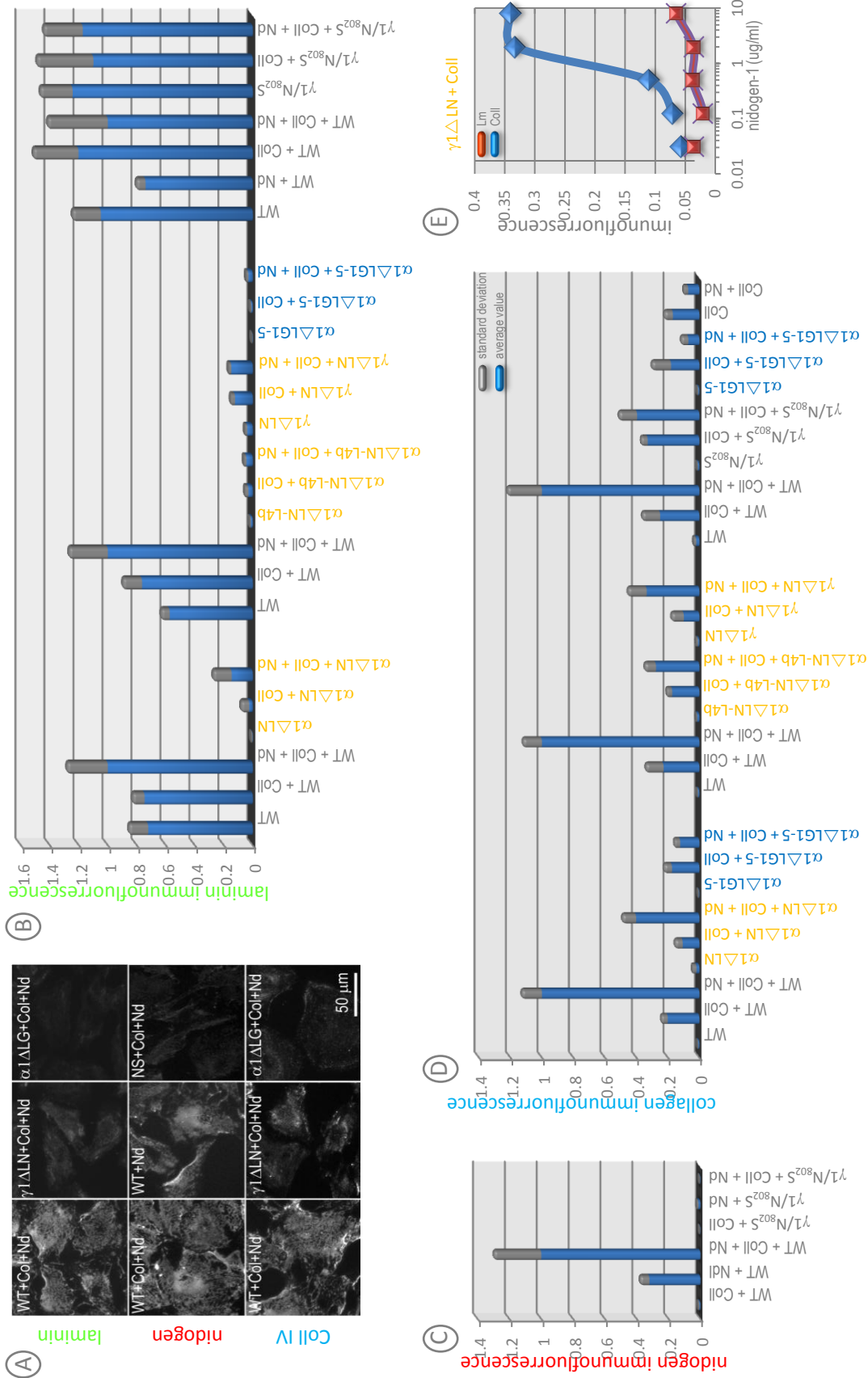
Appendix Figure 10 – αDystroglycan, nidogen-1, and type IV collagen expression in cultured Schwann Cells.

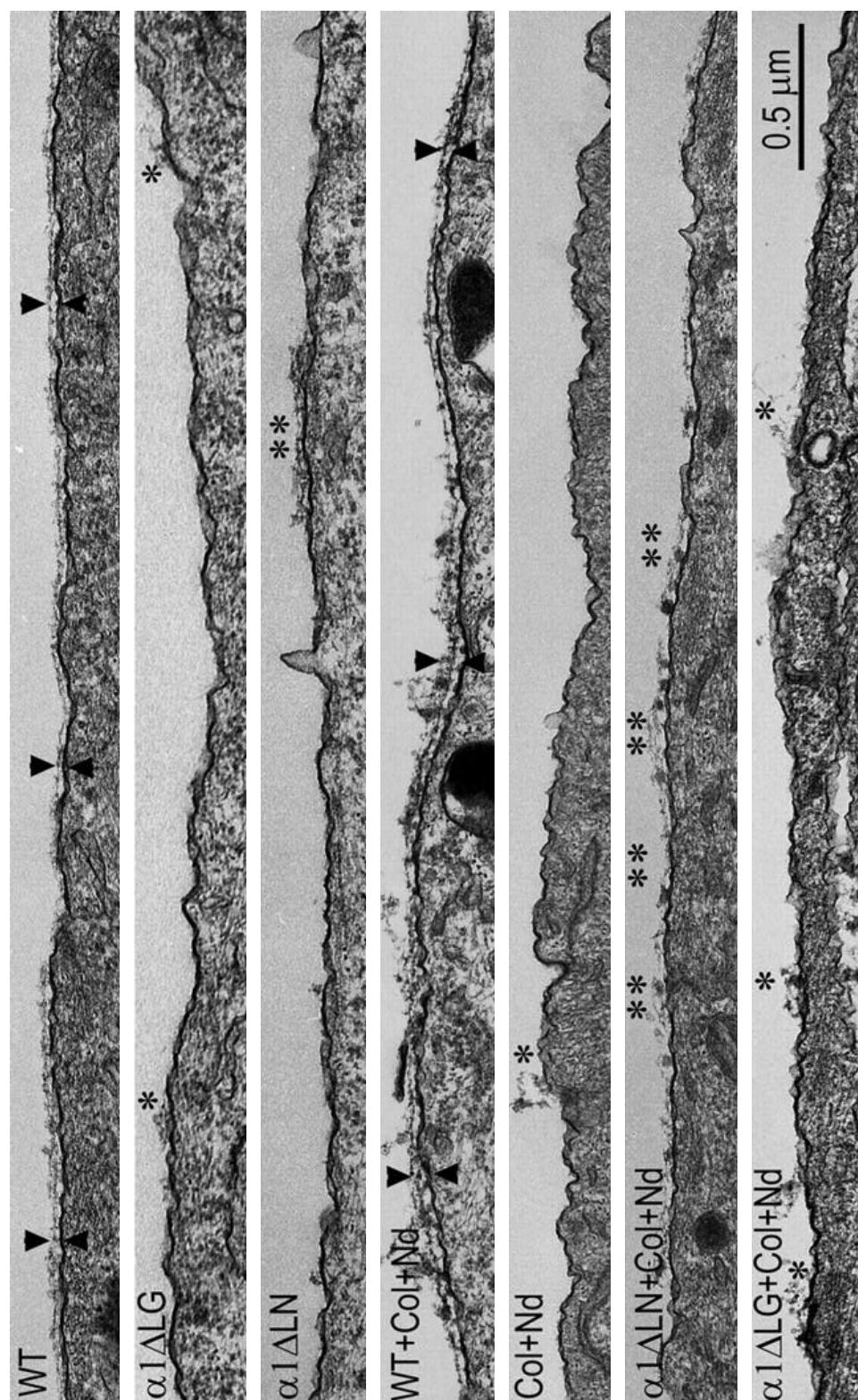


Appendix Figure 11 – Perlecan, syndecan-1, and syndecan-3 expression in cultured Schwann cells.

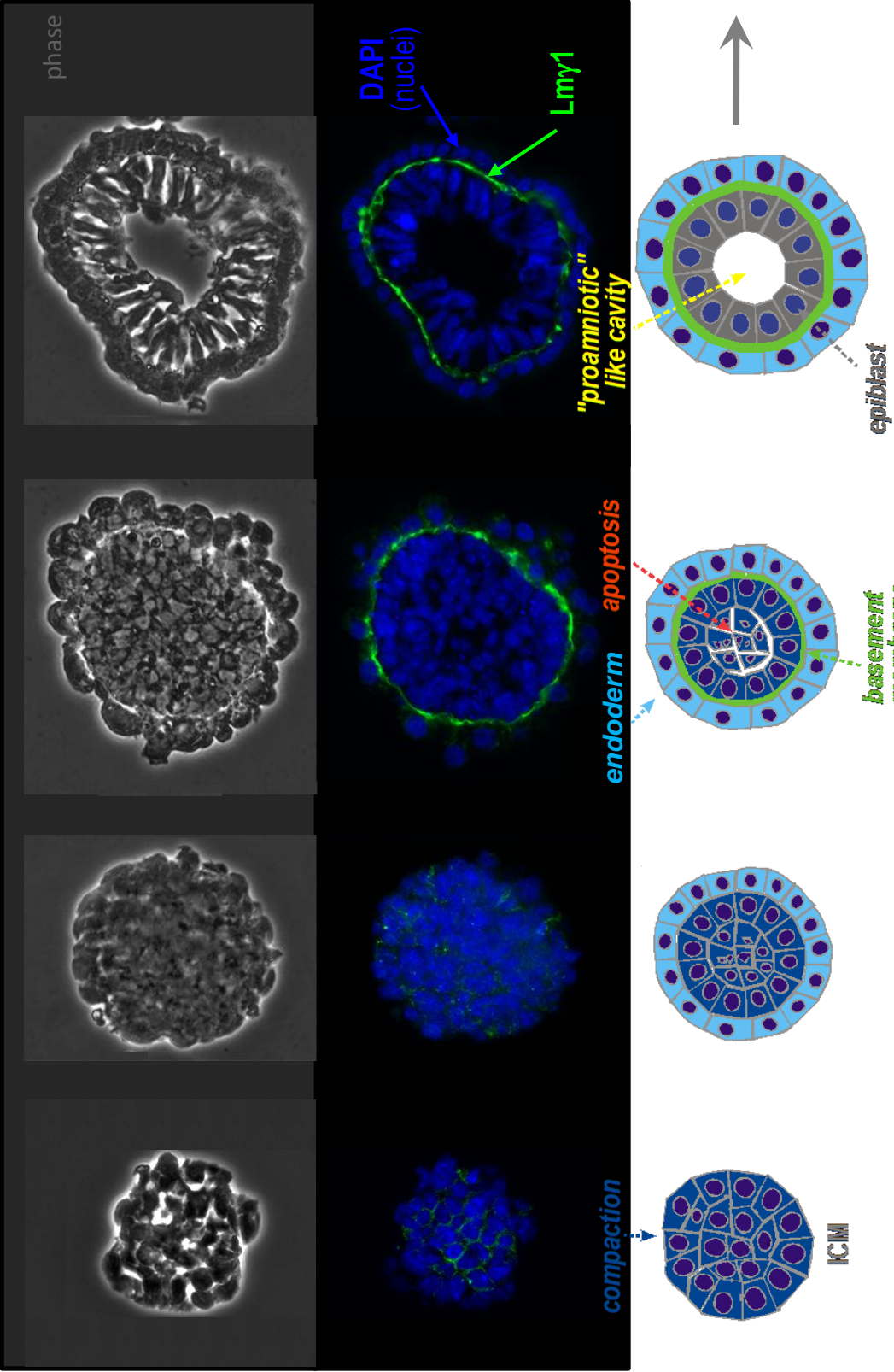


Appendix Figure 12 – β 1 integrin, sulfatide, and agrin expression in cultured Schwann cells.

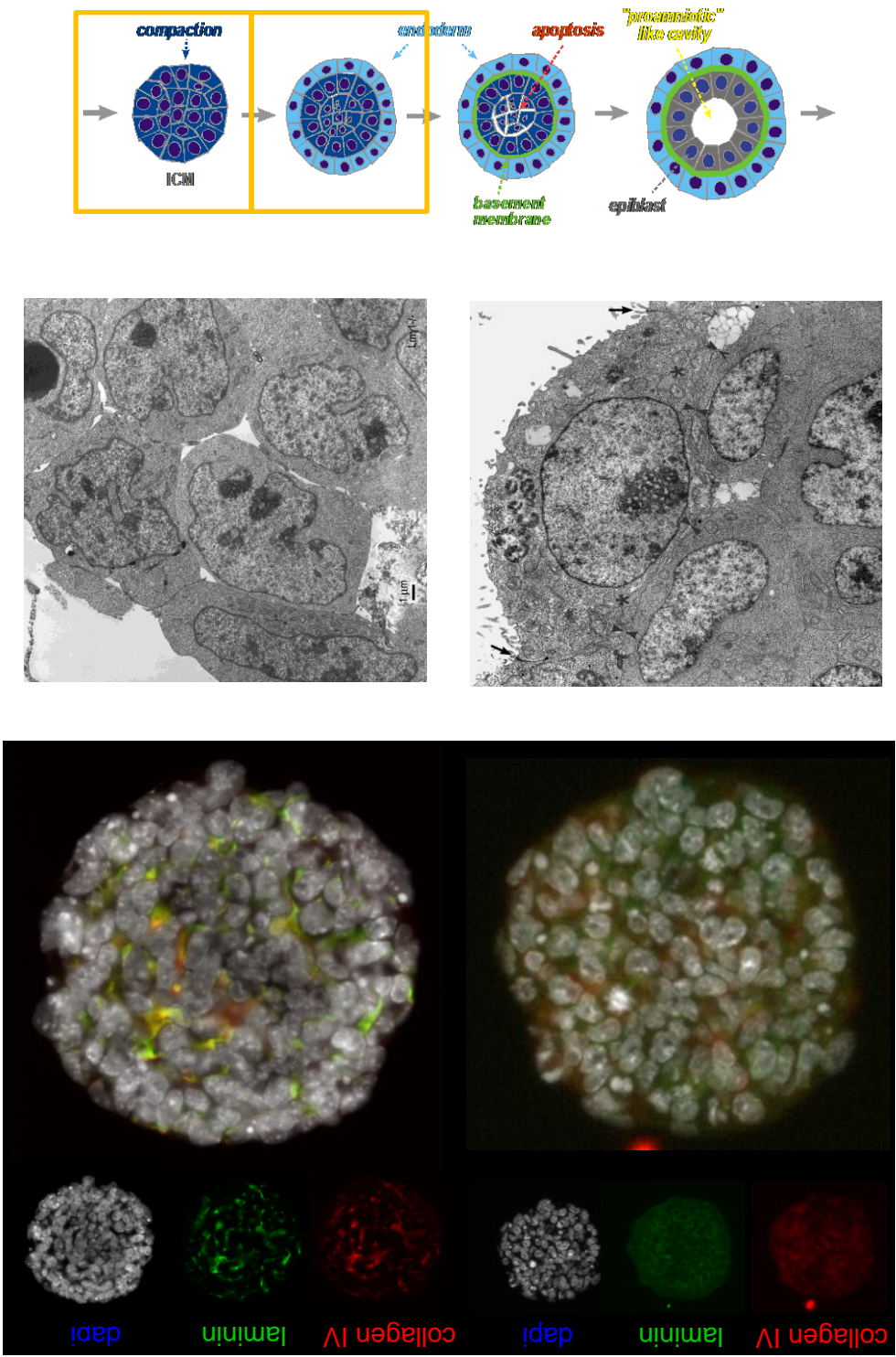




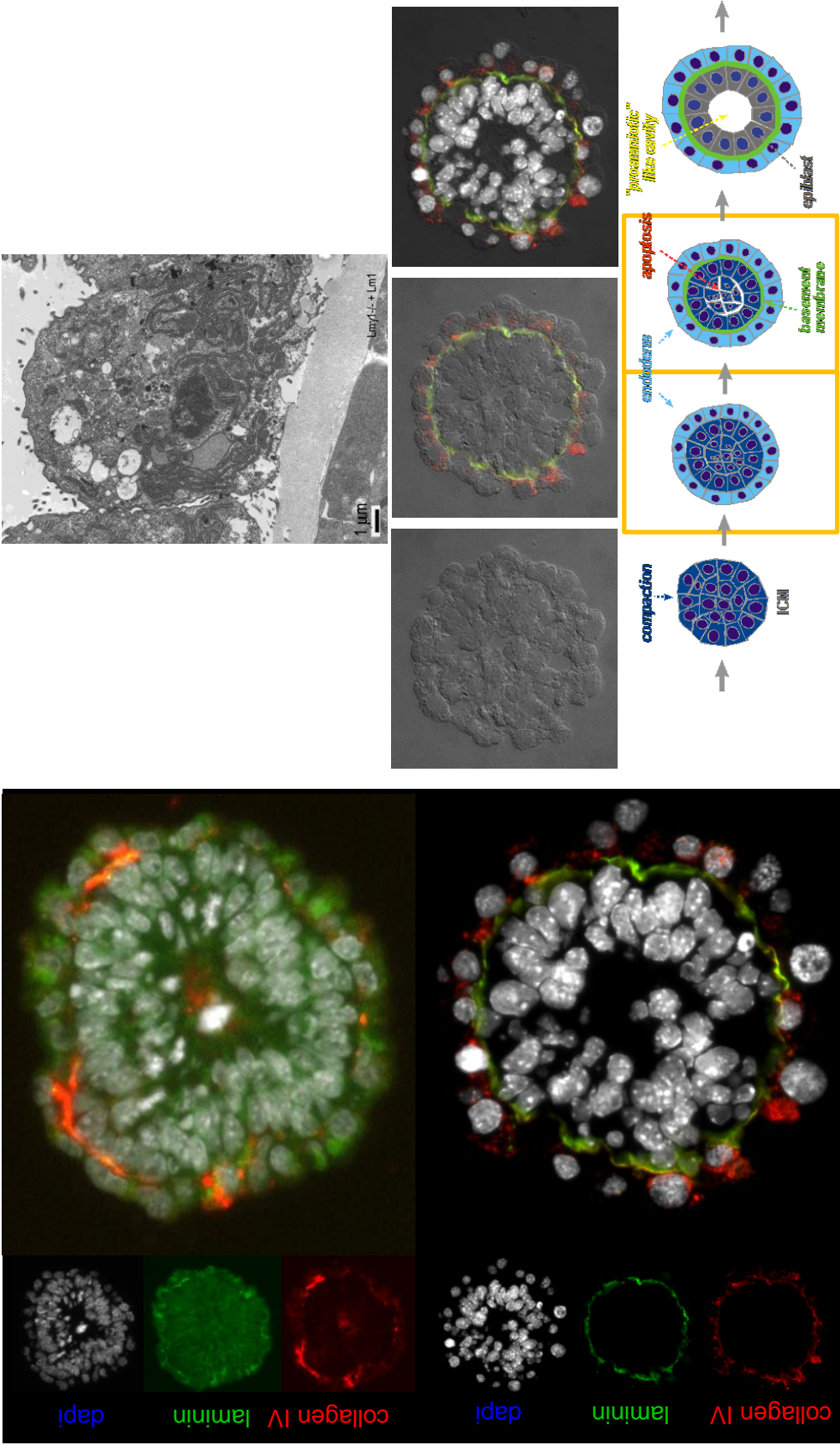
Appendix figure 14 – Electron microscopy images depicting the accumulation of recombinant heterotrimeric Lm-111s and BM formation on the cell surface of Schwann cells in the presence or absence of type IV collagen and nidogen-1.



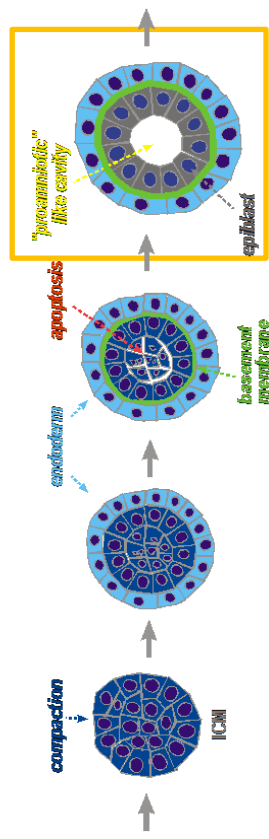
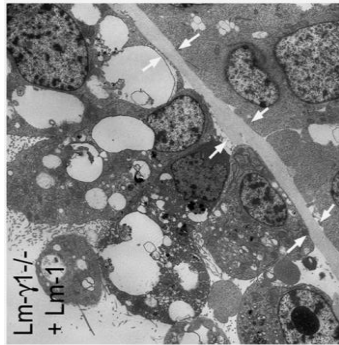
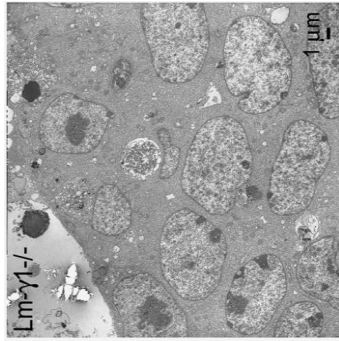
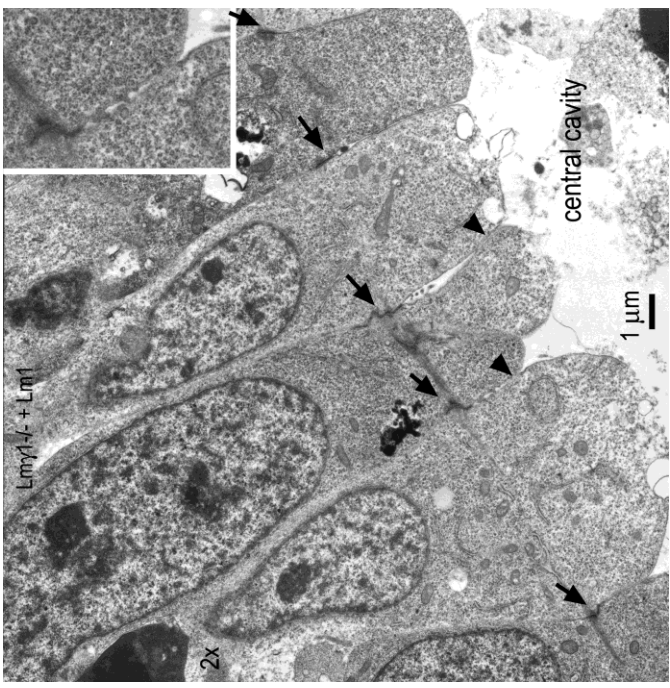
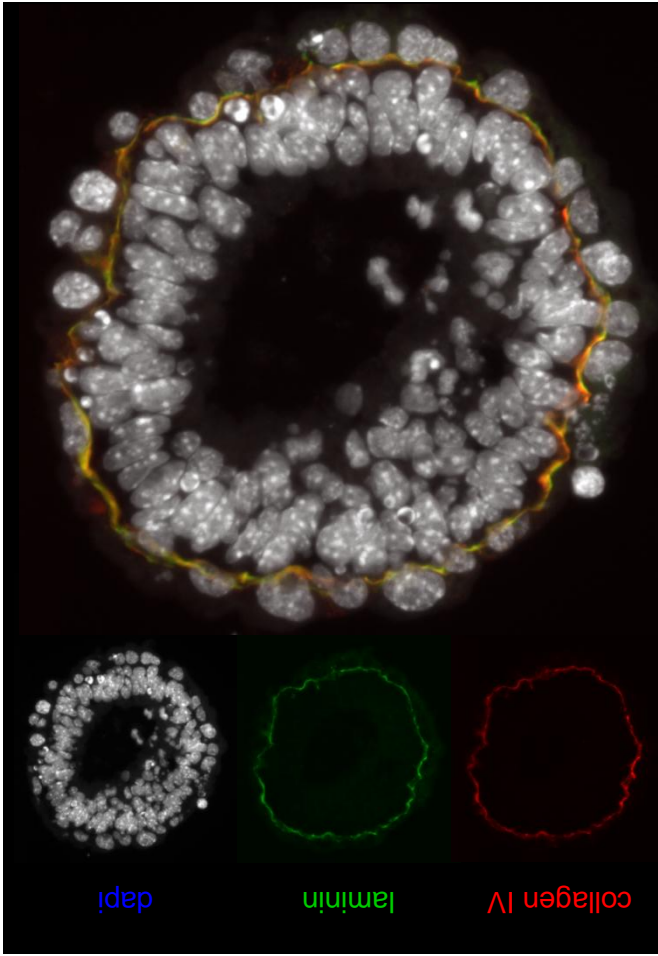
Appendix figure 15 – The different stages of differentiation and development WT ES cells undergo during embryoid body development.



Appendix Figure 16 – Immunofluorescence and electron microscopy of exogenous Laminin-111 induction of BM formation, epiblast differentiation, and cavitation in $\gamma 1$ laminin null EBs: aggregation and condensation.



Appendix Figure 17 – Immunofluorescence and electron microscopy of exogenous Laminin-111 induction of BM formation, epiblast differentiation, and cavitation in $\gamma 1$ laminin null EBs: BM formation, formation and elongation of epiblast layer.



Appendix Figure 18 – Immunofluorescence and electron microscopy of exogenous Laminin-111 induction of BM formation, epiblast differentiation, and cavitation in γ 1 laminin null EBs: cavitation.

Appendix figure 19 – Basement membrane formation and epiblast differentiation in $\gamma 1$ laminin null embryoid bodies treated with Lm-111, modified Lm-111, Lm-111 fragments, and recombinant Lm-111s.

Treatment	BM formation (%)	Epiblast differentiation (%)	Number counted
none	0	0	403
Lm-111	77 +/- 6	56 +/- 5	521
AEBSF Lm-111	0	0	203
Lm-111 + E1'	2 +/- 1	0	117
Lm-111 + AEBSF E1'	64 +/- 5	29 +/- 7	103
Lm-111 + E4	4 +/- 2	0	98
Lm-111 + AEBSF E4	70 +/- 8	35 +/- 4	109
Lm-111 ₀ Nh/Cf	23 +/- 4	6 +/- 4	223
Lm-111 _{Nm/Nh/O}	53 +/- 6	32 +/- 5	65
Lm-111 $\Delta\alpha$ LN _{Nm/Nh/Cf}	2 +/- 1	0	165
Lm-111 $\Delta\beta$ LN-LEa _{Nm/Nh/Cf}	6 +/- 3	0	135
Lm-111 _{Nm3/Nh/O}	3 +/- 2	0	147
Lm-111 + E8	43 +/- 5	22 +/- 3	145
Lm-111 + EHS E3	3 +/- 2	0	178
Lm-111 + AEBSF E3	65 +/- 6	39 +/- 4	166
Lm-111 $\Delta\alpha$ LG1-5 _{Nm/Nh/Cf}	0	0	143
Lm-111 _{Nm/Nh/O} + α 1LG4-5/WT	7 +/- 2	ND	133
Lm-111 _{Nm/Nh/O} + α 1LG4-5/ <u>RKR</u> ₂₇₂₁	9 +/- 5	ND	143
Lm-111 _{Nm/Nh/O} + α 1LG4-5/ <u>KRK</u> ₂₇₉₃	45 +/- 4	ND	145
Lm-111 *	60 +/- 4	38	211
Lm-111 + α 1LG4-5/WT _{Nf} *	8	ND	57
Lm-111 + α 1LG4-5/ <u>RKR</u> ₂₇₂₁ *	15	ND	53
Lm-111 + α 1LG4-5/ <u>KRK</u> ₂₇₉₃ *	38	ND	61

* = experiments done with EHS Lm and only performed by Dr. Shaohua Li.

Appendix Table 1. Crystallographic statistics for recombinant mouse $\alpha 1$ LG4-5. Various information concerning the data collection, modeling, and refinement for the crystal structure determination of mouse $\alpha 1$ LG4-5. Numbers in parentheses refer to data in the highest resolution shell.

Data collection and reduction	
space group	P2 ₁
unit cell dimensions	a = 70.53 Å°, b = 55.81 Å°,
	c = 100.99 Å°, β = 98.48°
resolution range (Å°)	20.0 (2.00) – 1.90
unique reflections	59682
multiplicity	2.6 (2.1)
completeness (%)	97.3 (91.5)
mean I/ σ (I)	10.2 (2.2)
R _{merge}	0.070 (0.333)

Refinement	
reflections (working set/test set)	56655/3015
atoms (protein/solvent)	5781/334
R _{cryst} /R _{free}	0.230/0.262
r.m.s. deviations	bond lengths (Å°)
	0.006
	bond angles (°)
B-factors (Å ²), ¹	1.4
	2.8
Ramachandran plot (%) ²	86.9/11.9/0.8/0.5

¹Difference in B-factors of covalently bonded atoms.

²Residues in most favored, additionally allowed, generously allowed, and disallowed regions (33). In both crystallographically independent molecules, two residues assume unfavorable main chain conformations: LY₅₂₇₉₁, which is part of the heparin binding site, and ARG₂₈₉₆, whose peptide carbonyl oxygen receives a hydrogen bond from a buried Lysine residue.

REFERENCES

1. Beck K, Hunter I, Engel J. (1990). Structure and function of laminin: anatomy of a multidomain glycoprotein. *FASEB* 4(2):148-160.
2. Cooper AR, MacQueen HA. (1983). Subunits of laminin are differentially synthesized in mouse eggs and early embryos. *Dev. Biol.* 96:467-471.
3. Aumailley M, Bruckner-Tuderman L, Carter WG, Deutzmann R, Edgar D, Ekblom P, Engel J, Engvall E, Hohenester E, Jones JC, Kleinman HK, Marinkovich MP, Martin GR, Mayer U, Meneguzzi G, Miner JH, Miyazaki K, Patarroyo M, Paulsson M, Quaranta V, Sanes JR, Sasaki T, Sekiguchi K, Sorokin LM, Talts JF, Tryggvason K, Uitto J, Virtanen I, von der Mark K, Wewer UM, Yamada Y, Yurchenco PD. (2005). A simplified laminin nomenclature. *Matrix Biol* 24(5): 326-332.
4. Beck K, Dixon TW, Engel J, Parry DA. (1993). Ionic interactions in the coiled-coil domain of laminin determine the specificity of chain assembly. *J Mol Biol* 231: 311-323.
5. Galliano MF, Aberdam D, Aguzzi A, Ortonne J P, Meneguzzi G. (1995). Cloning and complete primary structure of the mouse laminin alpha 3 chain. Distinct expression pattern of the laminin alpha 3A and alpha 3B chain isoforms. *J Biol Chem* 270: 21820-21826.
6. Kallunki P, Sainio K, Eddy R, Byers M, Kallunki T, Sariola H, Beck K, Hirvonen H, Shows TB, Tryggvason K. (1992). A truncated laminin chain homologous to the B2 chain: Structure, spatial expression, and chromosomal assignment. *J Cell Biol* 119: 679-693.
7. Talts JF, Timpl R. (1999). Mutation of a basic sequence in the laminin alpha2LG3 module leads to a lack of proteolytic processing and has different effects on beta1 integrin-mediated cell adhesion and alpha-dystroglycan binding. *FEBS Lett* 458: 319-323.
8. Ekblom P, Lonai P, Talts JF. (2003). Expression and biological role of laminin-1. *Matrix Biol* 22(1): 35-47.
9. Leivo I, Laurila P, Wahlstrom T, Engvall E. (1989). Expression of merosin, a tissue-specific basement membrane protein, in the intermediate trophoblast cells of choriocarcinoma and placenta. *Lab Invest* 60: 783-790.
10. Marinkovich MP, Lunstrum GP, Burgeson RE. (1992). The anchoring filament protein kalinin is synthesized and secreted as a high molecular weight precursor. *J Biol Chem* 267: 17900-6.
11. Miner, J. H., Patton, B. L., Lentz, S. I., Gilbert, D. J., Snider, W. D., Jenkins, N. A., Copeland, N. G., and Sanes, J. R. (1997). The laminin alpha chains: expression, developmental transitions, and chromosomal locations of alpha1-5, identification of heterotrimeric laminins 8-11, and cloning of a novel alpha3 isoform. *J Cell Biol* 137: 685-701.

12. Aumailley M, Smyth N, (1998). The role of laminins in basement membrane function. *J Anat* 193: 1–21.
13. Sasaki T, Göhring W, Mann K, Brakebusch C, Yamada Y, Fässler R, Timpl R. (2001). Short arm region of laminin-5 g2 chain: structure, mechanism of processing and binding to heparin and proteins. *J Mol Biol* 314: 751–763.
14. Talts JF, Sasaki T, Miosge N, Göhring W, Mann K, Mayne R, Timpl R. (2000). Structural and functional analysis of the recombinant G domain of the laminin $\alpha 4$ chain and its proteolytic processing in tissues. *J Biol Chem* 275: 35192–35199.
15. Sasaki T, Giltay R, Talts U, Timpl R, Talts JF. (2002). Expression and distribution of laminin $\alpha 1$ and $\alpha 2$ chains in embryonic and adult mouse tissues; an immunochemical approach. *Exp Cell Res* 275: 185–199.
16. Durbeej M, Fecker L, Hjalt T, Zhang HY, Salmivirta K, Klein G, Timpl R, Sorokin L, Ebendal T, Ekblom P, Ekblom M. (1996). Expression of laminin $\alpha 1$, $\alpha 5$ and $\beta 2$ chains during embryogenesis of the kidney and vasculature. *Matrix Biol* 15(6): 397–413.
17. Miner JH, Li C, Mudd JL, Go G, Sutherland AE (2004). Compositional and structural requirements for laminin and basement membranes during mouse embryo implantation and gastrulation. *Dev* 131(10): 2247–2256.
18. Schéele S, Falk M, Franzén A, Ellin F, Ferletta M, Lonai P, Andersson B, Timpl R, Forsberg E, Ekblom P. (2005). Laminin $\alpha 1$ globular domains 4–5 induce fetal development but are not vital for embryonic basement membrane assembly. *Proc Natl Acad Sci USA*. 102(5): 1502–6.
19. Falk M, Ferletta M, Forsberg E, Ekblom P. (1999). Restricted distribution of laminin $\alpha 1$ chain in normal adult mouse tissues. *Matrix Biol* 18: 557–568.
20. Erickson AC, Couchman JR. (2000). Still more complexity in mammalian basement membranes. *J Histochem Cytochem* 48: 1291–1306.
21. Mayer U, Kohfeldt E, Timpl R. (1998). Structural and genetic analysis of laminin-nidogen interaction. *Ann NY Acad Sci* 857: 130–142.
22. Barrett T, Troup DB, Wilhite SE, Ledoux P, Rudnev D, Evangelista C, Kim IF, Soboleva A, Tomashevsky M, Edgar R. (2007). NCBI GEO: mining tens of millions of expression profiles--database and tools update. *Nucleic Acids Res* 35(Database issue): D760–765.
23. Pontius JU, Wagner L, Schuler GD. (2003). UniGene: a unified view of the transcriptome. In: *The NCBI Handbook*. Bethesda (MD): National Center for Biotechnology Information.
24. Wheeler DL, Church DM, Federhen S, Lash AE, Madden TL, Pontius JU, Schuler GD, Schriml LM, Sequeira E, Tatusova TA, Wagner L. (2003). Database resources of

the National Center for Biotechnology. Nucl Acids Res 31: 28-33.

25. Engel J, Odermatt E, Engel A, Madri JA, Furthmayr H, Rohde H, Timpl R. (1981). Shapes, domain organizations and flexibility of laminin and fibronectin, two multifunctional proteins of the extracellular matrix. *J Mol Biol* 150: 97-120.

26. Sasaki M, Kato S, Kohno K, Martin GR, Yamada Y. (1987). Sequence of the cDNA encoding the laminin B1 chain reveals a multidomain protein containing cysteine-rich repeats. *Proc Natl Acad Sci USA* 84: 935-939.

27. Sasaki M, Kleinman HK, Huber H, Deutzmann R, Yamada Y. (1988). Laminin, a multidomain protein. The A chain has a unique globular domain and homology with the basement membrane proteoglycan and the laminin B chains. *J Biol Chem* 263: 16536-16544.

28. Sasaki M, Yamada Y. (1987). The laminin B2 chain has a multidomain structure homologous to the B1 chain. *J Biol Chem* 262: 17111-17117.

29. Timpl R, Rohde H, Robey PG, Rennard SI, Foidart JM, Martin GR. (1979). Laminin--a glycoprotein from basement membranes. *J Biol Chem* 254: 9933-9937.

30. Shim C, Kwon HB, Kim K. (1996). Differential expression of laminin chain-specific mRNA transcripts during mouse preimplantation embryo development. *Mol Reprod Dev* 44: 44-55.

31. Smyth N, Vatansever HS, Murray P, Meyer M, Frie C, Paulsson M, Edgar, D. (1999). Absence of Basement Membranes after Targeting the LAMC1 Gene Results in Embryonic Lethality Due to Failure of Endoderm Differentiation. *J Cell Biol* 144: 151-160.

32. Thorsteinsdottir S. (1992). Basement membrane and fibronectin matrix are distinct entities in the developing mouse blastocyst. *Anat Rec* 232: 141-149.

33. Wu TC, Wan YJ, Chung AE, Damjanov I. (1983). Immunohistochemical localization of entactin and laminin in mouse embryos and fetuses. *Dev Biol* 100: 496-505.

34. Ekblom M, Falk M, Salmivirta K, Durbeej M, Ekblom P. (1998). Laminin isoforms and epithelial development. *Ann. NY Acad. Sci.* 857: 194-211.

35. Colognato H, Yurchenco P. (2000). Form and function: the laminin family of heterotrimers. *Dev Dyn* 218: 213-234.

36. Virtanen I, Gullberg D, Rissanen J, Kivilaakso E, Kiviluoto T, Laitinen LA, Lehto VP, Ekblom P. (2000). Laminin $\alpha 1$ chain shows a restricted distribution in epithelial basement membranes of fetal and adult human tissues. *Exp Cell Res* 257: 298-309.

37. Nissinen M, Vuolteenaho R, Boot Handford R, Kallunki P, Tryggvason K. (1991). Primary structure of the human laminin A chain. Limited expression in human tissues. *Biochem J* 276: 369-379.

38. Salmivirta K, Sorokin LM, Ekblom P. (1997). Differential expression of laminin alpha chains during murine tooth development. *Dev Dyn* 210: 206-215.
39. Schuger L, Skubitz AP, Zhang J, Sorokin L, He L. (1997). Laminin alpha1 chain synthesis in the mouse developing lung: requirement for epithelial-mesenchymal contact and possible role in bronchial smooth muscle development. *J Cell Biol* 139: 553-562.
40. Sorokin LM, Pausch F, Durbeej M, Ekblom P. (1997). Differential expression of five laminin alpha (1-5) chains in developing and adult mouse kidney. *Dev Dyn* 210: 446-462.
41. Sorokin LM, Pausch F, Frieser M, Kroger S, Ohage E, Deutzmann R. (1997). Developmental regulation of the laminin alpha5 chain suggests a role in epithelial and endothelial cell maturation. *Dev Biol* 189: 285-300.
42. Timpl R, Brown JC. (1996). Supramolecular assembly of basement membranes. *BioEssays* 18: 123-132.
43. Tunggal P, Smyth N, Paulsson M, Ott MC. (2000). Laminins: structure and genetic regulation. *Microsc Res Tech* 51: 214-227.
44. Paulsson M. (1988). The role of Ca²⁺ binding in the self-aggregation of laminin-nidogen complexes. *J Biol Chem* 263: 5425-5430.
45. Yurchenco PD, Cheng YS. (1993). Self-assembly and calcium-binding sites in laminin. A three-arm interaction model. *J Biol Chem* 268: 17286-17299.
46. Yurchenco PD, Tsilibary EC, Charonis AS, Furthmayr H. (1985). Laminin polymerization in vitro. Evidence for a two-step assembly with domain specificity. *J Biol Chem* 260: 7636-7644.
47. Yurchenco PD. (1994). Assembly of laminin and type IV collagen into basement membrane networks. In *Extracellular Matrix Assembly and Structure*, Yurchenco PD, Birk DE, Mecham RP, eds. (New York: Academic Press), p. 351-388.
48. Yurchenco PD, Cheng YS, Colognato H. (1992). Laminin forms an independent network in basement membranes [published erratum appears in *J Cell Biol* 1992 118(2): 493]. *JCellBiol* 117: 1119-1133.
49. Yurchenco PD, O'Rear JJ. (1994). Basement membrane assembly. In: Ruoslahti E, Engvall E, editors. *Methods in enzymology* (Vol. 245). (New York: Academic Press), p. 489-518.
50. Kalb E, Engel J. (1991). Binding and calcium-induced aggregation of laminin onto lipid bilayers. *J Biol Chem* 266: 19047-19052.
51. Cheng YS, Champlaud MF, Burgeson RE, Marinkovich MP, Yurchenco PD. (1997). Self-assembly of laminin isoforms. *J Biol Chem* 272: 31525-31532.

52. Yurchenco PD and Ruben GC. (1987). Basement membrane structure in situ: Evidence for lateral associations in the type IV collagen network. *J Cell Biol* 105: 2559-2568.
53. Yurchenco PD, Ruben GC. (1988). Type IV collagen lateral associations in the EHS tumor matrix. Comparison with amniotic and in vitro networks. *Am J Pathol* 132: 278-291.
54. Friedrich MV, Gohring W, Morgelin M, Brancaccio A, David G, Timpl R (1999) Structural basis of glycosaminoglycan modification and of heterotypic interactions of perlecan domain V. *J Mol Biol* 294: 259–270.
55. Gesemann M, Brancaccio A, Schumacher B, Ruegg MA. (1998). Agrin is a high-affinity binding protein of dystroglycan in non-muscle tissue. *J Biol Chem* 273: 600-605.
56. Aumailley M, Wiedemann H, Mann K, Timpl R. (1989). Binding of nidogen and the laminin-nidogen complex to basement membrane collagen type IV. *Eur J Biochem* 184: 241-248.
57. Battaglia C, Mayer U, Aumailley M, Timpl R. (1992). Basement-membrane heparan sulfate proteoglycan binds to laminin by its heparan sulfate chains and to nidogen by sites in the protein core. *Eur J Biochem* 208: 359-366.
58. Brown JC, Sasaki T, Gohring W, Yamada Y, Timpl R. (1997). The C-terminal domain V of perlecan promotes beta1 integrin-mediated cell adhesion, binds heparin, nidogen and fibulin-2 and can be modified by glycosaminoglycans. *Eur J Biochem* 250: 39-46.
59. Fox JW, Mayer U, Nischt R, Aumailley M, Reinhardt D, Wiedemann H, Mann K, Timpl R, Krieg T, Engel J. (1991). Recombinant nidogen consists of three globular domains and mediates binding of laminin to collagen type IV. *EMBO J* 10: 3137-3146.
60. Poschl E, Fox JW, Block D, Mayer U, Timpl R. (1994). Two non-contiguous regions contribute to nidogen binding to a single EGF-like motif of the laminin gamma 1 chain. *EMBO J* 13: 3741-3747.
61. Mann K, Deutzmann R, Timpl R. (1988). Characterization of proteolytic fragments of the laminin-nidogen complex and their activity in ligand-binding assays. *Eur J Biochem* 178: 71-80.
62. Mayer U, Nischt R, Poschl E, Mann K, Fukuda K, Gerl M, Yamada Y, Timpl R. (1993). A single EGF-like motif of laminin is responsible for high affinity nidogen binding. *EMBO J* 12: 1879-1885.
63. Kim S, Wadsworth WG. (2000). Positioning of longitudinal nerves in *C. elegans* by nidogen. *Science* 288: 150-154.
64. Hall H, Deutzmann R, Timpl R, Vaughan L, Schmitz B, Schachner M. (1997). HNK-1 carbohydrate-mediated cell adhesion to laminin-1 is different from heparin-mediated and sulfatide-mediated cell adhesion. *Eur J Biochem* 246: 233-242.

65. Roberts DD, Rao CN, Magnani JL, Spitalnik SL, Liotta LA, Ginsburg V. (1985). Laminin binds specifically to sulfated glycolipids. *Proc Natl Acad Sci USA* 82: 1306-1310.
66. Burgeson RE, Chiquet M, Deutzmann R, Ekblom P, Engel J, Kleinman H, Martin GR, Meneguzzi G, Paulsson M, Sanes J, Timpl R, Tryggvason K, Burkin DJ, Kaufman SJ. (1999). The $\alpha 7 \beta 1$ integrin in muscle development and disease. *Cell Tissue Res* 296: 183-190.
67. Salmivirta K, Talts JF, Olsson M, Sasaki T, Timpl R, Ekblom P. (2002). Binding of mouse nidogen-2 to basement membrane components and cells and its expression in embryonic and adult tissues suggest complementary functions of the two nidogens. *Exp Cell Res* 279: 188–201.
68. Ervasti JM, Campbell KP. (1993). A role for the dystrophin-glycoprotein complex as a transmembrane linker between laminin and actin. *J Cell Biol* 122: 809-823.
69. Henry MD, Campbell KP. (1996). Dystroglycan: an extracellular matrix receptor linked to the cytoskeleton. *Curr Opin Cell Biol* 8: 625-631.
70. Li S, Harrison D, Carbonetto S, Fassler R, Smyth N, Edgar D, Yurchenco PD. (2002). Matrix assembly, regulation and survival functions of laminin and its receptors in embryonic stem cell differentiation *J Cell Biol* 157(7): 1279-1290.
71. Li S, Liquari P, McKee KK, Harrison D, Patel R, Lee S, Yurchenco PD. (2005). Laminin-sulfatide binding initiates basement membrane assembly and enables receptor signaling in Schwann cells and fibroblasts. *J Cell Biol* 169(1):179-189.
72. Spiro RG. (1967). Studies on the renal glomerular basement membrane. Preparation and chemical composition. *J Biol Chem* 242: 1915–1922.
73. Timpl R, Wiedemann H, van Delden V, Furthmayr H, Kuhn K. (1981). A network model for the organization of type IV collagen molecules in basement membranes. *Eur J Biochem* 120: 203–211.
74. Yurchenco PD, Furthmayr H. (1984). Self-assembly of basement membrane collagen. *Biochemistry* 23: 1839-1850.
75. Barker DF, Hostikka SL, Zhou J, Chow LT, Oliphant AR, Gerken SC, Gregory MC, Skolnick MH, Atkin CL, Tryggvason K. (1990). Identification of mutations in the COL4A5 collagen gene in Alport syndrome. *Science* 248: 1224–1227.
76. Spear PG. (1998). A welcome mat for leprosy and Lassa fever. *Science* 282: 1999-2000.
77. Spear GS, Slusser RJ. (1972). Alport's syndrome. Emphasizing electron microscopic studies of the glomerulus. *Am J Pathol* 69: 213–224.
78. Goodpasture EW. (1919). The significance of certain pulmonary lesions in relation to the etiology of influenza. *Am J Med Sci* 158: 863–870.

79. Gunwar S, Bejarano PA, Kalluri R, Langeveld JP, Wisdom BJ Jr, Noelken ME, Hudson BG. (1991). Alveolar basement membrane: molecular properties of the noncollagenous domain (hexamer) of collagen IV and its reactivity with Goodpasture autoantibodies. *Am J Respir Cell Mol Biol* 5: 107–112.
80. Hudson BG. (2004) The molecular basis of Goodpasture and Alport syndromes: beacons for the discovery of the collagen IV family. *J Am Soc Nephrol* 15(10): 2514–2527.
81. Hudson BG, Reeders ST, Tryggvason K. (1993). Type IV collagen: structure, gene organization, and role in human diseases. Molecular basis of Goodpasture and Alport syndromes and diffuse leiomyomatosis. *J Biol Chem* 268(35): 26033–26036.
82. Lerner RA, Glassock RJ, Dixon FJ. (1967). The role of anti-glomerular basement membrane antibody in the pathogenesis of human glomerulonephritis. *J Exp Med* 126: 989–1004.
83. Mayer U, Poschl E, Gerecke DR, Wagman DW, Burgeson RE, Timpl R. (1995). Low nidogen affinity of laminin-5 can be attributed to two serine residues in EGF-like motif gamma 2III4. *FEBS Lett* 365: 129–132.
84. Reinhardt D, Mann K, Nischt R, Fox JW, Chu M, Krieg T, Timpl R. (1993). Mapping of nidogen binding sites for collagen type IV, heparan sulfate proteoglycan, and zinc. *J Biol Chem* 268: 10881–10887.
85. Takagi J, Yang Y, Liu JH, Wang JH, Springer TA. (2003). Complex between nidogen and laminin fragments reveals a paradigmatic beta-propeller interface. *Nature* 424(6951): 969–974.
86. Cohen IR, Grassel S, Murdoch AD, Iozzo RV. (1993). Structural characterization of the complete human perlecan gene and its promoter. *Proc Nat Acad Sci* 90: 10404–10408.
87. Couchman JR, Kapoor R, Sthanam M, Wu RR. (1996). Perlecan and basement membrane-chondroitin sulfate proteoglycan (Bamacan) are two basement membrane chondroitin dermatan sulfate proteoglycans in the Engelbreth-Holm-Swarm tumor matrix. *J Biol Chem* 271: 9595–9602.
88. Dolan M, Horchar T, Rigatti B, Hassell JR. (1997). Identification of sites in domain I of perlecan that regulate heparan sulfate synthesis. *J Biol Chem* 272: 4316–4322.
89. Graham LD, Whitelock JM, Underwood PA. (1999). Expression of human perlecan domain I as a recombinant heparan sulfate proteoglycan with 20-Kda glycosaminoglycan chains. *Biochem Biophys Res Commun* 256: 542–548.
90. Groffen AJA, Buskens CA, Tryggvason K, Veerkamp JH, Monnens LA, Van Der Heuvel LPWJ. (1996). Expression and characterization of human perlecan domains I and II synthesized by baculovirus-infected insect cells. *Eur J Biochem* 241: 827–834.
91. Isemura M, Sato N, Yamaguchi Y. (1987). Isolation and characterization of fibronectin-binding proteoglycan carrying both heparan sulfate and dermatan sulfate chains from human placenta. *J Biol Chem* 262: 8926–8933.

92. Iozzo RV, Hassell JR. (1989). Identification of the precursor protein for the heparan sulfate proteoglycan of human colon carcinoma cells and its post-translational modifications. *Arch Biochem Biophys* 269: 239–349.
93. Kokenyesi R, Silbert JE. (1995). Formation of heparan sulfate or chondroitin/dermatan sulfate on recombinant domain of mouse perlecan expressed in Chinese hamster ovary cells. *Biochem Biophys Res Comm* 211: 262–267.
94. Ettner N, Gohring W, Sasaki T, Mann K, Timpl R. (1998). The N-terminal globular domain of the laminin alpha1 chain binds to alpha1beta1 and alpha2beta1 integrins and to the heparan sulfate- containing domains of perlecan. *FEBS Lett* 430: 217-221.
95. Hopf M, Gohring W, Mann K, Timpl R. (2001). Mapping of binding sites for nidogens, fibulin-2, fibronectin and heparin to different IG modules of perlecan. *J Mol Biol* 311: 529–541.
96. Couchman JR, Ljubimov AV, Sthanam M, Horchar T, Hassell JR. (1995). Antibody mapping and tissue localization of globular and cysteine-rich regions of perlecan domain III. *J Histochem Cytochem* 43: 955–963.
97. Murdoch AD, Liu B, Schwarting R, Tuan RS, Iozzo RV. (1994). Widespread expression of perlecan proteoglycan in basement membranes and extracellular matrices of human tissues as detected by a novel antibody against domain III and by in situ hybridization. *J Histochem Cytochem* 42: 239–249.
98. Tufvesson E, Westergren–Thorsson G. (2000). Alteration of proteoglycan synthesis in human lung fibroblasts induced by interleukin-1beta and tumor necrosis factor-alpha. *J Cell Biochem* 77: 298–309.
99. Mohan PS, Spiro RG. (1991). Characterization of heparan sulfate proteoglycan from calf lens capsule and proteoglycans synthesized by cultured lens epithelial cells: comparison with other basement membrane proteoglycans. *J Biol Chem* 266: 8567–8575.
100. Tapanadechopone P, Tumova S, Jiang X, Couchman JR. (2001). Epidermal transformation leads to increased perlecan synthesis with heparin-binding growth factor affinity. *Biochem J* 355: 517–527.
101. Knox S, Merry C, Stringer S, Melrose J, Whitelock J. (2002). Not all perlecans are created equal. Interactions with fibroblast growth factor (FGF) 2 and FGF receptors. *J Biol Chem* 277:14657–14665 .
102. SundarRaj N, Fite D, Ledbetter S, Chakravarti S, Hassell JR. (1995). Perlecan is a component of cartilage matrix and promotes chondrocyte attachment. *J Cell Sci* 108: 2663–2672.
103. Weiser MCM, Belknap JK, Grieshaber SS, Kinsella MG, Majack RA. (1996). Developmental regulation of perlecan gene expression in aortic smooth muscle cells. *Matrix Biol* 15: 331–340.

104. Aviezer D, Hecht D, Safran M, Eisinger M, David G, Yayon A. (1994). Perlecan, basal lamina proteoglycan, promotes basic fibroblast growth factor-receptor binding, mitogenesis, and angiogenesis. *Cell* 79: 1005–1013.
105. Aviezer D, Iozzo RV, Noonan DM, Yayon A. (1997). Suppression of autocrine and paracrine functions of basic fibroblast growth factor by stable expression of perlecan antisense cDNA. *Mol Cell Biol* 17: 1938–1946.
106. Gallagher JT. (2001). Heparan sulfate: growth control with restricted sequence menu. *J Clin Invest* 108: 357–361.
107. Turnbull JE, Fernig DG, Ke Y, Wilkinson MC, Gallagher JT. (1992). Identification of the basic fibroblast growth factor binding sequence in fibroblast heparan sulfate. *J Biol Chem* 267: 10337–10341.
108. Whitelock JM, Murdoch AD, Iozzo RV, Underwood PA. (1996). The degradation of human endothelial cell-derived perlecan and release of bound basic fibroblast growth factor by stromelysin, collagenase, plasmin, and heparanases. *J Biol Chem* 271: 10079–10086.
109. Yayon A, Klagsbrun M, Esko JD, Leder P, Ornitz DM. (1991). Cell surface, heparin-like molecules are required for binding of basic fibroblast growth factor to its high affinity receptor. *Cell* 64: 841–848.
110. Gitay-Goren H, Halaban R, Neufeld G. (1993). Human melanoma cells but not normal melanocytes express vascular endothelial growth factor receptors. *Biochem Biophys Res Commun* 190: 702–709.
111. Cohen T, Gitay-Goren H, Sharon R, Shibuya M, Halaban R, Levis B-Z, Neufeld G. (1995). VEGF₁₂₁, a vascular endothelial growth factor (VEGF) isoform lacking heparin binding ability, requires cell-surface heparan sulfate for efficient binding to the VEGF receptors of human melanoma cells. *J Biol Chem* 270: 11322–11326.
112. Gengrinovitch S, Berman B, David G, Witte L, Neufeld G. (1999). Glypican-1 is a VEGF₁₆₅ binding proteoglycan that acts as an extracellular chaperone for VEGF₁₆₅. *J Biol Chem* 274: 10816–10822.
113. Campanelli JT, Hoch W, Rupp F, Kreiner T, Scheller RH. (1991). Agrin mediates cell contact-induced acetylcholine receptor clustering. *Cell* 67: 909–916.
114. Denzer AJ, Brandenberger R, Gesemann M, Chiquet M, Ruegg MA. (1997). Agrin binds to the nerve-muscle basal lamina via laminin. *J Cell Biol* 137: 671–683.
115. Denzer AJ, Schulthess T, Fauser C, Schumacher B, Kammerer RA, Engel J, Ruegg MA. (1998). Electron microscopic structure of agrin and mapping of its binding site in laminin-1. *Embo J* 17: 335–343.
116. Gesemann M, Denzer AJ, Ruegg MA. (1995). Acetylcholine receptor-aggregating activity of agrin isoforms and mapping of the active site. *J Cell Biol* 128: 625–636.

117. Gesemann M, Cavalli V, Denzer AJ, Brancaccio A, Schumacher B, Ruegg MA. (1996). Alternative splicing of agrin alters its binding to heparin, dystroglycan, and the putative agrin receptor. *Neuron* 16: 755-67.
118. Ruegg MA, Tsim KW, Horton SE, Kroger S, Escher G, Gensch EM, McMahan UJ. (1992). The agrin gene codes for a family of basal lamina proteins that differ in function and distribution. *Neuron* 8: 691-699.
119. Rupp F, Ozcelik T, Linial M, Peterson K, Francke U, Scheller, R. (1992). Structure and chromosomal localization of the mammalian agrin gene. *J Neurosci* 12: 3535-3544.
120. Rupp F, Payan DG, Magill-Solc C, Cowan DM, Scheller RH. (1991). Structure and expression of a rat agrin. *Neuron* 6: 811-823.
121. DeChiara TM, Bowen DC, Valenzuela DM, Simmons MV, Poueymirou WT, Thomas S, Kinetz E, Compton DL, Rojas E, Park JS, Smith C, DiStefano PS, Glass DJ, Burden SJ, Yancopoulos GD. (1996). The receptor tyrosine kinase MuSK is required for neuromuscular junction formation in vivo. *Cell* 85: 501-512.
122. Finn AJ, Feng G, Pendergast AM. (2003). Postsynaptic requirement for Abl kinases in assembly of the neuromuscular junction. *Nature Neurosci.* 6: 717-723.
123. Wang J, Jing Z, Zhang L, Zhou G, Braun J, Yao Y, Wang ZZ. (2003). Regulation of acetylcholine receptor clustering by the tumor suppressor APC. *Nature Neurosci* 6: 1017-1018.
124. Khan AA, Bose C, Yam LS, Soloski MJ, Rupp F. (2001). Physiological regulation of the immunological synapse by agrin. *Science* 292: 1681-1686.
125. Gautam M, Noakes PG, Moscoso L, Rupp F, Scheller RH, Merlie JP, Sanes JR. (1996). Defective neuromuscular synaptogenesis in agrin-deficient mutant mice. *Cell* 85: 525-535.
126. McMahan, U J. (1990). The agrin hypothesis. *Cold Spring Harb Symp Quant Biol* 50: 407-418.
127. Kibbey MC, Jucker M, Weeks BS, Neve RL, Van Nostrand WE, Kleinman HK. (1993). Beta-amyloid precursor protein binds to the neurite-promoting IKVAV site of laminin. *Proc Natl Acad Sci USA* 90: 10150-10153.
128. Kleinman HK, Weeks BS, Cannon FB, Sweeney TM, Sephel GC, Clement B, Zain M, Olson MO, Jucker M, Burrous BA. (1991). Identification of a 110-kDa nonintegrin cell surface laminin-binding protein which recognizes an A chain neurite-promoting peptide. *Arch Biochem Biophys* 290: 320-325.
129. Hinek A, Rabinovitch M, Keeley F, Okamura Oho Y, Callahan J. (1993). The 67-kD elastin/laminin-binding protein is related to an enzymatically inactive, alternatively spliced form of beta-galactosidase. *J Clin Invest* 91: 1198-1205.

130. Runyan RB, Maxwell GD, Shur BD. (1986). Evidence for a novel enzymatic mechanism of neural crest cell migration on extracellular glycoconjugate matrices. *J Cell Biol* 102: 432-441.
131. El Nemer W, Gane P, Colin Y, Bony V, Rahuel C, Galacteros F, Cartron JP, Le Van Kim C. (1998). The Lutheran blood group glycoproteins, the erythroid receptors for laminin, are adhesion molecules. *J Biol Chem* 273: 16686-16693.
132. Colognato H, MacCarrick M, O'Rear JJ, Yurchenco PD. (1997). The laminin alpha2-chain short arm mediates cell adhesion through both the alpha1beta1 and alpha2beta1 integrins. *J Biol Chem* 272: 29330-29336.
133. Colognato-Pyke H, O'Rear JJ, Yamada Y, Carbonetto S, Cheng YS, Yurchenco PD. (1995). Mapping of network-forming, heparin-binding, and alpha 1 beta 1 integrin-recognition sites within the alpha-chain short arm of laminin- 1. *J Biol Chem* 270: 9398-9406.
134. Hall DE, Reichardt LF, Crowley E, Holley B, Moezzi H, Sonnenberg A, Damsky CH. (1990). The alpha 1/beta 1 and alpha 6/beta 1 integrin heterodimers mediate cell attachment to distinct sites on laminin. *J Cell Biol* 110: 2175-2184.
135. Languino LR, Gehlsen KR, Wayner E, Carter WG, Engvall E, Ruoslahti E. (1989). Endothelial cells use alpha 2 beta 1 integrin as a laminin receptor. *J Cell Biol* 109: 2455-2462.
136. Aumailley M, Timpl R, Sonnenberg A. (1990b). Antibody to integrin alpha 6 subunit specifically inhibits cell- binding to laminin fragment 8. *Exp Cell Res* 188: 55-60.
137. van der Flier A, Sonnenberg A. (2001). Function and interactions of integrins. *Cell Tissue Res* 305: 285-398.
138. Gee SH, Blacher RW, Douville PJ, Provost PR, Yurchenco PD, Carbonetto S. (1993). Laminin-binding protein 120 from brain is closely related to the dystrophin-associated glycoprotein, dystroglycan, and binds with high affinity to the major heparin binding domain of laminin. *J Biol Chem* 268: 14972-14980.
139. Kramer RH, Vu MP, Cheng YF, Ramos DM, Timpl R, Waleh N. (1991). Laminin-binding integrin alpha 7 beta 1: functional characterization and expression in normal and malignant melanocytes. *Cell Regul* 2: 805-817.
140. Lee EC, Lotz MM, Steele GDJ, Mercurio AM. (1992). The integrin alpha 6 beta 4 is a laminin receptor. *J Cell Biol* 117: 671-678.
141. Sonnenberg A, Modderman PW, Hogervorst F. (1988). Laminin receptor on platelets is the integrin VLA-6. *Nature*. 336: 487-489.
142. Deutzmann R, Aumailley M, Wiedemann H, Pysny W, Timpl R, Edgar D. (1990). Cell adhesion, spreading and neurite stimulation by laminin fragment E8 depends on maintenance of secondary and tertiary structure in its rod and globular domain. *Eur J Biochem* 191: 513-522.

143. George-Weinstein M, Foster RF, Gerhart JV, Kaufman SJ. (1993). In vitro and in vivo expression of alpha 7 integrin and desmin define the primary and secondary myogenic lineages. *Dev Biol* 156: 209-229.
144. Song WK, Wang W, Foster RF, Bielser DA, Kaufman SJ. (1992). H36-alpha 7 is a novel integrin alpha chain that is developmentally regulated during skeletal myogenesis [published erratum appears in *J Cell Biol* (1992) 118(1): 213]. *J Cell Biol* 117: 643-657.
145. Almeida EA, Huovila AP, Sutherland AE, Stephens LE, Calarco PG, Shaw LM, Mercurio AM, Sonnenberg A, Primakoff P, Myles DG, White JM. (1995). Mouse egg integrin alpha 6 beta 1 functions as a sperm receptor. *Cell* 8: 1095-1104.
146. Chen MS, Almeida EA, Huovila AP, Takahashi Y, Shaw LM, Mercurio AM, White JM. (1999). Evidence that distinct states of the integrin alpha6beta1 interact with laminin and an ADAM. *J Cell Biol* 144: 549-561.
147. Delwel GO, de Melker AA, Hogervorst F, Jaspars LH, Fles DL, Kuikman I, Lindblom A, Paulsson M, Timpl R, Sonnenberg A. (1994). Distinct and overlapping ligand specificities of the alpha 3A beta 1 and alpha 6A beta 1 integrins: recognition of laminin isoforms. *Mol Biol Cell* 5: 203-215.
148. Sonnenberg A. (1992). Laminin receptors in the integrin family. *Pathol Biol Paris* 40: 773-778.
149. Georges-Labouesse E, Messaddeq N, Yehia G, Cadalbert L, Dierich A, Le Meur M. (1996). Absence of integrin alpha 6 leads to epidermolysis bullosa and neonatal death in mice. *Nat Genet* 13: 370-373.
150. Georges-Labouesse E, Mark M, Messaddeq N, Gansmuller A. (1998). Essential role of alpha 6 integrins in cortical and retinal lamination [In Process Citation]. *Curr Biol* 8: 983-6.
151. Falk M, Salmivirta K, Durbeek M, Larsson E, Ekblom M, Vestweber D, Ekblom P. (1996). Integrin alpha 6B beta 1 is involved in kidney tubulogenesis in vitro. *J Cell Sci* 109: 2801-2810.
152. Kadoya Y, Kadoya K, Durbeek M, Holmvall K, Sorokin L, Ekblom P (1995). Antibodies against domain E3 of laminin-1 and integrin alpha 6 subunit perturb branching epithelial morphogenesis of submandibular gland, but by different modes. *J Cell Biol* 129: 521-534.
153. Sorokin L, Sonnenberg A, Aumailley M, Timpl R, Ekblom P. (1990). Recognition of the laminin E8 cell-binding site by an integrin possessing the alpha 6 subunit is essential for epithelial polarization in developing kidney tubules. *J Cell Biol* 111: 1265-1273.
154. Ibraghimov-Beskrovnaya O, Ervasti JM, Leveille CJ, Slaughter CA, Sernett SW, Campbell K P. (1992). Primary structure of dystrophin-associated glycoproteins linking dystrophin to the extracellular matrix. *Nature* 355: 696-702.

155. Ibraghimov Beskrovnaya O, Milatovich A, Ozcelik T, Yang B, Koepnick K, Francke U, Campbell KP. (1993). Human dystroglycan: skeletal muscle cDNA, genomic structure, origin of tissue specific isoforms and chromosomal localization. *Hum Mol Genet* 2: 1651-1657.
156. Campanelli JT, Roberds SL, Campbell KP, Scheller RH. (1994). A role for dystrophin-associated glycoproteins and utrophin in agrin-induced AChR clustering. *Cell* 77: 663-674.
157. Gee SH, Montanaro F, Lindenbaum MH, Carbonetto S. (1994). Dystroglycan-alpha, a dystrophin-associated glycoprotein, is a functional agrin receptor. *Cell* 77: 675-686.
158. Yamada H, Denzer AJ, Hori H, Tanaka T, Anderson LVB, Fujita S, Fukuta-Ohi H, Shimizu T, Ruegg MA, Matsumura K. (1996). Dystroglycan is a dual receptor for agrin and laminin-2 in Schwann cell membrane. *J Biol Chem* 271: 23418-23423.
159. Sealock R, Froehner SC. (1994). Dystrophin-associated proteins and synapse formation: is alpha-dystroglycan the agrin receptor? *Cell* 77: 617-619.
160. Brancaccio A, Schulthess T, Gesemann M, Engel J. (1995). Electron microscopic evidence for a mucin-like region in chick muscle alpha-dystroglycan. *FEBS Lett* 368: 139-142.
161. Chiba A, Matsumura K, Yamada H, Inazu T, Shimizu T, Kusunoki S, Kanazawa I, Kobata A, Endo T. (1997). Structures of sialylated O-linked oligosaccharides of bovine peripheral nerve alpha-dystroglycan. The role of a novel O-mannosyl-type oligosaccharide in the binding of alpha-dystroglycan with laminin. *J Biol Chem* 272: 2156-2162.
162. Andac Z, Sasaki T, Mann K, Brancaccio A, Deutzmann R, Timpl R. (1999). Analysis of heparin, alpha-dystroglycan and sulfatide binding to the G domain of the laminin alpha1 chain by site-directed mutagenesis. *J Mol Biol* 287(2): 253-264.
163. Hohenester E, Tisi D, Talts JF, Timpl R. (1999). The crystal structure of a laminin G-like module reveals the molecular basis of alpha-dystroglycan binding to laminins, perlecan, and agrin. *Mol Cell* 4: 783-792.
164. Matsumura K, Nonaka I, Campbell KP. (1993). Abnormal expression of dystrophin-associated proteins in Fukuyama-type congenital muscular dystrophy. *Lancet* 341: 521-522.
165. Matsumura K, Tome FMS, Ionasescu V, Ervasti JM, Anderson RD, Romero NB, Simon D, Recan D, Kaplan JC, Fardeau M, Campbell KP. (1993). Deficiency of dystrophin-associated proteins in Duchenne muscular dystrophy patients lacking COOH-terminal domains of dystrophin. *J Clin Invest* 92: 866-871.
166. Hayashi YK, Ogawa M, Tagawa K, Noguchi S, Ishihara T, Nonaka I, Arahata K. (2001). Selective deficiency of alpha-dystroglycan in Fukuyama-type congenital muscular dystrophy. *Neurology* 57: 115-121.

167. Esapa CT, Benson MA, Schroder JE, Martin-Rendon E, Brockington M, Brown SC, Muntoni F, Kroger S, Blake DJ. (2002). Functional requirements for fukutin-related protein in the Golgi apparatus. *Hum Molec Genet* 11: 3319-3331.
168. Kanagawa M, Saito F, Kunz S, Yoshida-Moriguchi T, Barresi R, Kobayashi YM, Muschler J, Dumanski JP, Michele DE, Oldstone MBA, Campbell KP. (2004). Molecular recognition by LARGE is essential for expression of functional dystroglycan. *Cell* 117: 953-964.
169. Michele DE, Barresi R, Kanagawa M, Saito F, Cohn RD, Satz JS, Dollar J, Nishino I, Kelley RI, Somer H, Straub V, Mathews KD, Moore SA, Campbell KP. (2002). Post-translational disruption of dystroglycan-ligand interactions in congenital muscular dystrophies. *Nature* 418: 417-422.
170. Williamson RA, Henry MD, Daniels KJ, Hrstka RF, Lee JC, Sunada Y, Ibraghimov-Beskrovnaya O, Campbell KP. (1997). Dystroglycan is essential for early embryonic development: disruption of Reichert's membrane in Dag1-null mice. *Hum Mol Genet* 6: 831-841.
171. Cote PD, Moukhles H, Lindenbaum M, Carbonetto S. (1999). Chimaeric mice deficient in dystroglycans develop muscular dystrophy and have disrupted myoneural synapses. *Nature Genet* 23: 338-342.
172. Henry MD, Satz JS, Brakebusch C, Costell M., Gustafsson E, Fassler R, Campbell KP (2001). Distinct roles for dystroglycan, beta1 integrin and perlecan in cell surface laminin organization. *J Cell Sci* 114(6): 1137-1144.
173. Durbeej M, Henry MD, Campbell KP. (1998). Dystroglycan in development and disease. *Curr Opin Cell Biol* 10: 594-601.
174. Roberts DD. (1986). Sulfatide-binding proteins. *Chem Phys Lipids* 42: 173-183.
175. Roberts DD, Wewer UM, Liotta LA, Ginsburg V. (1988). Laminin-dependent and laminin-independent adhesion of human melanoma cells to sulfatides. *Cancer Res* 48: 3367-3373.
176. Sung U, O'Rear JJ, Yurchenco PD. (1993). Cell and heparin binding in the distal long arm of laminin: identification of active and cryptic sites with recombinant and hybrid glycoprotein [published erratum appears in *J Cell Biol* 1993 123(6 Pt 1):1623]. *J Cell Biol* 123: 1255-1268.
177. Sung U, O'Rear JJ, Yurchenco PD. (1997). Localization of heparin binding activity in recombinant laminin G domain. *Eur J Biochem* 250: 138-43.
178. Yurchenco PD, Cheng YS, Schittny JC. (1990). Heparin modulation of laminin polymerization. *J Biol Chem* 265: 3981-3991.
179. Chou DKH, Ilyas AA, Evans JE, Costello C, Quarles RH, Jungalwala FB. (1986). Structure of sulfated glucuronyl glycolipids in the nervous system reacting with HNK-1 antibody and some IgM paraproteins in neuropathy. *J Biol Chem* 261: 11717-11725.

180. Voshol H, van-Zuylen CW, Orberger G, Vliegenthart JF, Schachner M. (1996). Structure of the HNK-1 carbohydrate epitope on bovine peripheral myelin glycoprotein P0. *J Biol Chem* 271: 22957-22960.
181. Ariga T, Kohriyama T, Freddo L, Latov N, Saito M, Kon K, Ando S, Suzuki M, Hemling ME, Rinehart KL, Kusunoki S, Yu RK. (1987). Characterization of sulfated glucuronic acid containing glycolipids reacting with IgM M-proteins in patients with neuropathy. *J Biol Chem* 262: 848-853.
182. Abo T, Balch CM. (1981). A differentiation antigen of human NK and K cells identified by a monoclonal antibody (HNK-1). *J Immunol* 127: 1024-1029.
183. Bakker H, Friedmann I, Oka S, Kawasaki T, Nifantev N, Schachner M, Mantei N. (1997). Expression Cloning of a cDNA Encoding a Sulfotransferase Involved in the Biosynthesis of the HNK-1 Carbohydrate Epitope. *J Biol Chem* 272: 29942-29946.
184. Kozutsumi Y, Takio K, Kawasaki, T. (1997). Cloning and functional expression of novel glucuronyltransferase involved in the biosynthesis of the carbohydrate epitope, HNK-1. *Proc. Natl. Acad. Sci. USA*, 94, 6093-6098.
185. Kruse J, Mailhammer R, Wernecke H, Faissner A, Sommer I, Goridis C, Schachner M. (1984). Neural cell adhesion molecules and myelin-associated glycoprotein share a common carbohydrate moiety recognized by monoclonal antibodies L2 and HNK-1. *Nature* 311: 153-155.
186. McGarry RC, Helfand SL, Quarles RH, Roder JC. (1983). Recognition of myelin-associated glycoprotein by the monoclonal antibody HNK-1. *Nature* 306: 376-378.
187. Yoshihara Y, Oka S, Nemoto Y, Watanabe Y, Nagata S, Kagamiyama H, Mori K. (1994). *Neuron* 12: 541-553.
188. Jungalwala FB. (1994). An ICAM-related neuronal glycoprotein, telencephalin, with brain segment-specific expression. *Neurochem Res* 19: 945-957.
189. Künemund V, Jungalwala FB, Fischer G, Chou DK, Keilhauer G, Schachner M. (1988). The L2/HNK-1 carbohydrate of neural cell adhesion molecules is involved in cell interactions. *J Cell Biol* 106: 213-223.
190. Nagase T, Nakamura S, Harii K, Osumi N. (2001). Ectopically localized HNK-1 epitope perturbs migration of the midbrain neural crest cells in Pax6 mutant rat. *Dev Growth Differ* 43: 683-692.
191. Schwarting GA, Jungalwala FB, Chou DK, Boyer AM, Yamamoto M. (1987). Sulfated glucuronic acid-containing glycoconjugates are temporally and spatially regulated antigens in the developing mammalian nervous system. *Dev Biol* 120: 65-76.
192. Yoshihara Y, Oka S, Watanabe Y, Mori K. (1991). Developmentally and spatially regulated expression of HNK-1 carbohydrate antigen on a novel phosphatidylinositol-anchored glycoprotein in rat brain. *J Cell Biol* 115: 731-744.

193. Bronner-Fraser M. (1987). Perturbation of cranial neural crest migration by the HNK-1 antibody. *Dev Biol* 123: 321-331.
194. Keilhauer G, Faissner A, Schachner M. (1985). Differential inhibition of neurone-neurone, neurone-astrocyte and astrocyte-astrocyte adhesion by L1, L2 and N-CAM antibodies. *Nature* 316: 728-730.
195. Martini R, Xin Y, Schmitz B, Schachner M. (1992). The L2/HNK-1 Carbohydrate Epitope is Involved in the Preferential Outgrowth of Motor Neurons on Ventral Roots and Motor Nerves. *Eur J Neurosci* 4: 628-639.
196. Mohan PS, Chou DKH, Jungalwala FB. (1990). Sulfoglucuronyl glycolipids bind laminin. *J. Neurochem.* 54, 2024-2031.
197. Needham LK, Schnaar RL. (1993). The HNK-1 reactive sulfoglucuronyl glycolipids are ligands for L-selectin and P-selectin but not E-selectin. *Proc Natl Acad Sci USA* 90: 1359-1363.
198. Bernfield M, Kokenyesi R, Kato M, Hinkes MT, Spring J, Gallo RL, Lose EJ. (1992). Biology of the syndecans: a family of transmembrane heparan sulfate proteoglycans. *Ann Rev Cell Biol* 8: 365-393.
199. Tkachenko E, Rhodes JM, Simons M. (2005). Syndecans: new kids on the signaling block. *Circ Res* 96(5): 488-500.
200. Rosenberg RD, Schworak NW, Lui J, Schwartz JJ, Zhang L. (1997). Heparan sulfate proteoglycans of the cardiovascular system. Specific structures emerge but how is synthesis regulated? *J Clin Invest* 99: 2062-2070.
201. Deepa SS, Yamada S, Zako M, Goldberger O, Sugahara K. (2004). Chondroitin sulfate chains on syndecan-1 and syndecan-4 from normal murine mammary gland epithelial cells are structurally and functionally distinct and cooperate with heparan sulfate chains to bind growth factors. A novel function to control binding of midkine, pleiotrophin, and basic fibroblast growth factor. *J Biol Chem* 279: 37368–37376.
202. Okamoto O, Bachy S, Odenthal U, Bernaud J, Rigal D, Lortat-Jacob H, Smyth N, Rousselle P. (2003). Normal human keratinocytes bind to the alpha3LG4/5 domain of unprocessed laminin-5 through the receptor syndecan-1. *J Biol Chem* 278: 44168–44177.
203. Hozumi K, Suzuki N, Nielsen PK, Nomizu M, Yamada Y. (2006). Laminin alpha1 chain LG4 module promotes cell attachment through syndecans and cell spreading through integrin alpha2beta1. *J Biol Chem* 281(43): 32929-32940.
204. Bachy S, Letourneur F, Rousselle P. (2008). Syndecan-1 interaction with the LG4/5 domain in laminin-332 is essential for keratinocyte migration. *J Cell Physiol* 214(1): 238-249.
205. Keum E, Kim Y, Kim J, Kwon S, Lim Y, Han I, Oh ES. (2004). Syndecan-4 regulates localization, activity and stability of protein kinase C-alpha. *Biochem J* 378(Pt 3): 1007-1014.

206. Oh ES, Woods A, Couchman JR. (1997). Multimerization of the cytoplasmic domain of syndecan-4 is required for its ability to activate protein kinase C. *J Biol Chem* 272: 11805–11811.
207. Horowitz A, Murakami M, Gao Y, Simons M. (1999). Phosphatidylinositol-4,5-bisphosphate mediates the interaction of syndecan-4 with protein kinase C. *Biochemistry* 38: 15871–15877.
208. Yuan K, Hong TM, Chen JJ, Tsai WH, Lin MT. (2004). Syndecan-1 up-regulated by ephrinB2/EphB4 plays dual roles in inflammatory angiogenesis. *Blood* 104: 1025–1033.
209. Irie F, Yamaguchi Y. (2004). EPHB receptor signaling in dendritic spine development. *Front Biosci* 9: 1365–1373.
210. Granes F, Urena J, Rocamora N, Vilaro S. (2000). Ezrin links syndecan-2 to the cytoskeleton. *J Cell Sci* 113: 1267–1276.
211. Kinnunen T, Kaksonen M, Saarinen J, Kalkkinen N, Peng HB, Rauvala H. (1998). Cortactin-Src kinase signaling pathway is involved in N-syndecan- dependent neurite outgrowth. *J Biol Chem* 273: 10702–10708.
212. Granes F, Berndt C, Roy C, Mangeat P, Reina M, Vilaro S. (2003). Identification of a novel Ezrin-binding site in syndecan-2 cytoplasmic domain. *FEBS Lett* 547: 212–216.
213. Cornelison DD, Wilcox-Adelman SA, Goetinck PF, Rauvala H, Rapraeger AC, Olwin BB. (2004). Essential and separable roles for syndecan-3 and syndecan-4 in skeletal muscle development and regeneration. *Genes Dev* 18: 2231–2236.
214. Brunetti A, Goldfine ID. (1990). Role of myogenin in myoblast differentiation and its regulation by fibroblast growth factor. *J Biol Chem* 265: 5960–5963.
215. Fuentealba L, Carey DJ, Brandan E. (1999). Antisense inhibition of syndecan-3 expression during skeletal muscle differentiation accelerates myogenesis through a basic fibroblast growth factor-dependent mechanism. *J Biol Chem* 274: 37876–37884.
216. Casar JC, Cabello-Verrugio C, Olguin H, Aldunate R, Inestrosa NC, Brandan E. (2004). Heparan sulfate proteoglycans are increased during skeletal muscle regeneration: requirement of syndecan-3 for successful fiber formation. *J Cell Sci* 117: 73–84.
217. Rapraeger AC. (2001). Molecular interactions of syndecans during development. *Cell & Dev Bio* 12: 107–116.
218. Filla MS, Dam P, Rapraeger AC. (1998). The cell surface proteoglycan syndecan-1 mediates fibroblast growth factor-2 binding and activity. *J Cell Physiol* 174: 310–321.

219. Saoncella S, Echtermeyer F, Denhez F, Nowlen JK, Mosher DF, Robinson SD, Hynes RO, Goetinck PF. (1999). Syndecan-4 signals cooperatively with integrins in a Rho-dependent manner in the assembly of focal adhesions and actin stress fibers. *Proc Natl Acad Sci USA* 96: 2805–2810.
220. Tkachenko E, Simons M. (2002). Clustering induces redistribution of syndecan-4 core protein into raft membrane domains. *J Biol Chem* 277: 19946–19951.
221. Fuki IV, Kuhn KM, Lomazov IR, Rothman VL, Tuszynski GP, Iozzo RV, Swenson TL, Fisher EA, Williams KJ. (1997). The syndecan family of proteoglycans. Novel receptors mediating internalization of atherogenic lipoproteins in vitro. *J Clin Invest* 100: 1611–1622.
222. Fuki IV, Meyer ME, Williams KJ. (2000). Transmembrane and cytoplasmic domains of syndecan mediate a multi-step endocytic pathway involving detergent-insoluble membrane rafts. *Biochem J* 351: 607–612.
223. Beardsley A, Fang K, Mertz H, Castranova V, Friend S, Liu J. (2004). Loss of caveolin-1 polarity impedes endothelial cell polarization and directional movement. *J Biol Chem* 280(5): 3541–3547.
224. Borset M, Hjertner O, Yaccoby S, Epstein J, Sanderson RD. (2000). Syndecan-1 is targeted to the uropods of polarized myeloma cells where it promotes adhesion and sequesters heparin-binding proteins. *Blood* 96: 2528–2536.
225. Baciuc PC, Goetinck PF. (1995). Protein kinase C regulates the recruitment of syndecan-4 into focal contacts. *Mol Biol Cell* 6: 1503–1513.
226. Shajahan AN, Timblin BK, Sandoval R, Tiruppathi C, Malik AB, Minshall RD. (2004). Role of Src-induced dynamin-2 phosphorylation in caveolae-mediated endocytosis in endothelial cells. *J Biol Chem* 279: 20392–20400.
227. Oh ES, Woods A, Couchman JR. (1997). Syndecan-4 proteoglycan regulates the distribution and activity of protein kinase C. *J Biol Chem* 272: 8133–8136.
228. Cheng ZJ, Singh RD, Marks DL, Pagano RE. (2006). Membrane microdomains, caveolae, and caveolar endocytosis of sphingolipids. *Mol Membr Biol* 23(1): 101–110.
229. Paine-Saunders S, Viviano BL, Saunders S. (1999). GPC6, a novel member of the glypican gene family, encodes a product structurally related to GPC4 and is colocalized with GPC5 on human chromosome 13. *Genomics* 57: 455–458.
230. Veugelers M, De Cat B, Ceulemans H, Bruystens AM, Coomans C, Durr J, Vermeesch J, Marynen P, David, G. (1999). Glypican-6, a new member of the glypican family of cell surface heparan sulfate proteoglycans. *J Biol Chem* 274: 26968–26977.
231. Veugelers M, Vermeesch J, Reekmans G, Steinfeld R, Marynen P, David G. (1997). Characterization of glypican-5 and chromosomal localization of human GPC5, a new member of the glypican gene family. *Genomics* 40: 24–30.

232. Beddington RSP, Robertson EJ. (1999). Axis development and early asymmetry in mammals. *Cell* 96: 195-209.
233. Beddington RSP, Robertson EJ. (1999). Anterior patterning in mouse *Trends Genet* 14(7): 277-284.
234. Brennan J, Lu CC, Norris DP, Rodriguez TA, Beddington RS, Robertson EJ. (2001). Nodal signalling in the epiblast patterns the early mouse embryo. *Nature* 411(6840): 965-969.
235. Lu CC, Brennan J, Robertson EJ. (2001). From fertilization to gastrulation: axis formation in the mouse embryo. *Curr Opin Genet Dev* 11(4): 384-392.
236. Ekblom P, Alitalo K, Vaheri A, Timpl R, Saxen L. (1980). Induction of a basement membrane glycoprotein in embryonic kidney: possible role of laminin in morphogenesis. *Proc Natl Acad Sci USA* 77: 485-489.
237. Schéele S, Nyström A, Durbeek M, Talts JF, Ekblom M, Ekblom P. (2007). Laminin isoforms in development and disease. *J Mol Med* 85(8): 825-386.
238. Miner JH, Yurchenco PD. (2004). Laminin functions in tissue morphogenesis. *Ann Rev Cell Dev Biol.* 20: 255-284.
239. Alpy F, Jivkov I, Sorokin L, Klein A, Arnold C, Huss Y, Keding M, Simon-Assmann P, Lefebvre O. (2005). Generation of a conditionally null allele of the laminin alpha1 gene. *Genesis* 43(2): 59-70.
240. Ringelmann B, Röder C, Hallmann R, Maley M, Davies M, Grounds M, Sorokin L. (1999). Expression of Laminin $\alpha 1$, $\alpha 2$, $\alpha 4$, and $\alpha 5$ Chains, Fibronectin, and Tenascin-C in Skeletal Muscle of Dystrophic 129ReJdy/dy Mice. *Exp Cell Res* 246(1): 165-182.
241. Murray P, Edgar D. (2000). Regulation of programmed cell death by basement membranes in embryonic development. *J Cell Biol* 150: 1215–1221.
242. Murray P, Edgar D. (2001). Regulation of the differentiation and behaviour of extra-embryonic endodermal cells by basement membranes. *J Cell Sci* 114(5): 931-939.
243. Colognato H, Galvin J, Wang Z, Relucio J, Nguyen, Harrison D, Yurchenco PD, ffrench-Constant C. (2007). Identification of dystroglycan as a second laminin receptor in oligodendrocytes, with a role in myelination. *Development* 134: 1723-1736.
244. Yu WM, Yu H, Chen ZL, Strickland S. (2008). Disruption of laminin in the peripheral nervous system impedes nonmyelinating Schwann cell development and impairs nociceptive sensory function. *Glia*. [Epub ahead of print].
245. Madrid RE, Jaros E, Cullen MJ, Bradley WG. (1975). Genetically determined defect of Schwann cell basement membrane in dystrophic mouse. *Nature* 257: 319-321.
246. Sunada Y, Bernier SM, Utani A, Yamada Y, Campbell KP. (1995). Identification of a novel mutant transcript of laminin alpha 2 chain gene responsible for muscular dystrophy and dysmyelination in dy2J mice. *Hum Mol Genet* 4: 1055-1061.

247. Sunada Y, Edgar TS, Lotz BP, Rust RS, Campbell KP. (1995). Merosin-negative congenital muscular dystrophy associated with extensive brain abnormalities. *Neurology* 45: 2084-2089.
248. Yu WM, Yu H, Chen ZL. (2007). Laminins in peripheral nerve development and muscular dystrophy. *Mol Neurobiol* 35(3): 288-297.
249. Xu H, Wu XR, Wewer UM, Engvall E. (1994). Murine muscular dystrophy caused by a mutation in the laminin alpha 2 (Lama2) gene. *Nat Genet* 8: 297-302.
250. Previtali SC, Dina G, Nodari A, Fasolini M, Wrabetz L, Mayer U, Feltri ML, Quattrini A. (2003) Schwann cells synthesize alpha7beta1 integrin which is dispensable for peripheral nerve development and myelination. *Mol Cell Neurosci* 23(2): 210-218.
251. Previtali SC, Nodari A, Taveggia C, Pardini C, Dina G, Villa A, Wrabetz L, Quattrini A, Feltri ML. (2003). Expression of laminin receptors in schwann cell differentiation: evidence for distinct roles. *J Neurosci* 23(13): 5520-5530.
252. Curcic R, Dhandayuthapani S, Deretic V. (1994). Gene expression in mycobacteria: transcriptional fusions based on xyle and analysis of the promoter region of the response regulator mtrA from *Mycobacterium tuberculosis*. *Mol Microbiol* 13(6):1057-1064.
253. Higgins D., Thompson J., Gibson T., Thompson J.D., Higgins D.G., Gibson T.J.(1994). CLUSTAL W: improving the sensitivity of progressive multiple sequence alignment through sequence weighting, position-specific gap penalties and weight matrix choice. *Nucleic Acids Research* 22: 4673-4680.
254. Larkin MA, Blackshields G, Brown NP, Chenna R, McGettigan PA, McWilliam H, Valentin F, Wallace IM, Wilm A, Lopez R, Thompson JD, Gibson TJ, Higgins DG. (2007). ClustalW and ClustalX version 2. *Bioinformatics* 23(21): 2947-2948.
255. Edgar RC. (2004). MUSCLE: a multiple sequence alignment method with reduced time and space complexity. *BMC Bioinformatics* 5(1): 113.
256. Edgar RC. (2004). MUSCLE: multiple sequence alignment with high accuracy and high throughput. *Nucleic Acids Research* 32(5): 1792-1797.
257. Pearson WR. (1990). Rapid and Sensitive Sequence Comparison with FASTP and FASTA. *Methods in Enzymology* 183: 63-98.
258. Pearson WR, Lipman DJ. (1988). Improved Tools for Biological Sequence Comparison. *PNAS* 85: 2444-2448.
259. Felsenstein J. (1989). PHYLIP - Phylogeny Inference Package (Version 3.2). *Cladistics* 5: 164-166.
260. Felsenstein J. (2005). PHYLIP (Phylogeny Inference Package) version 3.6. Distributed by the author. Department of Genome Sciences, University of Washington, Seattle.

261. Combet C, Blanchet C, Geourjon C, Deléage G. (2000). NPS@: Network Protein Sequence Analysis. TIBS 25(3): 147-150.
262. Deleage G, Roux B. (1987). An algorithm for protein secondary structure prediction based on class prediction. Protein Eng 1(4):289-294.
263. King RD, Sternberg MJ. (1996). Identification and application of the concepts important for accurate and reliable protein secondary structure prediction Protein Sci 5(11): 2298-2310.
264. Garnier J, Gibrat J-F, Robson B. (1996). GOR secondary structure prediction method version IV. Methods in Enzymology. RF Doolittle Ed. 266: 540-553.
265. Guermeur Y. (1997). Combinaison de classifieurs statistiques, Application a la prediction de structure secondaire des proteines. PhD Thesis
266. Rost B, Sander C. (1993). Prediction of protein secondary structure at better than 70% accuracy. J Mol Biol 232(2): 584-599.
267. Rost B, Sander C. (1994). Combining evolutionary information and neural networks to predict protein secondary structure. Proteins 19(1): 55-72.
268. Frishman D, Argos P. (1996). Incorporation of non-local interactions in protein secondary structure prediction from the amino acid sequence. Protein Eng 9(2):133-142.
269. Levin J. (1997). Exploring the limits of nearest neighbour secondary structure prediction. Protein Eng 7: 771-776.
270. Levin JM, Robson B, Garnier J. (1986). An algorithm for secondary structure determination in proteins based on sequence similarity. FEBS Lett 205(2): 303-308.
271. Geourjon C, Deleage G. (1994). SOPM: a self-optimized method for protein secondary structure prediction. Protein Eng 7(2): 157-164.
272. Geourjon C, Deleage G (1995). SOPMA: significant improvements in protein secondary structure prediction by consensus prediction from multiple alignments. Comput Appl Biosci 11(6):681-684.
273. Guermeur Y, Geourjon C, Gallinari P, Deleage G. (1999). Improved Performance in Protein Secondary Structure Prediction by Inhomogeneous Score Combination. Bioinformatics 15(5): 413-421.
274. Garnier J, Osguthorpe DJ, Robson B. (1978). Analysis of the accuracy and implications of simple methods for predicting the secondary structure of globular proteins. J Mol Biol 120(1): 97-120.
275. Gibrat JF, Garnier J, Robson B. (1987). Further developments of protein secondary structure prediction using information theory. New parameters and consideration of residue pairs. J Mol Biol 198(3): 425-443.

276. Guex N. (1996). Swiss-PdbViewer: A new fast and easy to use PDB viewer for the Macintosh. *Experientia* 52: A26.
277. Guex N, Diemand A, Peitsch MC. (1999). Protein modelling for all. *TiBS* 24: 364-367.
278. Guex N, Peitsch MC.(1996). Swiss-PdbViewer: A Fast and Easy-to-use PDB Viewer for Macintosh and PC. *Protein Data Bank Quaterly Newsletter* 77: 7.
279. Guex N, Peitsch MC. (1997). SWISS-MODEL and the Swiss-PdbViewer: An environment for comparative protein modeling. *Electrophoresis* 18: 2714-2723.
280. Šali A, Blundell TL. (1993). Comparative protein modelling by satisfaction of spatial restraints. *J Mol Biol* 234: 779-815.
281. Brooks BR, Bruccoleri RE, Olafson BD, States DJ, Swaminathan S, Karplus M. (1983) CHARMM: A Program for Macromolecular Energy, Minimization, and Dynamics Calculations. *J Comp Chem* 4: 187-217.
282. MacKerell AD, Brooks B, Brooks CL, Nilsson L, Roux B, Won Y, Karplus M. (1998) CHARMM: The Energy Function and Its Parameterization with an Overview of the Program, in *The Encyclopedia of Computational Chemistry* 1: 271-277. PVR Schleyer et al., editors (John Wiley & Sons: Chichester).
283. Case DA, Cheatham TE, Darden T, Gohlke H, Luo R, Merz KM, Onufriev A, Simmerling C, Wang B, Woods R. (2005). The Amber biomolecular simulation programs. *J Computat Chem* 26: 1668-1688.
284. Ponder JW, Case DA. (2003). Force fields for protein simulations. *Adv Prot Chem* 66: 27-85. Similar information for nucleic acids is given by Cheatham TE, Young MA. (2001). Molecular dynamics simulation of nucleic acids: Successes, limitations and promise. *Biopolymers* 56: 232-256.
285. Sorin EJ, Pande VS. (2005). Exploring the helix-coil transition via all-atom equilibrium ensemble simulations. *Biophys J* 88: 2472–2493.
286. Wang J, Cieplak P, Kollman PA. (2000). How well does a restrained electrostatic potential (RESP) model perform in calculating conformational energies of organic and biological molecules? *J Comput Chem* 21: 1049–1074.
287. Weiner SJ, Kollman PA, Case DA, Singh UC, Alagona G, Profeta S, Weiner P. (1984). "A new force field for the molecular mechanical simulation of nucleic acids and proteins". *J Am Chem Soc* 106: 765-784.
288. van Gunsteren WF, Billeter SR, Eising AA, Hunenberger PH, Kruger P, Mark AE, Scott WRP, Tironi IG. (1996). *Biomolecular Simulation: The GROMOS96 Manual and User Guide* (Univ Publ House, Zurich,).

289. Levitt M, Hirshberg M, Sharon R, Daggett V. (1995). Potential energy function and parameters for simulations of the molecular dynamics of proteins and nucleic acids in solution. *Comput Phys Commun* 91: 215–231.
290. Bashford D. (1997). An object-oriented programming suite for electrostatic effects in biological molecules. In Ishikawa Y, Rodney R, Oldehoeft JV, Reynders W, Tholburn M, editors, *Scientific Computing in Object-Oriented Parallel Environments 1343 of Lecture Notes in Computer Science*, pages 233-240, Berlin, 1997. ISCOPE97, Springer.
291. Appel RD, Bairoch A, Hochstrasser DF. (1994). A new generation of information retrieval tools for biologists: the example of the ExPASy WWW server. *Trends Biochem Sci* 19: 258-260.
292. Hooft RWW, Vriend G, Sander C, Abola EE. (1996). Errors in protein structures. *Nature* 381: 272-272.
293. Combs AC, Ervasti JM. (2005). Enhanced laminin binding by α -dystroglycan after enzymatic deglycosylation. *Biochem J* 390: 303-309.
294. McDearmon EL, Combs AC, Ervasti JM. (2003). Core 1 Glycans on α -Dystroglycan Mediate Laminin-induced Acetylcholine Receptor Clustering but Not Laminin Binding. *J Biol Chem* 278: 44868-44873.
295. Ervasti JM, Burwell AL, Geissler AL. (1997). Tissue-specific heterogeneity in alpha-dystroglycan sialoglycosylation. Skeletal muscle alpha-dystroglycan is a latent receptor for Vicia villosa agglutinin b4 masked by sialic acid modification. *J Biol Chem* 272: 22315-22321.
296. Smirnov SP, McDearmon EL, Li S, Ervasti JM, Tryggvason K, Yurchenco PD. (2002). Contributions of the LG modules and furin processing to laminin-2 functions. *J Biol Chem* 277(21):18928-18937.
297. Harrison D, Hussain SA, Combs AC, Ervasti JM, Yurchenco PD, Hohenester E. (2007). Crystal structure and cell surface anchorage sites of laminin alpha 1LG4-5. *JBC* 282(15): 11573-11581.
298. Watanabe R, Asakura K, Rodriguez M, Pagano RE. (1999). Internalization and sorting of plasma membrane sphingolipid analogues in differentiating oligodendrocytes. *J. Neurochem.* 73: 1375–1383.
299. Yurchenco PD, Quan Y, Colognato H, Mathus T, Harrison D, Yamada Y, O'Rear JJ. (1997). The alpha chain of laminin-1 is independently secreted and drives secretion of its beta- and gamma-chain partners. *Proc Natl Acad Sci USA* 94: 10189-10194.
300. Fredman P, Mattsson L, Andersson K, Davidsson P, Ishizuka I, Jeansson S, Mansson JE, and Svennerholm L. (1988). Characterization of the binding epitope of a monoclonal antibody to sulphatide. *Biochem J* 251: 17–22.

301. Yurchenco PD, Sung U, Ward MD, Yamada Y, O'Rear JJ. (1993). Recombinant laminin G domain mediates myoblast adhesion and heparin binding. *J Biol Chem* 268: 8356-8365.
302. Fassler R, Meyer M. (1995). Consequences of lack of beta 1 integrin gene expression in mice. *Genes Dev* 9: 1896-1908.
303. Fassler R, Pfaff M, Murphy J, Noegel AA, Johansson S, Timpl R, Albrecht R. (1995). Lack of beta 1 integrin gene in embryonic stem cells affects morphology, adhesion, and migration but not integration into the inner cell mass of blastocysts. *J Cell Biol* 128: 979-988.
304. Colognato H, Winkelmann DA, Yurchenco PD. (1999). Laminin polymerization induces a receptor-cytoskeleton network. *J Cell Biol* 145: 619-631.
305. Tisi D, Talts JF, Timpl R, Hohenester E. (2000). Structure of the C-terminal laminin G-like domain pair of the laminin alpha2 chain harbouring binding sites for alpha-dystroglycan and heparin. *EMBO J.* 19(7): 1432-1440.
306. Kozak M. (1987) An analysis of 5'-noncoding sequences from 699 vertebrate messenger RNAs. *NAR* 15(20): 8125-8148.
307. Harhay GP, Sonstegard TS, Keele JW, Heaton MP, Clawson ML, Snelling WM, Wiedmann RT, Van Tassell CP, Smith TP. (2005). Characterization of 954 bovine full-CDS cDNA sequences. *BMC Genomics* 6: 166.
308. Mignone F, Grillo G, Licciulli F, Iacono M, Liuni S, Kersey PJ, Duarte J, Saccone C, Pesole G. (2005) UTRdb and UTRsite: a collection of sequences and regulatory motifs of the untranslated regions of eukaryotic mRNAs. *Nucleic Acids Res* 33(Database issue): D141-146.
309. Ahn J, Gruen JR. (1999). The genomic organization of the histone clusters on human 6p21.3 Mamm. *Genome* 10(7): 768-770.
310. Marzluff WF, Gongidi P, Woods KR, Jin J, Maltais LJ.(2002). The human and mouse replication-dependent histone genes. *Genomics* 80(5): 487-498.
311. Griffiths-Jones S. (2004). The microRNA Registry. *Nucleic Acids Res* 32 (Database issue): D109-D111.
312. Griffiths-Jones S, Grocock RJ, van Dongen S, Bateman A, Enright AJ. (2006). miRBase: microRNA sequences, targets and gene nomenclature. *Nucleic Acids Res* 34 (Database issue): D140-D144.
313. International Human Genome Sequencing Consortium. (2004). Finishing the euchromatic sequence of the human genome. *Nature* 431: 931-945.
314. Humphray SJ, Oliver K, Hunt AR, Plumb RW, Loveland JE, Howe KL, Andrews TD, Searle S, Hunt SE, Scott CE, Jones MC, Ainscough R, Almeida JP, Ambrose KD, Ashwell RI, Babbage AK, Babbage S, Bagguley CL, Bailey J, Banerjee R, Barker DJ, Barlow KF, Bates K, Beasley H, Beasley O, Bird CP, Bray-Allen S, Brown AJ, Brown JY,

Burford D, Burrill W, Burton J, Carder C, Carter NP, Chapman JC, Chen Y, Clarke G, Clark SY, Clee CM, Clegg S, Collier RE, Corby N, Crosier M, Cummings AT, Davies J, Dhami P, Dunn M, Dutta I, Dyer LW, Earthrowl ME, Faulkner L, Fleming CJ, Frankish A, Frankland JA, French L, Fricker DG, Garner P, Garnett J, Ghorji J, Gilbert JG, Glison C, Grafham DV, Gribble S, Griffiths C, Griffiths-Jones S, Grocock R, Guy J, Hall RE, Hammond S, Harley JL, Harrison ES, Hart EA, Heath PD, Henderson CD, Hopkins BL, Howard PJ, Howden PJ, Huckle E, Johnson C, Johnson D, Joy AA, Kay M, Keenan S, Kershaw JK, Kimberley AM, King A, Knights A, Laird GK, Langford C, Lawlor S, Leongamornlert DA, Liversha M, Lloyd C, Lloyd DM, Lovell J, Martin S, Mashreghi-Mohammadi M, Matthews L, McLaren S, McLay KE, McMurray A, Milne S, Nickerson T, Nisbett J, Nordsiek G, Pearce AV, Peck AI, Porter KM, Pandian R, Pelan S, Phillimore B, Povey S, Ramsey Y, Rand V, Scharfe M, Sehra HK, Shownkeen R, Sims SK, Skuce CD, Smith M, Steward CA, Swarbreck D, Sycamore N, Tester J, Thorpe A, Tracey A, Tromans A, Thomas DW, Wall M, Wallis JM, West AP, Whitehead SL, Willey DL, Williams SA, Wilming L, Wray PW, Young L, Ashurst JL, Coulson A, Blocker H, Durbin R, Sulston JE, Hubbard T, Jackson MJ, Bentley DR, Beck S, Rogers J, Dunham I. (2004). DNA sequence and analysis of human chromosome 9. *Nature* 429(6990): 369-374.

315. Nichols RC, Raben N, Boerkoel CF, Plotz PH. (1995). Human isoleucyl-tRNA synthetase: sequence of the cDNA, alternative mRNA splicing, and the characteristics of an unusually long C-terminal extension. *Gene* 155(2): 299-304.

316. Strausberg RL, Feingold EA, Grouse LH, Derge JG, Klausner RD, Collins FS, Wagner L, Shenmen CM, Schuler GD, Altschul SF, Zeeberg B, Buetow KH, Schaefer CF, Bhat NK, Hopkins RF, Jordan H, Moore T, Max SI, Wang J, Hsieh F, Diatchenko L, Marusina K, Farmer AA, Rubin GM, Hong L, Stapleton M, Soares MB, Bonaldo MF, Casavant TL, Scheetz TE, Brownstein MJ, Usdin TB, Toshiyuki S, Carninci P, Prange C, Raha SS, Loquellano NA, Peters GJ, Abramson RD, Mullahy SJ, Bosak SA, McEwan PJ, McKernan KJ, Malek JA, Gunaratne PH, Richards S, Worley KC, Hale S, Garcia AM, Gay LJ, Hulyk SW, Villalón DK, Muzny DM, Sodergren EJ, Lu X, Gibbs RA, Fahey J, Helton E, Kettelman M, Madan A, Rodrigues S, Sanchez A, Whiting M, Madan A, Young AC, Shevchenko Y, Bouffard GG, Blakesley RW, Touchman JW, Green ED, Dickson MC, Rodriguez AC, Grimwood J, Schmutz J, Myers RM, Butterfield YS, Krzywinski MI, Skalska U, Smailus DE, Schnerch A, Schein JE, Jones SJ, Marra MA, Mammalian Gene Collection Program Team. (2002). Generation and initial analysis of more than 15,000 full-length human and mouse cDNA sequences. *Proc Natl Acad Sci USA* 99(26): 16899-16903.

317. Marques AC, Dupanloup I, Vinckenbosch N, Reymond A, and Kaessmann H. (2005). Emergence of young human genes after a burst of retroposition in primates. *PLoS Biol.* 3(11): E357.

318. Liu Z, Diaz LA, Haas AL, Giudice GJ. (1992). cDNA cloning of a novel human ubiquitin carrier protein. An antigenic domain specifically recognized by endemic pemphigus foliaceus autoantibodies is encoded in a secondary reading frame of this human epidermal transcript. *J Biol Chem* 267(22): 15829-15835.

319. Lowe TM, Eddy SR. (1997). tRNAscan-SE: a program for improved detection of transfer RNA genes in genomic sequence. *Nucleic Acids Res* 25(5): 955-964.

320. Vriend G. (1990). WHAT IF: A molecular modeling and drug design program. *J Mol Graph* 8: 52-56.
321. Levitt M. (1974). Energy refinement of hen egg-white lysozyme. *J Mol Biol* 82: 393-420.
322. Levitt M, Lifson S. (1969). Refinement of protein conformations using a macromolecular energy minimization procedure. *J Mol Biol* 46: 269-279.
323. Rodriguez R, Chinea G, Lopez N, Pons T, Vriend G. (1998). Homology modeling, model and software evaluation: three related resources. *CABIOS* 14: 523-528.
324. Talts JF, Andac Z, Gohring W, Brancaccio A, Timpl R. (1999). Binding of the G domains of laminin alpha1 and alpha2 chains and perlecan to heparin, sulfatides, alpha-dystroglycan and several extracellular matrix proteins. *EMBO J* 18(4): 863-870.
325. Ebara S, Shimura S, Nasu Y, Kaku H, Kumon H, Yang G, Wang J, Timme TL, Aguilar-Cordova E, Thompson TC. (2002). Gene therapy for prostate cancer: toxicological profile of four HSV-tk transducing adenoviral vectors regulated by different promoters. *Prostate Cancer Prostatic Dis* 5(4): 316-325.
326. Al-Dosari M, Zhang G, Knapp JE, Liu D. (2006). Evaluation of viral and mammalian promoters for driving transgene expression in mouse liver. *Biochem Biophys Res Commun* 339(2): 673-678.
327. Condreay JP, Witherspoon SM, Clay WC, Kost TA. (1999). Transient and stable gene expression in mammalian cells transduced with a recombinant baculovirus vector. *Proc Natl Acad Sci U S A*. 96(1): 127-132.
328. Boulos S, Meloni BP, Arthur PG, Bojarski C, Knuckey NW. (2006). Assessment of CMV, RSV and SYN1 promoters and the woodchuck post-transcriptional regulatory element in adenovirus vectors for transgene expression in cortical neuronal cultures. *Brain Res* 1102(1): 27-38.
329. Kawabata K, Sakurai F, Yamaguchi T, Hayakawa T, Mizuguchi H. (2005). Efficient gene transfer into mouse embryonic stem cells with adenovirus vectors. *Mol Ther* 12(3): 547-554.
330. Xu ZL, Mizuguchi H, Ishii-Watabe A, Uchida E, Mayumi T, Hayakawa T. (2001). Optimization of transcriptional regulatory elements for constructing plasmid vectors. *Gene* 272(1-2): 149-156.
331. Baldwin HS, Mickanin C, Buck C. (1997). Adenovirus-mediated gene transfer during initial organogenesis in the mammalian embryo is promoter-dependent and tissue-specific. *Gene Ther* 4(11): 1142-1149.
332. Sutherland LC, Williams GT. (1997). Viral promoter expression in CEM-C7 and Jurkat human T-lymphoid cell lines. *J Immunol Methods* 207(2): 179-183.

333. Matsui T. (1996). Differential activation of the murine laminin B1 gene promoter by RAR alpha, ROR alpha, and AP-1. *Biochem Biophys Res Commun* 220(2): 405-410.
334. Okano R, Mita T, Matsui T. (1992). Characterization of a novel promoter structure and its transcriptional regulation of the murine laminin B1 gene. *Biochim Biophys Acta* 1132(1): 49-57.
335. Vasios GW, Gold JD, Petkovich M, Chambon P, Gudas LJ. (1989). A retinoic acid-responsive element is present in the 5' flanking region of the laminin B1 gene. *Proc Natl Acad Sci USA* 86(23): 9099-9103.
336. Boado RJ, Pardridge WM. (1999). Amplification of gene expression using both 5'- and 3'-untranslated regions of GLUT1 glucose transporter mRNA. *Brain Res Mol Brain Res* 63: 371-374.
337. Boado RJ, Tsukamoto H, and Pardridge WM. (1996). Evidence for translational control elements within the 5'-untranslated region of GLUT1 glucose transporter mRNA. *J Neurochem* 67: 1335-1343.
338. Chappell SA, Edelman GM, and Mauro VP. (2000). A 9-nt segment of a cellular mRNA can function as an internal ribosome entry site (IRES) and when present in linked multiple copies greatly enhances IRES activity. *Proc Natl Acad Sci USA* 97: 1536-1541.
339. Hambræus G, Karhumaa K, Rutberg B. (2002). A 5' stem-loop and ribosome binding but not translation are important for the stability of *Bacillus subtilis* *aprE* leader mRNA. *Microbiology* 148: 1795-1803.
340. Pesole G, Liuni S, Grillo G, Licciulli F, Mignone F, Gissi C, Saccone C. (2002). UTRdb and UTRsite: specialized databases of sequences and functional elements of 5' and 3' untranslated regions of eukaryotic mRNAs. *Nucleic Acids Res* 30(1): 335-340.
341. Shalev A, Blair PJ, Hoffmann SC, Hirshberg B, Peculis BA, Harlan DM. (2002). A proinsulin gene splice variant with increased translation efficiency is expressed in human pancreatic islets. *Endocrinology* 143: 2541-2547.
342. Hoover DS, Wingett DG, Zhang J, Reeves R, Magnuson NS. (1997). Pim-1 protein expression is regulated by its 5'-untranslated region and translation initiation factor eIF-4E. *Cell Growth Differ* 8: 1371-1380.
343. Kos M, Denger S, Reid G, Gannon F. (2002). Upstream open reading frames regulate the translation of the multiple mRNA variants of the estrogen receptor alpha. *J Biol Chem* 277: 37131-37138.
344. Boado RJ, Pardridge WM. (1997). The 5'-untranslated region of GLUT1 glucose transporter mRNA causes differential regulation of the translational rate in plant and animal systems. *Comp Biochem Physiol Biochem Mol Biol* 118: 309-312.
345. Hua XJ, Van de Cotte B, Van Montagu M, Verbruggen N. (2001). The 5' untranslated region of the *At-P5R* gene is involved in both transcriptional and post-transcriptional regulation. *Plant J* 26: 157-169.

346. West CA, Arnett TR, Farrow SM. (1996). Expression of insulin-like growth factor I (IGF-I) mRNA variants in rat bone. *Bone* 19: 41–46.
347. Cannons AC, Cannon J. (2002). The stability of the *Chlorella* nitrate reductase mRNA is determined by the secondary structure of the 5'-UTR: implications for posttranscriptional regulation of nitrate reductase. *Planta* 214: 488–491.
348. De la Cruz BJ, Prieto S, Scheffler IE. (2002). The role of the 5' untranslated region (UTR) in glucose-dependent mRNA decay. *Yeast* 19: 887–902.
349. Decker CJ, Parker R. (1994). Mechanism of mRNA degradation in eukaryotes *Trends Biochem Sci* 19: 336–340.
350. Ganoza MC, Louis BG. (1994). Potential secondary structure at the translational start domain of eukaryotic and prokaryotic mRNAs. *Biochimie* 76(5): 428–439.
351. Kebaara B, Nazarenius T, Taylor R, Forch A, Atkin AL. (2003). The Upf-dependent decay of wild-type PPR1 mRNA depends on its 5'-UTR and first 92 ORF nucleotides. *Nucleic Acids Res* 31: 3157–3165.
352. McCarthy JEG, Kollmus H. (1995). Cytoplasmic mRNA–protein interactions in eukaryotic gene expression. *Trends Biochem Sci* 20: 191–197.
353. Wilhelm JE, Vale RD. (1993). RNA on the move: the mRNA localization pathway. *J Cell Biol* 123: 269–274.
354. Bashirullah A, Cooperstock RL, Lipshitz HD. (1998). RNA localization in development. *Annu Rev Biochem* 67: 335–394.
355. Singer RH. (1992). The cytoskeleton and mRNA localization. *Curr Opin Cell Biol* 4: 15–19.
356. Foyt HL, LeRoith D, Roberts CT. (1991). Differential association of insulin-like growth factor I mRNA variants with polysomes in vivo. *J Biol Chem* 266: 7300–7305.
357. Iida Y, Kanagu D. (2000). Quantification analysis of translation initiation signal in vertebrate mRNAs: effect of nucleotides at positions +4(-)+6 upon efficiency of translation initiation. *Nucleic Acids Symp Ser* (44): 77–78.
358. Kaufman RJ. (1994). Control of gene expression at the level of translation initiation. *Curr Opin Biotechnol* 5: 550–557.
359. Wang G, Guo X, Floros J. (2005). Differences in the translation efficiency and mRNA stability mediated by 5'-UTR splice variants of human SP-A1 and SP-A2 genes. *Am J Physiol Lung Cell Mol Physiol* 289(3): L497–508.
360. Rogers JT, Randall JD, Cahill CM, Eder PS, Huang X, Gunshin H, Leiter L, McPhee J, Sarang SS, Utsuki T, Greig NH, Lahiri DK, Tanzi RE, Bush AI, Giordano T, Gullans SR. (2002). An iron-responsive element type II in the 5'-untranslated region of the Alzheimer's amyloid precursor protein transcript. *J Biol Chem* 277: 45518–45528.

361. Zou Z, Eibl C, Koop HU. (2003). The stem-loop region of the tobacco psbA 5'UTR is an important determinant of mRNA stability and translation efficiency. *Mol Genet Genomics* 269: 340–349.
362. Gray NK, Wickens M. (1998). Control of translation initiation in animals. *Annu Rev Cell Dev Biol* 14: 399–458.
363. Klausner RD, Rouault TA, Harford JB. (1993). Regulating the fate of mRNA: the control of cellular iron metabolism. *Cell* 72: 19–28.
364. Pesole G, Grillo G, Larizza A, Liuni S. (2000). The untranslated regions of eukaryotic mRNAs: structure, function, evolution and bioinformatic tools for their analysis. *Brief Bioinform* 1(3): 236–249.
365. Pesole G, Mignone F, Gissi C, Grillo G, Licciulli F, Liuni S. (2001). Structural and functional features of eukaryotic mRNA untranslated regions. *Gene* 276: 73–81.
366. Van der Velden AW, Thomas AA. (1999). The role of the 5' untranslated region of an mRNA in translation regulation during development. *Int J Biochem Cell Biol* 31: 87–106.
367. Kozak M. (1984). Compilation and analysis of sequences upstream from the translational start site in eukaryotic mRNAs. *NAR* 12(2): 857–872.
368. Altschul SF, Gish W, Miller W, Myers EW, Lipman DJ. (1990). Basic local alignment search tool. *J Mol Biol* 215: 403–410.
369. Altschul SF, Madden TL, Schäffer AA, Zhang J, Zhang Z, Miller W, Lipman DJ. (1997). Gapped BLAST and PSI-BLAST: a new generation of protein database search programs. *Nucleic Acids Res* 25: 3389–3402.
370. Gish W, States DJ. (1993). Identification of protein coding regions by database similarity search. *Nature Genet* 3: 266–272.
371. Madden TL, Tatusov RL, Zhang J. (1996). Applications of network BLAST server. *Meth Enzymol* 266: 131–141.
372. Zhang J, Madden TL. (1997). PowerBLAST: A new network BLAST application for interactive or automated sequence analysis and annotation. *Genome Res* 7: 649–656.
373. Zhang Z, Schwartz S, Wagner L, Miller W. (2000). A greedy algorithm for aligning DNA sequences. *J Comput Biol* 7(1-2): 203–214.
374. Edgar R, Domrachev M, Lash AE. (2002). Gene Expression Omnibus: NCBI gene expression and hybridization array data repository. *Nucleic Acids Res* 30(1): 207–210.
375. von Heijne G. (1984). How signal sequences maintain cleavage specificity. *J Mol Biol* 173(2): 243–251.

376. von Heijne G. (1984). Analysis of the distribution of charged residues in the N-terminal region of signal sequences: implications for protein export in prokaryotic and eukaryotic cells. *EMBO J* 3(10): 2315-2318.
377. von Heijne G. (1985). Signal sequences. The limits of variation. *J Mol Biol* 184(1): 99-105.
378. Walter P, Ibrahimi I, Blobel G. (1981). Translocation of proteins across the endoplasmic reticulum. I. Signal recognition protein (SRP) binds to in-vitro-assembled polysomes synthesizing secretory protein. *J Cell Biol* 91: 545-50.
379. Gilmore R, Blobel G. (1983). Transient involvement of signal recognition particle and its receptor in the microsomal membrane prior to protein translocation. *Cell* 35: 677-685.
380. Hall MN, Gabay J, Schwartz M. (1983). Evidence for a coupling of synthesis and export of an outer membrane protein in *Escherichia coli*. *EMBO J* 2(1): 15-19.
381. Silhavy TJ, Benson SA, Emr SD. (1983). Mechanisms of protein localization. *Microbiol Rev* 47(3): 313-344.
382. von Heijne G. (1990). The signal peptide. *J Membr Biol* 115(3): 195-201.
383. von Heijne G. (1990). Protein targeting signals. *Curr Opin Cell Biol* 2(4): 604-608.
384. von Heijne G. (1986). Net N-C charge imbalance may be important for signal sequence function in bacteria. *J Mol Biol* 192(2): 287-290.
385. Vlasuk GP, Inouye S, Ito H, Itakura K, Inouye M. (1983) Effects of the complete removal of basic amino acid residues from the signal peptide on secretion of lipoprotein in *Escherichia coli*. *J Biol Chem*. 258(11): 7141-7148.
386. von Heijne G. (1983). Patterns of amino acids near signal-sequence cleavage sites. *Eur J Biochem* 133(1): 17-21.
387. Perlman D, Halvorson HO. (1983). A putative signal peptidase recognition site and sequence in eukaryotic and prokaryotic signal peptides. *J Mol Biol*. 167(2): 391-409.
388. Jagla B, Schuchhardt J. (2000). Adaptive encoding neural networks for the recognition of human signal peptide cleavage sites. *Bioinformatics* 16(3): 245-50.
389. Nielsen H, Engelbrecht J, Brunak S, von Heijne G. (1997) Identification of prokaryotic and eukaryotic signal peptides and prediction of their cleavage sites. *Protein Eng* 10(1): 1-6.
390. Nielsen H, Engelbrecht J, Brunak S, von Heijne G. (1997) A neural network method for identification of prokaryotic and eukaryotic signal peptides and prediction of their cleavage sites. *Int J Neural Syst* 8(5-6): 581-599.
391. Southern JA, Young DF, Heaney F, Baumgartner W, Randall RE. (1991). Identification of an Epitope on the P and V Proteins of Simian Virus 5 That Distinguishes

Between Two Isolates with Different Biological Characteristics. *J Gen Virol* 72: 1551-1557.

392. Esmon CT. (1987) The regulation of natural anticoagulant pathways. *Science* 235: 1348–1352.

393. Kisiel W, Ericsson LH, Davie EW. (1976). Proteolytic activation of protein C from bovine plasma. *Biochemistry* 15(22): 4893-4900.

394. Stearns DJ, Kurosawa S, Sims PJ, Esmon NL, Esmon CT. (1988). The interaction of a Ca^{2+} -dependent monoclonal antibody with the protein C activation peptide region. Evidence for obligatory Ca^{2+} binding to both antigen and antibody. *J Biol Chem* 263: 826–832.

395. Fiore MM, Neuenschwander PF, Morrissey JH. (1992). An unusual antibody that blocks tissue factor/factor VIIa function by inhibiting cleavage only of macromolecular substrates. *Blood* 80: 3127–3134.

396. Rezaie AR, Esmon CT. (1992). The function of calcium in protein C activation by thrombin and the thrombin-thrombomodulin complex can be distinguished by mutational analysis of protein C derivatives. *J Biol Chem* 267: 26104–26109.

397. Rezaie AR, Neuenschwander PF, Morrissey JH, Esmon CT. (1993). Analysis of the functions of the first epidermal growth factor-like domain of factor X. *J Biol Chem* 268: 8176–8180.

398. Rezaie AR, Esmon CT. (1994). Asp-70-->Lys mutant of factor X lacks high affinity Ca^{2+} binding site yet retains function. *J Biol Chem* 269: 21495–21499.

399. Rezaie AR, Esmon CT. (1994). Proline at the P2 position in protein C is important for calcium-mediated regulation of protein C activation and secretion. *Blood* 83: 2526–2531.

400. Rezaie AR, Fiore MM, Neuenschwander PF, Esmon CT, Morrissey JH. (1992). Expression and purification of a soluble tissue factor fusion protein with an epitope for an unusual calcium-dependent antibody. *Protein Expression and Purification* 3: 453–460.

401. Zheng Z, Katoh S, He Q, Oritani K, Miyake K, Lesley J, Hyman R, Hamik A, Parkhouse RM, Farr AG. (1995). Monoclonal antibodies to CD44 and their influence on hyaluronan recognition. *J Cell Biol* 130: 485–495.

402. Prickett KS, Amberg DC, Hopp TP. (1989). A calcium-dependent antibody for identification and purification of recombinant proteins. *BioTechniques* 7: 580–589.

403. Kreis TE. (1986). Microinjected antibodies against the cytoplasmic domain of vesicular stomatitis virus glycoprotein block its transport to the cell surface. *EMBO J* 5: 931–941.

404. Algrain M, Turunen O, Vaheri A, Louvard D, Arpin M. (1993). Ezrin contains cytoskeleton and membrane binding domains accounting for its proposed role as a membrane-cytoskeletal linker. *J Cell Bio* 120: 129–139.
405. Rivard N, McKenzie FR, Brondello JM, Pouyssegur J. (1995). The phosphotyrosine phosphatase PTP1D, but not PTP1C, is an essential mediator of fibroblast proliferation induced by tyrosine kinase and G protein-coupled receptors. *J Biol Chem* 270: 11017–11024.
406. Soldati T, Perriard JC. (1991). Intracompartamental sorting of essential myosin light chains: molecular dissection and in vivo monitoring by epitope tagging. *Cell* 66: 277–289.
407. van der Spek J, Hémaré A, Dautry-Varsat A, Boquet P, Murphy JR. (1994). Epitope tagging of DAB389IL-2: new insights into C-domain delivery to the cytosol of target cells. *Leukemia* 8 (supp 1): S144–S148.
408. Vouret-Craviari V, Grall D, Chambard JC, Rasmussen UB, Pouyssegur J, Van Obberghen-Schilling E. (1995). Post-translational and activation-dependent modifications of the G protein-coupled thrombin receptor. *J Biol Chem* 270: 8367–8372.
409. Wilson IA, Niman HL, Houghten RA, Cherenson AR, Connolly ML, Lerner RA. (1984). The structure of an antigenic determinant in a protein. *Cell* 37(3): 767-778.
410. Field J, Nikawa J, Broek D, MacDonald B, Rodgers L, Wilson IA, Lerner RA, Wigler M. (1988). Purification of a RAS-responsive adenylyl cyclase complex from *Saccharomyces cerevisiae* by use of an epitope addition method. *Mol Cell Biol* 8(5): 2159-2165.
411. Kolodziej PA, Young RA. (1991). Epitope tagging and protein surveillance. *Methods Enzymol* 194: 508-519.
412. Wadzinski BE, Eisfelder BJ, Peruski LF Jr, Mumby MC, Johnson GL. (1992). NH₂-terminal modification of the phosphatase 2A catalytic subunit allows functional expression in mammalian cells. *J Biol Chem* 267(24): 16883-16888.
413. Pines J, Hunter T. (1991). Human cyclins A and B1 are differentially located in the cell and undergo cell cycle-dependent nuclear transport. *J Cell Biol* 115(1): 1-17.
414. Malo D, Gros P, Bergmann A, Trask B, Mohrenweiser HW, Canfield VA, Levenson R. (1993). Genes encoding the H,K-ATPase alpha and Na,K-ATPase alpha 3 subunits are linked on mouse chromosome 7 and human chromosome 19. *Mamm Genome* 4(11): 644-649.
415. Antebi A, Fink GR. (1992). The yeast Ca²⁺-ATPase homologue, PMR1, is required for normal Golgi function and localizes in a novel Golgi-like distribution. *Mol Biol Cell* 3(6): 633-654.
416. Sherwood PW, Tsang SV, Osley MA. (1993). Characterization of HIR1 and HIR2, two genes required for regulation of histone gene transcription in *Saccharomyces cerevisiae*. *Mol Cell Biol* 13(1): 28-38.

417. Shen WC, Selvakumar D, Stanford DR, Hopper AK. (1993). The *Saccharomyces cerevisiae* LOS1 gene involved in pre-tRNA splicing encodes a nuclear protein that behaves as a component of the nuclear matrix. *J Biol Chem* 268(26): 19436-19444.
418. Herscovics A, Schneikert J, Athanassiadis A, Moremen KW. (1994). Isolation of a mouse Golgi mannosidase cDNA, a member of a gene family conserved from yeast to mammals. *J Biol Chem* 269(13): 9864-9871.
419. Manolson MF, Wu B, Proteau D, Taillon BE, Roberts BT, Hoyt MA, Jones EW. (1994). STV1 gene encodes functional homologue of 95-kDa yeast vacuolar H(+)-ATPase subunit Vph1p. *J Biol Chem* 269(19): 14064-14074.
420. Berkower C, Loayza D, Michaelis S. (1994). Metabolic instability and constitutive endocytosis of STE6, the a-factor transporter of *Saccharomyces cerevisiae*. *Mol Biol Cell* 5(11): 1185-1198.
421. Templeton DJ. (1992). Nuclear binding of purified retinoblastoma gene product is determined by cell cycle-regulated phosphorylation. *Mol Cell Biol* 12(2): 435-443.
422. Zhou Q, Lieberman PM, Boyer TG, Berk AJ. (1992). Holo-TFIID supports transcriptional stimulation by diverse activators and from a TATA-less promoter. *Genes Dev* 6(10): 1964-1974.
423. Emrich T, Förster R, Lipp M. (1993). Topological characterization of the lymphoid-specific seven transmembrane receptor BLR1 by epitope-tagging and high level expression. *Biochem Biophys Res Commun* 197(1): 214-220.
424. Malo D, Gros P, Bergmann A, Trask B, Mohrenweiser HW, Canfield VA, Levenson R. (1993). Genes encoding the H,K-ATPase alpha and Na,K-ATPase alpha 3 subunits are linked on mouse chromosome 7 and human chromosome 19. *Mamm Genome* 4(11): 644-649.
425. Chen YT, Holcomb C, Moore HP. (1993). Expression and localization of two low molecular weight GTP-binding proteins, Rab8 and Rab10, by epitope tag. *Proc Natl Acad Sci USA* 90(14): 6508-6512.
426. Niman HL, Houghten RA, Walker LE, Reisfeld RA, Wilson IA, Hogle JM, Lerner RA. (1983). Generation of protein-reactive antibodies by short peptides is an event of high frequency: implications for the structural basis of immune recognition. *Proc Natl Acad Sci USA* 80(16): 4949-4953.
427. Evan GI, Lewis GK, Ramsay G, Bishop JM. (1985). Isolation of monoclonal antibodies specific for human c-myc proto-oncogene product. *Mol Cell Biol* 5(12):3610-3616.
428. Cravchik A, Matus A. (1993). A novel strategy for the immunological tagging of cDNA constructs. *Gene* 137(1): 139-143.
429. Kolodziej PA, Young RA. (1991). Epitope tagging and protein surveillance. *Methods Enzymol* 194: 508-519.

430. Munro S, Pelham HR. (1987). A C-terminal signal prevents secretion of luminal ER proteins. *Cell* 48(5): 899-907.
431. Chiang CM, Roeder RG. (1993). Expression and purification of general transcription factors by FLAG epitope-tagging and peptide elution. *Pept Res* 6(2): 62-64.
432. Brizzard BL, Chubet RG, Vizard DL. (1994). Immunoaffinity purification of FLAG epitope-tagged bacterial alkaline phosphatase using a novel monoclonal antibody and peptide elution. *Biotechniques* 16(4): 730-735.
433. Ford CF, Suominen I, Glatz CE. (1991). Fusion tails for the recovery and purification of recombinant proteins. *Protein Expr Purif* 2(2-3): 95-107.
434. Hopp TP, Prickett KS, Price V, Libby RT, March CJ, Cerritti P, Urdal DL, Conlon PJ. (1988). A short polypeptide marker sequence useful for recombinant protein identification and purification. *BioTechnology* 6: 1205-1210.
435. Gerard NP, Gerard C. (1990). Construction and expression of a novel recombinant anaphylatoxin, C5a-N19, as a probe for the human C5a receptor. *Biochemistry* 29(39): 9274-9281.
436. Brizzard BL, Chubet RG, Vizard DL. (1994). Immunoaffinity purification of FLAG epitope-tagged bacterial alkaline phosphatase using a novel monoclonal antibody and peptide elution. *Biotechniques* 16(4): 730-735.
437. Schäfer K, Braun T. (1995). Monoclonal anti-FLAG antibodies react with a new isoform of rat Mg²⁺ dependent protein phosphatase beta. *Biochem Biophys Res Commun* 207(2): 708-714.
438. Keil B. (1971). Reaction of arginine residues in basic pancreatic trypsin inhibitor with phenylglyoxal. *FEBS Lett* 14(3): 181-184.
439. Prickett KS, Amberg DC, Hopp TP. (1989). A calcium-dependent antibody for identification and purification of recombinant proteins. *Biotechniques* 7(6):580-589.
440. Light A, Savithri HS, Liepnieks JJ. (1980). Specificity of bovine enterokinase toward protein substrates. *Anal Biochem* 106(1): 199-206.
441. Carrington JC, Dougherty WG. (1988). A viral cleavage site cassette: identification of amino acid sequences required for tobacco etch virus polyprotein processing. *Proc Natl Acad Sci USA* 85: 3391-3395.
442. Dougherty WG, Parks TD. (1989). Molecular genetic and biochemical evidence for the involvement of the heptapeptide cleavage sequence in determining the reaction profile at two tobacco etch virus cleavage sites in cell-free assays. *Virology* 172(1): 145-155.
443. Dougherty WG, Carrington JC, Cary SM, Parks TD. (1988). Biochemical and mutational analysis of a plant virus polyprotein cleavage site. *EMBO J* 7(5): 1281-1287.

444. Dougherty WG, Parks TD, Cary SM, Bazan JF, Fletterick RJ. (1989). Characterization of the catalytic residues of the tobacco etch virus 49-kDa proteinase. *Virology* 172(1): 302-310.
445. Dougherty WG, Cary SM, Parks TD. (1989). Molecular genetic analysis of a plant virus polyprotein cleavage site: a model. *Virology* 171: 356-364.
446. Kapust RB, Tözsér J, Copeland TD, Waugh DS. (2002). The P1' specificity of tobacco etch virus protease. *Biochem Biophys Res Commun* 294: 949-955.
447. Phan J, Zdanov A, Evdokimov AG, Tropea JE, Peters HPK, Kapust RB, Li M, Wlodawer A, Waugh DS. (2002). Structural basis for the substrate specificity of tobacco etch virus protease. *J Biol Chem* 277: 50564-50572.
448. Kapust RB, Tözsér J, Fox JD, Anderson DE, Cherry S, Copeland TD, Waugh DS. (2001). Tobacco etch virus protease: Mechanism of autolysis and rational design of stable mutants with wild-type catalytic proficiency. *Prot Eng* 14: 993-1000.
449. Lucast LJ, Batey RT, Doudna JA. (2001). Large-scale purification of a stable form of recombinant tobacco etch virus protease. *Biotechniques* 30: 544-550.
450. Bar-Nun S, Shneyour Y, Beckmann JS. (1983). G-418, an elongation inhibitor of 80 S ribosomes. *Biochim Biophys Acta* 741: 123-127.
451. Colbere-Garapin F, Horodniceanu F, Kourilsky P, Garapin AC. (1981). A new dominant hybrid selective marker for higher eukaryotic cells. *J Mol Biol* 150: 1-14.
452. Loebenberg D, Counels M, Waitz JA. (1975). G418, a new micromomospore-produced aminoglycoside with activity against protozoa and helminths: antiparasitic activity. *Antimicrob Agents Chemother* 7: 811-815.
453. Southern P, Berg P. (1982). Transformation of mammalian cells to antibiotic resistance with a bacterial gene under control of the SV40 early region promoter. *J Mol Biol* 1: 327-341.
454. Mulsant P, Gatignol A, Dalens M, Tiraby G. (1988). Phleomycin resistance as a dominant selectable marker in CHO cells. *Somatic Cell Mol Genet* 14: 243-252.
455. Sugiyama M, Thompson CJ, Kumagai T, Suzuki K, Deblaere R, Villarroel R, Davies J. (1994). Characterisation by molecular cloning of two genes from *Streptomyces verticillus* encoding resistance to bleomycin. *Gene* 151: 11-16.
456. Gritz L, Davies J. (1983). Plasmid-encoded hygromycin-B resistance: The sequence of hygromycin-B-phosphotransferase gene and its expression in *E. coli* and *S. cerevisiae*. *Gene* 25: 179-188.
457. Palmer TD, Hock RA, Osborne WRA, Miller AD. (1987). Efficient retrovirus-mediated transfer and expression of a human adenosine deaminase gene in diploid skin fibroblasts from an adenosine-deficient human. *Proc Natl Acad Sci USA* 84: 1055-1059.

458. De la Luna S, Sorina I, Pulido D, Ortin J, Jimenez A. (1988). Efficient transformation of mammalian cells with constructs containing a puromycin-resistance marker. *Gene* 62: 121-126.
459. Eyckerman S, Verhee A, der Heyden JV, Lemmens I, Ostade XV, Vandekerckhove J, Tavernier J. (2001). Design and application of a cytokine-receptor-based interaction trap. *Nat Cell Biol* 3(12): 1114-1119.
460. Tabuchi I. (2003). Next-generation protein-handling method: puromycin analogue technology. *Biochem Biophys Res Commun* 305(1): 1-5.
461. Izumi M, Miyazawa H, Kamakura T, Yamaguchi I, Endo T, Hanaoka F. (1991). Blasticidin S-resistance gene (bsr): a novel selectable marker for mammalian cells. *Exp Cell Res* 197: 229-233.
462. Kimura M, Takatsuki A, Yamaguchi I. (1994). Blasticidin S Deaminase Gene from *Aspergillus terreus* (BSD): A New Drug Resistance Gene for Transfection of Mammalian Cells. *Biochim Biophys ACTA* 1219: 653-659.
463. Mamoun CB, Gluzman IY, Goyard S, Beverley SM, Goldberg DE. (1999). A set of independent selectable markers for transfection of the human malaria parasite *Plasmodium falciparum*. *Proc Natl Acad Sci USA* 96(15): 8716-8720.
464. Takeuchi S, Hirayama K, Ueda K, Sakai H, Yonehara, H. (1958). Blasticidin S, A New Antibiotic. *The Journal of Antibiotics Series A* 11: 1-5.
465. Yamaguchi H, Yamamoto C, Tanaka N. (1965). Inhibition of Protein Synthesis by Blasticidin S. I. Studies with Cell-free Systems from Bacterial and Mammalian Cells. *J Biochem (Tokyo)* 57: 667-677.
466. Hozumi K, Suzuki N, Nielsen PK, Nomizu M, Yamada Y. (2006). Laminin alpha1 chain LG4 module promotes cell attachment through syndecans and cell spreading through integrin alpha2beta1. *J Biol Chem* 281(43): 32929-32940.
467. Wizemann H, Garbe JH, Friedrich MV, Timpl R, Sasaki T, Hohenester E. (2003). Distinct requirements for heparin and alpha-dystroglycan binding revealed by structure-based mutagenesis of the laminin alpha2 LG4-LG5 domain pair. *J Mol Biol* 332(3): 635-642.
468. Odenthal U, Haehn S, Tunggal P, Merkl B, Schomburg D, Frie C, Paulsson M, Smyth N. (2004). Molecular analysis of laminin N-terminal domains mediating self-interactions. *J Biol Chem* 279(43): 44504-44512.
469. Tsiper MV, Yurchenco PD. (2002). Laminin assembles into separate basement membrane and fibrillar matrices in Schwann cells. *J Cell Sci* 115(Pt 5): 1005-1015.
470. Paulsson M, Aumailley M, Deutzmann R, Timpl R, Beck K, Engel J. (1987). Laminin-nidogen complex. Extraction with chelating agents and structural characterization. *Eur J Biochem* 166: 11-19.

471. McKee KK, Harrison D, Capizzi S, and Yurchenco PD. (2007). Role of laminin terminal globular domains in basement membrane assembly. *JBC* 282(29): 21437-21447.
472. Aumailley M, Pesch M, Tunggal L, Gaill F, RF. (2000). Altered synthesis of laminin 1 and absence of basement membrane component deposition in (β)1 integrin-deficient embryoid bodies. *J Cell Sci* 113: 259-268.
473. Higgins D, Thompson J, Gibson T, Thompson JD, Higgins DG, Gibson TJ. (1994). CLUSTAL W: improving the sensitivity of progressive multiple sequence alignment through sequence weighting, position-specific gap penalties and weight matrix choice. *Nucleic Acids Research* 22: 4673-4680.
474. Singh RD, Puri V, Valiyaveetil JT, Marks DL, Bittman R, Pagano RE. (2003). Selective caveolin-1-dependent endocytosis of glycosphingolipids. *Mol Biol Cell*. 14(8): 3254-3265.
475. Mishra S, Joshi PG. (2007). Lipid raft heterogeneity: an enigma. *J Neurochem* 103 Suppl 1: 135-142.
476. Maggio B. (1997). Molecular interactions of the major myelin glycosphingolipids and myelin basic protein in model membranes. *Neurochem Res* 22(4): 475-481.
477. Maggio B, Yu RK. (1989). Interaction and fusion of unilamellar vesicles containing cerebroside and sulfatides induced by myelin basic protein. *Chem Phys Lipids*. 51(2): 127-36.
478. Kasahara K, Sanai Y. (1999). Possible roles of glycosphingolipids in lipid rafts. *Biophys Chem*. 82(2-3): 121-127.
479. Sotgia F, Razani B, Bonuccelli G, Schubert W, Battista M, Lee H, Capozza F, Schubert AL, Minetti C, Buckley JT, Lisanti MP. (2002). Intracellular retention of glycosylphosphatidyl inositol-linked proteins in caveolin-deficient cells. *Mol Cell Biol*. 22(11): 3905-3926.
480. Arvanitis DN, Min W, Gong Y, Heng YM, Boggs JM. (2005). Two types of detergent-insoluble, glycosphingolipid/cholesterol-rich membrane domains from isolated myelin. *J Neurochem* 94(6): 1696-1710.
481. Simons K, Toomre D. (2000). Lipid rafts and signal transduction. *Nat Rev Mol Cell Biol* 1(1): 31-39.
482. Wizemann H, Garbe JH, Friedrich MV, Timpl R, Sasaki T, Hohenester E. (2003). Distinct requirements for heparin and alpha-dystroglycan binding revealed by structure-based mutagenesis of the laminin alpha2 LG4-LG5 domain pair. *J Mol Biol* 332(3): 635-642.
483. Suzuki N, Ichikawa N, Kasai S, Yamada M, Nishi N, Morioka H, Yamashita H, Kitagawa Y, Utani A, Hoffman MP, Nomizu M. (2003). Syndecan binding sites in the laminin alpha1 chain G domain. *Biochemistry* 42(43): 12625-12633.

484. Hozumi K, Suzuki N, Nielsen PK, Nomizu M, Yamada Y. (2006). Laminin alpha1 chain LG4 module promotes cell attachment through syndecans and cell spreading through integrin alpha2beta1. *J Biol Chem* 281(43): 32929-32940.
485. Monti E, Preti A, Novati A, Aleo MF, Clemente ML, Marchesini S. (1992). Uptake and metabolism of a fluorescent sulfatide analogue in cultured skin fibroblasts. *Biochim Biophys Acta* 1124(1): 80-87.
486. Friedman Y, Arsenis C. (1972). The resolution of aryl sulfatase and heparin sulfamidase activities from various rat tissues. *Biochem Biophys Res Commun* 48(5): 1133-1139.
487. Waheed A, van Etten RL. (1980). Chemical characterization and substrate specificity of rabbit liver aryl sulfatase A. *Biochim Biophys Acta* 614(1): 92-101.
488. Schaapveld RQ, Schepens JT, Robinson GW, Attema J, Oerlemans FT, Fransen JA, Streuli M, Wieringa B, Hennighausen L, Hendriks WJ. (1997). Impaired mammary gland development and function in mice lacking LAR receptor-like tyrosine phosphatase activity. *Dev Biol* 188: 134-146.
489. Miyagoe Y, Hanaoka K, Nonaka I, Hayasaka M, Nabeshima Y, Arahata K, Nabeshima Y, Takeda S. (1997). Laminin alpha2 chain-null mutant mice by targeted disruption of the Lama2 gene: a new model of merosin (laminin 2)-deficient congenital muscular dystrophy. *FEBS Lett* 415: 33-39.
490. Ryan MC, Lee K, Miyashita Y, Carter WG. (1999). Targeted disruption of the LAMA3 gene in mice reveals abnormalities in survival and late stage differentiation of epithelial cells. *J Cell Biol* 145: 1309-1324.
491. Patton BL, Cunningham JM, Thyboll J, Kortessmaa J, Westerblad H, Edström L, Tryggvason K, Sanes JR. (2001). Properly formed but improperly localized synaptic specializations in the absence of laminin alpha4. *Nat Neurosci* 4(6): 597-604.
492. Thyboll J, Kortessmaa J, Cao R, Soininen R, Wang L, Iivanainen A, Sorokin L, Risling M, Cao Y, Tryggvason K. (2002). Deletion of the laminin alpha4 chain leads to impaired microvessel maturation. *Mol Cell Biol* 22(4): 1194-1202.
493. Miner JH, Cunningham J, Sanes JR. (1998). Roles for laminin in embryogenesis: Exencephaly, syndactyly, and placentopathy in mice lacking the laminin alpha5 chain. *J Cell Biol* 143: 1713-1723.
494. Miner JH, Li C. (2000). Defective glomerulogenesis in the absence of laminin alpha5 demonstrates a developmental role for the kidney glomerular basement membrane. *Dev Biol* 217: 278-289.
495. Noakes PG, Gautam M, Mudd J, Sanes JR, Merlie JP. (1995). Aberrant differentiation of neuromuscular junctions in mice lacking s- laminin/laminin beta 2. *Nature* 374: 258-262.

496. Noakes PG, Miner JH, Gautam M, Cunningham JM, Sanes JR, Merlie JP. (1995). The renal glomerulus of mice lacking s-laminin/laminin beta 2: nephrosis despite molecular compensation by laminin beta 1. *Nat Genet* 10: 400-406.
497. Patton BL, Miner JH, Chiu AY, Sanes JR. (1997). Distribution and function of laminins in the neuromuscular system of developing, adult, and mutant mice. *J Cell Biol* 139(6): 1507-1521.
498. Kuster JE, Guarnieri MH, Ault JG, Flaherty L, Swiatek PJ. (1997). IAP insertion in the murine Lamb3 gene results in junctional epidermolysis bullosa. *Mamm Genome* 8(9): 673-681.
499. Halfter W, Dong S, Yip YP, Willem M, Mayer U. (2002). A critical function of the pial basement membrane in cortical histogenesis. *J Neurosci* 22(14): 6029-6040.
500. Willem M, Miosge N, Halfter W, Smyth N, Jannetti I, Burghart E, Timpl R, Mayer U. (2002). Specific ablation of the nidogen-binding site in the laminin gamma1 chain interferes with kidney and lung development. *Development* 129(11): 2711-2722.
501. Meng X, Klement JF, Leperi DA, Birk DE, Sasaki T, Timpl R, Uitto J, Pulkkinen L. (2003). Targeted inactivation of murine laminin gamma2-chain gene recapitulates human junctional epidermolysis bullosa. *J Invest Dermatol* 121(4): 720-731.
502. Cosgrove D, Meehan DT, Grunkemeyer JA, Kornak JM, Sayers R, Hunter WJ, Samuelson GC. (1996). Collagen COL4A3 knockout: a mouse model for autosomal Alport syndrome. *Genes Dev* 10(23): 2981-2992.
503. Miner JH, Sanes JR. (1996). Molecular and functional defects in kidneys of mice lacking collagen alpha 3(IV): implications for Alport syndrome. *J Cell Biol* 135(5):1403-1413.
504. Arikawa-Hirasawa E, Watanabe H, Takami H, Hassell JR, Yamada Y. (1999). Perlecan is essential for cartilage and cephalic development. *Nature Genet* 23: 354-358.
505. Costell M, Gustafsson E, Aszodi A, Morgelin M, Bloch W, Hunziker E, Addicks K, Timpl R, Fassler R. (1999). Perlecan maintains the integrity of cartilage and some basement membranes. *J Cell Biol* 147: 1109-1122.
506. Murshed M, Smyth N, Miosge N, Karolat J, Krieg T, Paulsson M, Nischt R. (2000). The absence of nidogen 1 does not affect murine basement membrane formation. *Mol Cell Biol* 20(18): 7007-7012.
507. Dong L, Chen Y, Lewis M, Hsieh JC, Reing J, Chaillet JR, Howell CY, Melhem M, Inoue S, Kuszak JR, DeGeest K, Chung AE. (2002). Neurologic defects and selective disruption of basement membranes in mice lacking entactin-1/nidogen-1. *Lab Invest* 82(12): 1617-1630.
508. Schymeinsky J, Nedbal S, Miosge N, Pöschl E, Rao C, Beier DR, Skarnes WC, Timpl R, Bader BL. (2002). Gene structure and functional analysis of the mouse nidogen-2 gene: nidogen-2 is not essential for basement membrane formation in mice. *Mol Cell Biol* 22(19): 6820-6830.

509. Bader BL, Smyth N, Nedbal S, Miosge N, Baranowsky A, Mokkapati S, Murshed M, Nischt R. (2005). Compound genetic ablation of nidogen 1 and 2 causes basement membrane defects and perinatal lethality in mice. *Mol Cell Biol* 25(15): 6846-6856.
510. Gautam M, DeChiara TM, Glass DJ, Yancopoulos GD, Sanes JR. (1999). Distinct phenotypes of mutant mice lacking agrin, MuSK, or rapsyn. *Brain Res Dev Brain Res* 114: 171-178.
511. Stephens LE, Sutherland AE, Klimanskaya IV, Andrieux A, Meneses J, Pedersen RA, Damsky CH. (1995). Deletion of beta 1 integrins in mice results in inner cell mass failure and peri-implantation lethality. *Genes Dev* 9: 1883-1895.
512. Dowling J, Yu QC, Fuchs E. (1996). Beta4 integrin is required for hemidesmosome formation, cell adhesion and cell survival. *J Cell Biol* 134: 559-572.
513. Gardner H, Kreidberg J, Koteliensky V, Jaenisch R. (1996). Deletion of integrin alpha 1 by homologous recombination permits normal murine development but gives rise to a specific deficit in cell adhesion. *Dev Biol* 175: 301-313.
514. Chen J, Diacovo TG, Grenache DG, Santoro SA, Zutter MM. (2002). The alpha(2) integrin subunit-deficient mouse: a multifaceted phenotype including defects of branching morphogenesis and hemostasis. *Am J Pathol* 161(1): 337-344.
515. Holtkötter O, Nieswandt B, Smyth N, Müller W, Hafner M, Schulte V, Krieg T, Eckes B. (2002). Integrin alpha 2-deficient mice develop normally, are fertile, but display partially defective platelet interaction with collagen. *J Biol Chem* 277(13): 10789-10794.
516. DiPersio CM, Hodivala-Dilke KM, Jaenisch R, Kreidberg JA, Hynes RO. (1997). alpha3beta1 integrin is required for normal development of the epidermal basement membrane. *J Cell Biol* 137: 729-742.
517. Kreidberg JA, Donovan MJ, Goldstein SL, Rennke H, Shepherd K, Jones RC, Jaenisch R. (1996). Alpha 3 beta 1 integrin has a crucial role in kidney and lung organogenesis. *Development* 122: 3537-3547.
518. Mayer U, Saher G, Fassler R, Bornemann A, Echtermeyer F, von der Mark H, Miosge N, Poschl E, von der Mark K. (1997). Absence of integrin alpha 7 causes a novel form of muscular dystrophy. *Nat Genet* 17: 318-323.
519. Stepp MA, Gibson HE, Gala PH, Iglesia DD, Pajoohesh-Ganji A, Pal-Ghosh S, Brown M, Aquino C, Schwartz AM, Goldberger O, Hinkes MT, Bernfield M. (2002). Defects in keratinocyte activation during wound healing in the syndecan-1-deficient mouse. *J Cell Sci* 115(Pt 23): 4517-4531.
520. Kaksonen M, Pavlov I, Vöikar V, Lauri SE, Hienola A, Riekkari R, Lakso M, Taira T, Rauvala H. (2002). Syndecan-3-deficient mice exhibit enhanced LTP and impaired hippocampus-dependent memory. *Mol Cell Neurosci* 21(1): 158-172.

521. Cornelison DD, Wilcox-Adelman SA, Goetinck PF, Rauvala H, Rapraeger AC, Olwin BB. (2004). Essential and separable roles for Syndecan-3 and Syndecan-4 in skeletal muscle development and regeneration. *Genes Dev* 18(18): 2231-2236.
522. Ishiguro K, Kadomatsu K, Kojima T, Muramatsu H, Iwase M, Yoshikai Y, Yanada M, Yamamoto K, Matsushita T, Nishimura M, Kusugami K, Saito H, Muramatsu T. (2001). Syndecan-4 deficiency leads to high mortality of lipopolysaccharide-injected mice. *J Biol Chem* 276(50): 47483-47488.
523. Ishiguro K, Kadomatsu K, Kojima T, Muramatsu H, Matsuo S, Kusugami K, Saito H, Muramatsu T. (2001). Syndecan-4 deficiency increases susceptibility to kappa-carrageenan-induced renal damage. *Lab Invest* 81(4): 509-516.
524. Echtermeyer F, Streit M, Wilcox-Adelman S, Saoncella S, Denhez F, Detmar M, Goetinck P. (2001). Delayed wound repair and impaired angiogenesis in mice lacking syndecan-4. *J Clin Invest* 107(2): R9-R14.
525. Litwack ED, Ivins JK, Kumbasar A, Paine-Saunders S, Stipp CS, Lander AD. (1998). Expression of the heparan sulfate proteoglycan glypican-1 in the developing rodent. *Dev Dyn* 211(1): 72-87.
526. Cano-Gauci DF, Song HH, Yang H, McKerlie C, Choo B, Shi W, Pullano R, Piscione TD, Grisaru S, Soon S, Sedlackova L, Tanswell AK, Mak TW, Yeger H, Lockwood GA, Rosenblum ND, Filmus J. (1999). Glypican-3-deficient mice exhibit developmental overgrowth and some of the abnormalities typical of Simpson-Golabi-Behmel syndrome. *J Cell Biol* 146(1): 255-264.
527. Lin X, Perrimon N. (2000). Role of heparan sulfate proteoglycans in cell-cell signaling in *Drosophila*. *Matrix Biol* 19(4): 303-307.
528. Fujita N, Suzuki K, Vanier MT, Popko B, Maeda N, Klein A, Henseler M, Sandhoff K, Nakayasu H, Suzuki K. (1996). Targeted disruption of the mouse sphingolipid activator protein gene: a complex phenotype, including severe leukodystrophy and wide-spread storage of multiple sphingolipids. *Hum Mol Genet* 5(6): 711-725.
529. Hirahara Y, Bansal R, Honke K, Ikenaka K, Wada Y. (2004). Sulfatide is a negative regulator of oligodendrocyte differentiation: development in sulfatide-null mice. *Glia* 45(3): 269-277.
530. Schaapveld RQ, Schepens JT, Robinson GW, Attema J, Oerlemans FT, Fransen JA, Streuli M, Wieringa B, Hennighausen L, Hendriks WJ. (1997). Impaired mammary gland development and function in mice lacking LAR receptor-like tyrosine phosphatase activity. *Dev Biol* 188(1): 134-146.
531. Ren JM, Li PM, Zhang WR, Sweet LJ, Cline G, Shulman GI, Livingston JN, Goldstein BJ. (1998). Transgenic mice deficient in the LAR protein-tyrosine phosphatase exhibit profound defects in glucose homeostasis. *Diabetes* 47(3): 493-497.
532. Vuolteenaho R, Nissinen M, Sainio K, Byers M, Eddy R, Hirvonen H, Shows TB, Sariola H, Engvall E, Tryggvason K. (1994). Human laminin M chain (merosin): complete

primary structure, chromosomal assignment, and expression of the M and A chain in human fetal tissues. *J Cell Biol* 124: 381-394.

533. Ogawa M, Ikeuchi K, Watanabe M, Etoh K, Kobayashi T, Takao Y, Anazawa S, Yamazaki Y. (2005). Expression of matrix metalloproteinase 7, laminin and type IV collagen-associated liver metastasis in human colorectal cancer: immunohistochemical approach. *Hepatogastroenterology* 52(63): 875-880.

534. Ehrig K, Leivo I, Argraves WS, Ruoslahti E, Engvall E. (1990). Merosin, a tissue-specific basement membrane protein, is a laminin-like protein. *Proc Natl Acad Sci USA* 87: 3264-3268.

535. Sunada Y, Bernier SM, Kozak CA, Yamada Y, Campbell KP. (1994). Deficiency of merosin in dystrophic dy mice and genetic linkage of laminin M chain gene to dy locus. *J.Biol.Chem.* 269: 13729-13732.

536. McGrath JA, Kivirikko S, Ciatti S, Moss C, Dunnill GS, Eady RA, Rodeck CH, Christiano AM, Uitto J. (1995). A homozygous nonsense mutation in the alpha 3 chain gene of laminin 5 (LAMA3) in Herlitz junctional epidermolysis bullosa: Prenatal exclusion in a fetus at risk. *Genomics* 29: 282-284.

537. Ryan MC, Christiano AM, Engvall E, Wewer UM, Miner JH, Sanes JR, Burgeson RE. (1996). The functions of laminins: lessons from in vivo studies. *Matrix Biol* 15: 369-381.

538. Ryan MC, Tizard R, VanDevanter DR, Carter WG. (1994). Cloning of the LamA3 gene encoding the alpha 3 chain of the adhesive ligand epiligrin. Expression in wound repair. *J Biol Chem* 269: 22779-22787.

539. Iivanainen A, Korttesmaa J, Sahlberg C, Morita T, Bergmann U, Thesleff I, Tryggvason K. (1997). Primary Structure, Developmental Expression, and Immunolocalization of the Murine Laminin alpha4 Chain. *J Biol Chem* 272: 27862-27863.

540. Iivanainen A, Sainio K, Sariola H, Tryggvason K. (1995). Primary structure and expression of a novel human laminin alpha 4 chain. *FEBS Lett* 365: 183-188.

541. Richards A, Al-Imara L, Pope FM. (1996). The complete cDNA sequence of laminin alpha 4 and its relationship to the other human laminin alpha chains. *Eur J Biochem* 238: 813-821.

542. Richards AJ, al Imara L, Carter NP, Lloyd JC, Leversha MA, Pope FM. (1994). Localization of the gene (LAMA4) to chromosome 6q21 and isolation of a partial cDNA encoding a variant laminin A chain. *Genomics* 22: 237-239.

543. Patton BL, Chiu AY, Sanes JR. (1998). Synaptic laminin prevents glial entry into the synaptic cleft. *Nature* 393: 698-701.

544. Patton BL, Miner JH, Chiu AY, Sanes JR. (1997). Distribution and function of laminins in the neuromuscular system of developing, adult, and mutant mice. *J Cell Biol* 139: 1507-1521.

545. Hunter DD, Porter BE, Bullock JW, Adams SP, Merlie JP, Sanes JR. (1989). Primary sequence of a motor neuron-selective adhesive site in the synaptic basal lamina protein S-laminin. *Cell* 59: 905-913.
546. Hunter DD, Shah V, Merlie JP, Sanes JR. (1989). A laminin-like adhesive protein concentrated in the synaptic cleft of the neuromuscular junction. *Nature* 338: 229-234.
547. Pulkkinen L, Gerecke DR, Christiano AM, Wagman DW, Burgeson RE, Uitto J. (1995). Cloning of the beta 3 chain gene (LAMB3) of human laminin 5, a candidate gene in junctional epidermolysis bullosa. *Genomics* 25: 192-198.
548. Kuster JE, Guarnieri MH, Ault JG, Flaherty L, Swiatek PJ. (1997). IAP insertion in the murine LamB3 gene results in junctional epidermolysis bullosa. *Mamm Genome* 8(9): 673-681.
549. Pulkkinen L, Christiano AM, Airenne T, Haakana H, Tryggvason K, Uitto J. (1994). Mutations in the gamma 2 chain gene (LAMC2) of kalinin/laminin 5 in the junctional forms of epidermolysis bullosa. *Nat Genet* 6: 293-297.
550. Meng X, Klement JF, Leperi DA, Birk DE, Sasaki T, Timpl R, Uitto J, Pulkkinen L. (2003). Targeted inactivation of murine laminin gamma2-chain gene recapitulates human junctional epidermolysis bullosa. *J Invest Dermatol* 121(4): 720-731.
551. Koch M, Olson PF, Albus A, Jin W, Hunter DD, Brunken WJ, Burgeson RE, Champlaud MF. (1999). Characterization and Expression of the Laminin gamma3 Chain: A Novel, Non-Basement Membrane-associated, Laminin Chain. *J Cell Biol* 145: 605-618.

ABBREVIATIONS

Ab	-	antibody
AChR	-	acetyl choline receptor
α DG	-	alpha dystroglycan
AEBSF	-	4-(2-aminoethyl)benzenesulfonyl fluoride
BLAST	-	Basic Local Alignment Search Tool
BM	-	basement membrane
BODIPY	-	boron dipyrromethene difluoride
BODIPY-Cer	-	N-[5-(5,7-dimethyl BODIPY)-1-pentanoyl]-D-erythro-sphingosine
BSA	-	bovine serum albumin
Bt2cAMP	-	N ₆ ,O _{2'} -dibutyryl adenosine 3',5'-cyclic monophosphate
CAM	-	cell adhesion molecule
Cer	-	ceramide
CHAPS	-	3-[3-cholamidopropyl]-dimethylammonio]-1-propane-sulfonate: buffer
c-myc	-	transcription factor
CMV	-	cytomegalovirus
CNS	-	central nervous system
con2	-	the derived "consensus 2" 5' UTR sequence
CS	-	chondroitin sulfate
Cy3	-	cyanine 3; yellow-orange (~550 nm excitation, ~570 nm emission)
Cy5	-	cyanine 5; Cy5 is fluorescent in the red region (~650/670nm)
DAG	-	diacylglycerol
DAPI	-	4',6-diamidino-2-phenylindole; fluorescent stain binds strongly to DNA
DEPC	-	diethylpyrocarbonate: RNase inactivator
DF-BSA	-	defatted bovine serum albumin
DMEM	-	Dulbeccos minimum essential medium
DMF	-	dimethylformamide: organic solvent
DMSO	-	dimethyl sulfoxide: common solvent
DG	-	dystroglycan
DOC	-	deoxycholate: detergent
DTT	-	dithiothreitol: reducing agent
EB	-	embryoid body
ECM	-	extracellular matrix
EDTA	-	ethylenediaminetetraacetic acid: divalent metal chelator
EGF	-	epidermal growth factor
EHS	-	Englebreth-Holm-Sevard
EIA	-	enzyme immunoassay
eIF	-	eukaryotic initiation factor
EIF4A1 or eif4a1	-	human eukaryotic translation initiation factor 4A
EK	-	Enterokinase
ELISA	-	enzyme linked immunosorbent assay
EMBL	-	European Molecular Biology Laboratory
ES	-	embryonic stem
EST	-	expressed sequence tag
FAK	-	focal adhesion kinase
FBS	-	fetal bovine serum
FDFT1 or fdft1	-	human farnesyl-diphosphate farnesyltransferase 1
FGF	-	fibroblast growth factor
FITC	-	fluorescein isothiocyanate
GAG	-	glycosaminoglycan

GalCer	-	galactosylceramide
gal-sulfatide	-	HSO ₃ -3galactosylβ-1ceramide
GlcCer	-	glucosylceramide
glc-sulfatide	-	HSO ₃ -3glucosylβ-1ceramide
GPI	-	glycosylphosphatidylinositol
HA	-	Haemophilus hemagglutinin
HS	-	heparan sulfate
HSPG	-	heparan sulfate proteoglycan
H2B or h2b	-	human histone H2B
IARS or iars	-	human isoleucyl-tRNA synthetase
IB	-	immunoblot
ICM	-	inner cell mass
IP	-	immunoprecipitated
JEB	-	junctional epidermolysis bullosa
LacCer	-	lactosylceramide
Lm	-	laminin
mAb	-	monoclonal antibody
MAG	-	myelin-associated glycoprotein
MBP	-	myelin basic protein
MEF	-	mouse embryonic lung fibroblast
MOPS	-	morpholinepropanesulfonic acid: buffer
NCAM	-	neural cell adhesion molecule
NCBI	-	National Center for Biotechnology Information
NEB	-	New England BioLabs
NMJ	-	neuromuscular junction
OPD	-	o-phenylenediamine: HRP substrate (ELISA)
PAGE	-	polyacrylamide gel electrophoresis
PBS	-	phosphate buffered saline
pFAK	-	tyrosine phosphorylated focal adhesion kinase
PKC	-	protein kinase C
PMSF	-	phenylmethylsulfonyl fluoride: serine protease inhibitor
PNS	-	peripheral nervous system
polyHEMA	-	2-hydroxyethyl methacrylate
PVDF	-	polyvinylidene fluoride
RA	-	retinoic acid
RIPA	-	radioimmuno precipitation assay buffer
RSV	-	rous sarcoma virus
SC	-	Schwann cell
SDS	-	sodium dodecyl sulfate: ionic detergent
SFK	-	Src family kinase
SGGL-1	-	sulfoglucuronylneolactotetraosylceramide
TEV	-	tobacco etch virus protease
TGF-B	-	transforming growth factor-B
TMB	-	3,3',5,5'-tetramethylbenzidine: HRP substrate (ELISA)
TOMM7 or tomm7	-	human translocase of outer mitochondrial membrane 7 homolog
TRIS	-	tris (hydroxymethyl) aminomethane
TRIS-HCL	-	tris hydrochloride
TRITC	-	tetramethylrhodamine isothiocyanate
UBE2S or ube2s	-	human ubiquitin-conjugating enzyme E2S
5' UTR	-	5' untranslated region
VEGF	-	vascular endothelial growth factor

- V5 - 14 amino acid epitope derived from the P and V proteins of the paramyxovirus, SV5
- VSV-G - vesicular stomatitis virus G protein epitope
- XC - xylene cyanol
- X-gal - 5-bromo-4-chloro-3-indolyl-beta-D-galactoside: B-Gal substrate

ACKNOWLEDGEMENTS

Peter D. Yurchenco

Department of Pathology and Laboratory Medicine, Robert Wood Johnson Medical School, Piscataway, New Jersey 08854, USA

Principal Investigator whose laboratory the majority of this work was performed in, mentor, and person without whose patience and money I could not have had so much fun playing for so long.

Shaohua Li

Department of Surgery, Robert Wood Johnson Medical School, Piscataway, New Jersey 08854, USA

Lead investigator in ES/EB experiments, as well as, early Schwann and MEF experiments whose results were the spring board for my own experiments.

Sadaf-Ahmahni Hussain and Erhard Hohenester

Division of Cell and Molecular Biology, Imperial College London, London SW7 2AZ, UK

Performed the crystallization experiments and generated the structure for mouse $\alpha 1$ LG4-5, as well as making the expression construct which produced the recombinant protein which crystalized.

Ariana Combs and James M. Ervasti

Department of Biochemistry, Molecular Biology & Biophysics, University of Minnesota, Minneapolis, MN 55455, USA

For performing all the α DG binding analyses.

Karen McKee

Department of Pathology and Laboratory Medicine, Robert Wood Johnson Medical School, Piscataway, New Jersey 08854, USA

Performed the majority of polymerization assays, made both the $\gamma 1$ point mutations and domain swaps, helped with a number of recombinant proteins (transfections, screening, testing, purifications).

Segei Smirnov

Department of Pathology and Laboratory Medicine, Robert Wood Johnson Medical School, Piscataway, New Jersey 08854, USA

Provided various recombinant Lm-211 producing cell lines from which I was able to purify the various recombinant Lm-211 proteins from for experiments described in this thesis.

Raj Patel

Department of Pathology and Laboratory Medicine, Robert Wood Johnson Medical School, Piscataway, New Jersey 08854, USA

For help with electron microscopy and many lunches.

Patricia Liquari

Department of Pathology and Laboratory Medicine, Robert Wood Johnson Medical School, Piscataway, New Jersey 08854, USA

Stephanie Capizzi

Department of Pathology and Laboratory Medicine, Robert Wood Johnson Medical School, Piscataway, New Jersey 08854, USA

Gale Rhodes

Dept. of Chemistry, University of Southern Maine; Portland, Maine, USA

Manuel Peitsch, Torsten Schwede, and Nicolas Guex

For hosting a tutorial for DeepView/Swiss-Pdb Viewer Manuel Peitsch initiated SWISS-MODEL and is currently being developed by Torsten Schwede at the Structural Bioinformatics Group, Biozentrum (univ of Basel) within the SIB (Swiss Institute of Bioinformatics) and Nicolas Guex at GlaxoSmithKline.

Neil Smyth and **David Edgar** for the laminin $\gamma 1$ -/- ES cell line

Sal Carbonetto for the DG -/- ES cell line

*This work was supported by a Wellcome Senior Fellowship to E.H. and NIH grant R37-DK36425 to P.D.Y

The atomic coordinates and structure factors (code 2JD4) have been deposited in the Protein Data Bank (<http://www.rcsb.org>)